Simetría magnética aplicada al estudio de materiales magnéticos: nuevos programas del *Bilbao Crystallographic Server*

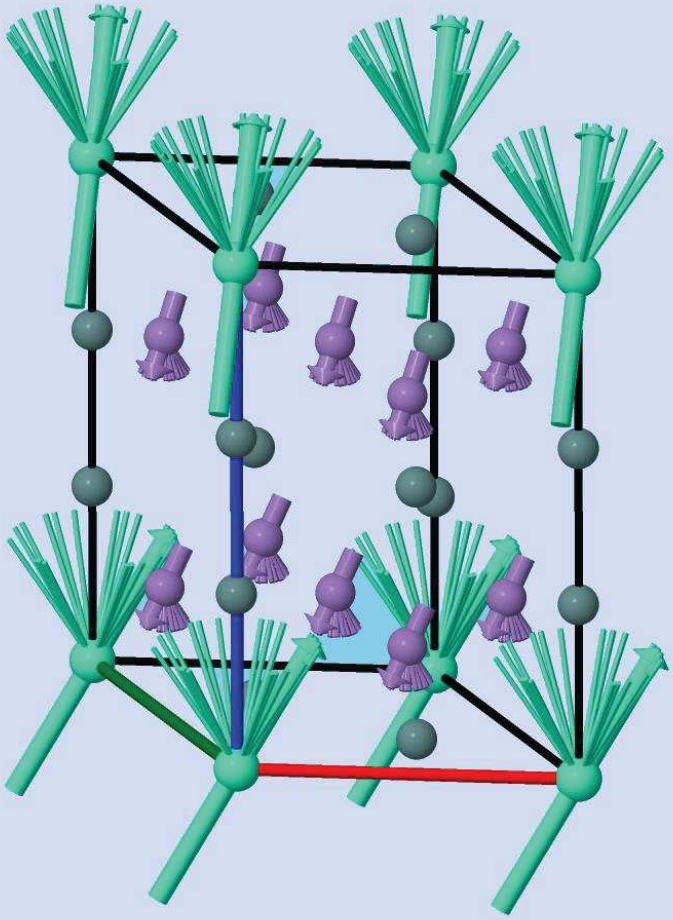

Samuel Vidal Gallego

Diciembre 2017

erman ta zabal zazu
Universidad del País Vasco
Euskal Herriko Unibertsitatea

SIMETRÍA MAGNÉTICA APLICADA AL ESTUDIO DE MATERIALES MAGNÉTICOS: NUEVOS PROGRAMAS DEL *BILBAO CRYSTALLOGRAPHIC SERVER*

ÍNDICE

SIMETRÍA MAGNÉTICA APLICADA AL ESTUDIO DE MATERIALES MAGNÉTICOS: NUEVOS PROGRAMAS DEL *BILBAO CRYSTALLOGRAPHIC SERVER*

1. INTRODUCCIÓN

Gran parte de las propiedades físicas de los sólidos dependen del orden presente en la disposición espacial de los átomos que componen dicho sólido. En las estructuras cristalinas, ya sean conmensurables o inconmensurables, los átomos están ordenados siguiendo un patrón concreto que o bien se repite periódicamente por todo el cristal, o bien sigue una pauta descrita por unos pocos parámetros. Esta distribución ordenada de los átomos implica que la correspondiente estructura permanece invariante ante diversas operaciones de simetría dentro de su rango de estabilidad termodinámica, y muchas propiedades físicas son consecuencia directa de dicha simetría. El estudio y determinación del orden presente en las estructuras cristalinas, de su simetría y de las propiedades físicas que de ella se derivan es la Cristalografía, a la que está dedicado el *Bilbao Crystallographic Server* [1-3].

El *Bilbao Crystallographic Server* (http://www.cryst.ehu.es) es un servidor web iniciado en 1997, disponible online de forma gratuita, cuyo objetivo es hacer uso de la computación para poner a disposición de investigadores de todo el mundo bases de datos, herramientas y programas interactivos relacionados con el uso práctico de la cristalografía en la investigación científica. Por un lado, el *Bilbao Crystallographic Server* proporciona bases de datos cristalográficas que contienen información similar a la disponible en *International Tables for Crystallography, Vol. A: Space-group Symmetry, Vol. A1: Symmetry Relations between Space Groups y Vol. E: Subperiodic Groups*, pero con diversas extensiones y ampliaciones asociadas a la flexibilidad que permite una base de datos digital. Por otro lado, contiene diversas aplicaciones, diseñadas para ser fáciles de utilizar por personas no necesariamente expertas, orientadas fundamentalmente a posibilitar, facilitar y mejorar diversos cálculos y tareas relacionados con la simetría y la teoría de grupos. Son tareas usuales en el campo de la ciencia de materiales, tales como determinación de estructuras cristalinas, estudio de transiciones de fase, análisis de modos de simetría, detección de pseudosimetría, indexación de patrones de difracción, determinación de reglas de selección y ausencias sistemáticas en experimentos de difracción o de *scattering* inelástico, descripción, determinación y recopilación de estructuras magnéticas, recopilación y visualización 3D de estructuras cristalinas, etc.

Con más de 300.000 usuarios únicos al año, el *Bilbao Crystallographic Server* se ha convertido en una herramienta ampliamente conocida entre los investigadores de materiales, que lo utilizan a menudo como parte de su investigación; hecho probado por las numerosas referencias al servidor que pueden encontrarse tanto en la

literatura científica como en las páginas web de instituciones como la *International Union of Crystallography* (IUCr), el *National Institute of Standards* (USA), y otros numerosos sitios web dedicados a diversas áreas relacionadas con la cristalografía, la ciencia de materiales o la física del estado sólido.

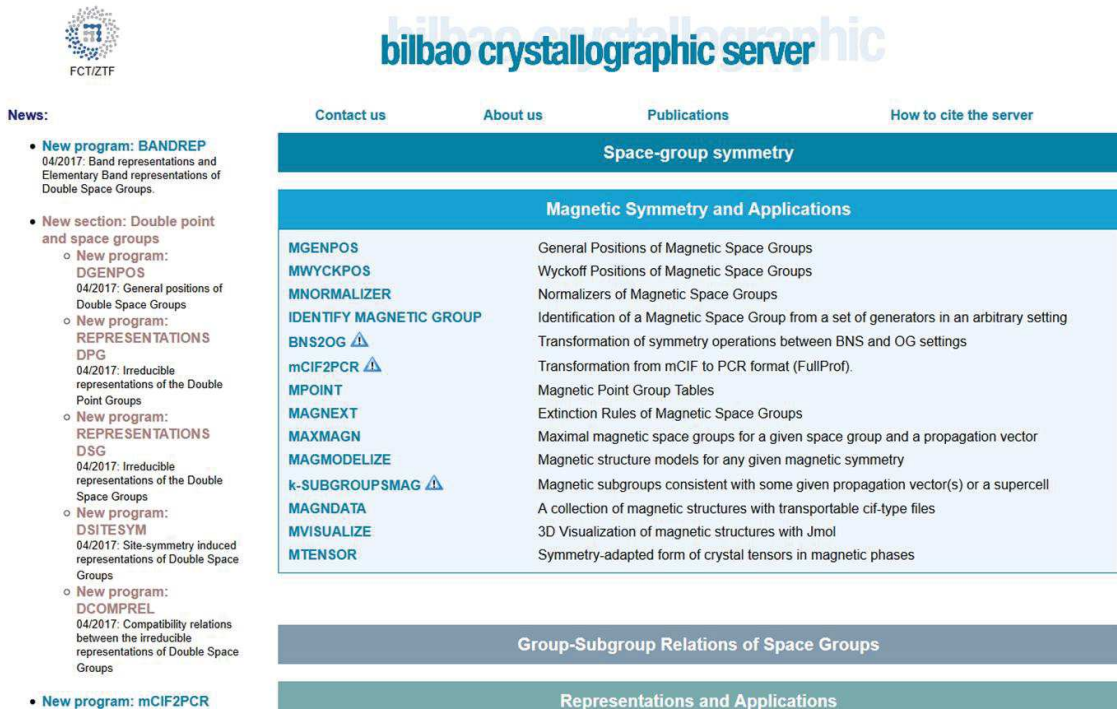

Figura 1. Página principal del *Bilbao Crystallographic Server*.

Esta tesis doctoral ha tenido como objetivo realizar un estudio exhaustivo de la simetría magnética y sus aplicaciones prácticas, desarrollando técnicas y métodos que faciliten su uso. Se han desarrollado diversas aplicaciones informáticas que implementan potentes métodos de análisis basados en la simetría magnética, y que están dirigidas a los investigadores en el campo de la determinación de estructuras magnéticas y el estudio de materiales magnéticos y sus propiedades, con especial énfasis en las propiedades tensoriales de materiales ferroicos y multiferroicos.

De forma general, la determinación de una estructura cristalina requiere el uso y consideración de la simetría cristalina de dicha estructura. Esto no es una excepción en el caso de las estructuras cristalinas magnéticas. No obstante, dicho uso resulta complejo en exceso sin herramientas computacionales adecuadas que simplifiquen los cálculos necesarios. Por ello, tradicionalmente se ha empleado casi en exclusiva el llamado "método de análisis de representaciones" o "*representation method*" [4]. Este método consiste principalmente en considerar la aparición de una fase ordenada magnéticamente (fase magnética) como el resultado de una transición de fase desde una fase paramagnética y, por tanto, como una distorsión de dicha fase paramagnética. De acuerdo con la teoría de Landau de las transiciones de fase, esa distorsión es consecuencia de la condensación de ondas de espín o "*spin waves*" que crean un ordenamiento con momentos magnéticos atómicos no nulos. Las amplitudes de estas ondas constituyen el llamado parámetro de orden que es nulo en la fase

paramagnética y no nulo en la fase magnética, y cuya aparición causa la transición de fase. La teoría de Landau postula entonces que el parámetro de orden asociado a la transición transforma según una única representación irreducible o *irrep* del grupo de simetría de la fase paramagnética. Este hecho permite que la identificación de la *irrep* asociada a la transición de fase baste para reducir el número de grados de libertad de la estructura magnética a refinar, al quedar éstos limitados a las amplitudes de las posibles *basis spin functions* o funciones base de espín que se transforman según esa *irrep*.

El *representation method* se ha considerado habitualmente más sencillo que el uso de la simetría magnética, ya que la ventaja principal del uso de la simetría magnética, que es la reducción en el número de grados de libertad del sistema, no compensaba la complejidad de su uso al no existir herramientas adecuadas que facilitasen su aplicación. Por estas razones, en las últimas décadas el uso de la simetría magnética en estudios experimentales ha llegado a ser puramente testimonial. Incluso, a menudo, se ha asumido que en general el *representation method* hacía innecesaria la simetría magnética del cristal, porque la asignación de una *irrep* a la transición de fase equivaldría a la asignación de un grupo espacial magnético a la estructura magnética. Y aunque efectivamente, el *representation method* puede resultar suficiente en casos sencillos, sin embargo, la noción de que puede dejarse de lado por completo la simetría magnética no es en modo alguno cierta (§C.3).

En general, el estudio y determinación de una estructura cristalina magnética sin hacer consideraciones de simetría resulta incompleto, especialmente debido a que no se conoce directamente el grupo espacial magnético de la estructura, ni por tanto el puntual, que se deriva de él, el cual es necesario para conocer la forma general adaptada a la simetría de las propiedades tensoriales del cristal. Además, cuando la *irrep* asociada a la transición de fase es multidimensional, el *representation method* no es lo suficientemente concluyente, y la suposición de que la asignación de *irrep* y la asignación de grupo espacial magnético son equivalentes no es en general cierta, siendo el uso de argumentos de simetría especialmente útil en estos casos.

En cualquier caso, ya sea para casos sencillos o complejos, el uso de la simetría magnética facilita enormemente la descripción y determinación de estructuras magnéticas, aportando información adicional complementaria a la que se obtiene del conocimiento de la *irrep* o *irreps* activas, reduciendo en muchos casos el número de parámetros libres a refinar, y aportando claridad, orden y elegancia a la descripción de una estructura magnética.

En definitiva, tanto el uso de *irreps* como de la simetría magnética son correctos y complementarios, siendo el uso conjunto de ambas técnicas lo más aconsejable a priori para determinar y describir estructuras magnéticas. De ahí la necesidad y utilidad de posibilitar el uso de la simetría magnética por medio de la creación de aplicaciones informáticas que permitan soslayar su complejidad técnica. Gracias a estas aplicaciones, el proceso de determinación de las estructuras magnéticas resulta mucho más sencillo, directo, preciso, elegante y claro, evitándose confusiones y errores comunes. Por ejemplo, resulta especialmente útil el ya mencionado descenso

del número de grados de libertad del ordenamiento de espines, que puede lograrse únicamente a partir del conocimiento de la simetría de la fase paramagnética y del vector de propagación del patrón de difracción magnética de neutrones. Ignorar este conocimiento y considerar todo ordenamiento como posible a priori durante el proceso de refinamiento puede llevar a considerar como posibles modelos erróneos para la estructura magnética, especialmente si los datos experimentales de que se dispone son escasos y/o poco precisos.

Por estas y otras razones, existe un creciente interés en el estudio de la simetría magnética y de los grupos puntuales y espaciales magnéticos. Debido a ello, por un lado, la comunidad científica ha realizado en los últimos años un esfuerzo por crear un estándar de descripción de estructuras magnéticas tanto conmensurables como inconmensurables en formato digital. El resultado de dichos esfuerzos es el desarrollo del formato magCIF [5] por parte de la *International Union for Crystallography* (IUCr), cuya versión definitiva ha sido aprobada recientemente. En esta tesis doctoral, no sólo se hace uso de ese formato magCIF, sino que se ha contribuido a su creación, habiendo sido los programas desarrollados en este trabajo uno de los principales bancos de pruebas de ese formato. Durante el proceso de elaboración de estos programas se ha hecho uso de las versiones preliminares de este formato, poniendo a prueba su efectividad y añadiendo elementos propios los cuales o bien se han incorporado al formato definitivo oficial o han quedado como elementos de uso local por parte de nuestros programas.

Por otro lado, numerosos trabajos de importancia se han realizado en los últimos años, o se están realizando actualmente, tanto para crear bases de datos y listados de grupos magnéticos [6, 7] como diversas herramientas que permitan tanto hacer uso de consideraciones de simetría magnética de forma análoga a como se hace para determinar estructuras no magnéticas, como determinar la forma adaptada a la simetría de las propiedades tensoriales de los materiales ferroicos y multiferroicos.

Un material ferroico es aquél que presenta multiestabilidad, de forma que puede ser conmutado, mediante un campo externo, entre diferentes configuraciones equivalentes (los denominados dominios [8]) que difieren por su orientación en el espacio, dando lugar a la conmutación de algún tipo de propiedad tensorial [9]. Una fase ferroica es necesariamente el resultado de una distorsión con respecto a una configuración de mayor simetría puntual, y en muchos casos surge tras una transición de fase gobernada por la aparición en la fase de baja simetría de un parámetro de orden primario no nulo, que causa la ruptura de la simetría del cristal. Dependiendo de la naturaleza del parámetro de orden, se puede dar uno de los cuatro órdenes ferroicos primarios: ferroeléctrico, ferroelástico, ferromagnético o ferrotoroídico, que pueden coexistir en la misma fase. El número de dominios posibles en una fase ferroica, su orientación relativa y su grupo espacial depende por entero de la relación entre su simetría y la simetría de la fase no distorsionada (real o virtual) en la que el parámetro de orden es nulo.

Los materiales multiferroicos fueron inicialmente definidos como aquellos con presencia de al menos dos órdenes ferroicos de los considerados originalmente

primarios (ferromagnetismo, ferroelectricidad o ferroelasticidad) [10]. Sin embargo, el término actualmente se utiliza para denominar cualquier material que presenta simultáneamente ordenamiento magnético y ferroelectricidad, y es en este sentido como se utiliza en esta tesis doctoral. Si además dicho ordenamiento magnético es tal que el tensor magnetoeléctrico lineal tiene componentes permitidas por simetría, el multiferroico será también magnetoeléctrico. Así pues, se consideran multiferroicos todos aquellos materiales con una fase magnética polar que se pueden derivar, en último término, de una fase paramagnética no polar. Estos materiales se pueden clasificar en dos tipos [11, 12]: los multiferroicos Tipo I son aquellos que resultan de pasar de la fase paramagnética a la magnética por medio de transiciones de fase separadas y diferenciadas, asociadas a diferentes parámetros de orden, que ocurren a diferentes temperaturas y que causan la aparición de ferroelectricidad y ordenamiento magnético por separado (la aparición de ferroelectricidad puede anteceder a la aparición de ordenamiento magnético o viceversa), mientras que los multiferroicos Tipo II son aquellos en los cuales la ferroelectricidad y la estructura magnética aparecen tras una única transición de fase, siendo la aparición de ferroelectricidad un efecto inducido por la aparición del orden magnético.

A pesar de que los materiales multiferroicos de tipo II no son tan comunes y conocidos como los de tipo I, resultan mucho más interesantes científica y tecnológicamente, ya que se espera razonablemente que aquellos materiales multiferroicos tipo II que sean también magnetoeléctricos, al ser la polarización un efecto inducido por el parámetro de orden magnético, presenten un acoplamiento más fuerte entre magnetización y polarización, y por tanto un efecto magnetoeléctrico mucho mayor que los multiferroicos tipo I. Así pues, los materiales multiferroicos, y especialmente los multiferroicos magnetoeléctricos, gozan de un creciente interés por parte de la comunidad científica, pues el hecho de que la magnetización pueda modificarse de forma estable y sencilla aplicando un campo eléctrico y, a su vez, la polarización eléctrica, aplicando un campo magnético al material tiene múltiples aplicaciones prácticas potenciales [13]. Se espera que estos materiales resulten útiles en un futuro para fabricar transductores, dispositivos de almacenamiento de memoria, aparatos de medida, instrumental óptico avanzado, etc.

La consecución de los objetivos de esta tesis doctoral ha tenido como resultado la creación de 11 programas informáticos que han sido incluidos en el *Bilbao Crystallographic Server*.

Todos los programas existentes en el *Bilbao Crystallographic Server* están divididos en diferentes secciones (*shells*) de acuerdo a su finalidad. Dichas secciones son:

Space-Group Symmetry: bases de datos relacionadas con los grupos espaciales, tales como posiciones generales y de Wyckoff, ausencias sistemáticas, subgrupos maximales, normalizadores, etc., así como herramientas de identificación de grupos espaciales y operaciones de simetría.

Magnetic Symmetry and Applications: es la sección dedicada por completo a la simetría magnética, su uso práctico para determinar estructuras magnéticas y sus propiedades tensoriales.

Group-Subgroup Relations of Space Groups: herramientas dedicadas a las relaciones grupo-subgrupo y al estudio de la ruptura de la simetría en transiciones de fase: subgrupos maximales y supergrupos minimales, grupos de Hermann, *splitting* de las posiciones de Wyckoff, descomposición en *cosets*, órbitas no características, etc.

Representations and Applications: utilidades relacionadas con las representaciones irreducibles de los grupos puntuales y espaciales.

Solid State Theory Applications: aplicaciones especializadas dedicadas a tareas habituales relacionadas con la teoría de grupos tales como el análisis de los modos de simetría en una transición de fase (AMPLIMODES), la búsqueda de pseudosimetría (PSEUDO), etc.

Structure Utilities: programas que permiten hacer cálculos y manipulaciones relacionadas con el *setting* y la visualización de estructuras, matrices de transformación, comparación de estructuras con simetría similar (COMPSTRU), etc.

Subperiodic Groups: Layer, Rod and Frieze Groups Retrieval Tools: bases de datos de las posiciones generales, posiciones de Wyckoff, etc., de los grupos subperiódicos.

Structure Databases: contiene la *Bilbao Incommensurate Crystal Structure Database*, una base de datos de estructuras inconmensurables publicadas. Todas las estructuras inconmensurables publicadas en las revistas de la *International Union for Cristallography* (IUCr) son depositadas en esta base de datos.

Raman and Hyper-Raman scattering: utilidades relacionadas con la espectroscopía Raman e Hyper-Raman de sólidos cristalinos: modos espectrales activos, tensores, reglas de selección, etc.

Point-group symmetry: posiciones generales y de Wyckoff de los grupos puntuales en 2 y 3 dimensiones.

Plane-group symmetry: posiciones generales, de Wyckoff y subgrupos maximales de los grupos planos.

Los programas creados como parte de esta tesis doctoral, que casi en su totalidad forman parte de la sección "*Magnetic Symmetry and Applications*" (ver Figura 1), son:

MGENPOS: base de datos interactiva de las posiciones generales de los grupos espaciales magnéticos.

MWYCKPOS: base de datos interactiva de las posiciones de Wyckoff de los grupos espaciales magnéticos.

MAGNEXT: base de datos interactiva de las ausencias sistemáticas en patrones de difracción de neutrones no polarizados para los grupos espaciales magnéticos, y herramienta de cálculo de dichas ausencias sistemáticas para grupos espaciales magnéticos en un *setting* no estándar y para grupos superespaciales magnéticos.

MPOINT: base de datos de los grupos puntuales magnéticos.

MSGNORM: base de datos de los normalizadores afín y euclídeo de los grupos espaciales magnéticos.

MAXMAGN: programa que proporciona, para una transición de fase entre una fase paramagnética y una fase magnética, a partir del vector de propagación del patrón de difracción magnética y del conocimiento del grupo espacial de la fase paramagnética, los grupos espaciales magnéticos compatibles con el vector de propagación que son maximales (llamados aquí k-maximales). Asimismo, MAXMAGN proporciona los modelos estructurales adaptados a las simetrías k-maximales que son posibles a priori, además de información adicional sobre dichos modelos, como estructuras equivalentes alternativas, ausencias sistemáticas, propiedades tensoriales, visualización 3D con Jmol [14], etc.

MAGMODELIZE: programa que permite explorar, para una estructura paramagnética dada, el modelo estructural consistente con la simetría magnética descrita por un grupo espacial magnético cualquiera.

MAGNDATA: una colección de más de 400 estructuras magnéticas conmensurables e inconmensurables extraídas de diferentes publicaciones, fundamentalmente de los últimos años, y que incluye, para cada una, archivos cristalográficos o "cifs" [15] magnéticos (magCIF) [5] descargables, así como datos, enlaces externos a otros programas del *Bilbao Crystallographic Server* relacionados con la simetría magnética y una herramienta de visualización con Jmol [14]. La aportación fundamental de esta base de datos es la introducción del uso sistemático de la simetría magnética tanto conmensurable como inconmensurable (grupos superespaciales magnéticos) para la descripción y clasificación de las estructuras. Esto supone un cambio cualitativo trascendental con respecto a los métodos tradicionales.

MVISUALIZE: programa que permite visualizar, por medio del programa Jmol [14], estructuras magnéticas tanto conmensurables como inconmensurables a partir de un archivo magCIF.

TENSOR y MTENSOR: programas que permiten consultar y calcular la forma adaptada a la simetría de los grupos puntuales y espaciales tanto no magnéticos (TENSOR) como magnéticos (MTENSOR) de tensores cristalinos. TENSOR no guarda relación con la simetría magnética, por lo que ha sido incluido en la sección "*Solid State Theory Applications*".

La sección "*Magnetic Symmetry and Applications*" incluye también otros dos programas que fundamentalmente son fruto del trabajo de Luis Elcoro. Estos programas no forman parte de esta tesis doctoral, pero están relacionados e interconectados con el resto de programas de la sección arriba mencionada. Estos programas son:

IDENTIFY MAGNETIC GROUP: programa que permite identificar un grupo espacial magnético a partir de un conjunto de generadores, por lo que es utilizado internamente por buena parte del resto de programas de la sección.

K-SUBGROUPSMAG: programa que permite obtener todos los subgrupos de un grupo espacial magnético, que sean compatibles con uno o varios vectores de propagación, o alternativamente, con una supercelda. Los subgrupos magnéticos proporcionados por K-SUBGROUPSMAG pueden ser organizados y filtrados de acuerdo a múltiples criterios adicionales.

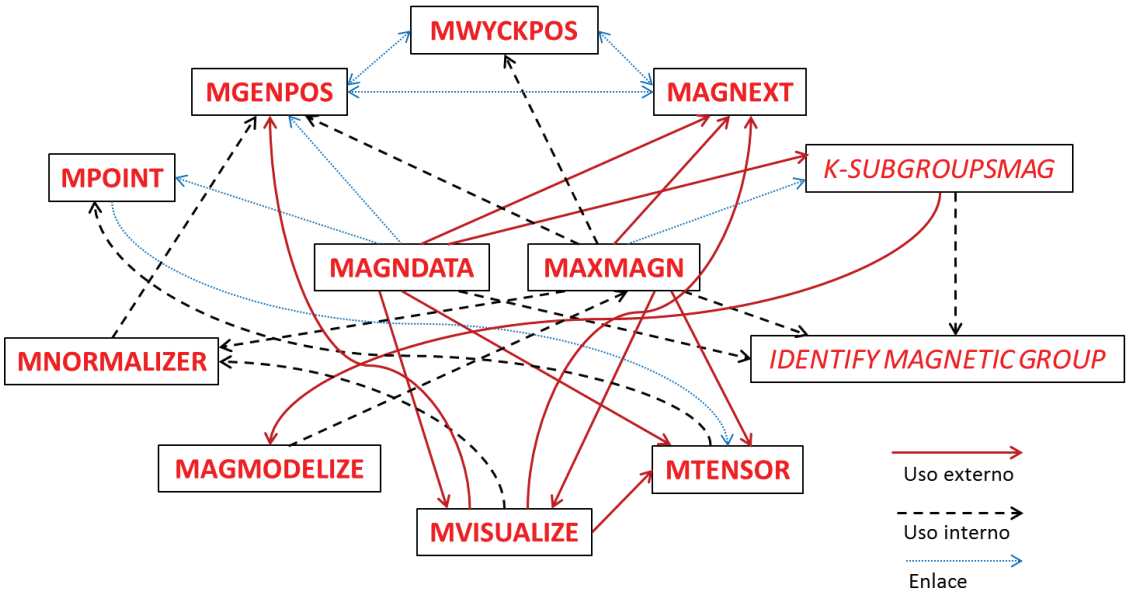

Figura 2. Interconexiones entre los programas del *Bilbao Crystallographic Server* relacionados con la simetría magnética. Los que no pertenecen a esta tesis doctoral están indicados en cursiva, el resto en negrita. Las interconexiones están clasificadas dependiendo de si un programa hace uso de otro de forma interna ("Uso interno"), con un enlace externo para hacer uso de sus funcionalidades con datos del programa de partida ("Uso externo"), o como un simple enlace para facilitar la navegación y la consulta de datos ("Enlace"). Algunas flechas son de doble sentido, indicando que ambos hacen uso uno del otro.

Los diferentes programas y bases de datos relacionados con la simetría magnética y fruto de esta tesis doctoral están estrechamente interrelacionados e interconectados, de forma que aquellos que tienen un propósito más práctico y son más cercanos al tratamiento directo de datos experimentales, tales como MAGNEXT, MAXMAGN, MAGMODELIZE o MTENSOR, hacen uso internamente de aquellos que son más básicos y teóricos y sirven principalmente como bases de datos interactivas, tales como

MGENPOS, MWYCKPOS, MSGNORM, etc. A su vez, algunos programas incluyen enlaces que permiten utilizar, en casos prácticos y concretos, las utilidades de unos programas desde otros. Por último, algunos programas incluyen enlaces a otros programas únicamente con el propósito de facilitar la navegación entre los programas o consultar casos particulares en las bases de datos. Un esquema gráfico de estas interconexiones entre los diferentes programas se muestra en la Figura 2.

Esta tesis doctoral se presenta en el formato "memoria de tesis por compendio de publicaciones y/o contribuciones". El texto presentado desarrolla, resume y complementa las 6 publicaciones existentes que son el resultado del proyecto de investigación vinculado a esta tesis doctoral. Estas publicaciones se recogen por orden cronológico en los Anexos A-F:

- **Anexo A**: Artículo sobre las reglas de ausencia sistemática para difracción magnética de neutrones no polarizados. Presenta, además de las bases de datos MGENPOS y MWYCKPOS, el programa MAGNEXT, explicando su funcionamiento y utilidad por medio de varios ejemplos prácticos.

Gallego S. V., Tasci E. S., de la Flor G., Perez-Mato J. M., Aroyo M. I. "Magnetic symmetry in the Bilbao Crystallographic Server: a computer program to provide systematic absences of magnetic neutron diffraction". *J. Appl. Crystallogr*. **45** 1236-47 (2012) DOI: 10.1107/S0021889812042185

- **Anexo B**: "*Comment*" de un artículo de Coh *et al*. [16] cuyo propósito es establecer una clasificación de las estructuras magnéticas de cristales aislantes con tensor magnetoeléctrico isótropo, definiendo para ello 30 estructuras magnéticas "canónicas". La aportación del *Comment* realizado es efectuar dicha búsqueda de estructuras magnéticas canónicas haciendo uso de la simetría magnética y más concretamente del programa MWYCKPOS, lo que tiene como resultado el hallazgo de 14 estructuras canónicas adicionales omitidas por error en el artículo original.

Comment on PRB: Perez-Mato J. M., Gallego S. V., Tasci E. S., Elcoro L., Aroyo M. I. "Comment on "Canonical magnetic insulators with isotropic magnetoelectric coupling"". *Phys. Rev. B* **90** 167101 (2014) DOI: 10.1103/PhysRevB.90.167101

- **Anexo C**: Artículo de "*Review*" consistente en un tutorial sobre la simetría magnética y su utilización para describir y determinar estructuras magnéticas. Presenta la mayoría de programas de la sección "*Magnetic Symmetry and Applications*" del *Bilbao Crystallographic Server*, y muestra cómo utilizarlos conjuntamente como alternativa y/o complemento del "*representation method*".

Perez-Mato J. M., Gallego S. V., Tasci E. S., Elcoro L., de la Flor G., Aroyo M. I. "Symmetry-Based Computational Tools for Magnetic Crystallography". *Annu. Rev. Mater. Res*. **45** 13.1-32 (2015) DOI: 10.1146/annurev-matsci-070214-021008

- **Anexo D**: Artículo que establece condiciones de simetría para estructuras magnéticas con propiedades multiferroicas de tipo II. Muestra cómo utilizar varios programas de la sección "*Magnetic Symmetry and Applications*" del *Bilbao Crystallographic Server* para comprobar el cumplimiento de estas condiciones para una estructura magnética, así como para buscar y predecir posibles materiales multiferroicos de tipo II.

Perez-Mato J. M., Gallego S. V., Elcoro L., Tasci E., Aroyo M. I. "Symmetry conditions for type II multiferroicity in commensurate magnetic structures". *J. Phys. Condens. Matter* **28** 286001 (2015) DOI: 10.1088/0953-8984/28/28/286001

- **Anexo E**: Artículo de presentación del programa MAGNDATA, una colección de estructuras magnéticas conocidas. Describe en detalle las características del programa para estructuras conmensurables.

Gallego S. V., Perez-Mato J. M., Elcoro L., Tasci E. S., Hanson R. M., Momma K., Aroyo M. I., Madariaga G. "MAGNDATA: towards a database of magnetic structures. I. The commensurate case". *J. Appl. Cryst*. **49**, 1750-76 (2016) DOI: 10.1107/S1600576716012863

- **Anexo F**: Artículo de presentación del programa MAGNDATA, una colección de estructuras magnéticas conocidas. Describe en detalle las características del programa para estructuras inconmensurables.

Gallego S. V., Perez-Mato J. M., Elcoro L., Tasci E. S., Hanson R. M., Aroyo M. I., Madariaga G. "MAGNDATA: towards a database of magnetic structures. II. The incommensurate case". *J. Appl. Cryst*. **49**, 1941-56 (2016) DOI: 10.1107/S1600576716015491

2. ESTRUCTURAS CRISTALINAS MAGNÉTICAS Y SU SIMETRÍA

2.1 Simetría magnética: grupos espaciales magnéticos

Las estructuras cristalinas conmensurables convencionales, es decir, no magnéticas, son invariantes ante un conjunto de operaciones de simetría espacial (operaciones rototraslacionales). Estas operaciones de simetría (rotaciones, inversiones, traslaciones y combinaciones de éstas) se denotan según la notación de Seitz [17] como $\{\boldsymbol{R}|\mathbf{t}\}$, donde $\boldsymbol{R}$ es la matriz de rotación o rotoinversión y $\mathbf{t}$ es el vector de traslación de la operación de simetría. El conjunto completo de operaciones de simetría espacial que dejan invariante al cristal forman el grupo espacial **G** del cristal.

Dos grupos espaciales $\mathbf{G_1}$ y $\mathbf{G_2}$ son equivalentes si es posible encontrar una transformación de *setting* ($\boldsymbol{N}$, $\mathbf{n}$) que cumpla la condición $\det(\boldsymbol{N}) > 0$, y que transforme el grupo $\mathbf{G_1}$ en $\mathbf{G_2}$; es decir, que se cumplan las relaciones:

$$\begin{aligned}\left(\boldsymbol{N},\mathbf{n}\right)^{-1}\mathbf{G_1}\left(\boldsymbol{N},\mathbf{n}\right)&=\mathbf{G_1}\\ \left(\boldsymbol{N},\mathbf{n}\right)^{-1}\mathbf{G_1}\left(\boldsymbol{N},\mathbf{n}\right)&=\mathbf{G_2}\end{aligned} \qquad (1)$$

Esta relación de equivalencia permite clasificar los grupos espaciales cristalográficos en los llamados 230 tipos de grupos espaciales [18], o simplemente grupos espaciales. Los grupos espaciales describen la simetría de las estructuras cristalinas convencionales, pero no la de las estructuras cristalinas magnéticas. La razón de esto es la simetría de inversión temporal.

La operación de simetría de inversión temporal, τ, es una operación de simetría discreta cuyo efecto es invertir la coordenada temporal del sistema: τ t = -t. Puede demostrarse, definiendo τ adecuadamente como un operador cuántico, que esta operación conmuta con las rotaciones, inversiones y traslaciones del grupo espacial del cristal y que su efecto sobre el momento magnético de los átomos es invertirlo [19]. Por ello, la aplicación de la inversión temporal sobre una estructura magnética (considerada clásicamente como un ordenamiento de momentos magnéticos atómicos en el espacio) tiene como único efecto la inversión del momento magnético.

En las estructuras no magnéticas, la ausencia de orden magnético implica que esta operación de simetría, denotada como $\{\boldsymbol{1}'|\mathbf{0}\}$, deja trivialmente invariante la estructura. Sin embargo, el orden magnético presente en las estructuras magnéticas rompe la simetría por inversión temporal. Es por ello que la simetría de las estructuras magnéticas está descrita por los grupos espaciales magnéticos (en adelante, MSGs), los cuales se derivan de combinar la operación de inversión temporal $\{\boldsymbol{1}'|\mathbf{0}\}$ con las operaciones rototraslacionales $\{\boldsymbol{R}|\mathbf{t}\}$ de los grupos espaciales convencionales.

La invariancia de una estructura cristalina no magnética bajo una operación de inversión temporal implica que es invariante tanto bajo las operaciones $\{\boldsymbol{R}|\mathbf{t}\}$ de su grupo espacial **G** (operaciones “no primadas”) como de las combinaciones de éstas con

la operación de inversión temporal, es decir, las operaciones {***R***'|**t**} (operaciones "primadas"). Por ello, la simetría magnética de una estructura no magnética viene descrita por el MSG **G1'**, que incluye las operaciones de simetría {***R***|**t**} de **G** así como sus correspondientes primadas {***R***'|**t**}, incluyendo la operación de inversión temporal, {***1***'|**0**}. Los elementos de simetría de un MSG pueden también expresarse en notación de Seitz modificada como {***R***,τ|**t**} (siendo τ igual a -1 ó +1, indicando si el elemento lleva asociada una operación de inversión temporal o no, respectivamente), y a menudo las operaciones primadas de los MSGs se denotan en color rojo para distinguirlas de las no primadas, en color negro.

Las estructuras magnéticas, en cambio, no son invariantes bajo la operación {***1***'|**0**}, y por tanto su simetría viene descrita por un subgrupo de **G1'** que no incluye {***1***'|**0**}. Esto implica que el MSG **M** de una estructura magnética se compone de operaciones tanto primadas como no primadas, de tal forma que la presencia en **M** de una operación particular no primada {$\boldsymbol{R}_i|\mathbf{t}_i$} implica la ausencia de la operación {$\boldsymbol{R}_i'|\mathbf{t}_i$}, y viceversa.

Los MSGs **M** pueden descomponerse de la siguiente forma [20]:

$$\mathbf{M} = \mathbf{D} + \left(\mathbf{G} - \mathbf{D}\right)1' \tag{2}$$

donde **D** es el grupo espacial formado por los elementos no primados de **M** y **G** es el grupo espacial efectivo de **M**, es decir, el grupo que se obtendría a partir de **M** si se obviara la operación de inversión temporal. El grupo **D** es o bien igual a **G**, o bien un subgrupo de **G** de índice 2. De las ecuaciones (1) y (2) se deduce que dos MSGs $\mathbf{M_1}$ y $\mathbf{M_2}$ serán equivalentes si es posible encontrar una transformación de *setting* (***N***, **n**), que cumpla la condición det(***N***) > 0, y que cumpla:

$$\begin{aligned}
\left(\boldsymbol{N},\mathbf{n}\right)^{-1}\mathbf{D}_1\left(\boldsymbol{N},\mathbf{n}\right) &= \mathbf{D}_1 \\
\left(\boldsymbol{N},\mathbf{n}\right)^{-1}\mathbf{G}_1\left(\boldsymbol{N},\mathbf{n}\right) &= \mathbf{G}_1 \\
\left(\boldsymbol{N},\mathbf{n}\right)^{-1}\mathbf{D}_1\left(\boldsymbol{N},\mathbf{n}\right) &\in \mathbf{D}_2 \\
\left(\boldsymbol{N},\mathbf{n}\right)^{-1}\mathbf{G}_1\left(\boldsymbol{N},\mathbf{n}\right) &\in \mathbf{G}_2
\end{aligned} \tag{3}$$

Esta relación de equivalencia permite clasificar los grupos espaciales magnéticos en 1651 tipos no cristalográficamente equivalentes: los llamados grupos espaciales magnéticos (MSG).

2.2 Estructuras cristalinas magnéticas y sus tipos

Independientemente de la situación en que se encuentren los diferentes electrones del cristal (es decir, ya sean electrones internos de los átomos, formen parte de las bandas de valencia o conducción en un metal o cualquier otra situación), en la mayoría de los casos la distribución de momento magnético en una estructura puede aproximarse considerando que el momento magnético está localizado en las

posiciones medias de los átomos, es decir, asignando a cada átomo un momento magnético neto, y siendo nulo en cualquier otro punto del cristal [21]. Este momento puede ser nulo o no nulo, lo que depende principalmente de la configuración electrónica de cada átomo.

Las propiedades magnéticas de un cristal dependen entonces de si los momentos magnéticos netos asociados a los átomos del cristal son nulos o no, así como de la magnitud y orientación relativa de estos momentos netos. Así, si la configuración electrónica de todos los átomos del cristal es tal que todos ellos poseen un momento magnético neto nulo, el cristal es diamagnético. Si por el contrario la configuración electrónica de algunos átomos del cristal es tal que poseen un momento magnético neto no nulo, lo cual es habitual en átomos o iones que tienen orbitales 3d (Cr^{3+}, Mn^{4+}, Fe^{3+}, Co^{2+}, Ni^{2+}, Cu^{2+}...) y 4f (Nd, Gd, Ho, Dy...) parcialmente ocupados, el cristal o bien es paramagnético, si los átomos con momentos magnéticos no nulos están orientados totalmente al azar, o bien presenta una estructura magnética de algún tipo (ferromagnética, antiferromagnética, ferrimagnética, etc.).

El ordenamiento magnético de una estructura magnética depende principalmente del balance entre la energía térmica del cristal, cuyo efecto es inducir desorden en la distribución de momentos magnéticos, y la intensidad de la interacción de intercambio entre los electrones de los átomos magnéticos del cristal, cuyo efecto es inducir a los momentos magnéticos a alinearse [21]. Así, si temperatura es suficientemente elevada el cristal será paramagnético, mientras que a bajas temperaturas se producirá en la mayoría de los casos un ordenamiento de los espines y el cristal presentará una estructura magnética. En estas estructuras, la interacción de intercambio, generalmente dominante, tiene como consecuencia una tendencia a la colinearidad de los momentos magnéticos de los átomos a lo largo de un eje (el llamado "*easy axis*"), con los momentos alineados paralela o antiparalelamente dependiendo de si su constante de intercambio es positiva o negativa. Esto implica que, habitualmente, las estructuras magnéticas son aproximadamente o rigurosamente colineales, con los momentos alineados a lo largo del *easy axis* y orientados paralela o antiparalelamente, lo que determina el carácter ferromagnético o antiferromagnético, respectivamente, de la estructura magnética. No obstante, la interacción de los electrones con el campo cristalino, así como el fenómeno de la frustración (incompatibilidad entre las configuraciones locales propiciadas por la interacción de intercambio), puede alterar o incluso romper la tendencia a la colinearidad dando lugar a una diversidad de tipos de estructuras magnéticas.

La onda de espín puede ser o no ser compatible con la periodicidad de la estructura nuclear. En el primer caso, la estructura magnética es conmensurable y existe una periodicidad espacial en el cristal, por lo que puede definirse una celda unidad y unos átomos y momentos magnéticos promedio dentro de la misma (§2.3). Si por el contrario la periodicidad de la onda de espín es incompatible con la de la red de traslaciones de la estructura nuclear, es decir, a lo largo de al menos una dirección espacial el cociente entre las periodicidades de la onda de espín y la estructura nuclear es un número irracional, la estructura magnética es inconmensurable y no existe periodicidad espacial, por lo que, aunque se pueden definir una celda unidad con los

átomos y momentos magnéticos de la estructura magnética promediada espacialmente, el momento magnético de cada átomo dentro de dicha celda unidad será diferente en cada celda del cristal, pues dependerá del valor de una función de modulación periódica inconmensurable (§2.4).

2.1.1 *Tipos de estructuras magnéticas*

En principio, los momentos magnéticos atómicos de una estructura magnética pueden estar orientados de cualquier manera. Sin embargo, la gran mayoría de las estructuras magnéticas se ajustan a alguno de los ordenamientos típicos más comunes [22]. Estos ordenamientos están ligados a ciertas propiedades físicas de los materiales que se ajustan a ellos. Los tipos de estructura magnética más habituales son (Figura 3):

- **Ferromagnética**: los momentos magnéticos de los átomos son colineales y paralelos. La magnetización neta del cristal es no nula y tiene la misma dirección y sentido que los momentos magnéticos de los átomos.

- **Antiferromagnética**: los momentos magnéticos de átomos contiguos son colineales y de igual tamaño, pero tienen sentidos opuestos, de forma que la magnetización neta del cristal es nula.

- **Ferrimagnética**: momentos magnéticos de diferente magnitud, asociados a átomos no equivalentes por simetría, se ordenan antiferromagnéticamente, resultando un ordenamiento parcialmente ferromagnético (magnetización neta del cristal no nula) y parcialmente antiferromagnético (momentos de átomos contiguos con sentidos opuestos).

- ***Canted***: los momentos magnéticos no son exactamente colineales y están inclinados (*canted*) con respecto al *easy axis*. Esto puede tener como consecuencia la aparición de una pequeña componente ferromagnética en una dirección perpendicular al *easy axis* en estructuras antiferromagnéticas, o de una pequeña componente antiferromagnética en una dirección perpendicular al *easy axis* en estructuras ferromagnéticas.

- **Frustrada:** Las configuraciones locales de los momentos magnéticos propiciadas por la interacción de intercambio son incompatibles entre sí, lo que no permite a los momentos ser colineales.

- **Incompleta**: algunos átomos magnéticos tienen momentos orientados al azar, de forma que no todos los átomos magnéticos tienen un momento magnético promedio no nulo. Este tipo de estructuras no es demasiado común, pues no son favorecidas por la interacción de intercambio.

- **Multiaxial**: estructuras magnéticas que poseen más de un *easy axis*, coexistiendo en el cristal ordenamientos ferromagnéticos o antiferromagnéticos a lo largo de estas direcciones.

- **Inconmensurable**: en estas estructuras, la razón entre la periodicidad de la onda de espín y la periodicidad de la estructura nuclear no es un número racional, no habiendo periodicidad espacial en el cristal (ver §2.4). La Figura 12 del Anexo C contiene los tipos de modulación magnética inconmensurable más comunes.

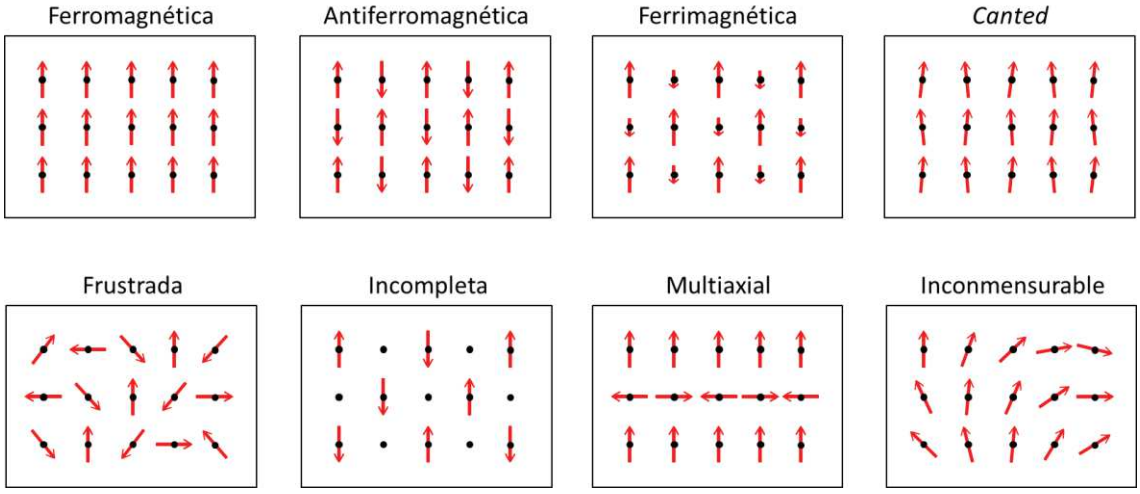

Figura 3. Tipos de estructuras cristalinas magnéticas más comunes.

2.3 Descripción de las estructuras magnéticas conmensurables

Para describir adecuadamente y sin ambigüedades una estructura magnética conmensurable es necesario describir las posiciones y momentos magnéticos promedio de sus átomos. Para conseguir esto es necesario y suficiente definir (ver §E.2):

a) La celda unidad de la red cristalina que define la periodicidad de la estructura magnética: la celda unidad magnética. Esta celda unidad debe reproducir la periodicidad de la estructura magnética completa, es decir, teniendo en cuenta tanto átomos como momentos magnéticos. Por ello, en el caso de las estructuras con MSG de tipo IV (§4.1) esta celda unidad difiere necesariamente de la celda unidad de la estructura nuclear, es decir, la celda que describe la periodicidad de la estructura si se ignoran los momentos magnéticos (Figura 4).

b) El MSG de la estructura magnética, que describe la simetría del cristal magnético.

c) Las posiciones atómicas promedio, en unidades relativas con respecto a la celda unidad, y los momentos magnéticos promedio asociados a cada átomo, de un conjunto de átomos no relacionados por simetría, que conforman la unidad asimétrica del cristal. Estos promedios son la media espacial y temporal de las posiciones atómicas y los momentos magnéticos de cada átomo de la unidad asimétrica y sus equivalentes por simetría en el cristal. Los momentos y posiciones del resto de átomos del cristal pueden derivarse a partir de la unidad asimétrica por medio de las operaciones de simetría del MSG de la estructura magnética.

El resultado de describir una estructura magnética definiendo lo descrito anteriormente puede visualizarse en la Figura 4, en la que se toma como ejemplo la estructura magnética del $CsFe_2Se_3$ [22]. Como puede observarse, las estructuras magnéticas difieren de las convencionales en que para describirlas es necesario asignar momentos magnéticos promedio a aquellos átomos de la unidad asimétrica que por su configuración electrónica poseen un momento magnético no nulo (lo que no significa necesariamente que el momento magnético promedio lo sea), átomos que en adelante serán llamados "átomos magnéticos". Como consecuencia, la periodicidad espacial de la estructura magnética y la estructura nuclear (la que se deriva ignorando los momentos magnéticos) es en general diferente.

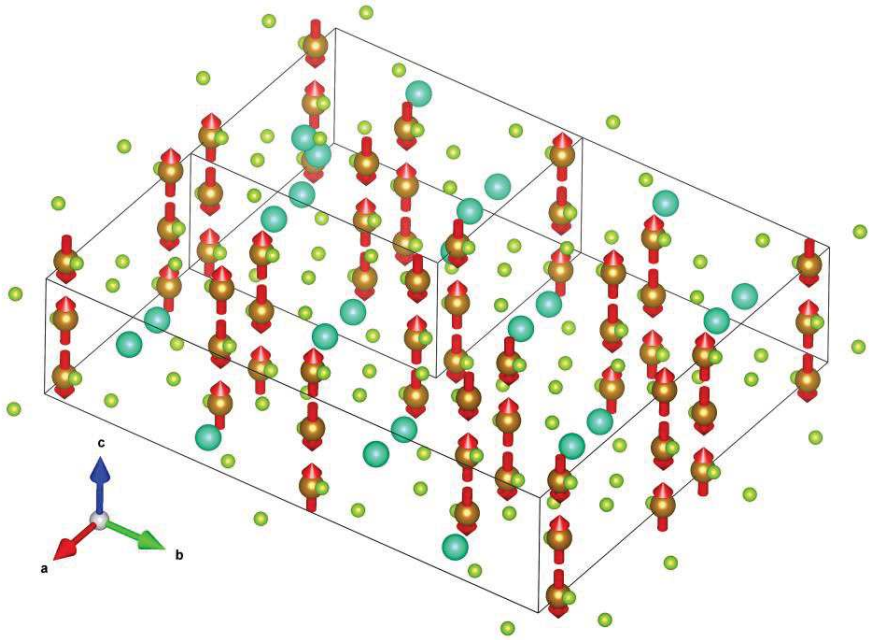

Figura 4. Modelo de estructura magnética del $CsFe_2Se_3$ [22]: queda especificada por medio de la definición de celda unidad, posiciones medias de los átomos de la unidad asimétrica, momentos magnéticos promedio y elementos de simetría. La celda unidad de la estructura magnética (grande) difiere de la de la estructura nuclear (pequeña). Figura obtenida con VESTA [23].

2.4 Descripción de las estructuras magnéticas inconmensurables

Como se ha mencionado, las estructuras magnéticas inconmensurables son aquellas en las que la razón entre las periodicidades de la estructura nuclear y el ordenamiento de espines a lo largo de al menos una dirección espacial (por sencillez, se supondrá en adelante que sólo una) es un número irracional (o, en la práctica, un número racional descrito por una fracción cuyo denominador no es reducible a unas pocas unidades). Es decir, el vector de propagación, que relaciona las celdas unidad en el espacio recíproco de la fase magnética y la fase no magnética de alta simetría del cristal tiene una componente irracional (ver salvedad antes mencionada) a lo largo de dicha dirección: el vector de propagación es inconmensurable. Estas estructuras magnéticas carecen de periodicidad espacial (o es excesivamente grande) y no tiene sentido

definir una celda unidad que describa la periodicidad de la estructura magnética en su conjunto. Por esta razón, la descripción de estructuras magnéticas establecida en §2.3 para las estructuras conmensurables no es válida para estas estructuras.

La descripción de una estructura magnética inconmensurable requiere de la utilización del formalismo superespacial [24] aplicado a las estructuras magnéticas. Según este formalismo, para describir una estructura magnética inconmensurable es necesario y suficiente definir (ver §F.2):

a) La celda unidad de la red cristalina que define la periodicidad de la estructura magnética promedio.

b) Un vector de propagación inconmensurable.

c) El grupo superespacial magnético (MSSG), que define la simetría de la estructura. Los MSSGs están formados por operaciones de simetría magnética como las que forman parte de los MSGs, pero con el añadido de una coordenada adicional x_4, correspondiente a la fase global de la función de modulación de los momentos magnéticos.

d) Las posiciones atómicas promedio, en unidades relativas con respecto a la celda unidad, y los momentos magnéticos promedio asociados a cada átomo, de un conjunto de átomos no relacionados por simetría, que conforman la unidad asimétrica del cristal. Estos promedios son la media espacial y temporal de las posiciones atómicas y los momentos magnéticos de cada átomo de la unidad asimétrica y sus equivalentes por simetría en el cristal. Los momentos y posiciones promedio del resto de átomos del cristal pueden derivarse a partir de la unidad asimétrica por medio de las operaciones de simetría del MSSG del cristal. Esta estructura magnética promedio, idéntica a la que describe una estructura magnética conmensurable, se denomina estructura magnética básica.

e) Las funciones de modulación de cada átomo magnético en la unidad asimétrica de la estructura magnética básica. En esta tesis doctoral, la forma escogida para representar estas funciones de modulación es especificar los coeficientes de uno o más términos del desarrollo en serie de Fourier de cada función de modulación (§F.A). A partir de unos valores iniciales, la aplicación de las operaciones del MSSG permite determinar el valor de dichas funciones de modulación para cualquier otro átomo en la celda unidad de la estructura básica.

La Figura 5 recoge un ejemplo de descripción de una estructura magnética y su MSSG. La descripción de las estructuras magnéticas inconmensurables se analiza en detalle §D.4 y §F.2. Asimismo, un estudio completo de la aplicación del formalismo superespacial a estructuras magnéticas puede encontrarse en [25].

Estructura magnética promedio:

Atom	Multiplicity	Symmetry constraints on M_0	M_{0x}	M_{0y}	M_{0z}	|M|
Dy1 Dy 0 0 0	1	0,0,m_z	0.0	0.0	3.932	**3.93**
Mn1 Mn 0.5 0 0.2510	6	0,0,m_z	0.0	0.0	-1.149	**1.15**

Función de modulación del momento magnético: $\mathbf{M}(x_4) = \mathbf{M}_0 + \sum_{n=1,\ldots} \left[\mathbf{M}_{\cos n} \cos(2\pi n x_4) + \mathbf{M}_{\sin n} \sin(2\pi n x_4) \right]$

Vector de propagación inconmensurable: k = (0, 0, 0.1651)

Valores de la función de modulación del momento magnético:

Atom	Mcos1		Msin1	
	Symmetry constraints	Values	Symmetry constraints	Values
Dy1	√3$M_x$sin1, 0, 0	6.195546, 0, 0	Mxsin1, Mxsin1, 0	3.577, 7.154, 0
Mn1	$M_x$cos1, $M_x$cos1, 0	-1.877, -0.206, 0	Mxsin1, Mysin1, 0	-0.846, -2.049, 0

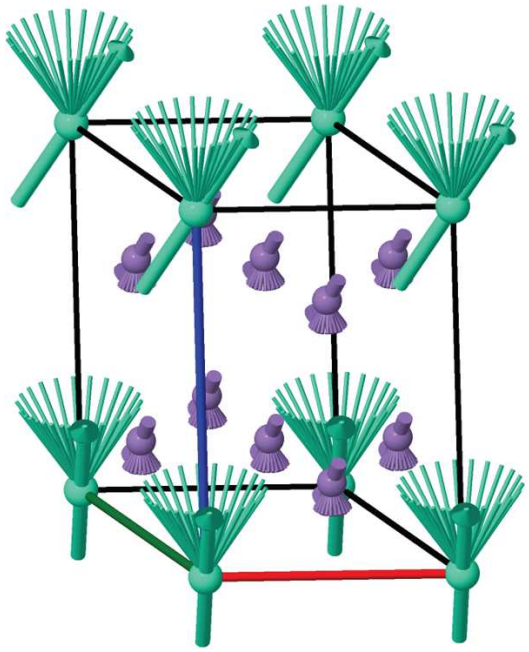

Grupo superespacial magnético (MSSG):
P62'2'(00γ)h00

Operaciones de simetría del MSSG:

N	(x1, x2, x3, x4)	Seitz notation
1	x1,x2,x3,x4,+1	{ 1 | 0 }
2	-x2,x1-x2,x3,x4+1/3,+1	{ 3^+_{001} | 0 0 0 1/3 }
3	-x1+x2,-x1,x3,x4+2/3,+1	{ 3^-_{001} | 0 0 0 2/3 }
4	-x1,-x2,x3,x4+1/2,+1	{ 2_{001} | 0 0 0 1/2 }
5	x2,-x1+x2,x3,x4+5/6,+1	{ 6^-_{001} | 0 0 0 5/6 }
6	x1-x2,x1,x3,x4+1/6,+1	{ 6^+_{001} | 0 0 0 1/6 }
7	x2,x1,-x3,-x4+5/6,-1	{ 2'110 | 0 0 0 5/6 }
8	x1-x2,-x2,-x3,-x4+1/2,-1	{ 2'100 | 0 0 0 1/2 }
9	-x1,-x1+x2,-x3,-x4+1/6,-1	{ 2'010 | 0 0 0 1/6 }
10	-x2,-x1,-x3,-x4+1/3,-1	{ 2'1-10 | 0 0 0 1/3 }
11	-x1+x2,x2,-x3,-x4,-1	{ 2'120 | 0 }
12	x1,x1-x2,-x3,-x4+2/3,-1	{ 2'210 | 0 0 0 2/3 }

Figura 5. Ejemplo de descripción de la estructura magnética inconmensurable del $DyMn_6Ge_6$ [26], obtenida del programa MAGNDATA (§9) (caso #1.1.10). Se especifican el vector de propagación inconmensurable, la estructura magnética promedio, la etiqueta y los elementos de simetría del MSSG, fórmula general de las funciones de modulación, tabla con los valores de los coeficientes de las funciones de modulación (en magnetones de Bohr), y la imagen de la estructura magnética inconmensurable, obtenida con VESTA [23]. La descripción de los nombres de las etiquetas de los MSSGs puede encontrarse en §F.2, apartado (e).

La descripción y estudio de las estructuras magnéticas inconmensurables y de los MSSGs dentro del marco de la aplicación del formalismo superespacial a las estructuras magnéticas inconmensurables queda más allá del propósito de esta tesis doctoral. La razón es que esto resultaría imposible, debido a la falta de estándares adecuados y a la inexistencia de una base de datos digital de MSSGs. No obstante, la abundancia y relevancia de las estructuras magnéticas inconmensurables, cuya existencia en la naturaleza es mucho más común, en proporción, que en el caso de estructuras no magnéticas, es motivo suficiente para incluir el estudio de las estructuras magnéticas inconmensurables en aquellas ocasiones en que dicha inclusión no requiera de un estudio detallado de los MSSGs. En concreto, se han incluido las

estructuras magnéticas inconmensurables en el estudio de las reglas de ausencia sistemática, y en la recopilación de estructuras magnéticas conocidas:

- El programa MAGNEXT (§5) incluye una herramienta para obtener las reglas de ausencia sistemática de estructuras magnéticas inconmensurables (1k) que se derivan de su MSSG. La inclusión de la posibilidad de utilizar MSSGs en MAGNEXT se debe a que la forma de obtener las reglas de ausencia sistemática para MSGs y MSSGs resulta ser muy similar, por lo que se puede incluir esta herramienta adicional sin necesidad de crear nuevos programas y bases de datos sobre los MSSGs ni elaborar algoritmos completamente nuevos.

- La recopilación de estructuras magnéticas conocidas y su inclusión en el programa MAGNDATA (§9) difícilmente podría haber excluido a las estructuras magnéticas inconmensurables sin haber quedado injustificadamente incompleta, por lo que no sólo se han incluido en la base de datos, implementándose los añadidos necesarios en la herramienta informática para permitir esta inclusión, sino que se ha realizado una publicación (Anexo F) dedicada en exclusiva a la descripción de estas estructuras dentro de MAGNDATA.

3. GRUPOS PUNTUALES MAGNÉTICOS: PROGRAMA MPOINT

3.1 Grupos puntuales magnéticos

Los grupos puntuales cristalográficos convencionales, **g**, se definen como el conjunto de operaciones de simetría que dejan invariante al menos un punto (el origen) y, además, dejan invariante la red de traslaciones del cristal, es decir, están sometidos al teorema de restricción cristalográfica. Los grupos puntuales se derivan de los espaciales obviando la parte traslacional de sus operaciones de simetría. De esta forma, de los 230 grupos espaciales se derivan los 32 tipos de grupos puntuales convencionales, que describen la simetría puntual de estructuras no magnéticas.

De forma similar, el grupo puntual magnético (MPG, en adelante), **m**, asociado a un MSG se obtiene considerando únicamente la parte rotacional o de rotoinversión de cada operación del MSG, obviando su parte traslacional. Los tipos de MPG se pueden deducir a partir de los grupos puntuales convencionales, combinando la operación de inversión temporal con las operaciones de simetría de los grupos puntuales convencionales. Dado que los MPGs que describen la simetría puntual de las estructuras no magnéticas han de incluir la inversión temporal, se forman añadiendo la inversión temporal como generador a los grupos puntuales **g**: son los grupos puntuales magnéticos grises **g1'**. Los MPGs que describen la simetría puntual de las estructuras magnéticas son subgrupos de los grupos puntuales cristalográficos grises que no contienen la inversión temporal, y en general contendrán tanto elementos primados como no primados.

La primera derivación de los MPGs fue llevada a cabo por Shubnikov [27] a partir de la introducción del concepto de antisimetría por parte de Heesch [28]. Si bien los MPGs pueden deducirse considerando las posibles combinaciones de los elementos de los grupos puntuales convencionales con la operación de inversión temporal, se pueden deducir de forma más sencilla obteniendo los subgrupos de índice 2 de los grupos puntuales grises **g1'** y construyendo los grupos tal como puede verse en la Figura 6.

Para cada MPG, **m**, existe un subgrupo de elementos no primados, **d**. Las características de **d** y su relación con **g** permiten establecer una clasificación de los MPGs en tres tipos. Los MPGs de tipo I (32) son aquellos que carecen de elementos primados, y por tanto son idénticos en forma a los grupos puntuales convencionales, aunque eso no significa que describan la simetría de estructuras no magnéticas; simplemente, sus elementos de simetría no llevan asociada una inversión temporal. La simetría puntual tanto de estructuras ferromagnéticas y ferrimagnéticas, etc., como de estructuras antiferromagnéticas puede venir descrita por MPGs tipo I.

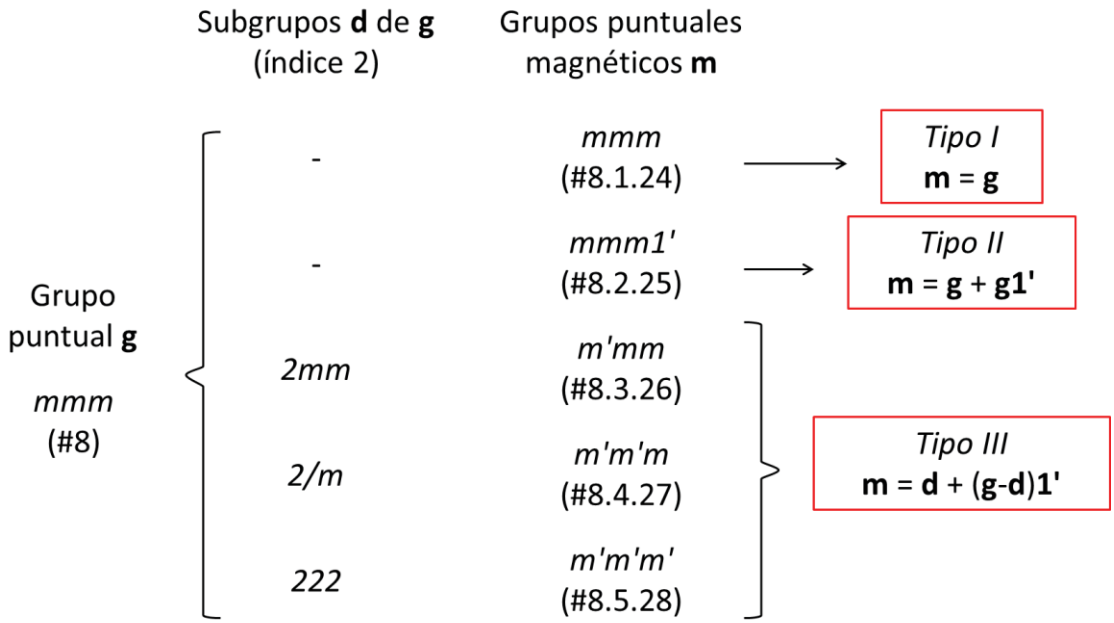

Figura 6. Derivación, notación y clasificación de los MPGs correspondientes al grupo puntual convencional *mmm*. Los MPGs de tipo 3 se pueden construir a partir de la *coset decomposition* de **g** en un subgrupo de índice 2 **d**, tomando **d** como subgrupo de elementos no primados y el resto de elementos de **g** como primados. La numeración de los grupos puntuales magnéticos utilizada en este trabajo proviene de Litvin [7].

Los MPGs que describen la simetría puntual de las estructuras no magnéticas, y por tanto contienen el elemento 1', son los de tipo II (32), también llamados grupos grises. En estos grupos, cada elemento de simetría no primado del grupo aparece también primado; se derivan, por tanto, de los grupos puntuales convencionales añadiendo el elemento 1' como generador. Por ello, además de las estructuras paramagnéticas y diamagnéticas, sólo las estructuras antiferromagnéticas, cuyo MSG es de tipo IV (ver §4.1), pueden tener una simetría puntual descrita por un grupo tipo II.

Por último, los MPGs de tipo III (58) o grupos *black-and-white* poseen tanto elementos primados como no primados, pero no contienen al elemento 1', por lo que un elemento rotacional que forma parte del grupo o bien forma parte de él primado o bien no primado. La simetría puntual tanto de estructuras ferromagnéticas y ferrimagnéticas, etc., como de estructuras antiferromagnéticas puede venir descrita por MPGs tipo III.

Algunos de los MPGs no pueden describir la simetría puntual de estructuras ferromagnéticas y ferrimagnéticas, cuya magnetización espontánea es no nula, al ser incompatibles con su existencia. Esto motiva la clasificación de los MPGs en ferromagnéticos (31) y no ferromagnéticos (91), siendo éstos últimos aquellos cuya simetría impide la existencia de magnetización espontánea (incluyendo los grupos grises). Por ejemplo, de los MPGs que se derivan del grupo *mmm* (ver Figura 6), sólo *m'm'm* (#8.4.27) es ferromagnético.

Para cada MPG puede definirse un grupo puntual efectivo **h**, formado por todos aquellos elementos que forman parte del grupo, primados o no primados, tomados como no primados: es el grupo resultante de obviar la presencia de inversión temporal asociada en los elementos de **m**. El grupo **h** es idéntico al grupo **g** del que **m** se deriva según el procedimiento expuesto en la Figura 6.

La notación y la elección del estándar para los MPGs (Figura 6) utilizada tanto en esta tesis doctoral como en los programas desarrollados proceden de Litvin [7]. El símbolo del grupo es similar al del grupo puntual convencional del que se derivan, añadiéndose una prima en aquellos generadores que estén primados, o bien el símbolo 1' al final del grupo para indicar que es gris, según sea el caso. La etiqueta del grupo consta de 3 números separados por puntos: el primero indica el grupo puntual efectivo, el segundo enumera los grupos que tienen el mismo grupo puntual efectivo, y el tercero es un número entre 1 y 122 que identifica unívocamente al MPG.

3.2 Programa MPOINT

Los grupos puntuales magnéticos o MPGs (§3.1) describen la simetría puntual macroscópica de las estructuras magnéticas. El MPG de una fase magnética, que es directamente deducible de su MSG o MSSG, restringe las propiedades tensoriales macroscópicas del cristal, por lo que su conocimiento resulta fundamental a la hora de caracterizar la propiedades tensoriales de los materiales magnéticos, y en particular de los materiales multiferroicos y/o magnetoeléctricos. En general, el tensor asociado a cualquier propiedad física de un material magnético debe ser invariante para todas las operaciones de simetría de su MPG. La aplicación de esta condición de invariancia permite hallar la forma general posible de cualquier tensor cristalino del material (§10).

El programa MPOINT (http://www.cryst.ehu.es/cryst/mpoint.html) ha sido desarrollado con el fin de recopilar los 122 grupos puntuales magnéticos existentes, que se recogen en una tabla en la página principal del programa (Figura 7).

1.1.1	1	1.2.2	11'	2.1.3	-1	2.2.4	-11'	2.3.5	-1'	3.1.6	2	3.2.7	21'	3.3.8	2'
4.1.9	m	4.2.10	m1'	4.3.11	m'	5.1.12	2/m	5.2.13	2/m1'	5.3.14	2'/m	5.4.15	2/m'	5.5.16	2'/m'
6.1.17	222	6.2.18	2221'	6.3.19	2'2'2	7.1.20	mm2	7.2.21	mm21'	7.3.22	m'm2'	7.4.23	m'm'2	8.1.24	mmm
8.2.25	mmm1'	8.3.26	m'mm	8.4.27	m'm'm	8.5.28	m'm'm'	9.1.29	4	9.2.30	41'	9.3.31	4'	10.1.32	-4
10.2.33	-41'	10.3.34	-4'	11.1.35	4/m	11.2.36	4/m1'	11.3.37	4'/m	11.4.38	4/m'	11.5.39	4'/m'	12.1.40	422
12.2.41	4221'	12.3.42	4'22'	12.4.43	42'2'	13.1.44	4mm	13.2.45	4mm1'	13.3.46	4'm'm	13.4.47	4m'm'	14.1.48	-42m
14.2.49	-42m1'	14.3.50	-4'2'm	14.4.51	-4'2m'	14.5.52	-42'm'	15.1.53	4/mmm	15.2.54	4/mmm1'	15.3.55	4/m'mm	15.4.56	4'/mm'm
15.5.57	4'/m'm'm	15.6.58	4/mm'm'	15.7.59	4/m'm'm'	16.1.60	3	16.2.61	31'	17.1.62	-3	17.2.63	-31'	17.3.64	-3'
18.1.65	32	18.2.66	321'	18.3.67	32'	19.1.68	3m	19.2.69	3m1'	19.3.70	3m'	20.1.71	-3m	20.2.72	-3m1'
20.3.73	-3'm	20.4.74	-3'm'	20.5.75	-3m'	21.1.76	6	21.2.77	61'	21.3.78	6'	22.1.79	-6	22.2.80	-61'
22.3.81	-6'	23.1.82	6/m	23.2.83	6/m1'	23.3.84	6'/m	23.4.85	6/m'	23.5.86	6'/m'	24.1.87	622	24.2.88	6221'
24.3.89	6'22'	24.4.90	62'2'	25.1.91	6mm	25.2.92	6mm1'	25.3.93	6'mm'	25.4.94	6m'm'	26.1.95	-6m2	26.2.96	-6m21'
26.3.97	-6'm'2	26.4.98	-6'm2'	26.5.99	-6m'2'	27.1.100	6/mmm	27.2.101	6/mmm1'	27.3.102	6/m'mm	27.4.103	6'/mmm'	27.5.104	6'/m'mm'
27.6.105	6/mm'm'	27.7.106	6/m'm'm'	28.1.107	23	28.2.108	231'	29.1.109	m-3	29.2.110	m-31'	29.3.111	m'-3'	30.1.112	432
30.2.113	4321'	30.3.114	4'32'	31.1.115	-43m	31.2.116	-43m1'	31.3.117	-4'3m'	32.1.118	m-3m	32.2.119	m-3m1'	32.3.120	m'-3'm
32.4.121	m-3m'	32.5.122	m'-3'm'												

Figura 7. Tabla de grupos puntuales magnéticos (obtenida del programa MPOINT).

Cada MPG de la tabla de la Figura 7 es un enlace a una página dedicada a cada MPG (Figura 8), que contiene una tabla con los elementos de simetría que componen el grupo puntual, expresados en formato *x*,*y*,*z*, formato matricial y notación de Seitz (ver §4.2), así como algunas características del grupo seleccionado: número de elementos de simetría (orden del grupo), centrosimétrico/no centrosimétrico, polar/no polar y permite/no permite ferromagnetismo.

En una transición de fase, la forma general de los tensores cristalinos para la fase de alta simetría está restringida a causa de su grupo puntual magnético. El MPG de la fase de baja simetría será un subgrupo de este MPG, por lo que los tensores consistentes con el MPG de la fase de baja simetría tendrán en general más coeficientes independientes; ambos tensores serán similares, salvo por la aparición de coeficientes adicionales, prohibidos en la fase de alta simetría, a causa de la ruptura de simetría. Por lo tanto, las relaciones grupo-subgrupo de los MPGs resultan relevantes a la hora de estudiar los tensores cristalinos de una fase magnética. Por ello, para cada MPG se incluye un enlace a una tabla que contiene sus subgrupos (Figura 9).

Number of elements of the group (order): **4**
This group is **not centrosymmetric**
This group is **polar**
This group is **compatible with ferromagnetism**

Symmetry operations of the group

N	(x,y,z) form	matrix form	Seitz symbol
1	x,y,z, +1 m_x,m_y,m_z	$\begin{pmatrix} 1 & 0 & 0 \\ 0 & 1 & 0 \\ 0 & 0 & 1 \end{pmatrix}$	1
2	x,-y,z, +1 $-m_x, m_y, -m_z$	$\begin{pmatrix} 1 & 0 & 0 \\ 0 & -1 & 0 \\ 0 & 0 & 1 \end{pmatrix}$	m_y
3	-x,-y,z, -1 $m_x, m_y, -m_z$	$\begin{pmatrix} -1 & 0 & 0 \\ 0 & -1 & 0 \\ 0 & 0 & 1 \end{pmatrix}'$	$2_z'$
4	-x,y,z, -1 $-m_x,m_y,m_z$	$\begin{pmatrix} -1 & 0 & 0 \\ 0 & 1 & 0 \\ 0 & 0 & 1 \end{pmatrix}'$	m_x'

Subgroups Table

Symmetry-adapted form of material tensors for the magnetic point group m'm2' (#7.3.22) via MTENSOR

Figura 8. Página de MPOINT del MPG *m'm2'* (#7.3.22).

Finalmente, MPOINT contiene un enlace que carga el grupo puntual en el programa MTENSOR (§10), donde puede obtenerse la forma general adaptada a la simetría de los tensores cristalinos para el MPG seleccionado.

Subgroup	Order	Index
1	1	4
2'	2	2
m	2	2
m'	2	2
m'm2'	4	1

Figura 9. Tabla de subgrupos puntuales del MPG *m'm2'* (#7.3.22), obtenida de MPOINT. Se indican el índice y el orden de cada grupo.

4. POSICIONES GENERALES Y POSICIONES DE WYCKOFF DE LOS GRUPOS ESPACIALES MAGNÉTICOS: PROGRAMAS MGENPOS Y MWYCKPOS

***NOTA**: Puede encontrarse información adicional a la expuesta en este capítulo en las publicaciones incluidas en los anexos A, B y C.*

4.1 Descripción y clasificación de los grupos espaciales magnéticos

Los MSGs fueron inicialmente derivados a partir de los grupos espaciales primero por Belov, Neronova y Smirnova [29] y más tarde por Opechowski y Guccione [30], de forma independiente y diferenciada. De estas dos derivaciones surgen los dos estándares, denominados BNS y OG por las siglas de sus autores, que existen para describir los MSGs; la descripción de ambos estándares y la discusión de sus diferencias se realizará más adelante. Posteriormente, recopilaciones más recientes de los MSGs y sus características han sido llevadas a cabo por Stokes [6] y Litvin [7] (ver Figura 10).

Los MSGs pueden derivarse construyendo todas las combinaciones matemáticas posibles de elementos primados y no primados que dan lugar a MSGs no equivalentes. Asimismo, de forma similar a los MPGs, los MSGs pueden derivarse a partir de los grupos espaciales de la forma expuesta en la Figura 11, para dar lugar a los 1651 grupos espaciales magnéticos, **M**. Las características del subgrupo **G** de elementos no primados y su relación con **M** permiten establecer una clasificación de los MSGs en 4 tipos claramente diferenciables, tal y como puede verse en la Figura 11. La nomenclatura de esta clasificación en 4 tipos de MSGs proviene de Bradley & Cracknell [31].

Los MSGs tipo I (230) son aquellos que carecen de elementos primados, y por tanto son idénticos en la forma a los grupos espaciales convencionales, aunque no por ello describen la simetría de estructuras no magnéticas; simplemente, sus elementos de simetría no llevan asociada una inversión temporal. La simetría espacial tanto de estructuras ferromagnéticas y ferrimagnéticas, etc., como de estructuras antiferromagnéticas puede venir descrita por MSGs tipo I.

Los MSGs tipo II o grupos grises (230) son aquellos que describen la simetría espacial de estructuras no magnéticas y, por tanto, contienen el elemento {***1***'|**0**}. En estos grupos, cada elemento de simetría no primado del grupo aparece también primado, y viceversa. Se derivan de los grupos espaciales convencionales añadiendo el elemento {***1***'|**0**} como generador. Sólo la simetría espacial de estructuras diamagnéticas y paramagnéticas puede venir descrita por grupos tipo II.

Los 1191 MSGs restantes poseen tanto elementos primados como no primados, pero no contienen al elemento {***1***'|**0**}, por lo que cada elemento de simetría aparece en el MSG o bien primado o bien sin primar. Estos MSGs se pueden obtener a partir de los

subgrupos de índice 2 de los grupos espaciales de la forma indicada en la Figura 11, que es similar a la empleada para grupos puntuales magnéticos (Figura 6). Además, estos MSGs se dividen en dos tipos dependiendo de si el subgrupo de **G** de índice 2, **D**, del que se derivan es un subgrupo *translationengleiche* (tiene la misma red traslacional que **G**) o *klassengleiche* (tiene el mismo grupo puntual que **G**) de **M**.

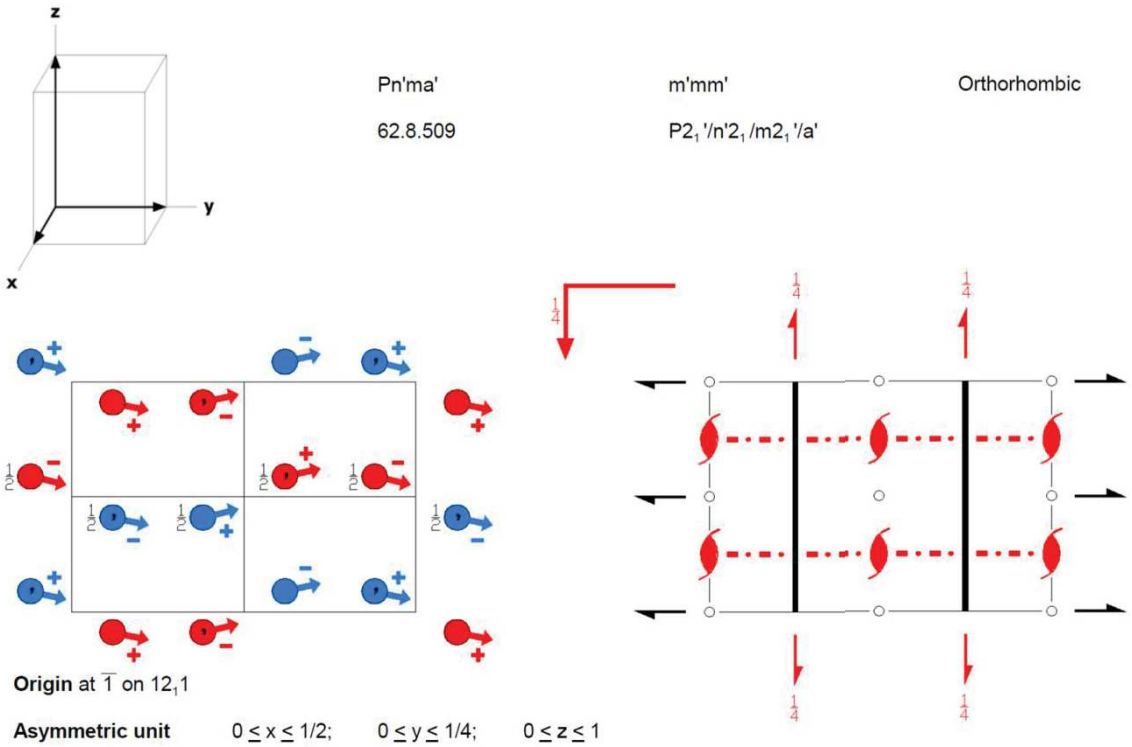

Positions

Multiplicity, Wyckoff letter, Site Symmetry.			Coordinates			
8	d	1	(1) x,y,z [u,v,w]	(2) $\bar{x}$+1/2,$\bar{y}$,z+1/2 [u,v,$\bar{w}$]	(3) $\bar{x}$,y+1/2,$\bar{z}$ [$\bar{u}$,v,$\bar{w}$]	(4) x+1/2,$\bar{y}$+1/2,$\bar{z}$+1/2 [$\bar{u}$,v,w]
			(5) $\bar{x}$,$\bar{y}$,$\bar{z}$ [u,v,w]	(6) x+1/2,y,$\bar{z}$+1/2 [u,v,$\bar{w}$]	(7) x,$\bar{y}$+1/2,z [$\bar{u}$,v,$\bar{w}$]	(8) $\bar{x}$+1/2,y+1/2,z+1/2 [$\bar{u}$,v,w]
4	c	.m.	x,1/4,z [0,v,0]	$\bar{x}$+1/2,3/4,z+1/2 [0,v,0]	$\bar{x}$,3/4,$\bar{z}$ [0,v,0]	x+1/2,1/4,$\bar{z}$+1/2 [0,v,0]
4	b	1̄	0,0,1/2 [u,v,w]	1/2,0,0 [u,v,$\bar{w}$]	0,1/2,1/2 [$\bar{u}$,v,$\bar{w}$]	1/2,1/2,0 [$\bar{u}$,v,w]
4	a	1̄	0,0,0 [u,v,w]	1/2,0,1/2 [u,v,$\bar{w}$]	0,1/2,0 [$\bar{u}$,v,$\bar{w}$]	1/2,1/2,1/2 [$\bar{u}$,v,w]

Figura 10. Ejemplo de descripción del MSG *Pn'ma'* (BNS: #62.448, OG: #62.8.509), incluyendo grupo puntual magnético, posiciones generales (elementos de simetría), posiciones de Wyckoff y descripción gráfica de sus elementos de simetría. Obtenido del listado de MSGs y sus propiedades de Litvin [7].

Los grupos tipo III (674) se derivan a partir de subgrupos *translationengleiche* de **G**, y, por tanto, poseen la misma red de traslaciones que **G**. Debido a la ausencia del

elemento {***1***'|**0**}, dos elementos de un grupo tipo III que tengan la misma parte rotacional pero distinta parte traslacional aparecen en el grupo o ambos primados o ambos sin primar, por lo que estos grupos no poseen traslaciones primadas: el segundo *coset representative* de **M** con respecto a **D** (Figura 11) no puede ser una traslación primada. La simetría espacial tanto de estructuras ferromagnéticas y ferrimagnéticas, etc., como de estructuras antiferromagnéticas puede venir descrita por MPGs tipo III.

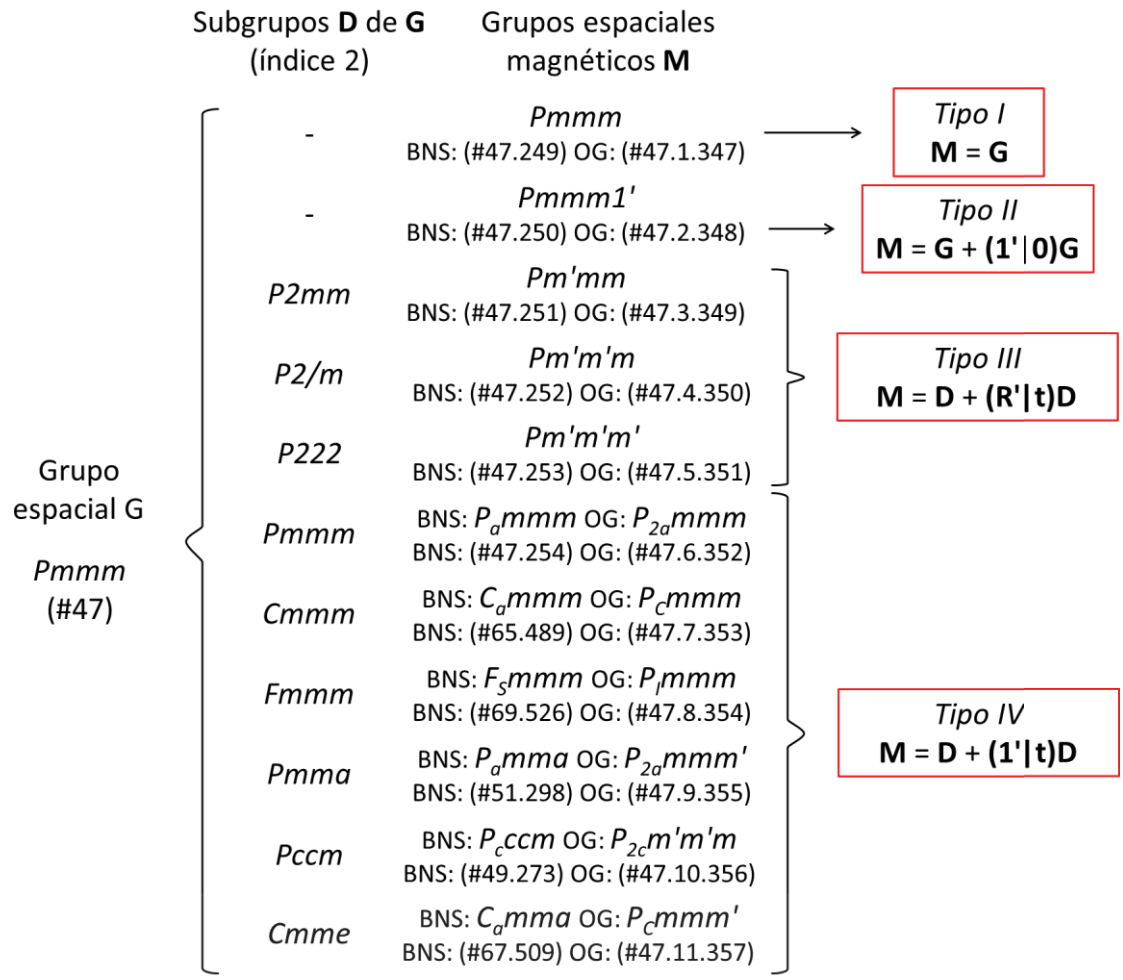

Figura 11. Derivación, notación y clasificación de los MSGs correspondientes al grupo espacial no magnético *Pmmm* (#47). Los MSGs de tipo III y IV se pueden construir a partir de la *coset decomposition* de **G** en un subgrupo de índice 2 **D**, tomando **D** como subgrupo de elementos no primados y los elementos de **G** que no pertenecen a **D** como primados.

Los grupos tipo IV (517) se derivan a partir de subgrupos *klassengleiche* de **G**; su red de traslaciones es un subgrupo de índice 2 de la de **G**, siendo las traslaciones de **G** que no forman parte de la red de traslaciones de **M** primadas: el MSG tiene asociada una red de traslaciones y traslaciones primadas o red *black-and-white*. A causa de esto, en el cristal cohabitan dos estructuras similares, que están desplazadas una respecto de la otra relacionadas por una traslación primada, y teniendo por tanto los momentos magnéticos invertidos una respecto de la otra. Esto implica necesariamente que sólo la simetría de estructuras antiferromagnéticas puede ser descrita por un MSG tipo IV. Además, esta coexistencia de dos estructuras similares con los momentos invertidos

implica que a cada MSG tipo IV se le puede asociar un vector de modulación **k** no nulo, tal que 2**k** es un vector de la red recíproca de **G** (§2.5, §5). La red *black-and-white* puede deducirse de este vector de modulación, y viceversa, evaluando la siguiente expresión:

$$\exp(2\pi i\, \vec{\mathbf{k}} \cdot \vec{\mathbf{t}}_i) \begin{cases} = 1 : \vec{\mathbf{t}}_i \in \mathbf{M},\ \vec{\mathbf{t}}_i{}' \notin \mathbf{M} \\ = -1 : \vec{\mathbf{t}}_i \notin \mathbf{M},\ \vec{\mathbf{t}}_i{}' \in \mathbf{M} \end{cases} \tag{4}$$

donde $\mathbf{t}_i$ y $\mathbf{t}_i'$ son, respectivamente, las traslaciones y traslaciones primadas de la red de traslaciones del MSG.

De esta forma, la red *black-and-white* puede especificarse alternativamente no como un conjunto de traslaciones primadas y no primadas sino como un conjunto de traslaciones (obviando la inversión temporal) y el vector de modulación **k**, que permite deducir cuáles son primadas y cuáles no.

Existen 14 tipos diferentes de redes de traslaciones o redes de Bravais asociadas a los grupos espaciales convencionales [32]. La red de traslaciones de los MSGs es también una de las redes de Bravais, pero en el caso de MSGs de tipo IV, la inclusión de traslaciones primadas permite definir 22 redes de Bravais *black-and-white* adicionales, que junto a los 14 tipos de redes de Bravais convencionales, componen los 36 tipos de redes de traslaciones y traslaciones primadas de los MSGs o redes de Bravais magnéticas [33, 34].

Para cada MSG puede definirse un grupo espacial efectivo **H**, formado por todos aquellos elementos que forman parte de **M**, primados o sin primar, tomados como no primados: es el grupo resultante de obviar la presencia de inversión temporal asociada en los elementos de **M**. El grupo **H** es idéntico al grupo no magnético **G** del que **M** se deriva según el procedimiento expuesto en la Figura 11.

4.1.1 *Descripciones estándar de los MSGs tipo IV: settings BNS y OG*

Como ya se ha mencionado, los MSGs fueron derivados de forma independiente por Belov, Neronova y Smirnova [29] (en adelante, BNS) y por Opechowski y Guccione [30] (en adelante, OG). En ambas fuentes se define una notación diferente para cada uno de los 1651 MSGs no equivalentes, y un *setting* estándar que coincide en el caso de MSGs de tipo I, II y III pero es diferente en el caso de MSGs de tipo IV. Eso es debido al diferente método utilizado para la obtención de los MSGs a partir de los grupos espaciales convencionales.

Como puede observarse en la Figura 11, todo MSG tiene asociado un grupo espacial efectivo **G** y un subgrupo de elementos no primados **D**, que es un subgrupo de índice 2 de **G**. Debido a esto, los MSGs pueden derivarse buscando todos los pares posibles de **G** y **D** y formando con ellos los MSGs de la forma expuesta en la Figura 11. En el caso del estándar BNS, este procedimiento se ha llevado a cabo tomando como **D** todos los

grupos espaciales, y buscando todos los supergrupos posibles de índice 2 de dichos grupos espaciales. Por el contrario, en el estándar OG se han tomado todos los grupos espaciales como **G**, y se han buscado todos los subgrupos de índice 2 de **G**. Es decir, la diferencia entre ambos estándares reside en que BNS toma como referencia el subgrupo y OG el supergrupo; es por esto que la notación de las etiquetas y símbolos de los MSGs en ambos estándares es diferente. Además, esta diferencia implica que, en el caso de MSGs de tipo IV, para los cuales **G** y **D** no están en el mismo *setting*, los *settings* definidos en los estándares BNS y OG, que coinciden, respectivamente, con el *setting* de los grupos **D** y **G** utilizados para deducir los MSGs, son en general diferentes.

Nótese que en el *setting* estándar OG la celda unidad de la red *black-and-white* de los MSGs coincide con la del grupo espacial efectivo. Esto, por un lado, resulta conveniente, ya que en numerosos casos las estructuras magnéticas proceden de una transición de fase desde una estructura paramagnética cuyo grupo espacial es el grupo espacial efectivo del MSG, por lo que en dichos casos la celda unidad de la fase paramagnética y la celda unidad OG del MSG coinciden, siendo ésta la celda unidad más apropiada para describir la estructura magnética desde un punto de vista práctico. Por otro lado, dado que el subgrupo de elementos no primados es un subgrupo *klassengleiche* de índice 2, algunas de las traslaciones básicas {***1***|1,0,0}, {***1***|0,1,0} y {***1***|0,0,1} pueden estar primadas. Si esto es así, la celda unidad de los MSGs expresados en el *setting* estándar OG no es una celda unidad válida para describir la simetría traslacional de cristal. Esto hace que el *setting* OG resulte engorroso desde el punto de vista matemático, ya que el conjunto de posiciones generales del MSG no puede definirse, en general, de una forma tal que la parte traslacional sea módulo 1; lo mismo sucede para las posiciones de Wyckoff (§2.4.2). El *setting* BNS no presenta estos problemas, ya que en él las traslaciones básicas definidas por la celda unidad utilizada son siempre no primadas.

Por tanto, salvo en algunos casos aislados en los que se hace uso de ambos *settings*, que se mencionarán expresamente, el *setting* utilizado como estándar, tanto en esta tesis doctoral como en los diversos programas desarrollados, es el *setting* BNS. Ésta es una elección propia de esta tesis doctoral, no un criterio global: las distintas publicaciones y programas informáticos relacionados con la simetría magnética hacen su propia elección de *setting* estándar. Por ejemplo, el listado de Stokes [6] de MSGs legibles por ordenador hace uso de ambos *settings*, mientras que el listado de tablas de los MSGs de Litvin [7] sólo hace uso del *setting* OG (Figura 10).

La notación del símbolo del grupo para ambos *settings* es similar a la de los grupos espaciales convencionales, añadiéndose una prima en aquellos generadores que estén primados, o bien el símbolo 1' al final del grupo para indicar que el grupo es gris, según sea el caso. La red de traslaciones está indicada al principio del símbolo del MSG; en el caso de los MSGs tipos I, II y III, por una letra mayúscula que identifica la red de Bravais; en el caso de los MSGs de tipo IV, por medio de un símbolo formado por una letra mayúscula y otra letra como subíndice que identifica la red de Bravais magnética (*black-and-white*). Los símbolos identificativos de la red de Bravais magnética son diferentes para los *settings* BNS y OG [33].

La etiqueta numérica de los MSGs en el *setting* BNS consta de 2 números separados por un punto: el primero indica el grupo espacial **D** del que el MSG se deriva, y el segundo enumera el grupo dentro de cada clase cristalina. La etiqueta de los MSGs en el *setting* OG consta de 3 números separados por puntos: el primero indica el grupo espacial efectivo **G** del que se deriva, el segundo enumera los grupos que tienen el mismo grupo espacial efectivo, y el tercero es un número entre 1 y 1651 que identifica unívocamente al MSG (Figuras 10 y 11).

4.1.2 Descripciones no estándar de los MSGs: transformaciones de setting

Cualquier MSG descrito por sus operaciones $\{\boldsymbol{R}|\mathbf{t}\}$ y $\{\boldsymbol{R}'|\mathbf{t}\}$ es siempre equivalente, mediante una transformación afín $(\boldsymbol{P},\mathbf{p})$, a uno de los 1651 posibles MSGs tal como están descritos en el *setting* estándar mencionado más arriba. La transformación (cambio de celda unidad y de origen $(\boldsymbol{P},\mathbf{p})$) que transforma las operaciones a su *setting* estándar no es única. El conjunto de transformaciones afines que dejan invariante las operaciones, manteniendo el MSG en su *setting* estándar, constituye el normalizador afín $\mathbf{N_A}$ de ese MSG (§6.1); y cualquier transformación $(\tilde{\boldsymbol{P}},\tilde{\mathbf{p}})$ relacionada con $(\boldsymbol{P},\mathbf{p})$ de la forma:

$$\left(\tilde{\boldsymbol{P}},\tilde{\mathbf{p}}\right)=\left(\boldsymbol{P},\mathbf{p}\right)\left(\boldsymbol{P}_{\mathrm{A}},\mathbf{p}_{\mathrm{A}}\right) \tag{5}$$

donde $(\boldsymbol{P}_{\mathrm{A}},\mathbf{p}_{\mathrm{A}})$ es cualquier elemento del normalizador afín $\mathbf{N_A}$ del MSG, permite también el paso al *setting* estándar del MSG.

Un MSG queda definido sin ambigüedad, salvo en el caso de los MSGs tipo IV en *setting* OG (§2.4), cuando se especifican sus posiciones generales (§2.4), que describen la actuación de las operaciones de simetría sobre el valor de una posición arbitraria (x,y,z), descrita en unidades relativas a la celda unidad, y sobre un momento magnético (m_x,m_y,m_z) localizado en ese punto. Esto es igualmente cierto para MSSGs (§2.5). Pero además, dado que un MSG es equivalente a un único MSG en *setting* estándar, cualquier MSG también queda definido sin ambigüedad indicando, por un lado, el símbolo o etiqueta del MSG en su *setting* estándar, y por otro, una transformación de *setting* $(\boldsymbol{P},\mathbf{p})$ que transforma dicho MSG al *setting* estándar; esta transformación puede ser cualquiera del conjunto $(\tilde{\boldsymbol{P}},\tilde{\mathbf{p}})$ definido en la ecuación (5).

Tanto en esta tesis doctoral como en los programas desarrollados, la forma de expresar una transformación $(\boldsymbol{P},\mathbf{p})$, que transforma el *setting* $(\mathbf{a},\mathbf{b},\mathbf{c})$ con origen en O en el *setting* $(\tilde{\mathbf{a}},\tilde{\mathbf{b}},\tilde{\mathbf{c}})$ con origen en $\tilde{\mathrm{O}}$, es en forma de matriz aumentada 4x4:

$$\left(\boldsymbol{P},\mathbf{p}\right)=\left(\begin{array}{ccc|c} & \boldsymbol{P} & & \mathbf{p} \\ \hline 0 & 0 & 0 & 1 \end{array}\right)=\left(\begin{array}{ccc|c} P_{11} & P_{12} & P_{13} & p_1 \\ P_{21} & P_{22} & P_{23} & p_2 \\ P_{31} & P_{32} & P_{33} & p_3 \\ \hline 0 & 0 & 0 & 1 \end{array}\right) \qquad \begin{aligned} \tilde{\mathbf{a}} &= P_{11}\mathbf{a}+P_{21}\mathbf{b}+P_{31}\mathbf{c} \\ \tilde{\mathbf{b}} &= P_{12}\mathbf{a}+P_{22}\mathbf{b}+P_{32}\mathbf{c} \\ \tilde{\mathbf{c}} &= P_{13}\mathbf{a}+P_{23}\mathbf{b}+P_{33}\mathbf{c} \\ \tilde{O} &= O+\mathbf{p} \end{aligned} \tag{6}$$

La transformación de *setting* en forma matricial puede indicarse ocasionalmente omitiendo la última línea de ceros y unos. La relación entre las posiciones atómicas, elementos de simetría y momentos magnéticos de los *settings* original y transformado es:

Operaciones de simetría:

$$\left(\begin{array}{ccc|c} & \tilde{\boldsymbol{R}} & & \tilde{\boldsymbol{t}} \\ \hline 0 & 0 & 0 & 1 \end{array}\right) = \left(\begin{array}{ccc|c} & \boldsymbol{P} & & \mathbf{p} \\ \hline 0 & 0 & 0 & 1 \end{array}\right)^{-1} \left(\begin{array}{ccc|c} & \boldsymbol{R} & & \boldsymbol{t} \\ \hline 0 & 0 & 0 & 1 \end{array}\right) \left(\begin{array}{ccc|c} & \boldsymbol{P} & & \mathbf{p} \\ \hline 0 & 0 & 0 & 1 \end{array}\right)$$

Posiciones atómicas:

$$\begin{pmatrix} \tilde{x} \\ \tilde{y} \\ \tilde{z} \\ 1 \end{pmatrix} = \left(\begin{array}{ccc|c} & \boldsymbol{P} & & \mathbf{p} \\ \hline 0 & 0 & 0 & 1 \end{array}\right)^{-1} \begin{pmatrix} x \\ y \\ z \\ 1 \end{pmatrix}$$

Momentos magnéticos:

$$\begin{pmatrix} \tilde{m}_x/\tilde{a} \\ \tilde{m}_y/\tilde{b} \\ \tilde{m}_z/\tilde{c} \end{pmatrix} = \boldsymbol{P}^{-1} \begin{pmatrix} m_x/a \\ m_y/b \\ m_z/c \end{pmatrix} \qquad (7)$$

Nótese que los momentos magnéticos de la ecuación (7) están divididos por los parámetros de red de ambos *settings*. La razón de esto es que los momentos asociados a los átomos magnéticos tienen componentes que no son adimensionales y, al contrario que las posiciones atómicas, no pueden expresarse en coordenadas relativas a la celda unidad, pues una transformación de *setting* que duplicara la celda unidad a lo largo de uno de los tres vectores de la base no debería provocar alteración alguna en los valores numéricos de las componentes de los momentos magnéticos. Sin embargo, una transformación de *setting* consistente en una rotación de los vectores de la base sí modificaría los valores de los momentos, pues la orientación de los vectores de la base cambia. Dicho de otro modo, las componentes de los momentos magnéticos son independientes de los parámetros de red, pero dependientes de la orientación de los vectores de la base; de ahí que sea necesario dividir los momentos magnéticos entre los parámetros de red antes de realizar la transformación de *setting*. Este hecho también se aplica a la relación entre las posiciones atómicas y momentos magnéticos de átomos magnéticos relacionados por un elemento $\{\boldsymbol{R},\tau|\mathbf{t}\}$ del MSG:

Posiciones atómicas:
$$\begin{pmatrix} \tilde{x} \\ \tilde{y} \\ \tilde{z} \\ 1 \end{pmatrix} = \left(\begin{array}{ccc|c} & \boldsymbol{R} & & \mathbf{t} \\ \hline 0 & 0 & 0 & 1 \end{array}\right) \begin{pmatrix} x \\ y \\ z \\ 1 \end{pmatrix}$$

Momentos magnéticos:
$$\begin{pmatrix} \tilde{m}_x/\tilde{a} \\ \tilde{m}_y/\tilde{b} \\ \tilde{m}_z/\tilde{c} \end{pmatrix} = \mathbf{det}(\boldsymbol{R}) \cdot \boldsymbol{\tau} \cdot \boldsymbol{R} \begin{pmatrix} m_x/a \\ m_y/b \\ m_z/c \end{pmatrix} \quad (8)$$

En esta tesis doctoral y en los programas desarrollados, los valores numéricos de las componentes de los momentos magnéticos se expresan tomando como unidad el magnetón de Bohr μ_B=9,27x10^{-24} J/T, como es habitual.

4.2 Posiciones Generales y Posiciones de Wyckoff de los grupos espaciales magnéticos

Las bases de datos de posiciones generales (elementos de simetría) y posiciones de Wyckoff (WP) de los MSGs utilizadas en los programas desarrollados como parte de esta tesis doctoral se han obtenido a partir de los listados de MSGs en *settings* BNS [29] y OG [30], que han sido recopilados en formato legible por ordenador por Stokes y Campbell [6]. Asimismo, el listado de Stokes y Campbell se basa en la base de datos de los MSGs realizada por Litvin [7], en cuyo trabajo de recopilación y estandarización de los MSGs se basa la notación de los MPGs y MSGs utilizada en esta tesis doctoral.

Partiendo de las fuentes mencionadas, se han creado los programas MGENPOS (http://www.cryst.ehu.es/cgi-bin/cryst/programs/magget_gen.pl) y MWYCKPOS (http://www.cryst.ehu.es/cgi-bin/cryst/programs/magget_wp.pl), que consisten en bases de datos interactivas de las posiciones generales y de Wyckoff, respectivamente, de los MSGs. Los datos procedentes de los listados de Stokes han sido leídos, procesados y almacenados internamente, no sólo para ser mostrados y utilizados en las bases de datos interactivas de MGENPOS y MWYCKPOS, sino también para ser utilizados internamente por otros programas de la sección "*Magnetic Symmetry and Applications*" del *Bilbao Crystallographic Server*. El capítulo 2 del Anexo A y el capítulo 2.1 del Anexo C contienen breves descripciones de MGENPOS y MWYCKPOS, que complementan lo expuesto en este capítulo.

4.2.1 *Posiciones generales de los MSGs*

Las posiciones generales de un MSG definen un conjunto de operaciones de simetría del MSG que permiten describir el grupo sin ambigüedad. Se definen, al igual que las

de un grupo espacial, como una elección particular de los *coset-representatives* de la *coset-decomposition* del MSG con respecto a un subgrupo **T** de traslaciones:

$$\mathbf{M} = \mathbf{T} + \left\{\boldsymbol{R}_1 \mid \mathbf{t}_1\right\}\mathbf{T} + \ldots + \left\{\boldsymbol{R}_n \mid \mathbf{t}_n\right\}\mathbf{T} \qquad (9)$$

Este subgrupo de traslaciones no es necesariamente la red de traslaciones, ya que, por simplicidad, algunos de los generadores de dicha red pueden ser incluidos en las posiciones generales como centrados. Para los MSG de tipos I, II y III y los MSG tipo IV en *setting* BNS, se elige como subgrupo **T** el conjunto de traslaciones básicas de la celda unidad y sus combinaciones, es decir, toda traslación con componentes enteros y mayores o iguales que uno. Esta elección es siempre posible, pues las traslaciones básicas de la celda unidad no están primadas en estos casos. Esta elección de **T**, común a todos los MSGs de estos tipos, permite que las operaciones $\{\boldsymbol{R}_i|\mathbf{t}_i\}$ (que se escogen de forma que las componentes de $\mathbf{t}_i$ sean menores que uno, y que pueden incluir centrados) caractericen unívocamente al MSG, de forma que estos MSGs puede ser descrito sin ambigüedad indicando únicamente sus posiciones generales.

Sin embargo, para los grupos tipo IV en *setting* OG, el grupo **T** no puede definirse siguiendo el criterio antes mencionado, pues en este caso las traslaciones básicas de la celda unidad pueden estar primadas. Esto implica que existe ambigüedad tanto en la elección del grupo **T**, que depende de qué traslaciones básicas estén primadas en cada MSG (y, por tanto, no es común a todos los MSGs de tipo IV en *setting* OG), como en la elección del conjunto de posiciones generales. A consecuencia de esta ambigüedad, las posiciones generales de un MSG de tipo IV en *setting* OG no lo caracterizan unívocamente, existiendo casos de MSGs en los cuales dos MSGs de tipo IV en *setting* OG diferentes tienen las mismas posiciones generales, diferenciándose únicamente en que sus redes *black-and-white* son diferentes (Figura 12). Por tanto, para definir unívocamente un MSG tipo IV en OG, la red *black-and-white* debe especificarse también.

En los listados de Stokes y Campbell [6] que se han utilizado como base en esta tesis doctoral, la descripción de la red *black-and-white* de los MSGs de tipo IV en *setting* OG presenta algunos problemas de ambigüedad o falta de cierta sistemática. Para evitar ambigüedades y confusiones, en esta tesis se ha seguido un criterio propio para elegir el grupo **T** y las posiciones generales en estos casos; además, tanto la red de traslaciones como la red *black-and-white* de estos MSGs se indican de la forma más explícita posible (Figura 12). Así pues, las posiciones generales proporcionadas por MGENPOS, así como las posiciones de Wyckoff proporcionadas por MWYCKPOS (por idénticas razones, §4.4.2) coinciden con las de los listados de Stokes y Campbell [6] salvo en los MSGs de tipo IV en *setting* OG, que han sido reelaborados.

El criterio empleado en esta tesis doctoral para definir las posiciones generales de los MSGs de tipo IV en *setting* OG es el siguiente: en los casos en que dos o más traslaciones básicas están primadas, se incluirá únicamente una traslación primada en las posiciones generales (la inclusión de más de una traslación básica primada implicaría incluir también los centrados $\{\boldsymbol{1}|1,1,0\}$, $\{\boldsymbol{1}|1,0,1\}$, y/o $\{\boldsymbol{1}|1,0,1\}$, hecho que

se trata de evitar). La traslación primada será elegida siguiendo el siguiente orden de preferencia: {***1***'|1,0,0}, {***1***'|0,1,0} y {***1***'|0,0,1}.

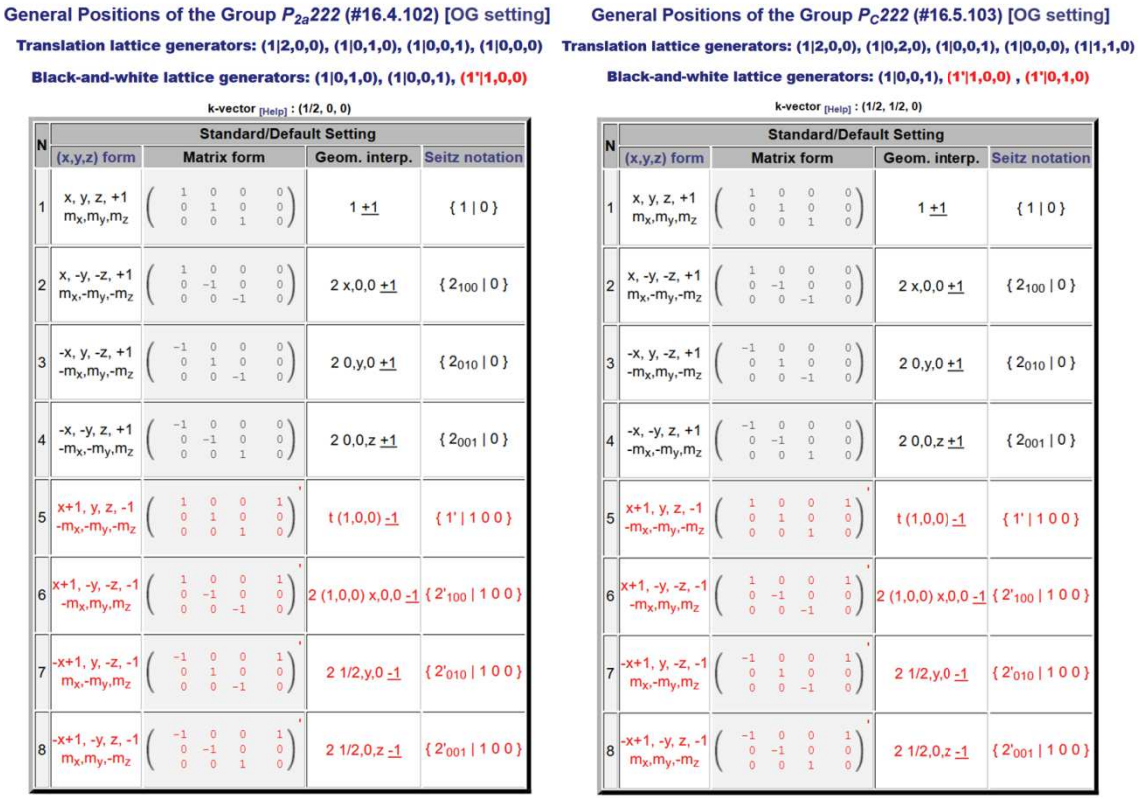

General Positions of the Group $P_{2a}222$ (#16.4.102) [OG setting]

Translation lattice generators: (1|2,0,0), (1|0,1,0), (1|0,0,1), (1|0,0,0)

Black-and-white lattice generators: (1|0,1,0), (1|0,0,1), (1'|1,0,0)

k-vector [Help] : (1/2, 0, 0)

N	Standard/Default Setting			
	(x,y,z) form	Matrix form	Geom. interp.	Seitz notation
1	x, y, z, +1 m_x,m_y,m_z	$\begin{pmatrix} 1 & 0 & 0 & 0 \\ 0 & 1 & 0 & 0 \\ 0 & 0 & 1 & 0 \end{pmatrix}$	1 +1	{ 1 | 0 }
2	x, -y, -z, +1 $m_x,-m_y,-m_z$	$\begin{pmatrix} 1 & 0 & 0 & 0 \\ 0 & -1 & 0 & 0 \\ 0 & 0 & -1 & 0 \end{pmatrix}$	2 x,0,0 +1	{ 2_{100} | 0 }
3	-x, y, -z, +1 $-m_x,m_y,-m_z$	$\begin{pmatrix} -1 & 0 & 0 & 0 \\ 0 & 1 & 0 & 0 \\ 0 & 0 & -1 & 0 \end{pmatrix}$	2 0,y,0 +1	{ 2_{010} | 0 }
4	-x, -y, z, +1 $-m_x,-m_y,m_z$	$\begin{pmatrix} -1 & 0 & 0 & 0 \\ 0 & -1 & 0 & 0 \\ 0 & 0 & 1 & 0 \end{pmatrix}$	2 0,0,z +1	{ 2_{001} | 0 }
5	x+1, y, z, -1 $-m_x,-m_y,-m_z$	$\begin{pmatrix} 1 & 0 & 0 & 1 \\ 0 & 1 & 0 & 0 \\ 0 & 0 & 1 & 0 \end{pmatrix}'$	t (1,0,0) -1	{ 1' | 1 0 0 }
6	x+1, -y, -z, -1 $-m_x,m_y,m_z$	$\begin{pmatrix} 1 & 0 & 0 & 1 \\ 0 & -1 & 0 & 0 \\ 0 & 0 & -1 & 0 \end{pmatrix}'$	2 (1,0,0) x,0,0 -1	{ $2'_{100}$ | 1 0 0 }
7	-x+1, y, -z, -1 $m_x,-m_y,m_z$	$\begin{pmatrix} -1 & 0 & 0 & 1 \\ 0 & 1 & 0 & 0 \\ 0 & 0 & -1 & 0 \end{pmatrix}'$	2 1/2,y,0 -1	{ $2'_{010}$ | 1 0 0 }
8	-x+1, -y, z, -1 $m_x,m_y,-m_z$	$\begin{pmatrix} -1 & 0 & 0 & 1 \\ 0 & -1 & 0 & 0 \\ 0 & 0 & 1 & 0 \end{pmatrix}'$	2 1/2,0,z -1	{ $2'_{001}$ | 1 0 0 }

General Positions of the Group P_C222 (#16.5.103) [OG setting]

Translation lattice generators: (1|2,0,0), (1|0,2,0), (1|0,0,1), (1|0,0,0), (1|1,1,0)

Black-and-white lattice generators: (1|0,0,1), (1'|1,0,0) , (1'|0,1,0)

k-vector [Help] : (1/2, 1/2, 0)

N	Standard/Default Setting			
	(x,y,z) form	Matrix form	Geom. interp.	Seitz notation
1	x, y, z, +1 m_x,m_y,m_z	$\begin{pmatrix} 1 & 0 & 0 & 0 \\ 0 & 1 & 0 & 0 \\ 0 & 0 & 1 & 0 \end{pmatrix}$	1 +1	{ 1 | 0 }
2	x, -y, -z, +1 $m_x,-m_y,-m_z$	$\begin{pmatrix} 1 & 0 & 0 & 0 \\ 0 & -1 & 0 & 0 \\ 0 & 0 & -1 & 0 \end{pmatrix}$	2 x,0,0 +1	{ 2_{100} | 0 }
3	-x, y, -z, +1 $-m_x,m_y,-m_z$	$\begin{pmatrix} -1 & 0 & 0 & 0 \\ 0 & 1 & 0 & 0 \\ 0 & 0 & -1 & 0 \end{pmatrix}$	2 0,y,0 +1	{ 2_{010} | 0 }
4	-x, -y, z, +1 $-m_x,-m_y,m_z$	$\begin{pmatrix} -1 & 0 & 0 & 0 \\ 0 & -1 & 0 & 0 \\ 0 & 0 & 1 & 0 \end{pmatrix}$	2 0,0,z +1	{ 2_{001} | 0 }
5	x+1, y, z, -1 $-m_x,-m_y,-m_z$	$\begin{pmatrix} 1 & 0 & 0 & 1 \\ 0 & 1 & 0 & 0 \\ 0 & 0 & 1 & 0 \end{pmatrix}'$	t (1,0,0) -1	{ 1' | 1 0 0 }
6	x+1, -y, -z, -1 $-m_x,m_y,m_z$	$\begin{pmatrix} 1 & 0 & 0 & 1 \\ 0 & -1 & 0 & 0 \\ 0 & 0 & -1 & 0 \end{pmatrix}'$	2 (1,0,0) x,0,0 -1	{ $2'_{100}$ | 1 0 0 }
7	-x+1, y, -z, -1 $m_x,-m_y,m_z$	$\begin{pmatrix} -1 & 0 & 0 & 1 \\ 0 & 1 & 0 & 0 \\ 0 & 0 & -1 & 0 \end{pmatrix}'$	2 1/2,y,0 -1	{ $2'_{010}$ | 1 0 0 }
8	-x+1, -y, z, -1 $m_x,m_y,-m_z$	$\begin{pmatrix} -1 & 0 & 0 & 1 \\ 0 & -1 & 0 & 0 \\ 0 & 0 & 1 & 0 \end{pmatrix}'$	2 1/2,0,z -1	{ $2'_{001}$ | 1 0 0 }

Figura 12. Definición de las posiciones generales de dos MSGs tipo IV en *setting* OG, $P_{2a}222$ (#16.4.102) y P_C222 (#16.5.103). El conjunto de posiciones generales es idéntico. Lo que permite distinguir ambos grupos son la red de traslaciones y la red *black-and-white*. Estas figuras están sacadas del programa MGENPOS (§4.3).

Además, debe notarse que la ambigüedad en la elección de las posiciones generales implica que la multiplicidad formal de las posiciones generales en *setting* OG puede ser distinta de la multiplicidad de dicho MSG en *setting* BNS. Lo mismo ocurre para las posiciones de Wyckoff (§4.4.2).

4.2.2 *Posiciones de Wyckoff de los MSGs: momentos magnéticos restringidos e importancia de los átomos no magnéticos*

Las posiciones de Wyckoff (WP) de los MSGs se definen igual que las de los grupos espaciales convencionales [35], con la particularidad de que, dado que los átomos de las estructuras magnéticas tienen asociado un momento magnético, cada WP de los MSGs tiene también asociada un momento magnético (Figura 10), que para posiciones especiales de Wyckoff puede estar restringido por simetría a ciertas direcciones, en incluso ser nulo obligatoriamente, debido a la invariancia de las posiciones especiales de Wyckoff bajo la acción de los elementos de simetría del *site-symmetry group* (SSG) de la posición de Wyckoff. Este hecho es importante, pues permite descartar, en el proceso de determinación de una estructura magnética, aquellos MSGs posibles a

priori cuyas restricciones en los momentos magnéticos de las WPs no permitan momentos magnéticos no nulos o sean incompatibles con los datos experimentales. Así pues, las restricciones que el SSG impone sobre los momentos magnéticos de los átomos en función de la WP que ocupen permiten determinar, una vez conocido el MSG de una estructura, la disposición y el máximo número de grados de libertad del ordenamiento de espines de los átomos magnéticos.

Además, el conocimiento de las WPs de los MSGs es también relevante en lo concerniente a los átomos no magnéticos. En general, la presencia en el cristal de átomos no magnéticos ubicados en WPs con SSGs de menor simetría que las SSGs de las WPs donde se ubican los átomos magnéticos, disminuye la simetría del cristal tanto en la fase no magnética como en la fase magnética. Por ello, la simetría de una estructura magnética puede ser menor que la simetría de su ordenamiento magnético considerado de forma aislada (es decir, teniendo en cuenta únicamente los átomos magnéticos), lo que puede influir en las propiedades físicas del material.

El análisis teórico y los ejemplos que pueden encontrarse en el capítulo 2.7 del Anexo C muestran la importancia que la presencia de átomos no magnéticos en WPs de baja simetría tiene a la hora de determinar el MSG y las propiedades físicas de las estructuras magnéticas. Asimismo, el Anexo D muestra en su capítulo 3 cómo las restricciones al momento magnético asociadas a las WPs se pueden utilizar para descartar MSGs que de otro modo no serían descartables, lo que resulta útil en la búsqueda de estructuras magnéticas multiferroicas; y en su capítulo 4, extiende estos argumentos a los átomos no magnéticos, cuya presencia causa una menor simetría que la que tendría por sí mismo el ordenamiento de espines. Todos estos argumentos muestran la importancia de la asignación de un MSG, la importancia de las restricciones de los momentos asociadas a los SSGs y el efecto en la simetría de los átomos no magnéticos. Sirva esto para prevenir contra la práctica habitual de determinar estructuras magnéticas y deducir sus propiedades calculando únicamente el ordenamiento de espines de los átomos magnéticos de la estructura, obviando tanto la presencia de átomos no magnéticos como las restricciones asociadas al SSG de cada WP ocupada por un átomo magnético.

Los momentos magnéticos de toda la órbita de una WP pueden derivarse a partir de los momentos de un representante de la WP aplicando los elementos de simetría del MSG sobre el momento magnético de dicho representante por medio de la fórmula (8).

4.3 Programa MGENPOS

El programa MGENPOS es una herramienta de consulta de las posiciones generales de los MSGs, tanto en *setting* BNS como OG. La página principal (Figura 13(a)) permite seleccionar un MSG y obtener sus posiciones generales tanto en *setting* estándar (botón "*Standard/Default Setting*") como en *setting* no estándar (botón "*Non-conventional setting*"). Se puede seleccionar un MSG bien introduciendo su etiqueta numérica correspondiente en el *setting* BNS u OG (§4.1.1) en el formulario indicado,

bien haciendo clic en el botón "*choose it*", lo que proporciona una lista de los 230 grupos espaciales convencionales para poder seleccionar, para cada uno, una lista de los MSGs que de él se derivan (Figura 13(b)), tanto en la forma de derivarlos de Belov, Neronova y Smirnova [29] como en la forma de Opechowski y Guccione [30].

(a)

(b)

The magnetic space groups derived from the Fedorov space group: Pmmm (#47)

Listed with respect to the BNS setting:

- #47.249 Pmmm [OG: Pmmm #47.1.347] *Type I (Fedorov)*
- #47.250 Pmmm1' [OG: Pmmm1' #47.2.348] *Type II (grey group)*
- #47.251 Pm'mm [OG: Pm'mm #47.3.349] *Type III (translationgleiche)*
- #47.252 Pm'm'm [OG: Pm'm'm #47.4.350] *Type III (translationgleiche)*
- #47.253 Pm'm'm' [OG: Pm'm'm' #47.5.351] *Type III (translationgleiche)*
- #47.254 $P_a$mmm [OG: P_{2a}mmm #47.6.352] *Type IV (klassengleiche)*
- #47.255 $P_C$mmm [OG: $C_P$mmm #65.9.553] *Type IV (klassengleiche)*
- #47.256 $P_I$mmm [OG: $I_P$mmm #71.6.626] *Type IV (klassengleiche)*

Listed with respect to the OG setting:

- #47.1.347 Pmmm [BNS: Pmmm #47.249] *Type I (Fedorov)*
- #47.2.348 Pmmm1' [BNS: Pmmm1' #47.250] *Type II (grey group)*
- #47.3.349 Pm'mm [BNS: Pm'mm #47.251] *Type III (translationgleiche)*
- #47.4.350 Pm'm'm [BNS: Pm'm'm #47.252] *Type III (translationgleiche)*
- #47.5.351 Pm'm'm' [BNS: Pm'm'm' #47.253] *Type III (translationgleiche)*
- #47.6.352 P_{2a}mmm [BNS: $P_a$mmm #47.254] *Type IV (klassengleiche)*
- #47.7.353 $P_C$mmm [BNS: $C_a$mmm #65.489] *Type IV (klassengleiche)*
- #47.8.354 $P_I$mmm [BNS: $F_S$mmm #69.526] *Type IV (klassengleiche)*
- #47.9.355 P_{2a}mmm' [BNS: $P_a$mma #51.298] *Type IV (klassengleiche)*
- #47.10.356 P_{2c}m'm'm [BNS: $P_c$ccm #49.273] *Type IV (klassengleiche)*
- #47.11.357 $P_C$mmm' [BNS: $C_a$mma #67.509] *Type IV (klassengleiche)*

Figura 13. (a) Formulario de consulta de las posiciones generales de los MSGs de la página principal del programa MGENPOS. (b) Página de selección de MSGs que se derivan del grupo espacial *Pmmm* (#47).

La tabla de posiciones generales proporcionada por MGENPOS cuando se selecciona un MSG en *setting* estándar puede verse en la Figura 14 para el MSG P_Cc (#7.6.37), así como en las Figuras 1 y 2 del Anexo A y en los ejemplos de la Figura 12 para diversos MSGs. En la página se indican la etiqueta y el símbolo del MSG para el *setting* (BNS/OG) seleccionado, así como la misma información para el *setting* no seleccionado. En el caso de que el MSG sea de tipo IV (Figura 14), se proporcionan además un enlace para seleccionar el *setting* BNS u OG alternativo al mostrado y un enlace a una página (Figura 15) que muestra la transformación de *setting* (una de las posibles) que debe realizarse para transformar el MSG del *setting* BNS al OG, y del OG al BNS. Las matrices de transformación OG->BNS son a menudo transformaciones sencillas que consisten en duplicar el tamaño de la celda unidad a lo largo de aquellos ejes según los cuales las traslaciones básicas en el *setting* OG están primadas; sin embargo, pueden ser más complejas. Dado que la celda unidad OG, que es igual que la del grupo espacial efectivo, es por definición igual o más pequeña que la celda unidad BNS, la parte lineal de las matrices de transformación OG->BNS tiene componentes

enteros, y su determinante es 1, 2, 4 u 8. Las transformaciones OG->BNS proporcionadas por MGENPOS provienen del listado de MSGs de Stokes [6], donde se indican explícitamente; invirtiendo éstas, se han obtenido las transformaciones BNS->OG.

General Positions of the Group P_Cc (#7.6.37) [OG setting]

To display the general positions in the BNS setting, please follow this link: C_ac (#9.41) [Transformation matrix]

Translation lattice generators: (1|2,0,0), (1|0,2,0), (1|0,0,1), (1|0,0,0), (1|1,1,0)

Black-and-white lattice generators: (1|0,0,1), (1'|1,0,0) , (1'|0,1,0)

k-vector [Help] : (1/2, 1/2, 0)

N	Standard/Default Setting			
	(x,y,z) form	Matrix form	Geom. interp.	Seitz notation
1	x, y, z, +1 m_x,m_y,m_z	$\begin{pmatrix} 1 & 0 & 0 & 0 \\ 0 & 1 & 0 & 0 \\ 0 & 0 & 1 & 0 \end{pmatrix}$	1 +1	{ 1 | 0 }
2	x, -y, z+1/2, +1 $-m_x,m_y,-m_z$	$\begin{pmatrix} 1 & 0 & 0 & 0 \\ 0 & -1 & 0 & 0 \\ 0 & 0 & 1 & 1/2 \end{pmatrix}$	c x,0,z +1	{ m_{010} | 0 0 1/2 }
3	x+1, y, z, -1 $-m_x, -m_y, -m_z$	$\begin{pmatrix} 1 & 0 & 0 & 1 \\ 0 & 1 & 0 & 0 \\ 0 & 0 & 1 & 0 \end{pmatrix}'$	t (1,0,0) -1	{ 1' | 1 0 0 }
4	x+1, -y, z+1/2, -1 $m_x,-m_y,m_z$	$\begin{pmatrix} 1 & 0 & 0 & 1 \\ 0 & -1 & 0 & 0 \\ 0 & 0 & 1 & 1/2 \end{pmatrix}'$	g (1,0,1/2) x,0,z -1	{ m'_{010} | 1 0 1/2 }

Go to the list of the Wyckoff Positions of the Group P_Cc (#7.6.37)
Go to the Systematic Absences for the Group P_Cc (#7.6.37)

Figura 14. Posiciones generales del MSG P_Cc (#7.6.37) [OG], obtenidas de MGENPOS.

OG to BNS Transformation matrix:

$$\begin{pmatrix} 2 & 0 & 0 & 0 \\ 0 & 2 & 0 & 0 \\ 0 & 0 & 1 & 0 \end{pmatrix}$$

BNS to OG Transformation matrix:

$$\begin{pmatrix} 1/2 & 0 & 0 & 0 \\ 0 & 1/2 & 0 & 0 \\ 0 & 0 & 1 & 0 \end{pmatrix}$$

Figura 15. Transformaciones de *setting* BNS->OG y OG->BNS para el MSG C_ac (#9.41) [BNS], P_Cc (#7.6.37) [OG], obtenidos de MGENPOS.

De igual forma, si el grupo seleccionado es de tipo IV (Figura 14), se especifican los generadores de la red de traslaciones y de la red *black-and-white* del grupo, indicando en ambos casos el conjunto completo de traslaciones y/o antitraslaciones dentro de la celda unidad (en el caso de los generadores de la red de traslaciones en *setting* OG, si alguna de las traslaciones básicas están primadas, se proporciona el conjunto completo de traslaciones y/o antitraslaciones dentro de la supercelda (*n***a**, *m***b**, *r***c**), donde *n*, *m* y *r* son 1 si la traslación básica a lo largo, respectivamente, de los ejes **a**, **b** y **c** es no primada, y 2 si es primada). De esta forma ambas redes quedan perfectamente definidas, tanto en *setting* BNS como OG, y se evita cualquier ambigüedad en la definición de las posiciones generales de los MSGs (§4.2.1).

Si además de ser de tipo IV, el MSG seleccionado está en *setting* OG, tal y como puede verse en la Figura 14 y en los ejemplos de la Figura 12, se indica el vector de propagación **k** asociado al MSG que fue descrito en §4.1 y que permite deducir si las traslaciones de la red *black-and-white* son primadas o no. Este vector de propagación permite describir un grupo en *setting* OG de la forma más sencilla posible: especificar el MSG de la forma habitual e indicar este vector es suficiente para describir el MSG sin ambigüedad. Por ello, este vector de propagación es también llamado "vector de onda OG".

Además, en casos sencillos, el vector de onda OG puede hacerse coincidir con el llamado vector de propagación experimental del ordenamiento magnético que se observaría en el patrón de difracción magnética correspondiente a una estructura magnética con ese MSG. Esto sucede si la celda primitiva de la fase magnética es el doble que la celda primitiva de la fase paramagnética; es decir, si se cumple, tanto para el vector de onda OG como para el vector de propagación experimental, que $2\mathbf{k} \in \mathbf{H}$, siendo **H** un vector cualquiera de la red recíproca del grupo de la fase paramagnética (en adelante, grupo padre). En ese caso, se puede hacer coincidir el vector de propagación con el vector de onda OG del MSG. Esta sencilla situación es habitual, y de darse el caso, el conocimiento del vector de onda OG de los MSGs permite descartar como posibles aquellos MSGs cuyo **k** asociado sea diferente (no equivalente). Esta asociación entre el vector de propagación y los MSGs en *setting* OG ilustra a la perfección la utilidad práctica del uso del *setting* OG en casos sencillos en los que este *setting* coincide con el *setting* del grupo padre.

El vector de onda OG **k** proporcionado por MGENPOS ha sido deducido de los generadores $\{1,\tau|\mathbf{t}\}$ de la red *black-and-white* (traslaciones básicas y centrados, primados o sin primar), y se obtiene aplicando para cada uno la condición:

$$\tau \exp\left(2\pi i \mathbf{k}\cdot\mathbf{t}\right) = 1 \qquad (10)$$

y tomando como **k** aquél de entre todos los que cumplen esta condición cuyas componentes sean sencillas.

Los elementos de simetría que componen las posiciones generales de los MSGs (Figura 14) se indican en color negro si son elementos no primados, y en rojo si son primados. Los elementos de simetría vienen dados en 4 formatos diferentes:

- **Formato *x,y,z***: es el formato clásico utilizado para definir las posiciones generales de los grupos espaciales. Para MSGs, se añade al final ",+1" si la operación es no primada y ",-1" si es primada, y además, se añade una segunda línea que indica cómo transforma el momento magnético (m_x, m_y, m_z) bajo la acción del elemento de simetría. Esta transformación, que se incluye para mayor claridad, es redundante, pues se deriva de la transformación de las coordenadas *x*, *y*, *z*: para un elemento de simetría $\{\boldsymbol{R},\tau|\mathbf{t}\}$, la transformación sobre el momento magnético (en realidad, dividida cada una de sus componentes entre los parámetros de red) es la que se indica en la ecuación (8).

- **Formato matricial**: se indican la matriz de rotación ***R*** 3x3 y la traslación **t** asociada en una columna a la derecha.

- **Interpretación geométrica**: interpretación geométrica del elemento de simetría, siguiendo el formato que puede hallarse en las Tablas Internacionales de Cristalografía [36], pero adaptado a la simetría magnética mediante la adición de un "-1" o "+1" al final, según sea el elemento primado o no, respectivamente (Figura 10). La interpretación geométrica de un elemento de simetría cualquiera puede obtenerse utilizando el programa SYMMETRY OPERATIONS (http://www.cryst.ehu.es/cryst/matrices.html) del *Bilbao Crystallographic Server*.

- **Notación de Seitz**: los elementos de simetría se especifican mediante un símbolo de Seitz, que indica el orden y eje de la rotación o rotoinversión, y la traslación asociada [17]. Este símbolo de Seitz ha sido adaptado a la simetría magnética incluyendo una prima en el símbolo rotacional cuando el elemento es primado.

Finalmente, al final de la página de cada MSG se proporcionan dos enlaces para consultar las páginas de MWYCKPOS (§4.4) y MAGNEXT (§5.2) correspondientes al MSG seleccionado.

MGENPOS puede utilizarse también para obtener las posiciones generales de un MSG en un *setting* no convencional, haciendo clic en el botón "*Non-conventional setting*" de la interfaz principal del programa (Figura 13(a)). Esto resulta útil en el caso de que se desee trabajar en un *setting* no estándar, lo cual es práctica común de muchos investigadores, ya sea por razones prácticas o por costumbre. Seleccionar esta opción redirige a un formulario donde introducir una transformación de *setting* (***P***,**p**), cuyo determinante debe ser mayor que cero. Entonces se muestra una página muy similar a la mostrada para *setting* estándar, pero indicando las redes de traslación y *black-and-white* de la estructura transformada (Figura 16), así como un enlace que permite visualizar la transformación introducida. Se muestran dos tablas con los elementos en el *setting* estándar y en el *setting* transformado. Estos elementos son los que resultan de la transformación directa del elemento en *setting* estándar $\{\boldsymbol{R}|\mathbf{t}\}$ por medio de la transformación (***P***,**p**) de la forma:

$$\{\boldsymbol{R}|\mathbf{t}\}' = (\boldsymbol{P},\mathbf{p})^{-1}\{\boldsymbol{R}|\mathbf{t}\}(\boldsymbol{P},\mathbf{p}) \qquad (11)$$

Los elementos de simetría así obtenidos se indican directamente, es decir, ni han sido sustituidos por sus equivalentes módulo 1, ni se indica tampoco el conjunto completo de las posiciones generales en el *setting* transformado, cuya multiplicidad podría variar fruto de la inclusión de centrados adicionales como generadores, o bien de la eliminación de centrados redundantes, si el determinante de la matriz de transformación fuese, respectivamente, mayor o menor que 1. Finalmente, los enlaces a MWYCKPOS (§4.4) y MAGNEXT (§5.2) redirigen a las páginas de estos programas correspondientes al MSG seleccionado en el *setting* transformado introducido.

N	Standard/Default Setting		Transformed	
	(x,y,z) form	matrix form	(x,y,z) form	matrix form
1	x, y, z, +1 m_x,m_y,m_z	$\begin{pmatrix} 1 & 0 & 0 & 0 \\ 0 & 1 & 0 & 0 \\ 0 & 0 & 1 & 0 \end{pmatrix}$	x, y, z, +1 m_x, m_y, m_z	$\begin{pmatrix} 1 & 0 & 0 & 0 \\ 0 & 1 & 0 & 0 \\ 0 & 0 & 1 & 0 \end{pmatrix}$
2	-x, y+1/2, -z, +1 $-m_x,m_y,-m_z$	$\begin{pmatrix} -1 & 0 & 0 & 0 \\ 0 & 1 & 0 & 1/2 \\ 0 & 0 & -1 & 0 \end{pmatrix}$	-x, -y, z+1/2, +1 $-m_x, -m_y, m_z$	$\begin{pmatrix} -1 & 0 & 0 & 0 \\ 0 & -1 & 0 & 0 \\ 0 & 0 & 1 & 1/2 \end{pmatrix}$
3	-x, -y, -z, +1 m_x,m_y,m_z	$\begin{pmatrix} -1 & 0 & 0 & 0 \\ 0 & -1 & 0 & 0 \\ 0 & 0 & -1 & 0 \end{pmatrix}$	-x, -y, -z, +1 m_x, m_y, m_z	$\begin{pmatrix} -1 & 0 & 0 & 0 \\ 0 & -1 & 0 & 0 \\ 0 & 0 & -1 & 0 \end{pmatrix}$
4	x, -y+1/2, z, +1 $-m_x,m_y,-m_z$	$\begin{pmatrix} 1 & 0 & 0 & 0 \\ 0 & -1 & 0 & 1/2 \\ 0 & 0 & 1 & 0 \end{pmatrix}$	x, y, -z+1/2, +1 $-m_x, -m_y, m_z$	$\begin{pmatrix} 1 & 0 & 0 & 0 \\ 0 & 1 & 0 & 0 \\ 0 & 0 & -1 & 1/2 \end{pmatrix}$
5	x+1/2, -y+1/2, -z+1/2, -1 $-m_x,m_y,m_z$	$\begin{pmatrix} 1 & 0 & 0 & 1/2 \\ 0 & -1 & 0 & 1/2 \\ 0 & 0 & -1 & 1/2 \end{pmatrix}'$	-x+1/2, y+1/2, -z+1/2, -1 $m_x, -m_y, m_z$	$\begin{pmatrix} -1 & 0 & 0 & 1/2 \\ 0 & 1 & 0 & 1/2 \\ 0 & 0 & -1 & 1/2 \end{pmatrix}'$
6	-x+1/2, -y, z+1/2, -1 $m_x,m_y,-m_z$	$\begin{pmatrix} -1 & 0 & 0 & 1/2 \\ 0 & -1 & 0 & 0 \\ 0 & 0 & 1 & 1/2 \end{pmatrix}'$	x+1/2, -y+1/2, -z, -1 $-m_x, m_y, m_z$	$\begin{pmatrix} 1 & 0 & 0 & 1/2 \\ 0 & -1 & 0 & 1/2 \\ 0 & 0 & -1 & 0 \end{pmatrix}'$
7	-x+1/2, y+1/2, z+1/2, -1 $-m_x,m_y,m_z$	$\begin{pmatrix} -1 & 0 & 0 & 1/2 \\ 0 & 1 & 0 & 1/2 \\ 0 & 0 & 1 & 1/2 \end{pmatrix}'$	x+1/2, -y+1/2, z+1/2, -1 $m_x, -m_y, m_z$	$\begin{pmatrix} 1 & 0 & 0 & 1/2 \\ 0 & -1 & 0 & 1/2 \\ 0 & 0 & 1 & 1/2 \end{pmatrix}'$
8	x+1/2, y, -z+1/2, -1 $m_x,m_y,-m_z$	$\begin{pmatrix} 1 & 0 & 0 & 1/2 \\ 0 & 1 & 0 & 0 \\ 0 & 0 & -1 & 1/2 \end{pmatrix}'$	-x+1/2, y+1/2, z, -1 $-m_x, m_y, m_z$	$\begin{pmatrix} -1 & 0 & 0 & 1/2 \\ 0 & 1 & 0 & 1/2 \\ 0 & 0 & 1 & 0 \end{pmatrix}'$

Figura 16. Tabla de MGENPOS de las posiciones generales del MSG en *setting* no convencional *Pb'n'm* (#62.448), o lo que es lo mismo, *Pn'ma'* (#62.448) en el *setting* no estándar (**c**,**a**,**b**; 0,0,0). El grupo espacial *Pbnm* es utilizado con cierta frecuencia en la literatura científica.

4.4 Programa MWYCKPOS

El programa MWYCKPOS es una herramienta de consulta de las WPs de los MSGs, tanto en *setting* BNS como OG. La página principal, de funcionamiento idéntico a la página principal de MGENPOS (Figura 13(a)), permite seleccionar un MSG y obtener sus WPs tanto en *setting* estándar (botón "*Standard/Default Setting*") como en *setting* no estándar (botón "*Non-conventional setting*"). Se puede seleccionar un MSG bien introduciendo su etiqueta correspondiente en el *setting* BNS u OG (§4.1.1) en el

formulario indicado, bien haciendo clic en el botón "*choose it*", lo que proporciona una lista de los 230 grupos espaciales convencionales para seleccionar, para cada uno, una lista de los MSGs que de él se derivan (Figura 13(b)).

La tabla de WPs y de *site-symmetry groups* (SSG) proporcionadas por MWYCKPOS cuando se selecciona un *setting* estándar puede verse en la Figura 17, así como en la Figura 3 del Anexo A, para el MSG *Pn'ma'* (#62.448) [BNS]. En la página se indican la etiqueta y el símbolo del MSG para el *setting* (BNS/OG) seleccionado, así como esa misma información sobre el *setting* alternativo no seleccionado. En el caso de que el MSG sea de tipo IV se proporciona un enlace para seleccionar el *setting* alternativo OG o BNS.

Wyckoff Positions of the Group *Pn'ma'* (#62.448)

For this space group, BNS and OG settings coincide.
Its label in the OG setting is given as: Pn'ma' (#62.8.509)

Multiplicity	Wyckoff letter	Coordinates
8	d	(x,y,z | m_x,m_y,m_z) (x+1/2,-y+1/2,-z+1/2 | -m_x,m_y,m_z) (-x,y+1/2,-z | -m_x,m_y,-m_z) (-x+1/2,-y,z+1/2 | m_x,m_y,-m_z) (-x,-y,-z | m_x,m_y,m_z) (-x+1/2,y+1/2,z+1/2 | -m_x,m_y,m_z) (x,-y+1/2,z | -m_x,m_y,-m_z) (x+1/2,y,-z+1/2 | m_x,m_y,-m_z)
4	c	(x,1/4,z | 0,m_y,0) (x+1/2,1/4,-z+1/2 | 0,m_y,0) (-x,3/4,-z | 0,m_y,0) (-x+1/2,3/4,z+1/2 | 0,m_y,0)
4	b	(0,0,1/2 | m_x,m_y,m_z) (1/2,1/2,0 | -m_x,m_y,m_z) (0,1/2,1/2 | -m_x,m_y,-m_z) (1/2,0,0 | m_x,m_y,-m_z)
4	a	(0,0,0 | m_x,m_y,m_z) (1/2,1/2,1/2 | -m_x,m_y,m_z) (0,1/2,0 | -m_x,m_y,-m_z) (1/2,0,1/2 | m_x,m_y,-m_z)

Site Symmetries of the Wyckoff Positions

WP	Representative	Site symmetry
4a	(0,0,0 | m_x,m_y,m_z)	-1
4b	(0,0,1/2 | m_x,m_y,m_z)	-1
4c	(x,1/4,z | 0,m_y,0)	.m.
8d	(x,y,z | m_x,m_y,m_z)	1

List the original elements of the orbits
List all the elements of the orbits

Go to the list of the Symmetry Operators of the Group *Pn'ma'* (#62.448)
Go to the Systematic absences for the Group *Pn'ma'* (#62.448)

Figura 17. Posiciones de Wyckoff del MSG *Pn'ma'* (#62.448) [BNS], obtenidas de MWYCKPOS.

La tabla de WPs incluye, si los hay, una línea superior que recoge los centrados y centrados primados que habrán de utilizarse para obtener el resto de posiciones de la

WP, pues en la tabla, por sencillez, no se incluyen aquellas posiciones derivadas de otras a través de centrados y centrados primados. Para cada WP, la tabla muestra la multiplicidad, que es diferente en general para los *settings* BNS y OG (§4.1.1), una letra identificadora de la WP y las posiciones de la WP, que incluyen la forma restringida por simetría del momento magnético (§4.2.2). La tabla de SSGs incluye, para cada WP, un símbolo identificativo del SSG y el representante de la WP al que corresponde. El símbolo es un enlace que redirige a una página (ver Figura 18) que muestra los elementos de simetría que componen el SSG, en los mismos 4 formatos usados para la tabla de las posiciones generales de MGENPOS (§4.3).

Site Symmetry Group .m. of the Wyckoff Position 4c

Magnetic Space Group: *Pn'ma'* (#62.448) [OG: *Pn'ma'* (#62.8.509)]

Representative: (x,1/4,z | 0,m_y,0)

Symmetry operations:

x, y, z, +1 m_x, m_y, m_z	(1|0,0,0)	$\begin{pmatrix} 1 & 0 & 0 & 0 \\ 0 & 1 & 0 & 0 \\ 0 & 0 & 1 & 0 \end{pmatrix}$	1
x, -y+1/2, z, +1 -m_x, m_y, -m_z	(m_y|0,1/2,0)	$\begin{pmatrix} 1 & 0 & 0 & 0 \\ 0 & -1 & 0 & 1/2 \\ 0 & 0 & 1 & 0 \end{pmatrix}$	m x,1/4,z

Figura 18. Elementos del s*ite-symmetry group .m.* correspondiente al representante (x,1/4,z|0,m_y,0) de la posición de Wyckoff 4c del MSG *Pn'ma'* (#62.448).

Los símbolos de los SSGs utilizados en MWYCKPOS han sido deducidos a partir de los elementos de simetría que lo componen, siguiendo los criterios adecuados para que coincidan con los SSGs del listado de MSGs de Litvin [7]. Estos símbolos son además similares a los símbolos de los SSGs de los grupos espaciales convencionales que se pueden encontrar en las Tablas Internacionales de Cristalografía [36] (Figura 10).

MWYCKPOS incluye el SSG correspondiente a todas las posiciones mostradas para cada WP. Cada posición de la tabla es un enlace que permite seleccionarla como el representante de la WP. Al hacerlo, se recargará la página, y dicha posición aparecerá en la tabla de SSGs como el representante de la WP; de esta forma el SSG correspondiente puede ser consultado. Los enlaces "*List the original elements of the orbits*" y "*List all the elements of the orbits*" bajo la tabla de SSGs permiten, respectivamente, deshacer las selecciones de representantes hechas hasta el momento (que el programa memoriza y acumula), e incluir en la lista de SSGs todas las posiciones de todas las WPs. Finalmente, se incluyen también enlaces a las páginas del MSG seleccionado en MGENPOS (§4.3) y MAGNEXT (§5.2).

Al igual que MGENPOS, y de la misma forma y por las mismas razones (§4.3), MWYCKPOS permite obtener las WPs de un MSG en un *setting* no convencional, haciendo clic en el botón "*Non-conventional setting*" de la interfaz principal del programa (Figura 13(a)). En este modo, MWYCKPOS muestra dos tablas con las WPs de

la estructura en el *setting* estándar y el *setting* transformado (Figura 19), así como una tabla de SSGs en la que figuran los SSGs de las WPs en el *setting* transformado.

Old Multiplicity	New Multiplicity	Wyckoff letter	Coordinates	
			Standard/Default Setting	Transformed
8	8	d	(x,y,z | m_x,m_y,m_z) (x+1/2,-y+1/2,-z+1/2 | -m_x,m_y,m_z) (-x,y+1/2,-z | -m_x,m_y,-m_z) (-x+1/2,-y,z+1/2 | m_x,m_y,-m_z) (-x,-y,-z | m_x,m_y,m_z) (-x+1/2,y+1/2,z+1/2 | -m_x,m_y,m_z) (x,-y+1/2,z | -m_x,m_y,-m_z) (x+1/2,y,-z+1/2 | m_x,m_y,-m_z)	(z,x,y | m_z,m_x,m_y) (-z+1/2,x+1/2,-y+1/2 | m_z,-m_x,m_y) (-z,-x,y+1/2 | -m_z,-m_x,m_y) (z+1/2,-x+1/2,-y | -m_z,m_x,m_y) (-z,-x,-y | m_z,m_x,m_y) (z+1/2,-x+1/2,y+1/2 | m_z,-m_x,m_y) (z,x,-y+1/2 | -m_z,-m_x,m_y) (-z+1/2,x+1/2,y | -m_z,m_x,m_y)
4	4	c	(x,1/4,z | 0,m_y,0) (x+1/2,1/4,-z+1/2 | 0,m_y,0) (-x,3/4,-z | 0,m_y,0) (-x+1/2,3/4,z+1/2 | 0,m_y,0)	(z,x,1/4 | 0,0,m_y) (-z+1/2,x+1/2,1/4 | 0,0,m_y) (-z,-x,3/4 | 0,0,m_y) (z+1/2,-x+1/2,3/4 | 0,0,m_y)
4	4	b	(0,0,1/2 | m_x,m_y,m_z) (1/2,1/2,0 | -m_x,m_y,m_z) (0,1/2,1/2 | -m_x,m_y,-m_z) (1/2,0,0 | m_x,m_y,-m_z)	(1/2,0,0 | m_z,m_x,m_y) (0,1/2,1/2 | m_z,-m_x,m_y) (1/2,0,1/2 | -m_z,-m_x,m_y) (0,1/2,0 | -m_z,m_x,m_y)
4	4	a	(0,0,0 | m_x,m_y,m_z) (1/2,1/2,1/2 | -m_x,m_y,m_z) (0,1/2,0 | -m_x,m_y,-m_z) (1/2,0,1/2 | m_x,m_y,-m_z)	(0,0,0 | m_z,m_x,m_y) (1/2,1/2,1/2 | m_z,-m_x,m_y) (0,0,1/2 | -m_z,-m_x,m_y) (1/2,1/2,0 | -m_z,m_x,m_y)

Figura 19. Tabla de MWYCKPOS de las posiciones de Wyckoff del MSG en *setting* no convencional *Pb'n'm* (#62.448), o lo que es lo mismo, *Pn'ma'* (#62.448) en el *setting* no estándar (**c**,**a**,**b**; 0,0,0).

Para un átomo ubicado en una WP de un MSG, MWCYKPOS permite conocer tanto la restricción por la simetría del MSG de su momento magnético asociado como el ordenamiento de espines correspondiente y, por tanto la correlación de signos de las componentes de los momentos dentro de la celda unidad, ya que la aplicación de las operaciones de simetría permite deducir los momentos magnéticos del resto de átomos equivalentes por simetría del cristal. Por ello, tal y como se indicó en §4.2.2, el conocimiento de las posiciones de Wyckoff de un MSG resulta útil para facilitar la asignación de un MSG a una estructura magnética a determinar, pues permite descartar aquellos MSGs cuyas WPs ocupadas por átomos magnéticos impongan condiciones inconvenientes o incompatibles con la existencia de la estructura magnética considerada. Por ejemplo, un MSG puede estar prohibido porque en la WP ocupada por el átomo magnético la simetría fuerza al momento magnético a ser cero; también, puede que el ordenamiento magnético asociado a la WP sea incompatible con lo observado porque, por ejemplo, la estructura analizada tenga propiedades ferromagnéticas y el ordenamiento de spines asociado a la WP sea antiferromagnético, o bien el ordenamiento de espines resultante tenga características poco habituales o improbables, como ordenamientos magnéticos incompletos, no colineales, etc., que quizá puedan considerarse descartables.

Igualmente, el conocimiento de las WPs resulta útil para deducir el ordenamiento de espines de estructuras magnéticas, pues una vez limitado el conjunto de posibles MSGs a unos pocos o sólo uno, el conocimiento de la WP ocupada por los átomos magnéticos puede reducir considerablemente el número de grados de libertad a considerar en el proceso de refinamiento de la estructura magnética, y quizá esclarecer las características generales de dicho ordenamiento en lo que respecta a completitud del ordenamiento magnético, colinearidad, carácter ferromagnético o antiferromagnético, *canting*, etc.

Algunos ejemplos del uso de las WPs en el proceso de determinación de estructuras magnéticas pueden encontrarse en el Anexo A. Particularmente ilustrativo resultan los

ejemplos 1 y 2 de las secciones §A.4.1.1 y §A.4.1.2 respectivamente, así como todos los ejemplos subsiguientes del Anexo A a excepción del ejemplo 3. El uso de las WPs es también habitual en varios de los numerosos ejemplos que se pueden encontrar en el Anexo C.

El conocimiento de las WPs de los MSGs tiene, en general, otras posibles aplicaciones, tanto reales como potenciales. Un buen ejemplo de aplicación práctica es la publicación recogida en el Anexo B de la presente memoria. Ésta consistió en un análisis y corrección de los resultados presentados en el artículo "*Canonical magnetic insulators with isotropic magnetoelectric coupling*" de Coh *et al*. [16], que presenta una recopilación de 20 estructuras magnéticas tipo que son susceptibles de presentar magnetoelectricidad isótropa. Dicha recopilación fue efectuada utilizando única y exclusivamente consideraciones de teoría de representaciones, sin tener en cuenta la simetría magnética. El trabajo aquí realizado lleva a cabo la misma recopilación, pero haciendo uso de argumentos de simetría basados en los posibles MSGs. La recopilación se realiza partiendo de aquellos MSGs cúbicos cuyo tensor magnetoeléctrico, que será isótropo, sea no nulo, recopilando a su vez aquellas WPs de estos grupos que resulten distinguibles (es decir, se obvian aquellas que pertenezcan a órbitas no características o que pertenezcan al mismo *set* de Wyckoff que otra WP ya recopilada). De esta forma se corrigieron los resultados del artículo comentado, dado que aparte de los 30 tipos de estructura que Coh *et al*. proponían, se pudo demostrar la existencia de 14 estructuras tipo adicionales.

5. AUSENCIAS SISTEMÁTICAS EN DIFRACCIÓN MAGNÉTICA DE NEUTRONES NO POLARIZADOS: PROGRAMA MAGNEXT

***NOTA**: Puede encontrarse información adicional a la expuesta en este capítulo en las publicaciones incluidas en los anexos A y C.*

5.1 Ausencias sistemáticas en difracción magnética de neutrones no polarizados

5.1.1 *Difracción magnética de neutrones no polarizados*

La técnica experimental habitual para determinar estructuras magnéticas es la difracción de neutrones no polarizados. La elección de neutrones se debe a que sus propiedades físicas (carga nula y espín no nulo) hacen que en el patrón de difracción, la intensidad proveniente de la interacción de los neutrones con los momentos magnéticos de la estructura magnética sea lo suficientemente grande en comparación con la intensidad proveniente de la interacción de los neutrones con los núcleos atómicos como para que la contribución magnética al patrón de difracción pueda ser observada con suficiente precisión. Además, la simetría de la estructura magnética y su relación con la simetría de la fase padre quedan reflejadas en el patrón de difracción.

Las intensidades que se observan en un patrón de difracción de neutrones no polarizados son el resultado de la superposición incoherente de las intensidades difractadas debidas a la estructura nuclear, por un lado (difracción no magnética o nuclear), y al ordenamiento de espines, por otro lado (difracción magnética). Para determinar la estructura magnética, es necesario cotejar este patrón de difracción experimental con el patrón de difracción teórico asociado a los diferentes modelos posibles a priori de la estructura magnética. Esto puede hacerse o bien deduciendo el patrón de difracción completo resultante de dichos modelos y cotejándolos con el obtenido experimentalmente, o bien obteniendo el patrón difracción magnética a partir del patrón de difracción completo obtenido experimentalmente. En este segundo caso, para obtener el patrón de difracción magnética se parte de los patrones de difracción correspondientes a las fases de baja y alta simetría, medidos por debajo y por encima de la temperatura de transición T_c o T_N (temperatura de Curie para estructuras ferromagnéticas, o de Neel para estructuras antiferromagnéticas) respectivamente, y se realiza una comparación entre ambos, sustrayendo la contribución nuclear (única presente en la fase paramagnética) al patrón de difracción de la fase de baja simetría (Figura 20).

Todos los vectores **H** de difracción del patrón de difracción magnética pueden describirse como:

$$\mathbf{H} = \mathbf{H_D} + m_1\mathbf{k_1} + \ldots + m_d\mathbf{k_d} \qquad (12)$$

donde $\mathbf{H_D}$ es un vector de la red recíproca del grupo padre, los coeficientes m_i son enteros y d un número finito. Los vectores $\mathbf{k_i}$, que en general no pertenecen a la red recíproca del grupo padre, son los vectores de propagación; en la gran mayoría de casos, el ordenamiento magnético se ajusta a un solo vector de propagación **k** (estructura 1k).

La comparación del patrón de difracción magnética con el patrón de difracción de la fase paramagnética permite distinguir dos tipos de patrones de difracción magnética. Por un lado, existen patrones de difracción en los cuales los vectores de difracción de las reflexiones pertenecen a la red recíproca del grupo padre (la coincidencia no es total, pues las ausencias sistemáticas son en general diferentes para ambas fases, como se explicará más adelante), es decir, ambos patrones de difracción están superpuestos: el vector de propagación **k** es 0. En estos casos, no hay pérdida de simetría traslacional asociada a la transición de fase, por lo que el MSG debe ser de tipo I o III.

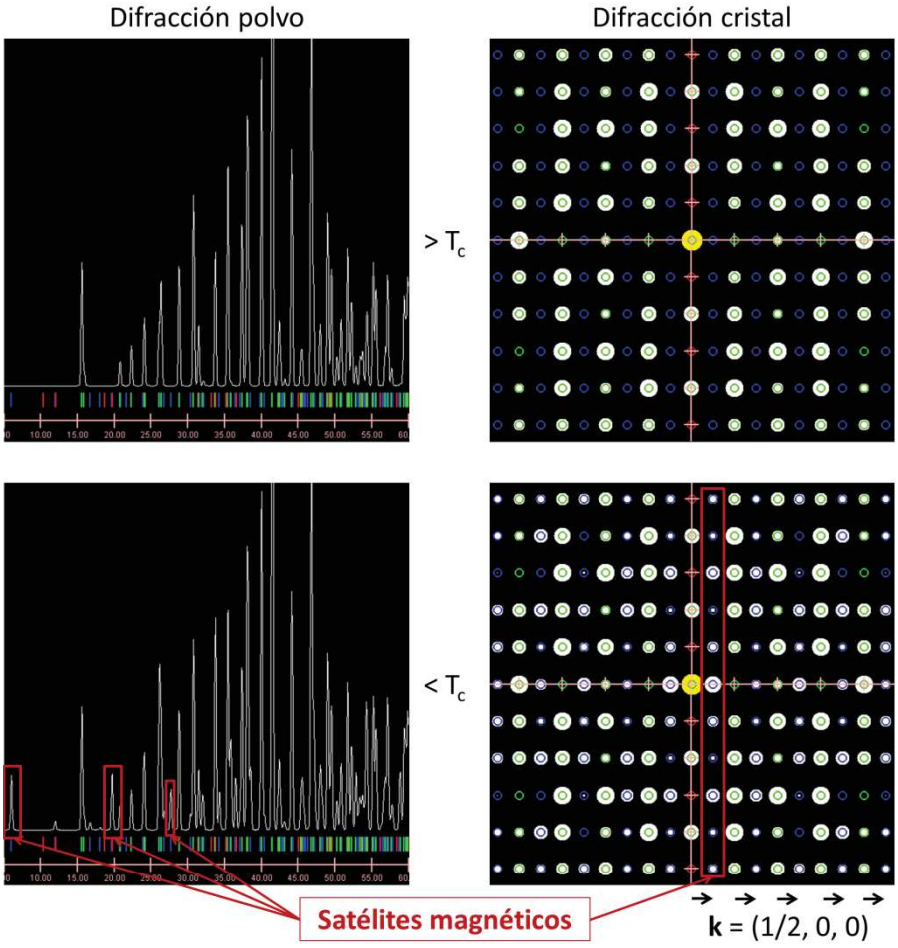

Figura 20. Obtención del patrón de difracción magnética en un experimento de difracción de neutrones no polarizados. Se observa la aparición de satélites magnéticos (h k l) para valores semienteros de h, de lo que se deduce que el vector de propagación es (1/2, 0, 0). Imágenes obtenidas con ISODISTORT [37].

Por otro lado, existen patrones de difracción en los cuales los vectores de difracción de ciertas reflexiones no pertenecen a la red recíproca del grupo padre, de forma que si se indexaran utilizando esta red recíproca como referencia, corresponderían o bien a índices de Miller fraccionarios o bien a vectores de difracción con índices enteros pero ausentes debido a centrados, que no son estrictamente vectores de red recíproca. Es decir, aparecen en el patrón de difracción los llamados "satélites magnéticos" (Figura 20), lo cual es un reflejo de la ruptura de la simetría traslacional en la transición de fase y de la posible conservación de algunas traslaciones perdidas como traslaciones primadas. En estos casos, **k** es distinto de 0, y además, para estructuras magnéticas conmensurables, se cumple que *n***k** es un vector de la red recíproca del grupo padre. Entonces, si *n* es un número par, ello implica que algunas de las traslaciones perdidas se conservan primadas; en estos casos, la estructura es antiferromagnética y su MSG es de tipo IV. Si en cambio n es un número impar, ninguna traslación perdida se conserva primada, y el MSG es de tipo I o III.

El vector de propagación **k** puede obtenerse a simple vista comparando los patrones de difracción por encima y por debajo de la temperatura de transición, por lo que es un dato habitualmente conocido. Además, el conocimiento de el o los vectores **k** permite especificar qué traslaciones han desaparecido o se conservan primadas en el MSG de la estructura magnética (ecuación (4), §4.1.1). Por último, si se puede considerar que el vector de propagación tiene componentes o bien irracionales o bien fraccionarias con un denominador grande a lo largo de algún eje, entonces se puede considerar que ninguna traslación a lo largo de ese eje se conserva, por lo que la estructura magnética será inconmensurable.

5.1.2 *Ausencias sistemáticas en el patrón de difracción de neutrones no polarizados*

En el patrón de difracción magnética correspondiente a una estructura magnética algunas reflexiones correspondientes a algunos vectores de difracción estarán ausentes como consecuencia de la invariancia de la estructura magnética bajo las operaciones de simetría de su MSG. Estas ausencias aparecen en ciertos subconjuntos de la red recíproca, es decir, están asociados a vectores de difracción de cierto tipo, y aparecen siguiendo patrones sistemáticos que se ajustan a una regla que se puede expresar paramétricamente como una relación entre los índices de Miller y un número entero *n* cualquiera. Por ejemplo, el patrón de difracción de la Figura 20, convenientemente indexado utilizando la base de la red recíproca del MSG (**a***/2, **b***, **c***) en lugar de la del grupo padre (**a***, **b***, **c***), presenta las siguientes reglas de ausencia sistemática:

$$\begin{aligned} &(hkl) && h = 2n \\ &(h00) && h = 2n+1 \\ &(0k0) && k = 2n+1 \end{aligned} \qquad (13)$$

Esto es, los vectores de difracción de tipo general (*hkl*) están ausentes si *h* es par; además, los de tipo (0*k*0) están ausentes si *k* es impar, y los de tipo (*h*00) están

ausentes también si *h* es impar, lo que unido a la regla de ausencia para vectores de tipo general implica que están ausentes para todo valor de *h*. Estas dos últimas reglas de (13) son también observables en el patrón de difracción de la fase paramagnética.

Las ausencias sistemáticas observadas en el patrón de difracción magnética están asociadas únicamente al MSG de la estructura magnética y pueden calcularse a partir de los elementos de simetría del MSG (§A.3). En general, la observación de estas ausencias sistemáticas no permite identificar unívocamente el MSG de una estructura, por lo que carecen del alto poder resolutivo de las ausencias sistemáticas asociadas a los grupos espaciales. No obstante, durante el proceso de determinación de una estructura, el conocimiento de las ausencias sistemáticas presentes en el patrón de difracción magnética de la estructura y su comparación con las ausencias sistemáticas asociadas a los MSGs puede permitir descartar algunos MSGs, lo que muy probablemente reducirá considerablemente el número de ordenamientos de espín posibles. De esta forma, las ausencias sistemáticas en patrones de difracción magnética de neutrones no polarizados resultan útiles a la hora de determinar estructuras magnéticas, pudiendo resultar claves en combinación con otras consideraciones.

Un buen ejemplo de la utilidad de las reglas de ausencia sistemática en la determinación de estructuras magnéticas se encuentra en la Tabla 9 del Anexo E, que consiste en una lista de parejas de estructuras diferentes recogidas en MAGNDATA (§9), y que han sido propuestas para la misma fase del mismo compuesto. Al menos una de las dos estructuras propuestas debe ser por tanto errónea. Según se muestra en la tabla, las ausencias sistemáticas de algunas de estas estructuras contradictorias son diferentes, por lo que su observación permitiría discernir cuál de las estructuras conflictivas es correcta y cuál es errónea.

Pese a que las ausencias sistemáticas son de uso habitual en la determinación de estructuras convencionales, las ausencias sistemáticas en patrones de difracción magnética de neutrones no polarizados han sido muy poco utilizadas en la determinación de estructuras magnéticas, debido, por un lado, a la escasez de datos relativos a las ausencias sistemáticas asociadas a los MSGs, y por otro, a la costumbre muy habitual de ignorar la simetría magnética en el estudio de estructuras magnéticas en favor del análisis de representaciones. Esta costumbre se basa en la creencia errónea de que la identificación de la *irrep* que interviene en la transición de fase equivale a la identificación del MSG del cristal, y de que el conocimiento explícito de este MSG no aporta información útil adicional.

5.2 Programa MAGNEXT

El propósito principal del programa MAGNEXT (http://www.cryst.ehu.es/cryst/magnext.html) es calcular para cualquier MSG las ausencias sistemáticas para la difracción de neutrones no polarizados, que se mencionan en la sección anterior.

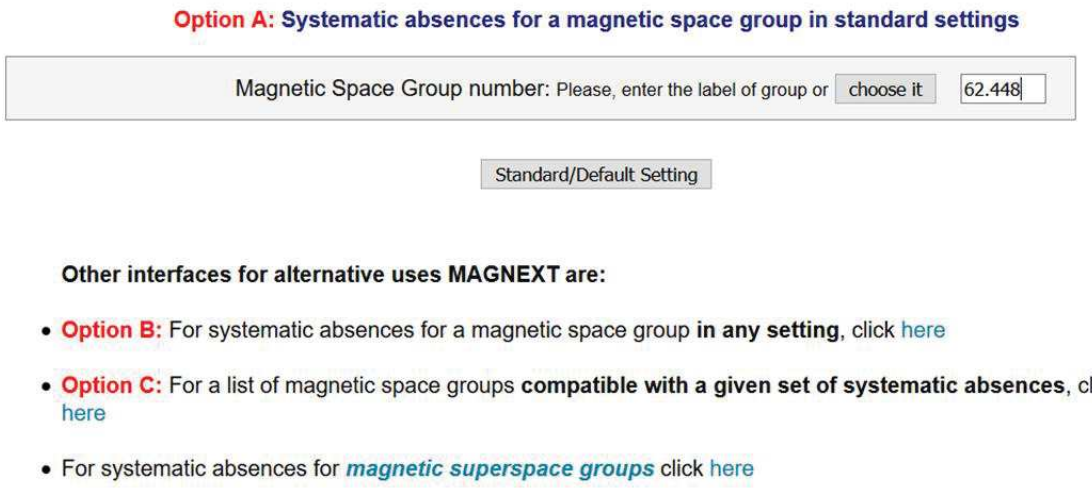

Figura 21. Página principal del programa MAGNEXT.

El Anexo A está dedicado principalmente a presentar los resultados obtenidos y describir el programa MAGNEXT. El capítulo §A.3.1 contiene un desarrollo teórico que describe las ecuaciones generales que permiten calcular las reglas de ausencia sistemática. El capítulo §A.3.2 contiene una explicación detallada del método utilizado para calcularlas utilizando proyectores [38]. Este método permite obtener las reglas de ausencia sistemática de forma más sencilla y elegante, obteniéndose además la forma restringida del factor de estructura magnético para los distintos tipos de vectores de difracción. En el capítulo §A.3.3 se incluyen algunas reglas de ausencia sistemática de validez general y se realiza una comparación general entre los patrones de difracción de neutrones magnética y no magnética según el tipo de MSG. En el capítulo §A.4 se incluyen numerosos ejemplos que describen cómo utilizar MAGNEXT y sus diversas opciones para facilitar la determinación de estructuras magnéticas. El ejemplo 1 del apartado §A.4.1.1 es un ejemplo de cálculo de las reglas de ausencia sistemática utilizando el método de proyectores descrito en el apartado §A.3.2.

Las reglas de ausencia sistemática de los MSGs son similares a las reglas de ausencia sistemática de los grupos espaciales convencionales para difracción de rayos X [36] que pueden encontrarse en el programa HKLCOND [2] del *Bilbao Crystallographic Server*, aunque presentan algunas diferencias sustanciales. En ambos casos, las reglas de ausencia sistemática se obtienen aplicando las operaciones de simetría del grupo al factor de estructura, del que depende la intensidad de los picos de difracción. No obstante, según lo expuesto en el capítulo §A.3, en el caso de la difracción magnética de neutrones no polarizados el factor de estructura magnético, que es la transformada de Fourier de la densidad de momento magnético dentro de la celda unidad (A.4), es un vector axial de componentes complejas (A.2). Además, la relación entre la intensidad de los picos de difracción y el factor de estructura magnético (A.1) es tal que un pico de difracción no sólo está ausente cuando el factor de estructura es nulo, sino también cuando es paralelo al vector de difracción.

Esto significa que, además de causar ausencias, la simetría descrita por el MSG puede restringir los valores de las componentes del factor de estructura, reduciendo sus parámetros libres. Asimismo, no es necesario que el valor del factor de estructura sea

nulo para que lo sea la intensidad. Como consecuencia, mientras que para difracción no magnética las ausencias sistemáticas se producen únicamente a causa de la presencia en el grupo de ejes helicoidales y planos de deslizamiento (exceptuando las reglas generales debidas a centrados), para difracción magnética de neutrones no polarizados no hay una regla general de este tipo: las ausencias pueden provenir de diversos elementos de simetría. Las Tablas 6 y 7 del Anexo A contienen una recopilación de todas las reglas de ausencia sistemática de todos los MSGs en *setting* estándar para cada tipo de vector de difracción, para los *settings* BNS y OG (sólo MSGs de tipo IV) respectivamente.

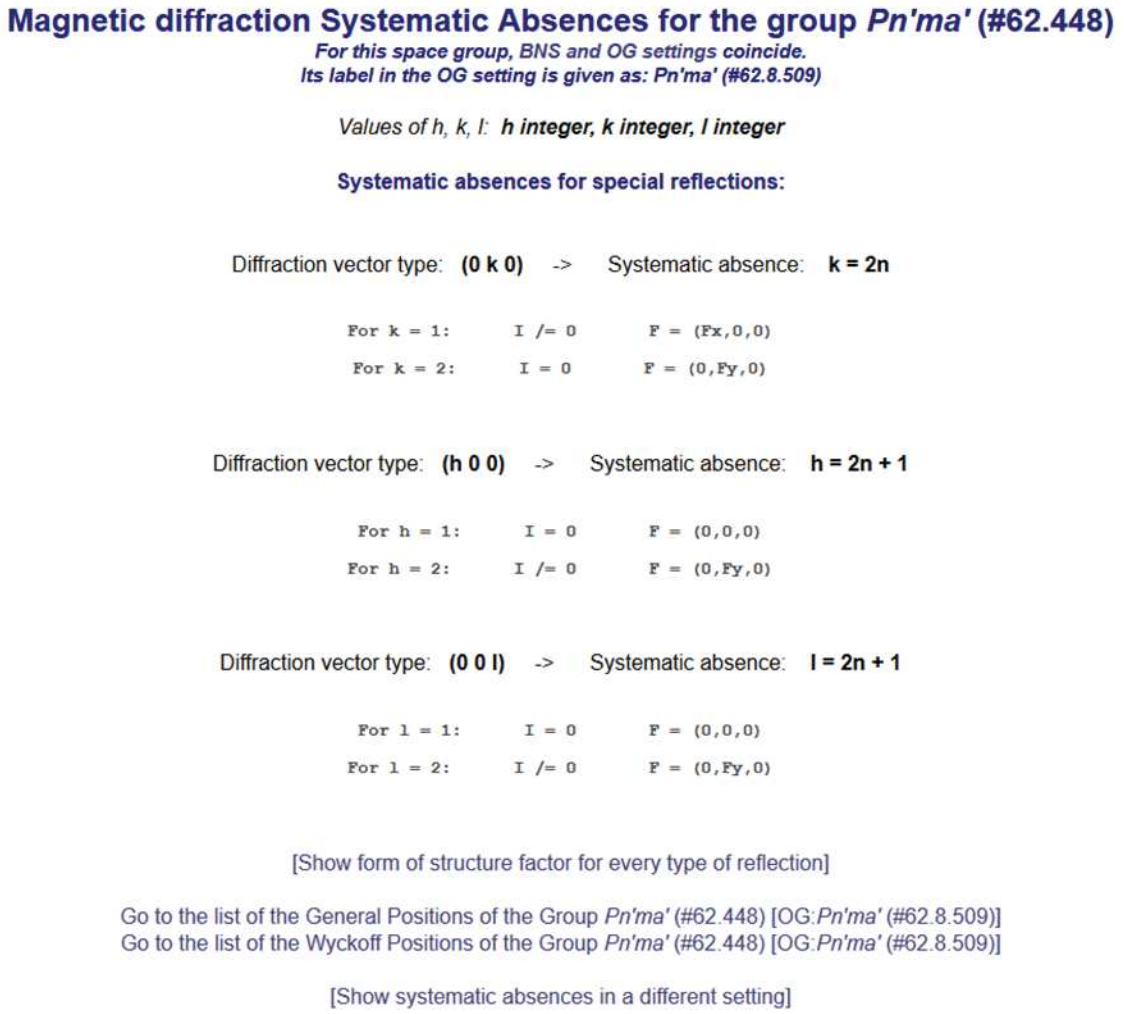

Figura 22. Página de MAGNEXT con las reglas de ausencia sistemática del grupo *Pn'ma'* (#62.448) [BNS].

La página principal del programa MAGNEXT (Figura 21) permite seleccionar una de las cuatro opciones de trabajo del programa. La opción A, que se describe en detalle en el capítulo §A.4.1, consiste en una recopilación de las reglas de ausencia sistemática asociadas a cada MSG en *setting* estándar, tanto BNS como OG. Una vez seleccionado un grupo, de forma idéntica a como se hace en MGENPOS y MWYCKPOS, se accede a la página que muestra las reglas de ausencia sistemática para el MSG seleccionado (Figura 22). Al principio de la página se indican los valores posibles de los índices de Miller *h*, *k* y *l* que definen la indexación correspondiente al MSG seleccionado. Para

MSGs tipo IV en *setting* OG, se incluye también el vector de onda OG asociado al MSG (§4.1).

Magnetic Space Group: *Pn'ma'* (#62.448) [OG: *Pn'ma'* (#62.8.509)]

Values of h, k, l: ***h integer, k integer, l integer***

Structure factors for general reflections (produced by centrings):

Diffraction vector type: **h,k,l**

For any h,k,l: I /= 0 F = (Fx,Fy,Fz)

Structure factors for special reflections:

Those diffraction vector types which are fully absent due to the general rule are not listed

Diffraction vector type: **0,k,0**

For k = 1: I /= 0 F = (Fx,0,0)

For k = 2: I = 0 F = (0,Fy,0)

Diffraction vector type: **h,0,l**

For h = 1, l = 1: I /= 0 F = (0,Fy,0)

For h = 1, l = 2: I /= 0 F = (0,Fy,0)

For h = 2, l = 1: I /= 0 F = (0,Fy,0)

For h = 2, l = 2: I /= 0 F = (0,Fy,0)

Diffraction vector type: **h,0,0**

For h = 1: I = 0 F = (0,0,0)

For h = 2: I /= 0 F = (0,Fy,0)

Diffraction vector type: **0,0,l**

For l = 1: I = 0 F = (0,0,0)

For l = 2: I /= 0 F = (0,Fy,0)

Diffraction vector type: **0,k,l**

For k = 1, l = 1: I /= 0 F = (0,Fy,Fz)

For k = 1, l = 2: I /= 0 F = (Fx,0,0)

For k = 2, l = 1: I /= 0 F = (Fx,0,0)

For k = 2, l = 2: I /= 0 F = (0,Fy,Fz)

Diffraction vector type: **h,k,0**

For h = 1, k = 1: I /= 0 F = (0,0,Fz)

For h = 1, k = 2: I /= 0 F = (0,0,Fz)

For h = 2, k = 1: I /= 0 F = (Fx,Fy,0)

For h = 2, k = 2: I /= 0 F = (Fx,Fy,0)

Figura 23. Página de MAGNEXT con las formas adaptadas a la simetría del factor de estructura magnético del grupo *Pn'ma'* (#62.448) (BNS) para los diversos tipos de vector de difracción.

El programa proporciona la lista de las reglas de ausencia sistemática para los distintos tipos de vector de difracción. La regla general debida a centrados y centrados

primados y el resto de reglas o "reflexiones especiales" se indican por separado. Para las reflexiones especiales, además de la regla sistemática, se proporcionan los valores del factor de estructura magnético y de la intensidad (nula o no nula) para un conjunto mínimo de valores relevantes de *h*, *k* y/o *l*. Debe notarse aquí que, para evitar redundancias, aquellas reglas de ausencia y valores relevantes de *h*, *k* y *l* que se deban por entero a la regla de ausencia general debida a centrados y centrados primados no son indicadas explícitamente; tampoco se indican aquellas reglas de ausencia que son casos particulares de reglas de ausencia para tipos de vector de difracción de dimensionalidad mayor. Por ejemplo, una regla de ausencia $l = 2n$ en (0 0 *l*) no se indicará expresamente si existen, por ejemplo, una regla de ausencia general $h + k + l = 2n$ o una regla de ausencia $k + l = 2n$ en (0 *k l*), de las cuales la primera regla no es sino un caso particular.

La forma adaptada a la simetría del factor de estructura magnético es una información relevante incluso para aquellos tipos de vector de difracción para los cuales no hay ausencias sistemáticas, pues en combinación con otras características de las estructuras magnéticas, tales como direcciones preferenciales conocidas de los momentos magnéticos, restricciones de los momentos debidas a la posición de Wyckoff ocupada por los átomos magnéticos, etc., las restricciones en el factor de estructura pueden ser causa de ausencias adicionales (de cumplimiento aproximado) a las debidas a la simetría magnética. Por ello, en la página de resultados de la Opción A (Figura 22) se incluye un enlace que permite obtener una lista de la forma adaptada a la simetría del factor de estructura magnético para todos los tipos de vector de difracción, incluidos aquellos sin ausencias o con ausencias redundantes y que por tanto son obviados en el listado de ausencias sistemáticas (Figura 23). Los ejemplos 1 y 2 del Anexo A son ejemplos del uso de la Opción A del programa MAGNEXT, así como de ausencias adicionales debidas a restricciones en el factor de estructura magnético junto con la existencia de una dirección preferencial de los momentos magnéticos y la posición especial de Wyckoff ocupada por los átomos magnéticos.

Por último, la página de resultados de la Opción A (Figura 22) de MAGNEXT incluye enlaces para consultar las posiciones generales y de Wyckoff del MSG seleccionado, así como un formulario que permite hallar las reglas de ausencia sistemática del MSG seleccionado en un *setting* alternativo (Figura 24); para ello, debe especificarse un cambio de base en el espacio recíproco.

La Opción B de MAGNEXT (Figura 24) está descrita en detalle en el capítulo §A.4.2. Esta opción permite obtener las reglas de ausencia sistemática de un MSG cualquiera, especificado por medio de un conjunto de generadores del mismo, expresados en formato *x*,*y*,*z* (§4.3). Dicho grupo puede estar expresado en un *setting* arbitrario, y además podrá ser de tipo *BNS-like* (todas las traslaciones básicas sin primar) u *OG-like* (algunas traslaciones básicas primadas). La interfaz de la Opción B de MAGNEXT permite seleccionar el tipo de *setting* y, en caso de elegirse *OG-like*, seleccionar qué traslaciones básicas están primadas (Figura 25).

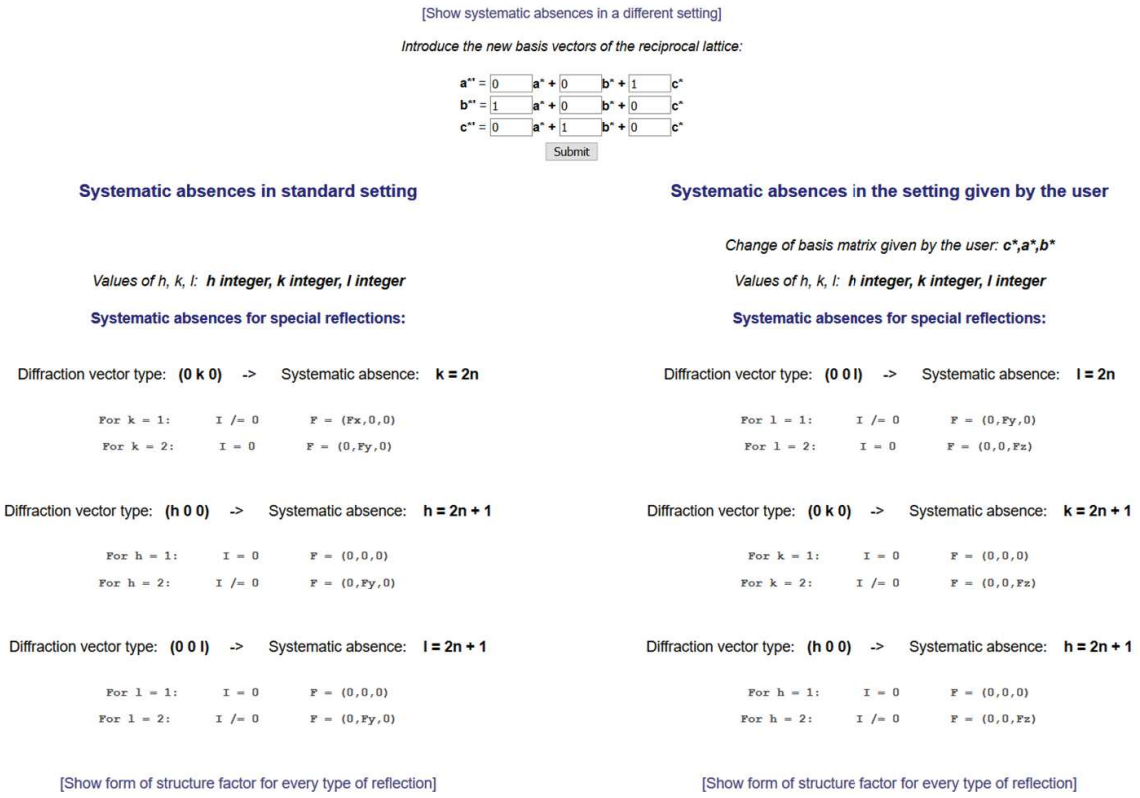

Figura 24. Interfaz de cambio de base y página de MAGNEXT con las reglas de ausencia sistemática del MSG en *setting* no convencional *Pb′n′m* (#62.448), o lo que es lo mismo, *Pn′ma′* (#62.448) en el *setting* no estándar (**c**,**a**,**b**; 0,0,0).

El resultado de la Opción B de MAGNEXT es muy similar al obtenido para la Opción A (Figura 22), e incluye también un enlace para obtener las formas adaptadas a la simetría del factor de estructura. Se indican además, al principio de la página, el conjunto de elementos de simetría introducidos y el conjunto total de elementos de simetría dentro de la celda unidad que se generan a partir de ellos.

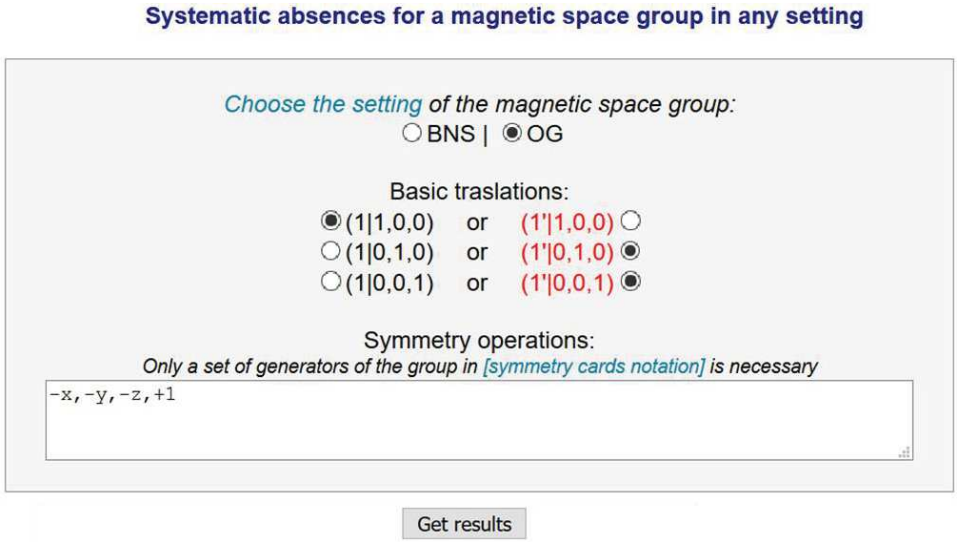

Figura 25. Interfaz de la Opción B de MAGNEXT. Los elementos de simetría introducidos son los generadores indicados en el Ejemplo 4 del Anexo A.

Como ilustran los ejemplos 3, 4 y 5 del Anexo A, la Opción B de MAGNEXT puede utilizarse para hallar las reglas debidas a uno o varios elementos de simetría conocidos (ejemplo 3), para obtener las reglas de ausencia sistemática en un *setting* no estándar (ejemplo 4), o para hallar las reglas de ausencia sistemática para átomos en posiciones especiales cuya simetría sea mayor que la de grupo del cristal, añadiendo estas operaciones de simetría como generadores adicionales (ejemplo 5).

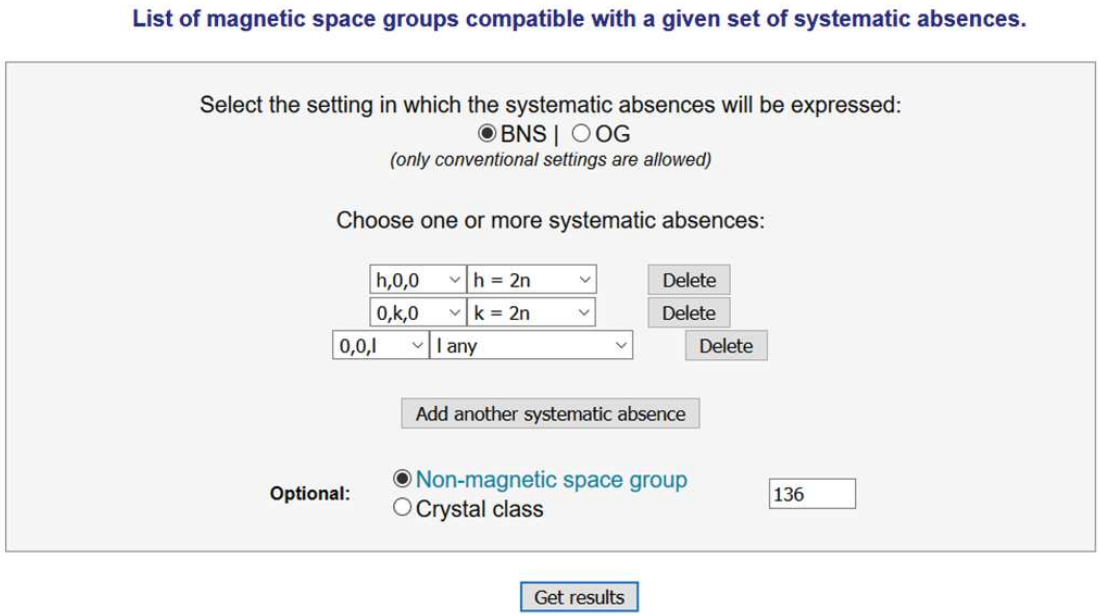

Figura 26. Interfaz y página de resultados de la Opción C de MAGNEXT, para el ejemplo 7 del Anexo A.

La Opción C de MAGNEXT (Figura 26) está descrita en detalle en el apartado §A.4.2. Esta opción consiste en un sencillo buscador que recopila todas las reglas de ausencia sistemática posibles para todos los tipos de vector de difracción posibles para todos los MSGs en *setting* BNS y OG (sólo MSGs de tipo IV) (ver Tablas 6 y 7 del Anexo A) y permite seleccionar una o más de estas reglas de ausencia sistemática para realizar

una búsqueda, cuyo resultado será una lista de todos los MSGs cuyas reglas de ausencia sistemática coincidan con las seleccionadas, para los tipos de vector de difracción seleccionados. Además, se puede especificar un grupo espacial indicando su etiqueta, o bien seleccionar un grupo puntual, para restringir la búsqueda. La lista resultante incluye el símbolo y etiqueta de los MSGs obtenidos, así como enlaces para consultar las posiciones generales, WPs y reglas de ausencia sistemática de dichos MSGs (Figura 26).

El propósito de esta opción de MAGNEXT es permitir realizar una búsqueda sencilla de qué grupos tienen asociadas unas reglas de ausencia sistemática coincidentes con las observadas; obviamente, esto sólo tiene utilidad si la indexación está realizada en un *setting* estándar. Los ejemplos 6 y 7 del Anexo A muestran la utilidad de esta opción de MAGNEXT. El ejemplo 6 muestra cómo se puede utilizar esta opción, junto con otras consideraciones de simetría, para determinar que las reglas de ausencia sistemáticas observadas para la estructura magnética conocida del $LaMnO_3$ del Ejemplo 1 del Anexo A sólo son compatibles con el MSG *Pn'ma'* (#62.448), es decir, el que realmente tiene la estructura. El ejemplo 7 (Figura 26) es un ejemplo hipotético en el que se parte del conjunto de reglas de ausencia sistemática observados y una posición de Wyckoff para el átomo magnético de una estructura magnética hipotética. Usando la Opción C de MAGNEXT, 4 MSGs posibles son obtenidos, de los cuales 2 son hallados incompatibles y descartados por tener asociadas ausencias sistemáticas incompatibles con las observadas. Para los dos restantes se calculan las ausencias sistemáticas adicionales de cumplimiento aproximado, distintas en ambos casos, causadas por la acción conjunta de las restricciones al momento magnético asociadas a la posición de Wyckoff del átomo magnético y las restricciones al factor de estructura que la Opción A de MAGNEXT provee para ambos grupos. De esta forma, la determinación del ordenamiento de espines se reduciría a determinar cuáles de estas ausencias sistemáticas se observan en el patrón de difracción.

Finalmente, MAGNEXT también permite calcular las reglas de ausencia sistemáticas y la forma adaptada a la simetría del factor de estructura magnético para MSSGs (§2.4) con un sólo vector de propagación inconmensurable. Para ello, debe tenerse en cuenta que en el patrón de difracción de una estructura inconmensurable se observan, además de las reflexiones habituales asociadas a vectores de difracción de la red recíproca, reflexiones adicionales asociadas al vector de propagación **k**, así como sus múltiplos. Dado que el vector de difracción es inconmensurable, estas reflexiones no pueden superponerse a las reflexiones asociadas a los vectores de difracción de la red recíproca del grupo padre. Estas reflexiones pueden presentar también ausencias sistemáticas. Para expresar paramétricamente las reglas de ausencia sistemática de patrones de difracción de estructuras magnéticas inconmensurables, es conveniente expresar el vector de difracción en función de 4 índices de Miller (*h k l m*):

$$\mathbf{H}_s = h\mathbf{a}^* + k\mathbf{b}^* + l\mathbf{c}^* + m\mathbf{k} = \mathbf{H} + m\mathbf{k} \qquad (14)$$

Esto permite calcular la forma adaptada a la simetría del factor de estructura magnético utilizando las fórmulas para el cálculo de las reglas de ausencia sistemáticas para MSGs utilizadas en los capítulos §A.3.1 y §A.3.2, pero adaptadas al formalismo

superespacial [24, 25]. Esto implica que las fórmulas (1-9) del capítulo 3 del Anexo A son aplicables a MSSGs haciendo las siguientes sustituciones:

$$\begin{aligned}\mathbf{t}=(t_x,t_y,t_z)&\longrightarrow\mathbf{t}_s=\left(t_1\left(=t_x\right),t_2\left(=t_y\right),t_3\left(=t_z\right),t_4\right)\\ \mathbf{r}=(x,y,z)&\longrightarrow\mathbf{r}_s=\left(x_1\left(=x\right),x_2\left(=y\right),x_3\left(=z\right),x_4\right)\\ \mathbf{H}&\longrightarrow\mathbf{H}_s=\mathbf{H}+m\mathbf{k}\end{aligned}\qquad(15)$$

Además, debe tenerse en cuenta que la ecuación (5) de §A.3.2, que permite hallar el tipo de vector para el cual se calcula la ausencia sistemática, debe modificarse de la siguiente forma:

$$\mathbf{H}\boldsymbol{R}=\mathbf{H}\longrightarrow\mathbf{H}_s\boldsymbol{R}=\mathbf{H}_s\Rightarrow\mathbf{H}\boldsymbol{R}=\mathbf{H},\ \mathbf{k}\boldsymbol{R}=\mathbf{k}\qquad(16)$$

De esta forma, se pueden obtener reglas de ausencia sistemática para los MSSGs similares a las obtenidas para los MSGs, diferenciándose únicamente en que su expresión paramétrica depende del índice de Miller *m*. Nótese que las definiciones expresadas en las ecuaciones (14) a (16) implican que esta herramienta de MAGNEXT ha sido simplificada de tal modo que actualmente no permite trabajar con vectores de propagación inconmensurables que tengan coordenadas racionales no nulas.

La ecuación (16) pone de manifiesto que, aunque los tipos de vectores de difracción para los cuales se deducen las reglas de ausencia sistemática no dependen de los valores de las componentes de **k**, sí dependen de la dirección de **k**, por lo que para calcular las reglas de ausencia sistemática debe conocerse, al menos, una forma paramétrica del vector de propagación **k** correspondiente al MSSG que permita conocer su dirección y permita aplicar la condición **k*R*** = **k**. Esta forma paramétrica puede calcularse a partir de los elementos de simetría del MSSG, pero dado que es un dato habitualmente conocido, MAGNEXT solicita que se especifique (Figura 27). Es más, MAGNEXT hará uso del vector en forma paramétrica especificado por el usuario, comprobando además que es compatible con el MSSG introducido para evitar inconsistencias.

La página principal de MAGNEXT (Figura 21) incluye un enlace a la sección del programa dedicada a las reglas de ausencia sistemática magnéticas para MSSGs. La interfaz de esta sección (Figura 27) permite especificar un MSSG en un *setting* cualquiera por medio de la introducción de un conjunto de generadores en formato x1,x2,x3,x4. Además, debe indicarse la forma general del vector de propagación inconmensurable en forma paramétrica (a,b,c) que corresponda al MSSG introducido, por las razones antes mencionadas.

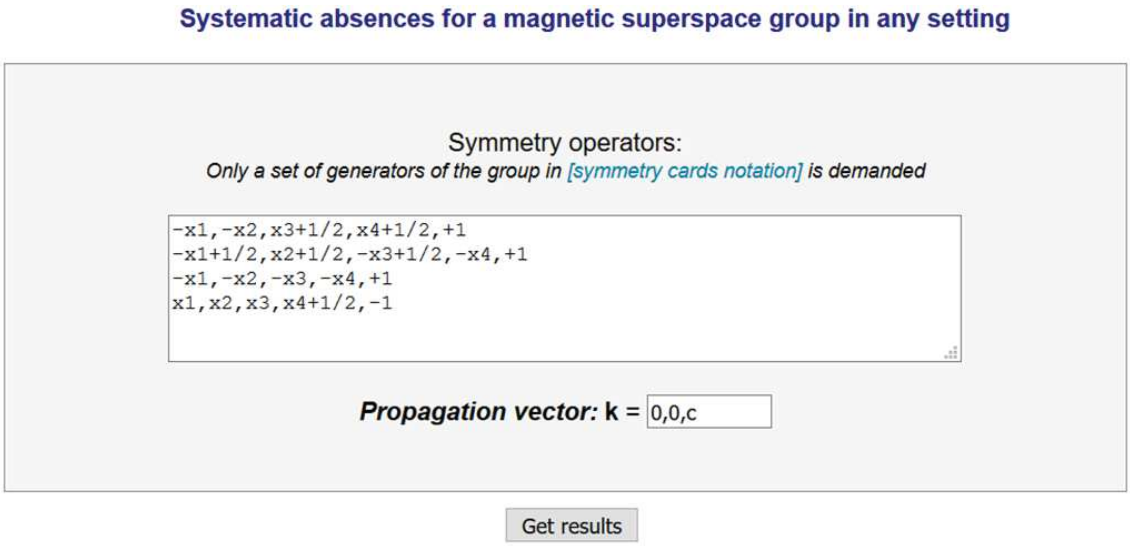

Figura 27. Interfaz de la sección de MAGNEXT para MSSGs. El MSSG introducido corresponde a la estructura inconmensurable del $CaCr_2O_4$ (caso 1.1.15 de MAGNDATA (§9)).

El resultado producido por MAGNEXT para MSSGs es muy similar al producido para MSGs, sólo que las reglas de ausencia sistemática mostradas incluyen en general el índice de Miller adicional *m* (Figura 28). De nuevo, se indican los datos introducidos y se incluye un enlace para consultar la forma adaptada a la simetría de los factores de estructura magnéticos.

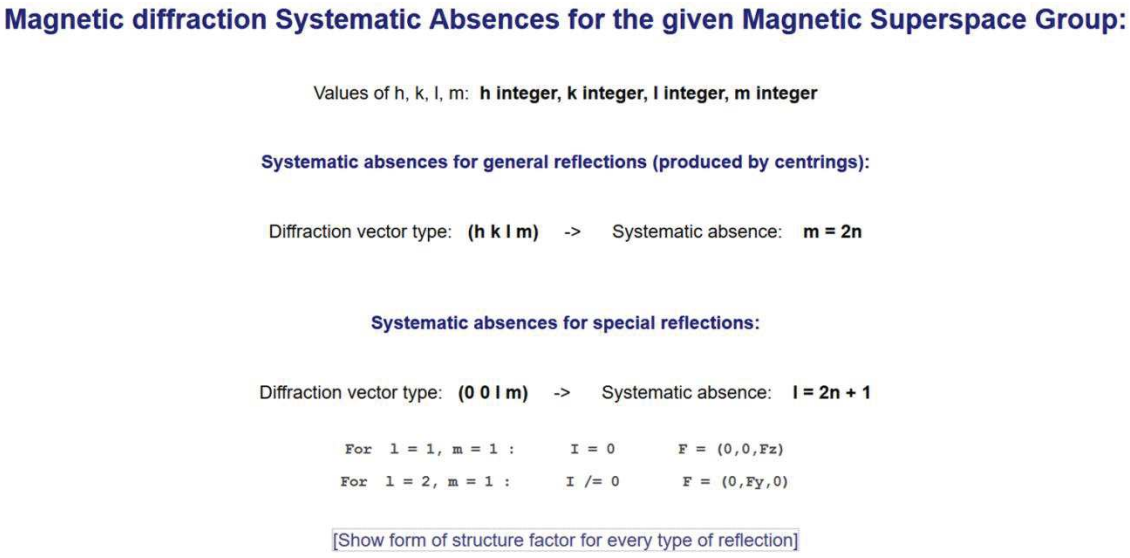

Figura 28. Página de MAGNEXT mostrando las reglas de ausencia sistemática de la estructura inconmensurable del $CaCr_2O_4$ (caso 1.1.15 de MAGNDATA (§9)).

Para finalizar, debe mencionarse que dado que el conocimiento de las reglas de ausencia sistemática magnéticas facilita significativamente la asignación del MSG de una estructura magnética y su determinación, se ha estimado conveniente facilitar el uso conjunto de MAGNEXT y del resto de programas desarrollados como parte de esta tesis doctoral. Por ello, los programas MAXMAGN (§7), MAGMODELIZE (§8), MVISUALIZE (§8) y MAGNDATA (§9) incluyen enlaces a MAGNEXT que permiten consultar las reglas de ausencia sistemática asociadas a los MSGs en diversas

situaciones. Un ejemplo de la utilidad de estos enlaces se encuentra en el Anexo C; en este anexo, que recoge una publicación cuyo propósito es servir de guía en el uso conjunto de las diversas herramientas sobre simetría magnética del *Bilbao Crystallographic Server*, se incluye la sección §C.2.4, que recoge un ejemplo de utilización de MAGNEXT desde MAXMAGN que permite descartar varios MSGs proporcionados como posibles por MAXMAGN para la estructura magnética del compuesto $Na_3Co(CO_3)_2Cl$.

6. NORMALIZADORES DE LOS GRUPOS ESPACIALES MAGNÉTICOS: PROGRAMA MNORMALIZER

Los normalizadores de los 230 grupos espaciales juegan un papel fundamental en la resolución de diversos problemas de teoría de grupos relacionados con la determinación de estructuras cristalinas [39]. La utilidad de los normalizadores está directamente relacionada con la aplicación de argumentos basados en la simetría, por lo que el escaso uso de la simetría magnética en la determinación de estructuras magnéticas por parte de la comunidad científica tiene como consecuencia que los normalizadores de los MSGs no hayan sido hasta ahora utilizados o recopilados. En esta tesis doctoral, la necesidad de utilizar los normalizadores afines de los MSGs surgió durante el desarrollo de los programas MAXMAGN (§7) y MAGMODELIZE (§8). En estos programas se utiliza el normalizador afín en las siguientes situaciones:

- Dado un MSG definido por su etiqueta y una transformación a su *setting* estándar, es conveniente en muchos casos obtener transformaciones de *setting* alternativas que definan exactamente el mismo MSG.
- A la hora de analizar los subgrupos de un determinado grupo padre es necesario comprobar si dos subgrupos del mismo tipo, definidos por medio de transformaciones al *setting* estándar diferentes, son el mismo subgrupo, o corresponden a dos subgrupos diferentes no equivalentes, o a dos subgrupos diferentes pero equivalentes por conjugación.

Esta necesidad de utilizar los normalizadores afines de los MSGs en los programas de aplicación ha sido la principal motivación para la realización de un cálculo más general y sistemático de los normalizadores tanto euclídeo como afín de todos los MSGs. Su resultado es el programa MNORMALIZER (http://www.cryst.ehu.es/cryst/msgnorm.html), que proporciona esta información de forma interactiva para cualquier MSG. El cálculo se ha realizado partiendo de los normalizadores de los grupos espaciales convencionales contenidos en el programa NORMALIZER (http://www.cryst.ehu.es/cryst/get_nor.html) del *Bilbao Crystallographic Server*.

6.1 Normalizadores afín y euclídeo de los MSGs

El normalizador $\mathbf{N_S(M)}$, de un MSG **M** y su supergrupo **S**, es a su vez un MSG, que se define como el conjunto de elementos de **S** que por medio de la conjugación dejan a **M** invariante. Si el supergrupo **S** es el grupo de transformaciones euclídeas $\mathbf{E\otimes 1'}$, o bien el grupo de transformaciones afines $\mathbf{A\otimes 1'}$, se obtienen el normalizador euclídeo $\mathbf{N_{E\otimes 1'}(M)}$ y el normalizador afín $\mathbf{N_{A\otimes 1'}(M)}$, respectivamente. Sean **G** y **D** el grupo espacial efectivo y el subgrupo de elementos no primados de **M**, respectivamente (Figura 11); entonces, los normalizadores afín y euclídeo de **M** se deducen de la siguiente forma:

$$\mathbf{N}_{\mathbf{A}\otimes\mathbf{1}'}(\mathbf{M}) := \left\{ s \in \mathbf{A}\otimes\mathbf{1}' \mid s^{-1}\mathbf{G}s = \mathbf{G} \ \wedge \ s^{-1}\mathbf{D}s = \mathbf{D} \right\}$$
$$\mathbf{N}_{\mathbf{E}\otimes\mathbf{1}'}(\mathbf{M}) := \left\{ s \in \mathbf{E}\otimes\mathbf{1}' \mid s^{-1}\mathbf{G}s = \mathbf{G} \ \wedge \ s^{-1}\mathbf{D}s = \mathbf{D} \right\} \quad (17)$$

Los normalizadores afín y euclídeo de los grupos espaciales convencionales **H** se definen de forma similar a como se definen en (17):

$$\mathbf{N}_{\mathbf{A}}(\mathbf{H}) := \left\{ s \in \mathbf{A} \mid s^{-1}\mathbf{H}s = \mathbf{H} \right\}$$
$$\mathbf{N}_{\mathbf{E}}(\mathbf{H}) := \left\{ s \in \mathbf{E} \mid s^{-1}\mathbf{H}s = \mathbf{H} \right\} \quad (18)$$

La condición en (18) de que los elementos *s* del normalizador, cuando son utilizados para conjugar **H**, deben dejarlo invariante, es la misma que deben cumplir en (17), sólo que aplicada a **G** y **D**. Esto implica que los normalizadores afín y euclídeo de **M**, $\mathbf{N}_{\mathbf{A}\otimes\mathbf{1}'}$ (**M**) y $\mathbf{N}_{\mathbf{E}\otimes\mathbf{1}'}$ (**M**), se pueden definir como:

$$\mathbf{N}_{\mathbf{A}\otimes\mathbf{1}'}(\mathbf{M}) = \left[\mathbf{N}_{\mathbf{A}}(\mathbf{G}) \cap \mathbf{N}_{\mathbf{A}}(\mathbf{D}) \right] \otimes \mathbf{1}'$$
$$\mathbf{N}_{\mathbf{E}\otimes\mathbf{1}'}(\mathbf{M}) := \left[\mathbf{N}_{\mathbf{E}}(\mathbf{G}) \cap \mathbf{N}_{\mathbf{E}}(\mathbf{D}) \right] \otimes \mathbf{1}' \quad (19)$$

Por tanto, los normalizadores afín y euclídeo de los MSGs **M** pueden calcularse haciendo uso de los normalizadores afines de los grupos espaciales convencionales **G** y **D**.

La operación de conjugación *s* que se aplica en (17) sobre los elementos de los grupos **G** y **D** es matemáticamente idéntica a una transformación de *setting* del grupo **M** por medio de una matriz de transformación (***N***,**n**) expresada en forma de matriz aumentada 4x4 (ecuación (6), §4.1.2). Debido a ello, los elementos de simetría del normalizador, cuando son utilizadas como transformaciones de *setting*, dejan **M** invariante. El normalizador afín, **S** = **A**⊗**1'**, es entonces el conjunto de todas las transformaciones afines que dejan **M** invariante, mientras que el normalizador euclídeo, **S** = **E**⊗**1'**, es el conjunto de todas las transformaciones euclídeas que dejan **M** invariante. Es precisamente esta cualidad del normalizador afín la que permite utilizarlo, como se mencionó anteriormente:

- Para obtener transformaciones de *setting* alternativas a una dada, utilizando elementos del normalizador afín como transformaciones de *setting* (ecuación (5), §4.1.2)
- Para deducir si dos MSGs $\mathbf{M_1}$ y $\mathbf{M_2}$ del mismo **M**, tipo definidos por transformaciones de *setting* distintas, ($\boldsymbol{P_1}$,$\mathbf{p_1}$) y ($\boldsymbol{P_2}$,$\mathbf{p_2}$), son MSGs distintos o idénticos. Serán idénticos si hay algún elemento (***N***,**n**) del normalizador afín de **M**, **N**(**M**), tal que se cumpla:

$$(\boldsymbol{P}_1, \mathbf{p}_1) = (\boldsymbol{P}_2, \mathbf{p}_2)(\boldsymbol{N}, \mathbf{n}) \quad (20)$$

El cálculo de los normalizadores afín y euclídeo de los MSGs puede realizarse siguiendo dos métodos o formas equivalentes y muy similares: el método de intersección y el método directo. El cálculo de los normalizadores afín y euclídeo de los MSGs se ha efectuado siguiendo ambos métodos, que se detallan a continuación.

6.2 Cálculo de los normalizadores afín y euclídeo de los MSGs: método directo y método de intersección

Para calcular los normalizadores afín y euclídeo de los MSGs, es necesario conocer los grupos **G** y **D** que corresponden a cada MSG, así como la matriz de transformación (***P***,**p**) entre **G** y **D** que define el *setting* de **D** (se utilizará el *setting* OG como estándar, lo que permite asumir que **G** está en el *setting* estándar de los grupos espaciales convencionales, ya que éste coincide con el *setting* estándar OG):

$$\left(\mathbf{a},\mathbf{b},\mathbf{c}\right)_{\mathbf{D}} = \left(\mathbf{a},\mathbf{b},\mathbf{c}\right)_{\mathbf{G}} \left(\boldsymbol{P},\mathbf{p}\right) \tag{21}$$

Todos estos datos han sido obtenidos por medio del programa MAXSUB del *Bilbao Crystallographic Server*. Utilizando este programa se han obtenido todos los subgrupos maximales de índice 2, **D**, de cada grupo espacial convencional **G** y sus correspondientes matrices de transformación de *setting* (***P***,**p**). Para saber a qué MSG **M** corresponde cada conjunto {**G**, **D**, (***P***,**p**)}, los elementos de simetría de los subgrupos maximales **D** han sido calculados en el *setting* del grupo **G** y cotejados con los subgrupos de elementos no primados de cada MSG derivado de **G** en *setting* OG. Así, se ha construido una base de datos interna que recoge los conjuntos {**G**, **D**, (***P***,**p**)} correspondientes a cada MSG.

Asimismo, es necesario conocer los normalizadores afín y euclídeo de los grupos espaciales convencionales. Éstos están disponibles en el programa NORMALIZER del *Bilbao Crystallographic Server*. En él, los normalizadores se especifican proporcionando una lista de *coset representatives* del normalizador con respecto al grupo espacial, los cuales son suficientes para especificar el normalizador completamente y sin ambigüedad. El punto de partida del cálculo para ambos métodos es la recolección de los *coset representatives* $(\boldsymbol{N},\mathbf{n})_{\mathbf{G}}$ del normalizador (afín o euclídeo) de **G**, **N**(**G**). A partir de aquí, se puede obtener el normalizador (afín o euclídeo) de **M**, **N**(**M**), calculando los *coset representatives* de **N**(**M**) respecto de **M** siguiendo cualquiera de los siguientes métodos:

- <u>*Método directo*</u>: los *coset representatives* de **N**(**M**) respecto de **M** son aquellos *coset representatives* $(\boldsymbol{N},\mathbf{n})_{\mathbf{G}}$ de **N**(**G**) respecto de **G** que dejan invariante al grupo **D** en *setting* OG, es decir, que cumplen:

$$\left(\boldsymbol{N},\mathbf{n}\right)_{\mathbf{G}}^{-1} \left\{\boldsymbol{R}\,|\,\mathbf{t}\right\}_{\mathbf{D}} \left(\boldsymbol{N},\mathbf{n}\right)_{\mathbf{G}} \in \mathbf{D} \tag{22}$$

- <u>*Método de intersección*</u>: se recopilan también los *coset representatives* de **N**(**D**) en **D**, $(\boldsymbol{N},\mathbf{n})_{\mathbf{D}}$. Éstos dejan invariante a **D** en el *setting* estándar de **D**, pero es necesario

expresarlos en el *setting* de **G**. Para ello, hay que transformarlos al *setting* estándar de **G** (es decir, el *setting* OG) utilizando la transformación de *setting* (***P***,**p**) que ha sido recopilada a tal efecto:

$$\left(\boldsymbol{P},\mathbf{p}\right)(\boldsymbol{N},\mathbf{n})_{\mathbf{D}}(\boldsymbol{P},\mathbf{p})^{-1}=(\boldsymbol{N},\mathbf{n})_{\mathbf{D}}^{\mathbf{G}} \qquad (23)$$

Entonces, los *coset representatives* de **N**(**M**) respecto de **M** son aquellos $(\boldsymbol{N},\mathbf{n})_{\mathbf{D}}^{\mathbf{G}}$ que pertenecen a **N**(**G**) como a $\mathbf{N}(\mathbf{D})_{\mathbf{G}}$, es decir, la intersección entre los normalizadores de **G** y **D** expresados en el *setting* de **G**.

Para ambos métodos, deben incluirse no sólo los *coset representatives* hallados, sino también sus equivalentes primados, de acuerdo con (20). Ambos métodos son equivalentes, y no son sino dos formas similares pero diferentes de hallar los normalizadores de los MSGs partiendo de los normalizadores de los grupos espaciales.

Ambos métodos han sido utilizados para obtener los normalizadores afín y euclídeo de los MSGs en *setting* OG, procediendo después a cotejar los resultados de ambos métodos, lo cual aporta mayor seguridad en la corrección de los cálculos efectuados. Al igual que con los normalizadores de los grupos espaciales convencionales, únicamente los *coset representatives* de **N**(**M**) respecto de **M** han sido calculados e incluidos en el programa MNORMALIZER, pues bastan para definir sin ambigüedad el normalizador. Los *coset representatives* de los normalizadores de los MSG tipo IV en *setting* BNS han sido calculados a partir de sus homólogos en *setting* OG utilizando la transformación entre los *settings* OG y BNS disponible en MGENPOS (§4.3, Figura 15).

6.3 Programa MNORMALIZER

El programa MNORMALIZER permite consultar los normalizadores afín y euclídeo de los MSGs en *setting* estándar BNS y OG. Para ello, debe seleccionarse un MSG en la interfaz de la página principal del programa haciendo uso del formulario dispuesto a tal efecto (similar al de la Figura 13) y seleccionando "*affine*" o "*euclidean* (*general metric*)" en dicho formulario.

La página del normalizador del MSG seleccionado puede verse en la Figura 29, donde se ha tomado como ejemplo el normalizador afín del MSG C_a222 (#21.43) en *setting* BNS. Esta página es similar para todos los normalizadores, con la excepción de los normalizadores afines de los MSGs monoclínicos y triclínicos (§6.4). Primero, para MSGs tipo IV, se indica la notación del MSG en el *setting* BNS u OG alternativo al elegido, incluyendo un enlace para consultar el normalizador del MSG en ese *setting*, así como un enlace para consultar las matrices de transformación entre los *settings* BNS y OG del MSG (Figura 15).

Affine normalizer of the magnetic space group C_a222 (#21.43)

To display the general positions in the OG setting, please follow this link: P_C222 (#16.5.103) [Transformation matrix]

Affine normalizer of C_a222 (a,b,c): *P4/mmm1'* (#123.340) (1/2a,1/2b,1/2c ; 0,0,0).

Index of C_a222 in *P4/mmm1'* (#123.340) (**1/2a,1/2b,1/2c ; 0,0,0**): 16 with i_L=2 and i_P=8

Left coset representatives of *P4/mmm1'* (#123.340) (**1/2a,1/2b,1/2c ; 0,0,0**) with respect to C_a222 (**a,b,c**)

Hint: *Normalizers of magnetic space groups are grey groups, so the elements with an associated time-reversal (-1) are also included*

(x,y,z) form	Matrix form	Geom. interp.	Seitz notation
x,y,z,+1	$\begin{pmatrix} 1 & 0 & 0 & 0 \\ 0 & 1 & 0 & 0 \\ 0 & 0 & 1 & 0 \end{pmatrix}$	1	{ 1 | 0 }
x,y,z+1/2,+1	$\begin{pmatrix} 1 & 0 & 0 & 0 \\ 0 & 1 & 0 & 0 \\ 0 & 0 & 1 & 1/2 \end{pmatrix}$	t (0,0,1/2)	{ 1 | 0 0 1/2 }
-x,-y,-z,+1	$\begin{pmatrix} -1 & 0 & 0 & 0 \\ 0 & -1 & 0 & 0 \\ 0 & 0 & -1 & 0 \end{pmatrix}$	-1 0,0,0	{ -1 | 0 }
-x,-y,-z+1/2,+1	$\begin{pmatrix} -1 & 0 & 0 & 0 \\ 0 & -1 & 0 & 0 \\ 0 & 0 & -1 & 1/2 \end{pmatrix}$	-1 0,0,1/4	{ -1 | 0 0 1/2 }
y,x,z,+1	$\begin{pmatrix} 0 & 1 & 0 & 0 \\ 1 & 0 & 0 & 0 \\ 0 & 0 & 1 & 0 \end{pmatrix}$	m x,x,z	{ $m_{1\text{-}10}$ | 0 }
y,x,z+1/2,+1	$\begin{pmatrix} 0 & 1 & 0 & 0 \\ 1 & 0 & 0 & 0 \\ 0 & 0 & 1 & 1/2 \end{pmatrix}$	c x,x,z	{ $m_{1\text{-}10}$ | 0 0 1/2 }
-y,-x,-z,+1	$\begin{pmatrix} 0 & -1 & 0 & 0 \\ -1 & 0 & 0 & 0 \\ 0 & 0 & -1 & 0 \end{pmatrix}$	2 x,-x,0	{ $2_{1\text{-}10}$ | 0 }
-y,-x,-z+1/2,+1	$\begin{pmatrix} 0 & -1 & 0 & 0 \\ -1 & 0 & 0 & 0 \\ 0 & 0 & -1 & 1/2 \end{pmatrix}$	2 x,-x,1/4	{ $2_{1\text{-}10}$ | 0 0 1/2 }

Figura 29. Página de MNORMALIZER correspondiente al normalizador afín en *setting* BNS del MSG C_a222 (#21.43).

Después se proporciona una definición del normalizador del grupo. Tal y como sucede con los normalizadores de los grupos espaciales convencionales [39], los normalizadores euclídeos, así como los normalizadores afines no monoclínicos ni triclínicos (para normalizadores afines monoclínicos y triclínicos, ver §6.4), son isomorfos a un grupo de isometrías en un espacio métrico [39], y por tanto, pueden ser expresados utilizando los símbolos de los MSGs. De hecho, al ser grupos grises, son equivalentes a MSGs de tipo II, con la excepción de la posible inclusión en el normalizador de traslaciones arbitrarias **r**, **s** y/o **t** a lo largo de cada uno de los tres ejes cristalográficos. Por ello, los símbolos de los normalizadores de los MSGs coinciden con los símbolos de los MSGs de tipo II, salvo quizá por la presencia de un conjunto infinito de traslaciones arbitrarias, cuya presencia se denotaría por medio de un superíndice 1, 2 ó 3 (indicando el número de ejes a lo largo de los cuales hay traslaciones arbitrarias) asociado a la letra que define la red de Bravais del grupo. Así pues, los normalizadores

de los MSGs pueden definirse de forma similar a los MSGs (§4.1.2), indicando para ello tanto un símbolo identificativo del tipo de grupo al que pertenece el normalizador como una transformación de *setting* al estándar. Nótese que esta transformación, que define el *setting* del normalizador, queda afectada por la posible presencia de las traslaciones arbitrarias mencionadas. Por ejemplo, el normalizador afín del MSG *Pm'm2'* (#25.59) incluye traslaciones arbitrarias a lo largo del eje *z*, por lo que su símbolo y etiqueta son P^1mmm1' (#47.250), y la transformación de *setting* al estándar es (1/2**a**, 1/2**b**, t**c**), siendo t el módulo de **t**.

Bajo la definición del normalizador, se indica el índice de la relación grupo-subgrupo entre el normalizador y el MSG, que es el producto del índice grupo-subgrupo entre los MPGs asociados a ambos (i_P) y del índice grupo-subgrupo entre las redes de traslaciones (i_L) de ambos, los cuales también se indican. El índice i_L, y por tanto el índice total, son infinitos si el normalizador contiene traslaciones arbitrarias.

Finalmente, se proporciona una tabla donde se indican los *coset representatives* del normalizador respecto del MSG, en los cuatro formatos descritos en §4.3. Esta lista puede incluir también traslaciones arbitrarias como generadores. Como se indica en la parte superior de la tabla, el hecho de que los normalizadores sean grupos grises implica que cada *coset representative* indicado en la lista forma parte del normalizador también primado. Estos *coset representatives* primados adicionales no se indican expresamente en el listado.

Para los MSGs cuyo grupo espacial efectivo sea un grupo espacial de Sohncke no enantiomórfico, como es el caso del grupo C_a222 (#21.43), los normalizadores afín y euclídeo contienen rotoinversiones como *coset representatives*. Dado que estos grupos pueden definir la simetría de estructuras quirales, cuando estos *coset representatives* del normalizador se utilizan como transformaciones de *setting* de una estructura magnética quiral, pese a que dejan invariante el MSG de la estructura, transforman la estructura en su imagen especular. Por ello, puede resultar útil conocer el normalizador "*chirality-preserving*" afín y euclídeo de estos grupos, por lo que MNORMALIZER proporciona dicho normalizador para este tipo de grupos debajo del normalizador convencional, de la misma manera que se hace para los grupos espaciales convencionales en el programa NORMALIZER del *Bilbao Crystallographic Server*.

6.4 Normalizadores afines de los MSGs monoclínicos y triclínicos

Aparte de los requisitos que en general la parte rotacional de los elementos de los normalizadores deben cumplir (determinante 1 o -1, coeficientes enteros), los normalizadores afines de los MSGs monoclínicos tienen la particularidad de que el único requisito adicional sobre la parte rotacional de sus elementos es que deje invariante el eje monoclínico. Este requisito ni siquiera es necesario en el caso de los MSGs triclínicos. Es por ello que los normalizadores afines de los grupos monoclínicos y triclínicos constituyen una excepción: al incluir elementos de simetría que no son isometrías en un espacio métrico, no son isomorfos a ningún grupo de isometrías en

un espacio métrico [39], por lo que no pueden ser expresados utilizando los símbolos de los MSGs de tipo II. De hecho, el subconjunto de elementos de simetría dentro de la celda unidad para este tipo de normalizadores contiene infinitos elementos, cuya parte rotacional y traslacional es parametrizable. Por ello, la mejor forma de expresar estos normalizadores es en forma de matriz 3x4 paramétrica, tal y como puede verse para el grupo C_ac (#9.41) en la Figura 30.

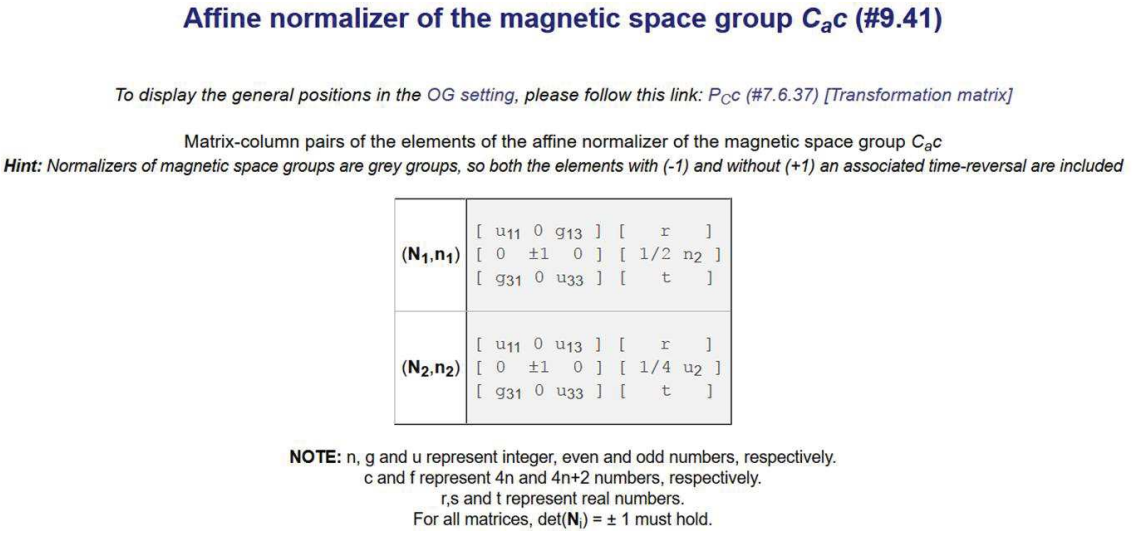

Affine normalizer of the magnetic space group C_ac (#9.41)

To display the general positions in the OG setting, please follow this link: P_Cc (#7.6.37) [Transformation matrix]

Matrix-column pairs of the elements of the affine normalizer of the magnetic space group C_ac

Hint: *Normalizers of magnetic space groups are grey groups, so both the elements with (-1) and without (+1) an associated time-reversal are included*

$(\mathbf{N_1},\mathbf{n_1})$	$\begin{bmatrix} u_{11} & 0 & g_{13} \\ 0 & \pm 1 & 0 \\ g_{31} & 0 & u_{33} \end{bmatrix} \begin{bmatrix} r \\ 1/2\ n_2 \\ t \end{bmatrix}$
$(\mathbf{N_2},\mathbf{n_2})$	$\begin{bmatrix} u_{11} & 0 & u_{13} \\ 0 & \pm 1 & 0 \\ g_{31} & 0 & u_{33} \end{bmatrix} \begin{bmatrix} r \\ 1/4\ u_2 \\ t \end{bmatrix}$

NOTE: n, g and u represent integer, even and odd numbers, respectively.
c and f represent 4n and 4n+2 numbers, respectively.
r,s and t represent real numbers.
For all matrices, det($\mathbf{N_i}$) = ± 1 must hold.

Figura 30. Página de MNORMALIZER con el normalizador afín del MSG monoclínico C_ac (#9.41) en *setting* BNS, expresado en forma paramétrica. En este caso particular, dos matrices son necesarias, correspondientes a dos conjuntos disjuntos de elementos de simetría que, tomados conjuntamente, forman el normalizador afín de C_ac (#9.41).

Así, los valores que cada componente de dicha matriz paramétrica pueden tener se expresan mediante una letra que especifica la condición que esa componente debe cumplir. El significado de estas letras puede consultarse en la leyenda que proporciona MNORMALIZER (Figura 30), así como en la leyenda disponible a tal efecto en la Tabla 2. Debe recordarse también que la condición de que el determinante debe ser 1 o -1 se cumple globalmente, así como el hecho de que cada elemento del normalizador afín también forma parte del normalizador como elemento primado. De esta forma, cualquier conjunto de valores que cumpla tanto estas condiciones como las restricciones en los valores de las componentes matriciales asociadas a su forma paramétrica (Figura 30) permite formar un elemento de simetría que forma parte del normalizador.

Los normalizadores monoclínicos y triclínicos de los MSGs han sido calculados a mano siguiendo los métodos directo y de intersección (§6.2) primero en *setting* OG, siendo luego transformados al *setting* BNS (sólo para MSGs tipo IV). Los resultados de estos cálculos manuales para todos los MSGs monoclínicos y triclínicos están recogidos en las Tablas 1 y 2.

Tabla 1. Tabla de los normalizadores afines de los MSGs triclínicos y monoclínicos en *setting* estándar BNS. Para los grupos tipo IV se incluye el normalizador afín en *setting* OG. Las parejas matriz-vector de la columna correspondiente vienen desglosadas en la Tabla G2.

Etiqueta	Símbolo	Matriz-vector	Etiqueta	Símbolo	Matriz-vector
1.1	*P1*	$\boldsymbol{M}_1$, $\mathbf{v}_1$	10.42	*P2/m*	$\boldsymbol{M}_4$, $\mathbf{v}_2$
1.2	*P11'*	$\boldsymbol{M}_1$, $\mathbf{v}_1$	10.43	*P2/m1'*	$\boldsymbol{M}_4$, $\mathbf{v}_2$
1.3	P_S1	$\boldsymbol{M}_2$, $\mathbf{v}_1$	10.44	*P2'/m*	$\boldsymbol{M}_4$, $\mathbf{v}_2$
1.3.3	$P_{2s}1$	$\boldsymbol{M}_3$, $\mathbf{v}_1$	10.45	*P2/m'*	$\boldsymbol{M}_4$, $\mathbf{v}_2$
2.4	*P-1*	$\boldsymbol{M}_1$, $\mathbf{v}_2$	10.46	*P2'/m'*	$\boldsymbol{M}_4$, $\mathbf{v}_2$
2.5	*P-11'*	$\boldsymbol{M}_1$, $\mathbf{v}_2$	10.47	P_a2/m	$\boldsymbol{M}_5$, $\mathbf{v}_2$
2.6	*P-1'*	$\boldsymbol{M}_1$, $\mathbf{v}_2$	10.6.54	$P_{2a}2/m$	$\boldsymbol{M}_6$, $\mathbf{v}_{11}$
2.7	P_S-1	$\boldsymbol{M}_2$, $\mathbf{v}_2$	10.48	P_b2/m	$\boldsymbol{M}_4$, $\mathbf{v}_2$
2.4.7	P_{2s}-1	$\boldsymbol{M}_3$, $\mathbf{v}_3$	10.7.55	$P_{2b}2/m$	$\boldsymbol{M}_4$, $\mathbf{v}_{12}$
3.1	*P2*	$\boldsymbol{M}_4$, $\mathbf{v}_4$	10.49	P_C2/m	$\boldsymbol{M}_5$, $\mathbf{v}_2$
3.2	*P21'*	$\boldsymbol{M}_4$, $\mathbf{v}_4$	12.7.72	C_P2/m	$\boldsymbol{M}_5$, $\mathbf{v}_2$
3.3	*P2'*	$\boldsymbol{M}_4$, $\mathbf{v}_4$	11.50	$P2_1/m$	$\boldsymbol{M}_4$, $\mathbf{v}_2$
3.4	P_a2	$\boldsymbol{M}_5$, $\mathbf{v}_4$	11.51	$P2_1/m1'$	$\boldsymbol{M}_4$, $\mathbf{v}_2$
3.4.11	$P_{2a}2$	$\boldsymbol{M}_6$, $\mathbf{v}_5$	11.52	$P2_1'/m$	$\boldsymbol{M}_4$, $\mathbf{v}_2$
3.5	P_b2	$\boldsymbol{M}_4$, $\mathbf{v}_4$	11.53	$P2_1/m'$	$\boldsymbol{M}_4$, $\mathbf{v}_2$
3.5.12	$P_{2b}2$	$\boldsymbol{M}_4$, $\mathbf{v}_4$	11.54	$P2_1'/m'$	$\boldsymbol{M}_4$, $\mathbf{v}_2$
3.6	C_P2	$\boldsymbol{M}_5$, $\mathbf{v}_4$	11.55	P_a2_1/m	$\boldsymbol{M}_5$, $\mathbf{v}_2$
5.5.23	P_C2	$\boldsymbol{M}_5$, $\mathbf{v}_4$	11.6.64	$P_{2a}2_1/m$	$\boldsymbol{M}_6$, $\mathbf{v}_{11}$
4.7	$P2_1$	$\boldsymbol{M}_4$, $\mathbf{v}_4$	11.56	P_b2_1/m	$\boldsymbol{M}_4$, $\mathbf{v}_2$
4.8	$P2_11'$	$\boldsymbol{M}_4$, $\mathbf{v}_4$	10.9.57	$P_{2b}2'/m$	$\boldsymbol{M}_4$, $\mathbf{v}_{12}$
4.9	$P2_1'$	$\boldsymbol{M}_4$, $\mathbf{v}_4$	11.57	P_C2_1/m	$\boldsymbol{M}_5$, $\mathbf{v}_2$
4.10	P_a2_1	$\boldsymbol{M}_5$, $\mathbf{v}_4$	12.9.74	C_P2'/m	$\boldsymbol{M}_5$, $\mathbf{v}_2$
4.4.18	$P_{2a}2_1$	$\boldsymbol{M}_6$, $\mathbf{v}_5$	12.58	*C2/m*	$\boldsymbol{M}_5$, $\mathbf{v}_2$
4.11	P_b2_1	$\boldsymbol{M}_4$, $\mathbf{v}_4$	12.59	*C2/m1'*	$\boldsymbol{M}_5$, $\mathbf{v}_2$
3.7.14	$P_{2b}2'$	$\boldsymbol{M}_4$, $\mathbf{v}_4$	12.60	*C2'/m*	$\boldsymbol{M}_5$, $\mathbf{v}_2$
4.12	P_C2_1	$\boldsymbol{M}_5$, $\mathbf{v}_4$	12.61	*C2/m'*	$\boldsymbol{M}_5$, $\mathbf{v}_2$
5.6.24	C_P2'	$\boldsymbol{M}_5$, $\mathbf{v}_4$	12.62	*C2'/m'*	$\boldsymbol{M}_5$, $\mathbf{v}_2$
5.13	*C2*	$\boldsymbol{M}_5$, $\mathbf{v}_4$	12.63	C_c2/m	$\boldsymbol{M}_7$, $\mathbf{v}_2$
5.14	*C21'*	$\boldsymbol{M}_5$, $\mathbf{v}_4$	12.6.71	$C_{2c}2/m$	$\boldsymbol{M}_8$, $\mathbf{v}_3$
5.15	*C2'*	$\boldsymbol{M}_5$, $\mathbf{v}_4$	12.64	C_a2/m	$\boldsymbol{M}_5$, $\mathbf{v}_2$
5.16	C_c2	$\boldsymbol{M}_7$, $\mathbf{v}_4$	10.8.56	P_C2/m	$\boldsymbol{M}_6$, $\mathbf{v}_{13}$
5.4.22	$C_{2c}2$	$\boldsymbol{M}_8$, $\mathbf{v}_6$	13.65	*P2/c*	$\boldsymbol{M}_6$, $\mathbf{v}_2$
5.17	C_a2	$\boldsymbol{M}_5$, $\mathbf{v}_4$	13.66	*P2/c1'*	$\boldsymbol{M}_6$, $\mathbf{v}_2$
3.6.13	P_C2	$\boldsymbol{M}_6$, $\mathbf{v}_5$	13.67	*P2'/c*	$\boldsymbol{M}_6$, $\mathbf{v}_2$
6.18	*Pm*	$\boldsymbol{M}_4$, $\mathbf{v}_7$	13.68	*P2/c'*	$\boldsymbol{M}_6$, $\mathbf{v}_2$
6.19	*Pm1'*	$\boldsymbol{M}_4$, $\mathbf{v}_7$	13.69	*P2'/c'*	$\boldsymbol{M}_6$, $\mathbf{v}_2$
6.20	*Pm'*	$\boldsymbol{M}_4$, $\mathbf{v}_7$	13.70	P_a2/c	$\boldsymbol{M}_7$, $\mathbf{v}_2$
6.21	P_am	$\boldsymbol{M}_5$, $\mathbf{v}_7$	13.6.82	$P_{2a}2/c$	$\boldsymbol{M}_9$, $\mathbf{v}_{11}$
6.4.28	$P_{2a}m$	$\boldsymbol{M}_6$, $\mathbf{v}_7$	13.71	P_b2/c	$\boldsymbol{M}_6$, $\mathbf{v}_2$

6.22	P_bm	$\boldsymbol{M}_4$, $\mathbf{v}_7$	13.7.83	$P_{2b}2/c$	$\boldsymbol{M}_6$, $\mathbf{v}_{12}$
6.5.29	$P_{2b}m$	$\boldsymbol{M}_4$, $\mathbf{v}_8$	13.72	P_c2/c	$\boldsymbol{M}_6$, $\mathbf{v}_2$
6.23	P_Cm	$\boldsymbol{M}_5$, $\mathbf{v}_7$	10.10.58	$P_{2c}2/m'$	$\boldsymbol{M}_5$, $\mathbf{v}_3$
8.5.42	C_P2	$\boldsymbol{M}_5$, $\mathbf{v}_7$	13.73	P_A2/c	$\boldsymbol{M}_6$, $\mathbf{v}_2$
7.24	Pc	$\boldsymbol{M}_6$, $\mathbf{v}_7$	12.10.75	C_P2/m'	$\boldsymbol{M}_5$, $\mathbf{v}_2$
7.25	$Pc1'$	$\boldsymbol{M}_6$, $\mathbf{v}_7$	13.74	P_C2/c	$\boldsymbol{M}_7$, $\mathbf{v}_2$
7.26	Pc'	$\boldsymbol{M}_6$, $\mathbf{v}_7$	15.6.97	C_P2/c	$\boldsymbol{M}_7$, $\mathbf{v}_2$
7.27	P_ac	$\boldsymbol{M}_7$, $\mathbf{v}_7$	14.75	$P2_1/c$	$\boldsymbol{M}_6$, $\mathbf{v}_2$
7.4.35	$P_{2a}c$	$\boldsymbol{M}_9$, $\mathbf{v}_7$	14.76	$P2_1/c1'$	$\boldsymbol{M}_6$, $\mathbf{v}_2$
7.28	P_cc	$\boldsymbol{M}_6$, $\mathbf{v}_7$	14.77	$P2_1'/c$	$\boldsymbol{M}_6$, $\mathbf{v}_2$
6.7.31	$P_{2c}m'$	$\boldsymbol{M}_5$, $\mathbf{v}_7$	14.78	$P2_1/c'$	$\boldsymbol{M}_6$, $\mathbf{v}_2$
7.29	P_bc	$\boldsymbol{M}_6$, $\mathbf{v}_7$	14.79	$P2_1'/c'$	$\boldsymbol{M}_6$, $\mathbf{v}_2$
7.5.36	$P_{2b}c$	$\boldsymbol{M}_6$, $\mathbf{v}_8$	14.80	P_a2_1/c	$\boldsymbol{M}_7$, $\mathbf{v}_2$
7.30	P_Cc	$\boldsymbol{M}_7$, $\mathbf{v}_7$	14.6.91	$P_{2a}2_1/c$	$\boldsymbol{M}_9$, $\mathbf{v}_{11}$
9.4.48	C_Pc	$\boldsymbol{M}_7$, $\mathbf{v}_7$	14.81	P_b2_1/c	$\boldsymbol{M}_6$, $\mathbf{v}_2$
7.31	P_Ac	$\boldsymbol{M}_6$, $\mathbf{v}_7$	13.9.85	$P_{2b}2'/c$	$\boldsymbol{M}_6$, $\mathbf{v}_{12}$
8.7.44	C_Pm'	$\boldsymbol{M}_5$, $\mathbf{v}_7$	14.82	P_c2_1/c	$\boldsymbol{M}_6$, $\mathbf{v}_2$
8.32	Cm	$\boldsymbol{M}_5$, $\mathbf{v}_7$	11.7.65	$P_{2c}2_1/m'$	$\boldsymbol{M}_5$, $\mathbf{v}_3$
8.33	$Cm1'$	$\boldsymbol{M}_5$, $\mathbf{v}_7$	14.83	P_A2_1/c	$\boldsymbol{M}_6$, $\mathbf{v}_2$
8.34	Cm'	$\boldsymbol{M}_5$, $\mathbf{v}_7$	12.11.76	C_P2'/m'	$\boldsymbol{M}_5$, $\mathbf{v}_2$
8.35	C_cm	$\boldsymbol{M}_7$, $\mathbf{v}_7$	14.84	P_C2_1/c	$\boldsymbol{M}_7$, $\mathbf{v}_2$
8.4.41	$C_{2c}m$	$\boldsymbol{M}_8$, $\mathbf{v}_7$	15.7.98	C_P2'/c	$\boldsymbol{M}_7$, $\mathbf{v}_2$
8.36	C_am	$\boldsymbol{M}_5$, $\mathbf{v}_7$	15.85	$C2/c$	$\boldsymbol{M}_7$, $\mathbf{v}_2$; $\boldsymbol{M}_{10}$, $\mathbf{v}_{14}$
6.6.30	P_Cm	$\boldsymbol{M}_6$, $\mathbf{v}_8$	15.86	$C2/c1'$	$\boldsymbol{M}_7$, $\mathbf{v}_2$; $\boldsymbol{M}_{10}$, $\mathbf{v}_{14}$
9.37	Cc	$\boldsymbol{M}_7$, $\mathbf{v}_7$; $\boldsymbol{M}_{10}$, $\mathbf{v}_9$	15.87	$C2'/c$	$\boldsymbol{M}_7$, $\mathbf{v}_2$; $\boldsymbol{M}_{10}$, $\mathbf{v}_{14}$
9.38	$Cc1'$	$\boldsymbol{M}_7$, $\mathbf{v}_7$; $\boldsymbol{M}_{10}$, $\mathbf{v}_9$	15.88	$C2/c'$	$\boldsymbol{M}_7$, $\mathbf{v}_2$; $\boldsymbol{M}_{10}$, $\mathbf{v}_{14}$
9.39	Cc'	$\boldsymbol{M}_7$, $\mathbf{v}_7$; $\boldsymbol{M}_{10}$, $\mathbf{v}_9$	15.89	$C2'/c'$	$\boldsymbol{M}_7$, $\mathbf{v}_2$; $\boldsymbol{M}_{10}$, $\mathbf{v}_{14}$
9.40	C_cc	$\boldsymbol{M}_7$, $\mathbf{v}_7$	15.90	C_c2/c	$\boldsymbol{M}_7$, $\mathbf{v}_2$
8.6.43	$C_{2c}m'$	$\boldsymbol{M}_8$, $\mathbf{v}_7$	12.8.73	$C_{2c}2/m'$	$\boldsymbol{M}_8$, $\mathbf{v}_3$
9.41	C_ac	$\boldsymbol{M}_7$, $\mathbf{v}_7$; $\boldsymbol{M}_{10}$, $\mathbf{v}_9$	15.91	C_a2/c	$\boldsymbol{M}_7$, $\mathbf{v}_2$; $\boldsymbol{M}_{10}$, $\mathbf{v}_{14}$
7.6.37	P_Cc	$\boldsymbol{M}_9$, $\mathbf{v}_8$; $\boldsymbol{M}_{11}$, $\mathbf{v}_{10}$	13.8.84	P_C2/c	$\boldsymbol{M}_9$, $\mathbf{v}_{13}$; $\boldsymbol{M}_{11}$, $\mathbf{v}_{15}$

Tabla 2. Matrices y vectores utilizados en la tabla G1 para definir los normalizadores afines monoclínicos y triclínicos de los grupos espaciales magnéticos. Todas las matrices deben cumplir $\det(M_i) = \pm 1$.

$$\boldsymbol{M}_1 = \begin{pmatrix} n_{11} & n_{12} & n_{13} \\ n_{21} & n_{22} & n_{23} \\ n_{31} & n_{32} & n_{33} \end{pmatrix} \quad \boldsymbol{M}_2 = \begin{pmatrix} n_{11} & n_{12} & g_{13} \\ n_{21} & n_{22} & g_{23} \\ n_{31} & n_{32} & u_{33} \end{pmatrix} \quad \boldsymbol{M}_3 = \begin{pmatrix} n_{11} & n_{12} & n_{13} \\ n_{21} & n_{22} & n_{23} \\ g_{31} & g_{32} & u_{33} \end{pmatrix} \quad \boldsymbol{M}_4 = \begin{pmatrix} n_{11} & 0 & n_{13} \\ 0 & \pm 1 & 0 \\ n_{31} & 0 & n_{33} \end{pmatrix}$$

$$\boldsymbol{M}_5 = \begin{pmatrix} u_{11} & 0 & n_{13} \\ 0 & \pm 1 & 0 \\ g_{31} & 0 & u_{33} \end{pmatrix} \quad \boldsymbol{M}_6 = \begin{pmatrix} u_{11} & 0 & g_{13} \\ 0 & \pm 1 & 0 \\ n_{31} & 0 & u_{33} \end{pmatrix} \quad \boldsymbol{M}_7 = \begin{pmatrix} u_{11} & 0 & g_{13} \\ 0 & \pm 1 & 0 \\ g_{31} & 0 & u_{33} \end{pmatrix} \quad \boldsymbol{M}_8 = \begin{pmatrix} u_{11} & 0 & n_{13} \\ 0 & \pm 1 & 0 \\ c_{31} & 0 & u_{33} \end{pmatrix}$$

$$\boldsymbol{M}_9 = \begin{pmatrix} u_{11} & 0 & c_{13} \\ 0 & \pm 1 & 0 \\ n_{31} & 0 & u_{33} \end{pmatrix} \quad \boldsymbol{M}_{10} = \begin{pmatrix} u_{11} & 0 & u_{13} \\ 0 & \pm 1 & 0 \\ g_{31} & 0 & u_{33} \end{pmatrix} \quad \boldsymbol{M}_{11} = \begin{pmatrix} u_{11} & 0 & f_{13} \\ 0 & \pm 1 & 0 \\ n_{31} & 0 & u_{33} \end{pmatrix}$$

$$\mathbf{v}_1 = \begin{pmatrix} r \\ s \\ t \end{pmatrix} \quad \mathbf{v}_2 = \begin{pmatrix} \frac{1}{2}n_1 \\ \frac{1}{2}n_2 \\ \frac{1}{2}n_3 \end{pmatrix} \quad \mathbf{v}_3 = \begin{pmatrix} \frac{1}{2}n_1 \\ \frac{1}{2}n_2 \\ n_3 \end{pmatrix} \quad \mathbf{v}_4 = \begin{pmatrix} \frac{1}{2}n_1 \\ s \\ \frac{1}{2}n_3 \end{pmatrix} \quad \mathbf{v}_5 = \begin{pmatrix} n_1 \\ s \\ \frac{1}{2}n_3 \end{pmatrix} \quad \mathbf{v}_6 = \begin{pmatrix} \frac{1}{2}n_1 \\ s \\ n_3 \end{pmatrix} \quad \mathbf{v}_7 = \begin{pmatrix} r \\ \frac{1}{2}n_2 \\ t \end{pmatrix} \quad \mathbf{v}_8 = \begin{pmatrix} r \\ n_2 \\ t \end{pmatrix}$$

$$\mathbf{v}_9 = \begin{pmatrix} r \\ \frac{1}{4}u_2 \\ t \end{pmatrix} \quad \mathbf{v}_{10} = \begin{pmatrix} r \\ \frac{1}{2}u_2 \\ t \end{pmatrix} \quad \mathbf{v}_{11} = \begin{pmatrix} n_1 \\ \frac{1}{2}n_2 \\ \frac{1}{2}n_3 \end{pmatrix} \quad \mathbf{v}_{12} = \begin{pmatrix} \frac{1}{2}n_1 \\ n_2 \\ \frac{1}{2}n_3 \end{pmatrix} \quad \mathbf{v}_{13} = \begin{pmatrix} n_1 \\ n_2 \\ \frac{1}{2}n_3 \end{pmatrix} \quad \mathbf{v}_{14} = \begin{pmatrix} \frac{1}{4}u_1 \\ \frac{1}{4}u_2 \\ \frac{1}{2}n_3 \end{pmatrix} \quad \mathbf{v}_{15} = \begin{pmatrix} \frac{1}{2}u_1 \\ \frac{1}{2}u_2 \\ \frac{1}{2}n_3 \end{pmatrix}$$

Leyenda:

n	Número entero
u	Número impar
g	Número par
c	Múltiplo de 4 (c = 4n)
f	Número impar duplicado (f = 4n + 2)
r, s, t	Números reales

7. SUBGRUPOS k-MAXIMALES Y MODELOS DE ESTRUCTURA MAGNÉTICA RESULTANTES: PROGRAMA MAXMAGN

***NOTA**: Puede encontrarse información adicional a la expuesta en este capítulo en las publicaciones incluidas en los anexos C (apartados 2.3, 2.4 y 2.5) y D.*

Habitualmente, el punto de partida del proceso de determinación de una estructura magnética y su simetría es la obtención del correspondiente patrón de difracción magnética y su indexación con respecto al *setting* del grupo espacial de la fase paramagnética o grupo padre (§5.1). Esa indexación permite identificar los vectores de modulación asociados con el ordenamiento magnético, los llamados vectores de propagación de la estructura magnética. En la mayoría de los casos, el ordenamiento magnético se ajusta a un solo vector de propagación (estructura 1k). El conocimiento del grupo padre **Gp** y de ese único vector de propagación **k** (si es conmensurable) es el punto de partida del programa MAXMAGN. MAXMAGN está diseñado para estructuras magnéticas 1k; el método a seguir para analizar estructuras magnéticas "multi-k" utilizando los programas del *Bilbao Crystallographic Server* se explica más adelante (§8.1). Es importante recalcar también que en MAXMAGN se consideran únicamente estructuras magnéticas conmensurables.

Haciendo uso de la simetría magnética, el conocimiento de **Gp** y **k** puede ser utilizado para facilitar la determinación de la estructura magnética y su simetría. El MSG de la estructura magnética debe ser un subgrupo no gris del MSG gris **Gp1'** asociado a la estructura paramagnética, es decir, el subgrupo puede ser de tipo I, III o IV. Pero el conocimiento de **k** restringe adicionalmente la posible simetría de la fase magnética, permitiendo clasificar todos los subgrupos no grises de **Gp1'** en compatibles y no compatibles con **k**, de forma que estos últimos se pueden descartar. Los subgrupos compatibles con **k** pueden clasificarse de acuerdo a su jerarquía grupo-subgrupo. Los de mayor simetría, es decir, aquellos que no son subgrupos de otros subgrupos compatibles con **k**, serán llamados en adelante MSGs k-maximales. A priori, cualquiera de los MSGs compatibles con **k** pueden describir la simetría de la estructura magnética, pero en general los sistemas tienden a conservar la máxima simetría posible y por tanto los MSGs k-maximales pueden considerarse más probables como posible simetría de la estructura magnética investigada. Proporcionar estos subgrupos k-maximales es el propósito principal de MAXMAGN. Si además se especifica la estructura de la fase paramagnética, MAXMAGN proporciona, para cada uno de los MSGs k-maximales, el modelo de estructura magnética más general posible para dicha simetría. MAXMAGN permite además visualizar y descargar en formato magCIF estos modelos estructurales.

Adicionalmente, MAXMAGN proporciona otras herramientas y enlaces a otros programas del *Bilbao Crystallographic Server* relacionados con la simetría magnética, con el objetivo de analizar los diferentes modelos de simetría maximal compatibles con el **k** observado. Estas opciones permiten contrastar las diferentes simetrías alternativas posibles con otros datos experimentales de los que se pueda disponer, tales como las reglas de ausencia sistemática del patrón de difracción o las

propiedades tensoriales del material, y así poder descartar aquellas simetrías que sean incompatibles con estos datos.

Otras opciones de MAXMAGN también permiten rebajar la simetría de las estructuras a subgrupos que no son k-maximales, consultar las posiciones generales de los MSGs, transformar el *setting* de los modelos obtenidos, obtener y enumerar todas las estructuras equivalentes relacionadas por maclaje, etc.

7.1 Compatibilidad con el vector de propagación y concepto de k-maximalidad

7.1.1 *Condiciones impuestas por la compatibilidad con **k***

El conocimiento del vector de propagación **k** del ordenamiento magnético permite deducir de forma exacta la red de traslaciones y traslaciones primadas o red *black-and-white* $\mathbf{T_M}$ del MSG **M** de la estructura magnética. La red de traslaciones y traslaciones primadas $\mathbf{T_M}$ es un subgrupo del grupo de traslaciones y traslaciones primadas **T** de **Gp1'**. Si $\mathbf{t_i} \in \mathbf{T}$ es una traslación de la red de Bravais de **Gp**, se puede deducir si $\mathbf{t_i}$ o $\mathbf{t_i'}$ pertenecen a $\mathbf{T_M}$ evaluando la siguiente expresión:

$$\exp(2\pi i\, \vec{\mathbf{k}}\cdot\vec{\mathbf{t}}_\mathbf{i})\begin{cases} = 1\colon \vec{\mathbf{t}}_\mathbf{i} \in \mathbf{T_M},\ \vec{\mathbf{t}}_\mathbf{i}{}' \notin \mathbf{T_M} \\ = -1\colon \vec{\mathbf{t}}_\mathbf{i} \notin \mathbf{T_M},\ \vec{\mathbf{t}}_\mathbf{i}{}' \in \mathbf{T_M} \\ \neq 1,\ \neq -1\colon \vec{\mathbf{t}}_\mathbf{i} \notin \mathbf{T_M},\ \vec{\mathbf{t}}_i{}' \notin \mathbf{T_M} \end{cases} \quad (24)$$

Este cálculo permite obtener la red *black-and-white* $\mathbf{T_M}$ de **M**. Sólo aquellos **M** < **Gp1'** que tengan $\mathbf{T_M}$ como red *black-and-white* son compatibles con **k**. Dependiendo del tipo de **k** y de la red *black-and-white* asociada, es posible distinguir 4 casos, tal como puede verse en la Figura 31:

- i) **k** = 0. Todas las traslaciones $\mathbf{t_i} \in \mathbf{T}$ se conservan no primadas.
- ii) $\mathbf{k} \notin \mathbf{H}$, $2\mathbf{k} \in \mathbf{H}$. Todas las traslaciones $\mathbf{t_i} \in \mathbf{T}$ se conservan, la mitad primadas y la otra mitad no primadas.
- iii) $\mathbf{k} \notin \mathbf{H}$, $2\mathbf{k} \notin \mathbf{H}$, $(2n+1)\mathbf{k} \in \mathbf{H}$. Algunas traslaciones $\mathbf{t_i} \in \mathbf{T}$ no se conservan, y ninguna se conserva primada.
- iv) $\mathbf{k} \notin \mathbf{H}$, $2\mathbf{k} \notin \mathbf{H}$, $(2n)\mathbf{k} \in \mathbf{H}$. Algunas traslaciones $\mathbf{t_i} \in \mathbf{T}$ no se conservan, y las que lo hacen, la mitad son primadas y la otra mitad no primadas.

Esta clasificación nace de considerar la relación entre los diversos vectores **k** posibles y la correspondiente conservación o pérdida en la fase magnética de traslaciones o traslaciones primadas. Nótese que los vectores **k** en los casos i) y iii) tienen asociada una red *black-and-white* carente de traslaciones primadas, lo que tiene como efecto que sólo MSGs de tipo I y III serán compatibles con dichos vectores **k**; asimismo, los vectores **k** en los casos ii) y iv) tienen asociada una red *black-and-white* sólo compatible con MSGs de tipo IV. Los vectores de los casos i) y iii), por un lado, y ii) y iv) por otro, dan por tanto lugar a simetrías magnéticas descritas por MSGs del mismo

tipo. La diferencia estriba en que en los casos i) y ii), todas las traslaciones de la fase paramagnética se conservan en la fase magnética en forma de traslación pura o como traslación primada, mientras que en los casos iii) y iv), hay traslaciones que se pierden por completo y esto se traduce en la posible existencia de armónicos en la modulación del ordenamiento magnético.

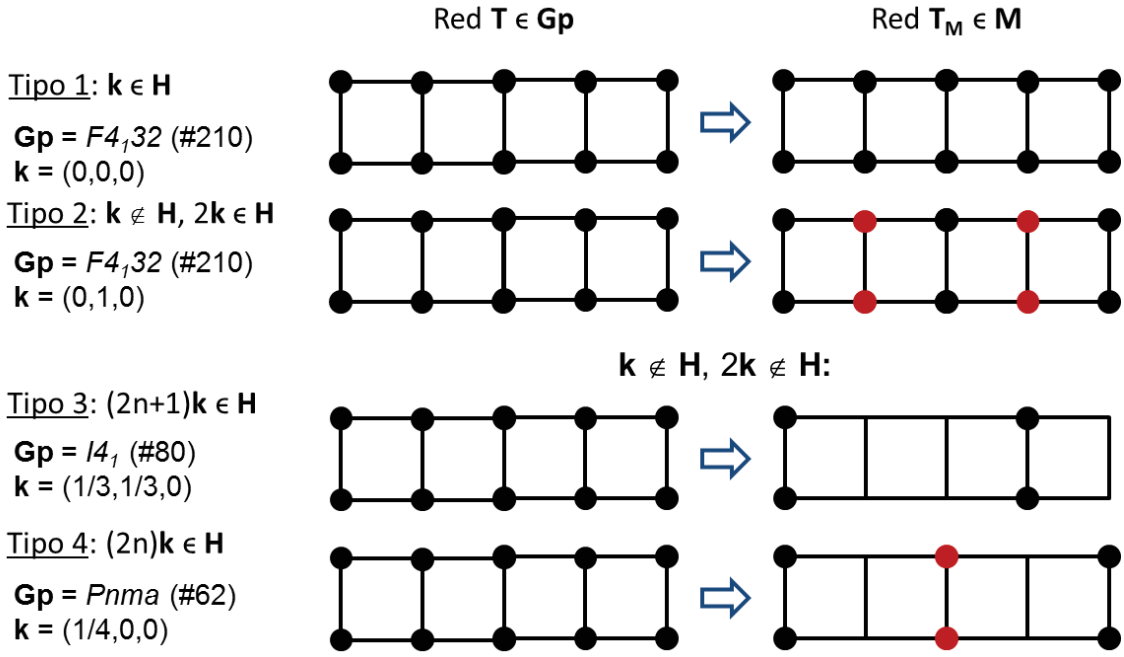

Figura 31. Tipos de vectores **k** y tipos de redes *black-and-white* asociados. Se indica un ejemplo de **Gp** y **k** para cada tipo de **k**. **H** representa al conjunto de vectores de la red recíproca de **Gp**.

Nótese que asumir que la estructura magnética es 1k implica asumir la ausencia de otros vectores de propagación de la estrella de **k** en el patrón de difracción, a excepción de -**k**, que estará presente en cualquier caso, incluso en sistemas sin centrosimetría, dado el carácter real de la modulación magnética. En muchos casos, **k** y -**k** son equivalentes (su diferencia es un vector de la red recíproca de **Gp1'**).

El criterio que permite evaluar la compatibilidad una operación $\{\boldsymbol{R},\tau|\mathbf{t}\}$ de **Gp1'** con **k** y con la red *black-and-white* correspondiente es que cumpla:

$$\mathbf{k}\cdot\boldsymbol{R}=\pm\mathbf{k}+\mathbf{H} \qquad (25)$$

donde **H** es un vector de la red recíproca de **Gp1'**. Los elementos que cumplen esta condición son aquellos que dejan invariante el conjunto de vectores {**k**, -**k**}. El subgrupo de operaciones de simetría de **Gp1'** que cumplen la condición (25) forman el llamado grupo pequeño extendido o *extended little group* $\mathbf{G_{k,-k}}$. $\mathbf{G_{k,-k}}$ es un grupo gris, ya que la operación de inversión temporal cumple con (25). El MSG **M** que describe la simetría de la estructura es necesariamente un subgrupo de $\mathbf{G_{k,-k}}$, y su simetría puntual **m** es un subgrupo del grupo puntual asociado a $\mathbf{G_{k,-k}}$, el *little co-group* $\mathbf{g_{k,-k}}$, estando descartado cualquier otro MSG **M** cuyo grupo puntual **m** no sea subgrupo de $\mathbf{g_{k,-k}}$. Por tanto, como consecuencia de la incompatibilidad con **k**, la simetría puntual de la fase magnética puede ser menor que la de la fase paramagnética.

Nótese que la condición (25) no es suficiente para asegurar que una operación de simetría de **Gp1'** sea compatible con **k** y con la red *black-and-white*. La razón es que algunos ejes helicoidales y planos de deslizamiento, si se conservan en la fase magnética, fuerzan la presencia de ciertas traslaciones o traslaciones primadas en el MSG de la fase magnética que pueden ser incompatibles con **k**, aun cuando cumplan con la condición (24). Esta incompatibilidad se describe en detalle en §D.2.

Por otro lado, de acuerdo con la ecuación (24), el vector de propagación **k** es un vector de la red recíproca de **M**. Es decir, si (***P***, **p**) es la matriz de transformación al *setting* estándar (en adelante, siempre en BNS) que define el subgrupo **M** (§4.1.2), debe cumplirse que:

$$\mathbf{k} \cdot \boldsymbol{P} = \mathbf{H}_{\mathbf{M}} \tag{26}$$

donde $\mathbf{H_M}$ es un vector de la red recíproca de **M** en *setting* estándar.

En conclusión, la exigencia conjunta de las condiciones mencionadas a las operaciones de simetría de **Gp1'** permite clasificar todos los subgrupos de **Gp1'** en compatibles e incompatibles con **k**, quedando estos últimos descartados.

7.1.2 *Tendencia a la maximalidad de la simetría magnética: k-maximalidad*

Existen tanto razones físicas (§C2.3) como evidencia fenomenológica (§E.5, §9) que implican que el MSG de una estructura magnética tiende a ser el de mayor simetría posible dentro del conjunto de todos los MSGs compatibles con los datos experimentales de los que se tenga constancia. Es decir, existe una tendencia a la maximalidad, en sentido amplio, en el MSG de las estructuras magnéticas, lo que implica que de todos los modelos de estructura magnética que son posibles a priori, los de mayor simetría son los primeros que deberían ser cotejados con los datos experimentales, debiéndose explorar modelos con simetrías menores sólo en caso de que los de mayor simetría resulten descartados.

Por esta razón, conocido **k**, el primer paso en el proceso de determinación de estructuras magnéticas y su simetría es la obtención de los subgrupos k-maximales de **Gp1'**, es decir, aquellos MSGs del conjunto de subgrupos no grises del grupo gris de la fase paramagnética compatibles con **k** que sean maximales, es decir, que no tengan supergrupos que pertenezcan a dicho conjunto. Los datos estadísticos provenientes de la evidencia fenomenológica recogida gracias a la creación de MAGNDATA (§9) indican que aproximadamente el 75% de las estructuras magnéticas conmensurables son k-maximales, por lo que, en general, al investigar una estructura magnética desconocida, es altamente probable que se ajuste a uno de los modelos estructurales de simetría k-maximal.

No obstante, no todas las estructuras magnéticas son k-maximales; aparte de **k**, existen otros datos y circunstancias que, de ser conocidos y considerados, pueden

conducir al descarte de todos los subgrupos k-maximales. En caso de que todos los MSGs k-maximales queden descartados es necesario obtener modelos correspondientes a subgrupos de los MSGs k-maximales. Es por esto que MAXMAGN permite descender a subgrupos de los grupos k-maximales. Subgrupos no k-maximales también pueden consultarse por medio de otros programas (§8.1).

MAXMAGN obtiene los subgrupos k-maximales haciendo uso internamente del programa K-SUBGROUPSMAG, que proporciona una lista de todos los subgrupos de **Gp1'** compatibles con **k**, estableciendo también la jerarquía grupo-subgrupo que existe entre ellos.

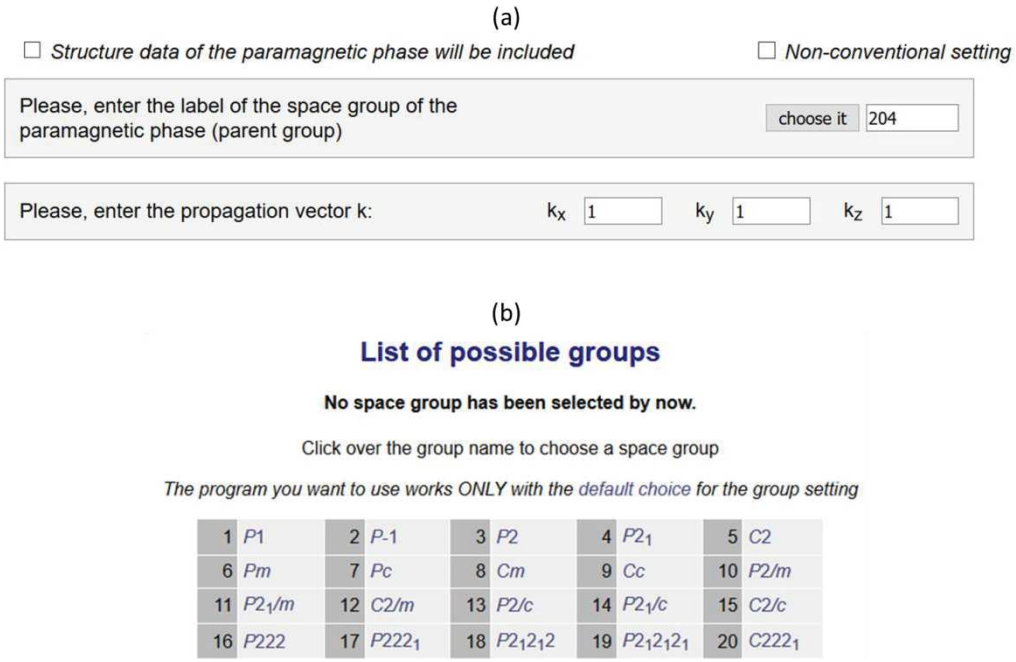

Figura 32. (a) Página principal del programa MAXMAGN. (b) Página de selección del grupo espacial de la fase paramagnética de MAXMAGN.

7.2 Programa MAXMAGN: obtención de subgrupos k-maximales

En su modo más simple, el programa MAXMAGN (http://www.cryst.ehu.es/cgi-bin/cryst/programs/msglist2.pl) permite obtener los subgrupos k-maximales que se obtienen a partir de un grupo espacial de la fase paramagnética o grupo padre **Gp** en *setting* estándar y un vector de propagación **k** determinados. Tal es el caso de la estructura magnética del $LaMn_3Cr_4O_{12}$ (caso #1.156 de MAGNDATA (§9)) [40], cuyo grupo padre **Gp** es *Im-3* (#204) en *setting* estándar, y su vector de propagación es **k** = (1, 1, 1). La página principal de MAXMAGN (Figura 32(a)) permite introducir estos datos. Se puede seleccionar un **Gp** bien introduciendo su etiqueta correspondiente (204) en el formulario indicado, bien haciendo clic en el botón "*choose it*", lo que proporciona una lista de los 230 grupos espaciales (Figura 32(b)) y permite cargar el grupo elegido en la página principal de MAXMAGN.

Tras hacer clic en el botón "*Submit*", MAXMAGN proporciona el listado de MSGs k-maximales correspondientes al **Gp** y **k** introducidos (Figura 33). Por razones prácticas, los MSGs proporcionados por MAXMAGN están siempre en *setting* tipo BNS (§4.1.1).

Maximal magnetic space groups for the parent space group 204 (*Im*-3) and the propagation vector k = (1, 1, 1)

N	Group (BNS)	Transformation matrix	General positions	Properties
1	P_Ia-3 (#201.21) Go to a subgroup	$\begin{pmatrix} 1 & 0 & 0 & 1/4 \\ 0 & 1 & 0 & 1/4 \\ 0 & 0 & 1 & 1/4 \end{pmatrix}$ Alternatives (domain-related)	Show	*Systematic absences* MAGNEXT *Tensor properties* MTENSOR
2	P_Im-3 (#200.17) Go to a subgroup	$\begin{pmatrix} 1 & 0 & 0 & 0 \\ 0 & 1 & 0 & 0 \\ 0 & 0 & 1 & 0 \end{pmatrix}$ Alternatives (domain-related)	Show	*Systematic absences* MAGNEXT *Tensor properties* MTENSOR
3	P_Immn (#59.416) Go to a subgroup	$\begin{pmatrix} 0 & 0 & -1 & 1/4 \\ 0 & 1 & 0 & 1/4 \\ 1 & 0 & 0 & 1/4 \end{pmatrix}$ Alternatives (domain-related)	Show	*Systematic absences* MAGNEXT *Tensor properties* MTENSOR
4	P_Innm (#58.404) Go to a subgroup	$\begin{pmatrix} 0 & 0 & -1 & 0 \\ 0 & 1 & 0 & 0 \\ 1 & 0 & 0 & 0 \end{pmatrix}$ Alternatives (domain-related)	Show	*Systematic absences* MAGNEXT *Tensor properties* MTENSOR

Figura 33. Subgrupos k-maximales del grupo *Im-3* (#204) para el vector **k** = (1, 1, 1), obtenidos con MAXMAGN.

Habitualmente, el conjunto de subgrupos k-maximales proporcionado por MAXMAGN no es muy numeroso, de forma que el número de modelos de estructura magnética de simetría k-maximal posibles a priori es reducido. En el ejemplo utilizado, tan sólo hay 4 subgrupos k-maximales posibles, y por lo tanto, 4 posibles modelos de estructura magnética no equivalentes de simetría k-maximal. Los subgrupos k-maximales proporcionados por MAXMAGN están agrupados por clase de conjugación, indicándose tan sólo un representante por clase de conjugación en el listado de la Figura 33. Para cada uno de estos representantes se indican la etiqueta y símbolo del MSG, así como la matriz de transformación entre el *setting* del grupo padre y el estándar del MSG, matriz que define el subgrupo (§4.1.2). Además, se proporcionan diversos botones que permiten utilizar tanto las diversas utilidades auxiliares de MAXMAGN como los programas externos accesibles desde MAXMAGN (§7.3, §7.4).

Los botones incluidos en la columna "*General positions*" del listado de la Figura 33 permiten consultar las posiciones generales correspondientes a cada uno de los MSG k-maximales. Éstas están expresadas tanto en el *setting* estándar del MSG como en el *setting* de trabajo, es decir, el *setting* en el que está expresado el subgrupo k-maximal (en este caso, coincide con el *setting* del grupo padre). Estas posiciones generales (Figura 34) están indicadas en formato *x*,*y*,*z*, formato matricial y notación de Seitz (ver §4.3). Encima de la tabla de posiciones generales se indica la matriz de transformación entre el *setting* del grupo padre y el *setting* de trabajo. Además, se incluye un enlace

que permite obtener, en texto plano, listas tanto del conjunto completo de posiciones generales del MSG (expresadas en el *setting* de trabajo) como de un conjunto de generadores (no minimal, en general), incluyendo o no las transformaciones de los momentos según se requiera. Estas listas facilitan la copia y el uso posterior en otros programas de estas posiciones generales.

General positions of the magnetic space group *P_In-3* (#201.21) in the basis (a, b, c; 0, 0, 0) of the parent space group 204 (*Im*-3)

Transformation matrix:

$$\begin{pmatrix} 1 & 0 & 0 & 1/4 \\ 0 & 1 & 0 & 1/4 \\ 0 & 0 & 1 & 1/4 \end{pmatrix}$$

General positions

[Get symmetry cards (parent-like setting (a, b, c; 0, 0, 0)) in plain text format]

	Standard setting			Parent-like setting (a, b, c; 0, 0, 0)		
N	(x,y,z) form	Matrix form	Seitz notation	(x,y,z) form	Matrix form	Seitz notation
1	x,y,z,+1 m_x,m_y,m_z	$\begin{pmatrix} 1 & 0 & 0 & 0 \\ 0 & 1 & 0 & 0 \\ 0 & 0 & 1 & 0 \end{pmatrix}$	{ 1 | 0 }	x,y,z,+1 m_x,m_y,m_z	$\begin{pmatrix} 1 & 0 & 0 & 0 \\ 0 & 1 & 0 & 0 \\ 0 & 0 & 1 & 0 \end{pmatrix}$	{ 1 | 0 }
2	x,-y-1/2,-z-1/2,+1 $m_x,-m_y,-m_z$	$\begin{pmatrix} 1 & 0 & 0 & 0 \\ 0 & -1 & 0 & -1/2 \\ 0 & 0 & -1 & -1/2 \end{pmatrix}$	{ 2_{100} | 0 -1/2 -1/2 }	x,-y,-z,+1 $m_x,-m_y,-m_z$	$\begin{pmatrix} 1 & 0 & 0 & 0 \\ 0 & -1 & 0 & 0 \\ 0 & 0 & -1 & 0 \end{pmatrix}$	{ 2_{100} | 0 }
3	-x-1/2,y,-z-1/2,+1 $-m_x,m_y,-m_z$	$\begin{pmatrix} -1 & 0 & 0 & -1/2 \\ 0 & 1 & 0 & 0 \\ 0 & 0 & -1 & -1/2 \end{pmatrix}$	{ 2_{010} | -1/2 0 -1/2 }	-x,y,-z,+1 $-m_x,m_y,-m_z$	$\begin{pmatrix} -1 & 0 & 0 & 0 \\ 0 & 1 & 0 & 0 \\ 0 & 0 & -1 & 0 \end{pmatrix}$	{ 2_{010} | 0 }
4	-x-1/2,-y-1/2,z,+1 $-m_x,-m_y,m_z$	$\begin{pmatrix} -1 & 0 & 0 & -1/2 \\ 0 & -1 & 0 & -1/2 \\ 0 & 0 & 1 & 0 \end{pmatrix}$	{ 2_{001} | -1/2 -1/2 0 }	-x,-y,z,+1 $-m_x,-m_y,m_z$	$\begin{pmatrix} -1 & 0 & 0 & 0 \\ 0 & -1 & 0 & 0 \\ 0 & 0 & 1 & 0 \end{pmatrix}$	{ 2_{001} | 0 }
5	z,x,y,+1 m_z,m_x,m_y	$\begin{pmatrix} 0 & 0 & 1 & 0 \\ 1 & 0 & 0 & 0 \\ 0 & 1 & 0 & 0 \end{pmatrix}$	{ 3^+_{111} | 0 }	z,x,y,+1 m_z,m_x,m_y	$\begin{pmatrix} 0 & 0 & 1 & 0 \\ 1 & 0 & 0 & 0 \\ 0 & 1 & 0 & 0 \end{pmatrix}$	{ 3^+_{111} | 0 }
6	y,z,x,+1 m_y,m_z,m_x	$\begin{pmatrix} 0 & 1 & 0 & 0 \\ 0 & 0 & 1 & 0 \\ 1 & 0 & 0 & 0 \end{pmatrix}$	{ 3^-_{111} | 0 }	y,z,x,+1 m_y,m_z,m_x	$\begin{pmatrix} 0 & 1 & 0 & 0 \\ 0 & 0 & 1 & 0 \\ 1 & 0 & 0 & 0 \end{pmatrix}$	{ 3^-_{111} | 0 }

Figura 34. Listado de posiciones generales del MSG *P_In-3* (#201.21), subgrupo k-maximal del grupo *Im-3* (#204) para el vector **k** = (1, 1, 1). A la izquierda se indican las operaciones de simetría del MSG en *setting* estándar BNS; a la derecha, en el *setting* de trabajo, que coincide con el del grupo padre en este caso. Obtenido con MAXMAGN.

En el ejemplo utilizado, el *setting* de trabajo del MSG de la Figura 34 coincide con el *setting* del grupo padre, por lo que la matriz de transformación que figura encima de la tabla de posiciones generales coincide con la indicada en el listado de subgrupos k-maximales (Figura 33). No obstante, en un caso general, el *setting* del grupo padre puede no ser válido para expresar los MSGs proporcionados por MAXMAGN, pues alguna de las traslaciones básicas del grupo padre podría no pertenecer al MSG (cosa que, de hecho, sucede siempre que el vector de propagación tenga componentes fraccionarias); en estos casos es necesario expresar el subgrupo k-maximal en un *setting* de trabajo alternativo.

Debido a que por razones experimentales es deseable que este *setting* sea muy parecido al *setting* del grupo padre, el *setting* de trabajo elegido por defecto por

MAXMAGN para expresar los MSGs k-maximales es el llamado "*setting parent-like*". Este *setting*, una supercelda del *setting* del grupo padre, es el *setting* válido más cercano al mismo. Se forma eligiendo como traslaciones básicas las traslaciones según *x*, *y*, y *z* más pequeñas de entre aquellas del grupo padre que también forman parte del MSG.

Maximal magnetic space groups for the parent space group 139 (*I4/mmm*) and the propagation vector k = (1/2, 1/2, 0)

N	Group (BNS)	Transformation matrix	General positions	Properties
1	C_Acca (#68.520) Go to a subgroup	$\begin{pmatrix} 0 & -1 & 1 & 0 \\ 0 & 1 & 1 & 1/2 \\ -1 & 0 & 0 & 0 \end{pmatrix}$ Alternatives (domain-related)	Show	Systematic absences MAGNEXT Tensor properties MTENSOR
2	C_Amma (#67.510) Go to a subgroup	$\begin{pmatrix} 0 & -1 & 1 & 0 \\ 0 & 1 & 1 & 1/2 \\ -1 & 0 & 0 & 0 \end{pmatrix}$ Alternatives (domain-related)	Show	Systematic absences MAGNEXT Tensor properties MTENSOR
3	C_Accm (#66.500) Go to a subgroup	$\begin{pmatrix} 0 & -1 & 1 & 7/4 \\ 0 & 1 & 1 & 1/4 \\ -1 & 0 & 0 & 1/4 \end{pmatrix}$ Alternatives (domain-related)	Show	Systematic absences MAGNEXT Tensor properties MTENSOR
4	C_Ammm (#65.490) Go to a subgroup	$\begin{pmatrix} 0 & -1 & 1 & 0 \\ 0 & 1 & 1 & 0 \\ -1 & 0 & 0 & 0 \end{pmatrix}$ Alternatives (domain-related)	Show	Systematic absences MAGNEXT Tensor properties MTENSOR
5	C_Amca (#64.480) Go to a subgroup	$\begin{pmatrix} 0 & -1 & 1 & 0 \\ 0 & 1 & 1 & 0 \\ -1 & 0 & 0 & 0 \end{pmatrix}$ Alternatives (domain-related)	Show	Systematic absences MAGNEXT Tensor properties MTENSOR
6	C_Amca (#64.480) Go to a subgroup	$\begin{pmatrix} 1 & 0 & -1 & 0 \\ -1 & 0 & -1 & 0 \\ 0 & 1 & 0 & 0 \end{pmatrix}$ Alternatives (domain-related)	Show	Systematic absences MAGNEXT Tensor properties MTENSOR
7	C_Amcm (#63.468) Go to a subgroup	$\begin{pmatrix} 1 & 0 & -1 & 1/4 \\ -1 & 0 & -1 & 1/4 \\ 0 & 1 & 0 & 1/4 \end{pmatrix}$ Alternatives (domain-related)	Show	Systematic absences MAGNEXT Tensor properties MTENSOR
8	C_Amcm (#63.468) Go to a subgroup	$\begin{pmatrix} 0 & -1 & 1 & 0 \\ 0 & 1 & 1 & 1/2 \\ -1 & 0 & 0 & 0 \end{pmatrix}$ Alternatives (domain-related)	Show	Systematic absences MAGNEXT Tensor properties MTENSOR

Figura 35. Subgrupos k-maximales del grupo *I4/mmm* (#139) para el vector **k** = (1/2, 1/2, 0), obtenidos con MAXMAGN.

Para ilustrar esto, sirva como ejemplo el caso del $CaFe_2As_2$ (caso #1.52 de MAGNDATA (§9)) [41], cuyo grupo padre **Gp** es *I4/mmm* (#139) en *setting* estándar y cuyo vector de propagación es **k** = (1/2, 1/2, 0). Para este caso (Figuras 35 y 36), las traslaciones {1|1,0,0} y {1|0,1,0} del grupo padre no forman parte de cualquier subgrupo k-maximal (Figura 36), por lo que el *setting* de trabajo establecido por defecto por MAXMAGN es el *setting parent-like* (2**a**, 2**b**, **c**), siendo (**a**, **b**, **c**) el *setting* del grupo padre. Tal y como puede verse en las Figuras 35 y 36, esto implica que la matriz de transformación indicada en el listado de subgrupos k-maximales (Figura 35) y la matriz indicada en el listado de posiciones generales (Figura 36) no coinciden, pues la primera es la transformación entre el *setting* del grupo padre y el *setting* estándar del MSG, mientras que la segunda es la transformación entre el *setting parent-like* y el *setting* estándar del MSG.

General positions of the magnetic space group $C_A mca$ (#64.480) in the basis (2a, 2b, c; 0, 0, 0) of the parent space group 139 (*I4/mmm*)

Transformation matrix:

$$\begin{pmatrix} 0 & -1/2 & 1/2 & 0 \\ 0 & 1/2 & 1/2 & 0 \\ -1 & 0 & 0 & 0 \end{pmatrix}$$

General positions

[Get symmetry cards (parent-like setting (2a, 2b, c; 0, 0, 0)) in plain text format]

	Standard setting			Parent-like setting (2a, 2b, c; 0, 0, 0)		
N	(x,y,z) form	Matrix form	Seitz notation	(x,y,z) form	Matrix form	Seitz notation
1	x,y,z,+1 m_x,m_y,m_z	$\begin{pmatrix} 1 & 0 & 0 & 0 \\ 0 & 1 & 0 & 0 \\ 0 & 0 & 1 & 0 \end{pmatrix}$	{ 1 | 0 }	x,y,z,+1 m_x,m_y,m_z	$\begin{pmatrix} 1 & 0 & 0 & 0 \\ 0 & 1 & 0 & 0 \\ 0 & 0 & 1 & 0 \end{pmatrix}$	{ 1 | 0 }
2	x,-y,-z,+1 $m_x,-m_y,-m_z$	$\begin{pmatrix} 1 & 0 & 0 & 0 \\ 0 & -1 & 0 & 0 \\ 0 & 0 & -1 & 0 \end{pmatrix}$	{ 2_{100} | 0 }	-x,-y,z,+1 $-m_x,-m_y,m_z$	$\begin{pmatrix} -1 & 0 & 0 & 0 \\ 0 & -1 & 0 & 0 \\ 0 & 0 & 1 & 0 \end{pmatrix}$	{ 2_{001} | 0 }
3	-x-1/2,y,-z+1/2,+1 $-m_x,m_y,-m_z$	$\begin{pmatrix} -1 & 0 & 0 & -1/2 \\ 0 & 1 & 0 & 0 \\ 0 & 0 & -1 & 1/2 \end{pmatrix}$	{ 2_{010} | -1/2 0 1/2 }	-y+1/4,-x+1/4,-z+1/2,+1 $-m_y,-m_x,-m_z$	$\begin{pmatrix} 0 & -1 & 0 & 1/4 \\ -1 & 0 & 0 & 1/4 \\ 0 & 0 & -1 & 1/2 \end{pmatrix}$	{ $2_{1\text{-}10}$ | 1/4 1/4 1/2 }
4	-x-1/2,-y,z+1/2,+1 $-m_x,-m_y,m_z$	$\begin{pmatrix} -1 & 0 & 0 & -1/2 \\ 0 & -1 & 0 & 0 \\ 0 & 0 & 1 & 1/2 \end{pmatrix}$	{ 2_{001} | -1/2 0 1/2 }	y+1/4,x+1/4,-z+1/2,+1 $m_y,m_x,-m_z$	$\begin{pmatrix} 0 & 1 & 0 & 1/4 \\ 1 & 0 & 0 & 1/4 \\ 0 & 0 & -1 & 1/2 \end{pmatrix}$	{ 2_{110} | 1/4 1/4 1/2 }
5	-x,-y,-z,+1 m_x,m_y,m_z	$\begin{pmatrix} -1 & 0 & 0 & 0 \\ 0 & -1 & 0 & 0 \\ 0 & 0 & -1 & 0 \end{pmatrix}$	{ -1 | 0 }	-x,-y,-z,+1 m_x,m_y,m_z	$\begin{pmatrix} -1 & 0 & 0 & 0 \\ 0 & -1 & 0 & 0 \\ 0 & 0 & -1 & 0 \end{pmatrix}$	{ -1 | 0 }
6	-x,y,z,+1 $m_x,-m_y,-m_z$	$\begin{pmatrix} -1 & 0 & 0 & 0 \\ 0 & 1 & 0 & 0 \\ 0 & 0 & 1 & 0 \end{pmatrix}$	{ m_{100} | 0 }	x,y,-z,+1 $-m_x,-m_y,m_z$	$\begin{pmatrix} 1 & 0 & 0 & 0 \\ 0 & 1 & 0 & 0 \\ 0 & 0 & -1 & 0 \end{pmatrix}$	{ m_{001} | 0 }

Figura 36. Listado de posiciones generales del MSG $C_A mca$ (#64.480), subgrupo k-maximal del grupo *I4/mmm* (#139) para el vector **k** = (1/2, 1/2, 0). Obtenido con MAXMAGN.

7.2.1 *Grupo padre en setting no estándar*

Adicionalmente, MAXMAGN permite también trabajar con grupos padre expresados en un *setting* no estándar, para permitir trabajar con facilidad con las numerosas estructuras publicadas que están descritas en un *setting* no estándar. Para indicar que se desea trabajar en un *setting* no estándar, es necesario seleccionar la casilla "*Non-conventional setting*" en la página principal de MAXMAGN (Figura 32(a)). Cuando esta opción está activa, MAXMAGN muestra una pantalla que permite introducir el grupo padre indicando un conjunto de generadores en formato *x*,*y*,*z* (Figura 37). Si en la pantalla principal se introdujo un grupo padre en la correspondiente casilla, éste será ignorado. MAXMAGN hace uso internamente del programa IDENTIFY GROUP del *Bilbao Crystallographic Server* (http://www.cryst.ehu.es/cgi-bin/cryst/programs/checkgr.pl?tipog=gesp) para identificar el grupo padre a partir de los generadores introducidos. El tipo de grupo padre y la transformación al *setting* estándar se indican en el listado de subgrupos k-maximales proporcionado por MAXMAGN, tal y como se muestra en la Figura 38 para el caso de la estructura magnética del La_2LiRuO_6 (caso #0.148 de MAGNDATA (§9)) [42], cuyo **Gp** es $P2_1/n$ (#14), o lo que es lo mismo, $P2_1/c$ (#14) (**a**, **b**, **a**+**c**) (ésta es la transformación al *setting* estándar), y cuyo vector de propagación es **k** = (0, 0, 0).

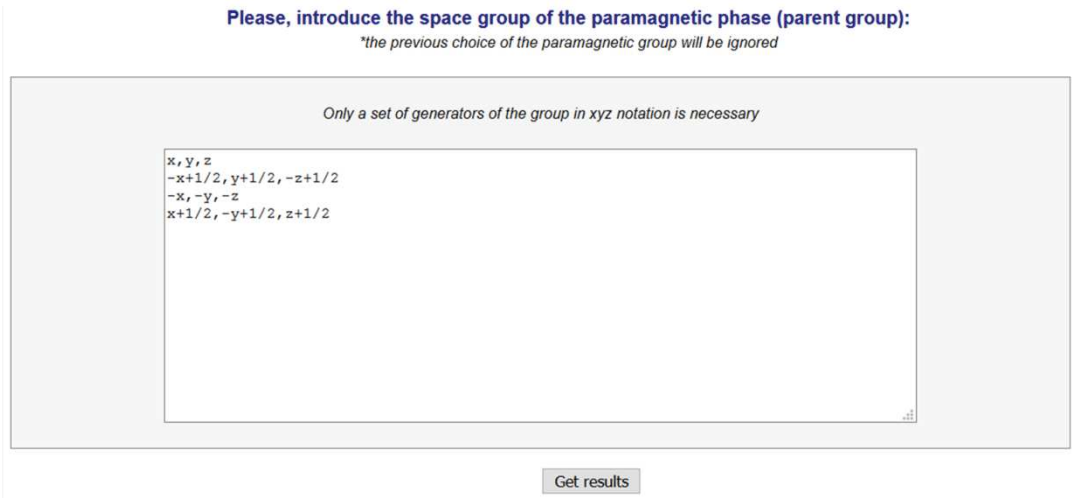

Figura 37. Formulario de introducción en MAXMAGN de un grupo padre en un *setting* no estándar.

Maximal magnetic space groups for the parent space group 14 ($P2_1/c$) and the propagation vector k = (0, 0, 0)

Parent space group in non-standard setting (a, b, a+c; 0, 0, 0)

N	Group (BNS)	Transformation matrix	General positions	Properties
1	$P2_1/c'$ (#14.79) Go to a subgroup	$\begin{pmatrix} 1 & 0 & 1 & 0 \\ 0 & 1 & 0 & 0 \\ 0 & 0 & 1 & 0 \end{pmatrix}$ Alternatives (domain-related)	Show	*Systematic absences* MAGNEXT *Tensor properties* MTENSOR
2	$P2_1/c'$ (#14.78) Go to a subgroup	$\begin{pmatrix} 1 & 0 & 1 & 0 \\ 0 & 1 & 0 & 0 \\ 0 & 0 & 1 & 0 \end{pmatrix}$ Alternatives (domain-related)	Show	*Systematic absences* MAGNEXT *Tensor properties* MTENSOR
3	$P2_1/c$ (#14.77) Go to a subgroup	$\begin{pmatrix} 1 & 0 & 1 & 0 \\ 0 & 1 & 0 & 0 \\ 0 & 0 & 1 & 0 \end{pmatrix}$ Alternatives (domain-related)	Show	*Systematic absences* MAGNEXT *Tensor properties* MTENSOR
4	$P2_1/c$ (#14.75) Go to a subgroup	$\begin{pmatrix} 1 & 0 & 1 & 0 \\ 0 & 1 & 0 & 0 \\ 0 & 0 & 1 & 0 \end{pmatrix}$ Alternatives (domain-related)	Show	*Systematic absences* MAGNEXT *Tensor properties* MTENSOR

Figura 38. Subgrupos k-maximales del grupo $P2_1/n$ ó $P2_1/c$ (**a**, **b**, **a+c**) (#14) para el vector **k** = (0, 0, 0), obtenidos con MAXMAGN. Sobre la tabla se indica que el grupo padre está en *setting* no estándar, y se indica la transformación al *setting* estándar.

7.3 Programa MAXMAGN: Modelos de estructura magnética con simetría k-maximal

Además de **Gp** y **k**, MAXMAGN permite especificar la estructura cristalina de la fase paramagnética por medio de la introducción de un archivo cristalográfico en formato CIF. De esta forma, se pueden obtener los modelos de estructura magnética compatibles con la simetría magnética de los subgrupos k-maximales proporcionados por MAXMAGN, así como utilizar desde MAXMAGN otros programas relacionados con

la simetría magnética para obtener información adicional que permita facilitar la determinación de la estructura magnética y su simetría.

Para introducir la estructura cristalina de la fase paramagnética, es necesario seleccionar la casilla "*Structure data of the paramagnetic phase will be included*" en la página principal de MAXMAGN (Figura 32(a)). Al hacerlo, se accede a una pantalla donde debe introducirse la estructura cristalina paramagnética, subiendo un archivo CIF que la contenga (Figura 39(a)). Tras introducir el archivo CIF y hacer clic en el botón "*Upload the file*", se muestra una pantalla con los átomos de la estructura procedentes del archivo CIF (Figura 39(b)). En dicha pantalla, debe seleccionarse el o los átomos que MAXMAGN deberá considerar magnéticos (debe seleccionarse al menos uno).

(a)

Parent paramagnetic structure cif file

Option 1: Please submit a structure file (CIF format):

Examinar... No se ha seleccionado ningún archivo. Upload the file

No space group provided. The space group indicated in the cif file will be taken.

(b)

Parent phase structure data: Magnetic Atoms

Parent space group: 204 (*Im*-3)
Lattice parameters (Angstroms and degrees): a=7.39800, b=7.39800, c=7.39800, alpha=90.0000, beta=90.0000, gamma=90.0000

Atoms: Please select the magnetic ones

N	Atom name	Atom type	Wyckoff Position	Coordinates	Magnetic?
1	La1	La	2a	0.00000 0.00000 0.00000	☐
2	Mn1	Mn	6b	0.00000 0.50000 0.50000	☑
3	Cr1	Cr	8c	0.25000 0.25000 0.25000	☑
4	O1	O	24g	0.00000 0.31040 0.17710	☐

Submit

Figura 39. Formularios de MAXMAGN para introducir (a) la estructura de la fase paramagnética por medio de un archivo CIF y (b) para seleccionar los átomos que se considerarán magnéticos. Los datos que figuran corresponden a la estructura magnética del $LaMn_3Cr_4O_{12}$ [40].

Debe tenerse en cuenta que de las diversas formas en que el grupo padre puede introducirse en MAXMAGN, el programa escoge, por orden de preferencia, el grupo padre correspondiente a los generadores del mismo incluidos en el archivo CIF (si se incluye), el grupo padre en *setting* estándar indicado en dicho CIF por medio del *tag* correspondiente (si dicho *tag* existe), y el elegido en el formulario de la página principal de MAXMAGN (si se eligió uno). Además, siempre que se desee introducir la estructura de la fase paramagnética en *setting* no estándar debe seleccionarse la casilla "*Non-conventional setting*" en la página principal de MAXMAGN (Figura 32(a)), pues de lo contrario el programa interpretará que la estructura está en *setting* estándar, incluso en el caso de que las operaciones del CIF introducido estén expresadas en un *setting* no estándar.

Excepcionalmente, puede introducirse también la estructura paramagnética utilizando los formularios a tal efecto que MAXMAGN provee (Figuras 40(a) y 40(b)); esta opción se muestra sólo en caso de que la casilla "*Non-conventional setting*" no esté seleccionada y se haya introducido un grupo padre en el formulario de la página principal de MAXMAGN.

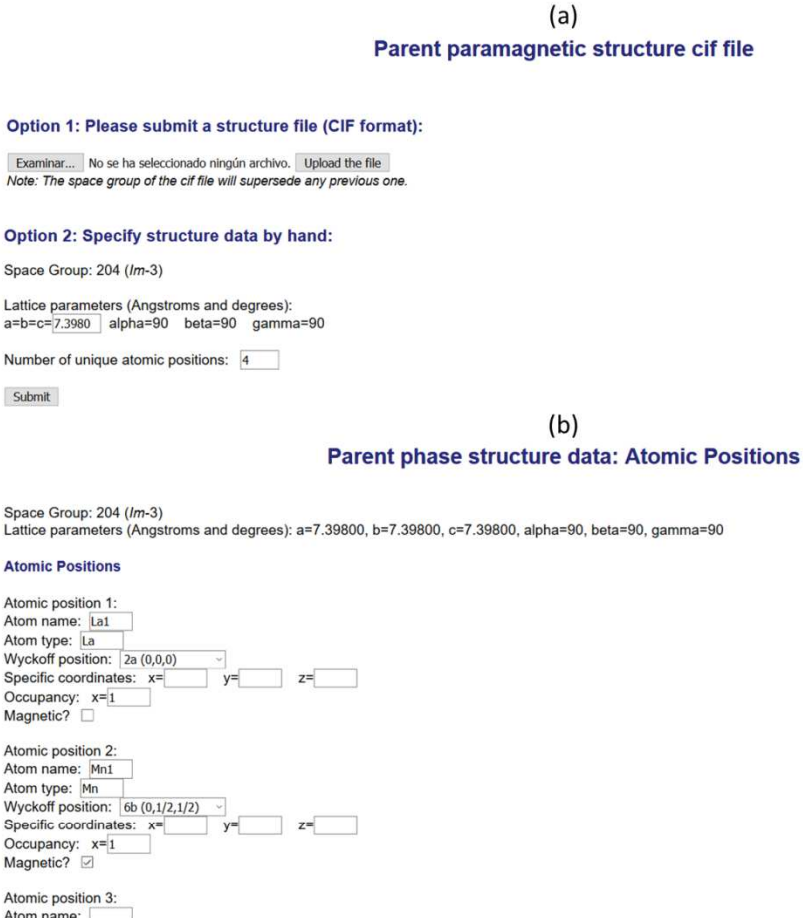

Figura 40. Formularios de MAXMAGN para introducir la estructura de la fase paramagnética: (a) parámetros de red y número de átomos independientes. (b) Átomos, posiciones atómicas, posiciones de Wyckoff, ocupación y especificación de qué átomos son magnéticos. Los datos que figuran corresponden a la estructura magnética del $LaMn_3Cr_4O_{12}$ [40].

Cuando la estructura paramagnética es especificada, MAXMAGN proporciona una lista de subgrupos k-maximales (Figura 41) similar a la dada cuando no se especifica la estructura de la fase paramagnética (Figuras 33, 35 y 38), con dos diferencias. Por un lado, aparece en la tabla una columna adicional titulada "*Magnetic Structure*", que permite consultar el modelo de estructura magnética correspondiente a cada MSG. Por otro lado, el fondo de las entradas de la tabla correspondientes a algunos subgrupos k-maximales aparece de color oscuro, indicando que para esos grupos, los momentos magnéticos de los átomos magnéticos están permitidos, es decir, podrían tener componentes de valor no nulo compatibles con la simetría magnética. Dicho de otra manera, aquellos que no aparecen en fondo oscuro son MSGs cuya simetría no permite la existencia de momentos no nulos en las WPs donde se ubican los átomos magnéticos y por tanto quedan descartados. Para el caso de la estructura magnética

del La_2LiRuO_6 (Figuras 38 y 41), puede verse que la especificación de la estructura de la fase paramagnética permite descartar los subgrupos k-maximales *P2₁/c'* (#14.78) y *P2₁'/c* (#14.77), permaneciendo los subgrupos *P2₁'/c'* (#14.79) y *P2₁/c* (#14.75) como únicos subgrupos k-maximales posibles.

Maximal magnetic space groups for the parent space group 14 (*P2₁/c*) and the propagation vector k = (0, 0, 0)

Parent space group in non-standard setting (a, b, a+c; 0, 0, 0)

Maximal subgroups which allow non-zero magnetic moments for at least one atom are coloured

N	Group (BNS)	Transformation matrix	General positions	Properties	Magnetic structure
1	*P2₁'/c'* (#14.79) Go to a subgroup	$\begin{pmatrix} 1 & 0 & 1 & 0 \\ 0 & 1 & 0 & 0 \\ 0 & 0 & 1 & 0 \end{pmatrix}$ Alternatives (domain-related)	Show	*Systematic absences* MAGNEXT *Tensor properties* MTENSOR	Show
2	*P2₁/c'* (#14.78) Go to a subgroup	$\begin{pmatrix} 1 & 0 & 1 & 0 \\ 0 & 1 & 0 & 0 \\ 0 & 0 & 1 & 0 \end{pmatrix}$ Alternatives (domain-related)	Show	*Systematic absences* MAGNEXT *Tensor properties* MTENSOR	Show
3	*P2₁'/c* (#14.77) Go to a subgroup	$\begin{pmatrix} 1 & 0 & 1 & 0 \\ 0 & 1 & 0 & 0 \\ 0 & 0 & 1 & 0 \end{pmatrix}$ Alternatives (domain-related)	Show	*Systematic absences* MAGNEXT *Tensor properties* MTENSOR	Show
4	*P2₁/c* (#14.75) Go to a subgroup	$\begin{pmatrix} 1 & 0 & 1 & 0 \\ 0 & 1 & 0 & 0 \\ 0 & 0 & 1 & 0 \end{pmatrix}$ Alternatives (domain-related)	Show	*Systematic absences* MAGNEXT *Tensor properties* MTENSOR	Show

Figura 41. Subgrupos k-maximales correspondientes a la estructura del La_2LiRuO_6 [42], obtenidos con MAXMAGN. Los MSGs 1 y 4 de la tabla permiten momentos magnéticos no nulos, mientras que el 2 y el 3 no los permiten y quedan descartados.

El modelo de estructura magnética compatible con la simetría de cada MSG de la tabla de subgrupos k-maximales puede obtenerse haciendo clic en el botón "*Show*" de la columna titulada "*Magnetic Structure*" (Figura 41). Esto permite obtener una pantalla que contiene una tabla con las posiciones atómicas, posiciones de Wyckoff y forma general compatible con la simetría de los momentos magnéticos asociados a los átomos magnéticos para el MSG consultado (Figura 42). Sobre la tabla, se indican algunos datos básicos, tales como el subgrupo elegido, el *setting* de trabajo, el grupo padre y los parámetros de red. Además se proporcionan enlaces que permiten cambiar de *setting*, descargar o visualizar la estructura magnética y descender a un grupo inferior no k-maximal.

Los átomos de la tabla de la Figura 42 se proporcionan agrupados en órbitas, indicándose la posición y momento permitido de cada átomo de la órbita. Los momentos magnéticos son indicados en forma paramétrica, es decir, son la forma más general compatible con la simetría que el momento de cada átomo puede tener. La forma general compatible con la simetría del momento magnético indicada en la columna "*Magnetic moment*" corresponde al primer átomo de la órbita indicada, y sólo se muestra para los átomos seleccionados como magnéticos. Por último, se indica la multiplicidad de cada órbita y se incluye una columna que permite especificar los valores de las componentes del momento magnético indicado en la columna

"*Magnetic moment*", definiendo así una estructura magnética particular que puede ser visualizada y exportada en forma de archivo cristalográfico magnético en formato magCIF.

Magnetic Structure

Selected magnetic space group: 4- $P2_1/c$ (#14.75)

Setting of the parent group

Parent space group 14 ($P2_1/c$), **in non-standard setting (a, b, a+c; 0, 0, 0)**

Lattice parameters: a=5.54430, b=5.59630, c=7.83030, alpha=90.000000, beta=90.034000, gamma=90.000000

[Go to setting standard (**a, b, a+c** ; 0, 0, 0)]
[Go to an alternative setting]

Export data to MCIF file/Visualize | Go to a subgroup

Atomic positions, Wyckoff positions and Magnetic Moments

N	Atom	New WP	Multiplicity	Magnetic moment	Values of M_x, M_y, M_z
1	La1 La 0.00830 0.95640 0.74910	(x,y,z | m_x,m_y,m_z) (-x+1/2,y+1/2,-z+1/2 | -m_x,m_y,-m_z) (-x,-y,-z | m_x,m_y,m_z) (x+1/2,-y+1/2,z+1/2 | -m_x,m_y,-m_z)	4	-	-
2	Li1 Li 0.50000 0.00000 0.00000	(1/2,0,0 | m_x,m_y,m_z) (0,1/2,1/2 | -m_x,m_y,-m_z)	2	-	-
3	Ru1 Ru 0.50000 0.00000 0.50000	(1/2,0,1/2 | m_x,m_y,m_z) (0,1/2,0 | -m_x,m_y,-m_z)	2	(M_x,M_y,M_z)	M_x = 0.0000(M_y = 0.0000(M_z = 0.0000(
4	O1 O 0.28090 0.69930 0.96000	(x,y,z | m_x,m_y,m_z) (-x+1/2,y+1/2,-z+1/2 | -m_x,m_y,-m_z) (-x,-y,-z | m_x,m_y,m_z) (x+1/2,-y+1/2,z+1/2 | -m_x,m_y,-m_z)	4	-	-
5	O2 O 0.20160 0.22120 0.95970	(x,y,z | m_x,m_y,m_z) (-x+1/2,y+1/2,-z+1/2 | -m_x,m_y,-m_z) (-x,-y,-z | m_x,m_y,m_z) (x+1/2,-y+1/2,z+1/2 | -m_x,m_y,-m_z)	4	-	-
6	O3 O 0.92420 0.51570 0.75650	(x,y,z | m_x,m_y,m_z) (-x+1/2,y+1/2,-z+1/2 | -m_x,m_y,-m_z) (-x,-y,-z | m_x,m_y,m_z) (x+1/2,-y+1/2,z+1/2 | -m_x,m_y,-m_z)	4	-	-

Figura 42. Modelo de estructura magnética correspondiente al MSG $P2_1/c$ (**a**, **b**, **a+c**) (#14.75), caso 4 de la tabla de grupos k-maximales de la Figura 41. Obtenido con MAXMAGN.

El *setting* de trabajo elegido por defecto es el *setting parent-like*; también se proporciona la estructura en el *setting* estándar del MSG: el enlace que hay bajo los parámetros de red (Figura 42) permite consultar alternativamente la estructura magnética en ambos *settings*. En el caso del La_2LiRuO_6, el *setting parent-like* coincide con el del grupo padre.

Con respecto a las estructuras magnéticas proporcionadas por MAXMAGN, debe subrayarse que tanto la métrica como las posiciones atómicas de las mismas son, en realidad, las de la estructura de la fase paramagnética, pues son éstas las que se han introducido en el programa. Por tanto, dichas posiciones atómicas son virtuales y no necesariamente coinciden con las posiciones atómicas reales de la estructura magnética, especialmente si existe un fuerte acoplamiento magnetoestructural. Esto significa que a la hora de comparar estas posiciones atómicas con las que realmente se calculen en el proceso de determinación de la estructura, debe tenerse en cuenta que pequeñas variaciones de las posiciones atómicas con respecto a los valores indicados por MAXMAGN son posibles siempre que no violen la simetría magnética de la estructura. A este respecto, debe notarse que debido a la pérdida de simetría puede haber un desdoblamiento o "*splitting*" en las órbitas de los átomos, *splitting* que

depende íntegramente del MSG consultado. Como puede verse en la Figura 42, se proporcionan las órbitas de los átomos, tanto magnéticos como no magnéticos, correspondientes al MSG seleccionado. La distribución en órbitas de los átomos asociada al MSG seleccionado en la fase de baja simetría debe tenerse en cuenta a la hora de considerar el modelo correspondiente como posible en el proceso de determinación de la estructura magnética investigada.

Adicionalmente, se proporciona el enlace "*Go to an alternative setting*", que despliega un formulario (Figura 43) que permite introducir una matriz de transformación alternativa, lo que permite obtener la estructura magnética en cualquier *setting* válido. La matriz de transformación debe ser la que relacione el *setting* del grupo padre y el *setting* deseado. Esta matriz debe ser válida, es decir, llevar a un *setting* en el que las traslaciones básicas de la nueva celda unidad sean traslaciones no primadas del MSG; la validez de la transformación introducida es comprobada, siendo las no válidas rechazadas. La matriz indicada en la Figura 43 es un ejemplo correspondiente al caso del La_2LiRuO_6. En este caso el grupo padre está expresado en un *setting* no estándar, que casualmente coincide con el *setting* de trabajo por defecto escogido por MAXMAGN para la estructura. Por ello, podría ser útil transformar la estructura obtenida al *setting* estándar del grupo padre. La matriz de transformación de *setting* necesaria para ello es (**a**, **b**, **a**+**c**). Introduciendo esta matriz en el formulario de la Figura 43 se obtiene una pantalla similar a la Figura 42 con la estructura magnética expresada en el *setting* estándar del grupo padre. En este caso particular, dicho *setting* coincide con el *setting* estándar del MSG.

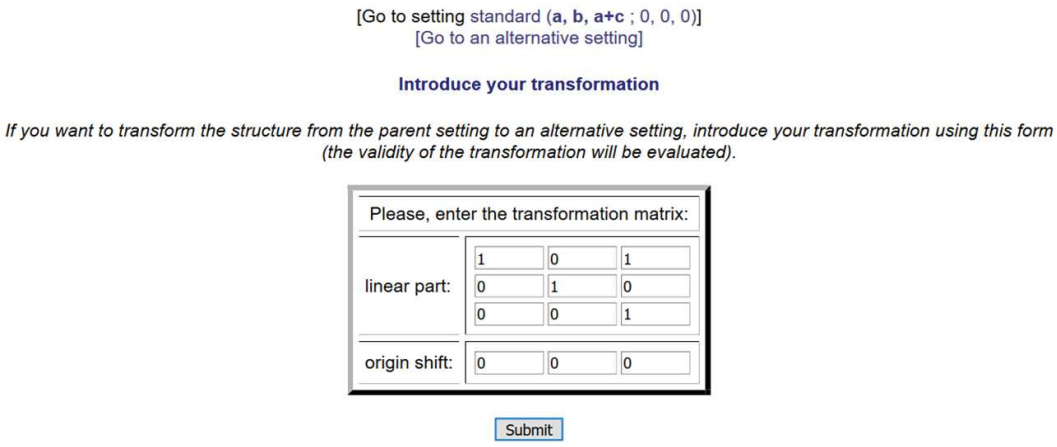

Figura 43. Formulario desplegable incluido en la página de MAXMAGN de la estructura magnética (Figura 42) que permite transformar la estructura a un *setting* cualquiera.

Una vez se han dado valores a las componentes de los momentos magnéticos de los átomos magnéticos, la estructura magnética puede ser exportada y visualizada. El botón "*Export data to MCIF file/Visualize*" conduce a una pantalla (Figura 44) que contiene un cuadro de previsualización del archivo magCIF (extensión .mcif), descargable a través del enlace ubicado sobre el cuadro. En estos archivos, al igual que en los archivos CIF de estructuras no magnéticas, se guarda información sobre la estructura cristalina en forma de "*tags*" o etiquetas [15]. MAXMAGN proporciona archivos magCIF que incluyen toda la información necesaria y relevante que el programa proporciona sobre la estructura magnética: parámetros de red, etiqueta y

símbolo del MSG, grupo padre, transformación de *setting* grupo-subgrupo, posiciones generales, posiciones atómicas, momentos magnéticos, forma adaptada a la simetría de los momentos magnéticos y vector de propagación. Además, se incluyen numerosos *tags* en blanco que el usuario puede rellenar con información experimental sobre la estructura magnética. Los archivos magCIF son el formato utilizado para la comunicación de estructuras magnéticas, y resultan legibles por la gran mayoría del *software* dedicado a la visualización y determinación de estructuras magnéticas, como por ejemplo JANA2006 [43], FULLPROF [44], ISOCIF [45], VESTA [23], Jmol [14], STRCONVERT [46] e ISODISTORT [37].

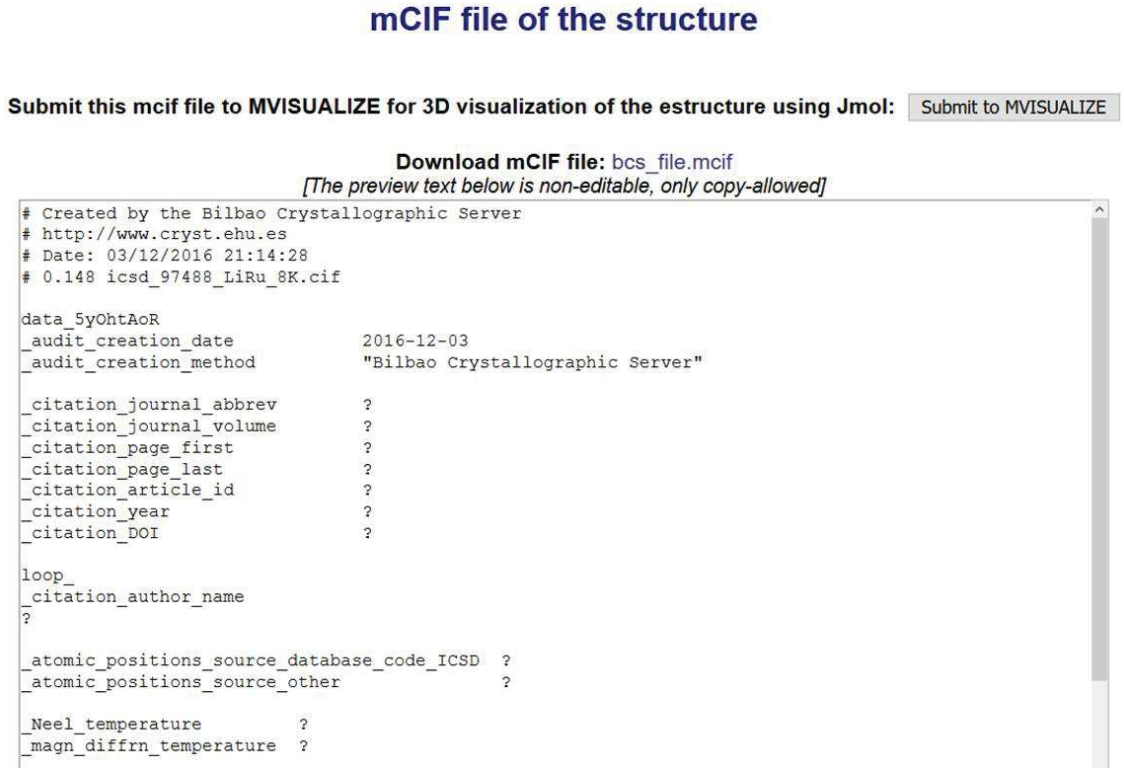

Figura 44. Formulario de descarga y visualización de estructuras magnéticas de MAXMAGN.

Asimismo, la pantalla de la Figura 44 incluye el botón "*Submit to MVISUALIZE*", que permite visualizar la estructura en 3D por medio del programa MVISUALIZE (§8.2). En la Figura 45 se pueden ver las estructuras magnéticas proporcionadas por MVISUALIZE correspondientes a los dos modelos k-maximales aún no descartados de entre los proporcionados por MAXMAGN (Figura 41). Estas estructuras han sido obtenidas de los correspondientes modelos asignando valores arbitrarios a las componentes permitidas de los momentos magnéticos, valores que pueden verse en la Figura 45.

Ambos modelos de simetría k-maximal son diferentes en varios aspectos. Aunque en ambos los átomos de Ru tienen momentos magnéticos permitidos en todas direcciones, los modelos difieren en sus características: mientras el modelo de la Figura 45(a), de MSG $P2_1/c$ (#14.75), es antiferromagnético a lo largo tanto del eje *x* como del *z*, estando permitida por simetría una componente ferromagnética a lo largo de *y*, el modelo de la Figura 45(b), de MSG $P2_1'/c'$ (#14.79), es antiferromagnético a lo largo de *y*, estando permitida por simetría una componente ferromagnética en el

plano *xz*. Por comparación con materiales similares, es posible suponer que esta estructura es antiferromagnética [42], por lo que las componentes ferromagnéticas, aunque permitidas por simetría, serán muy pequeñas en ambos modelos. Por tanto, el uso de MAXMAGN para analizar el caso del La_2LiRuO_6 permite concluir que su estructura magnética se ajustará a uno de los dos modelos (a) y (b) de la Figura 45, que presentan dos y un parámetros libres respectivamente que además resultan ser complementarios. Ambos modelos deberían ser considerados en el proceso de determinación de la estructura. Además, dado que las componentes ferromagnéticas están permitidas por simetría y son también complementarias, la observación de ferromagnetismo permitiría descartar uno de los modelos y confirmar el otro dependiendo de en qué dirección se observe la magnetización. Finalmente, como puede observarse en la correspondiente entrada de MAGNDATA (#0.148), esta estructura magnética se ajusta al modelo (a), cuyo MSG es *P2₁/c* (#14.75), siendo la componente ferromagnética permitida según *y* despreciable.

(a) *P2₁/c* (#14.75)

Ru1 Ru 0.50000 0.00000 0.50000	(1/2,0,1/2 | m_x,m_y,m_z) (0,1/2,0 | -m_x,m_y,-m_z)	2	(M_x,M_y,M_z)	M_x = 1.1000 M_y = 3.2000 M_z = 2.7000

(b) *P2₁'/c'* (#14.79)

Ru1 Ru 0.50000 0.00000 0.50000	(1/2,0,1/2 | m_x,m_y,m_z) (0,1/2,0 | m_x,-m_y,m_z)	2	(M_x,M_y,M_z)	M_x = 1.1000 M_y = 3.2000 M_z = 2.7000

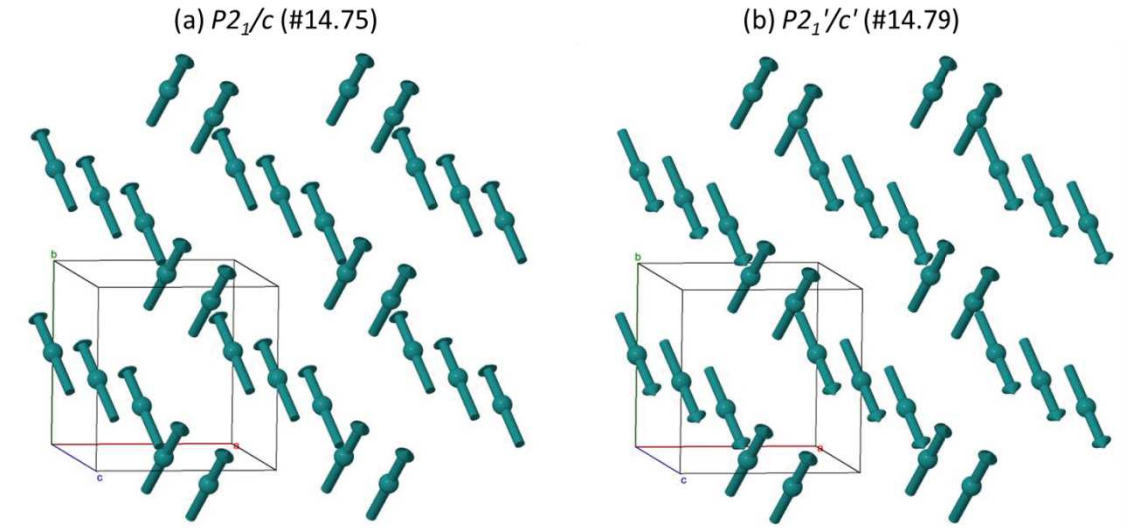

Figura 45. Modelos y estructuras magnéticas posibles para el La_2LiRuO_6, correspondientes a los subgrupos k-maximales (a) *P2₁/c* (#14.75) y (b) *P2₁'/c'* (#14.79). Obtenidos con MAXMAGN y MVISUALIZE.

En el caso del La_2LiRuO_6, se han deducido restricciones adicionales en los momentos gracias a la suposición de que la estructura magnética es antiferromagnética. En general, una vez obtenidos con MAXMAGN los posibles modelos k-maximales, un análisis de los mismos teniendo en cuenta el conocimiento de datos adicionales, la exigencia de características esperadas o la realización de aproximaciones razonables puede llevar a descartar algunos de estos modelos por incompatibilidades debidas a diversas causas: colinearidad, carácter ferromagnético o antiferromagnético,

direcciones preferentes en el momento magnético, polaridad, etc. Esto permite en muchos casos reducir aún más tanto el número de modelos k-maximales posibles como el número de parámetros libres de estos modelos.

Maximal magnetic space groups for the parent space group 204 (*Im*-3) and the propagation vector k = (1, 1, 1)

Maximal subgroups which allow non-zero magnetic moments for at least one atom are coloured

N	Group (BNS)	Transformation matrix	General positions	Properties	Magnetic structure
1	*P_In-3* (#201.21) Go to a subgroup	$\begin{pmatrix} 1 & 0 & 0 & 1/4 \\ 0 & 1 & 0 & 1/4 \\ 0 & 0 & 1 & 1/4 \end{pmatrix}$ Alternatives (domain-related)	Show	*Systematic absences* MAGNEXT *Tensor properties* MTENSOR	Show
2	*P_Im-3* (#200.17) Go to a subgroup	$\begin{pmatrix} 1 & 0 & 0 & 0 \\ 0 & 1 & 0 & 0 \\ 0 & 0 & 1 & 0 \end{pmatrix}$ Alternatives (domain-related)	Show	*Systematic absences* MAGNEXT *Tensor properties* MTENSOR	Show
3	*P_Immn* (#59.416) Go to a subgroup	$\begin{pmatrix} 0 & 0 & -1 & 1/4 \\ 0 & 1 & 0 & 1/4 \\ 1 & 0 & 0 & 1/4 \end{pmatrix}$ Alternatives (domain-related)	Show	*Systematic absences* MAGNEXT *Tensor properties* MTENSOR	Show
4	*P_Innm* (#58.404) Go to a subgroup	$\begin{pmatrix} 0 & 0 & -1 & 0 \\ 0 & 1 & 0 & 0 \\ 1 & 0 & 0 & 0 \end{pmatrix}$ Alternatives (domain-related)	Show	*Systematic absences* MAGNEXT *Tensor properties* MTENSOR	Show

Figura 46. Subgrupos k-maximales correspondientes a la estructura del $LaMn_3Cr_4O_{12}$, obtenidos con MAXMAGN. Los MSGs 1, 3 y 4 de la tabla son compatibles con la estructura magnética, mientras que el 2 es incompatible y queda descartado. Los MSGs 3 y 4 quedan también descartados por la falta de simetría trigonal polar a lo largo de la dirección [1 1 1].

Esta reducción de posibles modelos y parámetros libres es patente en el ejemplo de la estructura magnética del $LaMn_3Cr_4O_{12}$ [40]. Para este caso, la lista de subgrupos k-maximales proporcionada por MAXMAGN (Figura 46) permite descartar el subgrupo k-maximal *P_Im-3* (#200.17). Las características conocidas de la estructura magnética del $LaMn_3Cr_4O_{12}$ permiten, además, descartar los subgrupos *P_Immn* (#59.416) y *P_Innm* (#58.404). Esta fase magnética es el resultado de dos transiciones de fase diferenciadas y sucesivas asociadas a los átomos de Mn y Cr, por lo que las *irreps* asociadas a estas transiciones de fase son ambas primarias y además multidimensionales; por esta razón, no puede esperarse que, en este caso, la simetría sea k-maximal. Además, estas transiciones de fase magnéticas están acopladas con transiciones de fase ferroeléctricas que implican que esta fase del $LaMn_3Cr_4O_{12}$ es ferroeléctrica y, por tanto, polar, a lo largo de la dirección [1 1 1]. Esto implica que el MSG debe ser trigonal, con el eje trigonal a lo largo de la dirección [1 1 1], y es por esta causa por la que los subgrupos k-maximales *P_Immn* (#59.416) y *P_Innm* (#58.404), así como sus subgrupos no k-maximales quedan descartados. El único MSG superviviente es el *P_In-3* (#201.21), pero dado que es centrosimétrico, y además su ordenamiento magnético es incompleto (Figura 47), con momentos nulos para los átomos de Mn, también puede ser descartado; no así sus subgrupos, ni tampoco los subgrupos del *P_Im-3* (#200.17) que, aunque fue descartado porque no permite momentos magnéticos no nulos, sus subgrupos podrían permitirlos y deben ser reconsiderados al descartarse la k-maximalidad.

Al quedar descartados todos los MSGs k-maximales, todos los subgrupos de los subgrupos *P_In-3* y *P_Im-3* deberán ser explorados. La forma de hacer esto utilizando MAXMAGN se expondrá a continuación.

N	Atom	New WP	Multiplicity	Magnetic moment	Values of M_x, M_y, M_z
1	La1 La 0.00000 0.00000 0.00000	(0,0,0 | 0,0,0) (1/2,1/2,1/2 | 0,0,0)	2	-	-
2	Mn1 Mn 0.00000 0.50000 0.50000	(0,1/2,1/2 | 0,0,0) (1/2,0,1/2 | 0,0,0) (1/2,1/2,0 | 0,0,0) (1/2,0,0 | 0,0,0) (0,1/2,0 | 0,0,0) (0,0,1/2 | 0,0,0)	6	(0,0,0)	-
3	Cr1 Cr 0.25000 0.25000 0.25000	(1/4,1/4,1/4 | m_x,m_x,m_x) (3/4,3/4,1/4 | -m_x,-m_x,m_x) (3/4,1/4,3/4 | -m_x,m_x,-m_x) (1/4,3/4,3/4 | m_x,-m_x,-m_x) (3/4,3/4,3/4 | -m_x,-m_x,-m_x) (1/4,1/4,3/4 | m_x,m_x,-m_x) (1/4,3/4,1/4 | m_x,-m_x,m_x) (3/4,1/4,1/4 | -m_x,m_x,m_x)	8	(M_x,M_x,M_x)	M_x = 0.0000
4	O1 O 0.00000 0.31040 0.17710	(0,y,z | 0,m_y,m_z) (0,-y,z | 0,-m_y,m_z) (0,y,-z | 0,m_y,-m_z) (0,-y,-z | 0,-m_y,-m_z) (z,0,y | m_z,0,m_y) (z,0,-y | m_z,0,-m_y) (-z,0,y | -m_z,0,m_y) (-z,0,-y | -m_z,0,-m_y) (y,z,0 | m_y,m_z,0) (-y,z,0 | -m_y,m_z,0) (y,-z,0 | m_y,-m_z,0) (-y,-z,0 | -m_y,-m_z,0) (1/2,y+1/2,z+1/2 | 0,-m_y,-m_z) (1/2,-y+1/2,z+1/2 | 0,m_y,-m_z) (1/2,y+1/2,-z+1/2 | 0,-m_y,m_z) (1/2,-y+1/2,-z+1/2 | 0,m_y,m_z) (z+1/2,1/2,y+1/2 | -m_z,0,-m_y) (z+1/2,1/2,-y+1/2 | -m_z,0,m_y) (-z+1/2,1/2,y+1/2 | m_z,0,-m_y) (-z+1/2,1/2,-y+1/2 | m_z,0,m_y) (y+1/2,z+1/2,1/2 | -m_y,-m_z,0) (-y+1/2,z+1/2,1/2 | m_y,-m_z,0) (y+1/2,-z+1/2,1/2 | -m_y,m_z,0) (-y+1/2,-z+1/2,1/2 | m_y,m_z,0)	24	-	-

Figura 47. Modelo de estructura magnética correspondiente al MSG *P_In-3* (#201.21), caso 1 de la tabla de subgrupos k-maximales de la Figura 46, obtenido con MAXMAGN. La incompatibilidad de este MSG con la existencia de momentos no nulos en los átomos de Mn permite descartarlo.

7.4 Programa MAXMAGN: utilidades adicionales

7.4.1 Descenso a subgrupos no k-maximales

En aquellas ocasiones en que todos los modelos correspondientes a subgrupos k-maximales hayan sido descartados, será necesario descender a subgrupos no k-maximales. La mejor forma de hacer esto utilizando los programas del *Bilbao Crystallographic Server* es usar conjuntamente los programas K-SUBGROUPSMAG y MAGMODELIZE (§8.1). Sin embargo, MAXMAGN proporciona una herramienta adicional, accesible a través del botón "*Go to a subgroup*" incluido tanto en el listado de subgrupos k-maximales (Figura 46) como en la pantalla de estructura magnética (Figura 42), que permite descender a un subgrupo de un subgrupo k-maximal seleccionando algunas de sus operaciones de simetría como generadores. Esta pantalla (Figura 48) es similar a la pantalla que muestra las operaciones de simetría del MSG (Figura 36) y permite su selección. Incluye además un enlace a K-SUBGROUPSMAG que carga en este programa el grupo padre y el vector de propagación para obtener con él todos los subgrupos, tanto k-maximales como no k-maximales.

General positions of the magnetic space group P_Ibn-3 (#201.21) in the basis (a, b, c; 0, 0, 0) of the parent space group 204 (Im-3)

Obtain all (maximal and not maximal) magnetic subgroups compatible with these parent space group and propagation vector via K-SUBGROUPSMAG

Transformation matrix:

$$\begin{pmatrix} 1 & 0 & 0 & 1/4 \\ 0 & 1 & 0 & 1/4 \\ 0 & 0 & 1 & 1/4 \end{pmatrix}$$

Please, choose the generators of the subgroup

*Hint: In order to keep the black-and-white lattice derived from the given propagation vector **k**, the translations and antitranslations of the table are locked and included by default*

	Standard/Default Setting			Transformed Setting			Select
N	(x,y,z) form	Matrix form	Seitz notation	(x,y,z) form	Matrix form	Seitz notation	
1	x,y,z,+1 m_x,m_y,m_z	$\begin{pmatrix} 1 & 0 & 0 & 0 \\ 0 & 1 & 0 & 0 \\ 0 & 0 & 1 & 0 \end{pmatrix}$	{ 1 | 0 }	x,y,z,+1 m_x,m_y,m_z	$\begin{pmatrix} 1 & 0 & 0 & 0 \\ 0 & 1 & 0 & 0 \\ 0 & 0 & 1 & 0 \end{pmatrix}$	{ 1 | 0 }	☑
2	x,-y-1/2,-z-1/2,+1 $m_x,-m_y,-m_z$	$\begin{pmatrix} 1 & 0 & 0 & 0 \\ 0 & -1 & 0 & -1/2 \\ 0 & 0 & -1 & -1/2 \end{pmatrix}$	{ 2_{100} | 0 -1/2 -1/2 }	x,-y,-z,+1 $m_x,-m_y,-m_z$	$\begin{pmatrix} 1 & 0 & 0 & 0 \\ 0 & -1 & 0 & 0 \\ 0 & 0 & -1 & 0 \end{pmatrix}$	{ 2_{100} | 0 }	☐
3	-x-1/2,y,-z-1/2,+1 $-m_x,m_y,-m_z$	$\begin{pmatrix} -1 & 0 & 0 & -1/2 \\ 0 & 1 & 0 & 0 \\ 0 & 0 & -1 & -1/2 \end{pmatrix}$	{ 2_{010} | -1/2 0 -1/2 }	-x,y,-z,+1 $-m_x,m_y,-m_z$	$\begin{pmatrix} -1 & 0 & 0 & 0 \\ 0 & 1 & 0 & 0 \\ 0 & 0 & -1 & 0 \end{pmatrix}$	{ 2_{010} | 0 }	☐
4	-x-1/2,-y-1/2,z,+1 $-m_x,-m_y,m_z$	$\begin{pmatrix} -1 & 0 & 0 & -1/2 \\ 0 & -1 & 0 & -1/2 \\ 0 & 0 & 1 & 0 \end{pmatrix}$	{ 2_{001} | -1/2 -1/2 0 }	-x,-y,z,+1 $-m_x,-m_y,m_z$	$\begin{pmatrix} -1 & 0 & 0 & 0 \\ 0 & -1 & 0 & 0 \\ 0 & 0 & 1 & 0 \end{pmatrix}$	{ 2_{001} | 0 }	☐
5	z,x,y,+1 m_z,m_x,m_y	$\begin{pmatrix} 0 & 0 & 1 & 0 \\ 1 & 0 & 0 & 0 \\ 0 & 1 & 0 & 0 \end{pmatrix}$	{ 3^+_{111} | 0 }	z,x,y,+1 m_z,m_x,m_y	$\begin{pmatrix} 0 & 0 & 1 & 0 \\ 1 & 0 & 0 & 0 \\ 0 & 1 & 0 & 0 \end{pmatrix}$	{ 3^+_{111} | 0 }	☑
6	y,z,x,+1 m_y,m_z,m_x	$\begin{pmatrix} 0 & 1 & 0 & 0 \\ 0 & 0 & 1 & 0 \\ 1 & 0 & 0 & 0 \end{pmatrix}$	{ 3^-_{111} | 0 }	y,z,x,+1 m_y,m_z,m_x	$\begin{pmatrix} 0 & 1 & 0 & 0 \\ 0 & 0 & 1 & 0 \\ 1 & 0 & 0 & 0 \end{pmatrix}$	{ 3^-_{111} | 0 }	☐

Figura 48. Formulario de MAXMAGN para descender a subgrupos de los subgrupos k-maximales por medio de la selección de generadores. Las traslaciones y traslaciones primadas están fijadas para asegurar la compatibilidad con **k**.

En el caso del $LaMn_3Cr_4O_{12}$ (Figura 48), dado que el MSG de la estructura magnética es no k-maximal y además polar según [1 1 1], podría ser trigonal, con el eje 3 orientado en la dirección [1 1 1]. Será por tanto un subgrupo de P_Ibn-3 ó de P_Im-3, e incluirá probablemente el elemento $\{3_{111}^+|0\}$, que forma parte de ambos subgrupos k-maximales. Además, dado que el vector de propagación ya ha sido fijado por el usuario, y de él se deduce la red *black-and-white*, ésta formará parte obligatoriamente de cualquier subgrupo no k-maximal. Por ello, como puede verse en la Figura 48, todas las traslaciones y traslaciones primadas que aparecen en el listado de elementos de simetría están seleccionadas por defecto, y no pueden ser eliminadas, para asegurar la compatibilidad con **k**. La selección de cualquier otro generador, pertenezca bien a P_Ibn-3 bien a P_Im-3, o bien no generará ninguna operación adicional, o bien generará un MSG no polar, o bien generará todo el MSG k-maximal. Por tanto, la selección del elemento $\{3_{111}^+|0,0,0\}$, ya sea en el listado de operaciones de P_Ibn-3 o de P_Im-3, basta para seleccionar el subgrupo deseado, que es el de mayor simetría entre los posibles.

El resultado de seleccionar dicho subgrupo puede verse en la Figura 49(a), donde se muestra la pantalla intermedia que indica qué subgrupo ha sido seleccionado y cuáles

son sus operaciones de simetría. El grupo seleccionado, en este caso el *R*$_I$*3* (**a**-**b**, **b**-**c**, **a**+**b**+**c**) (#146.12) es detectado haciendo uso internamente del programa IDENTIFY MAGNETIC GROUP. Tras confirmar en esta pantalla que se elige dicho grupo, presionando el botón "*Choose*", el resultado es una tabla idéntica a la que contenía los subgrupos k-maximales (Figura 46), pero incluyendo únicamente el subgrupo seleccionado (Figura 49(b)). Ambas pantallas son idénticas e incluyen exactamente las mismas utilidades, por lo que todo aquello que puede hacerse en MAXMAGN para subgrupos k-maximales puede hacerse también para cualquier MSG obtenido gracias a la herramienta de descenso a subgrupos, incluida la posibilidad de descender a subgrupos aún menores.

(a)

Selected subgroup

The selected generators generate the magnetic space group:

***R*$_I$*3* (#146.12)**

Change of basis matrix form the parent setting to the standard setting of the group: (**a-b, b-c, a+b+c** ; 0, 0, 0)
Parent space group 204 (*Im*-3)

Selected generators:

x,y,z,+1
z,x,y,+1
x+1/2,y+1/2,z+1/2,-1

Full set of symmetry operations of the subgroup:

x,y,z,+1
z,x,y,+1
y,z,x,+1
x+1/2,y+1/2,z+1/2,-1
z+1/2,x+1/2,y+1/2,-1
y+1/2,z+1/2,x+1/2,-1

Choose

(b)

Selected magnetic space subgroup for the parent space group 204 (*Im*-3) and the propagation vector k = (1, 1, 1)

Subgroups which allow non-zero magnetic moments for at least one atom are coloured

N	Group (BNS)	Transformation matrix	General positions	Properties	Magnetic structure
1	*R*$_I$*3* (#146.12) Go to a subgroup	$\begin{pmatrix} 1 & 0 & 1 & 0 \\ -1 & 1 & 1 & 0 \\ 0 & -1 & 1 & 0 \end{pmatrix}$ Alternatives (domain-related)	Show	*Systematic absences* MAGNEXT *Tensor properties* MTENSOR	Show

Figura 49. (a) Pantalla informativa de MAXMAGN mostrando el MSG identificado y sus operaciones de simetría. (b) Tabla de MAXMAGN incluyendo únicamente dicho grupo, que permite acceder a las utilidades que proporciona MAXMAGN.

El modelo de estructura magnética correspondiente al MSG seleccionado es también accesible (Figura 50). Este modelo no presenta ninguna incompatibilidad adicional con los datos conocidos de la estructura magnética, por lo que es el de mayor simetría

entre los posibles y muy probablemente la estructura magnética concuerde con él. De hecho, es así, tal como puede verse en la correspondiente entrada de MAGNDATA (#1.156).

N	Atom	New WP	Multiplicity	Magnetic moment	Values of M_x, M_y, M_z
1	La1 La 0.00000 0.00000 0.00000	(0,0,0 | m_x,m_x,m_x) (1/2,1/2,1/2 | -m_x,-m_x,-m_x)	2	-	-
2	Mn1 Mn 0.00000 0.50000 0.50000	(0,1/2,1/2 | m_x,m_y,m_z) (1/2,1/2,0 | m_y,m_z,m_x) (0,1/2,0 | -m_z,-m_x,-m_y) (1/2,0,1/2 | m_z,m_x,m_y) (1/2,0,0 | -m_x,-m_y,-m_z) (0,0,1/2 | -m_y,-m_z,-m_x)	6	(M_x,M_y,M_z)	M_x = 0.00000 M_y = 0.00000 M_z = 0.00000
3	Cr1_1 Cr 0.25000 0.25000 0.25000	(1/4,1/4,1/4 | m_x,m_x,m_x) (3/4,3/4,3/4 | -m_x,-m_x,-m_x)	2	(M_x,M_x,M_x)	M_x = 0.00000
	Cr1_2 Cr 0.75000 0.75000 0.25000	(3/4,3/4,1/4 | m_x,m_y,m_z) (1/4,3/4,3/4 | m_y,m_z,m_x) (3/4,1/4,3/4 | m_z,m_x,m_y) (1/4,1/4,3/4 | -m_x,-m_y,-m_z) (1/4,3/4,1/4 | -m_y,-m_z,-m_x) (3/4,1/4,1/4 | -m_z,-m_x,-m_y)	6	(M_x,M_y,M_z)	M_x = 0.00000 M_y = 0.00000 M_z = 0.00000
4	O1_1 O 0.00000 0.31040 0.17710	(0,y,z | m_x,m_y,m_z) (z,0,y | m_z,m_x,m_y) (y,z,0 | m_y,m_z,m_x) (1/2,y+1/2,z+1/2 | -m_x,-m_y,-m_z) (z+1/2,1/2,y+1/2 | -m_z,-m_x,-m_y) (y+1/2,z+1/2,1/2 | -m_y,-m_z,-m_x)	6	-	-
	O1_2 O 0.00000 0.68960 0.17710	(0,-y,z | m_x,m_y,m_z) (z,0,-y | m_z,m_x,m_y) (-y,z,0 | m_y,m_z,m_x) (1/2,-y+1/2,z+1/2 | -m_x,-m_y,-m_z) (z+1/2,1/2,-y+1/2 | -m_z,-m_x,-m_y) (-y+1/2,z+1/2,1/2 | -m_y,-m_z,-m_x)	6	-	-
	O1_3 O 0.00000 0.31040 0.82290	(0,y,-z | m_x,m_y,m_z) (-z,0,y | m_z,m_x,m_y) (y,-z,0 | m_y,m_z,m_x) (1/2,y+1/2,-z+1/2 | -m_x,-m_y,-m_z) (-z+1/2,1/2,y+1/2 | -m_z,-m_x,-m_y) (y+1/2,-z+1/2,1/2 | -m_y,-m_z,-m_x)	6	-	-
	O1_4 O 0.00000 0.68960 0.82290	(0,-y,-z | m_x,m_y,m_z) (-z,0,-y | m_z,m_x,m_y) (-y,-z,0 | m_y,m_z,m_x) (1/2,-y+1/2,-z+1/2 | -m_x,-m_y,-m_z) (-z+1/2,1/2,-y+1/2 | -m_z,-m_x,-m_y) (-y+1/2,-z+1/2,1/2 | -m_y,-m_z,-m_x)	6	-	-

Figura 50. Estructura magnética correspondiente al subgrupo no k-maximal *R3* (#146.12). Obtenida con MAXMAGN.

En conclusión, para casos sencillos, la herramienta de descenso a subgrupos de MAXMAGN facilita la determinación de la estructura y la identificación de su MSG también para subgrupos no k-maximales. En el ejemplo escogido, el MSG queda completamente identificado y, gracias a ello, se conocen algunas de sus características: es una estructura polar, trigonal y no ferromagnética, y sus tensores cristalinos son deducibles vía MTENSOR (§7.4.4). Para determinar la estructura magnética basta con refinar los 7 parámetros libres del modelo hallado, quedando los momentos magnéticos de los átomos de cada órbita automáticamente fijados por la simetría magnética.

Con respecto a la herramienta de descenso a subgrupos, debe quedar claro que el descarte de un subgrupo k-maximal por ser incompatible con momentos no nulos en las WPs donde se ubican los átomos magnéticos (Figura 46) es válido única y exclusivamente mientras la búsqueda está restringida a los subgrupos k-maximales. Una vez se descarta la k-maximalidad, los subgrupos de aquellos subgrupos k-maximales descartados deben considerarse como posibles, pues la ausencia de los elementos de simetría que se pierden al descender al subgrupo puede causar que los momentos magnéticos dejen de estar prohibidos por simetría. Sirva como ejemplo ilustrativo de esta situación la estructura magnética del $LaMn_3V_4O_{12}$ (caso #1.119 de MAGNDATA (§9)) [47], un caso para el que MAXMAGN proporciona 4 subgrupos k-maximales de los cuáles sólo uno, ortorrómbico, permite momentos magnéticos no nulos para el átomo magnético de Mn (Figura 51). Sin embargo, existen datos adicionales que implican que la estructura es romboédrica y por tanto incompatible con el único subgrupo k-maximal superviviente, por lo que debe descenderse a subgrupos no k-maximales. El subgrupo no k-maximal que describe la simetría de la

estructura magnética resulta ser *R_I-3* (**a**+**c**, -**a**+**b**, -**a**-**b**+**c**) (#148.20), un subgrupo del subgrupo k-maximal *P_Im-3* (#200.17) (número 2 del listado de la Figura 51).

Maximal magnetic space groups for the parent space group 204 (*Im*-3) and the propagation vector k = (1, 0, 0)

Maximal subgroups which allow non-zero magnetic moments for at least one atom are coloured

N	Group (BNS)	Transformation matrix	General positions	Properties	Magnetic structure
1	*P_In-3* (#201.21) Go to a subgroup	$\begin{pmatrix} 1 & 0 & 0 & 1/4 \\ 0 & 1 & 0 & 1/4 \\ 0 & 0 & 1 & 1/4 \end{pmatrix}$ Alternatives (domain-related)	Show	*Systematic absences* MAGNEXT *Tensor properties* MTENSOR	Show
2	*P_Im-3* (#200.17) Go to a subgroup	$\begin{pmatrix} 1 & 0 & 0 & 0 \\ 0 & 1 & 0 & 0 \\ 0 & 0 & 1 & 0 \end{pmatrix}$ Alternatives (domain-related)	Show	*Systematic absences* MAGNEXT *Tensor properties* MTENSOR	Show
3	*P_Immn* (#59.416) Go to a subgroup	$\begin{pmatrix} 0 & 0 & -1 & 1/4 \\ 0 & 1 & 0 & 1/4 \\ 1 & 0 & 0 & 1/4 \end{pmatrix}$ Alternatives (domain-related)	Show	*Systematic absences* MAGNEXT *Tensor properties* MTENSOR	Show
4	*P_Innm* (#58.404) Go to a subgroup	$\begin{pmatrix} 0 & 0 & -1 & 0 \\ 0 & 1 & 0 & 0 \\ 1 & 0 & 0 & 0 \end{pmatrix}$ Alternatives (domain-related)	Show	*Systematic absences* MAGNEXT *Tensor properties* MTENSOR	Show

Figura 51. Subgrupos k-maximales correspondientes a la estructura del $LaMn_3V_4O_{12}$, obtenidos con MAXMAGN. Aunque el MSG 2 de la tabla queda descartado, la no k-maximalidad de la estructura hace que finalmente sea su subgrupo *R_I-3* (**a**+**c**, -**a**+**b**, -**a**-**b**+**c**) (#148.20) el que describe la simetría de la estructura magnética.

7.4.2 Modelos equivalentes alternativos: subgrupos conjugados correspondientes a dominios

Las listas de subgrupos proporcionadas por MAXMAGN (Figuras 33, 35, 38, 41, 46, 49(b) y 51) indican tan sólo un representante **M** de una clase de conjugación de subgrupos del grupo padre. Esto significa que por cada grupo indicado en dichas listas existe en general un conjunto de subgrupos conjugados $\mathbf{M_i}$ que pueden obtenerse a partir del representante **M** aplicando la operación de conjugación para todos los elementos g_i del grupo padre **Gp1'**:

$$\mathbf{M_i} = g_i^{-1}\mathbf{M}g_i \qquad \forall\, g_i \in \mathbf{Gp1'} \tag{27}$$

En la práctica, la aplicación de (27) para todos los elementos dentro de la celda unidad g_i de **Gp1'** es redundante: bastará con utilizar una selección particular de *coset representatives* g_j de la *coset decomposition* de **Gp1'** en **M**:

$$\mathbf{Gp1'} = \mathbf{M} + g_2\mathbf{M} + g_3\mathbf{M} + \ldots + g_j\mathbf{M} + \ldots \tag{28}$$

Estos *coset representatives*, cuando son utilizados para transformar la estructura magnética, dan lugar a los diferentes tipos de dominios de la fase ferroica, cuyo

número equivale al índice del subgrupo con respecto a **Gp1'**. Sin embargo, si el *coset representative* pertenece al normalizador afín de **M**, $\mathbf{N_M}$, $\mathbf{M_i}$ en (27) coincide con **M**, y la simetría del tipo de dominio resultante viene descrita por el mismo grupo **M**. Igualmente, dos *coset representatives* g_k y g_l tales que $g_k^{-1} \cdot g_l \in \mathbf{N_M}$ producirán dos dominios con la misma simetría. Por tanto, para calcular los subgrupos de la clase de conjugación y los modelos correspondientes no es necesario aplicar (27) para todos los g_i de (28), sino para los *coset representatives* g_k de la *coset decomposition* de **Gp1'** con respecto al subgrupo resultante de la intersección entre **Gp1'** y $\mathbf{N_M}$, que serán un subconjunto de los g_i de (28):

$$\mathbf{Gp1'} = (\mathbf{Gp1'} \cap \mathbf{N_M}) + g_2(\mathbf{Gp1'} \cap \mathbf{N_M}) + \ldots + g_j(\mathbf{Gp1'} \cap \mathbf{N_M}) + \ldots \qquad (29)$$

El grupo $\mathbf{Gp1'} \cap \mathbf{N_M}$ es un supergrupo de **M**. El número de *coset representatives* g_k en (29) es igual al número de *coset representatives* g_i en (28) dividido por el índice de **M** con respecto de $\mathbf{Gp1'} \cap \mathbf{N_M}$.

En la ecuación (29) puede observarse que tanto el grupo **Gp1'** como el grupo $\mathbf{Gp1'} \cap \mathbf{N_M}$ son grupos grises, por lo que la coset decomposition de la ecuación (29) es una coset decomposition entre dos grupos espaciales convencionales. Por ello, para obtener los *coset representatives* de la ecuación (29), MAXMAGN hace uso del programa COSETS (http://www.cryst.ehu.es/cryst/cosets.html) de la sección "*Group-Subgroup Relations of Space Groups*" del *Bilbao Crystallographic Server*, que permite calcular la *coset decomposition* para grupos espaciales convencionales. Además, dado que todo elemento de un *coset* es válido como *coset representative*, el programa, por un lado, trata de escoger siempre el elemento de simetría más "sencillo" posible, dando preferencia a traslaciones pequeñas y rotaciones de orden bajo; y por otro lado, nunca escoge elementos cuya parte rotacional sea una rotoinversión como *coset representative* si en el *coset* hay algún elemento cuya parte rotacional sea estrictamente una rotación.

Los subgrupos conjugados obtenidos aplicando (27) con los *coset representatives* g_k de (29) describen la simetría de los tipos de dominios cuya simetría viene descrita por un subgrupo de **Gp1'** diferente al escogido como representante de la clase de conjugación en los listados proporcionados inicialmente por MAXMAGN. MAXMAGN tiene una opción que permite cambiar el representante de la clase de conjugación elegido por el programa y cambiarlo por cualquiera de los subgrupos conjugados $\mathbf{M_i}$ que llevan asociado el mismo vector de propagación. Esta opción permite construir todos los modelos con el mismo vector de propagación y experimentalmente indistinguibles, pero diferentes y con simetrías descritas por subgrupos conjugados. Es importante resaltar que en esta opción no se incluyen los subgrupos conjugados por operaciones que impliquen una transformación del vector de propagación, y que corresponden a dominios con un vector de propagación relacionado por simetría, pero distinguible al introducido inicialmente en el programa.

Para el caso del compuesto $LaMn_3Cr_4O_{12}$ [40], cuya estructura magnética está descrita por el MSG *R_I3* (**a**-**b**, **b**-**c**, **a**+**b**+**c**) (#146.12) (Figura 49(b)), MAXMAGN proporciona el conjunto de subgrupos pertenecientes a la clase de conjugación de dicho MSG. Estos

subgrupos alternativos (Figura 52) se obtienen al hacer clic en el botón "*Alternatives (domain-related)*" que hay bajo las matrices de transformación de la columna "*Transformation matrix*" (Figura 49(b)). Para cada uno de estos subgrupos se indica la matriz de transformación al *setting* estándar que lo define, así como el *coset representative* g_i (columna "*Coset representative*"), expresado en formato *xyz* y notación de Seitz, cuya utilización en (27) permite obtenerlo. Los subgrupos de la misma clase de conjugación son casi siempre un MSG del mismo tipo que el representante, MSG que es indicado encima de la tabla (Figura 52). Un subgrupo de la clase podrá ser un MSG de otro tipo tan sólo en el caso de que el MSG del representante de la clase de conjugación sea enantiomórfico y además el *coset representative* que permite obtenerlo sea una rotoinversión; entonces, el MSG del subgrupo conjugado será el otro miembro del par enantiomórfico. En estos casos, la tabla de subgrupos conjugados proporcionada por MAXMAGN incluirá una columna adicional indicando el tipo de MSG al que pertenece cada subgrupo.

Conjugated (domain-related) subgroups and alternative transformations to standard setting

Selected magnetic space group: 1- R_I3 (#146.12)

Conjugated (domain-related) subgroups

The coset representatives used to derive the conjugated subgroups are expressed in the setting of the parent group

Conjugated subgroup	Coset representatives		Transformation matrix:	Alternative matrices	Choose matrix
	(x,y,z) form	Seitz notation			
1	x,y,z,+1	{1 | 0}	$\begin{pmatrix} 1 & 0 & 1 & 0 \\ -1 & 1 & 1 & 0 \\ 0 & -1 & 1 & 0 \end{pmatrix}$	Show	Choose
2	-x,-y,z,+1	$\{2_{001} \mid 0\}$	$\begin{pmatrix} -1 & 0 & -1 & 0 \\ 1 & -1 & -1 & 0 \\ 0 & -1 & 1 & 0 \end{pmatrix}$	Show	Choose
3	-x,y,-z,+1	$\{2_{010} \mid 0\}$	$\begin{pmatrix} -1 & 0 & -1 & 0 \\ -1 & 1 & 1 & 0 \\ 0 & 1 & -1 & 0 \end{pmatrix}$	Show	Choose
4	x,-y,-z,+1	$\{2_{100} \mid 0\}$	$\begin{pmatrix} 1 & 0 & 1 & 0 \\ 1 & -1 & -1 & 0 \\ 0 & 1 & -1 & 0 \end{pmatrix}$	Show	Choose

Figura 52. Lista de subgrupos obtenida con MAXMAGN de *Im-3* (#204) pertenecientes a la misma clase de conjugación que el MSG R_I3 (**a**-**b**, **b**-**c**, **a**+**b**+**c**) (#146.12).

La tabla de la Figura 52 incluye la columna "*Alternative matrices*" que permite obtener una lista de matrices de transformación equivalentes a la del subgrupo seleccionado que definen exactamente el mismo MSG (Figura 53). Dado que todos los elementos $\boldsymbol{P_N}$ del normalizador afín $\mathbf{N_M}$ del MSG, aplicados como matrices de transformación sobre el MSG, lo dejan invariante (§6.1), la aplicación conjunta de una matriz particular $\boldsymbol{P}$ y de cualquier $\boldsymbol{P_N} \in \mathbf{N_M}$ será equivalente a $\boldsymbol{P}$ y describirá el mismo subgrupo que $\boldsymbol{P}$. Por tanto, el conjunto de matrices equivalentes $\boldsymbol{P'}$ se obtiene aplicando:

$$\boldsymbol{P'} = \boldsymbol{P}\boldsymbol{P_N} \quad \forall \boldsymbol{P_N} \in \mathbf{N_M} \tag{30}$$

Alternative transformations to standard setting

Selected magnetic space group: 1- R_I3 (#146.12)

N	Transformation matrix:	Choose matrix
1	$\begin{pmatrix} 1 & 0 & 1 & 0 \\ -1 & 1 & 1 & 0 \\ 0 & -1 & 1 & 0 \end{pmatrix}$	Choose
2	$\begin{pmatrix} 1 & 0 & 1 & 1/2 \\ -1 & 1 & 1 & 1/2 \\ 0 & -1 & 1 & 1/2 \end{pmatrix}$	Choose
3	$\begin{pmatrix} 0 & 1 & -1 & 0 \\ 1 & -1 & -1 & 0 \\ -1 & 0 & -1 & 0 \end{pmatrix}$	Choose
4	$\begin{pmatrix} 0 & 1 & -1 & 1/2 \\ 1 & -1 & -1 & 1/2 \\ -1 & 0 & -1 & 1/2 \end{pmatrix}$	Choose

Figura 53. Lista de matrices de transformación de *setting* equivalentes a (**a**-**b**, **b**-**c**, **a**+**b**+**c**), obtenida con MAXMAGN.

Check your transformation

If you want to use your own choice of transformation to the subgroup or a conjugated one, use this form (the validity of the transformation matrix will be evaluated).

Please, enter the transformation matrix:			
linear part:	0	-1	1
	-1	1	1
	-1	0	-1
origin shift:	1/2	3/2	-1/2

Submit

The transformation matrix

$$\begin{pmatrix} 0 & -1 & 1 & 1/2 \\ -1 & 1 & 1 & 3/2 \\ -1 & 0 & -1 & -1/2 \end{pmatrix}$$

is ok as an alternative transformation matrix to the standard setting of the conjugated subgroup 2 of the table shown above

Choose

Figura 54. Resultado del formulario de comprobación de matrices de transformación de *setting* bajo la tabla de subgrupos conjugados de la Figura 52. La matriz alternativa introducida ha sido (-**b**-**c**, -**a**+**c**, **a**+**b**-**c**; 1/2, 3/2, -1/2), que resulta ser equivalente a la matriz del subgrupo conjugado número 2 de la tabla de la Figura 52. Obtenido con MAXMAGN.

MAXMAGN proporciona tan sólo algunas de estas matrices alternativas. En concreto, proporciona aquellas derivadas de utilizar como $\boldsymbol{P_N}$ aquellos *coset representatives* de (27) que pertenecen a $\mathbf{N_M}$ pero no a **M**. En el caso de MSGs monoclínicos y triclínicos, para los cuales existen infinitas matrices $\boldsymbol{P}'$, se indican sólo algunas de las más sencillas. El objetivo de este listado es únicamente proporcionar información útil en el caso de que el usuario desee pasar a un *setting* estándar del grupo y de la estructura

magnética correspondiente. En muchos casos, la transformación al *setting* estándar elegida arbitrariamente por el programa puede dar lugar a una celda unidad o un origen con características indeseadas desde un punto de vista práctico o estético, en cuyo caso este listado permite buscar una celda unidad y origen más adecuados dentro de los muchos posibles como *setting* estándar para el MSG.

Bajo la tabla de subgrupos conjugados se incluye un formulario que permite introducir una matriz de transformación para comprobar si es equivalente a alguna de las matrices de la clase de conjugación (Figura 54). Esta herramienta resulta útil si se conoce un MSG particular susceptible de describir la simetría magnética de la estructura y se quiere comprobar si es equivalente a alguno de los subgrupos de la clase de conjugación, o bien para utilizar en MAXMAGN un MSG definido por una matriz de transformación particular.

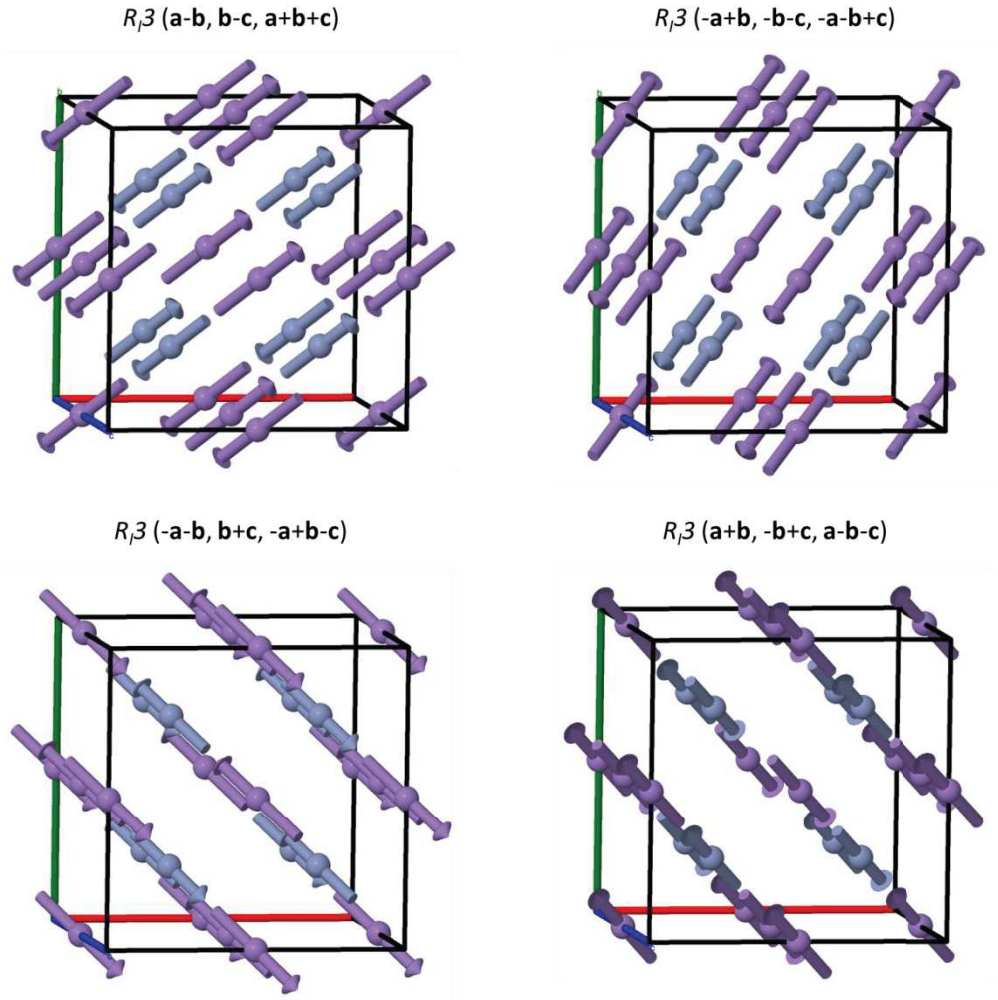

Figura 55. Estructuras magnéticas de los dominios asociados a los cuatro subgrupos conjugados de la tabla de la Figura 52, obtenidas con MVISUALIZE a través de MAXMAGN. Todas ellas están descritas en el *setting parent-like*.

Finalmente, al igual que en la utilidad de descenso a subgrupos (§7.4.1), tanto la tabla de la Figura 52 (columna "*Choose Matrix*") como los resultados de las Figuras 53 y 54 incluyen botones "*Choose*" que permiten seleccionar los diversos subgrupos definidos

por las diversas matrices. Esta selección carga el MSG elegido en MAXMAGN, de forma similar a como puede verse en la Figura 49(b), lo que permite utilizar con ellos las mismas utilidades que MAXMAGN ofrece para los subgrupos k-maximales, incluyendo por supuesto la obtención de los modelos de estructura magnética correspondientes. En la Figura 55 pueden verse representaciones gráficas obtenidas utilizando MVISUALIZE desde MAXMAGN de los cuatro modelos correspondientes a los cuatro subgrupos conjugados de la tabla de la Figura 52. Los valores de los momentos magnéticos escogidos para visualizar estos modelos equivalentes son los valores reales de la estructura magnética del $LaMn_3Cr_4O_{12}$ que figuran en la entrada #1.156 de MAGNDATA (§9). Como puede observarse, estas cuatro estructuras representan dominios con diferentes orientaciones de los momentos magnéticos, correspondientes a las cuatro direcciones trigonales del grupo padre cúbico.

7.4.3 Reglas de ausencia sistemática

Las listas de subgrupos proporcionadas por MAXMAGN (Figuras 33, 35, 38, 41, 46, 49(b) y 51) incluyen la columna "*Properties*", en la cual hay un botón que permite utilizar MAGNEXT desde MAXMAGN. Esto permite obtener las reglas de ausencia sistemática y la forma adaptada a la simetría del factor de estructura correspondientes a los MSG proporcionados por MAXMAGN.

En el ejemplo de la Figura 56, se puede ver el resultado de esta opción para el caso del La_2LiRuO_6 [42], en el que existen dos subgrupos k-maximales posibles (Figura 41): *P2'$_1$/c'* (#14.79) y *P2$_1$/c* (#14.75).

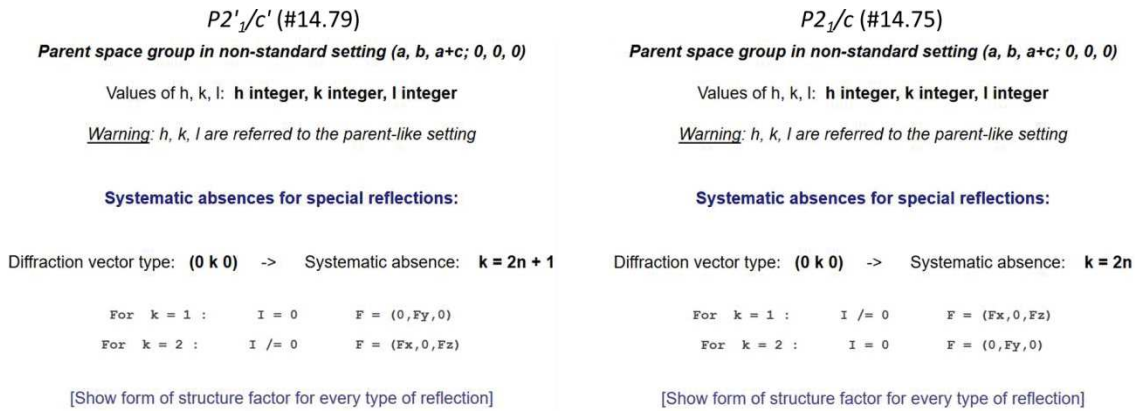

Figura 56. Reglas de ausencia sistemática correspondientes a los subgrupos k-maximales *P2'$_1$/c'* (#14.79) y *P2$_1$/c* (#14.75) del grupo padre *P2$_1$/c* (#14) para **k** = (0, 0, 0), caso que corresponde a la estructura magnética del La_2LiRuO_6. Obtenidas con MAGNEXT a través de MAXMAGN.

Como puede observarse, ambos subgrupos k-maximales poseen reglas de ausencia sistemática diferentes a lo largo de la dirección (0 *k* 0) del espacio recíproco, por lo que la observación de esta dirección en el patrón de difracción permitiría descartar uno de los grupos. En este caso particular, asumiendo que el MSG será k-maximal, la mera observación del cumplimiento o violación de una regla de ausencia sistemática

determina el MSG de la estructura magnética: la mera presencia de la reflexión (0 1 0) o (0 2 0) en el patrón de difracción magnética indica qué MSG es el correcto (en este caso, debe tenerse presente que las reflexiones (0 *k* 0) con *k* impar están prohibidas para las difracción no magnética, mientras que las de *k* par están presentes siempre). Aunque habitualmente las reglas de ausencia sistemática no son tan determinantes como en este ejemplo, es habitual que algunos MSGs tengan reglas de ausencia sistemática diferentes e incompatibles entre sí, por lo que el cotejado de los resultados de MAXMAGN con el patrón de difracción magnética de neutrones no polarizados permite en muchos casos reducir el número de modelos posibles. Otro ejemplo de la utilización conjunta de MAXMAGN y MAGNEXT para restringir el número de modelos estructurales compatibles con los datos experimentales se puede encontrar en §C2.4.

7.4.4 Propiedades tensoriales

La columna "*Properties*" en las listas de subgrupos proporcionadas por MAXMAGN (Figuras 33, 35, 38, 41, 46, 49(b) y 51) incluye también un botón que permite utilizar MTENSOR desde MAXMAGN. Con este botón se accede a la interfaz principal de MTENSOR (§10), en la cual el MPG correspondiente al MSG seleccionado aparece cargado. Mediante esta conexión entre MAXMAGN y MTENSOR, se puede obtener la forma restringida por simetría en el *setting parent-like* de cualquier tensor cristalino correspondiente a cualquier MSG proporcionado por MAXMAGN.

Por ejemplo, en el caso de La_2LiRuO_6 [42], puede observarse (Figura 57) que algunos tensores cristalinos tienen formas restringidas por simetría no sólo diferentes, sino complementarias, para cada MSG, de forma que la observación macroscópica de una sola componente de cualquier tensor cristalino que sea nula por simetría para uno de los MSGs y pueda ser no nula para el otro, permitiría determinar el MSG de la fase magnética. En este caso, la observación de cualquiera de las componentes de la magnetización y del tensor magnetoeléctrico de segundo orden sirve para discriminar entre ambos MSGs. Asimismo, puede observarse que las componentes 123 y 213 del efecto Hall (componentes antisimétricas del tensor de magnetorresistencia $\boldsymbol{R}_{ijk}$) son opuestas para el MSG $P2'_1/c'$, mientras que son diferentes para el MSG $P2_1/c$, debido a que una pequeña componente simétrica en *ij* asociada a la transición de fase magnética está permitida por simetría únicamente si el MSG es $P2_1/c$; la observación de esta violación de la antisimetría de estas componentes del efecto Hall permitiría, de nuevo, determinar el MSG de la estructura magnética.

7.5 Utilización de MAXMAGN en la búsqueda de materiales multiferroicos tipo II

***NOTA**: Puede encontrarse información adicional a la expuesta en este capítulo en la publicación recogida en el anexo D.*

El programa MAXMAGN puede ser utilizado para identificar situaciones en las cuales las restricciones impuestas a la simetría por el vector de propagación provocan un

escenario favorable a la existencia de propiedades multiferroicas de tipo II (§1). Los materiales multiferroicos de tipo II son de gran interés, al estar sus propiedades ferroeléctricas acopladas directamente con su ordenamiento magnético.

Tensor de magnetización

P2'$_1$/c' (#14.79)

M_i		
i	1	M_1
	2	0
	3	M_3

P2$_1$/c (#14.75)

M_i		
i	1	0
	2	M_2
	3	0

Efecto Hall (tensor de magnetorresistencia)

P2'$_1$/c' (#14.79)

R_{ijk}		k		
		1	2	3
ij	11	R_{111}	0	R_{113}
	12	R_{121}	R_{122}	R_{123}
	13	R_{131}	R_{132}	R_{133}
	21	$-R_{121}$	R_{122}	$-R_{123}$
	22	R_{221}	0	R_{223}
	23	R_{231}	R_{232}	R_{233}
	31	R_{131}	$-R_{132}$	R_{133}
	32	$-R_{231}$	R_{232}	$-R_{233}$
	33	R_{331}	0	R_{333}

P2$_1$/c (#14.75)

R_{ijk}		k		
		1	2	3
ij	11	0	R_{112}	0
	12	R_{121}	0	R_{123}
	13	0	R_{132}	0
	21	R_{211}	0	R_{213}
	22	0	R_{222}	0
	23	R_{231}	0	R_{233}
	31	0	R_{312}	0
	32	R_{321}	0	R_{323}
	33	0	R_{332}	0

Tensor magnetoeléctrico de segundo orden

P2'$_1$/c' (#14.79)

α_{ijk}		jk								
		11	12	13	21	22	23	31	32	33
i	1	α_{111}	0	α_{113}	0	α_{122}	0	α_{113}	0	α_{133}
	2	0	α_{212}	0	α_{212}	0	α_{223}	0	α_{223}	0
	3	α_{311}	0	α_{313}	0	α_{322}	0	α_{313}	0	α_{333}

P2$_1$/c (#14.75)

α_{ijk}		jk								
		11	12	13	21	22	23	31	32	33
i	1	0	α_{112}	0	α_{112}	0	α_{123}	0	α_{123}	0
	2	α_{211}	0	α_{213}	0	α_{222}	0	α_{213}	0	α_{233}
	3	0	α_{312}	0	α_{312}	0	α_{323}	0	α_{323}	0

Figura 57. Forma restringida por simetría de los tensores cristalinos (magnetización, efecto Hall y efecto magnetoeléctrico de segundo orden) correspondiente a los MPGs asociados a los MSGs k-maximales *P2'$_1$/c'* (#14.79) y *P2$_1$/c* (#14.75) para el caso de La_2LiRuO_6 [42]. Obtenidas con MAGNEXT a través de MAXMAGN.

El Anexo D recoge la publicación titulada "*Symmetry conditions for type II multiferroicity in commensurate magnetic structures*", en la cual se analizan estos escenarios favorables a la multiferroicidad tipo II desde el punto de vista de la simetría magnética, y se muestra cómo usar MAXMAGN para hallar este tipo de casos. El estudio, que está restringido, por sencillez, a estructuras 1k, muestra que las condiciones que hacen favorable la multiferroicidad tipo II son

- Grupo padre no polar, que sería polar de no ser por la presencia de ejes helicoidales y/o planos de deslizamiento
- Vector de propagación incompatible con la conservación, primados o sin primar, de dichos ejes helicoidales y/o planos de deslizamiento
- Átomos magnéticos ubicados en posiciones de Wyckoff compatibles con la existencia de momentos magnéticos no nulos y, a ser posible, con un ordenamiento de espines colineal asociado

Si se dan estas condiciones, la transición de fase magnética es una transición de fase entre una fase no polar y una polar, lo que implica que la aparición de ferroelectricidad a lo largo del eje polar de la fase de baja simetría podría ser un efecto magnéticamente inducido, pues de acuerdo con el principio de Neumann [48], todo ordenamiento magnético en un material aislante cuya aparición produzca una ruptura de simetría de un grupo puntual no polar a un grupo puntual polar es susceptible de presentar ferroelectricidad impropia. La identificación de estructuras magnéticas que encajan en el escenario descrito sirve para identificar materiales potencialmente multiferroicos de tipo II.

Los capítulos §D.2 y §D.3 exponen los argumentos teóricos que hay tras las condiciones antes expuestas, e incluyen diversos ejemplos de incompatibilidad entre vectores de propagación, ejes helicoidales/planos de deslizamiento y ciertas posiciones de Wyckoff. El capítulo §D.4 explica la importancia de los átomos no magnéticos de la estructura en la aparición de multiferroicidad, subrayando el error que constituye la falsa percepción habitual de que basta con considerar el ordenamiento de espines asociado a los átomos magnéticos para hallar las propiedades de una estructura magnética, pues muy a menudo la simetría puntual del ordenamiento de espines es superior a la del cristal considerado en su conjunto, siendo los átomos no magnéticos los responsables de disminuir la simetría del cristal, provocando en el caso que nos ocupa que la estructura magnética sea polar en situaciones en las que la estructura magnética no lo sería si se obviara la presencia de los átomos no magnéticos.

A continuación, el capítulo §D.5 analiza otros escenarios favorables que incrementan la probabilidad de multiferroicidad cuando la incompatibilidad entre vector de propagación y ejes helicoidales/planos de deslizamiento no basta: simetrías k-maximales polares, *irreps* multidimensionales con *epikernels* polares, reducción de simetría debida a la incompatibilidad de algunos elementos de simetría con dos o más posiciones de Wyckoff ocupadas por átomos magnéticos y ausencia de centro de inversión en grupos de alta simetría no polares. Finalmente, el capítulo §D.6 hace uso de la colección de estructuras magnéticas de MAGNDATA (§9) para analizar los escasos casos en los que o bien se dan las condiciones antes mencionadas pero la estructura

no presenta multiferroicidad tipo II, o bien la presenta pese a que no cumple las condiciones antes mencionadas. Estas excepciones se analizan, encontrándose que se deben o bien a probables errores, o bien a situaciones muy excepcionales. Mención aparte merece el interesante caso del aislante de Mott GeV_4S_8, que cumple las condiciones de multiferroicidad tipo II y además presenta una transición de fase a una fase ferroeléctrica previa a la fase magnética, por lo que es multiferroico tipo I. Este caso único presenta tanto ferroelectricidad intrínseca como magnéticamente inducida, por lo que es un caso intermedio entre multiferroico tipo I y multiferroico tipo II.

8. MODELIZACIÓN Y VISUALIZACIÓN DE ESTRUCTURAS MAGNÉTICAS: PROGRAMAS MAGMODELIZE Y MVISUALIZE

***NOTA**: Puede encontrarse información adicional a la expuesta en este capítulo en las publicaciones incluidas en los anexos C y E.*

Para casos sencillos, los subgrupos k-maximales y los modelos que les corresponden proporcionados por MAXMAGN son suficientes como punto de partida para la determinación de la estructura magnética y su simetría. MAXMAGN, proporcionando un conjunto de posibles modelos compatibles con los datos experimentales con alta probabilidad de corresponder a la estructura, permite acotar el problema y desde un principio limitar con éxito el número de parámetros libres a considerar. Sin embargo, existen situaciones para las cuales el uso de MAXMAGN no es suficiente. Existen casos en los que hay más de un vector de propagación asociado a la transición de fase magnética, o casos en que todos los subgrupos k-maximales ofrecidos por MAXMAGN no son compatibles con los datos experimentales, y es necesario descender a subgrupos no k-maximales. Estos casos evidencian la necesidad de disponer de una herramienta que permita analizar un MSG cualquiera, subgrupo del grupo padre, y obtener un modelo general de la estructura magnética consistente con él, de forma que se puedan utilizar para él las mismas utilidades que proporciona MAXMAGN.

Haciendo uso de los programas del *Bilbao Crystallographic Server*, la mejor forma de proceder en los casos en que los MSGs k-maximales quedan descartados es utilizar conjuntamente los programas K-SUBGROUPSMAG y MAGMODELIZE. El primero permite obtener una lista de todos los subgrupos, k-maximales o no, para un grupo padre gris **Gp1'** y uno o más vectores **k** dados. Estos subgrupos se pueden obtener también en forma de árbol, de forma que puede visualizarse la jerarquía grupo-subgrupo que existe entre ellos. Además, K-SUBGROUPSMAG incluye herramientas adicionales que permiten filtrar los subgrupos obtenidos, especificando datos adicionales tales como *irreps* activas, posiciones de Wyckoff ocupadas por los átomos magnéticos, etc.

Para analizar y modelizar una estructura bajo la simetría magnética descrita por un subgrupo cualquiera de **Gp1'**, ya sea uno proporcionado por K-SUBGROUPSMAG o uno obtenido por otros medios, y poder hacer uso con él de las mismas utilidades presentes en MAXMAGN se ha creado el programa MAGMODELIZE, un programa muy similar a MAXMAGN tanto en su formato como en las herramientas que incorpora. Por otro lado, K-SUBGROUPSMAG incorpora un sencillo formulario que permite enviar a MAGMODELIZE cualquier subgrupo proporcionado por dicho programa.

Por último, se ha creado una herramienta de visualización de estructuras magnéticas: el programa MVISUALIZE, cuyo propósito principal es visualizar estructuras magnéticas tanto conmensurables como inconmensurables en 3D. Para poder ser representadas por MVISUALIZE, las estructuras magnéticas deben ser introducidas en formato magCIF (con extensión .mcif en nuestros programas), que es el formato estándar de comunicación de estructuras magnéticas recientemente creado [5], o bien en formato

PNG-3D (imagen en formato PNG generado con Jmol que contiene en su interior un archivo magCIF comprimido). MVISUALIZE hace uso del programa Jmol [14] en su forma adaptada al lenguaje Javascript (JSmol) para representar en 3D las estructuras magnéticas. Los programas MAXMAGN (§7), MAGMODELIZE (§8.1) y MAGNDATA (§9) enlazan directamente con MVISUALIZE para representar las estructuras magnéticas que proporcionan. Además, MVISUALIZE incorpora herramientas adicionales y enlaces externos que permiten realizar tareas y obtener datos acerca de la estructura magnética cargada, tales como cambio de *setting*, obtención de tensores cristalinos vía MTENSOR (§10) y obtención de estructuras equivalentes asociadas a dominios (§8.3) y sus tensores cristalinos (§10).

8.1 Modelización de estructuras magnéticas: programa MAGMODELIZE

La utilización de MAGMODELIZE (http://www.cryst.ehu.es/cryst/magmodelize.html) resulta muy similar a la de MAXMAGN; por ello, todo lo expuesto en las secciones §7.2, §7.3 y §7.4 sobre el funcionamiento de MAXMAGN es también aplicable a MAGMODELIZE. La página principal de MAGMODELIZE (Figura 58) posee elementos comunes a la de MAXMAGN, que funcionan de la misma manera. Sin embargo, el formulario es diferente, pues en MAGMODELIZE en lugar del vector de propagación debe introducirse el tipo de MSG que corresponde al subgrupo que se desea analizar. Esto se hace introduciendo la etiqueta del MSG en el formulario correspondiente, o seleccionando dicho grupo en el formulario de selección de MSGs accesible haciendo clic en el botón "*Choose it*" (Figura 13(b)), e indicando a continuación la matriz de transformación desde el *setting* del grupo padre al *setting* estándar del MSG que corresponde al subgrupo.

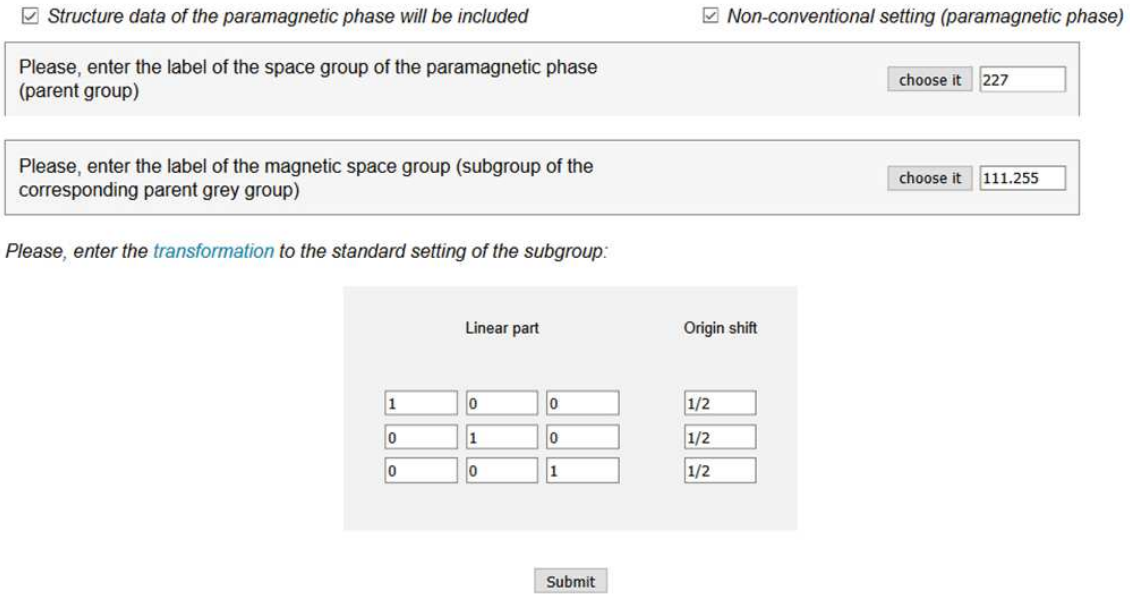

Figura 58. Interfaz de la página principal del programa MAGMODELIZE.

Por ejemplo, en el caso del $MgCr_2O_4$ (caso #3.4 de MAGNDATA (§9)) [49] la simetría de la estructura magnética está descrita por el MSG *P-42'm'* (**a**, **b**, **c**; 1/2, 1/2, 1/2)

(#111.255) siendo el grupo padre *Fd-3m* (**a**, **b**, **c**; -1/8, -1/8, -1/8) (#227). Estos datos, incluido un archivo CIF con la estructura de la fase paramagnética si procede, deben introducirse en el formulario de la página principal de MAGMODELIZE (Figura 58). En esta estructura magnética tetragonal, proveniente de una estructura paramagnética cúbica, el átomo magnético de Cr tiene los momentos alineados según las diagonales de la celda unidad cúbica de la fase paramagnética. Sin embargo, dado que su simetría es tetragonal, con el eje 4 según los ejes *x*, *y* o *z*, esta dirección particular de los momentos magnéticos sin duda no está estrictamente forzada por la simetría. Por ello, puede resultar interesante obtener el modelo de estructura magnética asociado a su MSG para así conocer cuáles son realmente los parámetros libres de dicho modelo, qué restricciones cumplen y qué desviaciones de los momentos con respecto a las direcciones de las diagonales del cubo son compatibles con la simetría magnética y por tanto teóricamente posibles. Para responder a estas cuestiones es necesario obtener con MAGMODELIZE el modelo de estructura magnética asociado al MSG de la estructura.

(a)

Selected magnetic space subgroup for the parent space group 227 (*Fd-3m*)

Parent space group in non-standard setting (a, b, c; 1/8, 1/8, 1/8)

Maximal subgroups which allow non-zero magnetic moments for at least one atom are coloured

N	Group (BNS)	Transformation matrix	General positions	Properties	Magnetic structure
1	*P-42'm'* (#111.255) Go to a subgroup	$\begin{pmatrix} 1 & 0 & 0 & 1/2 \\ 0 & 1 & 0 & 1/2 \\ 0 & 0 & 1 & 1/2 \end{pmatrix}$ Alternatives (domain-related)	Show	*Systematic absences* MAGNEXT *Tensor properties* MTENSOR	Show

(b)

3	Cr2_1 Cr 0.62500 0.62500 0.62500	0.5	(5/8,5/8,5/8 | m_x,m_x,m_z) (3/8,3/8,5/8 | -m_x,-m_x,m_z) (3/8,5/8,3/8 | m_x,-m_x,m_z) (5/8,3/8,3/8 | -m_x,m_x,m_z)	4	(M_x,M_x,M_z)	M_x = 0.00000 M_z = 0.00000
	Cr2_2 Cr 0.37500 0.87500 0.12500	0.5	(3/8,7/8,1/8 | m_x,m_y,m_z) (1/8,3/8,7/8 | m_y,-m_x,m_z) (5/8,1/8,1/8 | -m_x,-m_y,m_z) (1/8,5/8,1/8 | -m_y,-m_x,m_z) (7/8,3/8,1/8 | m_y,m_x,m_z) (7/8,5/8,7/8 | -m_y,m_x,m_z) (3/8,1/8,7/8 | -m_x,m_y,m_z) (5/8,7/8,7/8 | m_x,-m_y,m_z)	8	(M_x,M_y,M_z)	M_x = 0.00000 M_y = 0.00000 M_z = 0.00000
	Cr2_3 Cr 0.87500 0.12500 0.37500	0.5	(7/8,1/8,3/8 | m_x,-m_x,m_z) (1/8,1/8,5/8 | m_x,m_x,m_z) (7/8,7/8,5/8 | -m_x,-m_x,m_z) (1/8,7/8,3/8 | -m_x,m_x,m_z)	4	(M_x,-M_x,M_z)	M_x = 0.00000 M_z = 0.00000

Figura 59. (a) Listado de subgrupos en MAGMODELIZE, indicando el MSG introducido. (b) Átomos magnéticos del modelo de estructura magnética correspondiente al indicado en (a), obtenidos con MAGMODELIZE.

MAGMODELIZE proporciona una tabla de subgrupos con idénticas características que las tablas proporcionadas por MAXMAGN (Figuras 33, 35, 38, 41, 46, 49(b) y 51), pero donde figura únicamente el MSG introducido (Figura 59(a)). A partir de este punto, el funcionamiento y las utilidades de MAGMODELIZE son idénticas a las de MAXMAGN y no requieren mayores explicaciones. Al igual que MAXMAGN, MAGMODELIZE permite obtener el modelo de estructura magnética correspondiente al MSG introducido (Figura 59(b)), donde puede observarse en el ejemplo que, por un lado, la órbita del átomo magnético Cr_2 se divide en tres órbitas en la fase de baja simetría que, en teoría, al no estar ligadas por simetría admiten momentos de diferente tamaño; y por

otro lado, puede observarse que de los 16 átomos dentro de la celda unidad tan sólo 8 (pertenecientes a dos de las tres órbitas) presentan alguna restricción en su momento magnético, restricción que fuerza a los momentos a tener una dirección diagonal en el plano *xy*, siendo la componente *z* un parámetro libre.

Como se ha mencionado, MAGMODELIZE es también accesible desde K-SUBGROUPSMAG. La combinación de ambos programas permite llegar de forma fácil y sistemática a los modelos de estructura magnética y su simetría, que son relevantes en la mayoría de los casos, incluyendo los más complejos. Por ejemplo, la estructura magnética del TmAgGe (caso #3.1 de MAGNDATA (§9)) [50], cuyo grupo padre es *P-62m* (#189), es un caso de estructura magnética con 3 vectores de propagación, (1/2,0,0), (1/2,1/2,0) y (0,1/2,0). K-SUBGROUPSMAG permite obtener todos los subgrupos compatibles con este conjunto de vectores **k**. Además, estos subgrupos pueden ser filtrados especificando la o las WPs del grupo padre ocupadas por los átomos magnéticos (en este caso, la WP 3g) y especificando la *irrep* asociada a la fase magnética (en este caso, la *irrep* mM2). Introduciendo estos filtros en K-SUBGROUPSMAG, se obtiene una lista de los subgrupos compatibles con los datos introducidos (Figura 60).

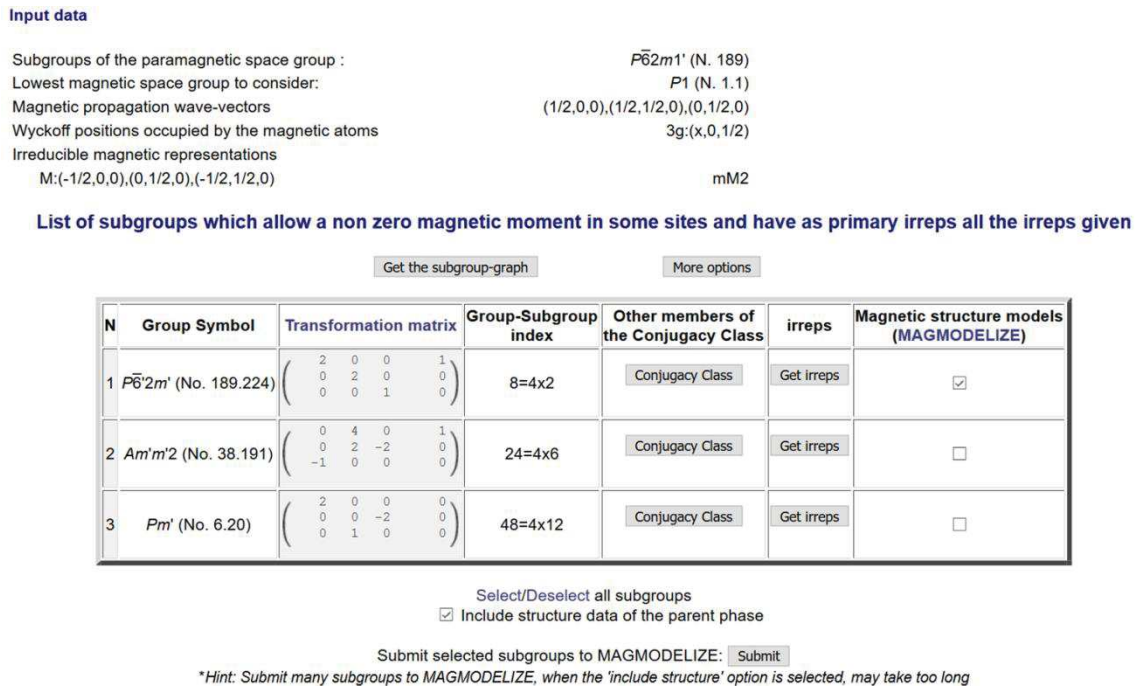

Input data

Subgroups of the paramagnetic space group :	$P\bar{6}2m1'$ (N. 189)
Lowest magnetic space group to consider:	$P1$ (N. 1.1)
Magnetic propagation wave-vectors	(1/2,0,0),(1/2,1/2,0),(0,1/2,0)
Wyckoff positions occupied by the magnetic atoms	3g:(x,0,1/2)
Irreducible magnetic representations	
M:(-1/2,0,0),(0,1/2,0),(-1/2,1/2,0)	mM2

List of subgroups which allow a non zero magnetic moment in some sites and have as primary irreps all the irreps given

Get the subgroup-graph More options

N	Group Symbol	Transformation matrix	Group-Subgroup index	Other members of the Conjugacy Class	irreps	Magnetic structure models (MAGMODELIZE)
1	$P\bar{6}'2m'$ (No. 189.224)	$\begin{pmatrix} 2 & 0 & 0 & 1 \\ 0 & 2 & 0 & 0 \\ 0 & 0 & 1 & 0 \end{pmatrix}$	8=4x2	Conjugacy Class	Get irreps	☑
2	$Am'm'2$ (No. 38.191)	$\begin{pmatrix} 0 & 4 & 0 & 1 \\ 0 & 2 & -2 & 0 \\ -1 & 0 & 0 & 0 \end{pmatrix}$	24=4x6	Conjugacy Class	Get irreps	☐
3	Pm' (No. 6.20)	$\begin{pmatrix} 2 & 0 & 0 & 0 \\ 0 & 0 & -2 & 0 \\ 0 & 1 & 0 & 0 \end{pmatrix}$	48=4x12	Conjugacy Class	Get irreps	☐

Select/Deselect all subgroups
☑ Include structure data of the parent phase

Submit selected subgroups to MAGMODELIZE: Submit
**Hint: Submit many subgroups to MAGMODELIZE, when the 'include structure' option is selected, may take too long*

Figura 60. Lista obtenida con K-SUBGROUPSMAG de subgrupos del grupo padre *P-62m* compatibles con los vectores de propagación (1/2,0,0), (1/2,1/2,0) y (0,1/2,0), con átomos magnéticos en la WP 3g y asociados a la *irrep* mM2.

Como puede observarse en la Figura 60, tan sólo hay 3 subgrupos de *P-62m* que cumplen las condiciones exigidas. De este conjunto, dada la tendencia general a la maximalidad de la simetría magnética (§7.1.2), los que son maximales entre ellos, es decir, que ningún otro de los subgrupos de la lista de la Figura 60 sea supergrupo suyo, se pueden considerar los que más probablemente describan la simetría de la fase investigada para la *irrep* relevante introducida en K-SUBGROUPSMAG. K-

SUBGROUPSMAG permite conocer la jerarquía grupo-subgrupo entre ellos, lo que permite saber cuáles son maximales. Basta con presionar el botón "*Get the subgroup-graph*" que hay sobre la tabla de la Figura 60. El resultado se plasma en la Figura 61, donde se ve que el subgrupo *P-6'2m'* (#189.224) es el único subgrupo maximal a considerar. Este subgrupo resulta ser el que efectivamente describe la simetría de la fase magnética.

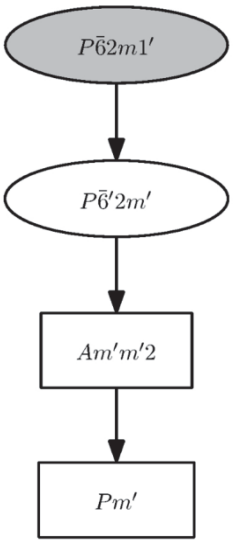

Figura 61. Árbol de subgrupos del grupo padre *P-62m*, indicado por un óvalo con el fondo relleno, obtenido con K-SUBGROUPSMAG. El MSG maximal *P-6'2m'* está indicado por un óvalo, y el resto de MSGs no maximales con un rectángulo.

La columna "*Magnetic structure models (MAGMODELIZE)*" en los listados de subgrupos proporcionados por k-SUBGROUPSMAG (Figura 60) permite seleccionar aquellos casos que se desean enviar a MAGMODELIZE. Bajo la tabla, los enlaces "*Select/Deselect*" permiten seleccionar y deseleccionar, respectivamente, todos los subgrupos de la tabla. La casilla "*Include structure data of the parent phase*" debe ser seleccionada si se desea especificar la estructura de la fase paramagnética; en caso de que se marque esta casilla, MAGMODELIZE pedirá especificar la estructura antes de cargar los subgrupos seleccionados, proceso que es idéntico al explicado para MAXMAGN en §7.3. De esta forma, podemos obtener modelos de estructura magnética consistentes con cualquiera de los subgrupos seleccionados.

El resultado es una tabla, similar a la de la Figura 59(a), que en esta ocasión incluye el subgrupo o subgrupos seleccionados en K-SUBGROUPSMAG (Figura 62(a)). La estructura magnética correspondiente al MSG obtenido se muestra en la Figura 62(b). Como puede verse, la determinación del MSG permite determinar parcialmente la estructura magnética, quedando únicamente 4 parámetros libres a refinar.

Más ejemplos sobre la utilización conjunta de MAGMODELIZE y K-SUBGROUPSMAG pueden encontrarse en las publicaciones recogidas en los Anexos C y E. Un ejemplo de utilización de estas herramientas para facilitar la determinación de una estructura con más de un vector de propagación puede encontrarse en §C2.6. Dos ejemplos que

incluyen el uso en K-SUBGROUPSMAG de los filtros de WPs e *irreps* pueden hallarse en §E.5.

(a)

Selected magnetic space subgroup for the parent space group 189 (*P-62m*)

Maximal subgroups which allow non-zero magnetic moments for at least one atom are coloured

N	Group (BNS)	Transformation matrix	General positions	Properties	Magnetic structure
1	*P-6'2m'* (#189.224) Go to a subgroup	$\begin{pmatrix} 2 & 0 & 0 & 1 \\ 0 & 2 & 0 & 0 \\ 0 & 0 & 1 & 0 \end{pmatrix}$ Alternatives (domain-related)	Show	*Systematic absences* MAGNEXT *Tensor properties* MTENSOR	Show

(b)

1	Tm1_1 Tm 0.28800 0.00000 0.50000	(x,0,1/2 | m_x,0,0) (-x,-x+1/2,1/2 | -m_x,-m_x,0) (1/2,x+1/2,1/2 | 0,m_x,0)	3	(M_x,0,0)	M_x = 0.0000
	Tm1_2 Tm 0.00000 0.28800 0.50000	(0,x,1/2 | m_x,m_y,0) (-x,-x,1/2 | m_x-m_y,-m_y,0) (x,1/2,1/2 | -m_x+m_y,-m_x,0) (0,x+1/2,1/2 | -m_x,-m_x+m_y,0) (x+1/2,1/2,1/2 | m_y,m_x,0) (-x+1/2,-x+1/2,1/2 | -m_y,m_x-m_y,0)	6	(M_x,M_y,0)	M_x = 0.0000 M_y = 0.0000
	Tm1_3 Tm 0.78800 0.00000 0.50000	(x+1/2,0,1/2 | m_x,0,0) (1/2,x,1/2 | 0,m_x,0) (-x+1/2,-x,1/2 | -m_x,-m_x,0)	3	(M_x,0,0)	M_x = 0.0000

Figura 62. (a) Subgrupo *P-6'2m'* (#189.224) cargado en MAGMODELIZE desde K-SUBGROUPSMAG. (b) Modelo de la estructura magnética correspondiente a dicho subgrupo, obtenido con MAGMODELIZE.

8.2 Visualización de estructuras magnéticas: programa MVISUALIZE

MVISUALIZE (http://www.cryst.ehu.es/cryst/mvisualize.html) es un programa de visualización de estructuras magnéticas conmensurables e inconmensurables. Las estructuras deben ser introducidas subiendo archivos en formato magCIF o PNG-3D (Figura 63). La pantalla de visualización de estructuras magnéticas de MVISUALIZE es diferente dependiendo de si la estructura magnética introducida es conmensurable o inconmensurable, característica que MVISUALIZE detecta automáticamente.

La Figura 64 muestra la pantalla de visualización de estructuras conmensurables de MVISUALIZE para el caso de la estructura magnética del TmAgGe [50], habiendo utilizado el archivo magCIF correspondiente que está disponible en MAGNDATA (#3.1).

La pantalla interactiva de visualización de estructuras magnéticas en 3D con JSmol aparece en el centro. En ella está representada la estructura magnética, incluyendo tanto átomos como momentos magnéticos. También se indican la celda unidad y los vectores de la base en la que está representada la estructura. Arriba a la izquierda se indican el símbolo del MSG de la estructura en *setting* BNS y el o los vectores de propagación. En el caso de que se esté mostrando más de una celda unidad, como es el caso de la Figura 64, se muestra abajo en el centro un texto indicando la supercelda escogida ((**a**, **b**, 2**c**) en este caso).

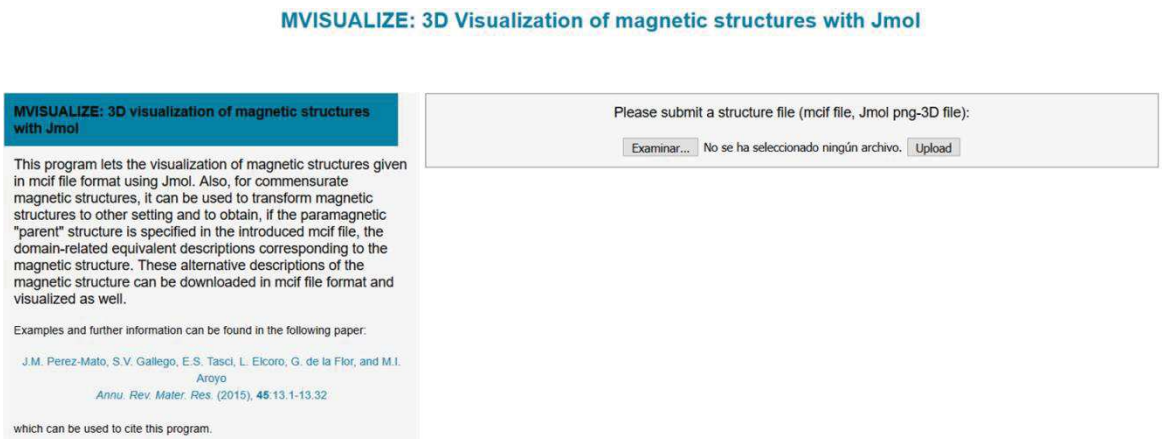

Figura 63. Página principal del programa MVISUALIZE con el formulario de carga de archivos magCIF o PNG-3D.

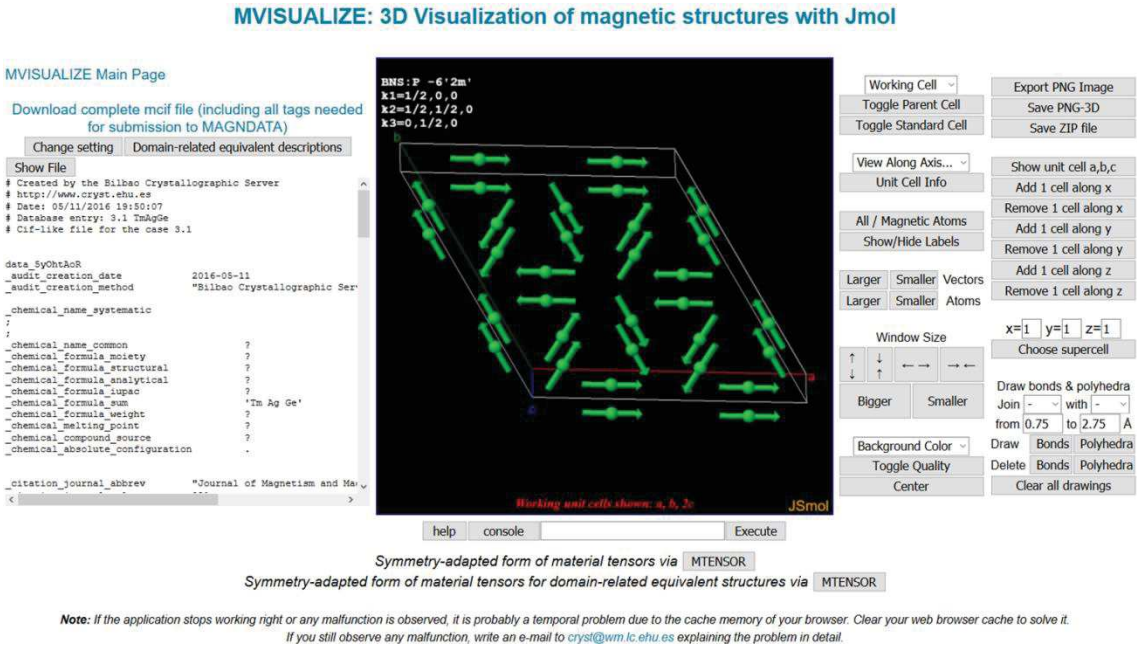

Figura 64. Página de visualización de estructuras magnéticas conmensurables de MVISUALIZE. Se muestra la estructura magnética del TmAgGe (sólo átomos magnéticos).

A izquierda y derecha, figuran numerosos botones o enlaces que permiten modificar la forma de visualizar la estructura, obtener información adicional sobre ella, descargar archivos, etc. En la parte izquierda de la Figura 64 hay un enlace titulado "*Download complete mcif file (including all tags needed for submission to MAGNDATA)*" que permite descargar un archivo magCIF "completo", es decir, un archivo magCIF que, además de incluir todos los *tags* presentes en el archivo magCIF introducido por el usuario, incluye muchos otros *tags* vacíos, que el usuario puede rellenar. Estos *tags*, algunos no oficiales y de carácter local solo usados por nuestro servidor, no son necesarios para que la estructura sea legible, pero son útiles para albergar información adicional sobre la estructura magnética. De esta forma, MVISUALIZE puede ser utilizado para obtener un archivo magCIF con todos los *tags* necesarios para poder introducir la estructura en MAGNDATA.

Existen también los botones "*Change setting*", que sirve para cambiar el *setting* de la estructura magnética, "*Domain-related equivalent descriptions*", que permite obtener las descripciones equivalentes asociadas a dominios de la estructura (§8.3) y el botón "*Show File*", que permite mostrar u ocultar el cuadro inferior, que está oculto por defecto y muestra el contenido exacto del archivo magCIF. Este cuadro de texto es no editable y se muestra únicamente con un propósito informativo.

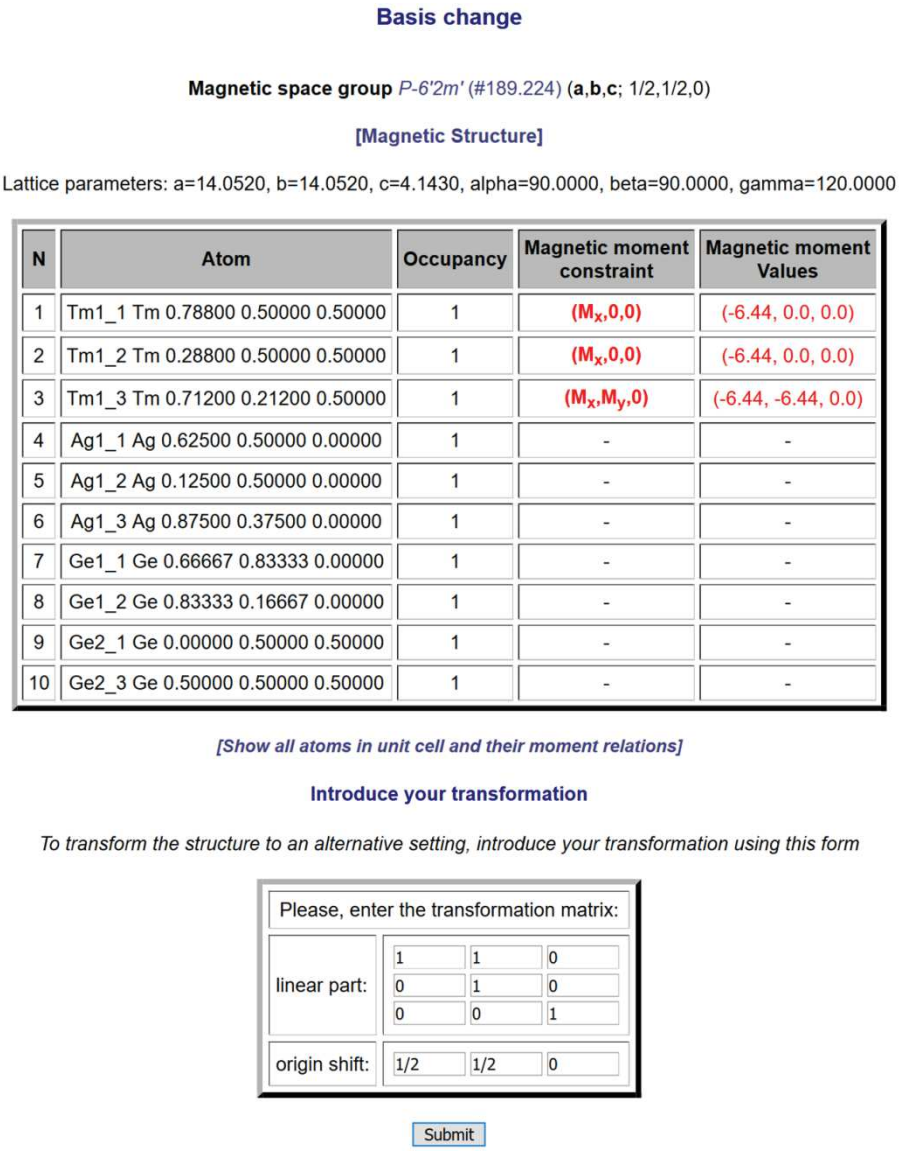

Basis change

Magnetic space group *P-6'2m'* (#189.224) (**a**,**b**,**c**; 1/2,1/2,0)

[Magnetic Structure]

Lattice parameters: a=14.0520, b=14.0520, c=4.1430, alpha=90.0000, beta=90.0000, gamma=120.0000

N	Atom	Occupancy	Magnetic moment constraint	Magnetic moment Values
1	Tm1_1 Tm 0.78800 0.50000 0.50000	1	(M_x,0,0)	(-6.44, 0.0, 0.0)
2	Tm1_2 Tm 0.28800 0.50000 0.50000	1	(M_x,0,0)	(-6.44, 0.0, 0.0)
3	Tm1_3 Tm 0.71200 0.21200 0.50000	1	(M_x,M_y,0)	(-6.44, -6.44, 0.0)
4	Ag1_1 Ag 0.62500 0.50000 0.00000	1	-	-
5	Ag1_2 Ag 0.12500 0.50000 0.00000	1	-	-
6	Ag1_3 Ag 0.87500 0.37500 0.00000	1	-	-
7	Ge1_1 Ge 0.66667 0.83333 0.00000	1	-	-
8	Ge1_2 Ge 0.83333 0.16667 0.00000	1	-	-
9	Ge2_1 Ge 0.00000 0.50000 0.50000	1	-	-
10	Ge2_3 Ge 0.50000 0.50000 0.50000	1	-	-

[Show all atoms in unit cell and their moment relations]

Introduce your transformation

To transform the structure to an alternative setting, introduce your transformation using this form

Please, enter the transformation matrix:

linear part:	1	1	0
	0	1	0
	0	0	1
origin shift:	1/2	1/2	0

Submit

Figura 65. Interfaz de la utilidad de cambio de *setting* de MVISUALIZE. Se muestran una tabla con los átomos independientes de la celda unidad del TmAgGe, un enlace para mostrar las órbitas asociadas a dichos átomos (ocultas por defecto) y la interfaz de introducción de la matriz de transformación al *setting* deseado.

A la derecha del cuadro de visualización se muestran dos columnas de botones cuyo propósito es adaptar la visualización de la estructura a los requerimientos del usuario. Los numerosos botones permiten:

- Seleccionar y visualizar alternativamente diversas celdas unidad: la original ("*Working*"), la del grupo padre ("*Parent*") y la estándar del MSG ("*Standard*").

- Mostrar la estructura proyectada a lo largo de cada uno de los tres ejes.
- Visualizar información sobre la celda unidad (parámetros de red).
- Mostrar alternativamente sólo los átomos magnéticos o todos los átomos.
- Mostrar u ocultar etiquetas con el nombre o el elemento químico de cada átomo.
- Variar el tamaño de átomos y momentos magnéticos.
- Variar el tamaño de la ventana de visualización.
- Elegir el color de fondo, la calidad de imagen, centrar la estructura.
- Descargar archivos: imagen PNG, archivo PNG-3D, archivo ZIP.
- Mostrar más de una celda unidad: elección de supercelda.
- Dibujar automáticamente o borrar enlaces entre átomos y/o poliedros.

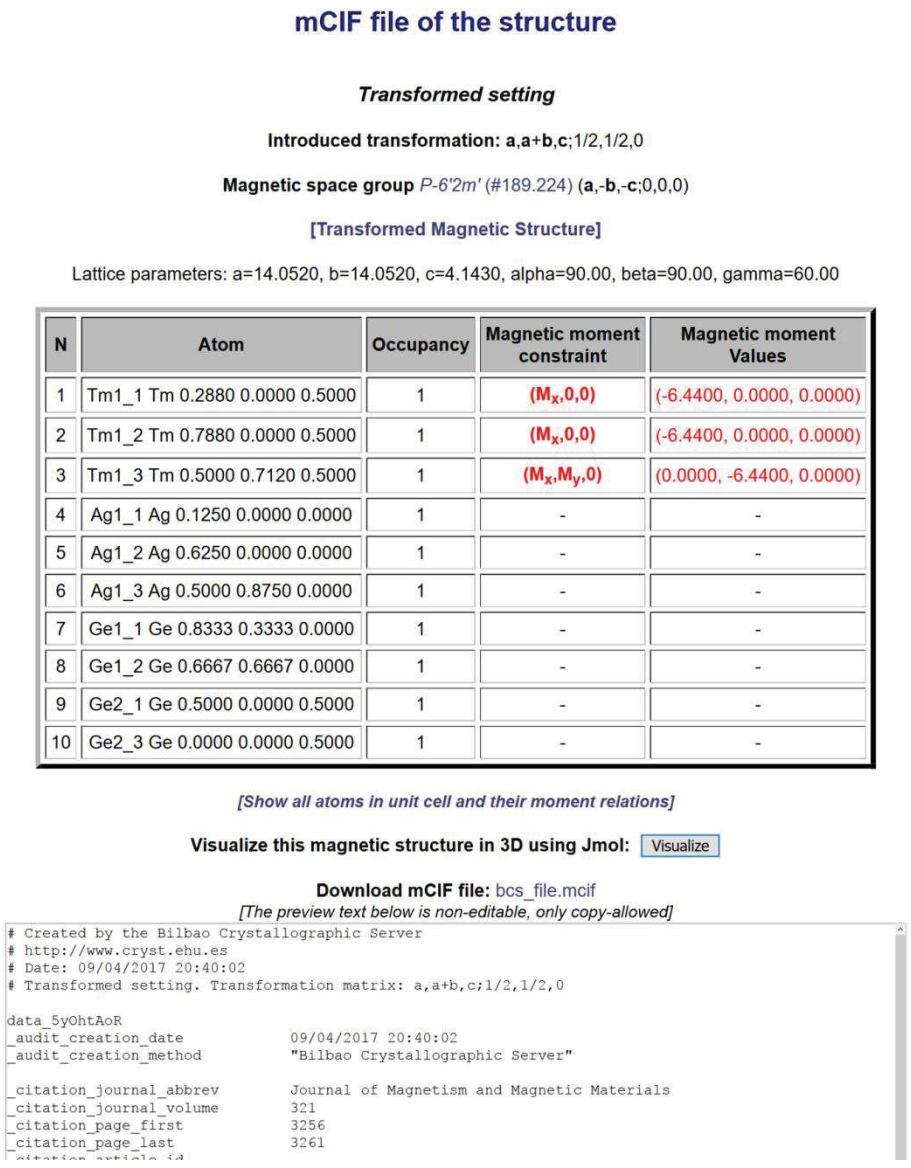

mCIF file of the structure

Transformed setting

Introduced transformation: a,a+b,c;1/2,1/2,0

Magnetic space group *P-6'2m'* (#189.224) (**a**,-**b**,-**c**;0,0,0)

[Transformed Magnetic Structure]

Lattice parameters: a=14.0520, b=14.0520, c=4.1430, alpha=90.00, beta=90.00, gamma=60.00

N	Atom	Occupancy	Magnetic moment constraint	Magnetic moment Values
1	Tm1_1 Tm 0.2880 0.0000 0.5000	1	(M_x,0,0)	(-6.4400, 0.0000, 0.0000)
2	Tm1_2 Tm 0.7880 0.0000 0.5000	1	(M_x,0,0)	(-6.4400, 0.0000, 0.0000)
3	Tm1_3 Tm 0.5000 0.7120 0.5000	1	(M_x,M_y,0)	(0.0000, -6.4400, 0.0000)
4	Ag1_1 Ag 0.1250 0.0000 0.0000	1	-	-
5	Ag1_2 Ag 0.6250 0.0000 0.0000	1	-	-
6	Ag1_3 Ag 0.5000 0.8750 0.0000	1	-	-
7	Ge1_1 Ge 0.8333 0.3333 0.0000	1	-	-
8	Ge1_2 Ge 0.6667 0.6667 0.0000	1	-	-
9	Ge2_1 Ge 0.5000 0.0000 0.5000	1	-	-
10	Ge2_3 Ge 0.0000 0.0000 0.5000	1	-	-

[Show all atoms in unit cell and their moment relations]

Visualize this magnetic structure in 3D using Jmol: Visualize

Download mCIF file: bcs_file.mcif

[The preview text below is non-editable, only copy-allowed]

```
# Created by the Bilbao Crystallographic Server
# http://www.cryst.ehu.es
# Date: 09/04/2017 20:40:02
# Transformed setting. Transformation matrix: a,a+b,c;1/2,1/2,0

data_5yOhtAoR
_audit_creation_date              09/04/2017 20:40:02
_audit_creation_method            "Bilbao Crystallographic Server"

_citation_journal_abbrev          Journal of Magnetism and Magnetic Materials
_citation_journal_volume          321
_citation_page_first              3256
_citation_page_last               3261
```

Figura 66. Estructura magnética transformada del TmAgGe mediante la transformación (**a**, **a+b**, **c**; 1/2, 1/2, 0), obtenida con MVISUALIZE. Se proporcionan un archivo magCIF descargable y un enlace para visualizar la estructura.

Bajo la pantalla de visualización, se incluyen varios botones que dan acceso a la documentación sobre JSmol ("*help*"), muestran un *pop-up* con una consola o ventana de comandos para poder introducir comandos de JSmol y ver el *output* correspondiente ("*console*") y permiten introducir comandos de JSmol de forma rápida (cuadro de texto y botón "*Execute*").

Finalmente, se incluyen dos botones que permiten utilizar el programa MTENSOR (§10) desde MVISUALIZE. El botón "*Symmetry-adapted form of material tensors via MTENSOR*" carga el MPG de la estructura en el programa MTENSOR para así poder obtener los diversos tensores cristalinos adaptados a la simetría de dicho MPG que MTENSOR permite consultar. El botón "*Symmetry-adapted form of material tensors for domain-related equivalent structures via MTENSOR*" permite hacer uso de la utilidad de MTENSOR que proporciona los tensores cristalinos adaptados a la simetría puntual de las descripciones equivalentes asociadas a los posibles dominios de la estructura.

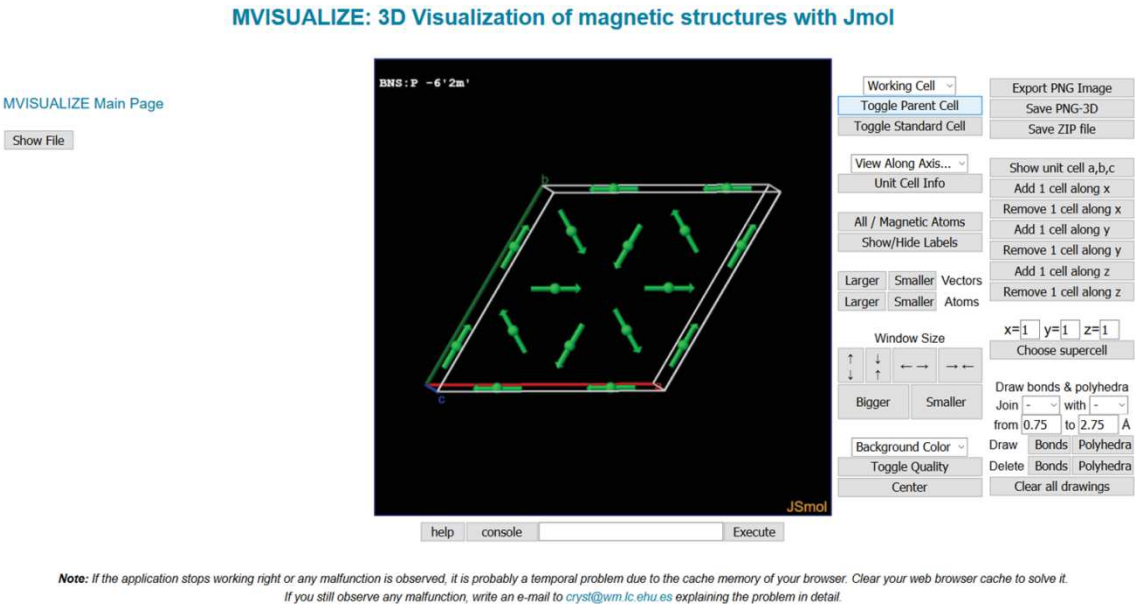

Figura 67. Visualización con MVISUALIZE de la estructura magnética transformada del TmAgGe mediante la transformación de *setting* (**a**, **a+b**, **c**; 1/2, 1/2, 0).

El botón "*Change Setting*" a la izquierda de la pantalla de visualización (Figura 64) da acceso a la utilidad de cambio de *setting* de MVISUALIZE. Primero, la interfaz de esta utilidad (Figura 65) proporciona la estructura magnética en forma de tabla de átomos independientes, así como la órbita completa asociada a cada átomo independiente (oculta por defecto); a continuación, incluye un formulario que permite transformar la estructura magnética a un *setting* alternativo introduciendo una matriz de transformación cualquiera. El único requisito es que dicha matriz lleve a un *setting* válido, es decir, uno en el que los elementos {1|1,0,0}, {1|0,1,0} y {1|0,0,1} estén presentes; MVISUALIZE comprobará si esto es así y rechazará la matriz en caso contrario. A modo de ejemplo, es posible obtener la estructura magnética del TmAgGe en un *setting* alternativo introduciendo la matriz de transformación (**a**, **a+b**, **c**; 1/2, 1/2, 0) (Figura 65). El resultado de esta operación puede verse en la Figura 66. Se proporcionan los átomos independientes y sus órbitas de la estructura magnética en el

setting transformado, así como un cuadro de texto no editable que contiene el archivo magCIF de la estructura transformada. Se incluyen, además, un enlace de descarga de dicho archivo magCIF y un botón "*Visualize*" que permite visualizar con MVISUALIZE la estructura transformada (Figura 67).

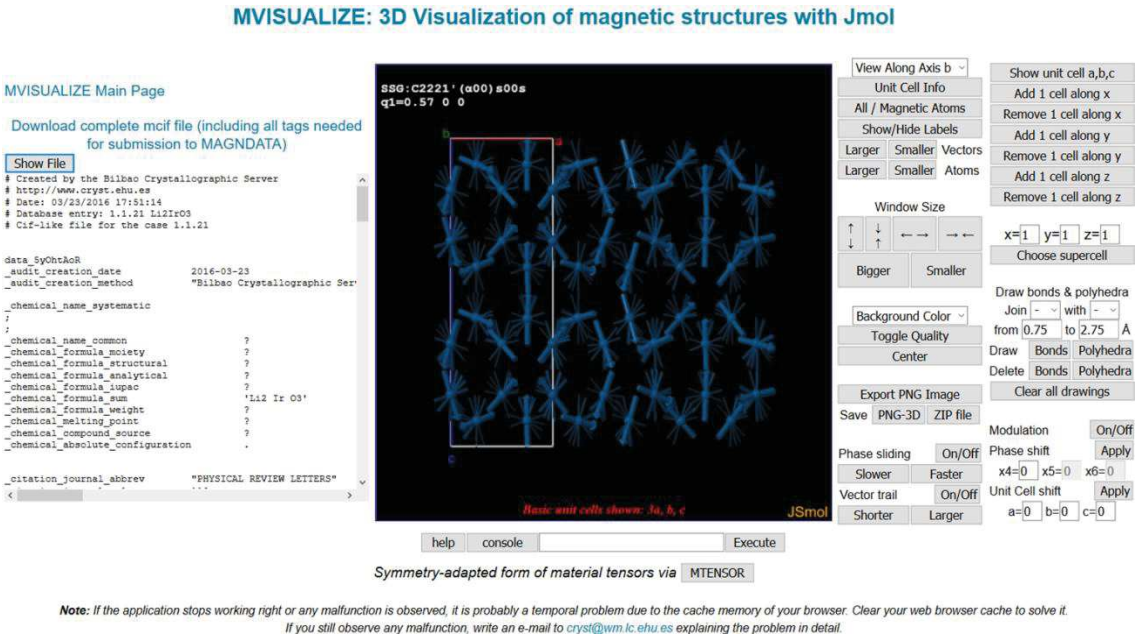

Note: *If the application stops working right or any malfunction is observed, it is probably a temporal problem due to the cache memory of your browser. Clear your web browser cache to solve it. If you still observe any malfunction, write an e-mail to cryst@wm.lc.ehu.es explaining the problem in detail.*

Figura 68. Página de visualización de estructuras magnéticas inconmensurables de MVISUALIZE. Se muestra la estructura magnética del Li_2IrO_3 [51] (sólo átomos magnéticos).

La Figura 68 muestra la pantalla de visualización de estructuras inconmensurables de MVISUALIZE para el caso de la estructura magnética del Li_2IrO_3 (caso #1.1.21 de MAGNDATA (§9)) [51]. El archivo magCIF utilizado se encuentra disponible en MAGNDATA. Esta pantalla es similar a la de las estructuras conmensurables (Figuras 64 y 67), presentando algunas diferencias. Por un lado, los enlaces a las secciones de cambio de *setting*, de obtención de descripciones equivalentes asociadas a dominios y de sus tensores cristalinos no se muestran para estructuras inconmensurables, ya que no funcionan para este tipo de estructuras.

Por otro lado, se incluyen algunas utilidades adicionales que permiten modificar la forma de visualizar la estructura magnética inconmensurable. El momento magnético de cada átomo en una estructura inconmensurable es el resultado de la adición de dos contribuciones (§2.4): por un lado, un momento magnético medio que, habitualmente, suele ser nulo; por otro lado, un momento magnético variable, distinto para cada átomo, procedente de una función periódica de periodo inconmensurable, cuyo valor particular depende del valor de su fase, es decir, de la coordenada inconmensurable x_4. La estructura magnética mostrada inicialmente corresponde a un valor nulo de dicha fase; variar esta fase equivale a mostrar el momento magnético asociado a otros átomos en otras ubicaciones del cristal. Por ello, MVISUALIZE incorpora las siguientes funcionalidades en la herramienta de visualización de estructuras magnéticas inconmensurables:

- Un botón ("*Modulation On/Off*") que permite mostrar/ocultar la contribución periódica inconmensurable a los momentos magnéticos. En modo *On*, se muestran los momentos que resultan de la adición de las dos contribuciones antes indicadas; en modo *Off*, tan sólo se muestran los momentos magnéticos promedio.
- Un selector ("*Phase shift*") del origen de la coordenada interna x_4 que permite variar el valor de la fase global de la función de modulación presente en el cristal. Aunque la mayoría de las estructuras magnéticas inconmensurables presentan sólo una modulación inconmensurable, MVISUALIZE permite la visualización de estructuras con hasta 3 modulaciones inconmensurables diferentes, permitiendo si procede variar el origen de las coordenadas internas x_4, x_5 y x_6.
- Un selector ("*Unit cell shift*") que permite modificar la o las coordenadas internas una cantidad equivalente a desplazarse a otra celda unidad. Dar valores a *a*, *b* y *c* (deben ser enteros) equivale a desplazarse a la celda unidad con un *origin shift* (*a*, *b*, *c*) para ver cuáles son los momentos magnéticos en dicha celda unidad en comparación con los de la celda original.
- Un botón "*Phase sliding On/Off*" que varía de forma continua en el tiempo el origen de la coordenada interna x_4 (sólo funciona para estructuras con una sola coordenada internas), produciendo una animación cuya velocidad es modificable (botones "*Slower/Faster*"), y que debe entenderse como un corrimiento de la fase global de la modulación en el cristal. El objetivo de esta utilidad es mostrar gráficamente los diversos valores de la dirección y módulo de los momentos magnéticos a lo largo de la modulación, y el grado de libertad (de coste energético nulo) asociado al corrimiento de fase de la modulación (fasón).
- Un botón "*Vector trail On/Off*" (sólo funciona si el *Phase sliding* está activo) que dibuja una "cola" de momentos magnéticos (Figura 68). Cada cierto tiempo, se dibuja el valor momentáneo del momento magnético, que queda preservado en la imagen durante un periodo de tiempo modificable (botones "*Shorter/Larger*"), formándose una cola de momentos magnéticos. Esto permite retener en pantalla las órbitas que describen los momentos cuando está activada la opción *Phase sliding*.

MVISUALIZE es utilizado tanto a nivel externo como interno por los programas MAXMAGN (§7), MAGMODELIZE (§8.1) y MAGNDATA (§9), para visualizar toda estructura magnética proporcionada por estos programas. Debe aclararse que cuando se utiliza MVISUALIZE desde alguno de estos programas, los botones y enlaces a las diversas utilidades de MVISUALIZE no siempre se muestran, pues algunas de estas utilidades resultan redundantes, al ser también accesibles desde el programa de partida. Los botones y enlaces que no se muestran siempre son el enlace para obtener un archivo magCIF completo, los enlaces a las secciones de cambio de *setting* y obtención de estructuras equivalentes asociadas a dominios y sus tensores, y el enlace que permite cargar el MPG de la estructura en el programa MTENSOR para poder obtener los diversos tensores cristalinos adaptados a la simetría.

8.3 Descripciones equivalentes relacionadas con dominios

***NOTA**: Puede encontrarse información adicional a la expuesta en este capítulo en el capítulo 4 del Anexo E*

MVISUALIZE incluye una utilidad adicional que permite obtener las estructuras magnéticas equivalentes a la introducida y que corresponden a los posibles dominios. Estas estructuras magnéticas físicamente equivalentes son diferentes desde el punto de vista orientacional y/o posicional con respecto a la estructura paramagnética padre. Son por tanto distinguibles, en un sistema de referencia fijo, de la estructura padre, con propiedades físicas posiblemente diferentes en dicho sistema de referencia. La transformación del sistema de una a otra de estas posibles estructuras equivalentes está en el origen de las propiedades de conmutación de estas fases. Estas estructuras se obtienen transformando la estructura magnética introducida utilizando como matriz de transformación aquellas operaciones de simetría de **Gp1'** que no pertenecen al MSG de la estructura introducida, **M** [8]. De hecho, para obtener todas las estructuras equivalentes distinguibles, basta con utilizar como posibles matrices de transformación una elección particular del conjunto de *coset representatives* de la *coset decomposition* de **Gp1'** en **M** (27). Por ello, el número de dominios o estructuras equivalentes distinguibles es igual al índice grupo-subgrupo entre **Gp1'** y **M**, y además el MSG de cada una de estas estructuras, $\mathbf{M}_i$, que puede calcularse a partir de **M** utilizando la ecuación (26), es un MSG del mismo tipo que **M**, salvo si **M** es enantiomórfico y el elemento $g_i \in$ **Gp1'** utilizado en (26) para obtener la estructura equivalente es una rotoinversión, en cuyo caso la estructura equivalente tiene un MSG $\mathbf{M}_i$ cuyo tipo es el otro miembro del par enantiomórfico de MSGs al que pertenece **M**.

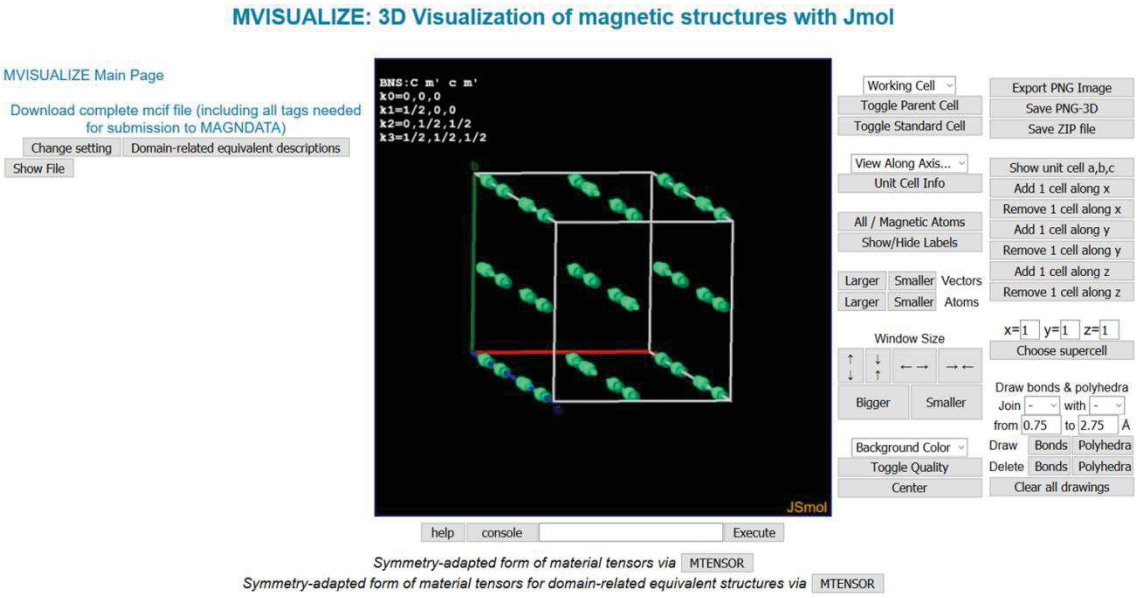

Figura 69. Estructura magnética del Ho_2RhIn_8 [52] obtenida con MVISUALIZE. El botón "*Domain-related equivalent descriptions*" permite obtener las estructuras equivalentes a la mostrada.

Esta utilidad de MVISUALIZE proporciona una tabla con las estructuras equivalentes asociadas a los posibles dominios, indicando para cada una de ellas un *coset representative* que permite obtenerlas a partir de la estructura introducida, su MSG, su unidad asimétrica y las órbitas de sus átomos. Además, permite visualizarlas con la herramienta de visualización de MVISUALIZE (§8.2).

Debe mencionarse que dicha tabla no contiene todas las estructuras equivalentes, pues no incluye aquellas estructuras triviales que se obtienen de las operaciones g_i ∈ **Gp1'** que son primadas. Dado que la operación de inversión temporal {1'|0,0,0} es siempre una de las operaciones perdidas en la transición de fase, los *coset representatives* g_i de la *coset decomposition* de **Gp1'** en **M** (27) pueden elegirse de tal forma que la mitad de ellos sean no primados y la otra mitad sean idénticos a éstos pero primados. De esta forma, la mitad de las estructuras equivalentes resultan triviales, al ser idénticas a la otra mitad salvo por tener todos los momentos magnéticos invertidos con respecto a éstas. Estas estructuras triviales se obvian en la tabla de estructuras equivalentes proporcionada por MVISUALIZE.

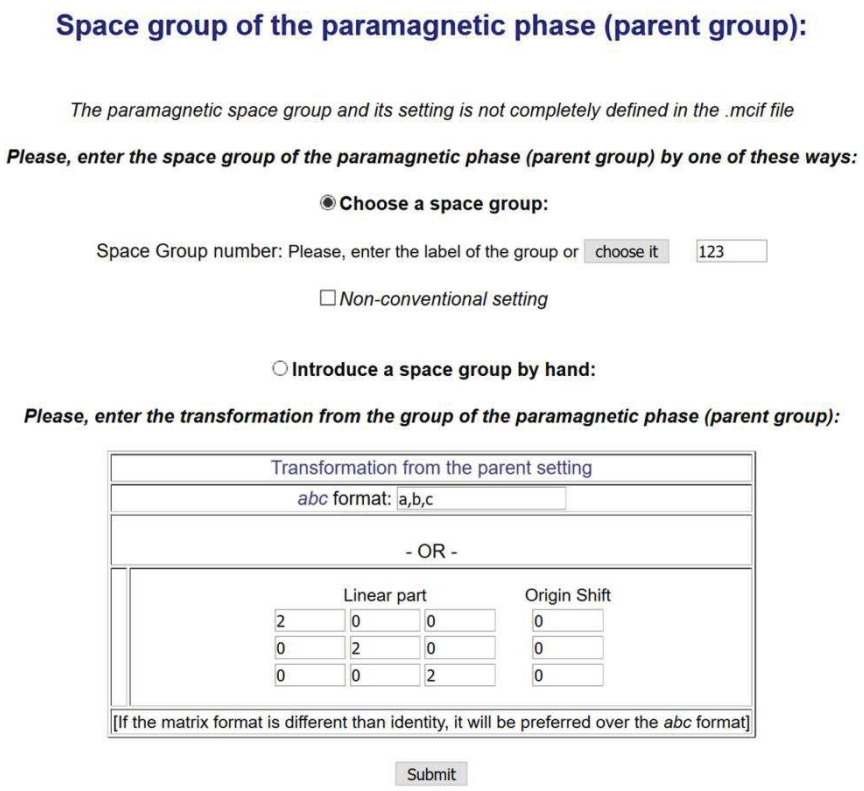

Figura 70. Interfaz de MVISUALIZE para introducir el grupo padre y la transformación entre su *setting* y el del MSG de la estructura. Los datos corresponden a la estructura del Ho_2RhIn_8 [52].

La estructura magnética del Ho_2RhIn_8 (caso #3.3 de MAGNDATA (§9)) [52] proporcionada por MVISUALIZE a partir de un archivo magCIF se muestra en la Figura 69. Las estructuras equivalentes correspondientes a los posibles dominios son accesibles a través del botón "*Domain-related equivalent descriptions*" de la Figura 69, que se muestra tan sólo para estructuras magnéticas conmensurables. Asimismo, son accesibles desde MAGNDATA (§9), que incluye un enlace externo a esta utilidad de MVISUALIZE para cada estructura magnética conmensurable contenida en esta

colección. Utilizar esta herramienta requiere definir el grupo padre, el MSG de la estructura y la transformación entre los *settings* en los que ambos están expresados, datos que, salvo el MSG, pueden no estar recogidos en el archivo magCIF introducido. Por ello, cuando se accede a esta herramienta a través de MAGNDATA (donde toda esta información está disponible), o bien cuando estos datos están definidos sin ambigüedad dentro del archivo magCIF introducido por los *tags* pertinentes, MVISUALIZE muestra directamente la tabla de estructuras equivalentes (Figura 71), mientras que en caso contrario, se muestra un formulario previo (Figura 70) donde deben especificarse el grupo padre y la transformación entre el *setting* del grupo padre y el *setting* de la estructura magnética.

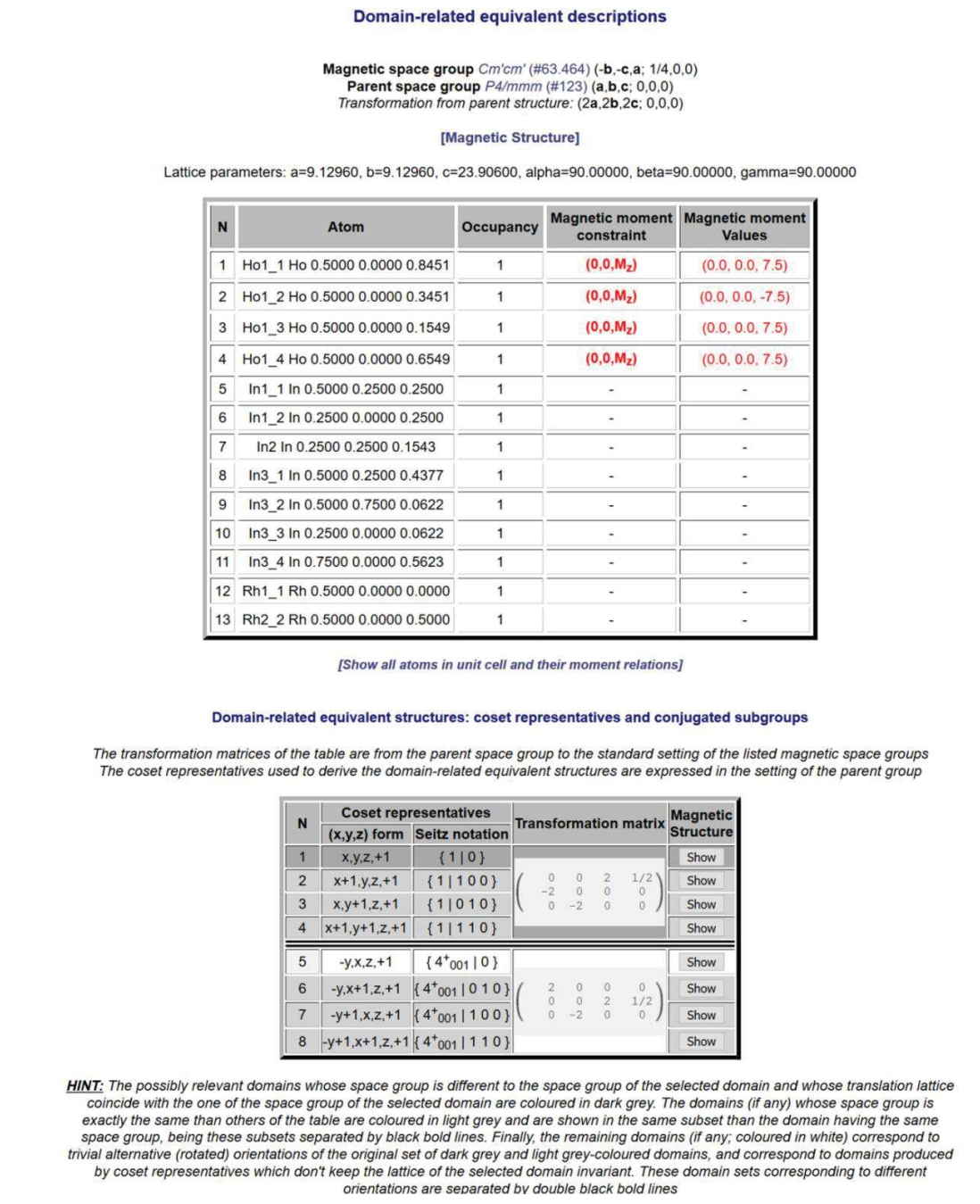

Domain-related equivalent descriptions

Magnetic space group *Cm'cm'* (#63.464) (**-b**,**-c**,**a**; 1/4,0,0)
Parent space group *P4/mmm* (#123) (**a**,**b**,**c**; 0,0,0)
Transformation from parent structure: (2**a**,2**b**,2**c**; 0,0,0)

[Magnetic Structure]

Lattice parameters: a=9.12960, b=9.12960, c=23.90600, alpha=90.00000, beta=90.00000, gamma=90.00000

N	Atom	Occupancy	Magnetic moment constraint	Magnetic moment Values
1	Ho1_1 Ho 0.5000 0.0000 0.8451	1	(0,0,M_z)	(0.0, 0.0, 7.5)
2	Ho1_2 Ho 0.5000 0.0000 0.3451	1	(0,0,M_z)	(0.0, 0.0, -7.5)
3	Ho1_3 Ho 0.5000 0.0000 0.1549	1	(0,0,M_z)	(0.0, 0.0, 7.5)
4	Ho1_4 Ho 0.5000 0.0000 0.6549	1	(0,0,M_z)	(0.0, 0.0, 7.5)
5	In1_1 In 0.5000 0.2500 0.2500	1	-	-
6	In1_2 In 0.2500 0.0000 0.2500	1	-	-
7	In2 In 0.2500 0.2500 0.1543	1	-	-
8	In3_1 In 0.5000 0.2500 0.4377	1	-	-
9	In3_2 In 0.5000 0.7500 0.0622	1	-	-
10	In3_3 In 0.2500 0.0000 0.0622	1	-	-
11	In3_4 In 0.7500 0.0000 0.5623	1	-	-
12	Rh1_1 Rh 0.5000 0.0000 0.0000	1	-	-
13	Rh2_2 Rh 0.5000 0.0000 0.5000	1	-	-

[Show all atoms in unit cell and their moment relations]

Domain-related equivalent structures: coset representatives and conjugated subgroups

The transformation matrices of the table are from the parent space group to the standard setting of the listed magnetic space groups
The coset representatives used to derive the domain-related equivalent structures are expressed in the setting of the parent group

N	Coset representatives (x,y,z) form	Coset representatives Seitz notation	Transformation matrix	Magnetic Structure
1	x,y,z,+1	{ 1 | 0 }		Show
2	x+1,y,z,+1	{ 1 | 1 0 0 }	$\begin{pmatrix} 0 & 0 & 2 & 1/2 \\ -2 & 0 & 0 & 0 \\ 0 & -2 & 0 & 0 \end{pmatrix}$	Show
3	x,y+1,z,+1	{ 1 | 0 1 0 }		Show
4	x+1,y+1,z,+1	{ 1 | 1 1 0 }		Show
5	-y,x,z,+1	{ 4^+_{001} | 0 }		Show
6	-y,x+1,z,+1	{ 4^+_{001} | 0 1 0 }	$\begin{pmatrix} 2 & 0 & 0 & 0 \\ 0 & 0 & 2 & 1/2 \\ 0 & -2 & 0 & 0 \end{pmatrix}$	Show
7	-y+1,x,z,+1	{ 4^+_{001} | 1 0 0 }		Show
8	-y+1,x+1,z,+1	{ 4^+_{001} | 1 1 0 }		Show

HINT: *The possibly relevant domains whose space group is different to the space group of the selected domain and whose translation lattice coincide with the one of the space group of the selected domain are coloured in dark grey. The domains (if any) whose space group is exactly the same than others of the table are coloured in light grey and are shown in the same subset than the domain having the same space group, being these subsets separated by black bold lines. Finally, the remaining domains (if any; coloured in white) correspond to trivial alternative (rotated) orientations of the original set of dark grey and light grey-coloured domains, and correspond to domains produced by coset representatives which don't keep the lattice of the selected domain invariant. These domain sets corresponding to different orientations are separated by double black bold lines*

Figura 71. Pantalla de MVISUALIZE que contiene las estructuras equivalentes relacionadas con dominios para el caso de la estructura magnética del Ho_2RhIn_8 [52].

Domain-related equivalent description

Selected parent symmetry operation transforming the initial structure: 2- { 1 | 1 0 0 }

Magnetic space group *Cm'cm'* (#63.464) (**-b**,**-c**,**a**; 1/4,0,0)
Parent space group *P4/mmm* (#123) (**a**,**b**,**c**; 0,0,0)

Setting (2**a**,2**b**,2**c**; 0,0,0) from parent group

Go to standard setting Change setting

[Transformed Magnetic Structure]

Lattice parameters: a=9.1296, b=9.1296, c=23.9060, alpha=90.00, beta=90.00, gamma=90.00

N	Atom	Occupancy	Magnetic moment constraint	Magnetic moment Values
1	Ho1_1 Ho 0.5000 0.0000 0.8451	1	**(0,0,M_z)**	(0.0000, 0.0000, 7.5000)
2	Ho1_2 Ho 0.5000 0.0000 0.3451	1	**(0,0,M_z)**	(0.0000, 0.0000, 7.5000)
3	Ho1_3 Ho 0.5000 0.0000 0.1549	1	**(0,0,M_z)**	(0.0000, 0.0000, 7.5000)
4	Ho1_4 Ho 0.5000 0.0000 0.6549	1	**(0,0,M_z)**	(0.0000, 0.0000, -7.5000)
5	In1_1 In 0.5000 0.2500 0.2500	1	-	-
6	In1_2 In 0.2500 0.0000 0.2500	1	-	-
7	In2 In 0.2500 0.2500 0.1543	1	-	-
8	In3_1 In 0.5000 0.2500 0.4378	1	-	-
9	In3_2 In 0.5000 0.7500 0.0623	1	-	-
10	In3_3 In 0.2500 0.0000 0.0623	1	-	-
11	In3_4 In 0.7500 0.0000 0.5623	1	-	-
12	Rh1_1 Rh 0.5000 0.0000 0.0000	1	-	-
13	Rh2_2 Rh 0.5000 0.0000 0.5000	1	-	-

[Show all atoms in unit cell and their moment relations]

Visualize this magnetic structure in 3D using Jmol: Visualize

Download mCIF file: bcs_file.mcif
[The preview text below is non-editable, only copy-allowed]

```
# Created by the Bilbao Crystallographic Server
# http://www.cryst.ehu.es
# Date: 25/12/2016 01:02:24
# Domain-related equivalent description. Coset representative: x+1,y,z,+1

data_5yOhtAoR
_audit_creation_date              25/12/2016 01:02:24
_audit_creation_method            "Bilbao Crystallographic Server"

_citation_journal_abbrev          PHYSICAL REVIEW B
_citation_journal_volume          91
_citation_page_first              ?
_citation_page_last               ?
_citation_article_id              144404
_citation_year                    2015
```

Figura 72. Pantalla de consulta y descarga de la estructura magnética equivalente número 2 de la tabla de la Figura 71. Obtenida con MVISUALIZE.

En el caso del Ho_2RhIn_8 el grupo padre es *P4/mmm* (#123), el MSG es *Cm'cm'* (**b**, **c**, **a**; 1/4, 0, 0) (#63.464) y la transformación de *setting* entre ambos es (2**a**, 2**b**, 2**c**). Cuando el grupo padre y la transformación han sido introducidos, MVISUALIZE muestra una pantalla que contiene las estructuras equivalentes a la estructura magnética del Ho_2RhIn_8 introducida (Figura 71).

En esta pantalla se indican el grupo padre, el MSG y la transformación entre ambos, y se incluye una tabla que enumera los átomos de la unidad asimétrica de la estructura magnética introducida, así como su órbita (oculta por defecto). Debajo, aparece la tabla de estructuras equivalentes, donde se indican los *coset representatives* utilizados para obtener dichas estructuras, en formato *x*,*y*,*z* y notación de Seitz (§4.3). En la columna "*Transformation matrix*" se indica la matriz de transformación al *setting* estándar de cada MSG. Si procede (MSGs enantiomórficos), se incluye una columna adicional que indica el símbolo y la etiqueta de cada MSG. Finalmente, la columna "*Magnetic Structure*" incluye un botón "Show" que permite consultar y visualizar cada estructura magnética, así como descargar el archivo magCIF correspondiente.

Al hacer clic en el botón "Show" se muestra una pantalla (Figura 72) que muestra los datos que definen la estructura equivalente seleccionada: *coset representative* que la produce, MSG y grupo padre, *setting* en el que está expresada, parámetros de red, átomos de la unidad asimétrica y sus órbitas (ocultas por defecto). Sobre la tabla de átomos de la unidad asimétrica se incluyen dos botones que permiten transformar la estructura, tanto al *setting* estándar (botón "*Go to standard setting*") como a un *setting* arbitrario (botón "*Change setting*") (§8.2). Bajo la tabla se incluyen botones que permiten visualizar la estructura con MVISUALIZE y descargar el archivo magCIF de la estructura, así como un cuadro de texto no editable que muestra el archivo magCIF.

Los *coset representatives* que producen las estructuras equivalentes son operaciones de simetría de **Gp1'** y por lo tanto se proporcionan expresadas en el *setting* de **Gp1'**. Dado que estas operaciones, salvo la correspondiente al primer *coset*, no pertenecen al MSG de la estructura introducida **M**, el MSG $\mathbf{M_i}$ de la estructura equivalente puede presentar diversas diferencias relevantes en comparación con la estructura introducida. Por un lado, el MSG $\mathbf{M_i}$ puede ser idéntico a **M** o no serlo, dependiendo de si g_i pertenece o no al normalizador de **M**. A su vez, en caso de que $\mathbf{M_i}$ sea distinto de **M**, la red de traslaciones de ambos MSGs puede coincidir o no y en general, dos estructuras cualesquiera del listado proporcionado por MVISUALIZE pueden tener o no la misma red de traslaciones. MVISUALIZE tiene en cuenta estas características, por un lado, para usarlas como base para clasificar las estructuras, y por otro lado, para elegir un *setting* en el que describir cada estructura:

Por un lado, las estructuras están divididas en conjuntos de estructuras cuya red de traslaciones es común y diferente de la red de traslaciones de las estructuras de otros conjuntos; estos conjuntos están divididos entre sí por una barra horizontal negra doble. A su vez, cada uno de estos conjuntos está dividido en subconjuntos cuyo MSG $\mathbf{M_i}$ es común (y, por tanto, comparten la misma matriz en la columna "*Transformation matrix*") y diferente del de otros subconjuntos; estos subconjuntos están divididos entre sí por una barra horizontal negra simple. Se emplea además el siguiente código de colores: dentro de cada subconjunto de estructuras de MSG común, todas menos la primera están denotadas con un fondo gris claro. Asimismo, la primera estructura de cada subconjunto está denotada con un fondo gris oscuro si su MSG $\mathbf{M_i}$ tiene la misma red de traslaciones que **M**, y con un fondo blanco si dicha red es diferente de la de **M**.

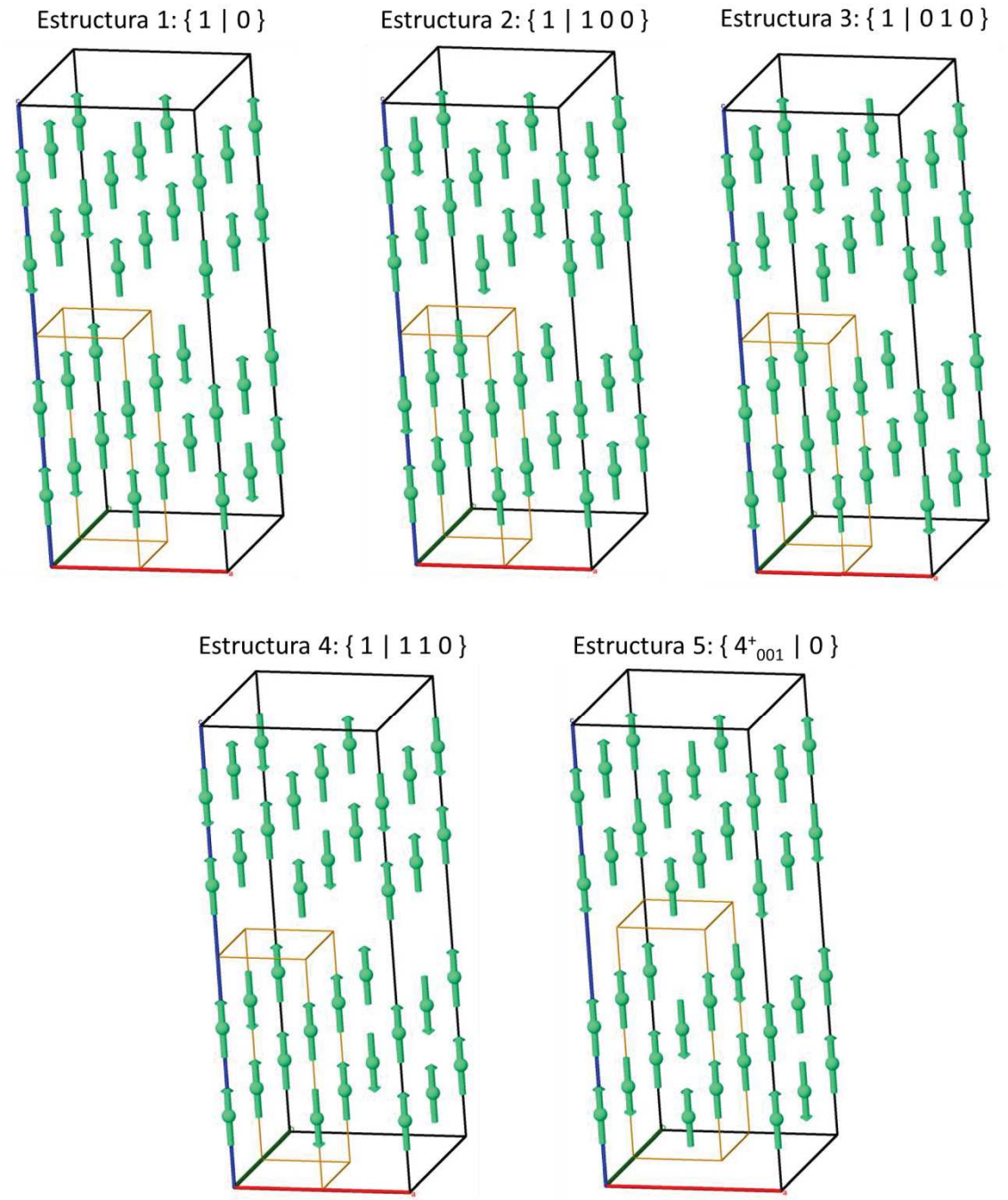

Figura 73. Estructuras equivalentes asociadas a dominios del Ho_2RhIn_8 [52] obtenidas con MVISUALIZE a partir de las estructuras equivalentes del 1 al 5 de la tabla de la Figura 71. Se muestra para cada estructura la celda unidad del grupo padre (celda pequeña).

Por otro lado, MVISUALIZE escoge el *setting* en el que describir cada estructura en función de si su red de traslaciones coincide con la de **M** o no. MVISUALIZE describe todas las estructuras cuya red de traslaciones coincide en el mismo *setting*, de forma que puedan observarse claramente las diferencias entre ellas. Por ello, aquellas estructuras cuya red de traslaciones coincida con la de **M** estarán expresadas en el *setting* de **M**. Sin embargo, el *setting* de **M** no es un *setting* válido para aquellas estructuras cuya red de traslaciones difiera de la de **M**. Por esta razón, en estos casos MVISUALIZE describe dichas estructuras en un *setting* alternativo.

Cada conjunto de estructuras cuya red de traslaciones es común y diferente de la de **M** corresponde a diferentes orientaciones posibles del conjunto original de estructuras con la misma red que **M**, y resultan triviales, pues son idénticas a dicho conjunto original; simplemente, su orientación cambia si se describen en el *setting* del grupo padre. De hecho, estas estructuras pueden obtenerse del conjunto original aplicando una operación de simetría de **Gp1'** que no forma parte de **M** y que no respeta su red de traslaciones; dicha operación es el *coset representative* asociado a la primera estructura del conjunto. MVISUALIZE expresa estas estructuras en un *setting* transformado por medio de dicha operación, de forma que al visualizar este conjunto de estructuras triviales no se observa diferencia alguna con respecto al conjunto original, salvo su diferente orientación con respecto a la celda unidad del grupo padre.

En el caso de la estructura magnética del Ho_2RhIn_8 de la Figura 71, existen 16 estructuras equivalentes, de las cuales figuran 8, al estar omitidas las estructuras triviales que se derivan de las 8 indicadas por medio de la operación {1'|0,0,0}. Las 4 primeras tienen el mismo MSG que la estructura introducida, y están expresadas en el *setting* de ese subgrupo; por ello, las estructuras 2, 3 y 4, por tener el mismo MSG que la 1, se denotan con fondo gris claro, mientras que la 1 se denota con fondo gris oscuro por tener la misma red que **M**. Estas 4 estructuras magnéticas constituyen el conjunto de estructuras magnéticas no triviales de la fase magnética que tienen la misma red de traslaciones que **M**; asimismo, constituyen el subconjunto de estructuras cuyo MSG coincide con **M** (en este caso, no hay estructuras con MSG distinto de **M** pero con la misma red; de haberlas, aparecerían separadas de las otras por una barra horizontal negra). Estas estructuras magnéticas se muestran en la Figura 73 (sólo átomos magnéticos). Las otras 4 estructuras son triviales, pues son idénticas a las 4 primeras, pero orientadas de forma alternativa. Para indicar esto, este subconjunto de estructuras están separadas del conjunto original por medio de una barra negra horizontal doble; además, la estructura 5, primera del subconjunto, está denotada con un fondo blanco (las estructuras 6, 7 y 8 están denotadas con fondo gris claro, indicando que tienen el mismo MSG que la estructura 5). La estructura número 5 se muestra en la Figura 73, donde se puede apreciar que es idéntica a la estructura número 1, salvo por su orientación con respecto a la celda unidad del grupo padre.

Debe quedar claro que esta herramienta de MVISUALIZE es diferente de las utilidades de MAXMAGN y MAGMODELIZE que permiten obtener modelos alternativos asociados a dominios (§7.4.2). Mientras éstas producen modelos con simetría descrita por subgrupos conjugados, que en el proceso de refinamiento de la estructura magnética pueden ser tenidos en cuenta como posibles descripciones equivalentes de una misma estructura, la herramienta de MVISUALIZE permite enumerar, describir y visualizar todas las estructuras equivalentes a una estructura magnética específica, incluyendo todas aquellas cuya simetría viene dada por el mismo subgrupo del grupo padre. Esta opción pretende ayudar a evitar confusiones a la hora de comparar estructuras alternativas propuestas por diferentes estudios u obtenidas en un mismo proceso de refinamiento, distinguiendo los modelos que son equivalentes de aquellos que realmente representan estructuras magnéticas físicamente distintas. Esta opción de MVISUALIZE puede también utilizarse para detectar pseudosimetría en la fase

magnética, y la posible relevancia de un modelo con simetría mayor. En efecto, en el caso de que la estructura difiera escasamente de un modelo con simetría mayor, alguna (o algunas) de las estructuras equivalentes enumeradas mediante esta herramienta serán muy similares a la estructura original, indicando que el *coset representative* utilizado para obtenerla está muy próximo a ser una operación de simetría de la estructura.

Esta herramienta de MVISUALIZE es utilizada internamente por MTENSOR (§10) para obtener los tensores cristalinos asociados a estas estructuras y así caracterizar las propiedades tensoriales de los diferentes dominios de la fase magnética.

9. MAGNDATA: hacia una base de datos de estructuras magnéticas

***NOTA**: Puede encontrarse información adicional a la expuesta en este capítulo en las publicaciones incluidas en los anexos E y F.*

Desde que la primera estructura magnética fue resuelta por medio de un experimento de difracción de neutrones y publicada en 1949 [53], se estima que alrededor de 5000 estructuras magnéticas han sido reportadas hasta la actualidad. Pese a ello, y salvo algunas recopilaciones aisladas [54, 55], no existe ninguna base de datos que contenga las estructuras magnéticas conocidas. Esto es, sin duda, debido a la falta de estándares adecuados a la hora de describir y publicar estructuras magnéticas, así como a la carencia de las herramientas necesarias, tanto teóricas como prácticas, para abordar el problema.

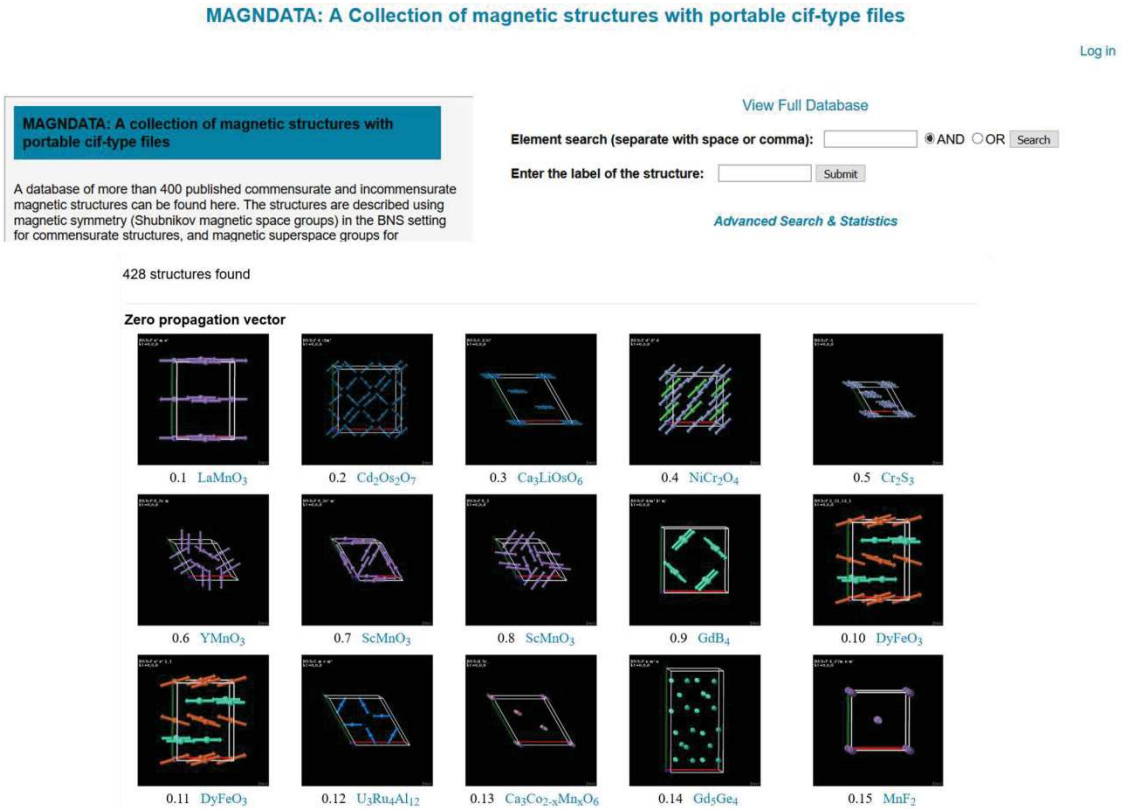

Figura 74. Página principal del programa MAGNDATA y listado de estructuras magnéticas.

Sin embargo, en los últimos años se han dado avances significativos que permitirían desarrollar dicha base de datos en formato digital: se han creado listas de grupos espaciales magnéticos legibles por ordenador [6, 7]; el formalismo superespacial ha sido extendido a estructuras magnéticas inconmensurables [56, 24]; el formato magCIF, una extensión del formato CIF para estructuras magnéticas tanto conmensurables como inconmensurables desarrollado durante estos últimos años [5], ha sido aprobado recientemente por la Unión Internacional de Cristalografía (IUCr) y

ya es utilizado por una proporción importante del software utilizado en el análisis y determinación de estructuras magnéticas.

La creación de una base de datos digital de estructuras magnéticas es un proceso necesario para establecer un estándar que asegure una adecuada descripción y comunicación de las estructuras magnéticas, así como para validar las estructuras magnéticas publicadas hasta ahora. La existencia de una base de datos digital permitiría a los investigadores tanto añadir estructuras nuevas a la base de datos como realizar comparaciones entre estructuras conocidas, encontrar características comunes a estructuras diversas, realizar estudios estadísticos, etc. Crear tal base de datos queda fuera del objetivo de esta tesis doctoral. Sin embargo, con el objetivo de establecer una prueba de concepto de que esa base de datos es posible cuando se utiliza una descripción basada en la simetría magnética, demostrando sus posibilidades y ventajas, se ha elaborado la colección de estructuras magnéticas MAGNDATA, que recopila más de 400 estructuras magnéticas, tanto conmensurables como inconmensurables, extraídas de diversas publicaciones (Figura 74). Esta colección pretende ser un punto de partida para la elaboración de esa más que necesaria base de datos digital de estructuras magnéticas.

Las estructuras incluidas en MAGNDATA han sido analizadas y descritas utilizando la simetría magnética, siempre que la estructura publicada estuviera reportada de forma clara y sin ambigüedades. Para ello, se ha hecho uso de los programas contenidos en el *Bilbao Crystallographic Server*, especialmente los de la sección "*Magnetic Symmetry and Applications*", así como de los programas ISODISTORT [37], JANA2006 [43], VESTA [23] y Jmol [14]. Dado que la gran mayoría de estructuras magnéticas son reportadas sin indicar el MSG o MSSG, estas estructuras han sido a menudo reinterpretadas, de forma que la descripción hecha en MAGNDATA difiere en general de la publicada, aunque la estructura coincida.

Cada entrada de MAGNDATA proporciona una descripción completa de la estructura magnética, describiendo la celda unidad, las posiciones generales, el grupo padre y los grupos espacial y puntual magnético de cada estructura. Además, se proporciona numerosa información adicional sobre las estructuras magnéticas recopiladas, así como archivos magCIF [5] y VESTA [23] descargables y enlaces externos a otros programas del "*Bilbao Crystallographic Server*", que permiten obtener información complementaria sobre la estructura magnética. Un ejemplo de entrada de MAGNDATA se muestra en la Figura 75 para la estructura magnética del $LaMn_3V_4O_{12}$ (#1.119) [47]. Nótese que la forma de describir y comunicar estructuras magnéticas es diferente dependiendo de si la estructura es conmensurable o inconmensurable, por lo que existen diferencias, en contenido y formato, entre las entradas correspondientes a unas y otras de MAGNDATA.

MAGNDATA incluye una herramienta de búsqueda avanzada que permite buscar entre las estructuras de la colección aplicando diversos filtros asociados con diversas características (Figura 76). Esta herramienta permite realizar estudios estadísticos y comparaciones entre las estructuras de la colección. Además, bajo la tabla de

resultados del buscador, se encuentra un sumario que contiene datos estadísticos agregados sobre la colección.

Con el objetivo de analizar las estructuras incluidas en MAGNDATA y describir exhaustivamente toda la información que este programa provee, se han elaborado dos artículos. Estos artículos, publicados recientemente, y recogidas en los Anexos E y F, describen en detalle el programa y analizan las estructuras magnéticas conmensurables (Anexo E) e inconmensurables (Anexo F) contenidas en él.

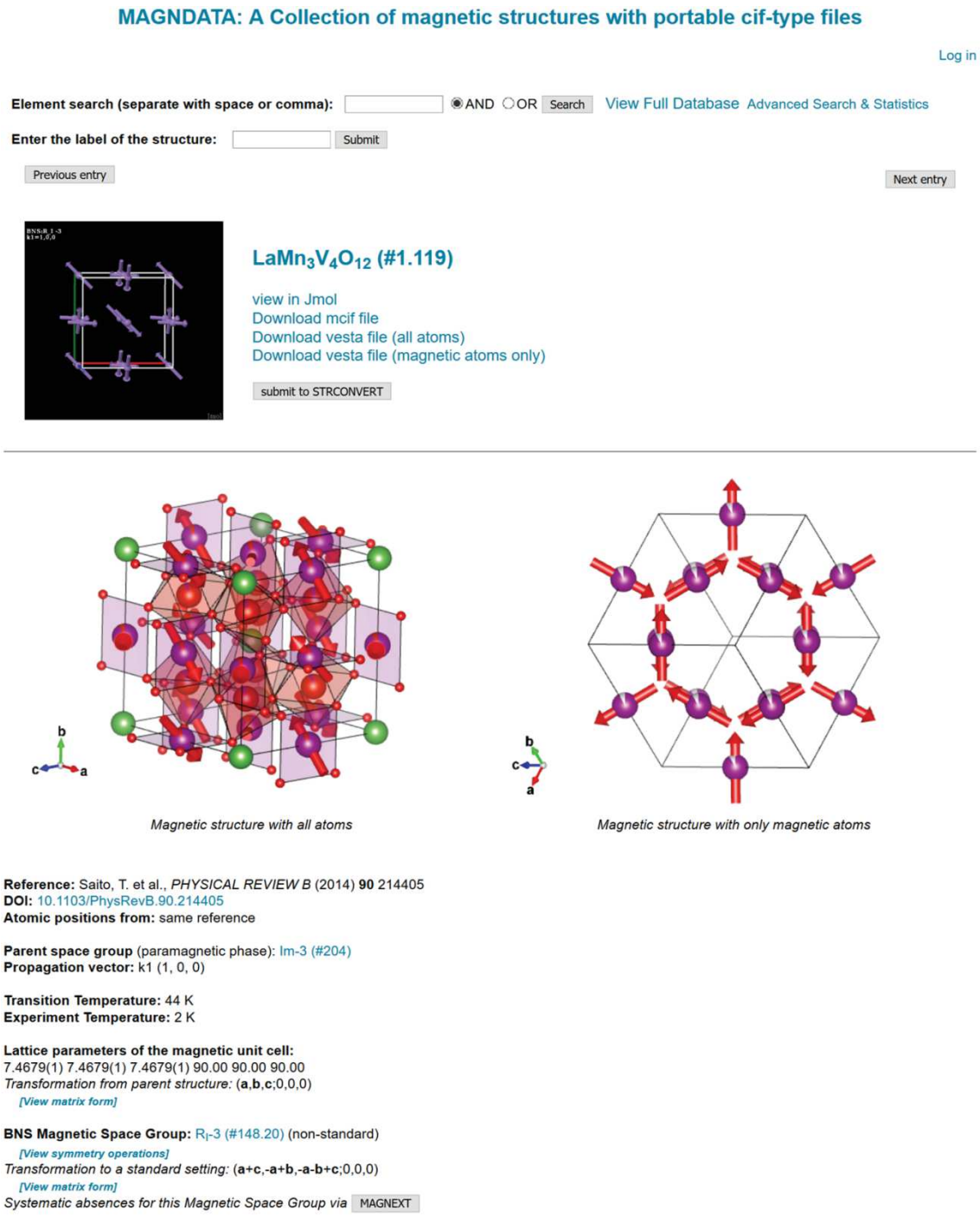

Figura 75. Entrada #1.119 de MAGNDATA, que contiene la estructura magnética del $LaMn_3V_4O_{12}$.

Magnetic Point Group: -31' (17.2.63)

[View symmetry operations]

Symmetry-adapted form of material tensors via MTENSOR

Symmetry-adapted form of material tensors for domain-related equivalent structures via MTENSOR

Positions and magnetic moments of symmetry independent atoms:

From now on, magnetic atoms are in boldface and colored in red. Magnetic moments are expressed in units of μB

[Show only magnetic atoms] *[Show all the atoms]* Go to standard **Use MVISUALIZE to:** Change setting Domain-related equivalent descriptions

Label	Atom type	x	y	z	Occupancy	Multiplicity	Symmetry constraints on M	M_x	M_y	M_z	|M|
Mn1	Mn	0.00000	0.50000	0.50000	0.92	6	m_x,m_y,m_z	0.0	2.95	2.95	4.17

[Show all magnetic atoms in unit cell and their moment relations]

Active Irreps: *Irrep decomposition via* Get_mirreps

label	dim. full irrep	dim. small irrep	direction	action	number of modes
mH4+	3	3	special	primary	3

Comments:

- NPD
- The original report reduces arbitrarily the parent symmetry to rombohedral for the representation analysis. Here the irreps of the actual parent symmetry are considered instead.
- The magnetic configuration can be understood as fully symmetry dictated by a single irrep of the space group of the Mn site, restricted to one of its epikernels.

Comments (symmetry):

- 1k magnetic structure
- magnetic representation contains only the irrep mH4+.
- Magnetic symmetry is one of the epikernels of the irrep mH4+
- The Mn1 moment is not forced by symmetry or by the irrep to have a special direction. But the Mn1 site has the higher symmetry Im-3m, and if this higher space group is taken as parent symmetry, the special direction for the Mn1 moment of the refined model corresponds a primary active irrep mH5+, while the negligible but symmetry-allowed,deviations from this direction correspond to a secondary irrep (mH4+) of Im-3m.
- Symmetry break to rombohedral. Possible induced rombohedral structural distortion not observed.

Figura 75 (cont.). Entrada #1.119 de MAGNDATA, que contiene la estructura magnética del $LaMn_3V_4O_{12}$.

La publicación dedicada a las estructuras conmensurables de MAGNDATA (Anexo E) comienza definiendo el estándar de comunicación y descripción de dichas estructuras (§E.2), estableciendo el conjunto mínimo de datos necesario para describir una estructura conmensurable y mostrando la forma en que éstos se recogen en MAGNDATA. Numerosos aspectos técnicos y cuestiones teóricas acerca de los datos recogidos en MAGNDATA y su interpretación son tratadas en §E.2: elección del *setting* de la estructura, importancia de los átomos no magnéticos, origen de las posiciones atómicas utilizadas y uso externo de los programas MAXMAGN (§7), MAGMODELIZE (§8) y K-SUBGROUPSMAG para obtener el MSG de las estructuras magnéticas, en el frecuente caso de que no haya sido identificado en la publicación original. Asimismo, se explica el proceso general seguido para obtener los archivos magCIF de cada una de las estructuras magnéticas recopiladas.

A continuación, el artículo describe el contenido de MAGNDATA. El capítulo §E.3 desgrana la información adicional sobre las estructuras magnéticas que MAGNDATA proporciona: MPG, grupo padre y descripción de su base, vectores de propagación, análisis de representaciones, *irreps* activas, temperaturas de transición y medición, referencias y comentarios específicos. En este capítulo se explica que el número y tipo de vectores de propagación es utilizado para establecer una clasificación de las estructuras recopiladas, la cual determina también la etiqueta asignada a cada estructura.

El capítulo §E.4 trata sobre los enlaces externos a otros programas del *Bilbao Crystallographic Server*. Por medio de estos enlaces, se puede transformar el *setting* de la estructura, obtener las estructuras equivalentes relacionadas con dominios (§8.3) y sus tensores cristalinos (§10), visualizar la estructura magnética vía MVISUALIZE (§8.2), obtener las reglas de ausencia sistemática para el grupo vía MAGNEXT (§5), la forma adaptada a la simetría de los tensores cristalinos para el MPG de la estructura (§10) y la descomposición en *irreps* asociada a la transición de fase desde la fase paramagnética vía K-SUBGROUPSMAG. Además, se puede enviar el archivo magCIF de la estructura al programa STRCONVERT (http://www.cryst.ehu.es/cgi-bin/cryst/programs/mcif2vesta/index.php) del *Bilbao Crystallographic Server*, que permite realizar tareas de edición y paso de la información a archivos en otros formatos.

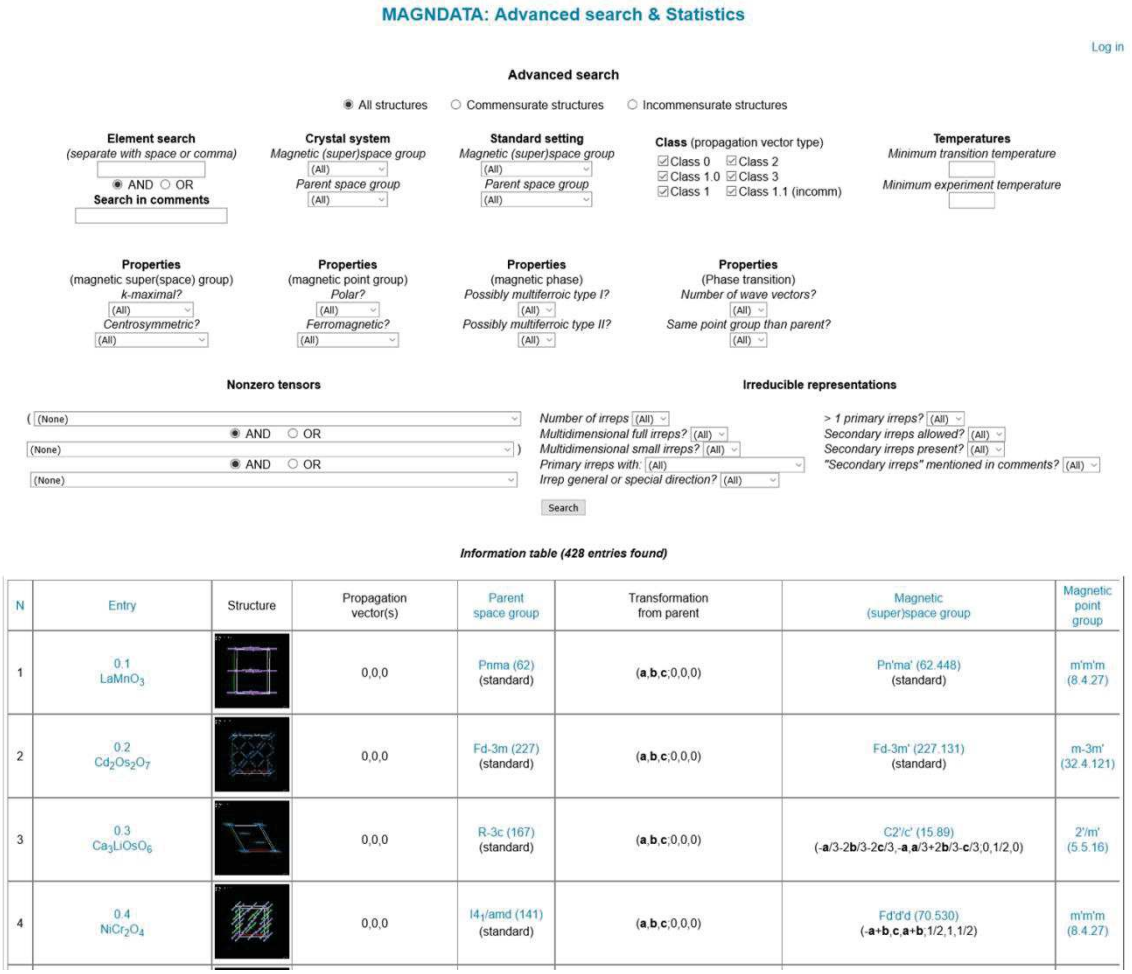

Figura 76. Herramienta de búsqueda avanzada de MAGNDATA, que permite buscar en la colección de estructuras aplicando diversos filtros.

Finalmente, el capítulo §E.5 hace uso de la información contenida en MAGNDATA para analizar la tendencia hacia la maximalidad (§7.1) de la simetría de las estructuras magnéticas de MAGNDATA, y el extenso capítulo §E.6 contiene un análisis completo de la colección de estructuras magnéticas fruto de una inspección minuciosa de las características comunes a algunas estructuras. En este capítulo se proporcionan datos

estadísticos que han sido obtenidos utilizando la sección de búsqueda avanzada de MAGNDATA (Figura 76). Estos dos últimos capítulos muestran que MAGNDATA se puede utilizar para mejorar la comprensión de las características de las estructuras magnéticas conocidas, aportando una visión de conjunto sobre las mismas que permite extraer conclusiones relevantes, como por ejemplo el predominio de estructuras 1k o con simetría k-maximal, la no equivalencia entre la asignación de *irrep* y MSG, la importancia de la asignación de un MSG en el caso de *irreps* multidimensionales o la presencia de *irreps* secundarias, etc. Asimismo, este análisis revela y analiza ciertas prácticas erróneas comunes, tales como la asunción de restricciones en los grados de libertad que no están forzadas por simetría, la no consideración y exploración de modelos válidos y equiprobables al propuesto o el error común de considerar distorsiones estructurales explicables por la aparición del orden magnético como una "transición estructural concomitante". En particular, se hace especial hincapié en el hecho de que en el proceso de refinamiento de las estructuras magnéticas se hacen con frecuencia asunciones no vinculadas ni a la simetría magnética ni a la o las *irreps* activas, asunciones cuya arbitrariedad queda patente cuando se utiliza la simetría magnética. Estas prácticas limitan la fiabilidad de algunas de las estructuras recogidas en MAGNDATA, que incluye estructuras diferentes, propuestas por distintos autores, para la misma fase de un material, y que claramente son contradictorias.

La publicación dedicada a las aproximadamente 40 estructuras magnéticas inconmensurables contenidas en MAGNDATA se encuentra en el Anexo F. Las estructuras magnéticas inconmensurables de MAGNDATA han sido descritas utilizando el formalismo superespacial, y por tanto asignándoles un MSSG, lo que asegura una descripción clara y sin ambigüedades. El capítulo §F.2 resume el formalismo superespacial y establece un estándar de descripción y comunicación de estructuras magnéticas inconmensurables, definiendo y describiendo en detalle el conjunto mínimo de datos (celda unidad promedio, MSSG, posiciones y momentos de la unidad asimétrica de la estructura promedio y funciones de modulación) necesario para definir una estructura magnética inconmensurable. Estos datos mínimos necesarios están contenidos tanto en MAGNDATA como en los archivos magCIF descargables de cada estructura (ver Tablas 1, 2 y 3 del Anexo F). En este capítulo se describen también las modulaciones estructurales, que MAGNDATA incluye también para aquellas estructuras magnéticas inconmensurables que las presentan, y se describe la herramienta de visualización de estructuras magnéticas inconmensurables de MVISUALIZE (§8.2) accesible desde el programa. El capítulo §F.3 complementa al capítulo §F.2 describiendo el resto de la información disponible en MAGNDATA para las estructuras magnéticas inconmensurables: MPG, grupo padre e *irreps* activas.

El análisis de las estructuras inconmensurables recogidas en MAGNDATA se realiza en los capítulos §F.4 y §F.5. En el capítulo §F.4, se realiza una comparativa entre el uso de la simetría magnética y el "*representation method*" para determinar y describir estructuras magnéticas inconmensurables, analizando los diferentes escenarios que pueden darse y comparando ambos métodos en cada posible situación, mostrando la complementariedad entre ambos métodos. Finalmente, el capítulo §F.5 recoge las 40

estructuras magnéticas inconmensurables presentes en MAGNDATA en el momento de la publicación, agrupándolas según sus características y analizándolas en detalle.

Por último, el Anexo D recoge, en las tablas 3 y 4, aquellas estructuras de MAGNDATA que, de acuerdo a los criterios establecidos en dicha publicación, cumplen con los requisitos para ser multiferroicos tipo II únicamente a causa de la incompatibilidad entre el vector de propagación y algunos ejes helicoidales o planos de deslizamiento del grupo padre, por lo que son (tabla 3) o son candidatos para ser (tabla 4) multiferroicos tipo II.

10. TENSORES CRISTALINOS ADAPTADOS A LA SIMETRÍA DE LOS GRUPOS PUNTUALES Y PUNTUALES MAGNÉTICOS: PROGRAMAS TENSOR Y MTENSOR

***Nota**: este capítulo resume brevemente los programas TENSOR y MTENSOR, y únicamente contiene una breve explicación de su objetivo, utilidad y funcionamiento. La descripción detallada de ambos programas se relega a una publicación futura.*

10.1 Introducción

Los programas TENSOR y MTENSOR contienen una base de datos que permite consultar la forma adaptada a la simetría de unas 100 propiedades tensoriales cristalinas conocidas, tanto de equilibrio como ópticas y de transporte (Figura 77).

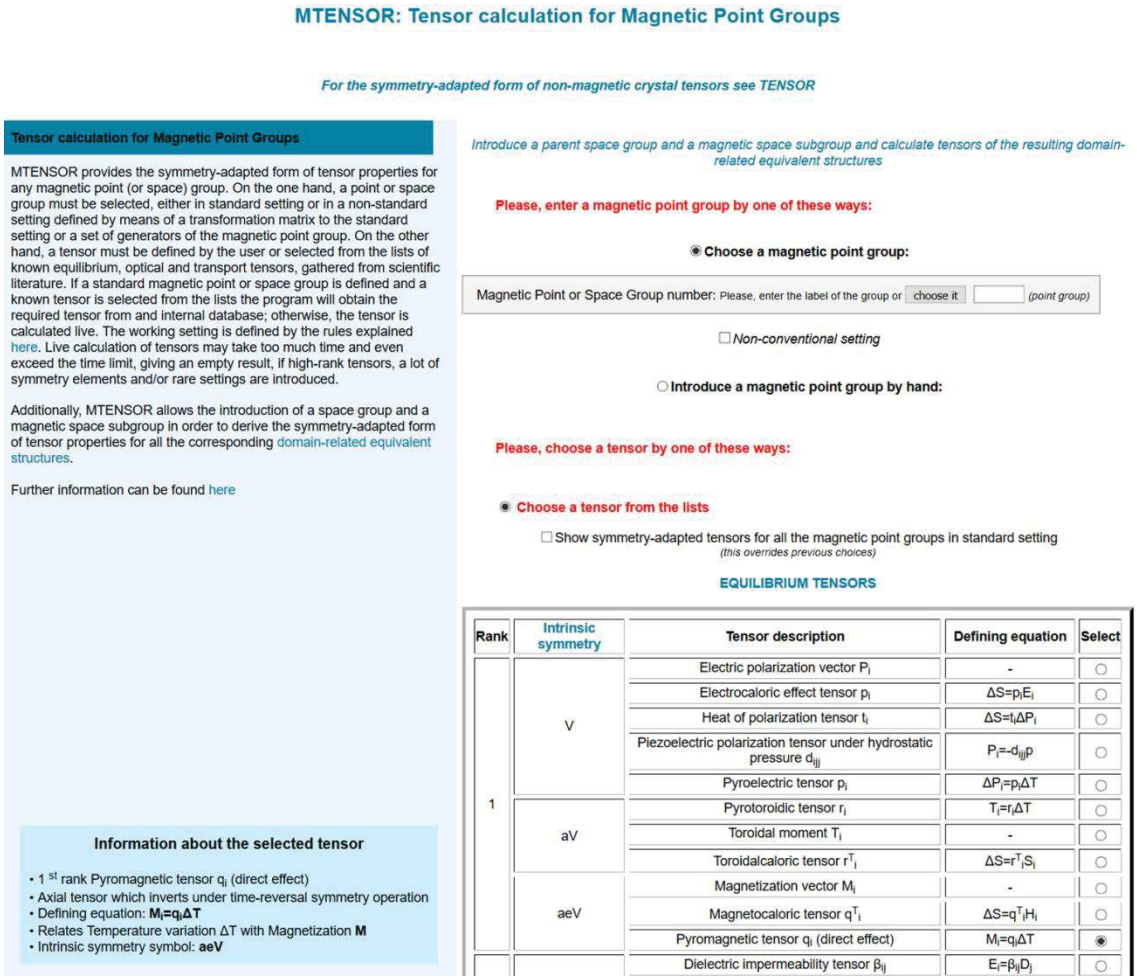

Figura 77. Página principal de MTENSOR, que contiene tres tablas que incluyen numerosas propiedades tensoriales cristalinas de equilibrio, ópticas y de transporte conocidas.

TENSOR y MTENSOR son programas muy similares, que se diferencian únicamente en que el primero considera propiedades tensoriales correspondientes a materiales no

magnéticos, y por tanto su simetría puntual puede ser descrita por un grupo puntual cristalográfico ordinario, mientras que MTENSOR es más general y proporciona información sobre las propiedades tensoriales de sistemas ordenados magnéticamente donde la simetría puntual relevante es necesariamente un grupo puntual magnético cristalográfico. Por ello, las propiedades tensoriales incluidas en ambos programas son las mismas, con la excepción de aquellas propiedades magnéticas prohibidas en sistemas no ordenados magnéticamente, y que no se incluyen lógicamente en el programa TENSOR. El programa MTENSOR en realidad proporciona para materiales no magnéticos la misma información que el programa TENSOR, si se introduce como simetría magnética el grupo gris magnético asociado a su simetría cristalográfica ordinaria.

En particular, el programa MTENSOR permite conocer las restricciones resultantes de la simetría magnética sobre las propiedades tensoriales de los materiales multiferroicos.

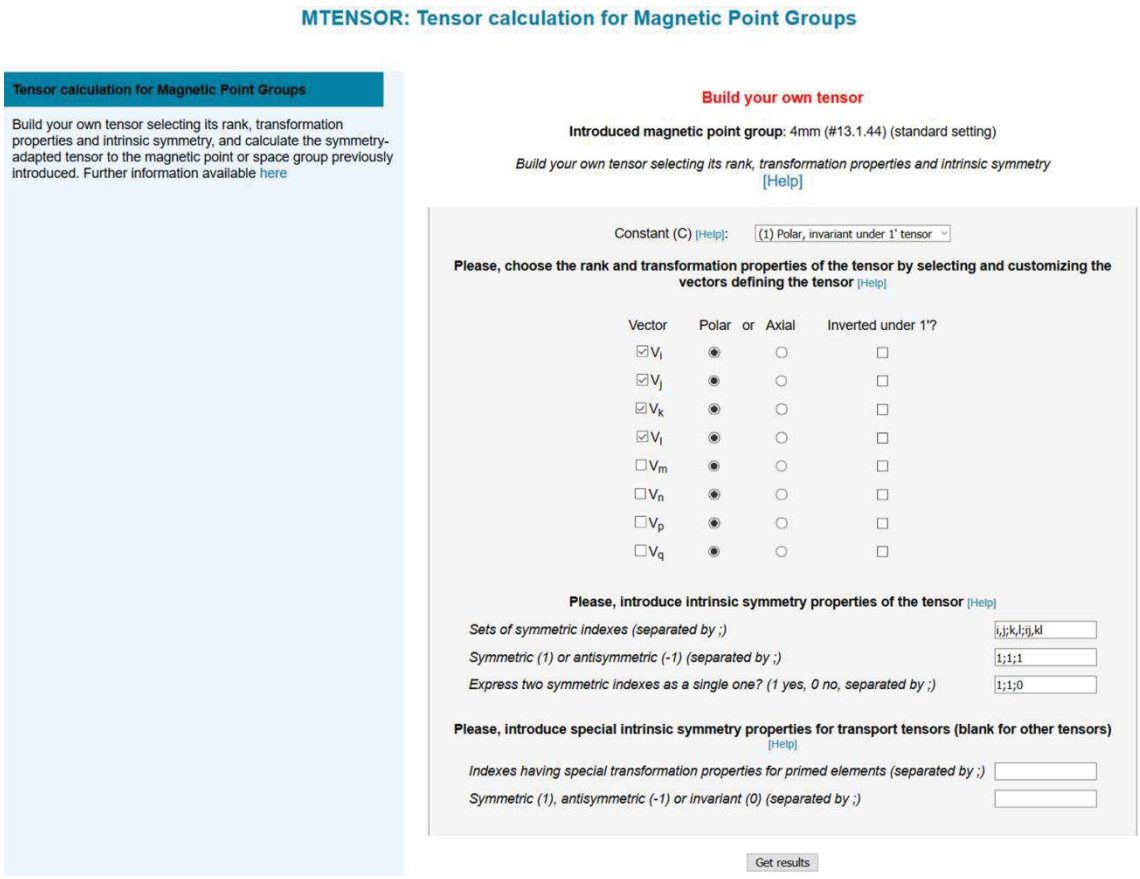

Figura 78. Interfaz de construcción de tensores de MTENSOR.

La forma adaptada a la simetría de los tensores cristalinos incluidos en las bases de datos de TENSOR y MTENSOR ha sido calculada para los diversos tipos de grupo puntual y puntual magnético, respectivamente. Dado que no existe un estándar para los grupos puntuales cristalográficos ordinarios y magnéticos, se han tomado como estándar los contenidos en los programas POINT (http://www.cryst.ehu.es/rep/point.html) y MPOINT (§3.2).

Asimismo, TENSOR y MTENSOR permiten consultar los tensores adaptados a la simetría puntual asociada a los grupos espaciales y los grupos espaciales magnéticos en *setting* estándar, respectivamente (BNS en el caso magnético), a través de la identificación del grupo puntual que les corresponde. La página principal de ambos programas permite seleccionar el grupo puntual o espacial, y además incluye una opción que permite obtener, para cada tensor, un listado de la forma adaptada a la simetría de todos los grupos puntuales o puntuales magnéticos. Ambos programas permiten también calcular la forma adaptada a la simetría de los tensores para un grupo puntual o espacial en un *setting* cualquiera, que debe definirse introduciendo o bien la matriz de transformación al *setting* estándar o bien un conjunto de generadores en formato *x*,*y*,*z*.

TENSOR y MTENSOR incluyen además una herramienta (Figura 78) que permite construir un tensor cualquiera de rango igual o menor que 8 y calcular su forma adaptada a la simetría de cualquier grupo puntual o puntual magnético.

10.2 Fundamentos básicos y método

Las propiedades tensoriales de los cristales son propiedades intrínsecas de los mismos, que están definidas por una ecuación constitutiva según la cual relacionan entre sí las componentes de dos o más magnitudes físicas, descritas también por medio de tensores. Por ejemplo, el tensor piezomagnético Λ_{ijk} tiene como ecuación constitutiva $M_i = \Lambda_{ijk}\, \sigma_{jk}$, y por tanto relaciona las componentes del tensor de esfuerzos σ_{jk} aplicado al material y la magnetización M_i inducida en el mismo como consecuencia de dicho esfuerzo.

Una propiedad tensorial de un cristal se describe mediante un tensor $T_{ijk\ldots n}$ de rango *n*. Dicho tensor, cuando se aplica un cambio de base por medio de una matriz de transformación $\boldsymbol{P} = P_{ij}$, transforma de la siguiente forma:

$$T'_{ijk\ldots n} = P_{ir} P_{js} P_{kt} \ldots P_{nm} T_{rst\ldots m} \qquad (31)$$

donde se usa el convenio de suma de Einstein. Esta expresión es válida sólo si el tensor está expresado en una base ortogonal. De (31) pueden deducirse las restricciones en las componentes del tensor debidas a la simetría cristalina, que dependen no sólo del MPG de la estructura magnética, sino de la simetría intrínseca del tensor.

En TENSOR y MTENSOR, la simetría intrínseca de los tensores se denota mediante un símbolo que la identifica. Se puede considerar que un tensor de rango *n* relaciona entre sí, en último término, las componentes de *n* vectores. Por ejemplo, el tensor magnetoeléctrico, definido por la ecuación constitutiva $M_i = \alpha_{ij}\, E_j$, relaciona entre sí dos vectores: la magnetización M_i y el campo eléctrico E_j. Asimismo, el tensor piezomagnético Λ_{ijk} relaciona el vector magnetización M_i con el tensor de esfuerzos σ_{ij}, tensor que a su vez relaciona dos vectores entre sí (un vector perpendicular a la superficie n_j y el vector de tensión mecánica T_i a través de dicha superficie: $T_i = \sigma_{ij}\, n_j$).

Así pues, para representar un tensor general de rango *n* se utiliza el símbolo V x V x V x ... x V = V^n, indicando que sus propiedades intrínsecas son las del número *n* de vectores que relaciona entre sí. Las propiedades de transformación de dichos vectores determinan cómo transforma el tensor cuando se aplica una operación de simetría. Si uno de dichos vectores es axial, dicho vector se denota como *e*V; si su sentido se invierte bajo una operación de inversión temporal, se denota como *a*V; y si se invierte bajo cualquiera de ambas operaciones, se denota como *ae*V. Puede pensarse en *e* como en una constante de carácter axial (pseudoescalar) y en *a* como una constante cuyo valor se invierte bajo inversión temporal. Entonces, se cumple que *a* x *a* = 1 y *e* x *e* = 1, por lo que un tensor cuyo símbolo sea $(aV)^2$ puede simplificarse haciendo $(aV)^2$ = (*a* x *a*) V^2 = V^2. La notación de estos símbolos proviene de [57].

Además, el símbolo de la simetría intrínseca de los tensores también refleja la simetría que algunos presentan cuando dos o más índices (asociados a vectores V) son permutados. Cuando un tensor es simétrico bajo la permutación de varios índices asociados a varios vectores V, esto se denota en el símbolo de simetría intrínseca rodeando los Vs con corchetes, y cuando es antisimétrico, con llaves. Así, el tensor magnetoeléctrico α_{ij}, dado que relaciona entre sí la magnetización M_i, un vector axial y que se invierte bajo inversión temporal (*ae*V), y el campo eléctrico E_j, un vector polar (V), tiene como símbolo *ae*V x V = aeV^2; por su parte, el tensor piezomagnético Λ_{ijk} relaciona la magnetización M_i (*ae*V) con el tensor de esfuerzos σ_{jk} (que relaciona entre sí dos vectores polares, y además es simétrico en los índices *j* y *k*, por lo que su símbolo es $[V^2]$) por lo que su símbolo es *ae*V$[V^2]$. Debe mencionarse que existen otras propiedades de transformación especiales que los tensores de transporte y ópticos pueden presentar, asociados a las relaciones de Onsager para estructuras magnéticas, y que serán detalladas en la futura publicación sobre TENSOR y MTENSOR.

El símbolo de la simetría intrínseca de un tensor es suficiente para determinar su forma restringida por la simetría de un MPG. Así, dos tensores con el mismo símbolo poseen la misma simetría intrínseca y, por tanto, la forma restringida de ambos tensores para el mismo MPG es idéntica. Dicho símbolo figura en la columna "*Intrinsic symmetry*" de la tabla de la Figura 77, donde puede observarse que aquellas propiedades tensoriales cuyo tensor tiene la misma simetría intrínseca figuran agrupadas, pues su forma adaptada a la simetría para los diferentes MSGs es idéntica. Igualmente, en la Figura 78 puede observarse que el formulario que permite obtener la forma restringida de un tensor cualquiera permite especificar la simetría intrínseca del tensor indicando las propiedades de transformación de los vectores que relaciona, así como indicando las propiedades de transformación globales del tensor y la simetría o antisimetría ante la permutación de índices.

Según el principio de Neumann, la invariancia de un cristal bajo la acción de una operación de simetría implica también la invariancia de sus propiedades físicas. De (31) se deduce que la invariancia del cristal bajo una operación de simetría $\{\boldsymbol{R},\tau\}$ de un MPG **m**, con $\boldsymbol{R}$ = a_{ij}, implica la siguiente condición para las componentes del tensor $T_{ijk...n}$, condición que depende de la simetría intrínseca del tensor:

$$
\begin{aligned}
&T_{ijk\ldots n} = a_{ir}a_{js}a_{kt}\ldots a_{nm}T_{rst..m} \quad \text{si } T_{ijk\ldots n} \text{ es polar y no invierte bajo } 1' \ (1)\\
&T_{ijk\ldots n} = \det(\boldsymbol{R})\, a_{ir}a_{js}a_{kt}\ldots a_{nm}T_{rst..m} \quad \text{si } T_{ijk\ldots n} \text{ es axial y no invierte bajo } 1' \ (e)\\
&T_{ijk\ldots n} = \tau a_{ir}a_{js}a_{kt}\ldots a_{nm}T_{rst..m} \quad \text{si } T_{ijk\ldots n} \text{ es polar e invierte bajo } 1' \ (a)\\
&T_{ijk\ldots n} = \tau \det(\boldsymbol{R})\, a_{ir}a_{js}a_{kt}\ldots a_{nm}T_{rst..m} \quad \text{si } T_{ijk\ldots n} \text{ es axial e invierte bajo } 1' \ (ae)
\end{aligned}
\tag{32}
$$

Así pues, para calcular la forma restringida de un tensor cristalino asociada a un MPG bastaría con aplicar la condición (32) para todas las operaciones de simetría del MPG. Sin embargo, calcular la forma restringida de los tensores de esa forma requiere resolver sucesivamente sistemas de ecuaciones homogéneos potencialmente muy grandes, y en muchos casos las restricciones impuestas por algunas operaciones del MPG **m** son redundantes frente a las más generales impuestas por otras. Por estas razones, se ha optado por proceder de forma similar a como se hizo para calcular las reglas de ausencia sistemática (§5) y utilizar un método basado en proyectores similar al descrito en el capítulo 3.2 del Anexo A, que permite calcular la forma adaptada a la simetría puntual de los tensores de forma elegante, sencilla y rápida.

Para aplicar este método, se ordenan las componentes del tensor $T_{ijk\ldots n}$ de menor a mayor *i*; aquellas que tengan el mismo *i*, de menor a mayor *j*; y así sucesivamente. De esta forma, se asigna un número ordinal *u* a las componentes del tensor, de forma que se pueden realizar las conversiones *ijk...n* -> *u* y *rst...m* -> *v* en (32) para así poder representar el tensor en forma de matriz columna T_u o T_v. Si se procede de esta manera, las condiciones (32) pueden reescribirse como:

$$
T_{ijk\ldots n} = Q_{ijk\ldots n\ rst\ldots m}(\boldsymbol{R},\tau)T_{rst..m} \quad \rightarrow \quad T_u = Q_{uv}(\boldsymbol{R},\tau)T_v \tag{33}
$$

con

$$
\begin{aligned}
&Q_{ijk\ldots n\ rst..m}(\boldsymbol{R},\tau) = a_{ir}a_{js}a_{kt}\ldots a_{nm} \quad \text{si } T_{ijk\ldots n} \text{ es polar y no invierte bajo } 1'\\
&Q_{ijk\ldots n\ rst..m}(\boldsymbol{R},\tau) = \det(\boldsymbol{R})\, a_{ir}a_{js}a_{kt}\ldots a_{nm} \quad \text{si } T_{ijk\ldots n} \text{ es axial y no invierte bajo } 1'\\
&Q_{ijk\ldots n\ rst..m}(\boldsymbol{R},\tau) = \tau a_{ir}a_{js}a_{kt}\ldots a_{nm} \quad \text{si } T_{ijk\ldots n} \text{ es polar e invierte bajo } 1'\\
&Q_{ijk\ldots n\ rst..m}(\boldsymbol{R},\tau) = \tau \det(\boldsymbol{R})\, a_{ir}a_{js}a_{kt}\ldots a_{nm} \quad \text{si } T_{ijk\ldots n} \text{ es axial e invierte bajo } 1'
\end{aligned}
\tag{34}
$$

Las matrices Q_{uv} son una representación, en general reducible, del MPG del cristal, adaptada a su vez a la simetría intrínseca del tensor. La ecuación (33) sólo puede cumplirse si la representación Q_{uv} contiene la representación irreducible identidad del MPG **m**. Para esta representación, puede construirse el proyector Q^1_{uv}, que proyecta un tensor T_u general en el subespacio asociado a la representación irreducible identidad:

$$
Q^1_{uv} = \left(1/|\mathbf{m}|\right) \sum_{\{\boldsymbol{R},\tau\}\in\mathbf{m}} Q_{uv}(\boldsymbol{R},\tau) \tag{35}
$$

donde |**m**| es el orden del MPG **m**. La forma restringida por el MPG **m** del tensor T_u, T^r_u se puede entonces obtener haciendo actuar este proyector de la forma:

$$T^r_u = Q^{|\mathbf{m}|}_{uv} T_u \tag{36}$$

donde T^r_u es un tensor general arbitrario. Finalmente, la posible simetría o antisimetría del tensor bajo una permutación de índices debe aplicarse al tensor T^r_u para obtener la forma final adaptada a la simetría intrínseca del tensor y restringida por el MPG **m**.

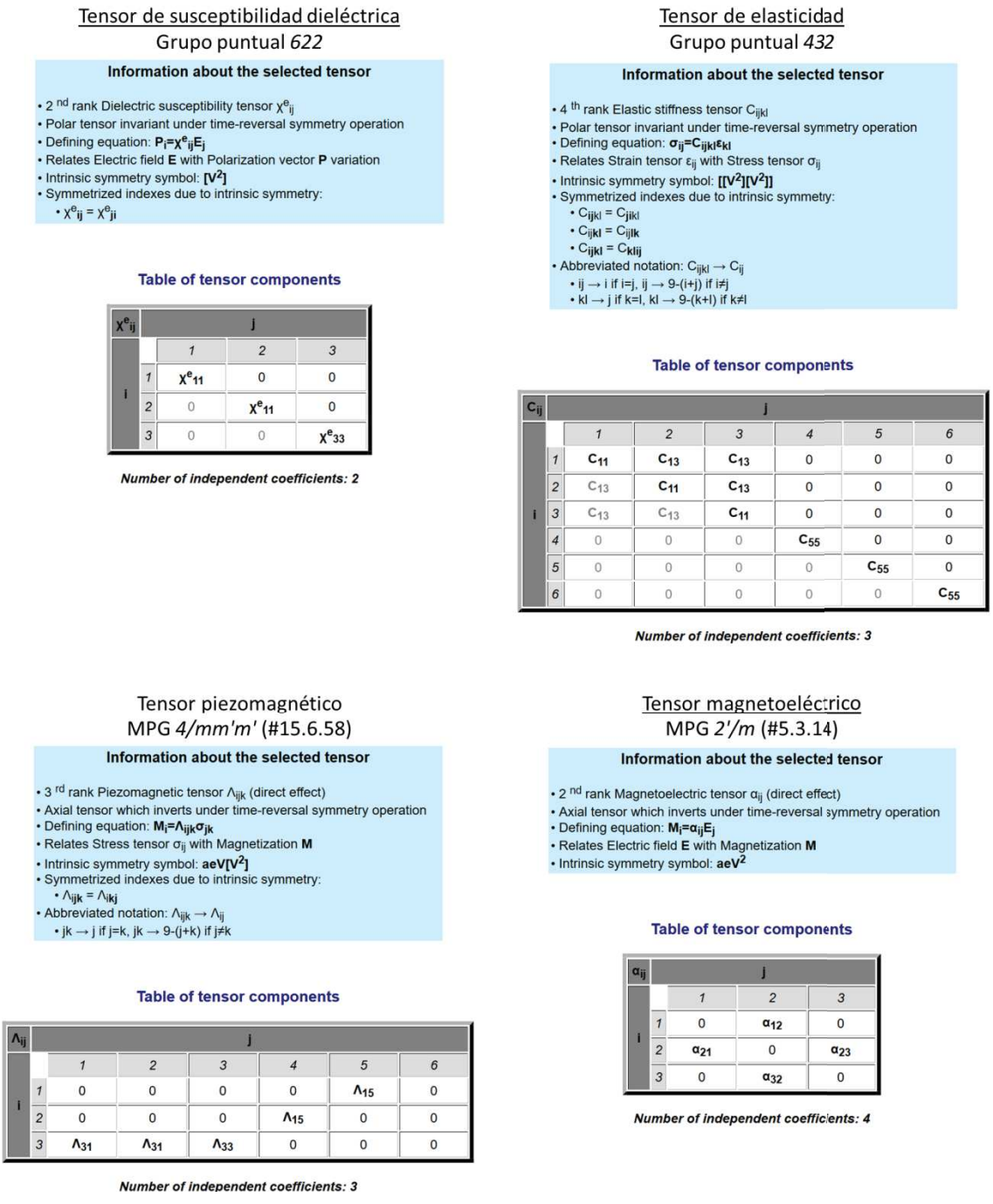

Figura 79. Ejemplos de tensores adaptados a la simetría de diversos grupos puntuales y puntuales cristalográficos ordinarios y magnéticos. Obtenidos con TENSOR y MTENSOR.

El método de cálculo anterior es igualmente válido tanto para MPGs como para grupos puntuales convencionales, por lo que éste es el método elegido para calcular la forma restringida de los tensores tanto en MTENSOR como en TENSOR. Para este último caso, simplemente la simetría intrínseca de los tensores es tal que las componentes del tensor jamás se invierten bajo una inversión temporal, y los grupos puntuales convencionales utilizados son los MPGs grises.

Ejemplos de tensores adaptados a la simetría de diversos grupos puntuales y puntuales magnéticos, calculados con el método arriba expuesto, pueden encontrarse en la Figura 79. El tensor se representa mediante una tabla bidimensional, que incluye en los ejes vertical y horizontal todos los índices del tensor y sus posibles valores (lo que permite representar tensores de cualquier rango) y que expresa los valores de las componentes del tensor y las relaciones entre ellas. Se incluye un recuadro que contiene información básica sobre la naturaleza de la propiedad tensorial y su simetría intrínseca, así como detalles técnicos sobre las propiedades del tensor. Finalmente, se indica el número de componentes independientes del tensor.

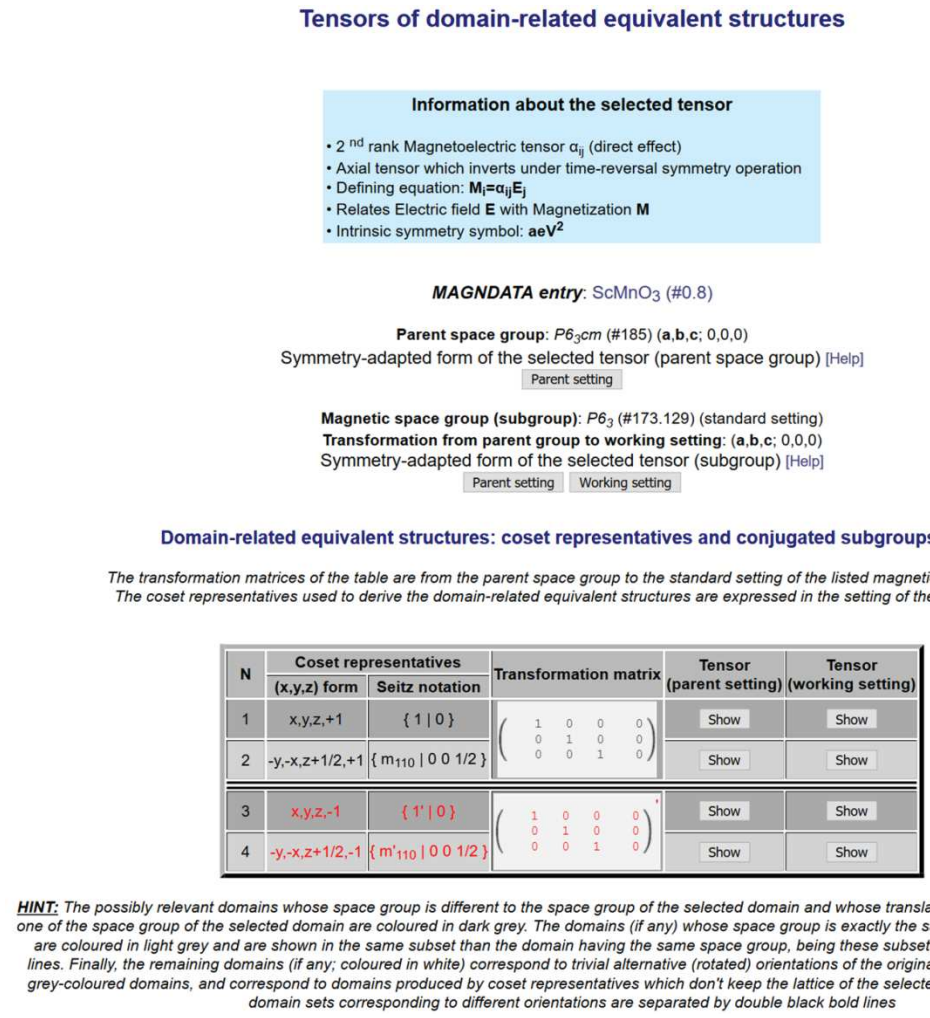

Tensors of domain-related equivalent structures

Information about the selected tensor

- 2 nd rank Magnetoelectric tensor α_{ij} (direct effect)
- Axial tensor which inverts under time-reversal symmetry operation
- Defining equation: $\mathbf{M_i=\alpha_{ij}E_j}$
- Relates Electric field **E** with Magnetization **M**
- Intrinsic symmetry symbol: $\mathbf{aeV^2}$

MAGNDATA entry: $ScMnO_3$ (#0.8)

Parent space group: $P6_3cm$ (#185) (**a**,**b**,**c**; 0,0,0)
Symmetry-adapted form of the selected tensor (parent space group) [Help]
Parent setting

Magnetic space group (subgroup): $P6_3$ (#173.129) (standard setting)
Transformation from parent group to working setting: (**a**,**b**,**c**; 0,0,0)
Symmetry-adapted form of the selected tensor (subgroup) [Help]
Parent setting | Working setting

Domain-related equivalent structures: coset representatives and conjugated subgroups [Help]

The transformation matrices of the table are from the parent space group to the standard setting of the listed magnetic space groups
The coset representatives used to derive the domain-related equivalent structures are expressed in the setting of the parent group

N	Coset representatives (x,y,z) form	Coset representatives Seitz notation	Transformation matrix	Tensor (parent setting)	Tensor (working setting)
1	x,y,z,+1	{ 1 | 0 }	(1 0 0 0 / 0 1 0 0 / 0 0 1 0)	Show	Show
2	-y,-x,z+1/2,+1	{ m_{110} | 0 0 1/2 }		Show	Show
3	x,y,z,-1	{ 1' | 0 }	(1 0 0 0 / 0 1 0 0 / 0 0 1 0)'	Show	Show
4	-y,-x,z+1/2,-1	{ m'$_{110}$ | 0 0 1/2 }		Show	Show

HINT: *The possibly relevant domains whose space group is different to the space group of the selected domain and whose translation lattice coincide with the one of the space group of the selected domain are coloured in dark grey. The domains (if any) whose space group is exactly the same than others of the table are coloured in light grey and are shown in the same subset than the domain having the same space group, being these subsets separated by black bold lines. Finally, the remaining domains (if any; coloured in white) correspond to trivial alternative (rotated) orientations of the original set of dark grey and light grey-coloured domains, and correspond to domains produced by coset representatives which don't keep the lattice of the selected domain invariant. These domain sets corresponding to different orientations are separated by double black bold lines*

Figura 80. Interfaz de MTENSOR que enumera las estructuras equivalentes asociadas a dominios para el caso del $ScMnO_3$ [58] y permite consultar la forma adaptada a la simetría de los tensores cristalinos de dichas estructuras.

Por último, TENSOR y MTENSOR incluyen una herramienta que permite obtener la forma adaptada a la simetría de los tensores cristalinos para todas las estructuras equivalentes asociadas a dominios, si se introduce la simetría puntual de la fase paramagnética como referencia. Esta sección es similar a que incluye MVISUALIZE y que se describe en §8.3. Al igual que en ella, es necesario especificar el grupo padre y la transformación entre su *setting* y el del grupo introducido. Para el caso de la estructura magnética del $ScMnO_3$ (caso #0.8 de MAGNDATA (§9)) [58], el resultado (Figura 80) es similar al que puede observarse en la Figura 71 (de hecho, procede de la misma herramienta de cálculo interna) con la salvedad de que, en el caso de MTENSOR, los dominios triviales asociados a *coset representatives* primados se incluyen, ya que para algunas propiedades tensoriales los tensores de estas estructuras equivalentes son diferentes (opuestos) a los tensores de los *coset representatives* no primados.

En la Figura 81 se muestra la forma adaptada a la simetría del tensor magnetoeléctrico para las cuatro estructuras equivalentes asociadas a dominios de la Figura 80. Los tensores de las estructuras equivalentes se calculan transformando con el *coset representative* correspondiente el tensor adaptado a la simetría para la estructura introducida (que coincide con el tensor número 1 de la Figura 81); es decir, las componentes α_{11}, α_{12} y α_{33} de la Figura 81 son iguales para los 4 tensores indicados.

1- {1|0,0,0}

α_{ij}	j		
i	1	2	3
1	α_{11}	α_{12}	0
2	$-\alpha_{12}$	α_{11}	0
3	0	0	α_{33}

2- {m_{110}|0,0,1/2}

α_{ij}	j		
i	1	2	3
1	α_{11}	$-\alpha_{12}$	0
2	α_{12}	α_{11}	0
3	0	0	α_{33}

3- {1'|0,0,0}

α_{ij}	j		
i	1	2	3
1	$-\alpha_{11}$	$-\alpha_{12}$	0
2	α_{12}	$-\alpha_{11}$	0
3	0	0	$-\alpha_{33}$

4- {m'_{110}|0,0,1/2}

α_{ij}	j		
i	1	2	3
1	$-\alpha_{11}$	α_{12}	0
2	$-\alpha_{12}$	$-\alpha_{11}$	0
3	0	0	$-\alpha_{33}$

Figura 81. Tensor magnetoeléctrico de las cuatro estructuras equivalentes asociadas a dominios de la Figura 80.

El programa MTENSOR es accesible desde los programas MPOINT (§3.2), MAXMAGN (§7.4.4), MAGMODELIZE (§8.1), MVISUALIZE (§8.2) y MAGNDATA (§9) para calcular la forma adaptada a la simetría de tensores cristalinos para las diversas estructuras y/o grupos puntuales magnéticos que proporcionan. Al mismo tiempo, la herramienta de

obtención de tensores cristalinos de las estructuras equivalentes asociadas a dominios es accesible desde MVISUALIZE (§8.3) y MAGNDATA (§9).

Los tensores cristalinos adaptados a la simetría de las estructuras equivalentes asociadas a dominios, que son proporcionados por TENSOR y MTENSOR, permiten conocer la relación entre las componentes tensoriales espontáneas en cada tipo de dominio de la fase ferroica, y de esa forma ayudan a caracterizar las propiedades de conmutación entre los diferentes dominios de la propiedad tensorial de que se trate.

11. CONCLUSIONES

En esta tesis doctoral se ha realizado un estudio de la simetría magnética y de los grupos espaciales y superespaciales magnéticos desde un punto de vista práctico, orientado al desarrollo de herramientas teóricas que faciliten el estudio, descripción y determinación de estructuras magnéticas y sus propiedades. Esta tesis doctoral pretende demostrar la conveniencia e idoneidad del uso de la simetría magnética en la determinación de estructuras magnéticas, concluyendo no sólo que es una metodología útil y complementaria al tradicional *representation method*, sino que a menudo resulta imprescindible para un análisis completo y riguroso. Como resultado, se han creado 11 programas informáticos que incluyen bases de datos y programas interactivos.

Los programas desarrollados permiten, entre otras cosas, explorar todas las posibles estructuras magnéticas compatibles con los datos experimentales disponibles, haciendo uso de forma consistente de su simetría magnética, así como obtener la forma restringida por simetría de sus propiedades tensoriales y las posibles estructuras equivalentes asociadas a dominios, junto con sus propiedades tensoriales de conmutación.

Las herramientas desarrolladas en este trabajo permiten extraer y aplicar de forma sistemática argumentos de simetría en la investigación de una estructura magnética, haciendo uso únicamente de datos experimentales elementales. Es de esperar que el paulatino incremento del interés en las posibilidades de la simetría magnética lleve a una utilización progresiva de estos programas. De esta forma, este trabajo pretende ser un paso adelante en el perfeccionamiento de los métodos utilizados en este campo, y se suma al esfuerzo realizado simultáneamente en la misma dirección por otros grupos dentro de la comunidad especializada, con la implementación de la simetría magnética en diversos programas como VESTA [23], Jmol [14], JANA2006 [43], ISODISTORT [37], ISOCIF [45], FULLPROF [44], etc...

Nuestro propósito ha sido contribuir a que la aplicación sistemática y rigurosa de argumentos de simetría, de forma complementaria al tradicional *representation method*, pase a ser habitual dentro de la comunidad especializada en este campo. Esto permitirá describir y determinar estructuras magnéticas de forma mucho más clara, elegante y sencilla, y posibilitará la creación de estándares de comunicación y descripción de estructuras magnéticas, como paso previo a la necesaria construcción de una base de datos completa y actualizada de estructuras magnéticas. Asimismo, esperamos que el uso de la simetría magnética de la forma aquí descrita y la utilización de los programas desarrollados faciliten la búsqueda de materiales multiferroicos y magnetoeléctricos, cuyas propiedades son objeto de un creciente interés científico y tecnológico.

Al iniciar esta tesis doctoral, el uso práctico de la simetría magnética era un campo casi inexplorado, y de hecho, durante la realización de este trabajo diversas aplicaciones de la simetría magnética han ido surgiendo de forma inesperada, como demuestran las publicaciones recogidas en los Anexos B y D. Es de esperar que en un futuro la

continuación de esta línea de investigación lleve a nuevas aplicaciones y sus correspondientes herramientas informáticas. La sección magnética del *Bilbao Crystallographic Server*, que este trabajo ha desarrollado cubre una buena parte de las posibles aplicaciones de la simetría magnética, pero está abierta a nuevas futuras aportaciones que hagan uso de sus programas y bases de datos. El desarrollo de herramientas relacionadas con la simetría magnética dentro del *Bilbao Crystallographic Server* no debería detenerse aquí.

REFERENCIAS

[1] Aroyo M. I., Perez-Mato J. M., Orobengoa D., Tasci E., De la Flor G., Kirov A. "Crystallography online: Bilbao Crystallographic Server". *Bulg. Chem. Commun*. **43(2)** 183-97 (2011)

[2] Aroyo M. I., Perez-Mato J. M., Capillas C., Kroumova E., Ivantchev S., Madariaga G., Kirov A., Wondratschek H. "Bilbao Crystallographic Server I: Databases and crystallographic computing programs". *Z. Krist*. **221**, 1, 15-27 (2006) DOI: 10.1524/zkri.2006.221.1.15

[3] Aroyo M. I., Kirov A., Capillas C., Perez-Mato J. M., Wondratschek H. "Bilbao Crystallographic Server II: Representations of crystallographic point groups and space groups". *Acta Cryst*. A **62**, 115-128 (2006) DOI: 10.1107/S0108767305040286

[4] Bertaut E. F. "Representation analysis of magnetic structures". *Acta Cryst*. A **24** 217–231 (1968) DOI: 10.1107/S0567739468000306

[5] *Int. Union Crystallogr*. "Commission on Magnetic Structures" (2015) http://www.iucr.org/iucr/commissions/magnetic-structures

[6] Stokes H. T., Campbell B. J. "ISO-MAG: table of magnetic space groups". *ISOTROPY Software Suite.* (2011) http://iso.byu.edu

[7] Litvin D. B. "Magnetic Group Tables: 1-, 2- and 3-Dimensional Magnetic Subperiodic Groups and Magnetic Space Groups". *Int. Union Crystallogr*. Chester, UK (2013) http://www.iucr.org/publ/978-0-9553602-2-0

[8] Janovec V., Privratska J. *International Tables for Crystallography*. Vol. D, Chapter 3.4, pp. 449–505 (2006)

[9] Wadhawan V. K. "Introduction to Ferroic Materials". Gordon and Breach Science Publishers (2000)

[10] Schmid H. "Multi-ferroic Magnetoelectrics". *Ferroelectrics* **162** 317-38 (1994) DOI: 10.1080/00150199408245120

[11] Khomski D. Classifying multiferroics: "Mechanisms and effects". *Physics* **2** 20 (2009) DOI: 10.1103/Physics.2.20

[12] Johnson R. D., Radaelli P. G. "Diffraction Studies of Multiferroics". *Annu. Rev. Mater. Res.* **44** 269–98 (2014) DOI: 10.1146/annurev-matsci-070813-113524

[13] Ortega N., Kumar A., Scott J. F., Katiyar R. S. "Multifunctional magnetoelectric materials for device applications". *J. Phys. Condens. Matter*. **27**(50) 504002 (2015) DOI: 10.1088/0953-8984/27/50/504002

[14] Hanson R. "Jmol: an open-source Java viewer for chemical structures in 3D". (2013) http://www.jmol.org/

[15] Hall S. R., Allen F. H., Brown I. D. “The Crystallographic Information File (CIF): a new standard archive file for crystallography”. *Acta Crystallogr. Sect. A* **47** 655–85 (1991)

[16] Coh S., Vanderbilt D. “Canonical magnetic insulators with isotropic magnetoelectric coupling”. *Phys. Rev*. B **88** 121106 (2014) DOI: 10.1103/PhysRevB.88.121106

[17] Glazer A. M., Aroyo M. I., Authier A. “Seitz symbols for crystallographic symmetry operations”. *Acta Crystallogr. Sect. A* **70** 300-2 (2014) DOI: 10.1107/S2053273314004495

[18] Souvignier B. “A general introduction to space groups”. *International Tables for Crystallography* Vol. A **1.3** 22-41 (2016)

[19] Birss R. R. “*Symmetry and Magnetism*“. North-Holland Publishing Co.: Amsterdam. Tema 3. (1964)

[20] Litvin D. B. “Magnetic subperiodic groups and magnetic space groups”. *International Tables for Crystallography* Vol. A **3.6** 852-865 (2016)

[21] Ashcroft, N. W., Mermin, N. D. “*Solid State Physics”*. Holt, Rinehart and Winston, New York. Capítulos 31-33 (1976)

[22] Du F., Ohgushi K., Nambu Y., Kawakami T., Avdeev M., Hirata Y., Watanabe Y., Sato T. J., Ueda Y. “*Stripelike magnetism in a mixed-valence insulating state of the Fe-based ladder compound* $CsFe_2Se_3$”. *Phys. Rev*. B **85** 214436 (2012) DOI: 10.1103/PhysRevB.85.214436

[23] Momma K., Izumi F. “VESTA 3 for three-dimensional visualization of crystal, volumetric and morphology data”. *J. Appl. Crystallogr*. **44** 1272-76 (2011)

[24] Janssen T, Janner A, Looijenga-Vos A and de Wolf P 2006. “Incommensurate and commensurate modulated structures”. *International Tables for Crystallography*. Vol C, chapter 9.8, pp 907–55 (Amsterdam: Kluwer)

[25] Perez-Mato J. M., Ribeiro J. L., Petricek V., Aroyo M. I. “Magnetic superspace groups and symmetry constraints in incommensurate magnetic phases”. *J. Phys.: Condens. Matter* **24** 163201 (2012)

[26] Rodriguez-Carvajal, J. & Bouree F. “Symmetry and magnetic structures”. *EPJ Web of Conferences* **22**, 00010 (2012) DOI: 10.1051/epjconf/20122200010

[27] Shubnikov A. V. “*Simmetriya i antisimmetriya konechnykh figur* (simetría y antisimetría de figuras finitas)”. Izd-vo AN SSSR: Moscow, Russia (1951)

[28] Heesch H. “Zur Strukturtheorie der Ebenen Symmetriegruppen” *Z. Kristallogr*. **71** 95-102 (1929) DOI: 10.1524/zkri.1929.71.1.95

[29] Belov N. V., Neronova N. N., Smirnova T. S. “Shubnikov groups”. *Sov. Phys. Crystallogr.* **2** 311–22 (1957)

[30] Opechowski W., Guccione R. “Magnetic symmetry”. In *Magnetism*, Vol. II, Part A, ed. Rado G. T., Suhl H., pp. 105–65. New York: Academic (1965)

[31] Bradley A. P, Cracknell C. J. “*Mathematical theory of symmetry in solids*”. Clarendon, Oxford. p.575 (1972)

[32] Dresselhaus M. S., Dresselhaus G., Jorio A. “*Group Theory”.* Springer, Berlin. Figura 9.3, p. 191 (2008)

[33] Stokes H. T., Campbell B. J. “ISO-MAG: table of magnetic space groups”. BNS and OG Lattice Symbols: http://stokes.byu.edu/iso/magneticspacegroupshelp.php

[34] Dresselhaus M. S., Dresselhaus G., Jorio A. “*Group Theory”.* Springer, Berlin. Figura 16.4, p. 417 (2008)

[35] Wondratschek H. *International Tables for Crystallography*. Vol. A, Chapter 8.3, pp. 732–740 (2006)

[36] *International Tables for Crystallography* Vol. A, Chapter 7, pp. 111–718 (2006)

[37] Campbell B. J., Stokes H. T., Tanner D. E., Hatch D. M. “ISODISPLACE: a web-based tool for exploring structural distortions”. *J. Appl. Crystallogr*. **39** 607-14 (2006) http://stokes.byu.edu/isodistort.html

[38] Dresselhaus M. S., Dresselhaus G., Jorio A. “*Group Theory”.* Springer, Berlin. Figura 4.3, p. 64 (2008)

[39] Koch E., Fischer W., Müller U. “Normalizers of space groups and their use in crystallography. International Tables for Crystallography”. *International Tables for Crystallography* Vol. A **15** 878 (2006)

[40] Wang X., Chai Y., Zhou L., Cao H., de la Cruz C., Yang J., Dai J., Yin Y., Yuan Z., Zhang S., Yu R., Azuma M., Shimakawa Y., Zhang H., Dong S., Sun Y., Jin C., Long Y. “Observation of Magnetoelectric Multiferroicity in a Cubic Perovskite System: $LaMn_3Cr_4O_{12}$”. *Phys. Rev. Lett*. **115** 087601 (2015)

[41] Goldman A. I., Argyriou D. N., Ouladdiaf B., Chatterji, T., Kreyssig A., Nandi S., Ni N., Bud’ko S. L., Canfield P. C., McQueeney R. J. “Lattice and magnetic instabilities in $CaFe_2As_2$: A single-crystal neutron diffraction study”. *Phys. Rev*. *B* **78** 100506(R) (2008)

[42] Battle, P. D., Grey C. P., Hervieu M., Martin C., Moore C. A., Paik Y. “Structural chemistry and magnetic properties of La_2LiRuO_6”. *Journal of Solid State Chemistry* **175** 20-26 (2003)

[43] Petricek, V., Dusek, M., Palatinus, L. “*Jana2006: The Crystallographic Computing System*”. http://jana.fzu.cz/ (2006)

[44] Rodríguez-Carvajal, J. “Recent advances in magnetic structure determination by neutron powder diffraction”. *Physica B* **192** 55–69 (1993)

[45] Stokes, H. T., Campbell, B. J. “*ISOCIF: create or modify CIF files. ISOTROPY Software Suite*”. http://iso.byu.edu (2014)

[46] Bilbao Crystallogr. Serv.. “STRCONVERT: structure data converter&editor”. *Bilbao Crystallographic Server*. http://www.cryst.ehu.es/cryst/strconvert (2014)

[47] Saito, T., Toyoda, M., Ritter, C., Zhang, S., Oguchi, T., Attfield, J. P., Shimakawa, Y. “Symmetry-breaking 60°-spin order in the A-site-ordered perovskite $LaMn_3V_4O_{12}$”. *Phys. Rev. B* **90** 214405 (2014)

[48] Nye, J. F. “Physical Properties of Crystals” (New York: Oxford University Press) pp. 20-24 (1957)

[49] Shaked, H., Hastings, J. M., Corliss, L. M. “Magnetic Structure of Magnesium Chromite”. *Phys. Rev. B* **1** 3116 (1970)

[50] Baran, S., Kaczorowski, D., Arulraj, A., Penc, B., Szytula, A. “Frustrated magnetic structure of TmAgGe”. *Journal of Magnetism and Magnetic Materials* **321** 3256-3261 (2009)

[51] Biffin, A., Johnson, R. D., Kimchi, I., Morris, R., Bombardi, A., Analytis, J. G., Vishwanath, A., Coldea, R. “Noncoplanar and Counterrotating Incommensurate Magnetic Order Stabilized by Kitaev Interactions in γ−Li_2IrO_3”. *Phys. Rev. Lett*. **113** 197201 (2014)

[52] Cermák, P., Prokes, K., Ouladdiaf, B., Boehm, M., Kratochvílová, M., Javorský, P. “Magnetic structures in the magnetic phase diagram of Ho_2RhIn_8”. *Phys. Rev. B* **91** 144404 (2015)

[53] Shull, C. G., Smart, J. S. “Detection of Antiferromagnetism by Neutron Diffraction”. *Phys. Rev*. **76** 1256–1257 (1949)

[54] Oles, A., Kajzar, P., Kucab, M., Sikora, W. “*Magnetic Structures Determined by Neutron Diffaction*”. Warszawa, Krakow: Panstwowe Wydawnictwo Naukowe. (1976)

[55] Dul, M., Lesniewska, B., Oles, A., Pytlik, L., Sikora, W. “Computer database of magnetic structures determined by neutron diffraction”. *Phys. B Condens. Matter*, **234–236**, 790–791. (1997)

[56] Petricek, V., Fuksa, J., Dusek, M. “Magnetic space and superspace groups, representation analysis: competing or friendly concepts?”. *Acta Cryst*. **A66**, 649–655. (2010)

[57] Litvin D. B. “Changes of physical properties in multiferroic phase transitions”. *Acta Cryst*. **A70**, 382–384 (2014)

[58] Muñoz, A., Alonso, J. A., Martínez-Lope, M. J., Casáis, M. T., Martínez, J. L., Fernández-Díaz, M. T. “Magnetic structure of hexagonal $RMnO_3$ (R=Y, Sc): Thermal evolution from neutron powder diffraction data”. *Phys. Rev. B* **62** 9498 (2000)

ANEXO A

S. V. Gallego, E. S. Tasci, G. de la Flor, J. M. Perez-Mato and M. I. Aroyo. *J. Appl. Cryst*. (2012). **45**, 1236-47

Magnetic symmetry in the Bilbao Crystallographic Server: a computer program to provide systematic absences of magnetic neutron diffraction

Samuel V. Gallego,[a] Emre S. Tasci,[a] Gemma de la Flor,[a] J. Manuel Perez-Mato[a]* and Mois I. Aroyo[a]

[a]Departamento de Fisica de la Materia Condensada, Universidad del País Vasco (UPV/EHU), Apartado 644, 48080 Bilbao, Spain
*Correspondence e-mail: jm.perez-mato@ehu.es

(Received 26 June 2012; accepted 8 October 2012; online 15 November 2012)

MAGNEXT is a new computer program available from the Bilbao Crystallographic Server (http://www.cryst.ehu.es) that provides symmetry-forced systematic absences or extinction rules of magnetic nonpolarized neutron diffraction. For any chosen Shubnikov magnetic space group, the program lists all systematic absences, and it can also be used to obtain the list of the magnetic space groups compatible with a particular set of observed systematic absences. Absences corresponding to specific ordering modes can be derived by introducing effective symmetry operations associated with them. Although systematic extinctions in neutron diffraction do not possess the strong symmetry-resolving power of those in nonmagnetic crystallography, they can be important for the determination of some magnetic structures. In addition, *MAGNEXT* provides the symmetry-adapted form of the magnetic structure factor for different types of diffraction vectors, which can then be used to predict additional extinctions caused by some prevailing orientation of the atomic magnetic moments. This program, together with a database containing comprehensive general information on the symmetry operations and the Wyckoff positions of the 1651 magnetic space groups, is the starting point of a new section in the Bilbao Crystallographic Server devoted to magnetic symmetry and its applications.

Keywords: magnetic nonpolarized neutron diffraction; systematic absences; extinction rules; Bilbao Crystallographic Server; *MAGNEXT*; computer programs.

1. Introduction

The investigation of complex magnetic and multiferroic materials and their properties requires a detailed knowledge of their symmetries, which in the case of commensurate magnetic orderings are determined by the so-called magnetic or Shubnikov space groups. The symmetry operations of the 1651 Shubnikov space-group types include the isometries of the 230 space groups and their combinations with the operation of time inversion 1’ which `inverts' the spin direction.

Apart from their essential role in the classification of magnetic symmetries, the magnetic space groups can be highly useful in the systematic description of magnetic

structures and their properties. Analogously to nonmagnetic diffraction, the symmetry of a magnetic material described by a magnetic space group is reflected in the symmetry of the magnetic neutron diffraction pattern. Magnetic Bragg reflections obtained by nonpolarized neutron diffraction experiments can present systematic absences in some directions caused by the magnetic symmetry of the crystal, *i.e.* by the existence of some specific symmetry operations. Such systematic absences can be derived directly from the magnetic space group, in a similar way to the derivation of nonmagnetic systematic absences from conventional space groups.

Unlike what happens in structural research, these systematic absences or systematic extinctions are seldom considered in the analysis of the diffraction of magnetic structures. One of the reasons is probably the lack of a comprehensive listing of reflection-condition data of the type found in *International Tables for Crystallography*, Vol. A (Hahn, 2002) for space groups. In fact, we could find very few articles on magnetic extinctions in the literature (Li, 1956; Ozerov, 1967, 1969). In his papers, Ozerov discusses and tabulates systematic extinctions of magnetic reflections in collinear magnetic materials and lists Shubnikov diffraction groups for triclinic and monoclinic magnetic structures. It is very likely that these results have been forgotten or, as the articles by Ozerov are written in Russian, generally ignored. Apart from obvious experimental difficulties when nuclear and magnetic diffraction peaks superpose, an additional general reason for the disregard of the information brought by magnetic diffracton extinctions may be related to the widespread (mis)understanding of the inefficiency of magnetic symmetry in comparison to the so-called representation analysis (Bertaut, 1968) of magnetic structures [for example, see Izyumov *et al.* (1991); it is worth noting that Ozerov is one of the co-authors of the book].

We think, however, that although magnetic systematic absences are not as conclusive as those of nonmagnetic crystallography, and in general cannot determine uniquely the magnetic space group of a crystal, they may provide some key information about the magnetic symmetry of the crystal and the type of magnetic ordering prior to any quantitative analysis of the diffraction data. Furthermore, in general, the use of the representation analysis method is no substitute for the identification of the symmetry of a magnetic phase. As the program *ISODISTORT* (Campbell *et al.*, 2006) nicely shows, the identification of an active irreducible representation(s) and of the magnetic space group provide complementary data, which allow one to obtain a full characterization of a magnetic structure and its properties.

Within this context the main aim of this contribution is to report on the development of an interactive program, *MAGNEXT*, for the study of the systematic absences of nonpolarized magnetic neutron diffraction in commensurate magnetic phases. The program *MAGNEXT* gives access to comprehensive listings of these absences and to the symmetry-adapted form of the structure factors for the different types of reflections associated with any of the 1651 magnetic space groups (§§A.3 and A.4). Alternatively, the program can be used to obtain a list of magnetic space groups compatible with a given set of systematic absences. Several illustrative examples, presented in §A.4, show how the information provided by *MAGNEXT* can be used in a systematic way to study possible systematic absences in the diffraction data,

identifying by this means the possible symmetry of the structure and its symmetry-forced features. The program is implemented in a new shell of the Bilbao Crystallographic Server (Aroyo, Perez-Mato *et al.*, 2006; Aroyo, Kirov *et al.*, 2006) which, in addition, contains databases and tools related to magnetic space groups and magnetic symmetry. The magnetic space-group database (introduced in §A.2 of the article) provides data on the symmetry operations of the 1651 magnetic groups, their generators, and general and special Wyckoff positions.

2. Database of magnetic space groups

Our recently constructed database of the 1651 magnetic space groups (Shubnikov groups) is freely available at the Bilbao Crystallographic Server (http://www.cryst.ehu.es) under the access tool MGENPOS. This database was built from the comprehensive computer-readable tables of Stokes & Campbell (2011), which were based on data extracted from the electronic book of Litvin (2011) and from the work of Bradley & Cracknell (1972).

MGENPOS provides a representative set of symmetry operations of any Shubnikov group, in four different formats: (i) as coordinate triplets of a general-position orbit of the magnetic group, including the components of an axial vector (magnetic moment) for each general-position point; (ii) as matrix–column pairs indicating the 3×3 roto-inversion matrices and the columns of components of the translation vectors associated with the operations; (iii) as a list of symmetry-operation symbols with the geometric interpretation of each operation, according to the notation of *International Tables for Crystallography*, Vol. A (Hahn, 2002); and (iv) using a generalized Seitz notation (Bradley & Cracknell, 1972), following the conventions proposed by Litvin (2011) and Litvin & Kopský (2011). The color red is used to distinguish the symmetry operations that combine with the operation of time inversion, which are primed following the generally accepted notation (see *e.g.* Litvin, 2011). Fig. 1 shows an example of the output of MGENPOS for the group *Pn'ma'* (62.448) [BNS].

In the case of type IV magnetic space groups [those containing operations of type (1' | **t**) but not (1' | 0)], for historical and practical reasons, there exist two alternative descriptions. These two different settings, called BNS (Belov, Neronova & Smirnova, 1957) and OG (Opechowski & Guccione, 1965), imply not only different labels for the space groups but also a quite different description of the symmetry operations, since the reference basis used is different. The OG description considers as reference the so-called black and white unit cell generating both the unprimed lattice translations (1 | **t**) and the primed lattice translations of type (1' | **t**) present in the group. In the BNS setting, instead, all translations refer to a unit cell corresponding to the actual translation lattice of the magnetically ordered crystal (usually called the magnetic unit cell), which is only formed by the operations of type (1 | **t**) so that primed translations always have fractional components. The different unit cells applied in the OG and BNS settings obviously imply different multiplicities for the corresponding Wyckoff position orbits (in general, the volume of the magnetic unit cell is a multiple of the volume of the paramagnetic unit cell). For a recent discussion and comparison of these alternative settings, see Grimmer (2009).

General Positions of the Group *Pn'ma'* (#62.448)

For this space group, BNS and OG settings coincide.
Its label in the OG setting is given as: Pn'ma' (#62.8.509)

N	Standard/Default Setting			
	(x,y,z) form	Matrix form	Geom. interp.	Seitz notation
1	x, y, z, +1 m_x,m_y,m_z	$\begin{pmatrix} 1 & 0 & 0 & 0 \\ 0 & 1 & 0 & 0 \\ 0 & 0 & 1 & 0 \end{pmatrix}$	1 +1	(1|0,0,0)
2	-x, -y, -z, +1 m_x,m_y,m_z	$\begin{pmatrix} -1 & 0 & 0 & 0 \\ 0 & -1 & 0 & 0 \\ 0 & 0 & -1 & 0 \end{pmatrix}$	-1 0,0,0 +1	(-1|0,0,0)
3	-x, y+1/2, -z, +1 $-m_x,m_y,-m_z$	$\begin{pmatrix} -1 & 0 & 0 & 0 \\ 0 & 1 & 0 & 1/2 \\ 0 & 0 & -1 & 0 \end{pmatrix}$	2 (0,1/2,0) 0,y,0 +1	(2_y|0,1/2,0)
4	x, -y+1/2, z, +1 $-m_x,m_y,-m_z$	$\begin{pmatrix} 1 & 0 & 0 & 0 \\ 0 & -1 & 0 & 1/2 \\ 0 & 0 & 1 & 0 \end{pmatrix}$	m x,1/4,z +1	(m_y|0,1/2,0)
5	x+1/2, -y+1/2, -z+1/2, -1 $-m_x,m_y,m_z$	$\begin{pmatrix} 1 & 0 & 0 & 1/2 \\ 0 & -1 & 0 & 1/2 \\ 0 & 0 & -1 & 1/2 \end{pmatrix}'$	2 (1/2,0,0) x,1/4,1/4 -1	($2_x'$|1/2,1/2,1/2)
6	-x+1/2, -y, z+1/2, -1 $m_x,m_y,-m_z$	$\begin{pmatrix} -1 & 0 & 0 & 1/2 \\ 0 & -1 & 0 & 0 \\ 0 & 0 & 1 & 1/2 \end{pmatrix}'$	2 (0,0,1/2) 1/4,0,z -1	($2_z'$|1/2,0,1/2)
7	-x+1/2, y+1/2, z+1/2, -1 $-m_x,m_y,m_z$	$\begin{pmatrix} -1 & 0 & 0 & 1/2 \\ 0 & 1 & 0 & 1/2 \\ 0 & 0 & 1 & 1/2 \end{pmatrix}'$	n (0,1/2,1/2) 1/4,y,z -1	(m_x'|1/2,1/2,1/2)
8	x+1/2, y, -z+1/2, -1 $m_x,m_y,-m_z$	$\begin{pmatrix} 1 & 0 & 0 & 1/2 \\ 0 & 1 & 0 & 0 \\ 0 & 0 & -1 & 1/2 \end{pmatrix}'$	a x,y,1/4 -1	(m_z'|1/2,0,1/2)

Figure 1
Example of the output of MGENPOS for the group *Pn'ma'*. Four different alternative descriptions of the symmetry operations are given (see text). The presence or absence of time inversion is indicated by a −1 or a +1, respectively, in columns 1 and 3; symmetry operations with time inversion are presented in red lettering.

MGENPOS works in either of the two settings and takes into account the practical consequences of the peculiarities of the OG setting, where the usual equivalence relationship by integer lattice translations is not valid in general. For these type IV groups, and in order to give complete information and avoid ambiguities, the output of the program includes an overcomplete set of generators of both the magnetic lattice and the black and white lattice. Fig. 2 shows an example of the output for the group labeled as C_ac (9.41) [BNS] and P_Cc (7.6.37) [OG] in the BNS and OG settings, respectively. It is important to stress that in the OG setting different magnetic space groups may have the same list of representative operations, except for the generators of the black and white lattice. This happens for instance with the group P_Cc (7.6.37) [OG] shown in Fig. 2 and the one labeled $P_{2a}c$ (7.4.35) [OG] (Litvin, 2011).

General Positions of the Group C_ac (#9.41) [BNS setting]

To display the general positions in the OG setting, please follow this link: P_{Cc} (#7.6.37) [Transformation matrix]

Translation lattice generators: (1|1,0,0), (1|0,1,0), (1|0,0,1), (1|1/2,1/2,0)

Black-and-white lattice generators: (1|1,0,0), (1|0,1,0), (1|0,0,1), (1|1/2,1/2,0), (1'|1/2,0,0) , (1'|0,1/2,0)

N	Standard/Default Setting			
	(x,y,z) form	Matrix form	Geom. interp.	Seitz notation
1	x, y, z, +1 m_x,m_y,m_z	$\begin{pmatrix} 1 & 0 & 0 & 0 \\ 0 & 1 & 0 & 0 \\ 0 & 0 & 1 & 0 \end{pmatrix}$	1 +1	(1|0,0,0)
2	x+1/2, y+1/2, z, +1 m_x,m_y,m_z	$\begin{pmatrix} 1 & 0 & 0 & 1/2 \\ 0 & 1 & 0 & 1/2 \\ 0 & 0 & 1 & 0 \end{pmatrix}$	t (1/2,1/2,0) +1	(1|1/2,1/2,0)
3	x, -y, z+1/2, +1 $-m_x,m_y,-m_z$	$\begin{pmatrix} 1 & 0 & 0 & 0 \\ 0 & -1 & 0 & 0 \\ 0 & 0 & 1 & 1/2 \end{pmatrix}$	c x,0,z +1	(m_y|0,0,1/2)
4	x+1/2, -y+1/2, z+1/2, +1 $-m_x, m_y, -m_z$	$\begin{pmatrix} 1 & 0 & 0 & 1/2 \\ 0 & -1 & 0 & 1/2 \\ 0 & 0 & 1 & 1/2 \end{pmatrix}$	n (1/2,0,1/2) x,1/4,z +1	(m_y|1/2,1/2,1/2)
5	x+1/2, y, z, -1 $-m_x,-m_y,-m_z$	$\begin{pmatrix} 1 & 0 & 0 & 1/2 \\ 0 & 1 & 0 & 0 \\ 0 & 0 & 1 & 0 \end{pmatrix}'$	t (1/2,0,0) -1	(1'|1/2,0,0)
6	x, y+1/2, z, -1 $-m_x, -m_y, -m_z$	$\begin{pmatrix} 1 & 0 & 0 & 0 \\ 0 & 1 & 0 & 1/2 \\ 0 & 0 & 1 & 0 \end{pmatrix}'$	t (0,1/2,0) -1	(1'|0,1/2,0)
7	x, -y+1/2, z+1/2, -1 $m_x,-m_y,m_z$	$\begin{pmatrix} 1 & 0 & 0 & 0 \\ 0 & -1 & 0 & 1/2 \\ 0 & 0 & 1 & 1/2 \end{pmatrix}'$	c x,1/4,z -1	(m_y'|0,1/2,1/2)
8	x+1/2, -y, z+1/2, -1 $m_x,-m_y,m_z$	$\begin{pmatrix} 1 & 0 & 0 & 1/2 \\ 0 & -1 & 0 & 0 \\ 0 & 0 & 1 & 1/2 \end{pmatrix}'$	n (1/2,0,1/2) x,0,z -1	(m_y'|1/2,0,1/2)

General Positions of the Group P_{Cc} (#7.6.37) [OG setting]

To display the general positions in the BNS setting, please follow this link: C_ac (#9.41) [Transformation matrix]

Translation lattice generators: (1|2,0,0), (1|0,2,0), (1|0,0,1), (1|1,1,0)

Black-and-white lattice generators: (1|0,0,1), (1'|1,0,0) , (1'|0,1,0)

N	Standard/Default Setting			
	(x,y,z) form	Matrix form	Geom. interp.	Seitz notation
1	x, y, z, +1 m_x,m_y,m_z	$\begin{pmatrix} 1 & 0 & 0 & 0 \\ 0 & 1 & 0 & 0 \\ 0 & 0 & 1 & 0 \end{pmatrix}$	1 +1	(1|0,0,0)
2	x, -y, z+1/2, +1 $-m_x,m_y,-m_z$	$\begin{pmatrix} 1 & 0 & 0 & 0 \\ 0 & -1 & 0 & 0 \\ 0 & 0 & 1 & 1/2 \end{pmatrix}$	c x,0,z +1	(m_y|0,0,1/2)
3	x+1, y, z, -1 $-m_x, -m_y, -m_z$	$\begin{pmatrix} 1 & 0 & 0 & 1 \\ 0 & 1 & 0 & 0 \\ 0 & 0 & 1 & 0 \end{pmatrix}'$	t (1,0,0) -1	(1'|1,0,0)
4	x+1, -y, z+1/2, -1 $m_x,-m_y,m_z$	$\begin{pmatrix} 1 & 0 & 0 & 1 \\ 0 & -1 & 0 & 0 \\ 0 & 0 & 1 & 1/2 \end{pmatrix}'$	g (1,0,1/2) x,0,z -1	(m_y'|1,0,1/2)

Figure 2

Example of the output of MGENPOS for a type IV group, showing its two alternative descriptions, with labels C_ac (9.41) [BNS] and P_{cc} (7.6.37) [OG]. The information includes a set of generators that define the unit cell (and its centerings) of both the actual periodic lattice of the group and its black and white lattice. Notice that the number of elements listed varies depending on the setting.

The choice of the BNS or OG setting implies important differences in the way the systematic absences for a type IV magnetic group must be described. Quite often the magnetic ordering implies a doubling of the magnetic primitive unit cell with respect to

that of the paramagnetic phase. In these cases, an OG description uses the lattice of the paramagnetic phase as reference, and in general magnetic reflections must be indexed with respect to their corresponding reciprocal lattice. This implies typically indexings with some half-integers. Thus, for these cases, the OG description is closer to the practice in experiments, where indexing is usually done with respect to the paramagnetic cell. The BNS setting, on the other hand, describes all properties using the unit cell, which is fully consistent with the actual periodic lattice of the magnetically ordered system, so that all translation components can be considered equivalent modulo 1. This has the advantage that it follows the usual crystallographic conventions and simplifies algebraic calculations, but it implies that magnetic diffraction peaks are indexed with respect to a magnetic unit cell, instead of using the natural reference given by the structural reciprocal lattice of the paramagnetic phase.

Wyckoff Positions of the Group *Pn'ma'* (#62.448)

For this space group, BNS and OG settings coincide.
Its label in the OG setting is given as: Pn'ma' (#62.8.509)

Multiplicity	Wyckoff letter	Coordinates
8	d	(x,y,z | m_x,m_y,m_z) (x+1/2,-y+1/2,-z+1/2 | -m_x,m_y,m_z) (-x,y+1/2,-z | -m_x,m_y,-m_z) (-x+1/2,-y,z+1/2 | m_x,m_y,-m_z) (-x,-y,-z | m_x,m_y,m_z) (-x+1/2,y+1/2,z+1/2 | -m_x,m_y,m_z) (x,-y+1/2,z | -m_x,m_y,-m_z) (x+1/2,y,-z+1/2 | m_x,m_y,-m_z)
4	c	(x,1/4,z | 0,m_y,0) (x+1/2,1/4,-z+1/2 | 0,m_y,0) (-x,3/4,-z | 0,m_y,0) (-x+1/2,3/4,z+1/2 | 0,m_y,0)
4	b	(0,0,1/2 | m_x,m_y,m_z) (1/2,1/2,0 | -m_x,m_y,m_z) (0,1/2,1/2 | -m_x,m_y,-m_z) (1/2,0,0 | m_x,m_y,-m_z)
4	a	(0,0,0 | m_x,m_y,m_z) (1/2,1/2,1/2 | -m_x,m_y,m_z) (0,1/2,0 | -m_x,m_y,-m_z) (1/2,0,1/2 | m_x,m_y,-m_z)

Site Symmetries of the Wyckoff Positions

WP	Representative	Site symmetry
4a	(0,0,0 | m_x,m_y,m_z)	-1
4b	(0,0,1/2 | m_x,m_y,m_z)	-1
4c	(x,1/4,z | 0,m_y,0)	.m.
8d	(x,y,z | m_x,m_y,m_z)	1

Figure 3
Example of the output of MWYCKPOS showing the general and special Wyckoff positions of the group *Pn'ma'*. Each Wyckoff position is specified by its multiplicity, Wyckoff letter and coordinate triplets and the corresponding components of the magnetic moments. The site-symmetry groups are designated by oriented point-group symbols.

As will be shown in §A.4, the calculation of the systematic absences in type IV groups has been done in the BNS setting using the procedure explained in the next section, but then the program can list them in either of the two alternative descriptions/indexings.

Additionally, we have developed a database of the Wyckoff positions of magnetic space groups, also freely available from the Bilbao Crystallographic Server, under the

MWYCKPOS program. This database was built from the same sources as the MGENPOS database (Stokes & Campbell, 2011; Litvin, 2011) and provides the Wyckoff positions of the magnetic space group types in both BNS and OG standard settings. Each Wyckoff position is specified by its Wyckoff letter, its multiplicity, and a set of coordinate and component triplets of the unit-cell points of the Wyckoff position orbit and their correlated magnetic moments. The site-symmetry groups are described by oriented magnetic point-group symbols, and optionally the program can calculate and list all symmetry operations of the site-symmetry magnetic group of a point. The Wyckoff positions provided by MWYCKPOS for the above-mentioned example, the magnetic space group *Pn'ma'* (62.448) [BNS], are shown in Fig. 3.

3. Magnetic systematic absences

3.1. General equations

The intensity of a diffraction peak due to the magnetic diffraction of unpolarized neutrons by an ordered magnetic crystal is given by (see *e.g.* Izyumov *et al.*, 1991)

$$I(\mathbf{H}) \propto \left|\mathbf{F}(\mathbf{H})\right|^2 - \left|\frac{\mathbf{H}}{|\mathbf{H}|}\cdot\mathbf{F}(\mathbf{H})\right|^2 \qquad \text{(A.1)}$$

where **H** is the corresponding diffraction vector and **F**(**H**) is the magnetic structure factor of the system. The magnetic structure factor is an axial (complex) vector, dependent on **H**, which can be defined as the Fourier transform of the average local magnetic moment density **M**(**r**) in the crystal:

$$\mathbf{F}(\mathbf{H}) = \int \mathbf{M}(\mathbf{r}) \exp(2\pi i \mathbf{H}\cdot\mathbf{r})\, \mathrm{d}\mathbf{r} \qquad \text{(A.2)}$$

The symmetry of the magnetic configuration, described by **M**(**r**), implies symmetry constraints on its corresponding structure factor. By definition, for any operation (***R***, θ | **t**) of the magnetic space (Shubnikov) group of the crystal (with ***R*** being a point-group operation, θ being −1 or +1 depending on whether the operation includes time inversion or not, and **t** being a translation) the magnetic moment density must satisfy

$$\mathbf{M}(\boldsymbol{R}\mathbf{r}+\mathbf{t}) = \theta \det(\boldsymbol{R})\, \boldsymbol{R}\mathbf{M}(\mathbf{r}) \qquad \text{(A.3)}$$

This condition implies for the magnetic structure factor that

$$\mathbf{F}(\mathbf{H}) = \theta \det(\boldsymbol{R}) \exp(2\pi i \mathbf{H}\cdot\mathbf{t})\, \boldsymbol{R}\mathbf{F}(\mathbf{H}\boldsymbol{R}) \qquad \text{(A.4)}$$

This equation becomes a constraint on the form of the structure factor and can then be the cause of some systematic absences for diffraction vectors such that

$$\mathbf{H}\boldsymbol{R} = \mathbf{H} \qquad \text{(A.5)}$$

According to equation (A.1), the diffraction intensity will be zero if this symmetry constraint forces **F**(**H**) to be either zero or parallel to **H**. Applying these considerations to each symmetry operation of the magnetic symmetry group of the crystal, all the

symmetry-forced systematic absences can be derived. Some types of diffraction vectors are invariant for more than one operation of the symmetry group, and the rules obtained in this way can be redundant or included in more general ones. A more systematic and consistent method is to apply group theoretical projector techniques to obtain the symmetry-adapted form of the magnetic structure factor for each symmetry-distinct type of diffraction vector **H**. This is the method employed by the program *MAGNEXT*, as explained below.

3.2. Projector method

The possible types of diffraction vectors **H** can be classified according to the symmetry point group P_{H} formed by the set of point-group operations (belonging to the magnetic point group of the crystal) that keep **H** invariant, *i.e.* they satisfy equation (A.5). For each symmetry type of diffraction vector some kind of systematic absence may occur. According to equation (A.4), for every symmetry operation (***R***, θ | **t**) of the crystal magnetic group, such that (***R***, θ) belongs to $P_{\mathbf{H}}$, the magnetic structure factor satisfies

$$\boldsymbol{T}\left(\boldsymbol{R},\theta\right)\mathbf{F}\left(\mathbf{H}\right)=\mathbf{F}\left(\mathbf{H}\right) \tag{A.6}$$

with

$$\boldsymbol{T}\left(\boldsymbol{R},\theta\right)=\theta\det\left(\boldsymbol{R}\right)\exp\left(2\pi i\mathbf{H}\cdot\mathbf{t}\right)\boldsymbol{R} \tag{A.7}$$

The matrices ***T***(***R***, θ) form a three-dimensional representation ***T*** of the magnetic point group $P_{\mathbf{H}}$, which is in general reducible. Thus, equation (A.6) can only be satisfied for a nonzero structure factor if this representation ***T*** contains the identity irreducible representation. As a consequence, the structure factor is identically zero if the decomposition of ***T*** into a direct sum of irreducible representations does not contain the identity irreducible representation A_1, *i.e.* if the multiplicity n_{A1} of A_1 in ***T*** is zero. According to standard group theory (see *e.g.* Bradley & Cracknell, 1972), this multiplicity can be obtained from the characters $\chi^{T}(\boldsymbol{R})$ of the representation ***T*** for all elements of $P_{\mathbf{H}}$:

$$\mathrm{n}_{A_1}=\frac{\mathbf{1}}{\left|P_{\mathbf{H}}\right|}\sum_{\boldsymbol{R}\in P_{\mathbf{H}}}\chi^{T}\left(\boldsymbol{R},\theta\right) \tag{A.8}$$

with $|P_{\mathbf{H}}|$ being the order of the group $P_{\mathbf{H}}$.

For n_{A1} = 2 or 3, any systematic absence coming from condition (A.6) can be discarded, as a nonzero magnetic structure factor can fulfill it without being restricted to having a fixed direction in space (the invariance space of the structure factor is two dimensional and three dimensional, respectively). Only in the case that n_{A1} = 1 does the symmetry condition (A.6) oblige **F**(**H**) to be restricted to a specific direction, and it is necessary then to check if this direction coincides with that of **H** or not, with a systematic absence occurring in the former case, according to equation (A.1).

Following standard group theory (see *e.g.* Bradley & Cracknell, 1972), the form of the structure factor required to satisfy equation (A.6) can be obtained using the projector P_1 on the subspace associated with the identity irreducible representation:

$$P_1 = \frac{\mathbf{1}}{|P_{\mathbf{H}}|} \sum_{\boldsymbol{R} \in P_{\mathbf{H}}} \boldsymbol{T}(\boldsymbol{R}, \theta) \tag{A.9}$$

Acting with P_1 on a generic axial vector, the most general form of an axial vector subject to condition (A.6) is obtained, *i.e.* the symmetry-adapted form of the magnetic structure factor for the type of diffraction vectors having $P_{\mathbf{H}}$ as symmetry group.

Following the scheme above, for each magnetic space group all symmetry types of diffraction vectors have been obtained, and for each of them the program *MAGNEXT* systematically uses equation (A.9) to obtain the symmetry-forced form of the magnetic structure factor. Then, equation (A.1) is applied to derive any resulting systematic absence.

3.3. Magnetic diffraction systematic absences of general validity

The systematic absences or extinction rules resulting from symmetry condition (A.6) also include those that are general and well known. Thus, equation (A.6) includes the trivial result that for any gray space group (Shubnikov group of type II; see *e.g.* Bradley & Cracknell, 1972) that is associated with magnetically disordered phases, magnetic diffraction is absent. Indeed, the presence of the time-inversion operation (1' | 0, 0, 0) in these groups implies according to equation (A.6) that **F**(**H**) = -**F**(**H**). Therefore, the fact that the magnetic structure factor is zero in these phases can be interpreted as a trivial consequence of their symmetry.

Magnetic orderings with a symmetry given by a type IV Shubnikov group contain symmetry operations with time inversion combined with some lattice translation, *i.e.* symmetry operations of type (1' | **t**). According to equations (A.6) and (A.7), a symmetry operation of this type implies that nonzero magnetic structure factors can only happen at diffraction vectors **H** such that exp(2πi**H**·**t**) = -1. On the other hand, the same operation (1' | **t**) in the case of nonmagnetic diffraction, caused by the nuclei or by the electron density in the case of X-ray diffraction (henceforth structural diffraction), forces a similar equation to (A.6) for its (scalar) structure factor $F_{scalar}(\mathbf{H})$, which taking into account that time inversion does not affect the nuclei positions reduces to

$$F_{scalar}(\mathbf{H}) = \exp(2\pi i \mathbf{H} \cdot \mathbf{t}) F_{scalar}(\mathbf{H}) \tag{A.10}$$

Here, the symmetry operation (1' | **t**) is equivalent to a lattice translation, so that diffraction only takes place when exp(2πi**H**·**t**) = 1. Hence we obtain the known general property that for type IV magnetic space groups, which are associated with antiferromagnetic orderings with a nonzero propagation vector, magnetic and nuclear diffraction peaks never coincide.

A completely different situation happens in type I and III magnetic space groups, corresponding to magnetic orderings where time-inversion symmetry is completely absent (type I), or only present when combined with point-group operations that are different from the identity (type III). In these groups, both nuclear and magnetic diffraction reflections can coincide. Only for certain types of diffraction vectors do we find systematic absences such that magnetic and nuclear diffraction peaks are not

superposed. This type of diffraction vector can also be determined using *MAGNEXT*, as demonstrated in the examples below.

4. MAGNEXT: main features and examples of application

There are three ways in which *MAGNEXT* can be used, depending on the type of input and output.

4.1. MAGNEXT option A

Option A is the default input choice. It provides a list of all (nonredundant) systematic absences for a magnetic space group in its conventional setting as described in MGENPOS. The group can be designated by first choosing one of the 230 crystallographic space groups and then selecting one of the magnetic space groups associated with it, either in the BNS or in the OG setting. The list of systematic absences is separated into two parts: first the absent reflections for any type of diffraction vector (produced by centerings and anti-translations, if existing), followed by systematic absences for specific symmetry types of diffraction vectors (**H** types). The program also provides a set of representative diffraction vectors and annotations that indicate whether the diffracted intensity is zero or nonzero and the kind of symmetry restriction existing on the forms of their magnetic structure factors.

The diffraction vectors are described with indices (*hkl*) with respect to the reciprocal basis of the basis used in direct space for describing the lattice translations. As a result of the properties discussed in the previous section (for type IV groups), the magnetic diffraction pattern, if described and indexed in the OG setting, may show reflections with half-integer values of *h*, *k* and/or *l*. Therefore, to avoid ambiguities, the output in all cases first indicates the type of allowed values for *h*, *k*, *l* in the diffraction diagram, showing explicitly if fractional values are allowed. In the case that the group is of type IV and described in the OG setting, the output also provides a formal propagation vector $\mathbf{k_0}$, described with respect to the reciprocal OG unit cell, which defines the black and white lattice in relation to the OG unit cell. Those OG lattice translations **t**that fulfill $\exp(2\pi i\mathbf{k_0}\cdot\mathbf{t}) = -1$ are necessarily accompanied by time inversion (anti-translations), while those satisfying $\exp(2\pi i\mathbf{k_0}\cdot\mathbf{t}) = 1$ are pure lattice translations.

The theoretical single propagation vector $\mathbf{k_0}$ that the program associates with each magnetic space group of type IV coincides with or is equivalent to the actual propagation vector considered in experiments in the case that the magnetic primitive unit cell is merely doubled with respect to that of the paramagnetic structure. In more complex orderings, the primitive paramagnetic unit cell will be smaller than the primitive OG unit cell by some integer factor, and the experimental indexing will differ from that provided by *MAGNEXT*. The experimental propagation vector is then related to the one provided by the program by the transformation matrix between the paramagnetic and OG unit cells. This transformation should be taken into account when interpreting the listed systematic absences.

Finally, the program also provides a list with all **H** types (including those where absences never occur) and the symmetry-restricted form of the structure factor for a set of relevant indices for each **H** type.

4.1.1. Example 1

Let us consider the magnetic space group *Pn'ma'* (62.448) [BNS] shown in Fig. 1, which is in fact realized in $LaMnO_3$, a well known distorted perovskite (see Fig. 4). The calculation of the systematic absences for this symmetry is made by *MAGNEXT* following the projector method described in §A.3.2. To calculate, for example, the systematic absences for reflection (0*k*0) the following operations keeping (0*k*0) invariant are to be used in the projector:

$$\left\{(1 \mid 0,\ 0,\ 0);\ \left(2_y \mid 0,\ \tfrac{1}{2},\ 0\right);\ \left(m_x \mid \tfrac{1}{2},\ \tfrac{1}{2},\ \tfrac{1}{2}\right);\ \left(m_z \mid \tfrac{1}{2},\ 0,\ \tfrac{1}{2}\right)\right\} \qquad \text{(A.11)}$$

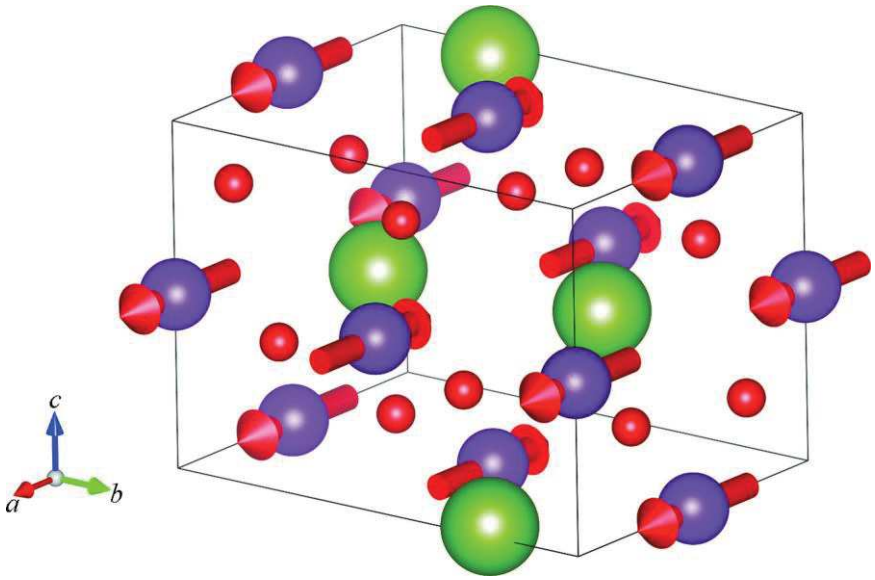

Figure 3
Scheme of the $LaMnO_3$ structure with a spin mode type A along the *x* direction in the *Pnma* setting, with magnetic symmetry given by the magnetic space group *Pn'ma'*.

Following the procedure described in §A.3.2, the symmetry-adapted form of the magnetic structure factor, **F**, is obtained:

$$\mathbf{F} = \mathscr{P}_1 \begin{pmatrix} F_x \\ F_y \\ F_z \end{pmatrix} = \frac{1}{2}\left[\begin{pmatrix} F_x \\ F_y \\ 0 \end{pmatrix} + \exp(i\pi k) \begin{pmatrix} -F_x \\ F_y \\ 0 \end{pmatrix} \right] \qquad \text{(A.12)}$$

We can determine for which values of *k* some components of the structure factor **F** will be zero:

$$\begin{aligned} F_x &= 0 \quad \text{if } k = 2n \\ F_y &= 0 \quad \text{if } k = 2n+1 \\ F_z &= 0 \quad \text{all } k \end{aligned} \qquad \text{(A.13)}$$

The component of the structure factor perpendicular to (0*k*0) is then restricted along the *x* direction, and therefore magnetic reflections will be absent for $k = 2n$. The null condition of the component F_y is the same as that of the nonmagnetic scalar structure factor, while for the component F_x it is the opposite. The fact that we obtain $F_z = 0$ for

any *k* illustrates the efficiency of the projector method. This nontrivial condition caused by the simultaneous fulfillment of equation (A.4) for all operations (A.11) is directly obtained by applying the projector.

Table 1 lists the resulting three types of systematic absences for this magnetic group. They originate in the screw rotations along the three crystallographic axes. Those along the *x* and *z* directions include time inversion and result in the same extinction rules as for nonmagnetic diffraction. On the other hand, the screw rotation along *y* results in an absence rule complementary to that of nonmagnetic diffraction.

Table 1
Systematic absences for the magnetic space group *Pn'ma'* (62.448) [BNS] as given by *MAGNEXT*

H type	Systematic absences
(*h*00)	Absent if $h = 2n + 1$
(0*k*0)	Absent if $k = 2n$
(00*l*)	Absent if $l = 2n + 1$

In many cases, overwhelming (super)exchange interactions favor a certain correlation of the orientations of the atomic magnetic moments beyond the restrictions of the relevant magnetic space group, such that magnetic moments have a prevailing direction. Thus, in $LaMnO_3$, the spin direction of the Mn atoms is mainly along *x* according to a so-called A-type ordering mode of the spins of the four atoms in the unit cell. This restriction, only fulfilled approximately, yields additional approximate absences, which can be derived directly from the knowledge of the symmetry-adapted form of the structure factor for each **H** type, also provided by *MAGNEXT* and reproduced in Table 2. One can derive directly from this table that, for magnetic moments essentially restricted to the *x* direction, the following additional approximate absences should occur:

$$\begin{aligned} &(h0l) \quad \text{all absent} \\ &(0kl) \quad \text{absent if } k + l = \text{even} \\ &(hk0) \quad \text{absent if } h = \text{odd} \end{aligned} \tag{A.14}$$

These additional absence rules are not forced by the magnetic symmetry; they are due to the prevailing direction of the spins, independently of the sites occupied by the magnetic atoms. Stronger rules can exist if the magnetic atoms are at special positions (see below).

Table 2
Form of the magnetic structure factor for each possible symmetry type of diffraction vector for space group *Pn'ma'* (62.448) [BNS]
Zero and nonzero structure factor components are explicitly listed.

H type	***h*, *k*, *l* values**	**Structure factors**
(*hkl*)	Any *h*, *k*, *l*	**F** = (F_x, F_y, F_z)
(*hk*0)	$h = 2n + 1$	**F** = (0, 0, F_z)

H type	*h*, *k*, *l* values	Structure factors
	$h = 2n$	**F** = (F_x, F_y, 0)
(*h*0*l*)	Any *h*, *l*	**F** = (0, F_y, 0)
(0*kl*)	$k + l = 2n$	**F** = (0, F_y, F_z)
	$k + l = 2n + 1$	**F** = (F_x, 0, 0)
(*h*00)	$h = 2n$	**F** = (0, F_y, 0)
	$h = 2n + 1$	**F** = (0, 0, 0)
(0*k*0)	$k = 2n$	**F** = (0, F_y, 0)
	$k = 2n + 1$	**F** = (F_x, 0, 0)
(00*l*)	$l = 2n$	**F** = (0, F_y, 0)
	$l = 2n + 1$	**F** = (0, 0, 0)

The absence rules provided by *MAGNEXT* are of very general validity, as they only depend on the magnetic symmetry of the system. However, one should stress that often magnetic phases can have additional systematic absences. These originate from the special position of the magnetic atoms, occupying so-called noncharacteristic orbits, which have higher symmetry than the actual symmetry of the whole structure (Engel *et al.*, 1984). These additional absences, which depend on the Wyckoff orbit(s) occupied by the magnetic atom(s), are not provided directly by the program. They can be derived, however, with *MAGNEXT* if it is used in conjunction with the program *NONCHAR*, also available from the Bilbao Crystallographic Server, which identifies noncharacteristic orbits and their symmetry.

$LaMnO_3$ is also an example of the presence of noncharacteristic absences, *i.e.* caused by the special position occupied by the Mn atom. It occupies the 4*a* Wyckoff orbit of *Pn'ma'* (62.448) [BNS] (see Fig. 3 and Table 3), and one can check using *NONCHAR* that this orbit is indeed noncharacteristic and has *Cmmm* symmetry. This is because the four positions of the orbit are consistent with the additional symmetry translations (1|1/2, 0, 1/2), (1|0, 1/2, 0) and their combination (1|1/2, 1/2, 1/2). These are indeed the additional symmetry translations that one has to consider for a spin arrangement of type F (spin component along **y**), where the spin component is equal in the four atoms. However, for spin arrangements of type A (component along **x**), the opposite signs of the spins of the two atoms related by the two last translations require that we consider (1|1/2, 0, 1/2), (1'|0, 1/2, 0) and (1'|1/2, 1/2, 1/2), *i.e.* two of the translations are combined with time inversion. Similarly, for the component along **z** of type G, the additional symmetry operations that can be included are (1|1/2, 0, 1/2), (1'|0, 1/2, 0) and (1|1/2, 1/2, 1/2). If indeed the spin ordering is approximately restricted to a single component, the presence of these additional centering translations or anti-translations among the atoms causing the magnetic diffraction is sufficient according to equation (A.6) to produce additional approximate absence rules. For instance, for the case of $LaMnO_3$, if the spins are exactly restricted to the A-type arrangement along the **x** direction, the following absence rules can be directly derived from equation (A.6) (see option B of the program):

$$\begin{aligned} &\text{From } (1' \mid 0,\ \tfrac{1}{2},\ 0) : (hkl) \quad \text{absent if } k = \text{even}, \\ &\text{From } (1 \mid \tfrac{1}{2},\ 0,\ \tfrac{1}{2}) : (hkl) \quad \text{absent if } h + l = \text{odd}. \end{aligned} \tag{A.15}$$

Table 3
Sign correlation of the components along the crystallographic axes of the magnetic moments of the atoms of a 4*a* Wyckoff orbit for the magnetic space group *Pn'ma'* (62.448) [BNS].
These relations can be obtained with the tool MWYCKPOS from the Bilbao Crystallographic Server (see Fig. 3). The labels A, F, G, C correspond to the commonly employed notation (Bertaut, 1968). Mode C is not allowed in this group.

	A	**F**	**G**	**C**
Atom	m_x	m_y	m_z	
(000)	1	1	1	1
(1/2 0 1/2)	1	1	−1	−1
(0 1/2 0)	−1	1	−1	1
(1/2 1/2 1/2)	−1	1	1	−1

These absence rules are again approximate in the sense that symmetry does not forbid *y* and *z* components in the spin arrangements, and according to the Von Neumann principle some weak nonzero spin components along these directions should be expected. Following a similar reasoning for the systematic absences caused by spin arrangements along **y** and **z**, one can easily see that the presence of magnetic diffraction peaks breaking the first of these two rules will be due to the F ordering along **y**, while the breaking of the second rule must be the result of the presence of the symmetry-allowed G-type ordering along **z**.

4.1.2. Example 2

Let us consider the type IV space group $C_Pm'c'a$ (64.14.541) [OG]. This is the magnetic symmetry of the antiferromagnetic phase reported for La_2CuO_4 (Freltoft *et al.*, 1987) and shown in Fig. 5. This group is generated by the operations (1'|1/2, 1/2, 0), (2_x|1/2, 1/2, 0), (2_y|1/2, 0, 1/2) and (-1|0, 0, 0) (see MGENPOS). Many type IV groups in the OG setting have half-integer indexings, as the propagation vector has half-integer components in the reciprocal basis of the OG setting. In the present case, however, the magnetic reflections are indexed with integers (*hkl*), as the magnetic ordering only breaks the C-centering and the propagation vector with respect to the *Cmca* OG unit-cell basis (coincident with the unit cell of the paramagnetic phase) can be chosen as (1, 0, 0). Two systematic absences are then provided by the program:

$$\begin{aligned} &(hkl) \quad \text{absent if } h+k = \text{even}, \\ &(0k0) \quad \text{absent for any } k. \end{aligned} \tag{A.16}$$

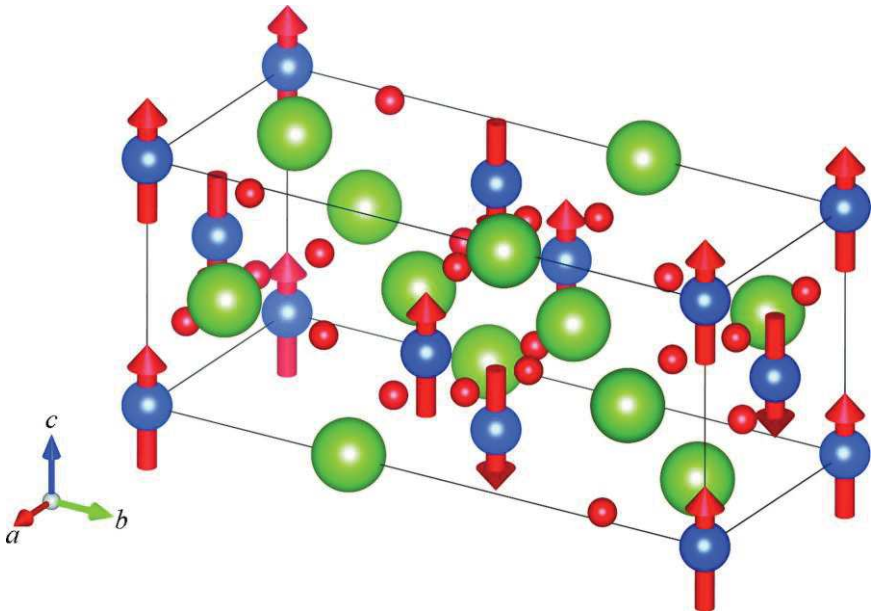

Figure 5
Magnetic structure of La_2CuO_4 with magnetic space group $C_Pm'c'a$ (64.14.541) [OG], according to Freltoft *et al.* (1987).

The first rule originates in the anticentering translation (1'|1/2, 1/2, 0), while the second is due to the operation (2_y|1/2, 0, 1/2), which forces the magnetic structure factor to have the form (0, F_y, 0) for diffraction vectors of type (0*k*0). The operations (2_x|1/2, 1/2, 0) and (2_z|0, 1/2, 1/2) would in principle also cause the absence of reflections of even index, for diffraction vectors of type (*h*00) and (00*l*), respectively, but these absences are subsumed within the first, much more general, one and as a consequence they are not listed separately.

Table 4 lists the symmetry-forced form of the magnetic structure factor for all symmetry types of diffraction vectors. In the case of La_2CuO_4 the magnetic moments are essentially directed along the *c* axis. From Table 4, one can then derive additional absences caused by this prevailing spin direction:

$$\begin{aligned} &(hk0) \quad \text{absent if } h = \text{even (or } k = \text{odd)}, \\ &(h0l) \quad \text{absent if } l \text{ odd}, \\ &(0k0) \quad \text{absent for any } k. \end{aligned} \tag{A.17}$$

Table 4
Form of the magnetic structure factor for each possible symmetry type of diffraction vector for space group $C_Pm'c'a$ (64.14.541) [OG].

H type	*h*, *k*, *l* values	Structure factors
(*hkl*)	$h + k = 2n$	**F** = (0, 0, 0)
	Elsewhere	**F** = (F_x, F_y, F_z)
(*hk*0)	$h = 2n + 1$ (or $k = 2n$)	**F** = (0, 0, F_z)
	$h = 2n$ (or $k = 2n + 1$)	**F** = (F_x, F_y, 0)
(*h*0*l*)	$l = 2n + 1$	**F** = (0, F_y, 0)

H type	*h*, *k*, *l* values	Structure factors
	$l = 2n$	**F** = (F_x, 0, F_z)
(0*kl*)	Any *l*	**F** = (0, F_y, F_z)
(*h*00)	Any *h*	**F** = (0, 0, F_z)
(0*k*0)	Any *k*	**F** = (0, F_y, 0)

As in the previous example, the independent magnetic atom Cu in La_2CuO_4 is at the origin and occupies the noncharacteristic orbit 4*a*. Complete information on this Wyckoff orbit $C_Pm'c'a$ (64.14.541) [OG], with indication of the relations among the magnetic moments of the atoms in the orbit, can be retrieved from MWYCKPOS in the Bilbao Crystallographic Server (or from the original sources; Litvin, 2011; Stokes & Campbell, 2011). This orbit can be described as (0, 0, 0|0, m_y, m_z), (1/2, 1/2, 0|0, -m_y, -m_z), (0, 1/2, 1/2|0, -m_y, m_z) and (1/2, 0, 1/2 | 0, m_y, -m_z). The magnetic components along **z** of these four atoms have therefore the following sign correlations: + − + −. This implies that this *z* component has as additional effective symmetry operation (1|0, 1/2, 1/2) and (1'|1/2, 0, 1/2), which according to equation (A.4) (see option B of the program) implies the following additional absence rules:

$$\begin{aligned} &\text{From } (1 \mid 0,\ \tfrac{1}{2},\ \tfrac{1}{2}) : (hkl) \quad \text{absent if } k+l = \text{odd}, \\ &\text{From } (1' \mid \tfrac{1}{2},\ 0,\ \tfrac{1}{2}) : (hkl) \quad \text{absent if } h+l = \text{even}. \end{aligned} \tag{A.18}$$

These two additional general absences include all those mentioned above for specific symmetry types of diffraction vectors. Their breaking can be taken as the signature of the presence of a nonzero *y* component in the atomic spins, which, as shown above, is allowed in this phase.

4.2. MAGNEXT option B

This option provides a list of all the systematic absences for a magnetic space group introduced in any arbitrary setting, using either a nonconventional BNS or OG type description. A set of generators expressed in coordinate triplet notation must be given. In the case of using an OG setting, the basic translations having associated time inversion must be indicated. This option can be used to monitor individually the extinction rules resulting from any possible symmetry operation described in any setting used by the user. It can also be employed to obtain specific absences due to particular spin ordering modes.

4.2.1. Example 3

If the paramagnetic phase of the systems is known to have a binary axis along the oblique direction [110], one can explore the possible signature of its conservation in the magnetic phase just by introducing in option B the coordinate triplet corresponding to this symmetry operation and adding time inversion or the lack of it, *i.e.* (*y*, *x*, −*z*, −1) or (*y*, *x* ,−*z*, 1). One can see then that if this binary rotation is conserved without time inversion, *i.e.* (2_{xy}|0, 0, 0), reflections of type (*hh*0) are all absent, while for the alternative conservation of the operation ($2'_{xy}$|0, 0, 0), which includes time inversion, these types of reflections are all allowed.

4.2.2. Example 4

The paramagnetic phase of Cl_2Cr has *Pnnm* symmetry. Cr atoms occupy the 2*a* Wyckoff position. The propagation vector of the magnetic ordering is (0, 1/2, 1/2) (Winkelmann *et al.*, 1997). Its magnetic space group has been considered to be P_{2s}-*1* (2.4.7) [OG] (Izyumov *et al.*, 1991). A standard triclinic cell for this magnetic space is necessarily oblique and clearly unpractical. The obvious approach is to maintain as working reference the setting of the orthorhombic paramagnetic phase. Keeping this setting, some nonstandard centering anti-translations have to be introduced in the space group to reproduce the black and white lattice resulting from the magnetic propagation vector. In the OG description and keeping the *Pnnm* setting, a propagation vector (0, 1/2, 1/2) is equivalent to the presence of the operations (1'|0, 1, 0) and (1'|0, 0, 1) in the magnetic space group. The introduction of these two operations and the inversion (-1|0, 0, 0) in option B is sufficient to produce the systematic absence rules for the group P_{2s}-*1* (2.4.7) [OG] in the unconventional setting corresponding to the paramagnetic *Pnmm* symmetry. One can see that this group has no specific systematic absences, except those caused by the anti-translations mentioned above, namely

$$\begin{aligned} &\text{Allowed values of } h, k, l: \\ &\qquad h \text{ integer}, k = n/2,\ l = n/2 \text{ (n integer)}, \\ &(hkl) \quad \text{absent if } k = n \text{ or } l = n. \end{aligned} \tag{A.19}$$

Magnetic diffraction peaks are therefore only located at (*hkl*) vectors with both *k* and *l* being half-integers. This is a trivial result in the sense that it just reproduces the equivalence of the anti-translation operations with the assignment of a propagation vector (0, 1/2, 1/2), but it is illustrative of how the selection rules caused by the existence of a single propagation vector are described as part of the set of systematic absences for a certain magnetic space group.

4.2.3. Example 5

Option B can also be used to derive systematic absences associated with noncharacteristic orbits and specific types of spin modes, by introducing additional effective symmetry operations which only apply to these specific orbits and spin modes. Let us consider for instance the mode of type C (Bertaut, 1968; Borovik-Romanov & Grimmer, 2003) for the cation *B* of a *Pnma* distorted perovskite, occupying a 4*a* Wyckoff orbit. The sign correlation of the magnetic moments of the four atoms in the *Pnma* unit cell corresponding to this mode is shown in Table 3. These correlations are equivalent to the introduction of an effective black and white lattice (translations and anti-translations) generated by the operations (1|0, 1/2, 0) and (1'|1/2, 0, 1/2). By introducing these operations in coordinate triplet notation (*x*, *y* + 1/2, *z*, +1) and (*x* + 1/2, *y*, *z* + 1/2, −1) in option B, we just obtain

$$(hkl) \quad \text{absent if } k = \text{odd or } h + l = \text{even}. \tag{A.20}$$

Table 5 summarizes the systematic absences obtained for the other types of modes listed in Table 3. This is just an example, and one can obtain automatically in a similar way the systematic absences corresponding to any type of mode in a Wyckoff orbit of

magnetic atoms, having higher translational and/or rotational symmetry than the whole crystal.

Table 5
Systematic absences for spin modes of type A, C, F and G (along any direction) for a 4*a* Wyckoff orbit of the group *Pnma*, as defined by the sign correlations described in Table 3.
These general absences can be obtained with option B (see text). This option can be used in general to obtain systematic absences resulting from any of the orbits occupied by the magnetic atoms.

Spin mode	H type	Systematic absences
A	(*hkl*)	$k = 2n$ or $h + l = 2n + 1$
F		$k = 2n + 1$ or $h + l = 2n + 1$
G		$k = 2n$ or $h + l = 2n$
C		$k = 2n + 1$ or $h + l = 2n$

These systematic absences depend on the spin mode type, and those coming from effective translations or anti-translations are independent of the direction taken by individual spins. They are not forced by the magnetic space group of the structure and can therefore be broken within the same magnetic phase by the presence of other spin mode types compatible with the actual magnetic symmetry of the phase.

4.3. MAGNEXT option C

As a result of the vectorial character of equations (A.1) and (A.6), the number of possible distinct symmetry-forced systematic absences is quite limited. In fact, apart from the absences resulting from centerings or anti-centering translations, only proper rotational symmetry operations can cause systematic absences that are independent of the specific spin arrangement. In option C we have collected all of them, expressed in the standard settings of the corresponding magnetic space groups (both BNS and OG settings). Tables 6 and 7 list all the possible distinct symmetry-forced systematic absences of any magnetic space group, in BNS and OG standard settings, respectively. Users can search the particular absence rules consistent with their observations and obtain the list of magnetic space groups compatible with them. This option is obviously only useful if the experimental diffraction diagram has been indexed in a standard setting (either OG or BNS). For magnetic orderings with nonzero modulation propagation wavevectors, this requires in general a deviation from the usual experimental labeling of magnetic diffraction peaks. In order to refine the search, the crystalline class or the space group associated with the searched magnetic space group in the OG setting can be specified.

Table 6
List of all the possible distinct symmetry-forced systematic absences of any magnetic space group in the BNS standard setting.
These systematic absences are the ones that can be provided as input in *MAGNEXT* option C.

H type	Systematic absences	
(*hkl*)	$h = 2n$	$h = 2n$ or $k + l = 2n$
	$k = 2n$	$h = 2n$ or $k + l = 2n + 1$

H type	Systematic absences	
	$l = 2n$	$h = 2n$ or $k = 2n$ or $l = 2n$
	$h + k = 2n$	$h + k = 2n$ or $l = 2n$
	$h + k = 2n + 1$	$h + k = 2n + 1$ or $l = 2n$
	$h + l = 2n$	$h + l = 2n$ or $k = 2n$
	$k + l = 2n$	$h + k = 2n$ or $h + l = 2n$
	$k + l = 2n + 1$	$h + k = 2n + 1$ or $h + l = 2n$
	$h + k + l = 2n$	$h + k = 2n + 1$ or $h + l = 2n + 1$
	$h + k + l = 2n + 1$	$2h + k + l \neq 3n$
	$h = 2n$ or $k = 2n$	$2h + k + l \neq 3n$ or $l = 2n$
	$k = 2n$ or $l = 2n$	
(h00)	$h = 2n$	h any
	$h = 2n + 1$	
(0k0)	$k = 2n$	k any
	$k = 2n + 1$	
(00l)	$l = 2n$	$l = 2n$ or $l = 3n$
	$l = 2n + 1$	$l = 2n + 1$ or $l = 3n$
	$l = 3n$	l any
(h h 0), (h -h 0)	h any (or k any)	
(h 0 h), (h 0 -h)		
(h -2h 0), (2h -h 0)		
(h h h), (h h -h)		
(h -h h), (h -h -h)		
(0 k k), (0 k -k)		

Table 7
List of all the possible distinct symmetry-forced systematic absences of any magnetic space group in the OG standard setting
These systematic absences are the ones that can be provided as input in *MAGNEXT* option C.

H type	Systematic absences	
(hkl)	$h = n$	$h = n$ or $k + l = 2n$
	$k = n$	$h = n$ or $k + l = 2n + 1$
	$l = n$	$h = n$ or $k = n$ or $l = n$
	$h + k = 2n$	$h + k = 2n$ or $l = n$
	$k + l = 2n$	$h + k = 2n + 1$ or $l = n$
	$h + k + l = 2n$	$h + k = 2n$ or $h + l = 2n$
	$h = n$ or $k = n$	$h + k = 2n + 1$ or $h + l = 2n$
	$k = n$ or $l = n$	$h + 2k + 2l \neq 3n$ or $l = n$
(00l)	$2l = 3n$	l any
(h00), (0k0)	h any (or k any)	
(h h 0), (h -h 0)		
(h h h), (h h -h)		

H type	Systematic absences
(*h* -*h h*), (*h* -*h* -*h*)	

When using option C, it must be taken into account that the systematic absences listed by the program are written in a nonredundant way, *i.e.* it is not necessary to introduce more specific absence rules that are contained in a more general one.

4.3.1. Example 6

Coming back to example 1, if we take the systematic absences of Table 1, we can check with option C that only two magnetic groups with *Pnma* as root space group are consistent with them, namely the group *Pn'ma'* (62.448) [BNS], as expected, but also the group *Pnm'a* (62.444) [BNS]. In the particular case of $LaMnO_3$ (see Fig. 4), however, the observation of the systematic absences would be sufficient to determine univocally the magnetic space group, as the second group can be discarded since it does not allow any magnetic moment for atoms in a 4*a* orbit (see MWYCKPOS). However, the approximate general absence rules, coming from the special symmetry of the Wyckoff orbit of magnetic atoms and the prevailing exchange-forced sign correlation of the moments, can make it difficult in practice to identify the specific exact absences due to the underlying magnetic symmetry. This happens in fact in this simple case of $LaMnO_3$, where the absence rules of the prevailing type A ordering (see Table 5) subsume the more specific absences caused by the group *Pn'ma'*. Even in this case, the systematic check of the presence of additional absence rules, besides that of type A ordering, is in fact sufficient for identifying the specific magnetic space group and with it the specific direction taken by the magnetic moments. For a type A ordering of a *Pnma* 4*a* Wyckoff orbit, magnetic reflections (*hkl*) will be absent if *k* = even or *h* + *l* = odd (see Table 5). This observation is then sufficient to know the sign correlation of the magnetic moments of the atoms in the orbit. A type A ordering along **x**, **y** or **z** implies, however, different magnetic space groups, which may have distinct additional systematic absences. A systematic check of their fulfillment can then be sufficient to determine the magnetic space group and with it the direction taken by the type A ordering mode. With option C, one can see that the only rules that can be added are (*a*) (*h*00) with *h* = even, (*b*) (0*k*0) with *k* = odd and (*c*) (00*l*) with *l* = even. Considering only groups that allow magnetic moments at the 4*a* Wyckoff positions, if rules (*a*) and (*b*) are detected (which combined with the type A absence rule means in practice that all magnetic reflections of these two types are absent) only the group *Pnm'a'* (62.447) [BNS] is possible, and inspecting with MWYCKPOS the 4*a* Wyckoff orbit for this group one can see that it implies that the type A mode must be along **y**. Similarly, rules (*a*) and (*c*) are only consistent with the group *Pnma* (62.441) [BNS], and this would correspond to an A-type spin mode along **z**. Finally rules (*b*) and (*c*) are only simultaneous in the group *Pn'm'a'* (62.446) [BNS], which is not compatible with an A-type spin mode. On the other hand, the group *Pn'ma'* (62.448) [BNS] corresponding to the type A ordering along **x** does not imply any additional absence rule, and this fact can then be used for identifying it as the relevant magnetic group.

One should be, however, cautious with option C. Some of the absences can correspond to reflections that are allowed for nuclear diffraction, and to detect unambiguously the rigorous fulfillment of the absence rule can be problematic. Furthermore, the list of

groups provided by option C does not include those groups for which the rules may be approximately fulfilled if the orbit of magnetic atoms is noncharacteristic and/or the direction of the atomic moments have within experimental accuracy special directions not forced by symmetry. Thus, as we have seen in example 1, rules (*a*) and (*b*) will also be satisfied by group *Pn'ma'* (62.448) [BNS] if the magnetic moments of the 4*a* atoms are strictly restricted to the **x** direction. The rules will, however, be broken if the symmetry-allowed spin canting is experimentally significant, while the absences must be strictly obeyed by any configuration with magnetic space group *Pnma* (62.441) [BNS].

4.3.2. Example 7

Let us consider a compound with space group $P4_2/mnm$ in the paramagnetic phase and only magnetic atoms in a 4*f* site. Let us also assume that from experiment we know that magnetic diffraction is absent for (*h*00) with *h* = even, (0*k*0) with *k* = even and (00*l*) for any *l*. Note that the first two absences are complementary to those of nuclear diffraction for the same diffraction vectors, implying that along these two axes nuclear and magnetic reflections are distinct spots depending on the parity of the index. These three rules introduced in option C provide a list of four possible magnetic groups with root OG space group $P4_2/mnm$. However, we can see immediately, calling to option A of the program for each of the groups, that two of them also include the absence of reflections of type (*hh*0) and (*h*-h0) for any *h*. They can therefore be excluded because this extinction is not realized in our system. The two remaining groups are $P4'_2/m'n'm$ (136.500) [BNS] and $P4'_2/mnm'$ (136.499) [BNS]. Looking at the Wyckoff positions of the two groups (MWYCKPOS) one can see that the first one constrains the magnetic moments in a 4*f* orbit to be in the basal plane, while the second group forces these moments to lie along the *z* axis. One can then inspect the symmetry-forced form of the structure factor provided by the program for any symmetry type of diffraction vector to check if the additional constraint of the spin direction is bound to cause additional distinctive systematic absences. In the case of the group $P4'_2/mnm'$ (136.499) [BNS], indeed, we can see that reflections of type (0*kl*) and *k* + *l* = even have a magnetic structure factor of the form (F_x, 0, 0). As the magnetic moments are along **z** in this group, F_x will necessarily be zero and these reflections must be absent. Similarly, by symmetry, reflections (*h*0*l*) with *h* + *l* = even would also be absent. On the other hand, for the group $P4'_2/m'n'm$ (136.500) [BNS], where the spins are constrained to the *xy* plane, no additional absence is expected. Therefore, the observation or not of this additional extinction rule is sufficient to determine univocally the magnetic space group of the structure, which in this simple example would imply a reduction of the structure refinement to a single parameter defining the magnitude of the magnetic moment of a single atom of the 4*f* orbit. A scheme showing the resulting magnetic orderings for both cases is shown in Fig. 6.

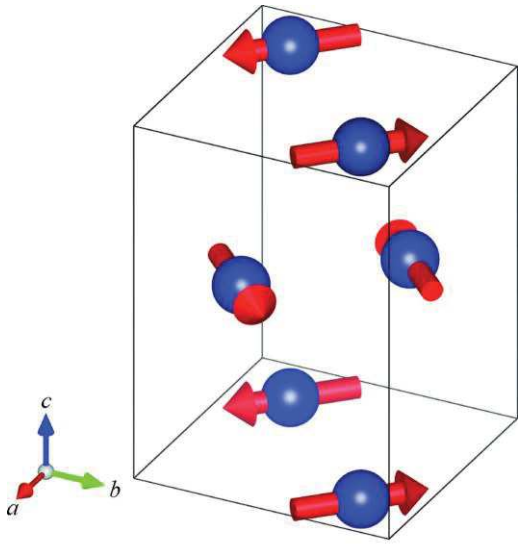

(*a*) $P4_2'/m'n'm$

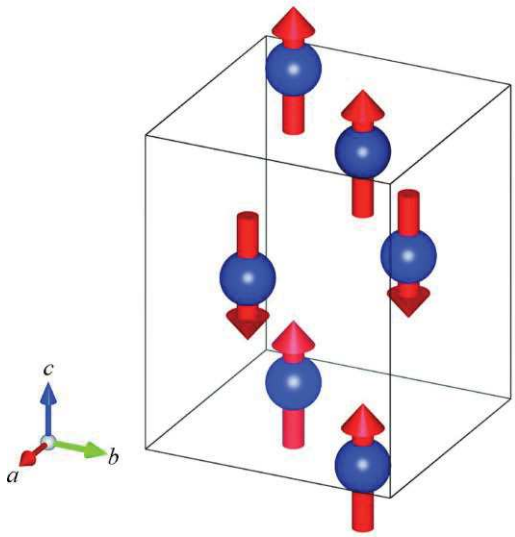

(*b*) $P4_2'/mnm'$

Figure 6
Schemes of two different magnetic orderings of a 4*f* orbit of atoms for the space group $P4_2/mnm$. The corresponding magnetic space groups are $P4'_2/m'n'm$ (136.500) [BNS] (*a*) and $P4'_2/mnm'$ (136.499) [BNS] (*b*). Both magnetic space groups exhibit the same absence rules: (*h*00) with *h* = even, (0*k*0) with *k* = even and (00*l*) for any *l*. However, the location of the magnetic atoms in the special Wyckoff position 4*f* forces the spins to be along the z direction in (*b*). This is sufficient to cause the additional systematic absences (*h*0*l*) with *h* + *l* = even and (0*kl*) with *k* + *l* = even (see text), which allow us to distinguish between the two types of ordering.

5. Conclusions

As part of a new shell at the Bilbao Crystallographic Server, dedicated to magnetic symmetry, an online tool called *MAGNEXT* has been developed, which provides systematic absences for any magnetic space group and allows the systematic use of this experimental information in the analysis of commensurate magnetic phases.

Through several examples we have shown its capabilities and the way the program can be helpful for determining magnetic structures. Although the number of distinct types of absences is quite limited, the observation or not of a specific extinction rule can be a key fact in discrimination between different competitive models of different symmetry, or in the decision to refine a model with less symmetry (more free parameters). Approximate absences due to magnetic ordering, which are restricted beyond the conditions forced by symmetry, or due to the special symmetry of the sites occupied by the magnetic atoms can also be derived.

As many magnetic structures are being determined and reported using the so-called representation method, without using magnetic symmetry, it is pertinent here to stress some basic points concerning the relation between the two approaches, which helps to show the utility of the program even in the case that the magnetic structure is being analyzed using the representation method. If the irreducible representation (irrep) associated with the basis modes (or basis functions) used in the description of the magnetic structure is one dimensional, the assignment of a magnetic space group is indeed equivalent to the identification of this specific irrep. However, in the case that the active irrep is multidimensional, the assignment of a magnetic space group is more restrictive than the identification of a relevant or active *n*-dimensional irrep. In these cases, the application of the restrictions of a magnetic space group is equivalent to some specific `symmetric' constraints on how the basis modes associated with the *n*-dimensional irrep should be linearly combined. These special linear combinations of the basis modes having an associated higher magnetic space-group symmetry may imply some additional systematic absence rule. In order to find the magnetic symmetry groups corresponding to a multidimensional irrep the program *ISODISTORT* (Campbell *et al.*, 2006; http://stokes.byu.edu/iso/isodistort.html) can be used. Once a magnetic space group is assigned, the relevant basis modes can be directly retrieved using MWYCKPOS from the listing of the Wyckoff orbit(s) corresponding to the magnetic atoms. These listings include the relations of the magnetic moments of the atoms in the orbit(s) and are automatically equivalent to the use of the basis modes (subject in general to specific symmetric linear combinations in the case of multidimensional irreps). In some cases, the degrees of freedom of the magnetic moments in the relevant Wyckoff orbits may also include some additional secondary basis modes corresponding to a different irrep, as a result of their compatibility with the magnetic symmetry.

Together with the databases MGENPOS and MWYCKPOS, which contain comprehensive information on the symmetry operations and the Wyckoff positions of the 1651 magnetic space groups, the development of *MAGNEXT* is the starting point of a new section of the Bilbao Crystallographic Server devoted to the study of magnetic symmetry and its applications.

Acknowledgements

This work has been supported by the Spanish Ministry of Science and Innovation (project MAT2008-05839) and the Basque Government (project IT-282-07). We thank H. Stokes and B. J. Campbell for valuable discussions and their help in processing their computer-readable listings of magnetic space groups and Wyckoff positions. We also

gratefully acknowledge helpful discussions with Daniel B. Litvin, and thank him for making freely available as an ebook his remarkable achievement of an extensive and detailed set of tables of the magnetic space groups. Structure figures were plotted using the *VESTA* package (Momma & Izumi, 2011).

References

Aroyo, M. I., Kirov, A., Capillas, C., Perez-Mato, J. M. & Wondratschek, H. (2006). *Acta Cryst.* A**62**, 115–128.

Aroyo, M. I., Perez-Mato, J. M., Capillas, C., Kroumova, E., Ivantchev, S., Madariaga, G., Kirov, A. & Wondratschek, H. (2006). *Z. Kristallogr.* **221**, 15–27.

Belov, N. V., Neronova, N. N. & Smirnova, T. S. (1957). *Sov. Phys. Crystallogr.* **2**, 311–322.

Bertaut, E. F. (1968). *Acta Cryst.* A**24**, 217–231.

Borovik-Romanov, A. S. & Grimmer, H. (2003). *International Tables for Crystallography*, Vol. D, edited by A. Authier, pp. 105–149. Dordrecht: Kluwer Academic Publishers.

Bradley, C. J. & Cracknell, A. P. (1972). *The Mathematical Theory of Symmetry in Solids.* Oxford: Clarendon Press.

Campbell, B. J., Stokes, H. T., Tanner, D. E. & Hatch, D. M. (2006). *J. Appl. Cryst.* **39**, 607–614.

Engel, P., Matsumoto, T., Steinmann, G. & Wondratschek, H. (1984). *Z. Kristallogr.* Suppl. Issue 1.

Freltoft, T., Fischer, J. E., Shirane, G., Moncton, D. E., Sinha, S. K., Vaknin, O., Remeika, J. P., Cooper, A. S. & Harshman, D. (1987). *Phys. Rev. B*, **36**, 826–828.

Grimmer, H. (2009). *Acta Cryst.* A**65**, 145–155.

Hahn, Th. (2002). (Editor). *International Tables for Crystallography* Vol. A, *Space-Group Symmetry*, 5th ed. Dordrecht: Kluwer Academic Publishers.

Izyumov, Yu. A., Naish, V. E. & Ozerov, R. P. (1991). *Neutron Diffraction of Magnetic Materials.* Dordrecht: Kluwer Academic Publishers.

Li, Y.-Y. (1956). *Acta Cryst.* **9**, 738–740.

Litvin, D. B. (2011). *Magnetic groups*, http://www.bk.psu.edu/faculty/litvin/Download.html .

Litvin, D. B. & Kopský, V. (2011). *Acta Cryst.* A**67**, 415–418.

Momma, K. & Izumi, F. (2011). *J. Appl. Cryst.* **44**, 1272–1276.

Opechowski, W. & Guccione, R. (1965). *Magnetism*, edited by G. T. Rado & H. Súhl, Vol. II, Part A, pp. 105–165. New York: Academic Press.

Ozerov, R. P. (1967). *Kristallografiya*, **12**, 239–251.

Ozerov, R. P. (1969). *Kristallografiya*, **14**, 393–403.

Stokes, H. & Campbell, B. J. (2011). *Table of Magnetic Space Groups*, http://stokes.byu.edu/magneticspacegroups.html .

Winkelmann, M., Baehr, M., Reehuis, M., Steiner, M., Hagiwara, M. & Katsumata, K. (1997). *J. Phys. Chem. Solids.* **58**, 481–489.

ANEXO B

J. M. Perez-Mato, Samuel V. Gallego, E. S. Tasci, L. Elcoro, and M. I. Aroyo. *Phys. Rev.* B **90**, 167101

Comment on "Canonical magnetic insulators with isotropic magnetoelectric coupling"

J. M. Perez-Mato[1,*], Samuel V. Gallego[1], E. S. Tasci[2], L. Elcoro[1] and M. I. Aroyo[1]
[1]Departamento de Fisica de la Materia Condensada, Universidad del Pais Vasco (UPV/EHU), Apartado 644, 48080 Bilbao, Spain
[2]Physics Department, Middle East Technical University, Ankara, Turkey
(Received 1 April 2014; published 8 October 2014)
*Corresponding author: jm.perez-mato@ehu.es

Coh *et al.* presented in [*Phys. Rev.* B **88**, 121106(R) (2013)] a systematic search of the simplest so-called "canonical" structures allowing isotropic magnetoelectric response, and reported a total of 30 such magnetic configurations. Using magnetic symmetry we show in this Comment that this listing is severely incomplete, and 14 additional distinct cases satisfying the same conditions should be added. The complete list of these elementary magnetic arrangements is then presented in a short and efficient form as distinct Wyckoff positions of some cubic magnetic space groups.

DOI: http://dx.doi.org/10.1103/PhysRevB.90.167101
PACS number(s): 75.85.+t, 03.65.Vf, 71.15.Rf

The Rapid Communication by Coh *et al.* [1] has reported a systematic search of the "simplest" structures, which allow isotropic magnetoelectric (ME) coupling. They listed a total of 30 such so-called "canonical" structures, which would represent the simplest configurations of atomic magnetic moments that have a symmetry-forced isotropic linear ME response. According to the Rapid Communication, this search was done by looking for distinct Wyckoff positions (WP) of cubic space groups with at most a free parameter. For each corresponding Wyckoff orbit, taken as a possible arrangement of the magnetic atoms, a representative canonical magnetic structure was obtained by associating an arrangement of magnetic moments according to the **k**=0 irreducible representation of the space group that allows nonzero ME coupling.

The method followed in Ref. [1] is in principle correct, but in fact these distinct elementary magnetic configurations can be compiled in a more straightforward manner by considering magnetic symmetry, i.e., magnetic space groups (Shubnikov groups) [2]. In the following we show how this simple alternative method is applied, with the important result (the main motivation of this comment) that a considerable number of cases are missing in the list of Ref. [1].

The derivation in the framework of magnetic symmetry of these simplest magnetic structures having isotropic ME coupling, is summarized as follows. Cubic symmetry is necessary to force an isotropic response. In addition it is well known (see, for instance, Ref. [3]), and it can be easily derived, that a nonzero linear ME effect requires that the

magnetic point group contains only proper rotations uncombined with time reversal and/or improper rotations combined with time reversal. Among the cubic point groups this is only fulfilled by the point groups 23, *m*′−3′, 432, −4′3*m*′, and *m*′−3′*m*′. This is equivalent to the condition introduced in Ref. [1] for the relevant irreducible representation and means that the magnetic space groups of the searched structures must have as point group one of the five listed above. This results in 36 possible cubic magnetic space groups from a total of 149. These groups are listed in the first column of Table 1.

Table 1
Cubic magnetic space groups allowing linear ME coupling. Each listed WP defines one elementary magnetic structure of the type proposed in Ref. [1]. The 14 additional cases not obtained in Ref. [1] are indicated in bold. The index assigned to each case includes, in brackets, the index used in Ref. [1], if any. The magnetic space groups (MSG) with a blank in the third column have only WPs that are noncharacteristic (see text).

MSG	Index	Magnetic Wyckoff position
*P*23	—	—
*F*23	—	—
*I*23	—	—
*P*213	1(1)	4*a* (*x*,*x*,*x*||*m*x,*m*x,*m*x)
*I*213	2(2)	12*b* (*x*,0,1/4||*m*x,0,0)
	3(3)	8*a* (*x*,*x*,*x*||*m*x,*m*x,*m*x)
Pm′−3′	4(4)	6f (*x*,0,1/2||*m*x,0,0)
Pn′−3′	—	—
Fm′−3′	—	—
Fd′−3′	—	—
Im′−3′	5(5)	12*e* (*x*,0,1/2||*m*x,0,0)
Pa′−3′	6(6)	8*c* (*x*,*x*,*x*||*m*x,*m*x,*m*x)
Ia′−3′	7(7)	24*d* (*x*,0,1/4||*m*x,0,0)
	8(8)	16*c* (*x*,*x*,*x*||*m*x,*m*x,*m*x)
*P*432	—	—
***P*4232**	**9**	**12k (1/4,y,−y+1/2||0,my,−my)**
*F*432	—	—
***F*4132**	**10**	**48g (1/8,y,−y+1/4||0,my,−my)**
***I*432**	**11**	**24i (1/4,y,−y+1/2||0,my,−my)**
*P*4332, *P*4132	**12**	**12d (1/8,y,−y+1/4||0,my,−my)**
	13(9)	8*c* (*x*,*x*,*x*||*m*x,*m*x,*m*x)
*I*4132	**14**	**24g (1/8,y,y+1/4||0,my,my)**
	15(10)	24*f* (*x*,0,1/4||*m*x,0,0)
	16(11)	16*e* (*x*,*x*,*x*||*m*x,*m*x,*m*x)
P-4′3*m*′	17(12)	4*e* (*x*,*x*,*x*||*m*x,*m*x,*m*x)
F-4′3*m*′	18(13)	16*e* (*x*,*x*,*x*||*m*x,*m*x,*m*x)
I-4′3*m*′	19(14)	8*c* (*x*,*x*,*x*||*m*x,*m*x,*m*x)
P-4′3*n*′	—	—
F-4′3*c*′	—	—
I-4′3*d*′	20(15)	24*d* (*x*,0,1/4||*m*x,0,0)
	21(16)	16*c*(*x*,*x*,*x*||*m*x,*m*x,*m*x)
Pm′−3′*m*′	**22**	**12i (0,y,y||0,my,my)**
	23(17)	12*h* (*x*,1/2,0||*m*x,0,0)
	24(18)	8*g* (*x*,*x*,*x*||*m*x,*m*x,*m*x)

MSG	Index	Magnetic Wyckoff position
	25(19)	6*e* (*x*,0,0||*m*x,0,0)
Pn′−3′*n*′	—	—-
Pm′−3′*n*′	**26**	**24j (1/4,y,y+1/2||0,my,my)**
	27(20)	12g (*x*,0,1/2||*m*x,0,0)
Pn′−3′*m*′	**28**	**24i (1/2,y,y+1/2||0,my,my)**
	29(21)	8*e* (*x*,*x*,*x*||*m*x,*m*x,*m*x)
Fm′−3′*m*′	**30**	**48h (0,y,y||0,my,my)**
	31(22)	32*f* (*x*,*x*,*x*||*m*x,*m*x,*m*x)
	32(23)	24*e* (*x*,0,0||*m*x,0,0)
Fm′−3′*c*′	—	—
Fd′−3′*m*′	**33**	**96h (0,y,−y||0,my,−my)**
	34(24)	48*f* (*x*,1/8,1/8||*m*x,0,0)
	35(25)	32*e* (*x*,*x*,*x*||*m*x,*m*x,*m*x)
***Fd*′-3′c**′	**36**	**96g (1/4,y,−y||0,my,−my)**
Im′−3′*m*′	**37**	**48i (1/4,y,−y+1/2||0,my,−my)**
	38	**24h (0,y,y||0,my,my)**
	39(26)	24*g* (*x*,0,1/2||*m*x,0,0)
	40(27)	16*f* (*x*,*x*,*x*||*m*x,*m*x,*m*x)
	41(28)	12*e* (*x*,0,0||*m*x,0,0)
Ia′−3′*d*′	**42**	**48g (1/8,y,−y+1/4||0,my,−my)**
	43(29)	48*f* (*x*,0,1/4||*m*x,0,0)
	44(30)	32*e* (*x*,*x*,*x*||*m*x,*m*x,*m*x)

Any cubic structure (simple or not), with atomic positions and ordering of magnetic moments following the relations of any of the magnetic space groups listed in Table 1 is bound to have a nonzero isotropic linear ME response. Their magnetic atoms may occupy general sites (where the magnetic moment of the independent atom has no restriction), or may be located at special WPs with restrictions both for the positions and magnetic moments. The possible different WPs and the symmetry restrictions of their corresponding orbits of atomic sites, both for magnetic moments and positions, of any magnetic space group have been tabulated and can be easily retrieved from freely available databases [2,4,5]. Thus, the knowledge that these 36 magnetic space groups are those allowing isotropic linear ME response, together with the mentioned tabulated WP orbits should be in principle sufficient as symmetry framework for searching real systems with isotropic ME coupling. But if one is interested in compiling the simplest structures in the sense considered in Ref. [1], then each Wyckoff orbit of atomic positions and moments of the magnetic space groups listed in Table 1, and having at most a free positional parameter, represents one distinct elementary structure for this collection, provided that duplicities and equivalences are avoided. This latter can be done by dropping noncharacteristic orbits, i.e., having higher symmetry than the corresponding space group, and orbits equivalent by a setting transformation (in the crystallographic language, Wyckoff orbits that belong to the same Wyckoff set). The set of magnetic WPs for the different magnetic space groups fulfilling these conditions, and therefore describing a complete set of elementary magnetic structures in the sense proposed in Ref. [1], are listed in Table 1.

As an example of the procedure followed to derive Table 1, let us consider the case of the group *Pm*′−3′*n*′. This group has five special WPs having one single free positional

parameter [2,4,5]: 12*f* (*x*,0,0||*m*x,0,0); 12*g* (*x*,0,1/2||*m*x,0,0); 12*h* (*x*,1/2,0||*m*x,0,0); 16*i* (*x*,*x*,*x*||*m*x,*m*x,*m*x); and 24*j* (1/4,*y*,*y*+1/2||0,*m*y,*m*y). From these we have to discard the WPs whose orbits are noncharacteristic, i.e., whose eigensymmetry is described by a supergroup of *Pm*′−3′*n*′. The eigensymmetry groups of the WPs of *Pm*′−3′*n*′ are trivially related with those of the WPs of the conventional (nonmagnetic) space group *Pm*−3*n* (available online in the *Bilbao Crystallographic Server* with the tool NONCHAR [6], and also in Table 14.2.3.2 of Ref. [7]). One can then see that the orbits of the WPs 12*f* and 16*i* are noncharacteristic: Their eigensymmetry is *Im*′−3′*m*′ and indeed their corresponding elementary magnetic configurations are listed as the WPs 12*e* (No. 41) and 16*f* (No. 40) of *Im*′−3*m*′ in Table 1. In addition, the WPs 12*g* and 12*h* of *Pm*′−3′*n*′ can be considered equivalent as they belong to the same Wyckoff set, which again can be deduced from the distribution of the orbits of the ordinary space group *Pm*−3*n* into Wyckoff sets (see Table 14.2.3.2 of Ref. [7] or use the tool WYCKSETS of the *Bilbao Crystallographic Server* [6]). We are therefore left with only two distinct WPs, 12*g* and 24*j*, of *Pm*′−3′*n*′ as distinct elementary magnetic structures in the sense proposed in Ref. [1]. They are therefore both included in Table 1 (see No. 27 and No. 26). Note that the second one is not among the elementary structures listed in Ref. [1].

Table 1 only lists the restrictions on the position and magnetic moment of a single representative atom of the Wyckoff orbit. This fully defines the searched elementary structure, as the positions and magnetic moments of the remaining atoms in the orbit are determined by the symmetry operations of the corresponding magnetic space group (listed in the above-mentioned tabulations [2,4,5]). For instance, the specific example discussed in detail in Ref. [1] corresponds to the WP 16*e* of the magnetic space group *F*−4′3*m*′ with the restricted position and magnetic moment of its representative atom being given by (*x*,*x*,*x*||*m*x,*m*x,*m*x), while the full orbit of 16 atomic positions and moments are (*x*,*x*,*x*||*m*x,*m*x,*m*x), (*x*,−*x*,−*x*||*m*x,−*m*x,−*m*x), (−*x*,*x*,−*x*||−*m*x,*m*x,−*m*x), and (−*x*,−*x*,*x*||−*m*x,−*m*x,*m*x), plus the 12 additional sites obtained by the *F* centering translations, as can be easily retrieved, for instance, from the database of magnetic WPs MWYCKPOS [6]. One can see in this example that the WP of the magnetic space groups, through its corresponding Wyckoff orbit, fully defines the elementary structure, with no representation analysis being necessary.

Apart from the 30 elementary structures reported in Ref. [1], Table 1 contains 14 additional ones [8]. All the cases that are missing in Ref. [1] correspond to WPs where the representative atom, chosen by convention, has as free parameter the coordinate *y*. This suggests that the derivation done in Ref. [1] using representation analysis seems to have systematically overlooked this type of site when selecting relevant WPs of cubic (nonmagnetic) space groups.

Table 1 also includes those magnetic space groups having no WP fulfilling the desired conditions, because it would be misleading to discard them as relevant in the search for isotropic linear ME response in systems with simple orbits of magnetic atoms. Although their WPs have higher magnetic symmetries and therefore are already included in some other group of the list, the actual magnetic symmetry of the system also depends on the positions of the nonmagnetic atoms, so that the actual space group could be any of them. These groups therefore represent perfectly valid symmetries for simple magnetic orderings with isotropic linear ME effect.

Summarizing, we have presented how the symmetry conditions for isotropic linear ME coupling that were discussed in Ref. [1] can be derived within the frame of Shubnikov space groups, and this shows that a good number of cases are missing in the listing of elementary magnetic configurations with such property that were reported there. We do not question the correctness of the method followed, but probably a systematic error was made at the early stages of the derivation, and this becomes evident when the problem is treated using magnetic symmetry. We hope to have shown that the use of well-established tabulated knowledge on the properties of magnetic space groups is an effective and efficient approach when dealing with this kind of problem.

References

[1] S. Coh and D. Vanderbilt, *Phys. Rev*. B **88**, 121106(R) (2013).

[2] Daniel B. Litvin, Magnetic Group Tables, International Union of Crystallography, 2013, www.iucr.org/publ/978-0-9553602-2-0.

[3] A. S. Borovik-Romanov, H. Grimmer, and M. Kenzelmann, *International Tables for Crystallography* (John Wiley & Sons, Chichester, 2013), Vol. D, Chap. 1.5, pp. 106–152.

[4] H. T. Stokes, D. M. Hatch, and B. J. Campbell, ISOTROPY Software Suite, iso.byu.edu.

[5] S. V. Gallego, E. S. Tasci, G. de la Flor, J. M. Perez-Mato, and M. I. Aroyo, *J. Appl. Crystallogr*. **45**, 1236 (2012).

[6] M. I. Aroyo, A. Kirov, C. Capillas, J. M. Perez-Mato, and H. Wondratschek, *Acta Crystallogr*. **A62**, 115 (2006).

[7] *International Tables for Crystallography*, *Vol. A, Space-Group Symmetry*, 5th ed., edited by Th. Hahn (Kluwer Academic, Dordrecht, 2002).

[8] We have considered enantiomorphic pairs as a single case, maintaining the criterion that seems to be applied in Ref. [1].

ANEXO C

Perez-Mato J. M., Gallego S. V., Tasci E. S., Elcoro L., de la Flor G., Aroyo M. I. *Annu. Rev. Mater. Res*. **45** 13.1-32 (2015) DOI: 10.1146/annurev-matsci-070214-021008

Symmetry-Based Computational Tools for Magnetic Crystallography

J.M. Perez-Mato[a], S. V. Gallego[a], E. S. Tasci[b], L. Elcoro[a], G. de la Flor[a] and M. I. Aroyo[a]

[a]Dpto. de Física de la Materia Condensada, Facultad de Ciencia y Tecnología, Universidad del País Vasco, UPV/EHU, Apdo. 644, 48080 Bilbao, Spain.
[b]Physics Department, Middle East Technical University, Ankara, Turkey.
Contact author email: jm.perez-mato@ehu.es

Keywords: magnetic crystallography, Bilbao Crystallographic Server, magnetic structure determination, magnetic space groups, magnetic symmetry software, magnetic superspace symmetry

Abstract

In recent years, two important advances have opened new doors for the characterization and determination of magnetic structures. Firstly, researchers have produced computer-readable listings of the magnetic or Shubnikov space groups. Secondly, they have extended and applied the superspace formalism, which is presently the standard approach for the description of nonmagnetic incommensurate structures and their symmetry, to magnetic structures. These breakthroughs have been the basis for the subsequent development of a series of computer tools that allow a more efficient and comprehensive application of magnetic symmetry, both commensurate and incommensurate. Here we briefly review the capabilities of these computation instruments and present the fundamental concepts on which they are based, providing various examples. We show how these tools facilitate the use of symmetry arguments expressed as either a magnetic space group or a magnetic superspace group and allow the exploration of the possible magnetic orderings associated with one or more propagation vectors in a form that complements and goes beyond the traditional representation method. Special focus is placed on the programs available online at the Bilbao Crystallographic Server (http://www.cryst.ehu.es).

1. Introduction

Magnetic ordering is a symmetry-breaking process, and, as in other fields of physics, the characterization of the involved symmetry reduction is an essential step for its comprehension. The symmetry of a magnetic phase is given by a magnetic space group (MSG) (also called a Shubnikov group) (1, 2), if commensurate, or by a magnetic superspace group (MSSG) (3–5), in the case of an incommensurate ordering. The symmetry group of a magnetic phase determines all structural and magnetic symmetry constraints that are thermodynamically obliged within its whole stability range. These symmetry-dictated properties can only be broken through an additional phase

transition or by applying a symmetry-breaking perturbation. By comparing the symmetry group of a magnetic phase with the symmetry group of the parent paramagnetic phase, one can also determine the set of possible domains and twin-related configurations. The symmetry characterization of magnetic phases, expressed in the form of a symmetry group, is especially important for predicting and understanding their magneto-structural properties. Furthermore, similar to what happens in conventional crystallography, the assignment of some symmetry to a magnetic structure implies very specific constraints on the possible magnetic moments and atomic positions, which can be unambiguously defined and distinguished from other features that are not symmetry protected.

The identification of the relevant magnetic symmetry and its constraints can therefore be considered an essential part of the characterization of a magnetic phase. However, magnetic symmetry considerations have been absent from most studies for decades because of the lack of computer-readable listings of MSGs and computational tools based on magnetic symmetry. In contrast, Bertaut (6, 7), and later Izyumov's group (8–11), developed the so-called representation method, and free efficient software was soon available for its application (12–14). Thus, the representational analysis has become the most popular method for determining and describing magnetic structures. In this method, the possible magnetic orderings are parameterized using spin modes, which transform according to one or more irreducible representations (*irreps*) of the space group of the paramagnetic phase. In the more general case of multidimensional *irreps*, this method neither uses nor controls the magnetic symmetry of the spin configurations. Therefore, magnetic structures are commonly reported without assigning any magnetic symmetry. In the case of incommensurate phases, this situation was inevitable, as ordinary MSGs are not applicable, and the specific use of superspace symmetry and MSSGs for magnetic structures was not considered in detail and translated into appropriate software until recently (4). In these circumstances, despite some early attempts (15), no comprehensive database of magnetic structures exists yet, although hundreds of such structures are reported each year. The development of such a database requires an unambiguous and unified description of magnetic structures and demands a systematic application of magnetic symmetry information. Also, the renewed interest in multiferroics in the past decade (16–19), for which symmetry-governed magneto-structural properties are especially important, has evidenced the need for a more comprehensive use of magnetic symmetry concepts.

In this context, a considerable number of free computational tools for the analysis of magnetic structures based on and/or applying magnetic symmetry have been developed during the past few years. Computer-readable listings of MSG data are now available, whereas refinement programs have been implemented in which models constrained by alternative possible MSGs or MSSGs can be derived and tested. These are complemented by various programs that allow the analysis of possible magnetic orderings for a given parent structure, with full consideration of symmetry properties, consistently including both magnetic symmetry groups and *irreps*. This novel extensive software has opened a new path in which magnetic symmetry is employed as a tool to both enumerate possible alternative magnetic models and store and retrieve, in a robust, unambiguous, and unified form, any magnetic structure, commensurate or incommensurate. Furthermore, under the auspices of the International Union of

Crystallography, the CIF (crystallographic information file) dictionary (20) is being extended to magnetic structures (21). The new symmetry-based computational tools use this so-called magCIF file format (in its preliminary form), which has also been adopted by some visualization programs. These developments have already permitted the creation of an incipient small database of commensurate and incommensurate magnetic structures, in which magnetic symmetry (in the form of an MSG or MSSG) is employed (22).

Here we briefly review these computation instruments, with a short introduction to their theoretical basis and some examples of their applications. We give special attention to the computer tools that have been developed by our group, namely those available at the Bilbao Crystallographic Server (23, 24).

Below, we use the Seitz notation for any symmetry operation as defined in Reference 25 but extended to magnetic groups by including time reversal with the symbol 1′ and writing any point-group operation **R** combined with time reversal as **R′**. The transformations to different bases or settings are expressed in the shorthand notation used in the *International Tables for Crystallography* (26). Following common practice in the field, the terms magnetic moment and spin are used here indistinctly as synonyms. Full information on the magnetic structures discussed below can be found in MAGNDATA (22), the aforementioned collection of magnetic structures, which is freely available on the Internet. Structure figures have been produced using either VESTA (27) or Jmol (28).

2. Commensurate magnetic structures

2.1. Magnetic Space Groups (Shubnikov Groups)

In the context of magnetic structures, average atomic magnetic moments can be considered real quantities, and the action of the time reversal operation simply changes the sign of all atomic magnetic moments in the structure while keeping unchanged the nonmagnetic degrees of freedom. By definition, a commensurately ordered magnetic phase breaks the time reversal symmetry operation that is present in the magnetically disordered paramagnetic phase. If *G* is the space group of the paramagnetic phase, its full symmetry, considering the presence of the disordered atomic spins, is given by the gray magnetic group *G1′*, which can be decomposed in *cosets* as *G1′* = *G* + {1′ | 0, 0, 0}*G*. Thus, the full symmetry group of the system includes, in addition to the operations of *G*, those obtained by multiplying all of them with {1′ | 0, 0, 0} (i.e., the time reversal operation with zero translation). The symmetry of a commensurately magnetically ordered phase is then described by a subgroup of this parent group *G1′*, say Ω, where {1′ | 0, 0, 0} is necessarily absent. This means that the MSG Ω may include nonidentity operations either combined or not combined with time reversal, but not both. Being commensurate, the lattice or a sublattice of the paramagnetic phase will also be maintained, and in general, Ω can be decomposed in *cosets* with respect to a subgroup *F* of *G* with the same lattice periodicity as Ω in one of the following three forms: Ω = *F*, Ω = *F* + {$\mathbf{R_o}$′ | **t**}*F*, or Ω = *F* + {1′ | **L**} *F*, where {$\mathbf{R_o}$′ | **t**} and {1′ | **L**} are operations of the gray group *G1′*, and **L** is a specific lattice translation of the paramagnetic phase. For consistency, {$\mathbf{R_o}$ | **t**}^{2} and {1 | 2**L**} must belong to *F*,

whereas {$\mathbf{R_o}$ | **t**} and {1 | **L**} belong to *G* but not to *F*. These three types of possible magnetic symmetry breakings correspond to the three types of MSGs known as type I, III, and IV, respectively (1, 2) (type II are the gray groups). Notice that all the symmetry operations present in MSGs of type I coincide with those of the ordinary space groups, but as magnetic groups, the existence within the symmetry of the system of the same operations combined with time reversal is explicitly discarded. Thus, for example, a paramagnetic phase with space group *Pnma* can transform into a magnetic phase with MSG *Pnma* as the result of a symmetry breaking *Pnma*1′ → *Pnma*, where all symmetry operations combined with time reversal, which are implicitly present in the paramagnetic phase, disappear.

As stressed in the introduction, the constraints coming from the MSG of a magnetic phase are robust (symmetry-protected) properties within the whole phase. Both atomic magnetic moments and atomic positions are subjected to it. Any operation {**R′** | **t**}, which includes time reversal, acts on the atomic positions in the same way as the operation {**R** | **t**} without time reversal; therefore, the effective symmetry that constrains the atomic positions can be described by an effective space group *H*, which is either *F*, *F* + {$\mathbf{R_o}$ | **t**}*F*, or *F* + {1 | **L**}*F*, depending on Ω being type I, III, or IV, respectively. In addition, the symmetry relations forced by the magnetic group on the atomic magnetic moments can be reduced to the following rule: If two atoms with nonzero magnetic moments have their atomic positions related by an operation of Ω, then their moments are related by the corresponding point-group operation **R** (transforming as axial vectors) with an additional change of sign if time reversal is included in the operation. For magnetic atoms at special positions, i.e., kept invariant by some of the operations of Ω, site-symmetry restrictions on the possible magnetic moments exist, and they are part of the definition of the Wyckoff positions of an MSG.

Litvin (29) recently tabulated the 1,651 mathematically distinct MSGs (1, 2) in a form analogous to that of the ordinary space groups in the *International Tables for Crystallography* (30). These tables of MSGs are freely available electronically and use the so-called Opechowski-Guccione (OG) description (31). This notation employs the space group *H*, defined above, as the reference to describe the symmetry operations, and therefore, in the case of type IV groups, the employed unit cell does not generate the lattice of the magnetic configuration. This is the essential difference with the alternative Belov-Neronova-Smirnova (BNS) description (32), in which the employed unit cell defines the lattice periodicity of the spin arrangement. Computer-readable tables of MSG data have been produced by Stokes & Campbell (33) in both the BNS and OG notations. Online retrieval tools at the Bilbao Crystallographic Server, based on these tables, allow access to the symmetry operations (MGENPOS) and Wyckoff positions (MWYCKPOS) of any chosen MSG (34). All these listings and tools keep the same conventions, and therefore they can be taken as standard. The MSGs in this review are given in BNS notation.

The MSG Ω defining the symmetry of a commensurate magnetic phase can be introduced without making any reference to the gray space group *G1′* defining the symmetry of its paramagnetic phase. In fact, the same group Ω, as a mathematical group type, can be relevant for different parent *G1′* groups. But, as in other ferroics, the domain and switching properties of the system are only defined if the parent group

G1′ is also known. Therefore, a full description of the symmetry properties of a magnetic phase requires the knowledge of both symmetries: *G1′* and its subgroup Ω. More concretely, if *H* is the effective space group of the nonmagnetic degrees of freedom, described above, and *s* is its index with respect to *G* (i.e., the factor relating the number of operations in *G* and *H*), then 2*s* is the index of Ω with respect to *G1′*, and one can choose *s* operations $\{g_j\}$ of *G* (*coset* representatives) not belonging to *H*, such that $G = H + g_2H + \cdots + g_sH$, and *s* equivalent, distinct, domain-related structures can be obtained by applying each operation g_j to the magnetic structure. An additional set of *s* trivially related domains, with reversed moments, corresponds to the application of the symmetry operations g_j'. The magnetic symmetry of a domain-related structure obtained by the action of g_j is given by the subgroup $g_j\Omega g_j^{-1}$ of *G1′*. This subgroup can coincide with Ω or be a distinct subgroup belonging to the same conjugacy class. Conjugate subgroups describe physically equivalent symmetry breakings. Below, if nothing is said to the contrary, an MSG Ω is implicitly taken as a representative of a class of conjugate subgroups with respect to a parent space group *G1′*.

2.2. Crystallographic Description of Commensurate Magnetic Structures

Following an approach similar to the one employed for nonmagnetic crystal structures, once the MSG is defined through its set of operations and its unit cell, a magnetic structure is unambiguously described by listing the atomic positions and magnetic moments of a set of symmetry-independent atoms within the unit cell, the so-called asymmetric unit. As an example, **Tables 1** and **2** describe the magnetic structure of $GdMn_2O_5$ (35), also shown in **Figure 1*a***. The directions of the spins (not explicitly given in the original reference) are only approximate. **Tables 1** and **2**, together with the unit cell parameters, are the essential information included in a magCIF file, and they are sufficient for the unambiguous definition of the atomic positions and moments of the whole structure. They can be generated from the atomic positions and moments listed in **Table 2** using the symmetry operations of **Table 1**. The MSG in **Table 1** is in a nonstandard setting, using a basis as close as possible to the one of the parent phase. The symmetry operations of all MSGs are freely available in a standard form in the references mentioned above, and therefore, the information in **Table 1** could be substituted with just the label of this MSG: $P_ac a 2_1$ (#29.104), together with the transformation from the employed unit cell basis (and origin) to the standard setting of the group. This transformation is indicated in **Figure 1** in a shorthand notation (26). Applying the inverse of this transformation to the operations of the standard MSG available in References 33 or 34, one can directly obtain the operations listed in **Table 1**. Below, we define any relevant magnetic subgroup by this means, i.e., with its standard BNS label plus a transformation to its standard setting.

Table 1
Operations that define the MSG of the magnetic structure of $GdMn_2O_5$ [a]

N	(x,y,z)[b]	(m_x,m_y,m_z)[c]	Seitz notation
1	x,y,z,+1	m_x,m_y,m_z	{ 1 | 0,0,0 }
2	-x+3/4,y+1/2,-z,+1	$-m_x,m_y,-m_z$	{ 2_{010} | 3/4,1/2,0 }
3	-x+1/4,y+1/2,z,+1	$m_x,-m_y,-m_z$	{ m_{100} | 1/4,1/2,0 }

4	x+1/2,y,-z,+1	$-m_x,-m_y,m_z$	{ m_{001} | 1/2,0,0 }
5	x+1/2,y,z,-1	$-m_x,-m_y,-m_z$	{ 1' | 1/2,0,0 }
6	-x+1/4,y+1/2,-z,-1	$m_x,-m_y,m_z$	{ $2'_{010}$ | 1/4,1/2,0 }
7	-x+3/4,y+1/2,z,-1	$-m_x,m_y,m_z$	{ m'_{100} | 3/4,1/2,0 }
8	x,y,-z,-1	$m_x,m_y,-m_z$	{ m'_{001} | 0,0,0 }

[a] These operations (modulo lattice translations) are a subset of those in *Pbam1'*, expressed in a setting (2$\mathbf{a}_p$,$\mathbf{b}_p$,$\mathbf{c}_p$;0,0,0), where {$\mathbf{a}_p$, $\mathbf{b}_p$, $\mathbf{c}_p$} is the parent *Pbam1'* basis. They define a subgroup of *Pbam1'*, which is the polar MSG P_ca2_1 (#29.104), but in a non-standard setting (see text).
[b] Operations are expressed in the usual crystallographic notation, but with the addition of the symbol -1/+1 to indicate the combination or not with time reversal.
[c] Transformation of a generic spin (m_x,m_y,m_z) associated with the general position (x,y,z).

Table 2 shows that the spin model reported for $GdMn_2O_5$ in Reference 35 has simplifying features that are not symmetry forced: Namely, the Mn1 moment is constrained to lie on the plane *ab*, whereas the spins of the two independent Mn2_1 and Mn2_2 sites are restricted to be exactly equal. Although these restrictions may be reasonable, it is important to have them clearly separated from the fundamental ones that are symmetry protected and are evidenced in **Table 2**. Lacking more precise details, the atomic positions listed in **Table 2** are those of the paramagnetic phase (36, 37) and therefore comply with the parent space group *Pbam* (#55), but the table shows that some atomic sites are split because of the symmetry reduction. Hence, in principle, these split sites could vary their positions independently within the magnetic phase if magneto-structural couplings are sufficiently large. Also, the Mn1 site, which does not split, transforms into a general position, with its three coordinates becoming free. Even if these new structural degrees of freedom triggered by the magnetic ordering remain negligible within experimental resolution, it is convenient to be aware of them. They are fundamental for monitoring any possible structural distortion induced by the magnetic ordering. The effective space group that governs the triggering of new structural degrees of freedom with respect to the paramagnetic phase is given by the operations listed in **Table 1**, disregarding the presence of time reversal in the operation. This is the space group $Pmc2_1$ (#26) in a nonstandard setting and with a centered unit cell doubled along *a*, the transformation to standard setting being (**c**, −**a**/2, −**b**; 3/8, 0, 0) [this can be directly obtained with the IDENTIFY GROUP tool in the Bilbao Crystallographic Server (38)]. This effective space group for the atomic positions is the space group that we have generically called *H* above. The magnetic ordering therefore implies for the atomic positional structure an effective symmetry breaking: *Pbam* → $Pmc2_1$ ($Pb2_1m$ in the setting used) without change of lattice. This is a transformation from a nonpolar phase to a polar one, with the polar axis along the *b* direction of the parent setting. According to the von Neumann principle, an induced electric polarization P_y should be expected.

Table 2
Symmetry-independent atoms of the magnetic structure of $GdMn_2O_5$

Label	Atom type	x[a]	y[a]	z[a]	Symmetry constraints on M	M_x[b]	M_y[b]	M_z[b]	|M|
Gd1_1	Gd	0.06975	0.17160	0.00000	$m_x,m_y,0$	4.87	1.63	0.0	5.14

Gd1_2	Gd	0.93025	0.82840	0.00000	$m_x,m_y,0$	-4.51	-1.5	0.0	4.75
Mn1	Mn	0.00000	0.50000	0.25510	m_x,m_y,m_z	-2.85	0.95	0.0	3.00
Mn2_1	Mn	0.20590	0.35180	0.50000	$m_x,m_y,0$	3.8	-1.27	0.0	4.01
Mn2_2	Mn	0.79410	0.64820	0.50000	$m_x,m_y,0$	3.8	-1.27	0.0	4.01
O1	O	0.00000	0.00000	0.26970	-	-	-	-	-
O2_1	O	0.07630	0.44860	0.00000	-	-	-	-	-
O2_2	O	0.92370	0.55140	0.00000	-	-	-	-	-
O3_1	O	0.07270	0.43560	0.50000	-	-	-	-	-
O3_2	O	0.92730	0.56440	0.50000	-	-	-	-	-
O4_1	O	0.19970	0.20760	0.24500	-	-	-	-	-
O4_2	O	0.80030	0.79240	0.24500	-	-	-	-	-

[a] Approximate atomic positions have been taken from entry 97046 of the ICSD database (36, 37), and are given in the basis ($2\mathbf{a}_p,\mathbf{b}_p,\mathbf{c}_p$;0,0,0), with $\mathbf{a}_p,\mathbf{b}_p,\mathbf{c}_p$ being the parent *Pbam* basis.
[b] Approximate magnetic moment components (μB) have been estimated from the model reported in Reference 35.

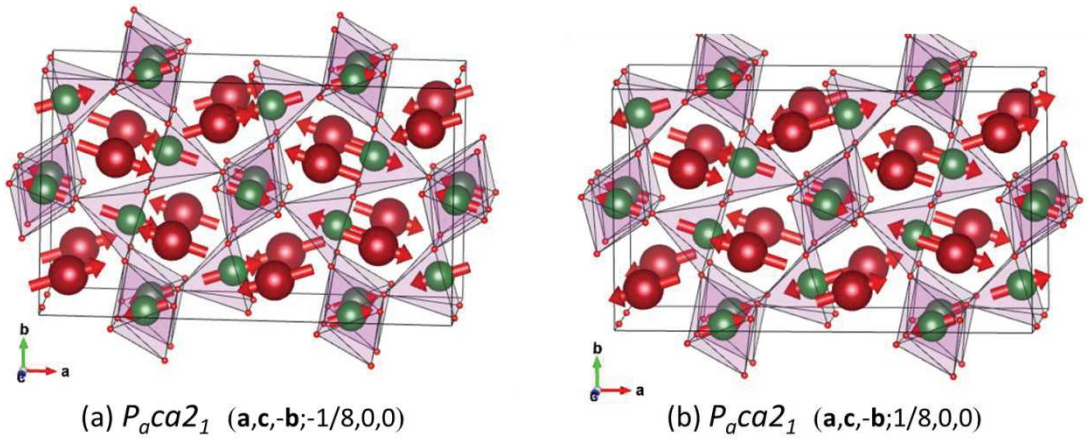

Figure 1
(*a*) Magnetic structure of $GdMn_2O_5$ (35) described in **Tables 1** and **2**. (*b*) Twin structure equivalent to panel *a*. The two configurations must have opposite, magnetically induced polarizations. Their symmetry is given by different but conjugate magnetic space groups indicated below.

Thus, without making appeal to any specific mechanism, the symmetry characterization of the magnetic structure allows one to infer that the system will behave as a multiferroic of type II, with a magnetically induced ferroelectricity (16, 18), in agreement with experimental evidence (35). Interestingly, researchers have proposed a similar spin model for $PrMn_2O_5$ (40), but these authors explicitly discard the existence of an electric polarization. The symmetry of the proposed magnetic ordering is, however, coincident with the one above, and some induced ferroelectricity, however small, is to be expected.

The index of the MSG of $GdMn_2O_5$ with respect to the parent symmetry *Pbam*1' is four. Thus, two distinct twin-related configurations exist, apart from their corresponding trivial twins with all spins reversed. The second nontrivial twin is shown in **Figure 1*b***. This configuration can be obtained by transforming the structure shown in **Figure 1*a*** with any lost operation of the parent space group *Pbam*. This means any operation of

the second *coset* in the *coset* decomposition of *Pbam* with respect to its subgroup $Pmc2_1$ (**c**, −**a**/2, −**b**; 3/8, 0, 0), such as the inversion operation {−1 | 0, 0, 0}: *Pbam* = $Pmc2_1$ + {−1 | 0, 0, 0}$Pmc2_1$. These operations switch the structural polarity, and therefore the two magnetic domains will have opposite orientations of P_y. Notice that the magnetic symmetry of the second domain-related configuration is given by a different MSG (specified in **Figure 1*b***).

The online editing tools ISOCIF (41) and STRCONVERT (42) are very useful in the field of describing and building up commensurate magnetic structures with full application of magnetic symmetry. They can be used to produce or edit the magCIF file of any real or hypothetical magnetic structure. If the MSG of a given magnetic structure is unknown, a model with all atomic positions and spins in the unit cell can be introduced or edited under the trivial symmetry *P*1. The actual magnetic symmetry of the structure and a description in accordance with it can then be obtained [the program FINDSYM (43) is applied by both tools]. ISOCIF has also a visualization tool and can transform the description of a magnetic structure to any setting, whereas STRCONVERT supports several file formats, including those of the ab initio code VASP (44), and is linked to MVISUALIZE (45) (also in the Bilbao Crystallographic Server) for direct visualization with Jmol (28).

2.3. *1k* Magnetic Structures and k-Maximal Magnetic Symmetries

Most of the reported commensurate magnetic structures are *1k* magnetic phases, i.e., their magnetic moment arrangements can be described as spin waves over the paramagnetic structure with a single independent propagation vector **k**. The wave may be anharmonic, but the symmetry break is fully defined by the first harmonic of the frozen spin wave. *1k* magnetic configurations include the frequent case of magnetic orderings with **k** = 0, in which the lattices of the magnetic and paramagnetic structures coincide. The propagation vector is directly accessible from diffraction experiments, and its value strongly restricts the possible magnetic symmetries. It is therefore very convenient to have tools that directly exploit this information. In general, the translation lattice of a *1k* magnetic ordering is given by those lattice translations **L** of the parent group *G1′*, such that $exp(i2\pi\mathbf{k}\cdot\mathbf{L}) = 1$. This condition defines a primitive supercell of a volume *n* times larger than that of the paramagnetic phase, with *n* being the minimal integer such that *n***k** is a reciprocal lattice vector. In the case of *n* being even, those lattice translations of the paramagnetic phase that satisfy $exp(i2\pi\mathbf{k}\cdot\mathbf{L}) = -1$ are also preserved in the magnetic configuration but combined with time reversal, i.e., they are maintained as antitranslations of type {1′ | **L**}. The resulting symmetry is therefore described by an MSG of type IV. When *n* is odd (including **k** = 0), no antitranslations are possible, and the subgroup of *G1′* describing the symmetry of the resulting structure is an MSG of type I or III.

The possible symmetries of a magnetic ordering with a propagation vector **k** are therefore limited to those compatible with the specific subgroup of lattice translations defined by **k** and, for even *n*, also with the additional set of antitranslations. This minimal symmetry is described by either the MSG *P*1 (lattice translations) for odd *n* or P_s1 for even *n* (lattice translations plus antitranslations). However, the propagation vector **k** is usually directed along special crystallographic directions, and larger subgroups of *G1′* can be relevant. In general, a hierarchy of possible subgroups of *G1′*

consistent with the **k** vector is possible. Among this set of **k**-consistent subgroups of *G1'*, those that do not have any supergroup fulfilling the same **k**-consistency conditions are the possible maximal symmetry groups of the magnetic structure. We call them k-maximal subgroups or k-maximal magnetic symmetries for a given parent space group G and a given magnetic propagation vector **k**. **Figure 2** depicts the k-maximal subgroups for *Pbam* and a magnetic propagation vector **k** = (1/2, 0, 0). This case is relevant for the magnetic structure of $GdMn_2O_5$ discussed above. Only four distinct types of magnetic ordering of k-maximal symmetry are possible, and one is in fact realized in $GdMn_2O_5$ (and other RMn_2O_5 compounds).

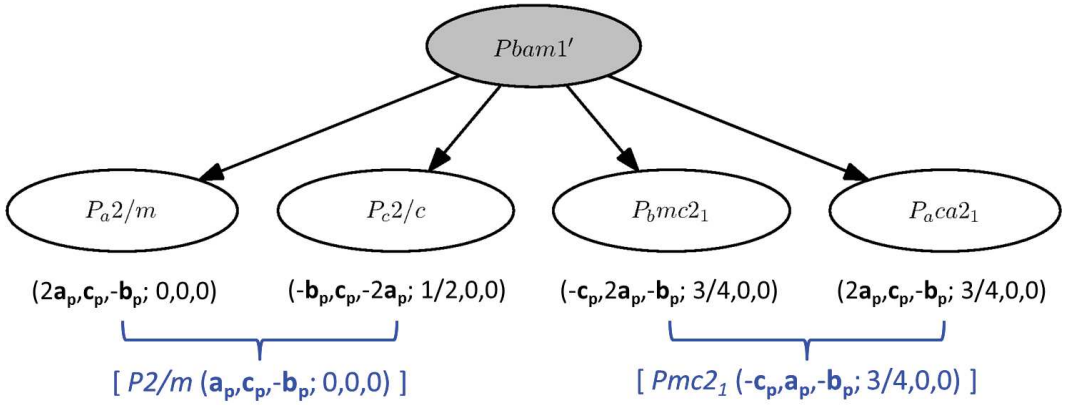

Figure 2
The four possible k-maximal magnetic symmetries for a magnetic ordering with propagation vector **k** = (1/2, 0, 0) on a paramagnetic phase with space group *Pbam*, as obtained with MAXMAGN. The transformation (from the parent *Pbam* basis) to the standard setting of each magnetic space group (MSG) is indicated. The index of the four subgroups is four. The corresponding effective space groups for the atomic positions (common to pairs of MSGs) are shown in gold.

From general physical arguments (symmetry-dictated energy extrema at symmetrical configurations and smoothness of the energy landscape), one expects that magnetic orderings generally tend to keep as much symmetry as possible or, reversely, that the symmetry reduction tends to be minimal. Indeed, one can associate a k-maximal MSG with the majority of the known magnetic structures. The example in **Figure 2** is very illustrative, as it shows that two of the four possible maximal symmetries for the known propagation vector are polar (in both cases, along the *b* axis of the *Pbam* setting). Therefore, the derivation of the k-maximal MSGs allows one to infer directly that the system, if an insulator, is likely to be multiferroic. In fact, this is a quite general property of nonsymmorphic centrosymmetric space groups with cell-duplicating propagation vectors along the direction of one of the intrinsic nonprimitive translations of the nonsymmorphic operations. One can easily check with MAXMAGN (46) that this is sufficient for having noncentrosymmetric groups, polar in most cases, among the k-maximal symmetries.

The number of k-maximal MSGs (a representative of each conjugacy class) is usually rather small, and each describes a possible, alternative, nonequivalent spin configuration. An efficient and intuitive first step in the process of determining a magnetic structure with a known propagation vector is to enumerate and construct these alternative models of maximal symmetry for their subsequent contrast with

experimental data or calculations. This first step can be done with the program MAXMAGN (46) in the Bilbao Crystallographic Server. This tool derives the k-maximal MSGs for any parent space group and any (reasonable) commensurate propagation vector. If the parent paramagnetic structure is introduced (in CIF format), it also produces the spin and structure models corresponding to each of the alternative k-maximal MSGs. These alternative models can be transported in magCIF format to refinement programs such as JANA2006 (47, 48) or FULLPROF (12) or to other computational tools for further analysis. These magCIF files can be visualized online with MVISUALIZE (45) or ISOCIF (41) or locally with VESTA (27) or Jmol (28).

As an example, **Figure 3** summarizes some of the results obtained for the case of $HoMnO_3$, a material with *Pnma* as the parent space group and propagation vector (1/2, 0, 0) (49). Of the four possible k-maximal symmetries, two are polar along *c*. Furthermore, the other two possible centrosymmetric monoclinic symmetries require that some of the Mn atoms remain with zero magnetic moment. Therefore, a full magnetic ordering of the Mn atoms with this propagation vector necessarily produces a symmetry breaking in which at least the *c* direction becomes polar. Thus, if the Mn atoms are fully ordered and the magneto-structural coupling is large enough, the material is bound to be a multiferroic with magnetically induced ferroelectricity (i.e., a type II multiferroic) (50). As in the preceding example, the index of the MSG is four, and there are two equivalent, nontrivial, twinned magnetic configurations related by inversion and with opposite electric polarizations.

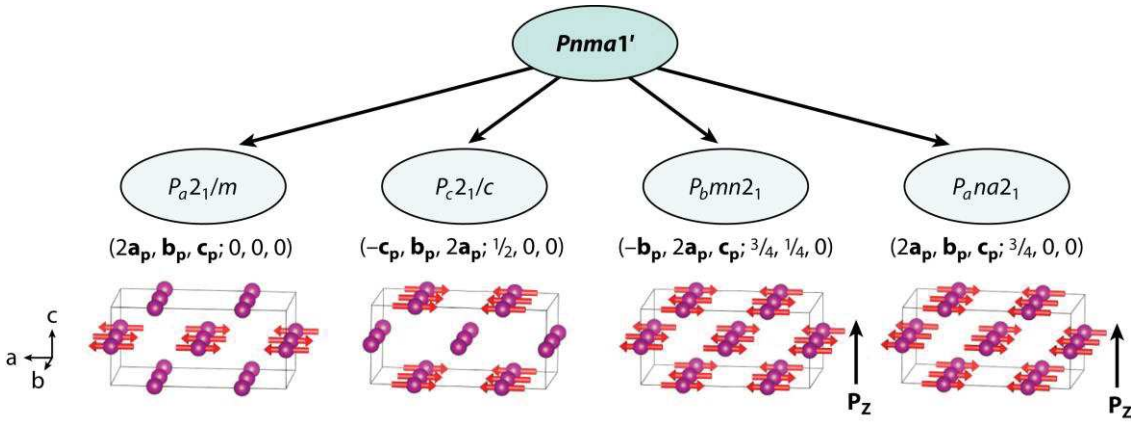

Figure 3
The four possible distinct magnetic orderings of maximal symmetry with propagation vector **k** = (1/2, 0, 0) for the Mn site in orthomanganites, as obtained with MAXMAGN, assuming that the spins are aligned along the *a* direction. The magnetic space group label associated with the magnetic symmetry of each structure is shown, together with the transformation (from the parent *Pnma*1′ basis) to its standard setting. The index of the four subgroups is four. The magnetic unit cell used in all figures is (2**a**$_p$, **b**$_p$, **c**$_p$; 0, 0, 0). The direction (with arbitrary sense) of the possible magnetically induced electric polarization P_z, when it is symmetry allowed, is indicated. The P_bmn2_1 ordering is the one observed in $HoMnO_3$ (22, 49). Abbreviation: P_z, possible magnetically induced electric polarization.

2.4. Systematic absences in the magnetic diffraction diagram

MAGNEXT (34) can be used to derive the symmetry-forced systematic absences of magnetic, nonpolarized neutron diffraction for any MSG or MSSG. The presence of these systematic absences can sometimes help reduce the possible magnetic

arrangements to be explored. Because MAGNEXT is directly accessed from MAXMAGN, the systematic absences for every alternative k-maximal magnetic symmetry can be consulted easily. Let us consider, for instance, the case of $Na_3Co(CO_3)_2Cl$ (51), which has a paramagnetic phase with space group *Fd-3* (#203) and a magnetic phase with zero propagation vector. In this compound, the Co atoms at the 16*c* Wyckoff position form a highly frustrated pyrochlore-type framework. Using MAXMAGN, we can see that there are four k-maximal magnetic subgroups of *Fd-31'*, but only two allow some nonzero spin for the Co atoms, namely *Fd-3* (#203.26) and *Fd'd'd* (#70.530) (the two subgroups are in their standard setting when using the parent unit cell). **Figure 4** shows a scheme of the spin arrangement for each of these two possible maximal symmetries. For *Fd-3* the spin of the single independent Co at the origin must have the direction (1, 1, 1); in the alternative *Fd'd'd* ordering, it can have any direction. When the (1, 1, 1) direction is also kept in this second arrangement, the two k-maximal symmetries basically correspond to spin orderings in the Co tetrahedra of the all-in/all-out and two-in/two-out types (**Figure 4**). These two alternative configurations are in fact often discussed as energetically favorable and have been observed in these pyrochlore-type materials. MAGNEXT shows that, in principle, they can be distinguished by the presence or lack in the magnetic diffraction of some systematic absences. For the subgroup *Fd-3*, all reflections of type (*h, h, h*) or (*h, 0, 0*) for any *h* value (and their cubic symmetry–related ones) are forbidden, whereas for the orthorhombic *Fd'd'd* model, only magnetic reflections of type (*0, 0, l*) are extinct. Twinning can, however, hamper the observation of these absences. In the case of the *Fd-3* symmetry, the subgroup is of index two, and only a trivial twin with all spins reversed is possible, having no consequence in the diffraction diagram. But in the case of the *Fd'd'd* structure, the subgroup index is six, and three nontrivial twinned configurations are expected to be superposed in the diffraction diagram, where the 3-fold rotation and its inverse could be taken as the twinning operations. The magnetic structure of $Na_3Co(CO_3)_2Cl$ reported in Reference 51 indeed possesses one of these two maximal symmetries, namely the MSG *Fd-3* (22).

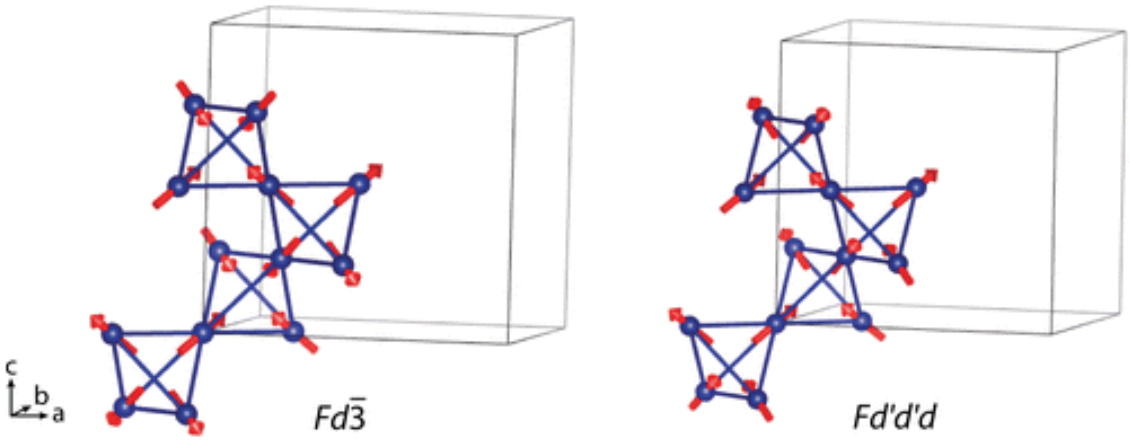

Figure 4

Scheme of the two possible magnetic models with zero propagation vector of maximal symmetry for the magnetic structure of $Na_3Co(CO_3)_2Cl$, as obtained with MAXMAGN. Only some Co atoms are depicted. These two maximal symmetries correspond to the so-called all-in/all-out and two-in/two-out models. Systematic absences in the diffraction pattern can distinguish the two models (see Section 2.4). The *Fd-3* model is the one proposed in Reference 51 for this compound.

2.5 Hierarchy of possible magnetic symmetries

If the models with k-maximal symmetry are not satisfactory to explain the experimental data, one can also use MAXMAGN to decrease the symmetry of the model in a controlled way. For this purpose, combining this program with the tool k-SUBGROUPSMAG (52) can be very helpful. This second program, also in the Bilbao Crystallographic Server, provides for any parent space group all possible magnetic symmetries consistent with one or more given propagation vectors, indicating their group-subgroup hierarchy. Let us consider, for instance, the magnetic structure of NiO (53). Its parent space group is *Fm-3m* (#225) and its magnetic propagation vector is (1/2, 1/2, 1/2). **Figure 5** shows possible MSGs consistent with this propagation vector, as obtained with k-SUBGROUPSMAG. All k-maximal subgroups are in this case centrosymmetric, and for simplicity, we have limited the descending graph to their centrosymmetric subgroups. Some MSG labels are repeated, as some subgroups belonging to different conjugacy classes are MSGs of the same type. One can in fact distinguish two branches of subgroups with identical labels. The difference between them can be seen by comparing the operations of the minimal subgroup of type P_s-*1* associated with each branch. In one of the branches, the inversion center at the origin is combined with time reversal, whereas in the other, it is not. The first branch is therefore not relevant for a full magnetic ordering of the Ni atoms, as the symmetry operation {−1′ | 0, 0, 0} would necessarily force a null spin for the Ni atom at the origin.

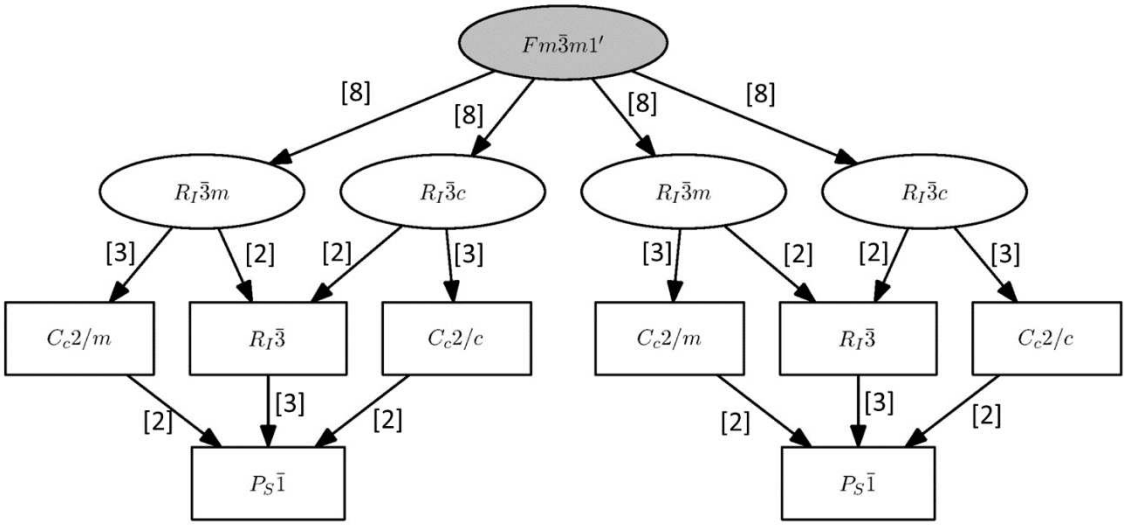

Figure 5
Graph obtained with k-SUBGROUPSMAG of all possible magnetic symmetries for a magnetic ordering with propagation vector (1/2, 1/2, 1/2) in a structure with space group *Fm-3m*. The subgroup index is indicated in brackets for each group-subgroup relation. The k-maximal magnetic space groups (MSGs) are highlighted with elliptical frames. Only one subgroup per conjugate class is shown, and the graph has been restricted to centrosymmetric subgroups. Subgroup labels only indicate the type and can be repeated. The MSG of NiO is one of the subgroups of type C_c2/c.

The magnetic structure of NiO (53) is depicted in **Figure 6**. Its symmetry is given by a monoclinic subgroup of type C_c2/c (*#15.90*) with the inversion center at the origin. Thus, it is not a k-maximal symmetry, and one has to go to a second level in the

subgroup hierarchy depicted in **Figure 5** to obtain the relevant MSG. **Table 3** lists the operations of this subgroup, showing that the monoclinic axis is along the (1, −1, 0) direction. The index of this subgroup is 24. Therefore, 12 nontrivial twinned configurations can superpose in a single crystal diffraction diagram; 3 have the same propagation vector but have the monoclinic axis directed along the equivalent directions (1, −1, 0), (0, 1, −1), and (1, 0, −1), whereas the rest correspond to analogous configurations with rotated propagation vectors equivalent to (1/2, 1/2, 1/2). In the chosen setting, the Ni spins are reported to be within a good approximation directed along the (1, 1, −2) direction (53). One can check, however, with MAXMAGN that for this MSG, the Ni spins are only constrained to lie on the plane perpendicular to the monoclinic axis, having the general form (m_x, m_x, m_z). This is a less restrictive condition, and a weak spin component along the direction (1, 1, 1), which reduces the spin direction to its more general symmetry-allowed form has indeed been reported (53, 54). The symmetry of NiO is also compatible with a monoclinic distortion of the lattice [the effective space group *H* for the atomic positions is *C*2/*m* (#12)], but to our knowledge, no monoclinic strain has been observed. But in the case of CoO, which has a similar spin arrangement, such induced strain is known (55). Thus, the identification of the magnetic symmetry automatically indicates the possible phenomena that are the consequence of the symmetry reduction, although their magnitude may be too weak to be observable.

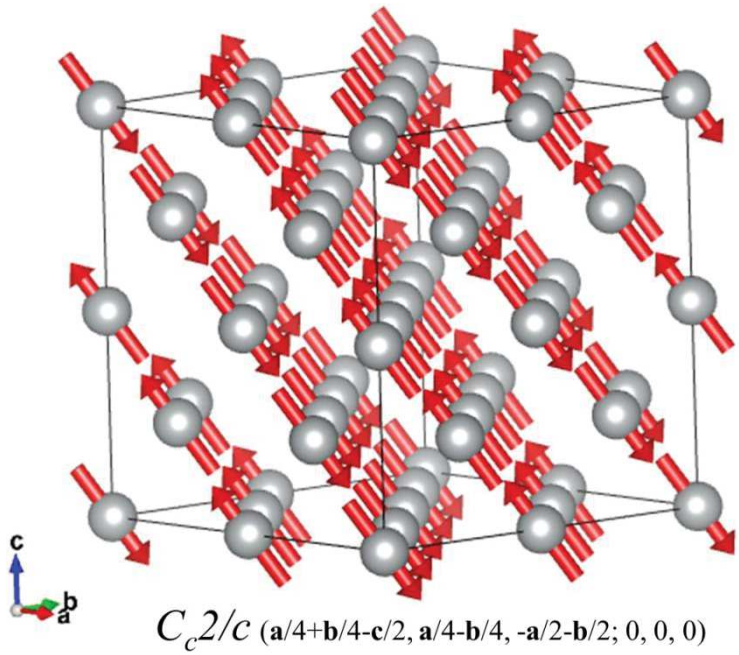

Figure 6
Magnetic structure of NiO (53) with indication of its magnetic space group. Only Ni atoms are shown.

Table 3
Operations that define the symmetry[a] of the magnetic phase of NiO[b]

N	(x,y,z)	Seitz notation
1	x,y,z,+1	{ 1 | 0,0,0 }
2	-y,-x,-z+1/2,+1	{ $2_{1\text{-}10}$ | 0,0,1/2 }
3	-x,-y,-z,+1	{ -1 | 0,0,0 }

4	y,x,z+1/2,+1	{ $m_{1\text{-}10}$ | 0,0,1/2 }
5	x,y,z+1/2,-1	{ 1' | 0,0,1/2 }
6	-y,-x,-z,-1	{ $2'_{1\text{-}10}$ | 0,0,0 }
7	-x,-y,-z+1/2,-1	{ -1' | 0,0,1/2 }
8	y,x,z,-1	{ $m'_{1\text{-}10}$ | 0,0,0 }

[a] The magnetic space group type is *Cc2/c*, in a nonstandard setting

[b] The symmetry operations (modulo lattice translations) are given in the setting ($2\mathbf{a}_p$, $2\mathbf{b}_p$, $2\mathbf{c}_p$; 0,0,0) being the parent cubic basis. The cell ($2\mathbf{a}_p$, $2\mathbf{b}_p$, $2\mathbf{c}_p$) includes 16 centering translations generated by {1 | 1/4, 3/4, 0}, {1 | 1/4, 0, 3/4}, and {1 | 0, 1/4, 3/4}. The transformation to the standard setting of C_c2/c is indicated in **Figure 6**.

2.6. Multiple-*k* magnetic structures

Most of the reported magnetic structures have a single independent propagation vector. However, in the case of wave vectors related by the parent point-group symmetry (i.e., belonging to the same k-vector star), the experimental distinction between single-*k* or multiple-*k* structures is difficult to make. In many cases, the *1k* arrangement is taken as the simplest option, although multiple-*k* ordering could also explain the experimental data. Possible multiple-*k* spin arrangements can be explored in a systematic and symmetry-hierarchical form using k-SUBGROUPSMAG combined with the tool MAGMODELIZE (56). The first program supplies all possible magnetic symmetries, together with their group-subgroup relations, for a given parent space group and a set of propagation vectors. Once one or several possible MSGs provided by k-SUBGROUPSMAG are chosen, the second program provides a model of the corresponding magnetic structures in magCIF format that can be tested and analyzed with other programs. As in the case of *1k* arrangements, the lattice is defined by the lattice translations **L** of the parent group *G1'* such that $exp(i2\pi\mathbf{k}_i\cdot\mathbf{L}) = 1$, for all the propagation vectors $\mathbf{k}_i$, whereas the set of translations (if any) satisfying $exp(i2\pi\mathbf{k}_i\cdot\mathbf{L}) = -1$ for all $\mathbf{k}_i$ are maintained in the possible magnetic groups as antitranslations {1' | **L**}. k-SUBGROUPSMAG calculates all possible magnetic subgroups of the parent *G1'* having this lattice of translations and antitranslations (if they exist), and their group-subgroup hierarchy.

Figure 7 shows the graph obtained for a parent symmetry *I4*/*mmm*1' and two wave vectors: $\mathbf{k}_1 = (-1/2, 0, 1/2)$ and $\mathbf{k}_2 = (0, 1/2, 1/2)$. This figure is relevant for $Sr_2F_2Fe_2OS_2$ (57), in which the magnetic ordering involves two of the wave vectors of the four-arms star of the point *N* in the Brillouin zone (58). The spin arrangement reported in Reference 57 is shown in **Figure 8**. Its symmetry is given by one of the k-maximal MSGs shown in **Figure 7**, namely the subgroup C_a2/m ($\mathbf{a}_p - \mathbf{b}_p - \mathbf{c}_p$, $2\mathbf{a}_p + 2\mathbf{b}_p$, $\mathbf{a}_p/2 - \mathbf{b}_p/2 + \mathbf{c}_p/2$; 0, 0, 0), demonstrating again the efficiency of looking for maximal compatible symmetry when searching probable spin orderings. A general magnetic structure complying with this MSG (or with any other subgroup of **Figure 7**) can be obtained in magCIF format using MAGMODELIZE (56). Although all other atoms split into two independent sites, the Fe site remains unsplit but becomes a general position, with its spin (and position) not constrained by symmetry. Thus, the aesthetically appealing tetragonal-like pattern of the model in **Figure 8*a*** is in fact not symmetry protected. Symmetry does not force an extreme of the energy map for this configuration. **Figure 8*b*** depicts a more general hypothetical arrangement with the same symmetry,

showing the freedom existing in this phase, where the three spin components of the symmetry-independent Fe atom must in principle be determined.

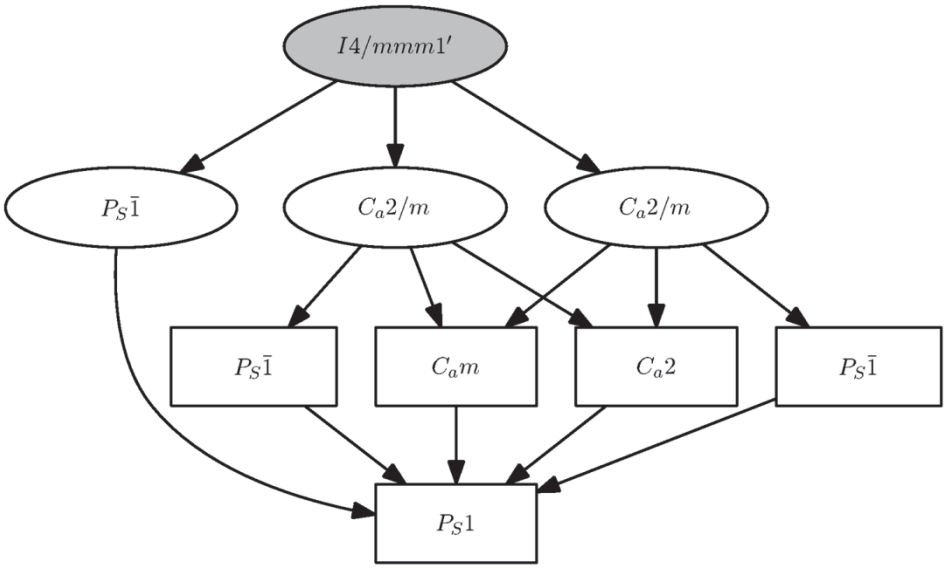

Figure 7
Graph (obtained with k-SUBGROUPSMAG) of all possible magnetic symmetries for a 2*k* magnetic ordering with propagation vectors (−1/2, 0, 1/2) and (0, 1/2, 1/2) on a paramagnetic structure with space group *I*4/*mmm*. The k-maximal magnetic space groups are highlighted with elliptical frames. Only one subgroup per conjugacy class is shown. The magnetic ordering reported for $Sr_2F_2Fe_2OS_2$ (57) (see **Figure 8**) corresponds to one of the k-maximal subgroups of type C_a2/m.

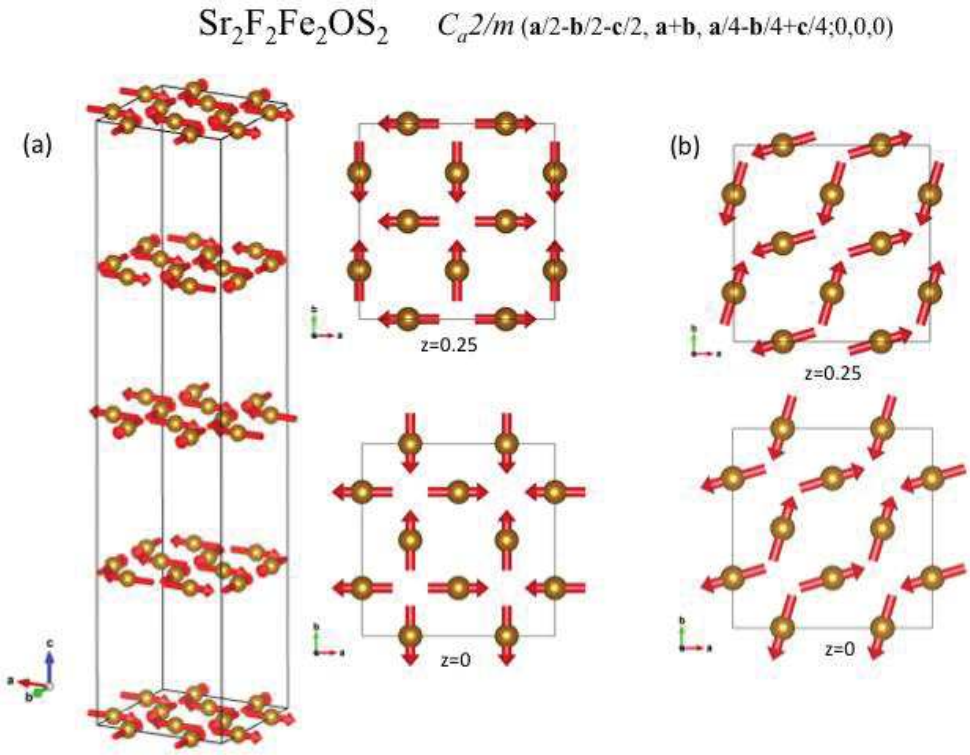

Figure 8

(*a*) 2*k* magnetic structure of $Sr_2F_2Fe_2OS_2$ (57) with a magnetic space group (MSG) of type C_a2/m (see **Figure 7**). The monoclinic axis is along the (1, 1, 0) direction. Only Ni atoms are shown. (*b*) Hypothetical structure with the same MSG as panel *a* showing the orientational freedom of the spins in this phase. A spin component along the *c* direction is also symmetry allowed.

2.7. Importance of Nonmagnetic Atoms

Magnetic atoms often occupy high-symmetry sites, and their spin arrangements are very simple, such that they can be described in simple terms without explicitly using an MSG or any specific symmetry consideration. However, to be able to predict and explain the properties of the resulting magnetic phase, one must be aware of the associated MSG, and this depends in general not only on the magnetic atoms but also on the actual positions of the nonmagnetic ones. Therefore, despite their irrelevance in magnetic diffraction, nonmagnetic atoms play an important role in the symmetry of a magnetic phase and its consequences.

Let us consider, for instance, the case of Gd_2CuO_4 (59). Its paramagnetic phase has been considered to have the space group *I*4/*mmm* (#139), with the magnetic Cu^{2+} occupying the Wyckoff position 2*a* (0, 0, 0). The reported magnetic ordering with propagation vector (1/2, 1/2, 0) is depicted in **Figure 9*a***. The magnetic symmetry of this simple spin arrangement of the body-centered Cu sublattice is given by the MSG C_Accm, again a k-maximal MSG for the observed propagation vector, and the collinearity of the spins along the (1, 1, 0) direction is symmetry protected. The magnetic point group of this MSG is *mmm*1′, i.e., a gray group, which forbids ferromagnetism. However, Gd_2CuO_4 is known to be a weak ferromagnet. This is due to the existence of a small structural distortion with the same wave vector (1/2, 1/2, 0) as the magnetic propagation vector, which decreases the effective parent space group symmetry from *I*4/*mmm* to *Cmce* (#64). This is sufficient to reduce the MSG to *Cm'ca'* (see **Figure 9*b***); the magnetic point group is then *m'mm'*, which allows a ferromagnetic component along the *b* direction of the standard setting, i.e., along the (1, −1, 0) direction in the tetragonal parent basis. The observed weak ferromagnetism is therefore a direct consequence of the orthorhombic structural distortion and is coupled with it. In terms of symmetry relations, the actual magnetic symmetry is the intersection of the subgroups *Cmce*1′ and C_Accm, corresponding to the structural and magnetic distortions. But the resulting symmetry is also compatible with the presence of a ferromagnetic component that alone would yield another intermediate subgroup. A scheme of the group-subgroup relations corresponding to this symmetry breaking is depicted in **Figure 10**. This graph has the characteristic topology of three different symmetry-breaking distortions that are necessarily trilinearly coupled. Their switching is correlated by pairs, similar to what happens in other ferroic systems (60–62). Under some conditions, the two primary distortions can condense simultaneously in a single phase transition (61, 62).

The simple spin ordering of **Figure 9*a*** could also be sufficient to produce a polar phase if the symmetry of the paramagnetic phase considering all atoms were limited to *I*-42*m* (#121). **Figure 9*c*** shows the structure of Ga_2MnSe_4 (63), which has this parent space group, with a hypothetical spin ordering of the type in **Figure 9*a***. The MSG of this hypothetical phase would be A_Bma2 (#40.210). The magnetic point group is then reduced to *mm*21′, with the polar direction along the tetragonal axis. Thus, if the

system were an insulator, this simple magnetic ordering could induce some ferroelectric polarization. These examples show the importance of identifying the magnetic symmetry, taking into account the nonmagnetic atoms, independently of the simplicity of the spin arrangement.

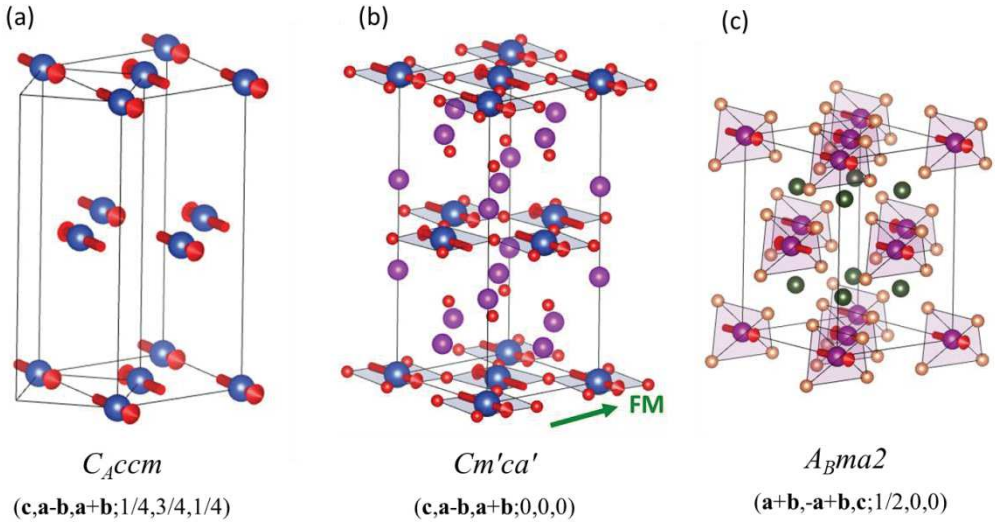

Figure 9
Simple spin arrangement in a body-centered tetragonal lattice of magnetic atoms, resulting in different symmetries and different magneto-structural properties depending on the parent space group of the structure as a whole: (*a*) *I*4/*mmm*, (*b*) *Cmce*, and (*c*) *I-42m*. The transformation from the tetragonal basis to the standard setting of each magnetic space group (MSG) is given below each MSG label. The case in panel *b* with weak ferromagnetism is realized in Gd_2CuO_4 (59), and the case in panel *c* is a hypothetical multiferroic with a parent structure similar to the one of Ga_2MnSe_4 (63).

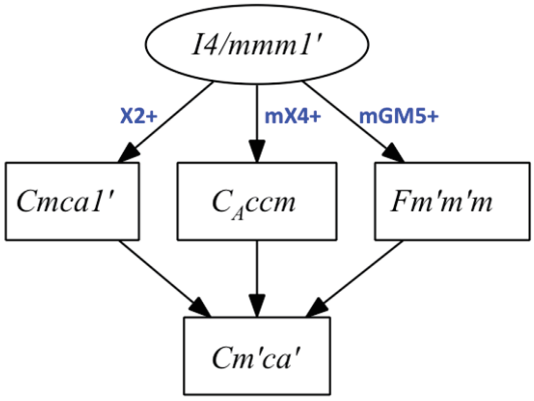

Figure 10
Scheme of the symmetry descent from the parent symmetry in the magnetic structure of Gd_2CuO_4 (59) showing the symmetry breakings of the primary structural and magnetic distortions and the triggering through symmetry compatibility of a ferromagnetic mode. The *irrep* labels of the distortions involved are indicated in gold (see Section 3). Notice that the group labels are the standard ones, and the orientations of their bases do not coincide.

3. Irreducible representations versus commensurate magnetic symmetry

In accordance with Landau theory, a magnetic ordering very often defines an order parameter with transformation properties given by a single *irrep* of the parent symmetry. This is the basis of the representation method developed by Bertaut (6, 7), in which the possible magnetic orderings are parameterized with basis modes transforming according to *irreps* of the parent space group. The basis spin modes are restricted to a single *irrep* or, if necessary, to a set of *irreps*. Originally, the *irreps* were considered representations of an ordinary space group, but if one includes the transformation properties of the spin modes under time reversal, they are in fact *irreps* of the parent gray MSG, being odd for time reversal. To distinguish them from those that are even for time reversal (associated, for instance, with phonon modes), we call them magnetic *irreps* and include a prefix *m* in their label.

The relationship between the representation method and magnetic symmetry was initially the subject of an intense discussion (64–66), which provoked a kind of splitting between two communities and some unfortunate misunderstandings that have persisted for decades. Today, however, the program ISODISTORT (67) allows a comprehensive application of the two approaches. The use of this program permits one to characterize any magnetic ordering, commensurate or incommensurate, in terms of both magnetic symmetry and *irreps*, showing their generally complex relationship. Below, we briefly summarize this relation and some of the capabilities of ISODISTORT in this context.

In the simplest case that the active *irrep* is one-dimensional (1-D) and real, the spin arrangement will either change sign or be invariant when transformed by any of the operations of the gray space group. If an operation of the parent space group has the character −1 associated, the analogous operation combined with time reversal will necessarily have +1 associated, and all operations of the parent space group G will therefore be conserved, either pure or combined with time reversal. A one-to-one correspondence thus exists between the assignment of a 1-D *irrep* and an MSG. The *irrep* determines the MSG and vice versa, and the *irrep* basis spin modes define the same restrictions for the spin arrangement as those that can be directly derived from the MSG. However, this simple scenario is no longer true if the *irrep* is multidimensional. In this general case, different magnetic symmetries can occur for a single *irrep*. An arbitrary combination of the *irrep* basis modes results in a minimal symmetry given by the operations of the parent gray space group to which the *irrep* associates the identity matrix. This is the so-called kernel of the *irrep* (4, 68). But for specific combinations of the spin modes (i.e., specific directions in the space of the *irrep* or order parameter directions), higher magnetic groups called epikernels can be realized (68). Thus, the assignment of one MSG corresponding to an *irrep* epikernel introduces more constraints than the assignment of just the *irrep*, as it limits the possible combinations of the *irrep* basis modes. Epikernels and kernels are also called *isotropy* subgroups (67).

Traditionally, the representation method has been applied considering the full set of *irrep* basis modes; this implies that the symmetry of the configuration space being explored was therefore generally the lowest one, i.e., the kernel of the *irrep*. Ad hoc restrictions in the basis modes introduced either a priori or as the result of the refinement could in fact make the spin model comply with one of the *irrep* epikernels,

but in general, the representation method has been applied without monitoring or controlling the resulting symmetry. This scenario changes if ISODISTORT is used. This powerful program calculates the epikernels and kernel of any possible *irrep* and provides the corresponding models of the magnetic structure complying with each of these alternative symmetries in the form of a magCIF file. It can also supply a basis of spin modes consistent with each possible epikernel or with the kernel of an *irrep*. The program is very general and can also supply similar information if several *irreps* are active, deriving all possible alternative magnetic symmetries and corresponding models for a given set of *irreps*. Furthermore, it can be used in a reverse approach to decompose a given magnetic structure in terms of spin *irrep* modes, including structural *irrep* modes if some significant structural distortion with respect to the paramagnetic phase exists.

If the active *irrep* of a magnetic ordering is multidimensional, one can distinguish two different, rather common situations that we illustrate with example cases analyzed with ISODISTORT. The *irrep* labels used below are those of this program. The definitions and details of any of the *irreps* considered here can be examined with the tool REPRES (24) of the Bilbao Crystallographic Server, which uses the same notation.

Case 1: The symmetry of the magnetic structure is an *irrep* epikernel and a k-maximal MSG. In this case, the description of the magnetic structure using its MSG reduces the number of spin degrees of freedom with respect to the usual representation method. As an example, we can take the case of $GdMn_2O_5$ discussed in Section 2, with parent space group *Pbam* and propagation vector **k** = (1/2, 0, 0). There are two two-dimensional (2-D) *irreps* for this wave vector (point *X* in the Brillouin zone), labeled *mX1* and *mX2*, and **Table 4** lists their epikernels and kernels. Taking into account the equivalence of the transformations to standard setting, one can see that the four possible epikernels coincide with the four k-maximal MSGs discussed in Section 2. As shown in **Table 4**, the $P_ac a 2_1$ (#29.104) magnetic structure of $GdMn_2O_5$ discussed in Section 2 corresponds to a spin arrangement according to the *irrep mX2* but is restricted to a special direction within the *irrep* space that limits the number of degrees of freedom to 11, instead of the 22 that exist for a general *mX2* spin configuration. Similar to what can be done with MAXMAGN, once the *irrep* epikernel $P_ac a 2_1$ is chosen as the tentative symmetry of the structure, a magnetic structure model complying with this symmetry can be supplied by ISODISTORT in magCIF format and introduced for refinement in JANA2006 or FULLPROF. As explained in Section 2 (see **Table 2**), the 11 spin degrees of freedom of this structure are automatically taken into account in the crystallographic description of the magCIF file that makes use of the MSG. In such cases, the use of *irrep* modes brings no advantage or additional information in what concerns the magnetic degrees of freedom of the structure. Furthermore, we have seen in the previous section that all *irrep* epikernels in this example can be directly derived as k-maximal symmetries.

Table 4
Epikernels and kernels of the magnetic irreps of *Pbam1'* at the point X[a]

Irrep	Order parameter direction	MSG	Transformation to standard	Number of spin degrees of freedom[b]

	(a,0)	$P_b mc2_1$ (#26.72)	($\mathbf{c}_p$, 2$\mathbf{a}_p$, $\mathbf{b}_p$; 1/4, 0, 0)	2 (Gd), 5 (Mn)
mX1	(a,a)	$P_a 2/m$ (#10.47)	(-2$\mathbf{a}_p$, $\mathbf{c}_p$, $\mathbf{b}_p$; - 1/2, 0, 0)	2 (Gd), 5 (Mn)
	(a,b)	$P_a m$ (#6.21)	(-2$\mathbf{a}_p$, $\mathbf{c}_p$, $\mathbf{b}_p$; 0, 0, 0)	4 (Gd), 10 (Mn)
	(a,0)	$P_a ca2_1$ (#29.104)	(-2$\mathbf{a}_p$, $\mathbf{c}_p$, $\mathbf{b}_p$; -3/4, 0, 0)	4 (Gd), 7 (Mn)
mX2	(a,a)	$P_c 2/c$ (#13.72)	($\mathbf{b}_p$, $\mathbf{c}_p$, 2$\mathbf{a}_p$; 0, 0, 0)	4 (Gd), 7 (Mn)
	(a,b)	$P_c c$ (#7.28)	($\mathbf{b}_p$, $\mathbf{c}_p$, 2$\mathbf{a}_p$;0,0,0)	8 (Gd), 14 (Mn)

[a] Epikernels and kernels that can be relevant for the magnetic ordering with a propagation vector (1/2,0,0) in $GdMn_2O_5$, as obtained with ISODISTORT.
[b] For the magnetic atoms in $GdMn_2O_5$.

Case 2: The symmetry of the magnetic structure is an *irrep* epikernel but not a k-maximal MSG. In general, all k-maximal MSGs are *irrep* epikernels, but the reverse is not true for cubic, hexagonal, and trigonal parent symmetries, for which some *irrep* epikernels may not be k-maximal symmetries. In these cases, the magnetic symmetry given by the *irrep* epikernel allows, in general, spin degrees of freedom corresponding to other *irreps*. The most efficient approach in such situations is to decompose the spin degrees of freedom into *irrep* spin modes that should be restricted or symmetry-adapted to the relevant MSG.

The magnetic structure of NiO discussed above is a simple example of this situation. There is only a single Ni atom per primitive unit cell, and therefore the *irrep* spin modes are defined by the spin of this single site. The magnetic representation of the Ni moments with propagation vector (1/2, 1/2, 1/2) (point *L* in the Brillouin zone) decomposes into *mL2+* $\oplus$ *mL3+*. The small *irreps* corresponding to *mL2+* and *mL3+*, relevant for *1k* spin arrangements, are 1-D and 2-D, respectively. Thus, the three spin degrees of freedom of the system decompose into a single spin mode of type *mL2+* and two spin modes for the *irrep mL3+*. **Table 5** shows that a magnetic model according to the *irrep mL2+* is equivalent to the assignment of the MSG R_I-*3c* (#167.108), which is one of the k-maximal MSGs shown in **Figure 5**. Under this symmetry, the Ni moment is constrained along the (1, 1, 1) direction, i.e., the *mL2+* spin Ni mode is just a spin directed along the (1, 1, 1) direction; this can be checked by applying the usual programs used in the representation method [BASIREPS (12), SARA*h* (13), or MODY (14)]. For the 2-D small *irrep mL3+*, the situation is quite different. The mentioned programs provide two basis spin modes for *mL3+*, and if both are used, the explored magnetic configurations have the lowest possible symmetry, namely the *irrep* kernel P_S-*1*. The Ni spin is then only restricted to lie on the plane perpendicular to the (1, 1, 1) direction. In order to restrict the *irrep* model to one of the epikernels, one must choose a specific linear combination of the two basis modes of *mL3+*. These epikernel-adapted modes can be obtained with ISODISTORT and are listed in **Table 5**. The MSG of the magnetic structure of NiO is C_c2/c (#15.90). Therefore, the active *irrep* is *mL3+* but is restricted to one of its epikernels, with the spin mode being along the (1, 1, −2) direction. We saw in the previous section, however, that the C_c2/c symmetry only restricts the Ni spin to lie on a plane of the form (m_x, m_x, m_z). This symmetry therefore also allows an orthogonal spin component along the (1, 1, 1) direction.

Hence, the symmetry assignment of the MSG C_c2/c (#15.90) restricts the spin configuration with respect to a general *mL3+* arrangement, but, at the same time, it allows the presence of a mode according to the *irrep mL2+*. The reason for the possible

presence of this secondary spin mode can be seen in **Figure 5**. C_c2/c is not a k-maximal symmetry but is in fact a subgroup of the epikernel of *mL2+*. Therefore, in accordance with von Neumann principle, the symmetry break produced by the primary *mL3+* order parameter allows the presence of an *mL2+* distortion as a symmetry-compatible secondary effect. Thus, the MSG automatically takes into account all degrees of freedom that are triggered by the symmetry break. From physical arguments, one should expect that the prevailing spin direction will comply with the *mL3+ irrep* but will be restricted to the relevant epikernel and will therefore be along the (1, 1, −2) direction, whereas the *mL2+* component along the (1, 1, 1) direction should be weak or even negligible. This is indeed what is observed.

Therefore, the most efficient approach in this type of case is to consider both the magnetic symmetry of the system represented by an MSG and the decomposition of the degrees of freedom in terms of *irrep* modes restricted to this MSG. In general, a physical hierarchy between the symmetry-compatible *irreps* will exist, and the degrees of freedom associated with the secondary *irreps* may be disregarded, reducing their number with respect to a description using only the MSG.

A more complex example is summarized in **Figure 11**, which shows all the possible **k** = 0 magnetic symmetries for the compound $Na_3Co(CO_3)_2Cl$, discussed in Section 2.4. The figure also indicates the possible *irrep* epikernels and kernels and the number of *irrep* basis modes in each case. For instance, a general spin configuration according to the *irrep mGM4+* requires nine basis modes, and its magnetic symmetry is the minimal one, *P-1*, but it allows three additional degrees of freedom corresponding to the secondary symmetry-compatible *irreps mGM1+* and *mGM2+* $\oplus$ *GM3+* (a physically irreducible *irrep*). But the *irrep mGM4+* can also yield the MSG *R-3* (#148.17), and under this symmetry, the number of free spin parameters is four. But this MSG restricted to the *irrep mGM4+* only requires three basis modes, whereas the fourth degree of freedom corresponds to the symmetry-compatible mode for the *irrep mGM1+* of symmetry *Fd-3* (#203.26).

Table 5
Epikernels and kernels of the magnetic irreps of *Fm-3m1'* at the L point[a] of the Brillouin zone

Irrep	Order parameter direction	MSG	Transformation to standard	Spin degrees of freedom[b]	Ni spin basis modes
mL2+	(a)	R_I*-3c* (#167.108)	(-**a**$_p$/2+**c**$_p$/2,**b**$_p$/2-**c**$_p$/2,-2**a**$_p$-2**b**$_p$-**2**c$_p$;0,0,0)	1	(1,1,1)
	(a,0)	C_c*2/m* (#12.63)	(**a**$_p$/2+**b**$_p$/2-**c**, **a**$_p$/2-**b**$_p$/2, -**a**$_p$-**b**$_p$;0,0,0)	1	(1,-1,0)
mL3+	(a,a)	C_c*2/c* (#15.90)	(**a**$_p$/2+**b**$_p$/2-**c**, **a**$_p$/2-**b**$_p$/2, -**a**$_p$-**b**$_p$;0,0,0)	1	(1,1,-2)
	(a,b)	P_S*-1* (#7.28)	(-**b**$_p$/2+**c**$_p$/2, **a**$_p$/2-**b**$_p$/2, **a**$_p$+**c**$_p$;0,0,0)	2	(1,-1,0) (1,1,-2)

[a] Epikernels and kernels which can be relevant in the magnetic phase of NiO with propagation vector (1/2,1/2,1/2), as obtained with ISODISTORT (only 1k configurations are included).
[b] For the Ni atoms.

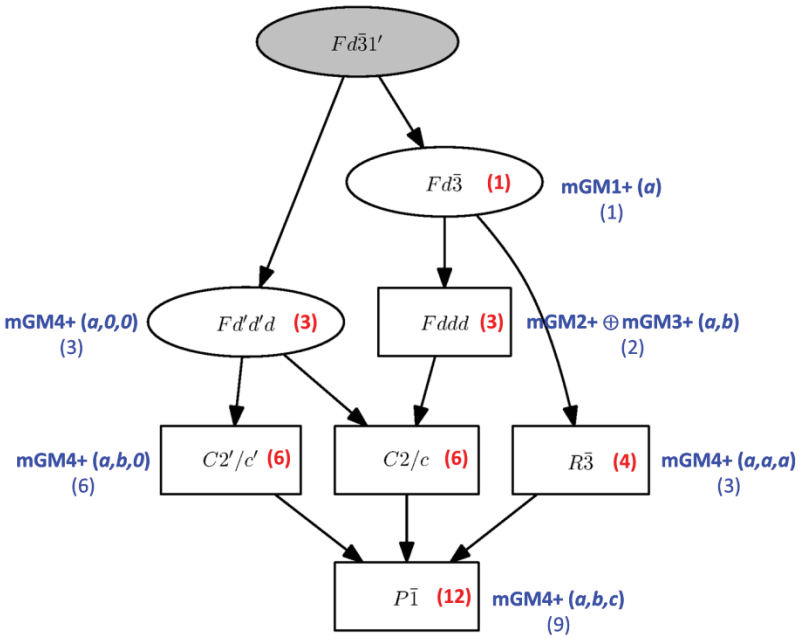

Figure 11
Group-subgroup graph of all possible magnetic symmetries for a structure with parent space group *Fd-3* (#203), propagation vector zero, and a magnetic atom at the origin. The k-maximal magnetic space groups are highlighted with elliptical frames. Only one subgroup per conjugacy class is shown. The subgroups that are epikernels for some irreducible representations (*irreps*) have at their side the corresponding *irrep* label with the order parameter direction in the ISODISTORT notation. The number of spin degrees of freedom is indicated in red for each group, and the number of symmetry-restricted *irrep* basis modes is written in gold below the *irrep*.

4. Incommensurate magnetic structures and superspace symmetry

The superspace symmetry formalism, developed between 1974 and 1985, has become the standard method for the analysis and determination of nonmagnetic modulated structures, both incommensurate and commensurate (5, 69–74). Nearly all quantitative structural studies of these systems employ the refinement program JANA2006 (47, 48), which is based on this formalism. A superspace group defines all the structural constraints that are symmetry forced and are protected within an incommensurate phase, playing the role that an ordinary space group does for commensurate phases. Since the beginning of its development, it was pointed out that superspace symmetry can be extended to magnetic systems (5), but in fact only a few testimonial works have applied this formalism to magnetic structures (75). The situation has drastically changed in the past few years with the development of computational tools specific for magnetic structures that make use of superspace symmetry, in particular the extension of JANA2006. Hence, the number of reported incommensurate magnetic structures refined, described, or both using superspace symmetry is increasing steadily (76–87). For the sake of simplicity, we restrict the discussion to *1k* incommensurate structures but we stress that superspace symmetry can also be considered in more general cases with several independent, incommensurate wave vectors.

In practical terms, the characterization of a *1k* incommensurate phase using a superspace group is reduced to the description of the local aperiodic atomic positions and atomic properties (as the magnetic moments) by means of periodic modulation functions of a continuous variable, say x_4, with period 1. The actual value of an atomic property of an atom at a position **r** is then given by the value of the corresponding modulation function at $x_4 = \mathbf{k}\cdot\mathbf{r}$. The continuous variable of these functions is associated with the additional dimension in a mathematical superspace, which is introduced in the definition of the symmetry operations. A symmetry operation of an incommensurate structure is, in general, an ordinary symmetry operation of the reference parent structure, say, {**R** | **t**} followed by a certain global shift τ of all the modulation functions, such that the transformed system with the atomic positions and local properties given by these shifted modulation functions becomes undistinguishable from the original one. The operation is then represented by {**R** | **t**, τ_0}, with $\tau_0 = \tau + \mathbf{k}\cdot\mathbf{t}$ being the k-independent part of the phase shift. Thus, the symmetry group of an incommensurate crystal is obtained by adding the possibility of shifting the global phase of all the modulation functions to the ordinary rotations, roto-inversions, and translations. A generalization to magnetic crystals is immediate by just including among the possible operations the combination with time reversal, yielding the MSSGs. As ordinary magnetic symmetry, MSSGs are robust in the sense that they can be associated with the properties of the system within a whole thermodynamic phase. The point-group symmetry constraining the tensor physical properties of the phase is then formed by the point-group operations that form part of the symmetry operations of the MSSG.

Following the basic principles explained above, deriving the magnetic point-group symmetry of a chain of spins with an incommensurate modulation of any type is straightforward. **Figure 12** shows the point-group symmetries of the most representative incommensurate spin modulations along a periodic atomic chain. In nearly all cases, the point group is gray, i.e., it contains time reversal, and linear magneto-structural couplings are therefore not possible. Only those spin modulations that include a **k** = 0 component in addition to the incommensurate frozen spin wave have nongray point groups. This is a general property: Any *1k* incommensurate modulation possesses the superspace symmetry operation {1′ | 0, 0, 0, 1/2} because, after switching the spins to opposite signs by the action of time reversal, a phase shift of 1/2 of the spin modulation as a whole recuperates the original spin arrangement.

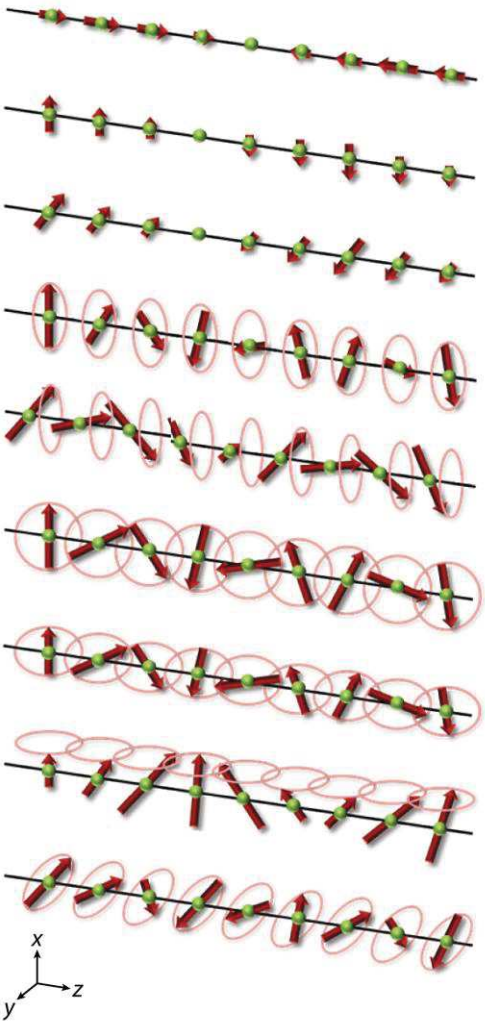

	Point group		
	No lattice	Cubic lattice	Hexagonal lattice
Collinear longitudinal	∞/*mm*1′	4/*mmm*1′	6/*mmm*1′
Collinear transversal	*mmm*1′	*mmm*1′	*mmm*1′
Collinear transversal oblique	12/*m*11′	12/*m*11′	12/*m*11′
Proper screw	∞21′	4221′	6221′
Conical screw	∞2′	42′2′	62′2′
Cycloid	2*mm*1′	2*mm*1′	2*mm*1′
Elliptical cycloid	2*mm*1′	2*mm*1′	2*mm*1′
Transverse cone	2′*mm*′	2′*mm*′	2′*mm*′
Elliptical oblique cycloid	1*m*11′	1*m*11′	1*m*11′

Figure 12
Representative spin modulations along a periodic chain of atoms with indication of their point-group symmetries according to their superspace symmetry groups. The first column is the point group of a single chain, whereas the second and third columns list those for three-dimensional cubic and hexagonal monoatomic arrangements of these chains, the chains being along the *c* direction.

Many of the point groups of the incommensurate spin chains in **Figure 12** include inversion, or other operations transforming **k** into **−k**. Only the cycloid arrangements and the transverse conical modulation break the symmetry into noncentrosymmetric polar groups. The polarity of a circular spin cycloid is along the direction perpendicular to **k** and within the plane of the cycloid. Thus, symmetry is sufficient to predict the polar character (and its direction) for this type of spin arrangement. Notice, however, that in the case of an elliptical oblique cycloid, with the main axes of the cycloid ellipse along arbitrary directions, the symmetry is reduced to *m*1′, with the mirror plane being the one of the cycloid. Hence, in this case, the possible induced polarization can take an arbitrary direction within this plane.

It is important to stress that a proper screw modulation, with the spins rotating on the plane perpendicular to the propagation vector, also breaks inversion but keeps any

binary axis perpendicular to the chain. Thus, this type of spin arrangement in high-symmetry lattices gives way to a noncentrosymmetric but nonpolar chiral symmetry. This is, for instance, the case of $MnAu_2$ (22, 88), with space group *I*4/*mmm* (#139) in the paramagnetic phase and MSSG *I*4221′*(00γ)q00s* (point group 4221′) in its incommensurate magnetic phase. However, if these types of screw spin chains are embedded in a structure lacking binary axes perpendicular to the direction of the modulation, the magnetic symmetry will be polar along the chain, and in the case of an insulator, an induced ferroelectric polarization along the direction of the propagation vector is possible.

4.2. Crystallographic Description of Incommensurate Magnetic Structures

A CIF dictionary for incommensurate (nonmagnetic) structures based on superspace symmetry already exists (89), and its extension to magnetic structures within the magCIF dictionary is straightforward. In the simplest case of a harmonic modulation, the spin modulation functions of a magnetic atom in the asymmetric unit are given by a combination of sine and cosine functions for each spin component. If the site lies in a special position, then the modulation is subject to site-symmetry constraints, whereas the spin modulation functions of the symmetry-related atoms are derived by the operations of the superspace group. A detailed review of the application of MSSGs in magnetic structures can be found in Reference 3.

As an example, we consider the very simple structure of Ce_2Pd_2Sn (90, 91), shown in **Figure 13**. This is a sinusoidal transversal spin modulation, of the Ce magnetic moments along *c*, with parent space group *P*4/*mbm* (#127) and propagation vector **k** = (0.105, 0, 0). The superspace symmetry of this spin arrangement is given by the MSSG *Pbam*1′*(α00)0s0s* (22), maintaining the parent setting for the average structure. This means that the structure is centrosymmetric, and its average symmetry is reduced from tetragonal to *Pbam*1′, which implies the possible liberation of structural degrees of freedom with respect to the parent phase through magneto-structural coupling. The 4*h* Ce site in the parent tetragonal phase remains a 4*h* site in the *Pbam*1′ average structure, and only the spin modulation of one atom, Ce1, is independent. The representative operations of *Pbam*1′*(α00)0s0s* are $\{2_{100} \mid 1/2, 1/2, 0, 1/2\}$, $\{2_{010} \mid 1/2, 1/2, 0, 1/2\}$, $\{2_{001} \mid 0, 0, 0, 0\}$, $\{-1 \mid 0, 0, 0, 0\}$, $\{m_{100} \mid 1/2, 1/2, 0, 1/2\}$, $\{m_{010} \mid 1/2, 1/2, 0, 1/2\}$, and $\{m_{001} \mid 0, 0, 0, 0\}$, plus those obtained by combining all these operations with {1′ | 0, 0, 0, 1/2} (22). The symmetry invariance of the Ce1 site for the operation $\{m_{001} \mid 0, 0, 1, 0\}$ constrains its spin modulation to be along the *c* direction:

$$\vec{M}_{Ce1}\left(x_4\right) = \left(0,0,M_{z\cos 1}\right)\cos\left(x_4\right) + \left(0,0,M_{z\sin 1}\right)\sin\left(x_4\right)$$

The spin modulation therefore has two free parameters. The modulation functions of the other three Ce atoms in the parent unit cell, Ce1_2, Ce1_3, and Ce1_4, are obtained through the operations $\{m_{010} \mid 1/2, 1/2, 0, 1/2\}$, $\{m_{100} \mid 1/2, 1/2, 0, 1/2\}$, and $\{-1 \mid 0, 0, 0, 0\}$, respectively (see Reference 3). Hence, Ce1_2 has the same modulation function as Ce1_1, whereas the other two atoms have the same cosine term but an opposite sine component. This implies that symmetry allows a phase shift between the modulations of the Ce atoms that are related by operations transforming **k** into −**k** but

constrains all amplitudes to be equal. According to the model reported in References 90 and 91, the parameter M_{zsin1} is negligible, and the four modulations are in phase.

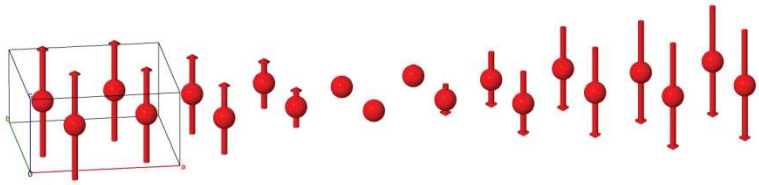

Figure 13
Incommensurate magnetic structure of Ce_2Pd_2Sn (54) with superspace group *Pbam1'(a00)0s0s.*

4.3. Irreducible Representations Versus Magnetic Superspace Groups

The relationship of the representation approach with the MSSGs is similar to the one discussed above between *irreps* and MSGs in commensurate structures (3). If the small *irrep* associated with the spin modulation is 1-D, there is a one-to-one correspondence between the MSSG and the *irrep*, but for multidimensional small *irreps* in general, several distinct MSSGs can be realized in the incommensurate phase depending on the direction taken by the order parameter within the representation space. Hence, different magnetic symmetries can result from the same *irrep*, constituting the epikernels and kernel of the *irrep*.

However, an important difference exists with respect to the commensurate case. For 1-D small *irreps*, even if only one MSSG is possible, this MSSG generally includes operations that transform the vector **k** into −**k** (if these operations exist in the paramagnetic phase). **Figure 14** shows the four MSSGs corresponding to the four possible *irreps* of *P*4/*mbm* for an incommensurate wave vector (α, 0, 0), which could be relevant for the case of Ce_2Pd_2Sn described above. All are centrosymmetric. Among the wave vector's superspace symmetry operations, the MSSGs keep all point-group operations of the parent symmetry that either maintain **k** invariant or transform it to −**k**. This is an important difference from the traditional representation approach, which has usually considered that atoms related by operations of the parent symmetry that transform **k** into −**k** become split in the incommensurate phase, yielding independent suborbits of atoms. In practice, some correlations between the parameters of these supposedly independent atoms are often introduced and justified with various arguments not related to symmetry. However, this example shows that, according to the MSSG associated with any active *irrep*, the modulations of atoms related by these −**k** operations remain symmetry related in the incommensurate phase. The spin arrangement of Ce_2Pd_2Sn complies with the *irrep mDT4* (see **Figure 14**), and the representation method yields three free parameters for this *irrep* (91) (one amplitude and phase per suborbit of Ce atoms, minus one free phase that can be fixed arbitrarily). Thus, in principle the method allows different amplitudes of the spin modulations of the two suborbits, although in practice they are made equal (91). The MSSG associated with the *irrep* shows that this is not just an additional reasonable assumption or approximation but is part of the restrictions for a single *irrep* distortion, i.e., a single order parameter. One can always derive them from the *irrep* transformation properties, as done in Reference 92, for instance, but the identification of the MSSG associated with the active *irrep* provides automatically all constraints,

including those of possible higher modulation harmonics, both magnetic and structural. The usual disregard of the symmetry constraints coming from the operations changing **k** into −**k** implies that more general spin arrangements are being considered, which represent the incoherent (phase-shifted) superposition of more than one *irrep* mode for the same *irrep*. Notice, for instance, that in the case of Ce_2Pd_2Sn, the constraint coming from the **k** to −**k** transforming operations is essential to keep the system centrosymmetric.

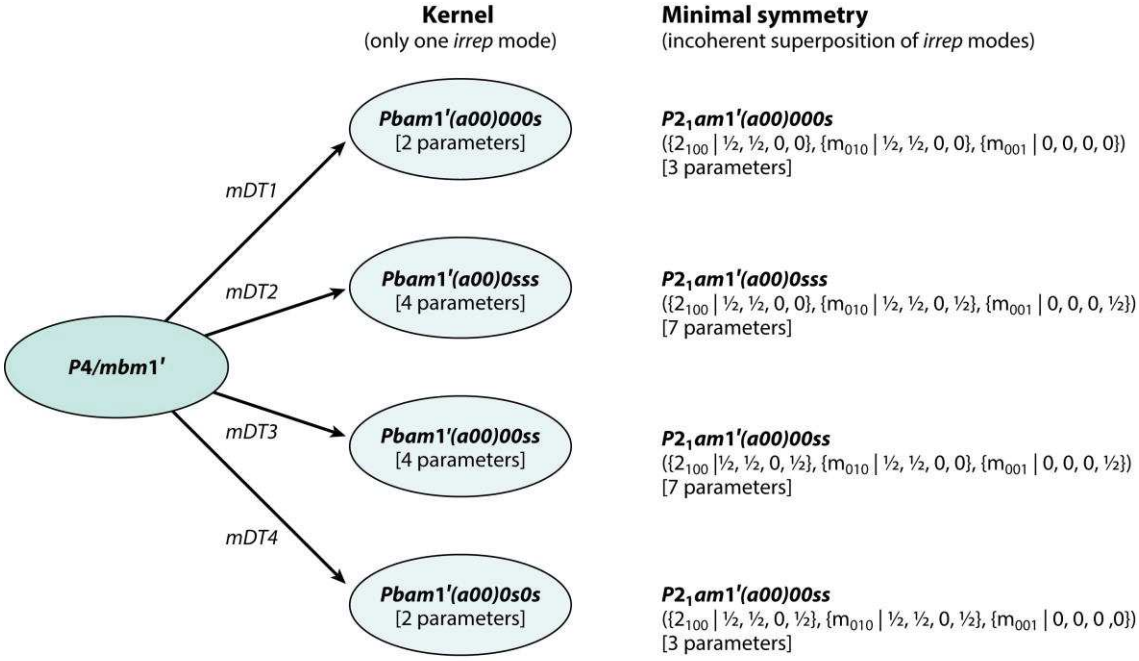

Figure 14
Possible magnetic superspace groups for an incommensurate magnetic modulation with propagation vector of type (α, 0, 0) on a parent structure with space group *P*4/*mbm,* if restricted to a single irreducible representation (*irrep*) mode, as can be obtained in JANA2006 or ISODISTORT. The number of free magnetic parameters for each case is indicated in brackets. A set of generators is listed for each symmetry, with the exception of {−1 | 0, 0, 0, 0} and {1′ | 0, 0, 0, 1/2}, present in all. The minimal superspace symmetry, corresponding to an incoherent superposition of more than one *irrep* mode, is shown on the right. Notice that the superspace groups are described here in the parent setting, in contrast with the default output of ISODISTORT.

ISODISTORT or JANA2006 provide the epikernels and kernel of any incommensurate *irrep* in the form of a list of possible MSSGs, and they can supply the corresponding symmetry-adapted magnetic structure models for visualization or any further analysis. The models are portable using incommensurate magCIF files, which are fully supported by the visualization program Jmol. JANA2006 can in principle refine any incommensurate *1k* magnetic structure under any chosen MSSG, and the program includes the calculation tool of epikernels and kernels for the possible *irreps* as a preliminary step to explore and construct all possible models of different superspace symmetry that can be confronted with the experimental data. Once one *irrep* epikernel (or kernel) is chosen, the program works in a crystallographic way using the corresponding MSSG to analyze the symmetry of the diffraction data and constrain both magnetic and structural parameters. This allows a systematic search of the

incommensurate magnetic structure in a symmetry-hierarchical way. It works by default in the parent setting, but it can be changed by the user. By contrast, ISODISTORT supplies the different possible MSSG models in their standard setting, which can strongly differ from the one of the parent phase, including a different choice of the propagation vector. This program focuses on the mode analysis of both the magnetic and structural degrees of freedom of the different possible phases and supplies a parameterization in terms of *irrep* basis modes adapted to the relevant MSSG. This is very important when several *irreps* are symmetry allowed, as one can distinguish primary *irrep* modes from weak or negligible secondary ones.

Figure 15 summarizes the case of $RbFe(MoO_4)_2$ (82, 93). This compound has a paramagnetic phase with space group *P-3*, and it orders with an incommensurate propagation vector (1/3, 1/3, γ) [line *P* in the Brillouin zone (58)]. Having the Fe atom at the origin, a spin arrangement with this propagation vector in the most general case would require five parameters (the amplitude and phase for the three spin components, minus one phase that can be chosen arbitrarily). However, the modulation of the spin component along *c* transforms according to the *irrep mP1*, whereas those on the *ab* plane correspond to the *irrep mP2P3* (a physically irreducible *irrep*). The *irrep mP2P3* has two possible epikernels. This means that two different alternative MSSGs of maximal symmetry are possible for this *irrep*. Their labels are indicated in **Figure 15**, together with the mathematical form of the spin modulation function and a graphical scheme. The system can either maintain the 3-fold axis and lose the space inversion symmetry or keep the centrosymmetry but break the 3-fold axis. In the first case, the MSSG forces the spin modulation to have two orthogonal components in quadrature on the *ab* plane; this is sufficient to acquire a typical 120° arrangement on the *ab* plane, whereas the spins rotate along *c*, forming a screw with a pitch determined by the propagation vector. If this MSSG is assigned, the determination of the corresponding spin configuration requires a single parameter. A magnetic phase with this superspace symmetry has 31’ as point-group symmetry. It is therefore polar along *c*, with domains related by the lost space inversion. Induced ferroelectricity, i.e., a multiferroic of type II, should be expected (93).

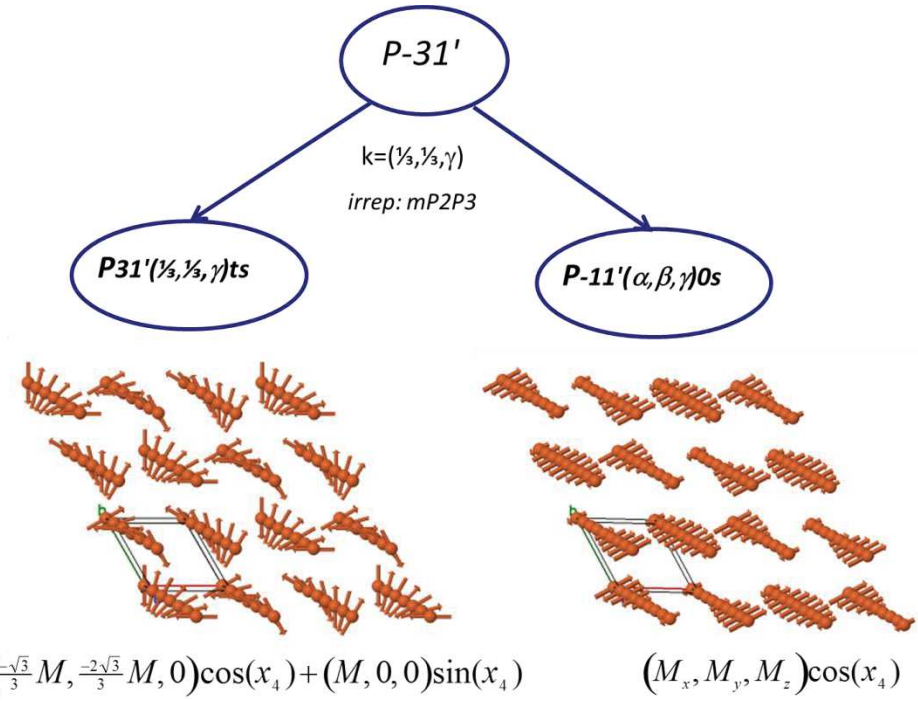

Figure 15

Epikernels of the irreducible representation (*irrep*) *mP2P3* (physically irreducible) with a propagation vector of type (1/3, 1/3, γ) for a parent space group *P-3* (#147) and corresponding spin arrangements for an atom at the origin, as obtained from JANA2006 or ISODISTORT. The general form of the spin modulation is also indicated for each case. These two alternative k-maximal symmetries are realized in the phase diagram of $RbFe(MoO_4)_2$ (82, 93).

The other alternative maximal symmetry is a collinear arrangement in which the modulations of the three moment components are in phase. This second MSSG has three free spin parameters, but one of them is the M_z component (see **Figure 15**), which corresponds to the *irrep mP1*. As in the commensurate case, the magnetic symmetry allows degrees of freedom corresponding to symmetry-compatible secondary modes associated with *irreps* having as epikernel (or kernel) one supergroup of the actual MSSG. This is the case of the M_z modulation that can be present, as a secondary *mP1* distortion, in a model complying with this MSSG *P-11'(α, β, γ)0s*, provided it is in phase with the primary *mP2P3* collinear distortion on the *ab* plane. This second component can be small enough to be negligible, reducing the number of free parameters to two. Notice that for this MSSG, the *x* and *y* components of the propagation vector are no longer forced to have the rational value 1/3, as explicitly indicated in the group label. This second alternative maximal superspace symmetry is realized in the phase diagram under magnetic field.

The kernel of *mP2P3*, i.e., the lowest superspace symmetry possible, is the intersection of the two alternative k-maximal superspace symmetries for *mP2P3* discussed above. It reduces to the MSSG *P11'(α,β,γ)0s*; i.e., only the ubiquitous operation {1' | 0, 0, 0, 1/2} is kept. This is the superspace symmetry of an arbitrary *mP2P3* modulation built up with all the *irrep* basis modes.

In simple cases such as the one above, the incommensurate spin configurations of higher symmetry are intuitively clear, and they are often tested in the refinements without appealing to concrete symmetry arguments. But for more general cases, the

enumeration for a given *irrep* of distinct spin arrangements of higher symmetry is not obvious. The application of superspace symmetry allows the systematic exploration of these possible privileged configurations, distinguishing them from simplifying features that are not symmetry dictated. For an atom in a general position, the superspace symmetry of the phase does not restrict the form of its spin modulation, and it is only the relation of its (arbitrary) modulation with those of the other symmetry-related atoms in the average unit cell that is forced by the MSSG.

If the magnetic modulation is anharmonic or the magneto-structural coupling is strong enough to induce a structural modulation, the knowledge of the superspace symmetry of the magnetic phase is especially important, as it dictates the features of all induced effects. For *1k* structures, the presence of the superspace symmetry operation {1′ | 0, 0, 0, 1/2} in the MSSG ensures that the spin modulation can only have odd harmonics, whereas any magnetically induced structural modulation is restricted to even harmonics of the primary propagation vector. Hence, the existence of this very simple superspace symmetry operation is the reason for this general property satisfied by magnetically induced structural modulations. Higher harmonics of both the spin and the structural modulation are subject to the same MSSG as the first harmonic, but this in general implies transformation properties corresponding to *irreps* different from the one of the first harmonic. For instance, for the case of $RbFe(MoO_4)_2$ under the trigonal MSSG *P*31′*(1/3, 1/3, γ)ts,* the presence of the symmetry operation $\{3^+ \mid 0, 0, 0, 1/3\}$ not only enforces the helical spin arrangement for the first harmonic but also restricts the third harmonic (actually all 3*n* harmonics) to be a modulation with the spin component along *c*, i.e., an *mP1* distortion. Similarly, any induced structural distortion should comply with the MSSG, and this means specific restrictions on each induced harmonic modulation. For instance, the Fe atoms can suffer a displacive modulation with wave vector 2**k**, but it is restricted to the *ab* plane (82).

Conversely, if the paramagnetic phase is itself incommensurate owing to a structural modulation, the symmetry of the paramagnetic phase is then given by a gray superspace group, and the propagation vector of the magnetic ordering can be commensurate with the incommensurate wave vector of the structural modulation. The MSSG of the magnetic phase is then related directly to the one of the paramagnetic phase (86).

5. CONCLUSIONS

Various computational tools developed during the past few years have made possible the relatively simple, systematic, and comprehensive application of magnetic symmetry in the analysis of magnetic structures, both commensurate and incommensurate. In the incommensurate case, the symmetry constraints of these phases are efficiently described and handled using superspace symmetry concepts with the introduction of MSSGs. A principle of maximal symmetry underlies most of the observed magnetic structures and their traditional description using *irreps*. The new computational instruments go beyond the traditional representation method and exploit the symmetry hierarchy among possible ordering models, such that a full characterization of the relevant symmetry breaking becomes a straightforward process. We have outlined this novel scenario by reviewing several examples and

explaining the main concepts involved. We hope to have clearly shown that the representation method and a symmetry-based description of magnetic structures should be considered as complementary, and not alternative, approaches. The assignment of a magnetic symmetry in the form of an MSG or MSSG is not equivalent to the assignment of an *irrep*, except for 1-D *irreps*. Also, contrary to common belief, the assignment of an *irrep*, if multidimensional, generally introduces fewer constraints than an MSG. In complex situations, the most appropriate approach is a comprehensive application of both magnetic symmetry and *irrep* modes, and this is facilitated by the computational tools reviewed here and summarized in **Table 6**.

Table 6
Databases and programs to analyze magnetic structures using magnetic symmetry[a]

Program or database	Program description
Magnetic group tables (30)	Tables of MSGs with illustrations and data analogous to those of the ordinary space groups in the *International Tables for Crystallography*. They are set in OG notation and are not computer readable.
ISO-MAG (33)	Computer-readable tables and data of MSGs in both BNS and OG notations.
MGENPOS, MWYCKPOS (34)	Database of symmetry operations and Wyckoff positions of MSGs in both BNS and OG notations.
IDENTIFY MAGNETIC GROUP (39)	Identifies a magnetic space group (commensurate) from a set of generators in an arbitrary setting.
ISOCIF (41), FINDSYM (43)	Editor to create or modify a magCIF file of a commensurate magnetic structure. It transforms to any desired setting and automatically finds the actual MSG of a structure introduced enumerating all atoms and spins in the unit cell. It includes an online visualization tool.
STRCONVERT (42)	Editor to convert, edit, or both a commensurate magnetic structure into different file formats, including magCIF. Using FINDSYM, it finds the MSG of the structure if transformed or given in *P*1 symmetry. VASP files for or from ab initio calculations are also supported.
ISODISTORT (67)	Comprehensive online program to enumerate and describe possible magnetic structures caused by one or more active *irreps*. The magCIF format is supported. It provides possible epikernels and kernels (isotropy subgroups) of any magnetic *irrep* or set of *irreps* and can yield the mode decomposition of any commensurate magnetic structure if given in magCIF format. Standard settings are required for input data, but the resulting models of the magnetic structures can be obtained in any chosen setting.
MAXMAGN (46)	Generates all possible magnetic symmetries and the corresponding magnetic structures for a given propagation vector, starting with those of maximal symmetry.

k-SUBGROUPSMAG (52)	Provides all possible magnetic symmetries for a known space group of the paramagnetic phase and a set of one or more propagation vectors. Their group-subgroup hierarchy is also provided in a graphic form.
MAGNEXT (34)	Provides symmetry-forced systematic absences of nonpolarized neutron magnetic diffraction, along with the symmetry-adapted form of the magnetic structure factor, for any MSG or MSSG. Nonstandard settings are also supported.
MAGMODELIZE (56)	For any parent structure, provides the magnetic structure model corresponding to any MSG given by the user, as well as all domain-equivalent ones. It can be combined with k-SUBGROUPSMAG to explore all possible magnetic arrangements for a known propagation vector following a stepwise symmetry descent.
JANA2006 (47, 48)	General refinement program that includes a tool to construct for each *irrep* possible alternative models with their symmetries given by the possible *irrep* epikernels and kernel. It can deal both with commensurate and incommensurate structures. Magnetic structures can be uploaded or retrieved using magCIF files.
FULLPROF (12)	General refinement program that supports magCIF files both as input and output. A console application provides information on MSGs. Any MSG symmetry can be implemented in the model to be refined.
MVISUALIZE (45)	Online visualization using Jmol of any magnetic structure (commensurate or incommensurate) if uploaded as a magCIF file.
VESTA (27)	Visualization program that supports magnetic structures in magCIF format and magnetic symmetry (only commensurate structures).
Jmol (28)	Visualization program that supports magnetic structures (both commensurate and incommensurate) in magCIF format and magnetic symmetry.
MAGNDATA (22)	A collection of more than 250 magnetic structures (commensurate and incommensurate) described using magnetic symmetry and magCIF files.

[a]This is a summary of the most important free databases, computer tools, and programs for the analysis of magnetic structures that use (or are based on) magnetic symmetry.

ACKNOWLEDGMENTS

The authors thank Vaclav Petricek, Juan Rodriguez-Carvajal, Branton Campbell, and Harold Stokes for helpful comments, their permanent receptivity to suggestions regarding their programs, and their efforts to achieve a common communication

format. We are also very grateful to Koichi Momma and Robert Hanson for adapting their visualization programs to this format and in this way joining the endeavor for a robust and unambiguous communication of magnetic structures. This work has been supported by the Spanish Ministry of Science and Innovation (project MAT2012-34740) and the Government of the Basque Country (project IT779-13).

LITERATURE CITED

1. Koptsik VA. 1966. *Shubnikov Groups. Handbook on the Symmetry and Physical Properties of Crystal Structures.* Moscow: Moscow Univ. Press. In Russian
2. Bradley CJ, Cracknell AP. 1972. *The Mathematical Theory of Symmetry in Solids*. Oxford, UK: Clarendon
3. Perez-Mato JM, Ribeiro JL, Petricek V, Aroyo MI. 2012. Magnetic superspace groups and symmetry constraints in incommensurate magnetic phases. *J. Phys. Condens. Matter.* 24:163201
4. Petříček V, Fuksa J, Dušek M. 2010. Magnetic space and superspace groups, representation analysis: competing or friendly concepts? *Acta Crystallogr. Sect. A* 66:649–55
5. Janner A, Janssen T. 1980. Symmetry of incommensurate crystal phases. I. Commensurate basic structures. *Acta Crystallogr. Sect. A* 36:399–408
6. Bertaut EF. 1968. Representation analysis of magnetic structures. *Acta Crystallogr. Sect. A* 24:217–31
7. Bertaut EF. 1971. Magnetic structure analysis and group theory. *J. Phys. Colloques* 32:C1–462–70
8. Izyumov YA, Naish VE. 1979. Symmetry analysis in neutron diffraction studies of magnetic structures: 1. A phase transition concept to describe magnetic structures in crystals. *J. Magn. Magn. Mater.* 12:239–48
9. Izyumov YA, Naish VE, Ozerov RP. 1991. *Neutron Diffraction of Magnetic Materials*. Dordrecht, Neth.: Kluwer Acad.
10. Izyumov YA, Naish VE, Syromiatnikov VN. 1979. Symmetry analysis in neutron diffraction studies of magnetic structures: 2. Changes in periodicity at magnetic phase transitions. *J. Magn. Magn. Mater.* 12:249–61
11. Izyumov YA, Naish VE, Petrov SB. 1979. Symmetry analysis in neutron diffraction studies of magnetic structures: 3. An example: the magnetic structure of spinels. *J. Magn. Magn. Mater.* 13:267–74
12. Rodríguez-Carvajal J. 1993. Recent advances in magnetic structure determination by neutron powder diffraction. *Physica B* 192:55–69
13. Wills AS. 2000. A new protocol for the determination of magnetic structures using simulated annealing and representational analysis (SARA*h*). *Physica B* 276–78:680–81
14. Sikora W, Białas F, Pytlik L. 2004. MODY: a program for calculation of symmetry-adapted functions for ordered structures in crystals. *J. Appl. Crystallogr.* 37:1015–19
15. Dul M, Lesniewska B, Oles A, Pytlik L, Sikora W. 1997. Computer database of magnetic structures determined by neutron diffraction. *Physica B* 234–36:790–91
16. Schmid H. 2008. Some symmetry aspects of ferroics and single phase multiferroics. *J. Phys. Condens. Matter* 20:434201
17. Fiebig M. 2005. Revival of the magnetoelectric effect. *J. Phys. D* 38:R123–52

18. Johnson RD, Radaelli PG. 2014. Diffraction studies of multiferroics. *Annu. Rev. Mater. Res.* 44:269–98
19. Kimura T. 2007. Spiral magnets as magnetoelectrics. *Annu. Rev. Mater. Res.* 37:387–413
20. Hall SR, Allen FH, Brown ID. 1991. The Crystallographic Information File (CIF): a new standard archive file for crystallography. *Acta Crystallogr. Sect. A* 47:655–85
21. Int. Union Crystallogr. 2015. *Commission on Magnetic Structures.* **http://www.iucr.org/iucr/commissions/magnetic-structures**
22. Bilbao Crystallogr. Serv. 2014. MAGNDATA: a collection of magnetic structures with portable cif-type files. *Bilbao Crystallographic Server.* **http://www.cryst.ehu.es/magndata/**
23. Aroyo MI, Perez-Mato JM, Capillas C, Kroumova E, Ivantchev S, et al. 2006. Bilbao Crystallographic Server: I. Databases and crystallographic computing programs. *Z. Krist.* 221 1:15–27
24. Aroyo MI, Kirov A, Capillas C, Perez-Mato JM, Wondratschek H. 2006. Bilbao Crystallographic Server: II. Representations of crystallographic point groups and space groups. *Acta Crystallogr. Sect. A* 62:115–28
25. Glazer AM, Aroyo MI, Authier A. 2014. Seitz symbols for crystallographic symmetry operations. *Acta Crystallogr. Sect. A* 70:300–2
26. Wondratschek H, Müller U, eds. 2011. *International Tables for Crystallography*, Vol. A1: *Symmetry Relations Between Space Groups*. Dordrecht, Neth.: Kluwer Acad.
27. Momma K, Izumi F. 2011. *VESTA 3* for three-dimensional visualization of crystal, volumetric and morphology data. *J. Appl. Crystallogr.* 44:1272–76
28. Hanson R. 2013. *Jmol: an open-source Java viewer for chemical structures in 3D*. **http://www.jmol.org/**
29. Litvin DB. 2013. *Magnetic Group Tables: 1-, 2- and 3-Dimensional Magnetic Subperiodic Groups and Magnetic Space Groups*. Chester, UK: Int. Union Crystallogr. **http://www.iucr.org/publ/978-0-9553602-2-0**
30. Hahn T, ed. 2002. *International Tables for Crystallography*, Vol. A: *Space-Group Symmetry*. Dordrecht, Neth.: Kluwer Acad. 5th ed.
31. Opechowski W, Guccione R. 1965. Magnetic symmetry. In *Magnetism*, Vol. II, Part A, ed. GT Rado, H Suhl, pp. 105–65. New York: Academic
32. Belov NV, Neronova NN, Smirnova TS. 1957. Shubnikov groups. *Sov. Phys. Crystallogr.* 2:311–22
33. Stokes HT, Campbell BJ. 2011. ISO-MAG: table of magnetic space groups. *ISOTROPY Software Suite.* **http://iso.byu.edu**
34. Gallego SV, Tasci ES, de la Flor G, Perez-Mato JM, Aroyo MI. 2012. Magnetic symmetry in the Bilbao Crystallographic Server: a computer program to provide systematic absences of magnetic neutron diffraction. *J. Appl. Crystallogr.* 45:1236–47
35. Lee N, Vecchini C, Choi YJ, Chapon LC, Bombardi A, et al. 2013. Giant tunability of ferroelectric polarization in $GdMn_2O_5$. *Phys. Rev. Lett.* 110:137203
36. FIZ Karlsruhe. 2014. *ICSD: Inorganic Crystal Structure Database*. Eggenstein-Leopoldshafen, Ger. **http://icsd.fiz-karlsruhe.de**
37. Kagomiya I, Kohn K, Uchiyama T. 2002. Structure and ferroelectricity of RMn_2O_5. *Ferroelectrics* 280:131–43

38. Bilbao Crystallogr. Serv. 2014. IDENTIFY GROUP: identification of a space group from a set of generators in an arbitrary setting. *Bilbao Crystallographic Server.* **http://www.cryst.ehu.es/cryst/identify_group**
39. Bilbao Crystallogr. Serv. 2014. IDENTIFY MAGNETIC GROUP: identification of a magnetic space group from a set of generators in an arbitrary setting. *Bilbao Crystallographic Server.* **http://www.cryst.ehu.es/cryst/identify_mgroup**
40. Doubrovsky C, André G, Gukasov A, Auban-Senzier P, Pasquier CR, et al. 2012. Magnetic phase transitions in $PrMn_2O_5$: Importance of ion-size threshold size effects in RMn_2O_5 compounds (*R* = rare earth). *Phys. Rev. B* 86:174417
41. Stokes HT, Campbell BJ. 2014. ISOCIF: create or modify CIF files. *ISOTROPY Software Suite*. **http://iso.byu.edu**
42. Bilbao Crystallogr. Serv. 2014. STRCONVERT: structure data converter & editor. *Bilbao Crystallographic Server.* **http://www.cryst.ehu.es/cryst/strconvert**
43. Stokes HT, Campbell BJ. 1998. FINDSYM: identify the space group of a crystal, given the positions of the atoms in a unit cell. *ISOTROPY Software Suite*. **http://iso.byu.edu**
44. Kresse G, Furthmüller J. 1996. Efficient iterative schemes for ab initio total-energy calculations using a plane-wave basis set. *Phys. Rev. B* 54:11169–86
45. Bilbao Crystallogr. Serv. 2014. MVISUALIZE: 3D visualization of magnetic structures with Jmol. *Bilbao Crystallographic Server.* **http://www.cryst.ehu.es/cryst/mvisualize**
46. Bilbao Crystallogr. Serv. 2013. MAXMAGN: maximal magnetic space groups for a given a propagation vector and resulting magnetic structural models. *Bilbao Crystallographic Server.* **http://www.cryst.ehu.es/cryst/maxmagn**
47. Petricek V, Dusek M, Palatinus L. 2006. *Jana2006: The Crystallographic Computing System*. **http://jana.fzu.cz/**
48. Petříček V, Dušek M, Palatinus L. 2014. Crystallographic computing system JANA2006: general features. *Z. Krist.* 229(5):345–52
49. Muñoz A, Casais MT, Alonso JA, Martinez-Lope MJ, Martinez JL, et al. 2001. Complex magnetism and magnetic structures of the metastable $HoMnO_3$ perovskite. *Inorg. Chem.* 40:1020–28
50. Lee N, Choi YJ, Ramazanoglu M, Ratcliff W, Kiryukhin V, Cheong SW. 2011. Mechanism of exchange striction of ferroelectricity in multiferroic orthorhombic $HoMnO_3$ single crystals. *Phys. Rev. B* 84:020101
51. Fu Z, Zheng Y, Xiao Y, Bedanta S, Senyshyn A, et al. 2013. Coexistence of magnetic order and spin-glass-like phase in the pyrochlore antiferromagnet $Na_3Co(CO_3)_2Cl$. *Phys. Rev.* 87:214406
52. Bilbao Crystallogr. Serv. 2014. k-SUBGROUPSMAG: magnetic subgroups consistent with some given propagation vector(s) or a supercell. *Bilbao Crystallographic Server.* **http://www.cryst.ehu.es/cryst/k_subgroupsmag**
53. Ressouche E, Kernavanois N, Regnault LP, Henry JY. 2006. Magnetic structures of the metal monoxides NiO and CoO re-investigated by spherical neutron polarimetry. *Physica B* 385–86:394–97
54. Herrmann-Ronzaud D, Burlet P, Rossat-Mignod J. 1978. Equivalent type-II magnetic structures: CoO, a collinear antiferromagnet. *J. Phys. C: Solid State Phys.* 11:2123–37
55. Jauch W, Reehuis M, Bleif HJ, Kubanek F, Pattison P. 2001. Crystallographic symmetry and magnetic structure of CoO. *Phys. Rev. B* 64:052102

56. Bilbao Crystallogr. Serv. 2014. MAGMODELIZE: magnetic structure models for any given magnetic symmetry. *Bilbao Crystallographic Server.* **http://www.cryst.ehu.es/cryst/magmodelize**
57. Zhao LL, Wu S, Wang JK, Hodges JP, Broholm C, Morosan E. 2013. Quasi-two-dimensional noncollinear magnetism in the Mott insulator $Sr_2F_2Fe_2OS_2$. *Phys. Rev. B* 87:020406
58. Aroyo MI, Orobengoa D, de la Flor G, Perez-Mato JM, Wondratschek H. 2014. Brillouin-zone databases on the Bilbao Crystallographic Server. *Acta Crystallogr. Sect. A* 70:126–37
59. Chattopadhyay T, Brown PJ, Roessli B, Stepanov AA, Barilo SN, Zhigunov DI. 1992. Magnetic ordering of Cu in Gd_2CuO_4. *Phys. Rev. B* 46:5731–34
60. Perez-Mato JM, Aroyo MI, García A, Blaha P, Schwarz K, et al. 2004. Competing structural instabilities in the ferroelectric Aurivillius compound $SrBi_2Ta_2O_9$. *Phys. Rev. B* 70:214111
61. Etxebarria I, Perez-Mato JM, Boullay P. 2010. The role of trilinear couplings in the phase transitions of Aurivillius compounds. *Ferroelectrics* 401:17–23
62. Ghosez P, Triscone JM. 2011. Multiferroics: coupling of three lattice instabilities. *Nat. Mater.* 10:269–70
63. Quintero M, Morocoima M, Guerrero E, Ruiz J. 1994. Temperature variation of lattice parameters and thermal expansion coefficients of the compound $MnGa_2Se_4$. *Phys. Status Solidi A* 146:587–93
64. Opechowski W, Dreyfus T. 1971. Classifications of magnetic structures. *Acta Crystallogr. Sect. A* 27:470–84
65. Opechowski W. 1971. Analyse des structures magnétiques et théorie des groupes: on two classifications of magnetic structures. *J. Phys. Colloques* 32:C1–457–61
66. Opechowski W, Litvin DB. 1977. Error corrections corrected, remarks on Bertaut's article “Simple derivation of magnetic space groups”. *Ann. Phys.* 2:121–25
67. Campbell BJ, Stokes HT, Tanner DE, Hatch DM. 2006. *ISODISPLACE*: a web-based tool for exploring structural distortions. *J. Appl. Crystallogr.* 39:607–14. **http://stokes.byu.edu/isodistort.html**
68. Ascher E. 1977. Permutation representations, epikernels and phase transitions. *J. Phys. C Solid State Phys.* 10:1365–77
69. de Wolff PM. 1974. The pseudo-symmetry of modulated crystal structures. *Acta Crystallogr. Sect. A* 30:777–85
70. Janner A, Janssen T. 1980. Symmetry of incommensurate crystal phases. II. Incommensurate basic structure. *Acta Crystallogr. Sect. A* 36:408–15
71. Janssen T, Janner A. 2014. Aperiodic crystals and superspace concepts. *Acta Crystallogr. Sect. B* 70:617–51
72. Janssen T, Janner A, Looijenga-Vos A, de Wolff PM. 2006. Incommensurate and commensurate modulated structures. In *International Tables for Crystallography*, Vol. C: *Mathematical, Physical and Chemical Tables*, ed. E. Prince, pp. 907–55. Dordrecht, Neth.: Kluwer Acad.
73. Janssen T, Chapuis G, de Boissieu M. 2007. *Aperiodic Crystals: From Modulated Phases to Quasicrystals*. IUCr Monogr. Crystallogr. No. 20. Oxford, UK: Oxford Univ. Press
74. Van Smaalen S. 2007. *Incommensurate Crystallography.* IUCr Monogr. Crystallogr. No. 21. Oxford, UK: Oxford Univ. Press

75. Schobinger-Papamantellos P, Janssen T. 2006. The symmetry of the incommensurate magnetic phase of $ErFe_4Ge_2$. *Z. Krist.* 221:732–34
76. Schönleber A, van Smaalen S, Palatinus L. 2006. Structure of the incommensurate phase of the quantum magnet TiOC. *Phys. Rev. B* 73:214410
77. Slawinski W, Przenioslo R, Sosnowska I, Bieringer M, Margiolaki I, Suard E. 2009. Modulation of atomic positions in $CaCu_xMn_{7-x}O_{12}$ (x < 0.1). *Acta Crystallogr. Sect. B* 65:535–42
78. Meddar L, Josse M, Deniard P, La C, Andre G, et al. 2009. Effect of nonmagnetic substituents Mg and Zn on the phase competition in the multiferroic antiferromagnet $MnWO_4$. *Chem. Mater.* 21:5203–14
79. Ribeiro JL, Vieira LG. 2010. Landau model for the phase diagrams of the orthorhombic rare-earth manganites $RMnO_3$ (R = Eu, Gd, Tb, Dy, Ho). *Phys. Rev. B* 82:064410
80. Ribeiro JL. 2010. Symmetry, incommensurate magnetism and ferroelectricity: the case of the rare-earth manganites $RMnO_3$. *J. Phys. Conf. Ser.* 226:012013
81. Janoschek M, Fischer P, Schefer J, Roessli B, Pomjakushin V, et al. 2010. Single magnetic chirality in the magnetoelectric $NdFe_3(^{11}BO_3)_4$. *Phys. Rev. B* 81:094429
82. Ribeiro JL, Perez-Mato JM. 2011. Symmetry and magnetic field driven transitions in the 2D triangular lattice compound $RbFe(MoO_4)_2$. *J. Phys. Condens. Matter* 23:446003
83. Abakumov AM, Tsirlin AA, Perez-Mato JM, Petříček V, Rosner H, et al. 2011. Spiral ground state against ferroelectricity in the frustrated magnet $BiMnFe_2O_6$. *Phys. Rev. B* 83:214402
84. Urcelay-Olabarria I, Perez-Mato JM, Ribeiro JL, García-Muñoz JL, Ressouche E, et al. 2013. Incommensurate magnetic structures of multiferroic $MnWO_4$ studied within the superspace formalism. *Phys. Rev. B* 87:014419
85. Terada N, Khalyavin DD, Perez-Mato JM, Manuel P, Prabhakaran D, et al. 2014. Magnetic and ferroelectric orderings in multiferroic α-$NaFeO_2$. *Phys. Rev. B* 89:184421
86. Prokeš K, Petříček V, Ressouche E, Hartwig S, Ouladdiaf B, et al. 2014. (3 + 1)-dimensional crystal and antiferromagnetic structures in CeRuSn. *J. Phys. Condens. Matter* 26:122201
87. Orlandi F, Righi L, Ritter C, Pernechele C, Solzi M, et al. 2014. Superspace application on magnetic structure analysis of the Pb_2MnWO_6 double perovskite system. *J. Mater. Chem. C* 2:9215–23
88. Herpin A, Meriel P. 1961. Étude de l'antiferromagnétisme helicoidal de $MnAu_2$ par diffraction de neutrons. *J. Phys. Radium.* 22:337–48
89. Brown ID, McMahon B. 2002. CIF: the computer language of crystallography. *Acta Crystallogr. Sect. B* 58:317–24
90. Laffargue D, Fourgeot F, Bourée F, Chevalier B, Roisnel T, et al. 1996. The antiferromagnetic-ferromagnetic transition of $Ce_2Pd_{2.04}Sn_{0.96}$ stannide. *Solid State Commun.* 100:575–79
91. Rodríguez-Carvajal J, Bourée F. 2012. Symmetry and magnetic structures. *EPJ Web Conf.* 22:00010
92. Biffin A, Johnson RD, Choi S, Freund F, Manni S, et al. 2014. Unconventional magnetic order on the hyperhoneycomb Kitaev lattice in *β*-Li_2IrO_3: full solution via magnetic resonant X-ray diffraction. *Phys. Rev. B* 90:205116

93. Kenzelmann M, Lawes G, Harris AB, Gasparovic G, Broholm C, et al. 2007. Direct transition from a disordered to a multiferroic phase on a triangular lattice. *Phys. Rev. Lett.* 98:267205

ACRONYMS AND DEFINITIONS

MSG: Magnetic space group, also called Shubnikov group
MSSG: Magnetic superspace supergroup
Irrep: Irreducible representation of a group
Representation method: Method to parameterize and determine magnetic structures using basis functions adapted to the irreps of the space group of the paramagnetic phase.
CIF: Crystallographic information file. Standard text file format for crystallographic data exchange developed and sponsored by the International Union of Crystallography (IUCr)
magCIF: extension of the crystallographic information file format to magnetic structures (under development)
Grey group: MSG of a paramagnetic phase; it includes the time reversal operation.
Effective space group *H*: Space group that defines the symmetry constraints on the atomic positions of a commensurate magnetic structure. It is directly derived from the MSG of the structure.
BNS notation: standard notation of a MSG where the unit cell used defines the lattice periodicity of the magnetic structure.
OG notation: standard notation for a MSG where the unit cell used is the one of the effective space group *H*.
Antitranslations: Translation operations combined with time reversal
k-maximal magnetic symmetry: magnetic symmetry for a given propagation vector ***k***, which is a subgroup of the grey group of the paramagnetic phase with no intermediate supergroup also compatible with ***k***.

ANEXO D

Perez-Mato J. M., Gallego S. V., Elcoro L., Tasci E., Aroyo M. I. *J. Phys. Condens. Matter* **28** 286001 (2015)

Symmetry conditions for type II multiferroicity in commensurate magnetic structures

J.M. Perez-Mato[1], S. V. Gallego[1], L. Elcoro[1], E. Tasci[2] and M.I. Aroyo[1]

[1]Departamento de Fisica de la Materia Condensada, Facultad de Ciencia y Tecnología, Universidad del País Vasco (UPV/EHU), Apartado 644, 48080 Bilbao, Spain

[2]Department of Physics, Middle East Technical University, 06800 Ankara, Turkey

E-mail: jm.perez-mato@ehu.es

Abstract: Type II multiferroics are magnetically ordered phases that exhibit ferroelectricity as a magnetic induced effect. We show that in *single-k* magnetic phases the presence in the paramagnetic phase of non-symmorphic symmetry combined with some specific type of magnetic propagation vector can be sufficient for the occurrence of this type of multiferroic behaviour. Other symmetry scenarios especially favourable for spin driven multiferroicity are also presented. We review and classify known type II multiferroics under this viewpoint. In addition, some other magnetic phases which due to their symmetry properties can exhibit type II multiferroicity are pointed out.

Keywords: Multiferroics, Symmetry of magnetic structures, Bilbao Crystallographic Server

1. Introduction

The term multiferroicity, originally designed for systems having simultaneously at least two different primary ferroic orders (ferromagnetism, ferroelectricity or ferroelasticity) [1], is presently being used in a quite different sense, namely as synonym for the simultaneous presence of any kind of magnetic ordering and ferroelectricity. If the two phenomena are caused by independent physical mechanisms with different transitions temperatures, one speaks of type I multiferroicity, while the materials where the ferroelectricity is induced by the magnetic order are called type II multiferroics [2, 3].

In type II multiferroics the induction of ferroelectricity by the ordered spins has been attributed at the atomic level to different mechanisms depending on the material [4]. But in all cases the ferroelectric polarization can be considered a side effect of the symmetry break caused by the magnetic ordering. Type II multiferroics can be considered to be part of the so-called improper ferroelectrics, where the spontaneous polarization is a secondary degree of freedom unclenched by the symmetry break. Its non-zero value originates in its symmetry-allowed linear coupling with some power of the actual order parameter [5]. According to Neumann's principle [6] any magnetic

ordering in an insulator that breaks the symmetry from a non-polar to a polar magnetic point group can have some improper ferroelectricity. Therefore magnetic phases appropriate for type II multiferroicity can in principle be identified by just checking the symmetry break accompanying the magnetic ordering [7]. Of course, the magnitude of the expected spontaneous polarization cannot be predicted from symmetry considerations, and it may be very weak. But to our knowledge the majority of insulating magnetic phases fulfilling a non-polar/polar symmetry break have evidenced, when investigated, some observable ferroelectricity.

Most of the reported magnetic structures are 'single-*k*' magnetic phases. This means that the Fourier spectrum of their magnetic spin arrangement includes either a single wave vector, the so-called propagation vector, and in some cases odd harmonics of it. One can consider single-*k* structures both those where **k** and −**k** are equivalent through a reciprocal lattice vector of the parent phase, and those where both **k** and −**k** are necessarily present in the magnetic spin wave as distinct non-equivalent wave vectors. The propagation vector, easily observable in diffraction experiments, partially determines the magnetic symmetry and drastically reduces the possible symmetries of a single-*k* magnetic structure. In this context, we have recently developed computer tools to determine and explore all possible symmetry breaks consistent with a known commensurate propagation vector. These tools are freely available online at the Bilbao Crystallographic Server (www.cryst.ehu.es) [8]. Using the results of the systematic application of these programs to different examples, we present here symmetry conditions for the parent space group and the magnetic propagation vector that can lead to a break into polar symmetry. We show that the knowledge of the propagation vector is often sufficient to infer a high probability of (and in some cases to predict univocally) a polar symmetry for the magnetic ordering. Thus, elementary data as parent space group, Wyckoff positions of magnetic atoms and propagation vector permit to identify those magnetic materials having favourable conditions for being type II multiferroics. In particular, we demonstrate that a non-symmorphic space group symmetry of the paramagnetic phase in conjunction with some propagation vectors is one of these favourable scenarios. The commensurate type II multiferroics reported up to now are briefly reviewed under this perspective. Finally, a set of reported magnetic structures, which fulfill the symmetry conditions for being type II multiferroics, but have not been yet investigated from this viewpoint, are pointed out.

2. Polar magnetic symmetries due to the incompatibility of the propagation vector with some screw or glide operation.

The propagation vector of a single-*k* commensurate magnetic ordering defines the set of translations and antitranslations that are maintained by the spin arrangement, i.e. it determines the *black&white* lattice of its magnetic space group (MSG), also called Shubnikov group [8–10]. This MSG must be a subgroup of the grey MSG of the paramagnetic phase, and in general its consistency with this *k*-defined lattice reduces the number of possible MSGs to a small finite set. The enumeration and identification of all these possible MSGs is a well-defined bounded mathematical problem. The program *k*-SUBGROUPSMAG at the Bilbao Crystallographic Server solves it for any parent space group and any reasonable commensurate propagation vector [8]. The

possible magnetic symmetries for a given propagation vector are obtained and classified in a hierarchical way according to their group–subgroup relations, and then, the corresponding models for the magnetic structure can be derived using other programs of the server [8].

It is an empirical fact that most of the reported magnetic structures fulfill a principle of minimal symmetry break (or maximal magnetic symmetry), in the sense that they tend to keep as much symmetry as possible, and therefore their symmetry is usually given by one of the larger subgroups of the grey parent symmetry group that are possible for the active propagation vector. Therefore, the group–subgroup hierarchy of possible magnetic symmetries obtained with *k*-SUBGROUPSMAG can be considered a descending hierarchy for the probability of being physically realised. The uppermost subgroups, what we call *k*-maximal symmetries [8], can be taken as the most probable symmetries for the magnetic structure. The assumption of a *k*-maximal symmetry is closely related with the assumption of a single active representation (irrep) for the magnetic order, but they are not equivalent (see [8] for a detailed discussion of their relation).

Through the systematic exploration of the possible magnetic symmetries for a given propagation vector one can observe some general conditions that favour a non-polar/polar symmetry break. Figure 1(a) for instance summarizes the possible MSGs for the case of a parent space group *P2₁/c* and a magnetic propagation vector (1/2,0,1/2). From the two possible *k*-maximal symmetries one of them breaks the inversion center and is polar along the monoclinic axis. This contrasts with the results obtained for the same propagation vector, but with parent space group *P2₁/m* (for the magnetic atom lying at the origin) depicted in figure 1(b), where all *k*-maximal MSGs are centrosymmetric. One can conclude that in the case of a magnetic phase with *P2₁/c* parent symmetry and propagation vector (1/2,0,1/2), the possibility of having a polar phase, with the polar direction along *b*, is high, while in the case of the *P2₁/m* parent symmetry, the inversion center cannot be broken. In fact we will see below that in the first case, the centrosymmetric subgroup does not allow magnetic ordering of all magnetic atoms, if those sit at the special Wyckoff positions *2a*, *2b*, *2c* or *2d*, and therefore in these cases, the break into polar symmetry is obliged for a full magnetic order.

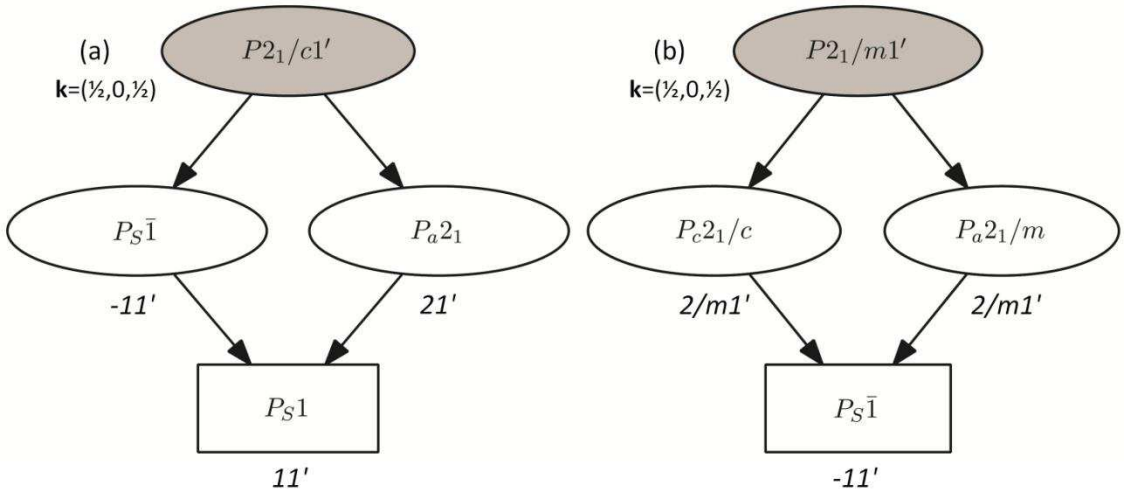

Figure 1

Possible magnetic symmetries resulting from a magnetic ordering having propagation vector (1/2,0,1/2) for a parent structure with space group $P2_1/c$ (a) or $P2_1/m$ (b) and with the magnetic atoms at the Wyckoff position *2a* (origin). The special position of the magnetic atoms implies a restriction with respect to a more general graph only in (b). *k*-compatible symmetries are shown as subgroups of the parent grey MSG using standard BNS labels [8–10]. Only one MSG for each equivalent conjugacy class is shown. Magnetic point groups are indicated below each MSG. (Obtained with *k*-SUBGROUPSMAG [8]).

This simple example shows how the knowledge of the propagation vector can be determinant for assessing the possibility of type II multiferroicity. In this example, it is the incompatibility of the wave vector with the *c* glide plane that makes the difference between the two cases. The incompatibility of the magnetic wave vector with some glide plane or some screw axes is in fact one of the general scenarios that favour the existence of a non-polar/polar symmetry break. This incompatibility can be explained in the following way:

Consider a spin arrangement with a commensurate propagation vector **k**, such that $n\mathbf{k}$ is a reciprocal lattice vector of the paramagnetic phase, with n being an even integer. Such type of magnetic order maintains the lattice translations $\{1|\mathbf{L}\}$ of the paramagnetic phase that satisfy $\exp(i2\pi\mathbf{k}\cdot\mathbf{L}) = 1$, but it also keeps the antitranslations $\{1'|\mathbf{L}\}$ of the grey symmetry of the paramagnetic phase that fulfill $\exp(i2\pi\mathbf{k}\cdot\mathbf{L}) = -1$ (for the employed notation see [7, 8]). The MSG describing the symmetry of the magnetic phase must be consistent with this set of translations and antitranslations. If it were not the case, the magnetic arrangement could not be explained as a magnetic ordering with a single propagation vector [8]. This implies strong restrictions for glide planes or screw rotations. Let us take for instance any pair of symmetry operations, say $\{\mathbf{R}|\mathbf{t}\}$ and $\{\mathbf{R}'|\mathbf{t}\}$, of the parent grey MSG associated with the paramagnetic phase, and that only differ by the combination or not with time reversal. If m is the order of the operation **R**, then $\{\mathbf{R}|\mathbf{t}\}^m = \{1|\mathbf{L}\}$, with **L** a lattice vector of the paramagnetic phase. If $\{\mathbf{R}|\mathbf{t}\}$ is a glide or a screw operation, **t** is necessarily different from zero, and also **L**, for any possible **t**. Therefore the preservation of any operation $\{\mathbf{R}|\mathbf{t}\}$ would also necessarily imply the maintenance of the lattice translation $\{1|\mathbf{L}\}$, while if instead $\{\mathbf{R}'|\mathbf{t}\}$ is kept, then $\{1|\mathbf{L}\}$ or $\{1'|\mathbf{L}\}$ should also be part of the MSG, if m is even or odd, respectively. Thus, both symmetry operations $\{\mathbf{R}|\mathbf{t}\}$ and $\{\mathbf{R}'|\mathbf{t}\}$ are necessarily lost if m is even and if the **k**-vector of the magnetic ordering is such that $\exp(i2\pi\mathbf{k}\cdot\mathbf{L}) \neq +1$ Similarly, both symmetry operations $\{\mathbf{R}|\mathbf{t}\}$ and $\{\mathbf{R}'|\mathbf{t}\}$ are necessarily lost if m is odd, and $\exp(i2\pi\mathbf{k}\cdot\mathbf{L}) \neq +1$ or -1. Hence, for example, the screw rotations $\{2_{001}|0\ 0\ 1/2\}$ and $\{2'_{001}|0\ 0\ 1/2\}$ (m even) are not compatible with a propagation vector **k** = (0 0 1/2), and the symmetry operations $\{3_{001}|0\ 0\ 1/3\}$ and $\{3'_{001}|0\ 0\ 1/3\}$ (m odd) are not compatible with a propagation vector **k** = (0 0 1/3). This incompatibility can occur for all possible translations **t** in the set of operations $\{\mathbf{R}|\mathbf{t}\}$ and $\{\mathbf{R}'|\mathbf{t}\}$ and in this case a point group symmetry reduction is obliged, with the disappearance of the operations **R** and **R**' from the resulting magnetic symmetry. The space inversion cannot be lost by this mechanism, but it can become incompatible with the presence of other symmetry operations, which, if alternatively kept, can give place to polar symmetries. This incompatibility between wave vector and some rotational operations can only happen for operations with an intrinsic non-zero translations, i.e. glide and screw operations.

Coming back to our example, i.e. a magnetic ordering with propagation vector having k_z = 1/2 on a parent phase with space group $P2_1/c$ (*b* unique axis), this *k*-vector implies the preservation of the antitranslation {1'|0,0,1} and the translation {1|0,0,2} with a duplication of the unit cell along *c*, and the breaking of the lattice translation {1|0,0,1}. On the other hand, the grey group corresponding to the paramagnetic phase includes a *c* glide plane and its combination with time reversal, i.e. the operations $\{m_{010}|0,1/2,1/2\}$ and $\{m'_{010}|0,1/2,1/2\}$. As $\{m_{010}|0,1/2,1/2\}^2 = \{m'_{010}|0,1/2,1/2\}^2 = \{1|0,0,1\}$ (see figure 2), the preservation of any of the two operations is incompatible with such propagation vector. The same argument is valid for the operations $\{m_{010}|0,1/2,3/2\}$ and $\{m'_{010}|0,1/2,3/2\}$, etc. Therefore the glide plane is necessarily broken and the system can either keep the two fold axis or the inversion center, but not both. Thus, the possible MSGs are very limited, as shown in figure 1(a).

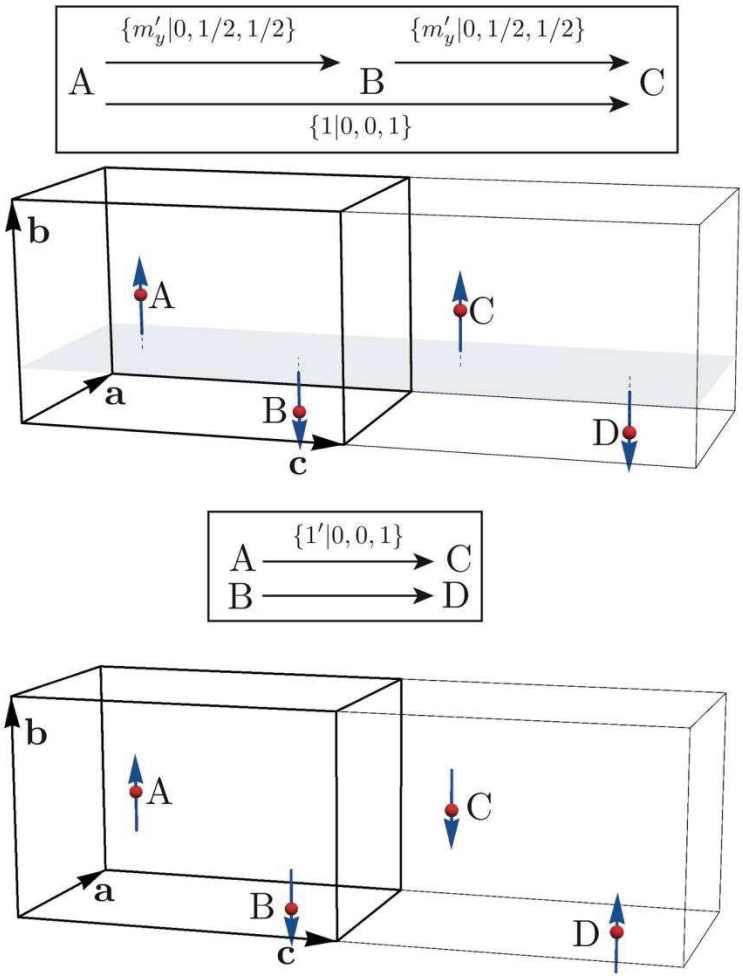

Figure 2

Simple scheme showing the incompatibility of a primed *c* glide plane with a magnetic propagation vector **k** having k_z = 1/2. This propagation vector forces the presence of the *antitraslation* {1'|0 0 1} in the parent setting, i.e. opposite spins in contiguous parent unit cells, while the existence of the glide plane is only compatible with equal spins in subsequent unit cells.

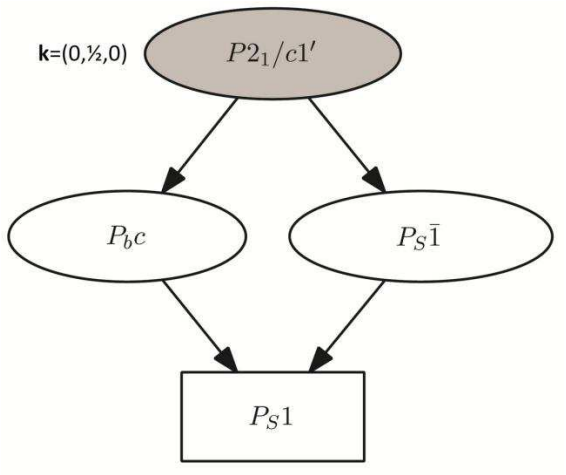

Figure 3
Possible magnetic symmetries resulting from a magnetic ordering with propagation vector (0,1/2,0) for a parent structure with space group *P2₁/c*. *k*-compatible symmetries are shown as subgroups of the parent grey MSG using standard BNS labels. Only one MSG for each equivalent conjugacy class is shown (Obtained with *k*-SUBGROUPSMAG [8]).

A similar situation occurs for the propagation vector **k** = (0,1/2,0) and the same parent space group. In this case, it is the two fold screw rotation that becomes incompatible with the propagation vector, and again only two possible *k*-maximal symmetries are possible (see figure 3), one of them being polar on the *ac* plane. This scenario, favourable for multiferroicity, with an unavoidable symmetry break of the point group symmetry, contrasts with the case **k** = (1/2,0,0). This wave vector does not have any incompatibility with the screw or glide operations and can therefore keep the whole point group symmetry of the parent phase. As shown in figure 4, the set of possible magnetic symmetries is then much more numerous, with the four possible *k*-maximal symmetries keeping the centrosymmetry; actually they maintain the whole point group, *2/m1*', of the parent phase, and if the magnetic atom lies at a centrosymmetric site, the centrosymmetry of the structure is necessarily maintained for any arbitrary spin configuration.

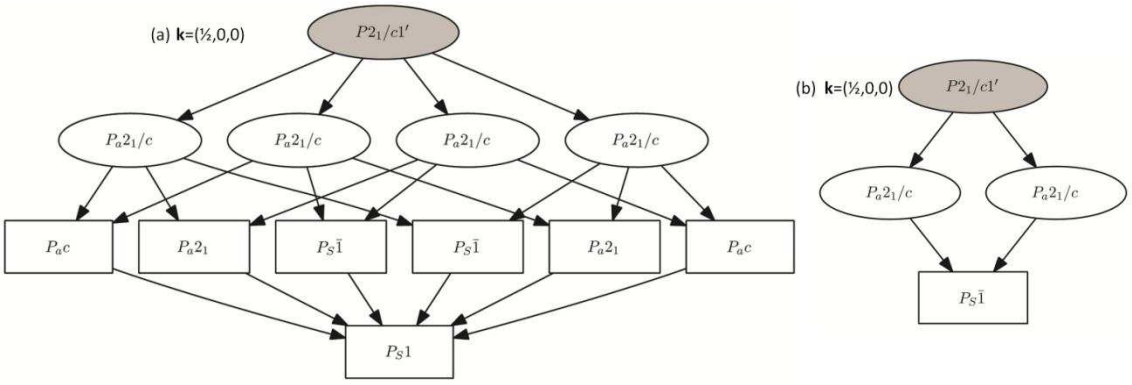

Figure 4
(a) Possible magnetic symmetries resulting from a magnetic ordering having propagation vector (1/2,0,0) for a parent structure with space group *P2₁/c*. *k*-compatible symmetries are shown as subgroups of the parent grey MSG using standard BNS labels. Some of the subgroups correspond to the same MSG type and have identical labels, but represent different inequivalent subgroups. (b) The same as (a) but for structures with the magnetic atoms at either the special Wyckoff position *2a*, *2b*, *2c* or *2d* (Obtained with *k*-SUBGROUPSMAG [8]).

From the viewpoint of representation analysis, symmetry breaks with respect to the point-group symmetry of the propagation vector **k** of the magnetic ordering may be obliged in the case that the associated small irrep is multidimensional. Even for very low symmetries, small irreps for some wave vectors are necessarily multidimensional if the space group is non-symmorphic. This is what happens in the example above, where one can see that the small irreps of $P2_1/c$ with wave vector (0,1/2,0) or (0,0,1/2) are 2D, while those for (1/2,0,0) are 1D. The symmetry argument using MSGs is however more general, and includes for instance, cases as **k** = (0,1/4,0), for which the small irreps are 1D for example both for a symmorphic *P2/m* or a non-symmorphic $P2_1/c$ parent space group. Because of the reasons explained above, if the parent space group is *P2/m*, the point-group symmetry *2/m* of the pair (**k**, −**k**) can be kept in the magnetic phase, but if instead the parent space group is $P2_1/c$ this point-group symmetry is necessarily broken.

3. Effect of magnetic atoms at special Wyckoff positions. Monoclinic and orthorhombic examples.

The fact that the magnetic atoms often lie at special Wyckoff positions of the paramagnetic structure is an additional factor that can favour a polar magnetic symmetry. If for instance, the magnetic atom sits on a site with point group symmetry *−1* in the paramagnetic phase (*−11'* considering its full magnetic symmetry), this site can split into orbits with local symmetry *−1* and *−1'*, if the inversion operation is maintained in the MSG. The magnetic moment must be zero at sites with *−1'* symmetry, and therefore keeping space inversion will not be compatible with the presence of magnetic order at all magnetic sites. Therefore, full magnetic order is only compatible with the non-centrosymmetric arrangement with the alternative polar symmetry (see for instance figure 3 of [8] where the particular case of $HoMnO_3$ is graphically summarized). This is what happens also in the example above with parent space group $P2_1/c$, where only special positions with site symmetry *−1* exist. Table 1 lists the possible *k*-maximal symmetries for all parent P-lattice centrosymmetric monoclinic space groups and the most frequent propagation vectors (i.e. symmetry points at the border of the Brillouin zone), with the resulting constraints for special Wyckoff positions.

Table 1
Possible maximal magnetic point-group symmetries resulting from magnetic orderings on a parent structure with a P-lattice centrosymmetric monoclinic space group (first column) and having as propagation vector a symmetry point at the border of the Brillouin zone.

SG	**Y (1/2,0,0)**	**Z (0,1/2,0)** **C (1/2,1/2,0)**	**B (0,0,1/2)** **A (1/2,0,1/2)**	**D (0,1/2,1/2)** **E (1/2,1/2,1/2)**
P2/m (10)	-	-	-	-
$P2_1/m$ (11)	-	***m1'*** (nc: *2e*) *-11'* (≠*2a*,*2b*,*2c*,*2d*)	-	***m1'*** (nc: *2e*) *-11'* (≠*2a*,*2b*,*2c*,*2d*)
P2/c (13)	-	-	***21'*** (nc: *2e*,*2f*) *-11'* (≠*2a*,*2b*,*2c*,*2d*)	***21'*** (nc: *2e*,*2f*) *-11'* (≠*2a*,*2b*,*2c*,*2d*)
$P2_1/c$ (14)	-	***m1'***	***21'***	*-11'*

-11' (≠*2a*,*2b*,*2c*,*2d*)	*-11'* (≠*2a*,*2b*,*2c*,*2d*)

Note: Only the cases where the maximal point groups are lower than the one of the parent phase (*2/m1*') are indicated. Besides each symmetry, Wyckoff positions that cannot be fully magnetically ordered or cannot order collinearly under it are indicated with the symbols '≠' and 'nc:', respectively. Polar symmetries are highlighted with bold characters. (Results derived using MAXMAGN [8]). Propagation vectors having equal results are indicated in the same column.

One can see that, because of the mentioned *−1*, *−1*' splitting, if space inversion is kept, magnetic atoms at Wyckoff sites *2a*, *2b*, *2c* or *2d*, which have site point-group symmetry *−1*, can only be fully magnetically ordered according to a polar MSG in the case of propagation vectors incompatible with some of the screw or glide operations. In contrast, sites *2e* or *2f*, with site point groups *m1*' or *21*' depending on the space group, split in the case of the polar MSGs into orbits with *m* and *m*' site symmetries (or *2* and *2*'), and therefore magnetic atoms at these sites must have magnetic moments with different directions, precluding a collinear magnetic ordering. One can then infer that for magnetic atoms at these non-centrosymmetric sites, if exchange interaction is dominant, polar symmetry will be unfavourable and the alternative centrosymmetric symmetry, where the spin arrangement can be collinear, is more probable. It should be noticed however that in the case of the parent space group $P2_1/c$, magnetic orderings with propagation vectors either (0,1/2,1/2) or (1/2,1/2,1/2), break both the screw rotation and the glide plane, and the only possible maximal point-group symmetry of any magnetic ordering is reduced to *−11*'. As shown in table 1, in such cases centrosymmetric collinear ordering is also possible for *2a*, *2b*, *2c* or *2d* sites.

From the above consideration it becomes clear that some propagation vectors in conjunction with some non-symmorphic parent space groups, specially if the magnetic atoms sit at some special Wyckoff positions, favour the symmetry break into polar symmetries and therefore the occurrence of type II multiferroicity. Orthorhombic systems are specially favourable for this scenario, and it can indeed be identified in many of the known orthorhombic commensurate type II multiferroics. This is the case for instance of the compounds RMnO$_3$ (R = Ho, Lu), with parent space group *Pnma* and **k** = (1/2,0,0) [11, 12], or the family RMn$_2$O$_5$ (R = Dy, Gd, Pr), with parent space group *Pbam* and **k** = (1/2,0,0) [13, 14], whose symmetry was discussed in [8]. Table 2 lists the possible *k*-maximal magnetic point-group symmetries for three representative orthorhombic non-symmorphic space groups (*Pmma*, *Pbam* and *Pnma*), and a propagation vector at one of the symmetry points of the Brillouin zone. Their compatibility with the Wyckoff positions is also indicated. One can see that as in the monoclinic case, the location of the magnetic atoms at centrosymmetric Wyckoff positions can favour polar magnetic symmetries over centrosymmetric ones, while magnetic atoms at other Wyckoff positions can favour the maintenance of space inversion, if collinear order prevails. For the parent space group *Pmma*, the point-group symmetry reduction, if it exists, is the same for all propagation vectors, with the polarity along *c*. But for the other two parent space groups in table 2, the polar direction depends on the direction of the propagation vector, and can be even extended to the plane *bc* or *ac* (see parent *Pnma* with propagation vector (1/2,1/2,1/2)). Tables 1 and 2 have been derived using MAXMAGN [8]. This program provides for any specific parent structure and any commensurate propagation vector,

the possible *k*-maximal MSGs and the models for the corresponding spin arrangements, with their symmetry constraints, orbit splittings, etc.

Table 2
Possible maximal magnetic point-group symmetries resulting from magnetic orderings on a parent structure with space group *Pmma*, *Pbam* or *Pnma* and having as propagation vector a symmetry point at the border of the Brillouin zone.

SG	X (1/2,0,0)	Y (0,1/2,0)	Z (0,0,1/2)	S (1/2,1/2,0)	U (1/2,0,1/2)	T (0,1/2,1/2)	R (1/2,1/2,1/2)
Pmma (51)	***mm21'*** (nc: *2e*,*2f*,*4k*) *12/m11'* (≠*2a*,*2b*,*2c*,*2d*) (nc: *4g*,*4h*)	-	-	***mm21'*** (nc: *2e*,*2f*,*4k*) *12/m11'* (≠*2a*,*2b*,*2c*,*2d*) (nc: *4g*,*4h*)	***mm21'*** (nc: *2e*,*2f*,*4k*) *12/m11'* (≠*2a*,*2b*,*2c*,*2d*) (nc: *4g*,*4h*)	-	***mm21'*** (nc: *2e*,*2f*,*4k*) *12/m11'* (≠*2a*,*2b*,*2c*,*2d*) (nc: *4g*,*4h*)
Pbam (55)	***m2m1'*** *112/m1'* (≠*4a*,*4b*,*4c*,*4d*) (nc: *4e*,*4f*)	***mm21'*** *112/m1'* (≠*4a*,*4b*,*4c*,*4d*) (nc: *4e*,*4f*)	-	*112/m1'*	***m2m1'*** *112/m1'* (≠*4a*,*4b*,*4c*,*4d*) (nc: *4e*,*4f*)	***2mm1'*** *112/m1'* (≠*4a*,*4b*,*4c*,*4d*) (nc: *4e*,*4f*)	*112/m1'*
Pnma (62)	***mm21'*** *12/m11* (≠*4a*,*4b*)	***2mm1'*** (nc: *4c*) *112/m1'* (≠*4a*,*4b*)	***2mm1'*** *12/m11'* (≠*4a*,*4b*)	***1m11'*** (nc: *4c*) ***1121'*** -11' (≠*4a*,*4b*)	***12/m11'***	***2mm1'*** (nc: *4c*) *2/m111'* (≠*4a*,*4b*)	***m111'*** ***1m11'*** (nc: *4c*) *-11'* (≠*4a*,*4b*)

Note: Only the cases where the maximal point groups are lower than the one of the parent phase (*mmm1'*) are indicated. Wyckoff positions that cannot be fully magnetically ordered or cannot order collinearly under one point-group symmetry are indicated with the symbols '≠' and 'nc:', respectively. The point groups that force polar symmetries for some Wyckoff positions are highlighted with bold characters. (Results derived using MAXMAGN [8]).

4. Dependence of the symmetry break on the non-magnetic atoms

Although the location of the magnetic atoms at special sites can favour a polar symmetry for the magnetic structure, it is important to realise that a fundamental part of the symmetry reduction is sometimes caused by the positions of the non-magnetic atoms, while the actual spin arrangement, if considered alone, has in fact a higher non-polar symmetry. This is illustrated in figure 5(a), where the magnetic structure of the double perovskite Lu_2MnCoO_6 [15], a known type II multiferroic, is shown with and without the non-magnetic atoms, and their corresponding MSGs are indicated. Its parent space group is $P2_1/c$, the Mn and Co atoms sit at positions *2c* and *2d*, and the propagation vector is (1/2,0,1/2). This material has been reported to be multiferroic, as expected from its symmetry P_a2_1, with point group *21'*, in agreement with the general results summarized in figure 1(a) and table 1. However, the virtual structure formed by the magnetic atoms alone has a higher centric symmetry, given by the MSG P_c2_1/c, with point group *2/m1'*. Therefore, the polar character of this phase, and its magnetically induced ferroelectricity paradoxically relies on the non-magnetic atoms, which reduce the parent symmetry and as a consequence also the symmetry of the magnetic phase. Lu_2MnCoO_6 is also an example of the need to avoid naive misconceptions coming from considering the form of the spin arrangements only at a

local level, and the convenience of applying rigorous symmetry arguments that include the whole structure. The structure of Lu_2MnCoO_6 has Mn–Co chains along the *c* direction with a spin configuration ++−−, and this kind of chains, are known to be polar along the chain direction. In fact, they are considered as a typical example of a spin configuration yielding electric polarization along the chain, via exchange striction [4, 16, 17]. Based on these considerations the measured electric polarization in polycrystalline samples of Lu_2MnCoO_6 has been assumed to be directed along *c* [15]. But in fact the monoclinic *b* direction is the polar direction of this magnetic structure, as shown in figure 5(a). This means that the possible direction of the polarization is perpendicular to the spin chains. These spin chains are in fact interrelated by binary rotations around the *b* axis, and the possible polarization along c resulting from exchange striction within each chain cancels out when summed for the two symmetry-related chains within a unit cell. As stressed in the figure, the chains of magnetic atoms are even related by space inversion at (1/4,1/4,1/8). It is only the presence of the non-magnetic atoms at positions of lower symmetry that reduces the symmetry of the system and makes it polar.

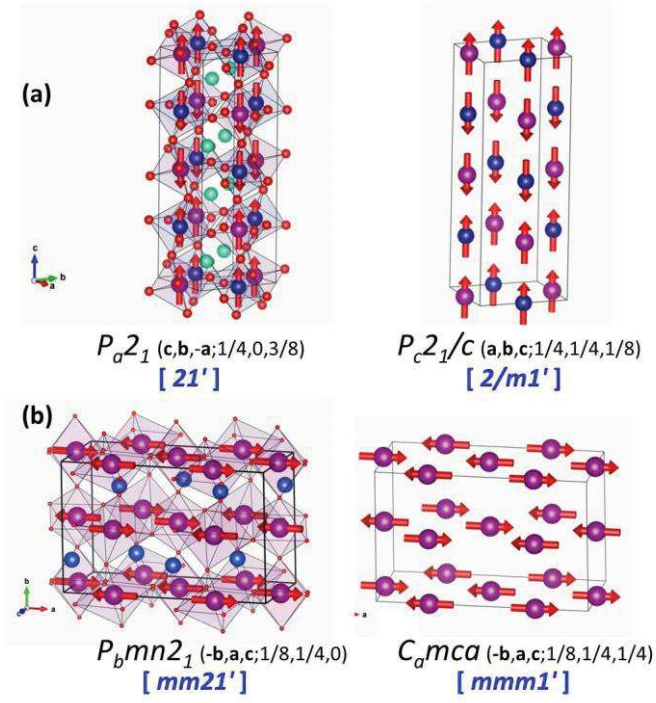

Figure 5
Magnetic structures of multiferroics Lu_2MnCoO_6 (a) and $HoMnO_3$ (b) with indication of its MSG and magnetic point group (in brackets). On the right, the same structures, but restricted to the magnetic atoms, with indication of the MSG and magnetic point group that these spin arrangements would have if standing alone. The monoclinic axis in (a) is along *b*. In each case, the transformation to the standard setting of the MSG is written in brackets.

Another example of the importance of non-magnetic atoms for spin driven ferroelectricity is the case of $HoMnO_3$ [11], with parent space group *Pnma*, Mn atoms at *4b* and propagation vector (1/2,0,0) (see figure 5(b)). The symmetry of its magnetic structure is given by the polar MSG P_bmn2_1 (point group *mm21*'), as one would expect from the rules summarized in table 2. But the Mn atoms alone form a spin arrangement whose MSG, if considered isolated, would be C_amca (point group

mmm1'). The non-magnetic atoms are therefore necessary to break the inversion symmetry and yield a polar magnetic symmetry. This means that the exchange striction mechanism assumed to be at the origin of the observed spontaneous electric polarization, would be impossible without the asymmetry of the superexchange constants caused by the non-magnetic atoms. In general, the non-magnetic atoms reduce the parent symmetry and as a consequence also the resulting symmetry of the magnetic structure.

5. Other favourable symmetry scenarios for type II multiferroicity.

The incompatibility of glide and screw operations with some propagation vectors also applies to structures that belong to crystalline classes with higher symmetry than those of monoclinic and orthorhombic systems. There are examples where this incompatibility can make that very symmetric propagation vectors paradoxically yield drastic symmetry breaks. For instance, a propagation vector **k** = (0,0,1/2) on a tetragonal parent phase with parent space group $P4_122$ has only two possible maximal symmetries with their magnetic point group reduced to *21*' in both cases. Due to incompatibility of the screw operation along ***c*** with the propagation vector, the system can only keep either the binary axis along <1,0,0> or along <1,1,0>. Thus, the non-polar/polar symmetry break is obliged. Similarly, a parent space group $P3_121$ with **k** = (0,0,1/3) has only as *k*-maximal point group symmetries *2* or *2*' along <1,0,0> , while for **k** = (0,0,1/2) all *k*-maximal symmetries keep the parent point group *321*'.

In general, however, the larger number of symmetry operations in the parent space group often yields that all k-maximal magnetic point-groups remain non-polar, despite some of them being non-centrosymmetric because of the incompatibility of some operations with the *k*-vector. As an example, figure 6 compares two parent space groups with the same point-group symmetry *4/mmm1*' and the same propagation vector. In both cases the incompatibility between the propagation vector and the *b* glide plane yields non-centrosymmetric *k*-maximal symmetries, but in one case they are polar and in the other not, depending on the parent space group.

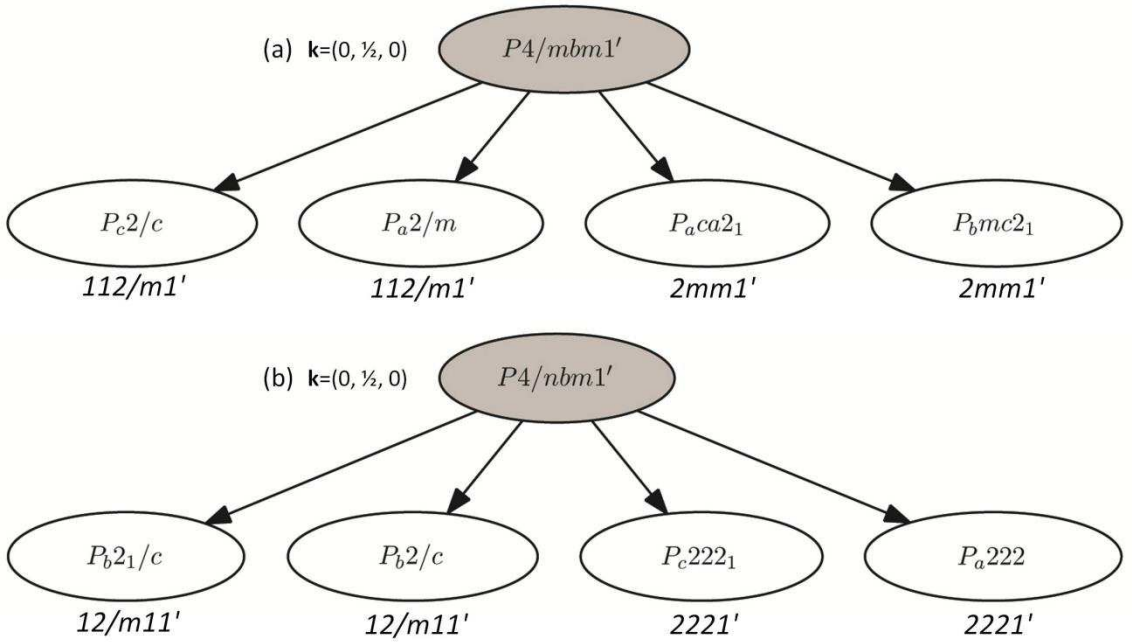

Figure 6

Possible *k*-maximal MSGs resulting from a magnetic ordering having propagation vector (0,1/2,0) for a parent structure with space group *P4/mbm* (a) or *P4/nbm* (b). The symmetries are shown as subgroups of the parent grey MSG giving their standard BNS labels. Only one MSG for each equivalent conjugacy class is shown. Notice that the BNS standard setting for each MSG in general does not coincide with the one of the parent space group. The magnetic point-group associated with each MSG in the orientation of the parent setting is also indicated (Obtained with *k*-SUBGROUPSMAG [8]).

Therefore, for high symmetries the incompatibility of some screw or glide operations with the propagation vector does not lead to simple general rules. In such cases, one can however derive the *k*-maximal subgroups and all possible *k*-compatible magnetic subgroups with tools such as MAXMAGN or *k*-SUBGROUPSMAG [8], and this permits to detect in a straightforward way situations that are susceptible of yielding a polar magnetic phase from only the knowledge of the paramagnetic structure and the active propagation vector. One can distinguish among these favourables cases several types of scenarios, which we describe below, taking as examples the symmetry properties of some wellknown multiferroics.

5.1. Some of the k-maximal magnetic symmetries are polar

This is the situation that may result from the incompatibility of the propagation vector and some screw or glide operations, as discussed in previous sections, but the existence of *k*-maximal polar symmetries can also happen for other reasons. This is the case of the multiferroics $Ba_3MnNb_2O_9$ [19], $Ba_3Nb_2NiO_9$ [20] and $Ba_2CoGe_2O_7$ [21]. For instance $Ba_3MnNb_2O_9$ has parent space group *P-3m1*, propagation vector (1/3,1/3,0) and the Mn atoms are located at *1b* (0,0,1/2). The number of non-equivalent *k*-maximal MSGs are: *P-31m*', *P-3*'*1m*', *P-3*'*1m*, *P-31m*, *P31m*' and *P31m*. The two last ones are polar along the *c* direction, and therefore the possibility of a minimal symmetry break into polar symmetry is already there. But among the other four maximal symmetries, two, namely *P-3*'*1m*' and *P-31m* can be discarded as they force the site *1b* to have zero moment. In addition the subgroup *P-3*'*1m* splits the magnetic

site into two, with one of the sites constrained to zero moment. Therefore although it cannot be fully discarded, this symmetry can be considered less favourable, as it does not allow the magnetic ordering of all magnetic atoms. We are therefore left with only three possible maximal symmetries that allow magnetic order of all magnetic atoms, and two of them are polar (see figure 7). One of them (*P31m*) is in fact the one realized in $Ba_3MnNb_2O_9$. The index of this subgroup with respect to the parent symmetry is 12, and therefore 12 is the number of different domains to be expected. Figure 7 shows only the spin arrangement corresponding to one of them. The equivalent configuration obtained by application of the lost space inversion corresponds to a domain with opposite electric polarization. The remaining domains are trivial as they can be derived by transformations with the lost lattice translations (antiphase domains) and/or time reversal (opposite spins). It is remarkable that the alternative maximal MSG *P31m*' shown in figure 7 allows a ferromagnetic component (FM) along *c*, and therefore a weak FM can be expected for this spin arrangement. One can therefore infer that a magnetic field along *c* may stabilize this alternative phase. It is important to note that again here the polar character of some of the maximal symmetries fully depend on the non-magnetic atoms, which reduce the symmetry of the structure. The spin arrangements in figure 7 as isolated entities are all centrosymmetric.

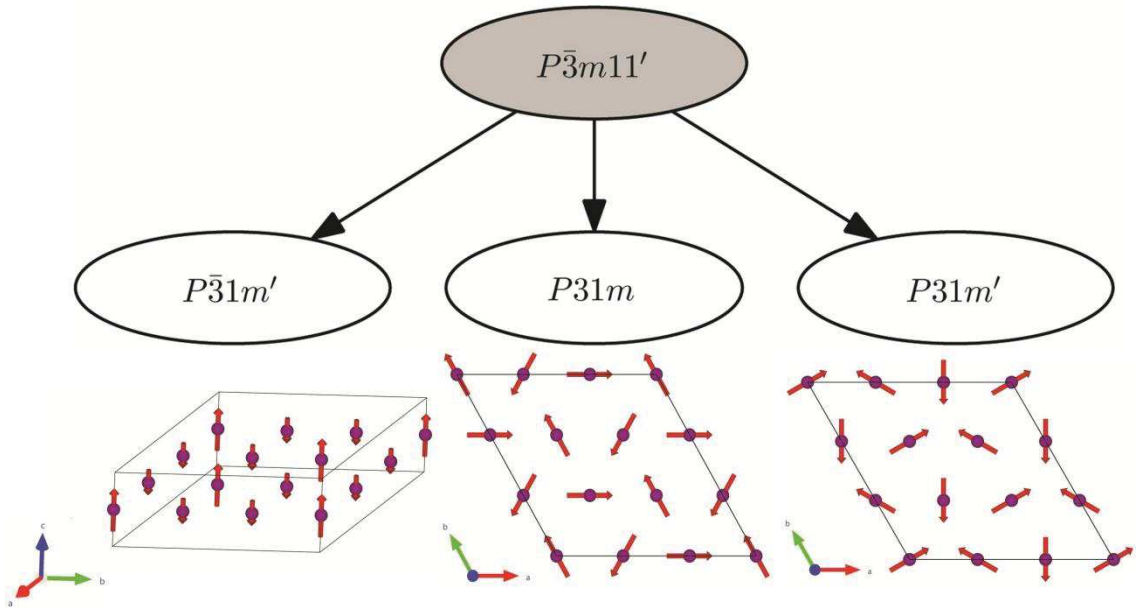

Figure 7

Possible *k*-maximal symmetries resulting from a magnetic ordering having propagation vector (1/3,1/3,0) on a parent structure with space group *P-31m* and the magnetic atom at Wyckoff position *1b*. A scheme of the spin arrangement corresponding to each symmetry is also shown. In the case of the MSG *P-31m*', the *1b* site splits into two; this is graphically stressed with two different arbitrary spin values. The MSG *P31m*' allows a FM **k** = 0 component along *c*, not shown. The graphic shows the MSGs of the full structure including also the non-magnetic atoms. The spin arrangements, considered isolated, have all higher centrosymmetric MSGs.

A very similar scenario to $Ba_3MnNb_2O_9$ can be found in $Ba_3Nb_2NiO_9$ [20]. In this case, the propagation vector is (1/3,1/3,1/2). This means that the magnetic symmetry necessarily has antitranslations and therefore the point groups include time reversal. This forbids the existence of ferromagnetism in all cases, but again there are three possible *k*-maximal symmetries, and two of them are polar.

Another example of a multiferroic with its symmetry being a *k*-maximal MSG is the case of $Ba_2CoGe_2O_7$ [21], where the parent space group *P-42₁m* is already non-centrosymmetric, and this is the fundamental reason behind the existence in this case of a *k*-maximal polar symmetry. For **k** = (0,0,0) and the Co atom sitting at *2a* [(0,0,0) and (1/2,1/2,0) positions], four *k*-maximal symmetries are possible: two are tetragonal and non-polar, with the spins along the *c* direction, and two are orthorhombic (*Cm*'*m2*' and *P2₁2₁*'*2*), with the spins on the basal plane. The polar point group symmetry *m*'*m2*' appears therefore as one of the four possible ones and is the one realised in this compound.

5.2. Some maximal irrep epikernels are polar

In many cases, magnetic phases fulfill the Landau assumption that the magnetic order parameter transforms according to a single irrep of the parent symmetry group. But for multidimensional irreps different MSGs can be realized depending on the direction taken by the magnetic order parameter. These possible alternative MSGs for a single irrep are called irrep epikernels, being the irrep kernel the minimal MSG corresponding to an arbitrary direction of the order parameter [8]. Usually the magnetic symmetry realized in the magnetic phase is one of the possible irrep epikernels of maximal symmetry, i.e. a maximal irrep epikernel. All *k*-maximal MSGs are maximal epikernels for one irrep (trivially fulfilled in the case of 1D irreps), but the reverse is not true, and there can be maximal irrep epikernels for multidimensional irreps that are not *k*-maximal. There are cases where all possible *k*-maximal symmetries are non-polar, but one of the irreps that can be active in the magnetic ordering has as possible maximal epikernel [8] a polar symmetry. This means that a spin configuration according to this irrep, despite its tendency to maximize the broken symmetry, has a high probability of realizing a non-polar/polar symmetry break. This the case of Cu_2OSeO_3 [22], where the parent space group is *P2₁3*, and the active irrep is the 3D mGM4, at **k** = 0. The epikernels of this irrep, i.e. the possible invariance subgroups of the grey group *P2₁31*' that can be maintained by an order parameter transforming according to this irrep are: *P2₁*'*2₁*'*2₁*, *R3*, *P2₁*' and *P1*. These irrep epikernels follow the group–subgroup hierarchy shown in figure 8(b) [23]. Therefore, one of the two maximal symmetries that can result for this irrep is the polar *R3*, which is the one realized in Cu_2OSeO_3. In this particular case, the intrinsic symmetry of the spin arrangement is not higher, and the polar character of the magnetic ordering does not depend on the non-magnetic atoms. Epikernels of magnetic irreps for **k** = 0 of centrosymmetric groups are in most cases centrosymmetric. In this example, the fact that the parent symmetry, although non-polar, lacks space inversion is a fundamental feature that favours the existence of a polar irrep epikernel.

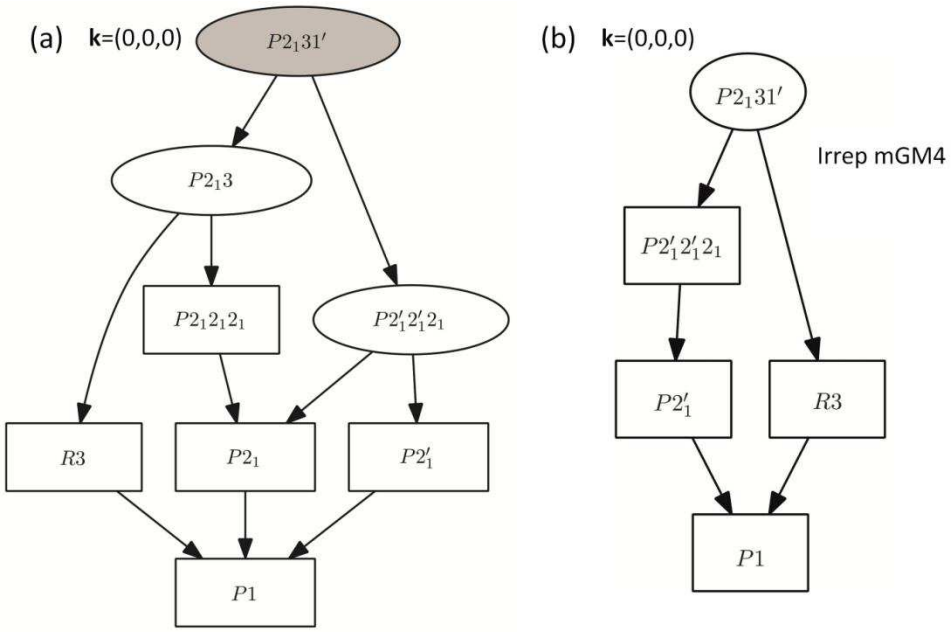

Figure 8

(a) Possible symmetries resulting from magnetic ordering having propagation vector (0,0,0) on a parent structure with space group *P2₁3*. The symmetries are shown as subgroups of the parent grey MSG, with their standard BNS labels, showing that all *k*-maximal symmetries are non-polar (b) The same as in (a), but considering only magnetic orderings according to the irrep mGM4, showing that one of the maximal symmetries (irrep epikernels) is polar (Obtained with k-SUBGROUPSMAG [8]).

5.3. Reduction to polar symmetry by symmetry incompatibility of different magnetic sites

This is the situation in $LaMn_3Cr_4O_{12}$, which has been recently reported as multiferroic [24]. This double perovskite, with chemical order both in the A and B sites, has as parent symmetry the cubic space group *Im-3* and a ground state phase where both Mn and Cr are magnetically ordered with a propagation vector (1,1,1). The Mn atoms sit at the site *6b* while the Cr atoms at *8c*. The possible MSGs for each of these sites are shown in figures 9(a) and (b). In both cases, space inversion is preserved by any spin ordering, the minimal symmetry being *P_s-1*. But the preserved inversion centers have different locations depending on the site. In the case of a magnetic order in the *8c* site, the inversion center is at (1/4,1/4,1/4), while in the case of the *6b* site, it is the inversion center at the origin that is preserved. There is no common subgroup in the subgroup graphs shown in figures 9(a) and (b). Thus, the presence of magnetic order on both sites should yield a symmetry given by the intersection of two subgroups, one taken from each graph. Space inversion is therefore necessarily broken. All the possible symmetries when both sites are magnetically ordered, are shown in figure 9(c). From the viewpoint of representational analysis, the magnetic representations for the *8c* and the *6b* sites do not have any common irrep, and therefore magnetic order on both sites necessarily implies the superposition of two different irreps, with a symmetry reduction resulting from the intersection of their corresponding epikernels.

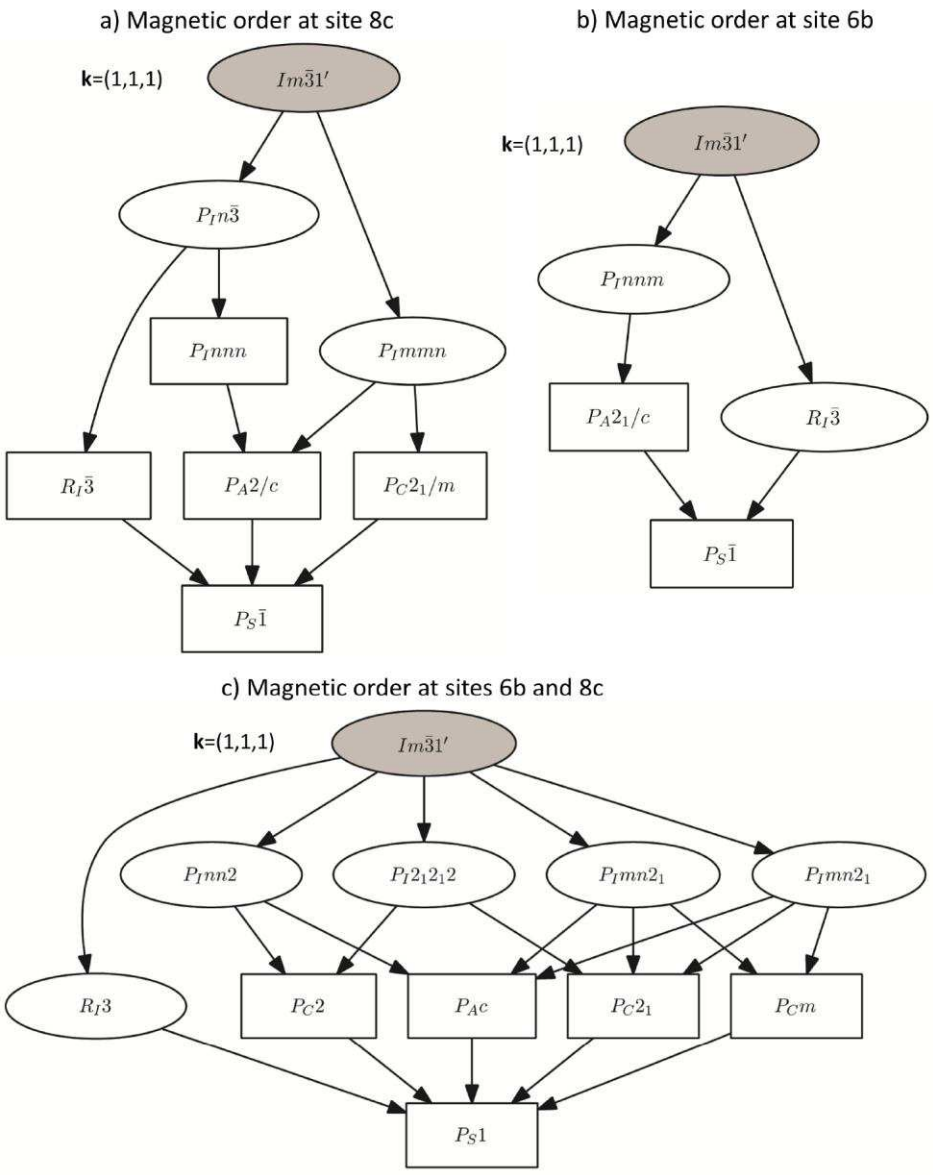

Figure 9
(a) Possible symmetries resulting from magnetic ordering having propagation vector (1,1,1) on a parent structure with space group *Im-3* if the magnetic atoms are located at the *8c* site (a), at the *6b* site (b), or at both sites (c). The symmetries are shown as subgroups of the parent grey MSG giving their standard BNS labels (Obtained with *k*-SUBGROUPSMAG [8]).

The case of $Ca_3Co_{2-x}Mn_xO_6$, with parent symmetry *R-3c*, magnetic atoms at *6a* and *6b*, and **k** = (0,0,0) can also be classified within this scenario: all *k*-maximal subgroups allowing full magnetic order either at *6a* or *6b* are centrosymmetric, but if magnetic order should be present on both sites, the possible maximal symmetries reduce to three, namely *R-3c*', *R3c* or *C2/c*. One of them is therefore polar along *c*, and it is the symmetry of the magnetic structure that has been observed [17].

Site symmetry incompatibility forcing the presence of more than one irrep for the existence of magnetic order at all magnetic sites can also happen in cases where the parent structure has only a single symmetry-independent atomic site. This is the case of $La_2O_2Fe_2OSe_2$ [46] (see next section).

6. Survey of the symmetry properties of known type II multiferroics and of some potential ones

We have shown that the knowledge of the parent structure and the magnetic propagation vector of a magnetic phase can be sufficient for identifying single-*k* magnetic structures with a high probability of exhibiting type II multiferroicity. Table 3 presents a comprehensive list of the materials that are known to be type II multiferroics, extracted from the MAGNDATA database [8, 25]. From the 19 compounds (or family of compounds), 16 can be assigned to one of the favourable symmetry scenarios that have been described above. In most cases, there exist polar symmetries among the *k*-maximal ones, and the reported structure corresponds to one of them (case (i) in the previous section). In general, these polar *k*-maximal symmetries are the result of magnetic arrangements transforming according to a single multidimensional irrep, but with the spin irrep basis functions combined in a specific form corresponding to a polar irrep epikernel. In a few cases, no *k*-maximal symmetry is polar, but one of the possible active irreps has some maximal epikernel of polar character, and the multiferroic phase corresponds to its realization (case (ii)). Finally, in three cases, the magnetic atoms occupy two different sites with some incompatibility on their maximal symmetries, and the symmetry reduction into a polar symmetry is due to the intersection of the *k*-maximal symmetries allowed for the different magnetic sites (case (iii)).

The compounds RMn$_2$O$_5$ (R = Ho,Tb) [26], with parent *Pbam* space group and **k** = (1/2,0,1/4), require a special comment. These systems can be readily identified as being propitious for type II multiferroicity due to the incompatibility of the propagation vector with the parent screw binary axis along *a*. This incompatibility causes that two *k*-maximal symmetries are polar among the possible six ones, both with point group *m2m1*' (see figure 10). The polarity in both cases is along *b*, which agrees with the experimental observation. However, the magnetic structures proposed for these phases have a much lower symmetry, namely a subgroup of one of the polar *k*-maximal ones: a subgroup with MSG C_am and point group *11m1*', which in principle would have an induced electric polarization in a general direction on the plane *ab*. The assumption of a single active irrep does not introduce in this case any restriction on the spin configuration, as there is only one irrep possible for this propagation vector. From the viewpoint of magnetic symmetry, however, the irrep spin basis modes for this wave vector can combine with different constraints and yield magnetic orderings fulfilling any of the various magnetic symmetries enumerated in figure 10. As the traditional representational method does not control magnetic symmetry and the assumption of a single irrep does not introduce any constraint, the magnetic structures reported for these two compounds were obtained introducing only ad hoc restrictions on the spin degrees of freedom. In view that the observed polarization is consistent with an orthorhombic point group *m2m1*', it may be worth to revisit these structures and explore in a systematic way the possible models corresponding to the higher symmetries indicated in figure 10, specially the one corresponding to the MSG C_amc2_1, which would be consistent with the observed macroscopic properties. A similar situation occurs in the case of the magnetic structure reported for BiMn$_2$O$_5$.

The Mott insulator GeV_4S_8 [32] has also particular interest. In table 3 we have considered as parent structure its cubic phase at room temperature, but a structural transition into a ferroelectric phase, previous to the magnetic ordering, has been reported [38]. Hence, strictly speaking this multiferroic should be considered of type I, with the ferroelectric instability being independent of the magnetic one. However, the four possible *k*-maximal subgroups of the parent cubic symmetry are all polar. This means that independently of the presence of the intermediate ferroelectric phase, the magnetic ordering also breaks the symmetry into the polar one. The system is bound to have some spin driven polarization, despite having an intrinsic ferroelectric distortion. This is quite exceptional in type I multiferroics and situates this material in an intermediate class, having some of the features of type II multiferroics, and for this reason it is included in the table.

There are only three multiferroics in table 3 where the reported break into polar symmetry could not be inferred from the value of the propagation vector. One of them ($DyFeO_3$) is a phase stabilized under magnetic field [27], and therefore it is outside the framework of the symmetry arguments discussed here. The other two multiferroic phases ($HoFe_3(BO_3)_4$ [28] and $Cu_3Mo_2O_9$ [29]) are the result of the superposition of spin modes corresponding to two different irreps. Although in both cases there are several magnetic sites, no symmetry incompatibility forces the lowering of the symmetry to those reported, and some supergroups would also be posible. In $HoFe_3(BO_3)_4$ (parent space group $P3_121$, **k** = (0,0,1/2)) one of the active irreps (mA3) has in fact polar epikernels with MSG C_c2, which would restrict the polarization to be along the <1,0,0> direction. This is in fact the MSG of the magnetic structure that has been reported for the similar compound $YFe_3(BO_3)_4$ [28] (see table 4). But in the case of $HoFe_3(BO_3)_4$ the reported magnetic structure has only P_s1 symmetry, i.e. it only keeps the antitranslation associated with the propagation vector. However, it seems that a comparative refinement controlling the symmetry and imposing the possible higher MSG C_c2 has not been attempted. The case of $Cu_3Mo_2O_9$ is also intriguing, since below T_N the electric polarization appears along *c* [29], but none of the several models proposed for the magnetic structure [30, 31] are consistent with this observation. Two possible polar structures have been considered in [30], but their polar direction would be either *a* or *b*. The symmetry break in these two materials can therefore be considered exceptional and their reported properties have controversial features. For this reason they deserve to be reinvestigated.

Table 3
Commensurate magnetic structures present in the database MAGNDATA [8] that are known to exhibit ferroelectricity, and according to their symmetry can be classified as type II multiferroics.

Compound	N[a]	Parent MSG	Multiferroic phase MSG	Ferroic species [7]	Propagation vector	Symmetry type[b]	Intr. pol[c]	REF[d]
$LaMn_3Cr_4O_{12}$	1.156	*Im-31'*	R_I3	*m-31'F31'*	(1, 1, 1)	Site incomp. >1 irrep	Yes	[24]
GeV_4S_8	1.86	*F-43m1'*	$P_an a2_1$	*-43m1'Fmm21'*	(1/2, 1/2 ,0)	*k*-max. sym.	Yes	[32]
Cu_2OSeO_3	0.35	$P2_131'$	*R3*	*231'F3*	(0, 0, 0)	Max. epikernel	Yes	[22]
$Ca_3Co_{2-x}Mn_xO_6$	0.13	*R-3c1'*	*R3c*	*-3m1'F3m*	(0, 0, 0)	Site incomp. >1 irrep	Yes	[17]
$NdFe_3(BO_3)_4$	1.7	*R321'*	C_c2	*321'F21'*	(0, 0 ,3/2)	Max. epikernel	Yes	[37]

$DyFeO_3$*	0.11	*Pnma1'*	*Pn'a'2₁*	*mmm1'Fm'm'2*	(0, 0, 0)	>1 irrep, H≠0	Yes	[27]
$Ba_3MnNb_2O_9$	1.0.8	*P-3m11'*	*P31m*	*-3m1'F3m*	(1/3, 1/3, 0)	*k*-max. sym.	No	[19]
$Ba_3Nb_2NiO_9$	1.13	*P-3m11'*	*P$_c$31c*	*-3m1'F3m1'*	(1/3, 1/3,1/2)	*k*-max. sym.	No	[20]
$HoFe_3(BO_3)_4$*	1.93	*P3₁211'*	*P$_s$1*	*321'F11'*	(0, 0, 1/2)	>1 irrep	Yes	[28]
$Ba_2CoGe_2O_7$	0.56	*P-42₁m1'*	*Cm'm2'*	*-42m1'Fm'm2'*	(0, 0, 0)	*k*-max. sym.	No	[21]
$Cu_3Mo_2O_9$*	0.130	*Pnma1'*	*Pm'c2₁'*	*mmm1'Fm'm2'*	(0, 0, 0)	>1 irrep	Yes	[29]
$BaFe_2Se_3$	1.120	*Pnma1'*	*C$_a$c*	*mmm1'Fm1'*	(1/2, 1/2, 1/2)	*k*-max. sym.	Yes	[33]
$RMnO_3$ (R: Ho,Lu)	1.20; 1.101	*Pnma1'*	*P$_b$mn2₁*	*mmm1'Fmm21'*	(1/2, 0, 0)	*k*-max. sym.	No	[11,12]
RMn_2O_5 (R:Dy,Gd,Pr)	1.76; 1.54; 1.19	*Pbam1'*	*P$_a$ca2₁*	*mmm1'Fmm21'*	(1/2, 0, 0)	*k*-max. sym.	Yes	[13,14]
$BiMn_2O_5$	1.74; 1.75	*Pbam1'*	*C$_a$m/C$_a$mc2₁*	*mmm1'Fm1'*	(1/2, 0, 1/2)	*k*-max. sym.	Yes	[34,42]
RMn_2O_5 (R:Ho,Tb)	1.109; 1.108	*Pbam1'*	*C$_a$m/C$_a$mc2₁*	*mmm1'Fm1*	(1/2, 0, 1/4)	*k*-max. sym.	Yes	[26]
$HoNiO_3$	1.48	*P2₁/c1'*	*P$_a$2₁*	*2/m1'F21'*	(1/2, 0, 0)	Site incomp >1 irrep	No	[36]
Lu_2MnCoO_6	1.32	*P2₁/c1'*	*P$_a$2₁*	*2/m1'F21'*	(1/2, 0, 1/2)	k-max. sym.	No	[15]

Note: Materials where the parent structure plus propagation vector are not sufficient to identify them as favourable cases for type II multiferroicity are distinguished with an asterisk. [a] Entry number in MAGNDATA [8, 25]. [b] Comment that indicates whether the MSG is a *k*-maximal symmetry, a maximal irrep epikernel, the result of site symmetry incompatibility, or the result of the action of several irreps. [c] Indication if the spin arrangement is intrinsically polar. [d] Reference of the magnetic structure.

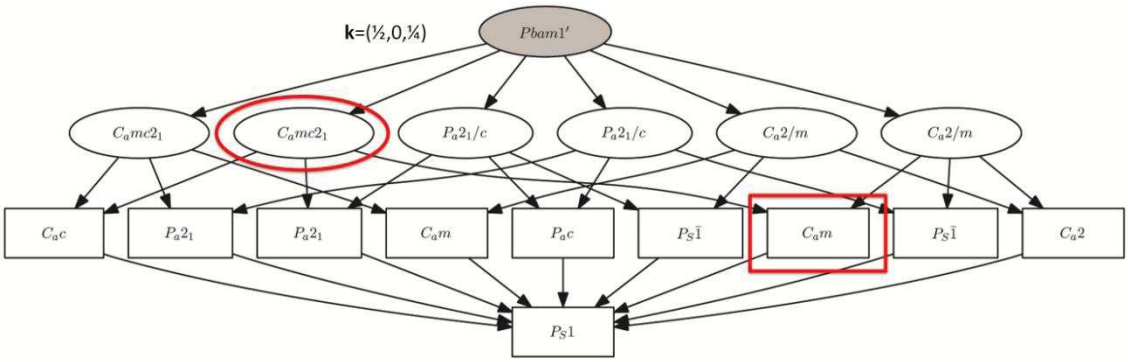

Figure 10
Possible magnetic symmetries resulting from a magnetic ordering having propagation vector (1/2,0,1/4) in a structure with space group *Pbam*. The symmetries shown are subgroups of the grey MSG of the paramagnetic phase, and are identified using standard BNS labels. Only one MSG for each conjugacy class is shown. Some of the subgroups correspond to the same mathematical MSG and have identical labels, but represent different inequivalent subgroups (obtained with *k*-SUBGROUPSMAG [8]). The point groups associated with the six possible k-maximal symmetries can only be either *mm21*' (*m2m1*' in the parent setting) or *2/m1*' (*12/m11*' or *112/m1*' in the parent setting). The MSG C_am (2a,-4c,b;0,0,0) of the magnetic structures reported for $TbMn_2O_5$ and $HoMn_2O_5$ [26] is highlighted with a red box. The polar *k*-maximal MSG, supergroup of this one, which is more consistent with the apparent restriction of the polarization along the *b* direction, is highlighted with a red ellipse.

Among the more than 360 commensurate magnetic structures stored in MAGNDATA, apart from the known type II multiferroics discussed above, one can identify some additional structures having a non-polar/polar symmetry break. These materials, in the case of being insulators, can be considered potential multiferroics of type II. They are

summarized in table 4. Four of the seven cases fulfill one of the favourable symmetry conditions discussed above, the polar symmetry being a *k*-maximal symmetry (two cases) or at least an irrep epikernel (one case). The second case ($La_2O_2Fe_2OSe_2$) fits into the third scenario with a site symmetry incompatibility forcing a further reduction of the symmetry in the case of magnetic order on all magnetic sites.

The symmetry break in $YFe_3(BO_3)_4$ has already been mentioned above as contrast to that of $HoFe_3(BO_3)_4$. Although this family of compounds has been intensively investigated because of its magnetoelectric properties, to our knowledge there exist no report yet of spin driven ferroelectricity in $YFe_3(BO_3)_4$.

The nickelates $RNiO_3$ (*R*:Nd,Pr) have been reported to have a charge ordering transition that decreases its paramagnetic space group to $P2_1/c$ [39] and with this alternative parent symmetry they are included in table 3 for $HoNiO_3$ [40]. The magnetic structures of these two compounds were however originally reported without considering any monoclinic distortion [35], and the propagation vector is along a different direction than in $HoNiO_3$ [40]. The reported magnetic ordering for these two compounds implies a polar/non-polar symmetry break and induced electric polarization should be expected along the *b* axis of the *Pbnm* setting of the parent symmetry. This is one of the favourable cases listed in table 2, with a *k*-maximal polar symmetry. Therefore, in contrast with the case of $HoNiO_3$ listed in table 3, the symmetry reduction of the parent phase due to charge ordering does not play a determinant role in the polar character of the spin ordering in these two compounds.

The compound Na_2MnF_5 has $P2_1/c$ as parent symmetry and a propagation vector (0,1/2,0). It is therefore a realization of the case represented in figure 3 and listed in table 1. The Mn atoms occupy the sites *2a* and *2b*, and as indicated in table 1, full magnetic ordering requires the break of space inversion, with *m1*' as maximal point-group symmetry. This is indeed the symmetry observed in the magnetic arrangement that has been reported [41], and therefore, one can expect to observe type II multiferroicity, if the magnetically induced electric polarization is large enough.

The case of $La_2O_2Fe_2OSe_2$ [46], although having seminconducting properties, has been included in the table because of its very special symmetry restrictions. The Fe atom occupies a single *4c* Wyckoff position of the parent space group *I4/mmm*, but one can easily check that no possible irrep for the observed propagation vector allows a non-zero magnetic moment at all Fe sites. Full magnetic order therefore requires the presence of at least two irrep distortions, with the possible resulting MSGs being polar in all cases, even for collinear arrangements. This non-polar/polar symmetry break can therefore be considered among those predictable from the knowledge of the propagation vector and the parent structure.

Table 4 includes three cases where the parent structure and the propagation vector does not seem to have specially favourable features for a symmetry break into a polar magnetic phase. In two of these structures ($CsCoBr_3$ [43] and $NiTa_2O_6$ [44]) the polar symmetry occurs because of the unpredictable presence of two irreps in the magnetic ordering. The case of Cs_2CoCl_4 [45] is rather peculiar. With *Pnma* as parent space group and propagation vector (0,1/2,1/2), it is one of the favourable scenarios listed in table 2, but with the exception of magnetic sites *4c*, for which the polar maximal symmetry

forces a non-collinear arrangement with orthogonal spins. The Wyckoff position occupied by the Co atoms is in fact *4c*, and therefore the alternative centrosymmetric *k*-maximal MSG, which allows collinearity, would be more favourable. The structure reported for Cs_2CoCl_4 indeed deviates only slightly through a small canting from a centrosymmetric collinear arrangement. It is this weak canting that reduces the symmetry further to the polar kernel of the active 2D irrep. This is one of the very few cases where the structure realized by a multidimensional magnetic order parameter does not correspond to one of the maximal irrep epikernels. The magnitude of this canting component is however close to its standard deviation. As the authors did not seem to be aware of the symmetry break that this canting represents, a new study of the structure would be convenient in order to confirm or discard this peculiar behaviour.

It is remarkable that the non-collinear magnetic structure reported for $CsCoBr_3$ deviates also scarcely from a collinear arrangement with centrosymmetric symmetry and with a single active irrep. In contrast, the proposed polar magnetic structure for $NiTa_2O_6$ is collinear but non-centrosymmetric, and it requires the superposition of two spin waves transforming according to two different irreps for the same propagation vector. The magnetic structure of this compound is also controversial, as there is a more recent model, which despite being similar, has a different non-polar magnetic symmetry.

Table 4
Commensurate magnetic structures present in the database MAGNDATA [8] that according to their symmetry fulfill the conditions for being type II multiferroics (if they are insulators), but have not been reported as such.

Compound	N[a]	Parent MSG	Multiferroic phase MSG	Ferroic species [7]	Propagation vector	Symm. type[b]	Intr. pol[c]	REF [d]
$YFe_3(BO_3)_4$	1.90	*P3₁2₁1'*	*C$_c$2*	*321'F21'*	(0, 0 ,1/2)	Max. epikernel	Yes	[28]
$La_2O_2Fe_2OSe_2$	1.58	*I4/mmm1'*	*C$_c$c*	*4/mmm1'Fm1'*	(1/2, 0, 1/2)	>1 irrep site incomp.	No	[46]
$RNiO_3$ (R:Nd, Pr)	1.44, 1.45	*Pnma1'*	*C$_a$mc2$_1$*	*mmm1'Fmm21'*	(0, 1/2 ,1/2)	*k*-max. sym.	Yes	[35]
Na_2MnF_5	1.55	*P2$_1$/c1'*	*P$_b$c*	*2/m1'Fm1'*	(0, 1/2 ,0)	*k*-max. sym.	No	[41]
$CsCoBr_3$*	1.0.3	*P63/mmc1'*	*Cm'c2$_1$'*	*6/mmm1'Fm'm2'*	(1/3, 1/3 ,0) (0, 0, 0)	>1 irrep	Yes	[43]
$NiTa_2O_6$*	1.172	*P4$_2$/mnm1'*	*A$_b$ba2*	*4/mmm1'Fmm21'*	(1/4, 1/4 ,1/2)	>1 irrep	No	[44]
Cs_2CoCl_4*	1.51	*Pnma1'*	*P$_a$2$_1$*	*mmm1'F21'*	(0, 1/2, 1/2)	Not max. epikernel	Yes	[45]

Note: Compounds which are known or are expected to have conductor or seminconductor properties are not included. Materials where the parent structure plus propagation vector are not sufficient to identify them as favourable cases for type II multiferroicity are distinguished with an asterisk. [a] Entry number in MAGNDATA [8, 25]. [b] Comment that indicates whether the MSG is a *k*-maximal symmetry, a maximal irrep epikernel, the result of site symmetry incompatibility, or the result of the action of several irreps. [c] Indication if the spin arrangement is intrinsically polar. [d] Reference of the magnetic structure used to identify the MSG.

7. Conclusions

The symmetry conditions for a commensurate magnetic phase to behave as a type II multiferroic have been reviewed. We have shown that in many cases the knowledge of the space group of the paramagnetic phase, the propagation vector, and the special sites occupied by the magnetic atoms can be sufficient to detect materials with favourable conditions for exhibiting this type of multiferroic behaviour. Most of the known type II multiferroics satisfy one of the favourable symmetry scenarios presented in this work. Finally, based on the symmetry properties of the magnetic structures reported, we identify some additional materials, which fullfil the necessary symmetry conditions for exhibiting spin driven ferroelectricity.

Acknowledgements

The authors thank Branton Campbell and Harold Stokes for their permanent improvement and extension of their program ISODISTORT that has been used for some parts of the analyses done in this work. One of us (JMPM) is also specially indebted to J L Ribeiro for helpful comments and interchange of information at the early stages of this work. This work has been supported by the Spanish Ministry of Economy and Competitiveness and FEDER funds (project MAT2012-34740) and the Government of the Basque Country (project IT779-13).

References

[1] Schmid H 1994 *Ferroelectrics* **162** 317–38
[2] Khomski D 2009 *Physics* **2** 20
[3] Johnson R D and Radaelli P G 2014 *Annu. Rev. Mater. Res.* **44** 269–98
[4] Tokura Y, Seki S and Nagaosa N 2014 *Rep. Prog. Phys*. **77** 076501
[5] Levanyuk A P and Sannikov D G 1974 *Sov. Phys. - Usp.* **17** 199–214
[6] Nye J F 1957 *Physical Properties of Crystals* (New York: Oxford University Press) pp 20–4
[7] Schmid H 2008 *J. Phys.: Condens. Matter* **20** 434201
[8] Perez-Mato J M, Gallego S V, Tasci E S, Elcoro L, de la Flor G and Aroyo M I 2015 *Annu. Rev. Mater. Res.* **45** 13.1–32
[9] Litvin D B 2013 *Magnetic Group Tables: 1-, 2- and 3-Dimensional Magnetic Subperiodic Groups and Magnetic Space Groups* (Chester: International Union of Crystallography) www.iucr.org/publ/978-0-9553602-2-0
[10] Stokes H T and Campbell B J 2011 ISO-MAG: table of magnetic space groups *ISOTROPY Software Suite* http://iso.byu.edu
[11] Munoz A, Casais M T, Alonso J A, Martinez-Lope M J, Martinez J L and Fernandez-Diaz M T 2001 *Inorg. Chem*. **40** 1020–8
[12] Okamoto H, Imamura N, Hauback B C, Karppinen M, Yamauchi H and Fjellvag H 2007 *Solid State Commun*. **146** 152–6
[13] Lee N, Vecchini C, Choi Y J, Chapon L C, Bombardi A, Radaelli P G and Cheong S W 2013 *Phys. Rev. Lett*. **110** 137203
[14] Doubrovsky C, Andre G, Gukasov A, Auban-Senzier P, Pasquier C R, Elkaim E, Li M, Greenblatt M, Damay F and Foury-Leylekian P 2012 *Phys. Rev*. B **86** 174417
[15] Yanez-Vilar S et al 2011 *Phys. Rev*. B **84** 134427
[16] Cheong S W and Mostovoy M 2007 *Nat. Mater*. **6** 13–20

[17] Choi Y J, Yi H T, Lee S, Huang Q, Kiryukhin V and Cheong S W 2008 *Phys. Rev. Lett*. **100** 047601
[18] Hearmon A J, Fabrizi F, Chapon L C, Johnson R D, Prabhakaran D, Streltsov S V, Brown P J and Radaelli P G 2012 *Phys. Rev. Lett*. **108** 237201
[19] Lee M, Choi E S, Huang X, Ma J, Dela Cruz C R, Matsuda M, Tian W, Dun Z L, Dong S and Zhou H D 2014 *Phys. Rev*. B **90** 224402
[20] Hwang J, Choi E S, Ye F, Dela Cruz C R, Xin Y, Zhou H D and Schlottmann P 2012 *Phys. Rev. Lett*. **109** 257205
[21] Hutanu V, Sazonov A, Meven M, Murakawa H, Tokura Y, Bordacs S, Kezsmarki I and Nafradi B 2012 *Phys. Rev*. B **86** 104401
[22] Bos J W G, Colin C V and Palstra T T M 2008 *Phys. Rev*. B **78** 094416
[23] Campbell B J, Stokes H T, Tanner D E and Hatch D M 2006 ISODISPLACE: a web-based tool for exploring structural distortions *J. Appl. Crystallogr*. **39** 607–14 http://stokes.byu.edu/isodistort.html
[24] Wang X et al 2015 *Phys. Rev*. *Lett*. **115** 087601
[25] Bilbao Crystallogr. Serv. 2014 MAGNDATA: a collection of magnetic structures with portable cif-type files (Bilbao Crystallographic Server) www.cryst.ehu.es/magndata/
[26] Blake G R, Chapon L C, Radaelli P G, Park S, Hur N, Cheong S W and Rodríguez-Carvajal J 2005 *Phys. Rev*. B **71** 214402
[27] Tokunaga Y, Iguchi S, Arima T and Tokura Y 2008 *Phys. Rev. Lett*. **101** 097205
[28] Ritter C, Vorotynov A, Pankrats A, Petrakovskii G, Temerov V, Gudim I and Szymczak R 2008 *J. Phys.: Condens. Matter* **20** 365209
[29] Kuroe H et al 2011 *J. Phys. Soc. Japan* **80** 083705
[30] Hase M, Kuroe H, Pomjakushin V Y, Keller L, Tamura R, Terada N, Matsushita Y, Donni A and Sekine T 2015 *Phys. Rev*. B **92** 054425
[31] Vilminot S, Andre G and Kurmoo M 2009 *Inorg. Chem*. **48** 2687–92
[32] Müller H, Kockelmann W and Johrendt D 2006 *Chem. Mater*. **18** 2174–80
[33] Caron J M, Neilson J R, Miller D C, Llobet A and McQueen T M 2011 *Phys. Rev*. B **84** 180409(R
[34] Muñoz A, Alonso J A, Casais M T, Martínez-Lope M J, Martínez J L and Fernández-Díaz M T 2002 *Phys. Rev*. B **65** 144423
[35] Garcia-Munoz J L, Rodriguez-Carvajal J and Lacorre P 1994 *Phys. Rev*. B **50** 978
[36] Fernandez-Diaz M T, Alonso J A, Martinez-Lope M J, Casais M T and Garcia-Munoz J L 2001 *Phys. Rev*. B **64** 144417
[37] Janoschek M, Fischer P, Schefer J, Roessli B, Pomjakushin V, Meven M, Petricek V, Petrakovskii G and Bezmaternikh L 2010 *Phys. Rev*. B **81** 094429
[38] Singh K, Simon C, Cannuccia E, Lepetit M B, Corraze B, Janod E and Cario L 2014 *Phys. Rev. Lett*. **113** 137602
[39] Medarde M, Fernandez-Diaz M T and Lacorre P 2008 *Phys. Rev*. B **78** 212101
[40] Giovannetti G, Kumar S, Khomskii D, Picozzi S and van den Brink J 2009 *Phys. Rev. Lett*. **103** 156401
[41] Nunez P, Roisnel T and Tressaud A 1994 *Solid State Commun*. **92** 601–5
[42] Vecchini C, Chapon L C, Brown P J, Chatterji T, Park S, Cheong S-W and Radaelli P G 2008 *Phys. Rev*. B **77** 134434
[43] Yelon W B, Cox D E and Eibschütz M 1975 *Phys. Rev*. B **12** 5007

[44] Ehrenberg H, Wltschek G, Rodriguez-Carvajal J and Vogt T 1998 *J. Magn. Magn. Mater*. **184** 111–5
[45] Kenzelmann M, Coldea R, Tennant D A, Visser D, Hofmann M, Smeibidl P and Tylczynski Z 2002 *Phys. Rev*. B **65** 144432
[46] Free D G and Evans J S O 2010 *Phys. Rev*. B **81** 214433

ANEXO E

Gallego S. V., Perez-Mato J. M., Elcoro L., Tasci E. S., Hanson R. M., Momma K., Aroyo M. I., Madariaga G. *J. Appl. Cryst*. **49**, 1750-76 (2016) DOI: 10.1107/S1600576716012863

MAGNDATA: towards a database of magnetic structures. I. The commensurate case

Samuel V. Gallego[a], J. Manuel Perez-Mato[a]*, Luis Elcoro[a], Emre S. Tasci[b], Robert M. Hanson[c], Koichi Momma[d], Mois I. Aroyo[a] and Gotzon Madariaga[a]

[a]Departamento de Fisica de la Materia Condensada, Facultad de Ciencia y Tecnología, Universidad del País Vasco (UPV/EHU), Apartado 644, 48080 Bilbao, Spain, [b]Department of Physics Engineering, Hacettepe University, 06800 Ankara, Turkey, [c]Department of Chemistry, St Olaf College, Northfield, MN 55057, USA and [d] National Museum of Nature and Science, 4-1-1 Amakubo, Tsukuba, Ibaraki 305-0005, Japan. *Correspondence e-mail: jm.perez-mato@ehu.es

Edited by G. Kostorz, ETH Zurich, Switzerland (Received 13 July 2016; accepted 9 August 2016; online 29 September 2016)

Keywords: magnetic structures database; *MAGNDATA*; commensurate magnetic structures; magnetic space groups; Bilbao Crystallographic Server; magnetic symmetry; irreducible representations.

Abstract:

A free web page under the name *MAGNDATA*, which provides detailed quantitative information on more than 400 published magnetic structures, has been developed and is available at the Bilbao Crystallographic Server (http://www.cryst.ehu.es). It includes both commensurate and incommensurate structures. This first article is devoted to explaining the information available on commensurate magnetic structures. Each magnetic structure is described using magnetic symmetry, *i.e.* a magnetic space group (or Shubnikov group). This ensures a robust and unambiguous description of both atomic positions and magnetic moments within a common unique formalism. A non-standard setting of the magnetic space group is often used in order to keep the origin and unit-cell orientation of the paramagnetic phase, but a description in any desired setting is possible. Domain-related equivalent structures can also be downloaded. For each structure its magnetic point group is given, and the resulting constraints on any macroscopic tensor property of interest can be consulted. Any entry can be retrieved as a magCIF file, a file format under development by the International Union of Crystallography. An online visualization tool using *Jmol* is available, and the latest versions of *VESTA* and *Jmol* support the magCIF format, such that these programs can be used locally for visualization and analysis of any of the entries in the collection. The fact that magnetic structures are often reported without identifying their symmetry

and/or with ambiguous information has in many cases forced a reinterpretation and transformation of the published data. Most of the structures in the collection possess a maximal magnetic symmetry within the constraints imposed by the magnetic propagation vector(s). When a lower symmetry is realized, it usually corresponds to an epikernel (isotropy subgroup) of one irreducible representation of the space group of the parent phase. Various examples of the structures present in this collection are discussed.

1. Introduction

The quantitative characterization of the magnetic ordering realized in magnetic phases is an essential part of research into the magnetic properties of solids. It is certainly fundamental for the cross-checking of theoretical models and for the exploration of complex solid-state magnetic phenomena. Furthermore, the determination of magnetic structures, mainly using neutron diffraction data, is a fundamental step in the search for functional materials for magnetic and/or magnetostructural applications. Since the first report of a magnetic structure determined from neutron diffraction data in 1949 (Shull & Smart, 1949), the magnetic structures of thousands of compounds have been investigated and reported. In 1976, an important effort was made to gather information available on all the magnetic structures known at that point, and a compilation of about 1000 magnetic structures was published (Oles *et al.*, 1976). This effort continued with an additional listing of about 100 structures in 1984 (Oles *et al.*, 1984). Since then, experimental facilities, instruments and analysis methods have improved enormously, and hundreds of magnetic structures are being reported each year. We estimate that, at the moment, there must be about 5000 published magnetic structures. In this scenario, the convenience of a digital database of magnetic structures seems clear, but despite some early work in this direction (Dul *et al.*, 1997), the lack of standards in the description and communication of magnetic structures has precluded the development of an appropriate computer database.

Two recent developments have, however, opened up new possibilities for the systematic application of magnetic symmetry and the achievement of a standardized framework for the description and digital storage of magnetic structures. Firstly, computer-readable listings of the magnetic space groups (or Shubnikov groups) have been made available (Litvin, 2013; Stokes & Campbell, 2011). Secondly, the superspace formalism (the standard approach for the quantitative description of non-magnetic incommensurate structures) has been extended in detail to incommensurate magnetic structures (Petříček *et al.*, 2010; Perez-Mato *et al.*, 2012). These fundamental steps have been the basis for the development of a series of computer tools for a comprehensive application of magnetic symmetry properties that allow an efficient crystallography-like methodology in the analysis and description of commensurate and incommensurate magnetic phases (Perez-Mato *et al.*, 2015). This methodology not only permits the exploration of the possible magnetic orderings associated with one or more propagation vectors in a form that complements and goes beyond the traditional representation method, but can also be employed to store and retrieve any magnetic structure in a robust and unambiguous form analogous to that employed for ordinary non-magnetic crystalline structures.

Another milestone has been the development by the Commission on Magnetic Structures of the IUCr (International Union of Crystallography, 2015) of the so-called magCIF format, *i.e.* an extension of the CIF (crystallographic information file) format (Brown & McMahon, 2002), which provides a robust and unambiguous file format for the archiving and exchange of magnetic structure information. Its preliminary version is already supported by the above-mentioned new symmetry-based computer tools.

Within this framework, we have collected at the Bilbao Crystallographic Server, under the name *MAGNDATA*, comprehensive information on more than 400 commensurate and incommensurate magnetic structures (Fig. 1). *MAGNDATA* is intended to be a benchmark and starting point for a complete database of magnetic structures, where magnetic symmetry is systematically employed and the magCIF format is the communication file format. Here, we present and discuss its main features for the case of commensurate structures. We concentrate on the information made available for each structure, and the way this information can be retrieved and analysed.

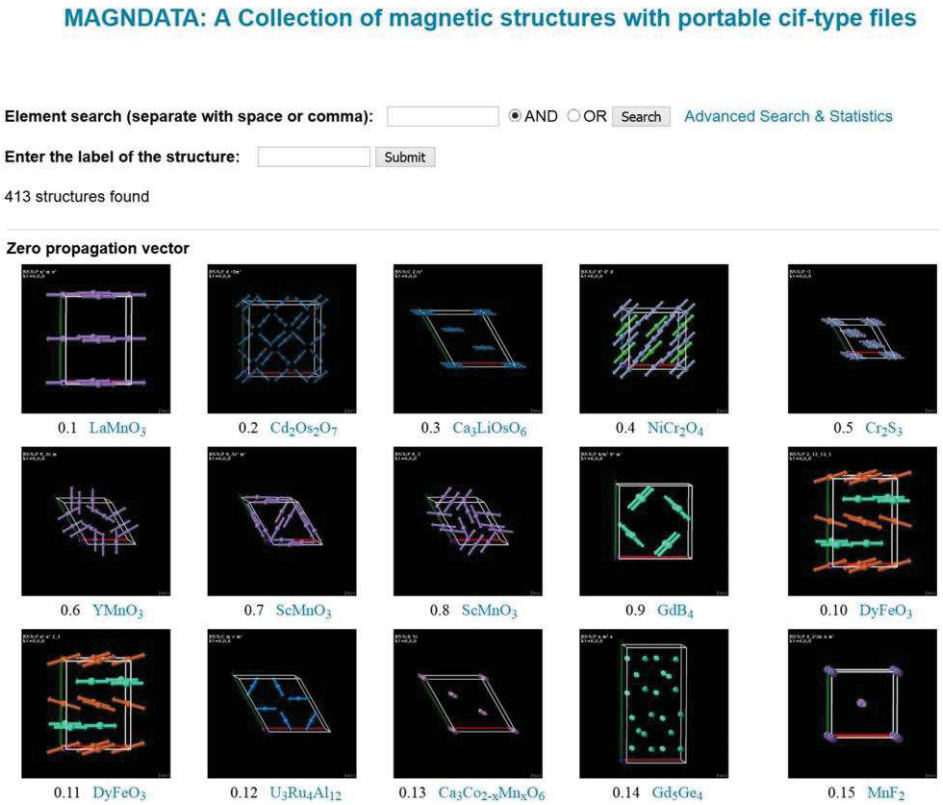

Figure 1
A screenshot showing a partial view of the online list with icons of the magnetic structures stored in *MAGNDATA*.

2. Description of commensurate magnetic structures

A magnetically long-range ordered structure can be considered fully determined if the available information unambiguously defines the average position of any atom and its average magnetic moment. In the case of a commensurate magnetic ordering, this can be achieved by providing three basic data items:

(i) The lattice unit cell that defines the periodicity of the magnetic ordering, *i.e.* the so-called magnetic unit cell.

(ii) The magnetic space group (MSG) or Shubnikov group, with the lattice described by (i), which defines the symmetry of the phase.

(iii) The atomic positions (in relative units with respect to the unit cell) and magnetic moments (if the atom is magnetic) of a set of atoms in the unit cell that are not symmetry related and form an asymmetric unit. From these symmetry-independent atomic positions and magnetic moments, the position and magnetic moment of any other atom in the unit cell can be derived through the application of the symmetry operations of the MSG defined in (ii).

This is the basic information that is stored for any of the commensurate magnetic structures compiled in *MAGNDATA*, and it is an essential part of the corresponding magCIF file that can be downloaded. These magCIF files are supported by various programs, for example for visualization using *VESTA* (Momma & Izumi, 2011) and *Jmol* (Hanson, 2013), for editing using *ISOCIF* (Stokes & Campbell, 2015) or *STRCONVERT* (Perez-Mato *et al.*, 2015), for analysis using *ISODISTORT* (Campbell *et al.*, 2006), or for further refinement using experimental data and *FullProf* (Rodríguez-Carvajal, 1993) or *JANA* (Petříček *et al.*, 2014).

Table 1
Symmetry operations of the MSG describing the symmetry of the magnetic structure of $Ba_2CoGe_2O_7$ (#0.56; Hutanu *et al.*, 2012). These operations correspond to the MSG *Cm'm2'* (No. 35.167) in a non-standard setting. The transformation to a standard setting is (**a**+**b**,-**a**+**b**,**c**; 1/2,0,0).

N	(*x*,*y*,*z*)	(m_x,m_y,m_z)	Seitz notation
1	*x*,*y*,*z*,+1	m_x,m_y,m_z	{1|0}
2	*y*+1/2,*x*+1/2,*z*,+1	-m_y,-m_x,-m_z	{$m_{1\text{-}10}$|1/2,1/2,0}
3	-*x*,-*y*,*z*,-1	m_x,m_y,-m_z	{2'$_{001}$|0}
4	-*y*+1/2,-*x*+1/2,*z*,-1	-m_y,-m_x,m_z	{m'_{110}|1/2,1/2,0}

Table 2
Positions and magnetic moments of symmetry-independent atoms in the magnetic structure of $Ba_2CoGe_2O_7$ (#0.56; Hutanu *et al.*, 2012). Unit cell *a* = 8.46600 Å, *b* = 8.46600 Å, *c* = 5.44500 Å, *α* = 90°, β = 90°, γ = 90°. MSG: *Cm'm2'* (**a**+**b**,-**a**+**b**,**c**; 1/2,0,0). Magnetic moment components are given in Bohr magnetons.

Magnetic atoms:

Label	Atom type	*x*	*y*	*z*	Multiplicity	Symmetry constraints on M	M_x	M_y	M_z	|M|
Co	Co	0.0	0.0	0.0	2	m_x,m_y,0	2.05	2.05	0.0	2.90

Non-magnetic atoms:

Label	Atom type	*x*	*y*	*z*	Multiplicity
Ba_1	Ba	0.83464	0.33466	0.50765	2
Ba_2	Ba	0.33464	0.16536	0.49235	2

Ge_1	Ge	0.64073	0.14073	0.95981	2
Ge_2	Ge	0.14073	0.35927	0.04019	2
O1_1	O	0.00000	0.50000	0.15942	1
O1_2	O	0.50000	0.00000	0.84058	1
O2_1	O	0.63791	0.13793	0.27045	2
O2_2	O	0.13791	0.36209	0.72955	2
O3_1	O	0.07906	0.18446	0.18857	4
O3_2	O	0.18446	0.92094	0.81143	4

As an example, Tables 1 and 2 present these three basic data items for the magnetic structure of $Ba_2CoGe_2O_7$ (Hutanu *et al.*, 2012), which is depicted in Fig. 2(*a*), as retrieved from *MAGNDATA*, where it is entry 0.56. In the following, the entry number of each example in *MAGNDATA* will be indicated in parentheses with the symbol #, *e.g.* (#0.56). With respect to the data in these tables the following remarks are important.

2.1. Symmetry operations

The listed symmetry operations fully define the MSG of the structure. They are given in a similar form to the symmetry operations of space groups in conventional crystallography. Each symmetry operation is described by the corresponding transformation of a general position (*x*, *y*, *z*) (Hahn, 2002) (second column in Table 1) or in the Seitz notation (Glazer *et al.*, 2014) (last column in Table 1). These operations in the first format are the only obligatory data concerning symmetry in a magCIF file. The only difference with respect to the symmetry operations of ordinary space groups is that the presence or not in the symmetry operation of the action of time reversal is also indicated: in the first format this is achieved by means of an additional symbol, −1 or +1, while in the Seitz notation a prime symbol is added or not to the rotation or roto-inversion symbol. As additional (redundant) information, the transformation of a magnetic moment (given in relative components with respect to the unit-cell basis) through the action of the symmetry operation is also listed (third column). The symmetry operations are described with respect to the magnetic unit cell that defines the lattice periodicity of the spin arrangement. In this sense, we use in all cases the Belov–Neronova–Smirnova (BNS) notation (Belov *et al.*, 1957). In the case of MSGs with antitranslations (*i.e.* operations combining a translation and time reversal), the alternative Opechowski–Guccione (OG) notation (Opechowski & Guccione, 1965) uses unit cells that are often closer to the reference lattice used in experiment, but in general they do not define the lattice periodicity of the MSG. The OG notation therefore requires a deviation from a straightforward extension of the group theoretical methods of ordinary crystallography, where symmetry operations and atomic variables are processed `modulo 1' with respect to the employed unit cell. We have preferred to avoid this complication and therefore *MAGNDATA* has been developed in all aspects using the BNS approach.

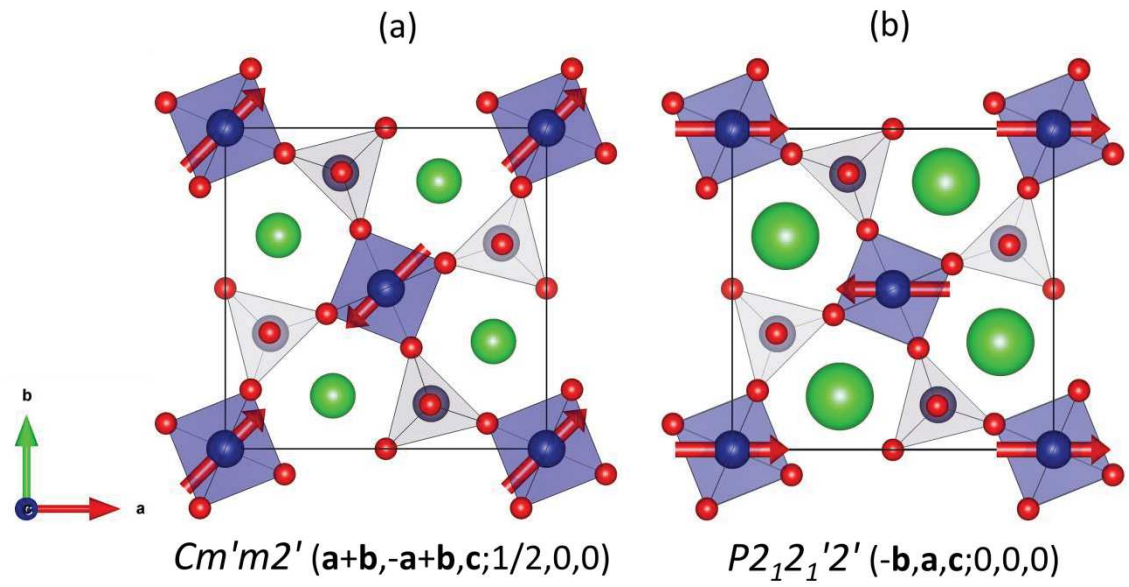

Figure 2
(*a*) The magnetic structure of multiferroic $Ba_2CoGe_2O_7$ (Hutanu *et al.*, 2012) retrieved from *MAGNDATA* (#0.56). A magnetically induced ferroelectric polarization along **c** is symmetry allowed. (*b*) An alternative model with the same but rotated spin arrangement, which has different magnetic symmetry and no multiferroic character. The associated MSG is indicated below each panel. The basis transformation in parentheses beside the MSG label transforms the MSG to its standard setting.

2.2. Magnetic space groups

In most cases we have used a unit cell that keeps the origin and orientation of the crystallographic axes of the paramagnetic phase. This is the reason why, in most cases, as in this example, the MSG is in a non-standard setting. As the symmetry information provided by *MAGNDATA* is the list of symmetry operations in this non-standard basis, this causes no particular problem and no ambiguity exists. The transformation from the used basis to a basis correponding to the standard setting of the MSG is given for each entry in the collection under the heading `Transformation to standard setting'.

In other words, the MSG defined by the listed operations in Table 1 is necessarily one of the 1651 Shubnikov groups, but its setting, *i.e.* the form of the operations, does not necessarily coincide with the one that is used in the listings of the MSGs that we can take as standard (Litvin, 2013; Stokes & Campbell, 2011; Bilbao Crystallographic Server, 2013). In the example above, if the change in unit cell and origin (**a** + **b**, −**a** + **b**, **c**; 1/2, 0, 0) is done, the symmetry operations transform into the BNS standard form of the MSG with the label *Cm*′*m*2′ and BNS number 35.167 (Bilbao Crystallographic Server, 2013). This means that the $\mathbf{a}_o$ and $\mathbf{b}_o$ basis vectors of the standard orthorhombic unit cell are given by the oblique vectors **a** + **b** and −**a** + **b**, respectively, while the origin should be shifted by **a**/2. We can summarize this information by saying, in short, that the symmetry of this structure is given by the MSG *Cm*′*m*2′ (**a** + **b**, −**a** + **b**, **c**; 1/2, 0, 0). Having computer-readable standard listings of all MSGs, this is the notation that can be used to define unambiguously any MSG under any setting. Notice, however, that the transformation to the standard setting is in general not unique, and different choices of unit cell and origin are possible for a standard setting of the MSG. In general, the

transformation to standard setting given in each case is just one of the many possible ones.

The label provided for the relevant MSG is in fact not needed for describing the structure, as the listed set of symmetry operations of the MSG is sufficient to define the MSG that should be used to build up the full structure. The assignment of a standard label and a transformation to the MSG standard setting are, however, included in the magCIF file and in the database as additional complementary information. This summarizes the symmetry properties of the structure in a short unambiguous form and, for instance, the list of symmetry operations in Table 1 could be obtained by the application of the inverse of the transformation (**a** + **b**, −**a** + **b**, **c**; 1/2, 0, 0) to the BNS standard form of the operations of the MSG *Cm*′*m*2′ (No. 35.167), which are retrievable from the databases available on the internet (Bilbao Crystallographic Server, 2013; Stokes & Campbell, 2011). Thus Table 2, with its heading that defines the unit cell, and the MSG label together with the transformation to its standard setting, can be considered a complete, unambiguous and robust form to report the magnetic structure, without the need for Table 1.

2.3. The metrics of the unit cell

As the paramagnetic phase is tetragonal and no orthorhombic strain has been detected, the unit cell of the example above has tetragonal metrics despite the MSG being orthorhombic. This is a common situation, as magnetoelastic couplings are usually very weak and the symmetry break, which in principle is relevant for all degrees of freedom, is often not observed in the lattice. However, it is important to know that, according to the symmetry of the phase, an orthorhombic strain of the unit cell is possible. From the orientation of the standard unit cell of the MSG, one can see that this symmetry-allowed strain is in fact a shear strain, namely a deviation of the γ angle from 90°, while the *a* and *b* parameters must keep equal values.

2.4. Positions and magnetic moments of the symmetry-independent magnetic atoms

The magnetic moments of the magnetic atoms are given as components (in Bohr magnetons) along the **a**, **b** and **c** unit-cell basis vectors. Other alternative parameterizations of the magnetic moments are included in the magCIF dictionary, but they have not been implemented in this database. As shown in Table 2, we list not only the positions and magnetic moments of the symmetry-independent magnetic atoms, but also the symmetry constraints acting on the magnetic moments. It can then be seen that, although according to the model the magnetic moments are aligned along the (1, 1, 0) direction, a deviation from this direction is symmetry-allowed.

Table 3
Full set of symmetry-related atoms in the unit cell, and their magnetic moments, generated from the symmetry-independent Co atom listed in Table 2 (*MAGNDATA* #0.56), as retrieved from *MAGNDATA*.

Atom	*x*	*y*	*z*	Symmetry constraints on M	M_x	M_y	M_z
1	0.00000	0.00000	0.00000	m_x,m_y,0	2.05	2.05	0.0
2	0.50000	0.50000	0.00000	-m_y,-m_x,0	-2.05	-2.05	0.0

2.5. Positions and magnetic moments of all atoms in the unit cell

Optionally, *MAGNDATA* provides the positions and magnetic moments of all the atoms in the unit cell. They are derived from those in the asymmetric unit using the symmetry operations of the MSG: if **r** and **m** are the position and magnetic moment, respectively, of an atom in the asymmetric unit, a symmetry operation $\{\boldsymbol{R}|\mathbf{t}\}$ implies the presence of another atom of the same species at $\mathbf{r}' = \boldsymbol{R}\mathbf{r} + \mathbf{t}$, with magnetic moment given by $\det(\boldsymbol{R})\boldsymbol{R}\cdot\mathbf{m}$, while if the symmetry operation is $\{\boldsymbol{R}'|\mathbf{t}\}$, *i.e.* it includes time reversal, the magnetic moment has an additional change of sign and is given by $-\det(\boldsymbol{R})\boldsymbol{R}\cdot\mathbf{m}$. The listing that can be retrieved for the magnetic atoms of our example is shown in Table 3. One can see in this table that the additional symmetry-allowed moment component in the orthogonal direction (1, -1, 0) breaks the collinearity of the spin configuration and is ferromagnetic. Thus, one can predict from the symmetry assignment that this structure is bound to exhibit weak ferromagnetism on the *ab* plane, more specifically along (1, -1, 0). The possible existence of weak ferromagnetism can also be derived directly from the magnetic point group symmetry associated with the MSG (see below).

2.6. Atomic positions of non-magnetic atoms

In principle, the MSG of a commensurate magnetically ordered phase describes the symmetry constraints of all degrees of freedom, not only of the magnetic ones. Thus, the atomic positions of all the non-magnetic atoms are also derived from those listed within the asymmetric unit by the action of the MSG operations, knowing that the presence or not of time reversal in the operation is irrelevant for the non-magnetic degrees of freedom. The positions and occupancies of all atomic sites are therefore subject to an effective ordinary space group that can be derived from the relevant MSG by eliminating the presence or not of time reversal in its operations. The effective space group in the above example is therefore *Cmm2* (**a** + **b**, -**a** + **b**, **c**; 1/2, 0, 0), with the same transformation to its standard description as for the MSG. As the parent paramagnetic phase of this compound has space group $P\text{-}42_1m$, some atomic sites are split with respect to the paramagnetic structure, and this is reflected in the listing of Table 2 with the split atoms having composite numbers in their labels, such as O1_1, O1_2 *etc.* Also, the unsplit Co atomic site acquires some additional freedom, as the position is now free along the polar **c** direction. The atomic positions listed in Table 2 reflect all the positional degrees of freedom released by the magnetic ordering that could in principle be relevant if the magnetostructural coupling becomes important. It is in the framework of this effective symmetry break $P\text{-}42_1m$ -> *Cmm2* for the non-magnetic degrees of freedom that the multiferroic properties of this material can be explained (Perez-Mato & Ribeiro, 2011).

In most cases, the magnetostructural coupling is very weak and the symmetry break for the positional structure associated with the magnetic ordering, even if formally present, remains undetected within the accuracy of the experimental data. Thus, it is usual that the atomic positions of a magnetic structure are modelled within a good approximation using the constraints associated with the symmetry of the paramagnetic phase, independently of the magnetic ordering producing or not a symmetry break for the atomic positions. Most magnetic structures are therefore refined considering the positional structure and the spin configurations as two

separate phases, with the positional structure being modelled under the space group of the paramagnetic phase. Often, the positional structure is even assumed to be identical to that determined in the paramagnetic phase. Although this type of approximation is often justified, a unique common rigorous approach to all structures, including those where a significant magnetostructural coupling is observed, seemed more appropriate for a database. We have therefore preferred to describe in all cases all the degrees of freedom, both for atomic positions and magnetic moments, under the symmetry constraints of the MSG that is relevant for the reported magnetic arrangement. This is the case for the example above where, despite having an observable electric polarization, the accompanying structural distortion was too weak to be detected and the positional structure was reported under the space group *P-42$_1$m*. Therefore, the symmetry-split atomic sites in Table 2 corresponding to an effective *Cmm2* space group are only virtual and have been derived from the reported *P-42$_1$m* positional structure. This may seem inefficient for some purposes, but it has the advantage of making explicit the structural degrees of freedom that become free in the magnetic phase and which must be taken into account in any eventual investigation of magnetostructural effects.

2.7. Transformation from the original published data

A good number of the magnetic structures published in the past or being published at present are determined using the representation method (Bertaut, 1968; Izyumov *et al.*, 1991) without making use of or identifying the MSG of the resulting magnetic structure. This has meant that, in many cases, we had to reinterpret the spin arrangement of the original article and transform it to the crystallographic symmetry-based description explained above. In this process, the identification of the symmetry group of the reported structure was essential.

In order to identify the relevant MSG, instead of applying a brute force search, a deductive process starting from the knowledge of the parent symmetry and the propagation vector(s) was followed. In most cases, this basic knowledge was sufficient to reduce the possible MSGs to a quite limited set of subgroups of the grey magnetic group associated with the parent phase. These MSGs have a hierarchy according to their group–subgroup relations, and are readily obtained using computer tools such as *MAXMAGN* or *k-SUBGROUPSMAG*, also available on the Bilbao Crystallographic Server (Perez-Mato *et al.*, 2015). Using these programs, combined if necessary with *MAGMODELIZE*, also available there, the different spin-ordering models corresponding to the alternative possible symmetries could be obtained in a straightforward manner and compared with the reported structure. In this way, the relevant symmetry was in general easily identified, and in most cases it was one of the (few) maximal subgroups in the hierarchical tree of possible MSGs (see §E.5 for an example). Once the appropriate magnetic symmetry had been identified, the above-mentioned tools were also employed to produce an appropriate magCIF file of the magnetic structure.

2.8. Visualization and analysis

The output page for each structure includes a pair of figures obtained with *VESTA* (Momma & Izumi, 2011). One of the figures depicts all the atoms, while the second reduces the graphical representation to the magnetic atoms. The *VESTA* files

corresponding to these figures can also be downloaded, but in any case the latest versions of *VESTA* support the magCIF format and commensurate magnetic symmetry. Therefore, the magCIF file provided by *MAGNDATA* can be used directly as input for *VESTA*, which can be used to visualize/analyse the structures.

A direct link to an online three-dimensional viewer that uses *Jmol* (Hanson, 2013) is also available (see Fig. 3). This online tool makes directly accessible the simplest and most important commands of *Jmol* through specific buttons, while the innumerable commands available to manipulate and analyse the graphical representation can be applied through a command window or pop-up console. The latest version of *Jmol* fully supports MSGs and accepts magCIF files as input files. Therefore, *Jmol* can also be used locally if the magCIF file of the sructure is downloaded, provided that the user has previously installed this free program.

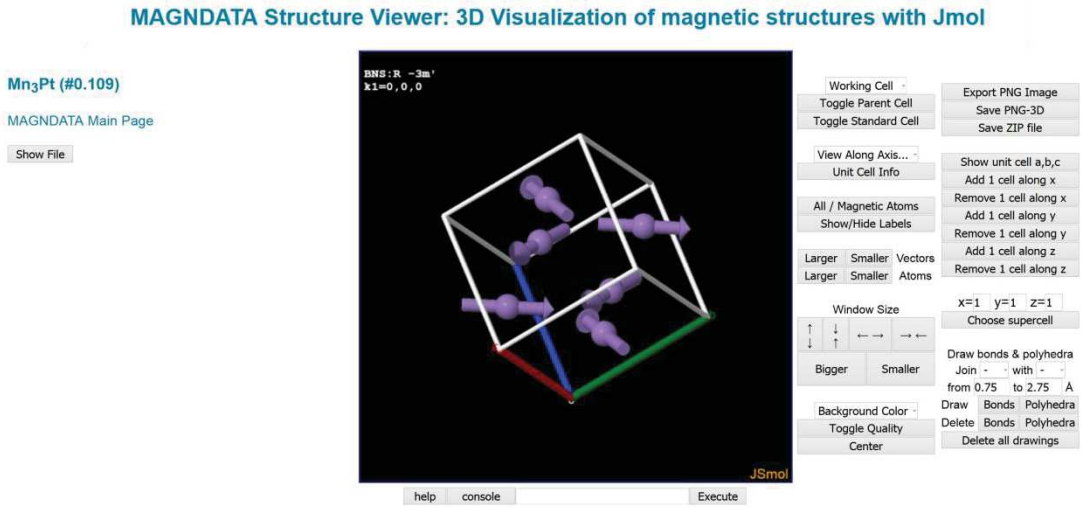

Figure 3
Screenshot of the online visualization of Mn_3Pt (Krén *et al.*, 1967) (#0.109).

3. Additional information

Apart from the minimal information necessary to build up the magnetic structure in three-dimensional space, *MAGNDATA* provides additional important data. This information is also included in the corresponding magCIF file that can be retrieved (local tags beyond the official magCIF dictionary are used for some of the items). We list and discuss here the most important items

3.1. Magnetic point group

The magnetic point group (MPG) associated with a commensurate magnetic structure can be derived in a straightforward manner from the knowledge of its MSG, simply by taking the rotation or roto-inversion operations combined (or not) with time reversal present in the group. This is a very important piece of information, as the magnetic point group governs the macroscopic crystal tensor properties. For instance, the point group of $Ba_2CoGe_2O_7$ (#0.56) discussed above is *m*'*m*2' (No. 7.3.2) (Litvin, 2013) (in a non-standard setting). *MAGNDATA* explicitly lists the operations of the magnetic point group in the used setting (see Table 4).

Table 4
Symmetry operations of the magnetic point group of $Ba_2CoGe_2O_7$ (Hutanu *et al.*, 2012) as given in MAGNDATA (#0.56). These operations form the magnetic point group *m'm2'* (No. 7.3.2) in a non-standard setting. The transformation to a standard setting is **a** + **b**, -**a** + **b** ,**c**.

N	(*x*,*y*,*z*)	(m_x,m_y,m_z)	Seitz notation
1	*x*,*y*,*z*,+1	m_x,m_y,m_z	1
2	*y*,*x*,*z*,+1	-m_y,-m_x,-m_z	m_{1-10}
3	-*x*,-*y*,*z*,-1	m_x,m_y,-m_z	$2'_{001}$
4	-*y*,-*x*,*z*,-1	-m_y,-m_x,m_z	m'_{110}

A direct link to *MTENSOR* (another program on the Bilbao Crystallographic Server) then allows the user to explore, for this specific point group and the setting used, the symmetry-adapted form of any macroscopic tensorial magnetic, structural or magnetostructural property (see next section). For the simplest properties in this example the results are rather obvious: the point group is polar along the **c** direction, while it allows ferromagnetism along the **b** direction of the standard unit cell, *i.e.* the (-1, 1, 0) direction in the basis used. The parent symmetry being non-polar, the magnetic point group symmetry is thus sufficient for the characterization of the system as having a non-polar/polar symmetry break and therefore as a type II multiferroic, where one can expect some induced electric polarization and some weak ferromagnetism, in accordance with the discussion in §E.2.

One must be aware that, in general, the point group symmetry of a magnetic structure not only is determined by the spin arrangement but also depends on the positions of the non-magnetic atoms: the simple spin arrangement depicted in Fig. 2(*a*), if considered in a purely mono-atomic Co structure, would have implied a rather different MSG and point group, which would forbid both ferroelectricity and weak ferromagnetism. Only the presence of the non-magnetic atoms reduces the parent symmetry, and as a consequence also the symmetry of the magnetic structure, to the MSGs discussed above.

It is also important to remark that both the MSG and the corresponding magnetic point group, and therefore also the multiferroic properties of this particular example, depend on the orientation of the collinear spin arrangement (see Fig. 2). The MSG, and as a consequence the magnetic point group, change if this orientation is changed. For instance, if the spins align along the **a** direction, the MSG changes to $P2_12_1'2'$ (−**b**, **a**, **c**; 0, 0, 0), with point group 2′2′2 (**a**, −**c**, **b**), which is non-polar, but it also has a ferromagnetic (FM) component allowed along the **b** direction, perpendicular to the direction of the antiferromagnetic (AFM) arrangement (Perez-Mato & Ribeiro, 2011). An electric polarization is not possible for this configuration and therefore magnetically induced ferroelectricity, which can be present for the oblique orientation of the spins, is forbidden for this alternative orientation. One can then predict that an external magnetic field rotating on the *ab* plane, through its coupling with the weak FM component, should induce the rotation of the AFM spin arrangement and a switch between the two limiting polar and non-polar symmetries, producing a sinusoidal oscillation of the induced electric polarization along **c**. This is indeed what is observed experimentally (Murakawa *et al.*, 2010).

Although the magnetic anisotropy may favour some specific direction, and hence some specific MSGs, it is sometimes difficult, as in this example, to determine the absolute orientation of the spins and, even if that is experimentally feasible, this orientation may be easily manipulated with external fields. In practice, this can mean some uncertainty over the actual MSG of the magnetic phase and the corresponding point group. In these ambiguous cases, we have generally assumed a spin orientation that maximizes the resulting magnetic symmetry. Known macroscopic properties, as shown in this example, can help to avoid ambiguities over the relevant MSG.

3.2. Parent space group and relation of the basis used with the one of the parent phase

By definition, a magnetic structure is distorted with respect to a so-called parent structure without magnetic order. This is independent of the magnetic phase being accessible directly from a paramagnetic phase or being bordered in the phase diagram by other magnetic phases. Although a magnetic structure is in principle fully defined using the data discussed in the previous section, the knowledge of the symmetry of its parent paramagnetic structure is fundamental to characterize the possible domains and the switching properties of the system. Therefore, this parent space group is included as additional information. If the parent structure has been considered in a non-standard setting, the transformation of its basis to the standard setting is also given.

In the above example of $Ba_2CoGe_2O_7$ (#0.56), the parent space group is *P-42₁m*, with the same unit cell and origin as those employed to describe the magnetic structure. This means that the magnetic phase results from a symmetry break that can be represented as

$$P-42_1m \longrightarrow Cm'm2'\left(\mathbf{a}_\mathrm{p}+\mathbf{b}_\mathrm{p},-\mathbf{a}_\mathrm{p}+\mathbf{b}_\mathrm{p},\mathbf{c}_\mathrm{p};\tfrac{1}{2},0,0\right) \qquad \text{(E.1)}$$

where the transformation to the standard setting is now described with respect to the basis of the parent phase. The index of the MSG *Cm*′*m*2′, as a subgroup of the parent grey tetragonal magnetic space group *P-42₁m1'* of the paramagnetic phase, is 4, and therefore four domain types are possible. Removing the trivial ones related by time reversal and having all spins reversed, one has to consider two distinct non-trivial domains related, for instance, by the lost operation {-4$_{001}$|0,0,0}. This means that the two domains will have their spins rotated by 90° and opposite electric polarization along **c**. This switching property is directly related to the symmetry of the parent phase. A magnetic structure with the same symmetry *Cm*′*m*2′, and for instance a parent space group *Cmmm*1′, would have different switching properties, having the spins in the two non-trivial domains related by space inversion.

The database includes information about the relation of the bases used for the reference parent phase and the magnetic unit cell. This is given under the heading `Transformation from parent structure'. In the example above this transformation is the identity, *i.e.* (**a**, **b**, **c**; 0, 0, 0). As a more complex example, we show in Fig. 4 the case of $Ba_3Nb_2NiO_9$ (Hwang *et al.*, 2012) (#1.13). Here, the parent space group is *P*-3*m*1 and the propagation vector of the magnetic ordering is (1/3,1/3,1/2). The magnetic unit cell that we use keeps the orientation and origin of the parent unit cell. Therefore,

the indicated `Transformation from parent structure' is (3**a**, 3**b**, 2**c**; 0, 0, 0). This is not a standard setting for the MSG $P_c31c$ of the structure, and under the heading `Transformation to a standard setting' the transformation (2/3**a**+1/3**b**,-1/3**a**+1/3**b**,**c**;1/9,2/9,0) is indicated. One should be aware that the first transformation refers to the parent basis, while the second one refers to the working magnetic unit cell that is being used for the MSG. The three bases/unit cells can be visualized online, as shown in Fig. 4. Combining the two basis transformations (from parent unit cell to the used magnetic unit cell, and from the used magnetic unit cell to a magnetic unit cell in a standard setting), the symmetry break between the parent and the magnetic phase is fully defined. Thus, in this example, the symmetry break is

$$P-3m1\,1' \longrightarrow P_c31c\left(2\mathbf{a}_\mathrm{p}+\mathbf{b}_\mathrm{p},-\mathbf{a}_\mathrm{p}+\mathbf{b}_\mathrm{p},2\mathbf{c}_\mathrm{p};\tfrac{1}{3},\tfrac{2}{3},0\right) \qquad \text{(E.2)}$$

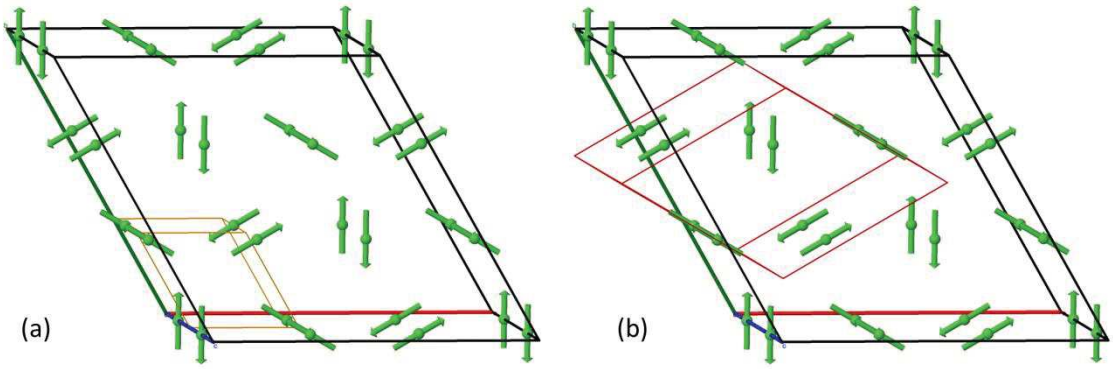

Figure 4
The spin arrangement in the magnetic structure of $Ba_3Nb_2NiO_9$ (#1.13) reported by Hwang *et al.* (2012), as given by the online *Jmol* visualization tool of *MAGNDATA*, showing (*a*) the magnetic unit cell used and the parent unit cell, and (*b*) the magnetic unit cell used and that corresponding to the standard setting of the MSG.

In most cases, the parent space group is clearly defined, as it corresponds to the symmetry of the experimental paramagnetic phase, and this structure is usually known and used as a reference for the subsequent determination of the magnetic structure. However, if the paramagnetic structure also includes some structural distortion with respect to a higher symmetry, the concept of parent symmetry becomes ambiguous and the formal choice of a parent space group is not unique. In these cases, we have usually considered as the parent structure the one that was used as a reference for the magnetic diffraction in the article reporting the structure. However, in some exceptional cases a better choice was detected and a different parent symmetry has been considered. This may happen, for instance, in magnetic phases where the presence of a concomitant structural distortion has led to the use of the distorted structure as a reference for the refinement of the magnetic diffraction data.

3.3. Propagation vector(s)

The propagation vectors that are active as primary wavevectors of the magnetic ordering are part of the characterization of a magnetic phase. These wavevectors can be derived in a straightforward manner from knowledge of the MSG and the parent space group of the magnetic structure, and the relation of their respective unit-cell

bases. In practice, however, the propagation vectors are directly accessible in diffraction experiments, and knowledge of them is usually the first step in the process of determining the magnetic structure. Thus, although the form in which the magnetic structures are described in *MAGNDATA* does not require the explicit definition of these propagation vectors, this information is included as an important complementary feature which is directly related to the experiment. If the magnetic arrangement includes spin waves with wavevectors corresponding to harmonics of a primary propagation vector, they are also listed.

The components of the propagation vectors are given in the reciprocal conventional basis of the parent space group. In our first example of Fig. 1, the propagation vector is **k** = (0, 0, 0), which means that magnetic ordering keeps the lattice of the parent structure, and neutron magnetic diffraction peaks will superpose with the nuclear ones. In Fig. 4, the propagation vector is (1/3,1/3,1/2).

The propagation vectors are used in this collection as the most basic feature for classifying the magnetic structures, and this is reflected in the entry labels. The structures are divided into six fundamental classes:

Class 0. Magnetic structures with a null propagation vector [**k** = (0, 0, 0)] which keep the lattice of the parent structure, and their MSG is necessarily of type I or III (Bradley & Cracknell, 1972), which means that the MSG does not include antitranslations of type {1′|**t**} (*i.e.* combinations of translations with time reversal).

Class 1. Commensurate magnetic structures with a single primary nonzero propagation vector **k**, such that *n***k** is a reciprocal lattice vector of the parent space group, with *n* even. The MSGs of these structures are necessarily of type IV (Bradley & Cracknell, 1972), *i.e.* they contain anti-translations of type {1′|**t**}. Higher harmonics with wavevectors *m***k** (*m* odd) may be present in the spin arrangement (if these vectors are not equivalent to **k**). The point group of these materials includes time reversal, *i.e.* it is a grey point group, and therefore linear magnetostructural effects are not possible.

Class 1.0. Commensurate magnetic structures with a single primary nonzero propagation vector **k**, such that *n***k** is a reciprocal lattice vector of the parent space group, with *n* odd. The MSGs of these structures are necessarily of type I or III (Bradley & Cracknell, 1972), as in Class 0, but some lattice translations of the parent structure are lost and the lattice of the magnetic structure is described by a supercell of the parent unit cell. As in the previous class, higher harmonics with wavevectors *m***k** (*m* odd) can be present in the spin arrangement, and in this case these possible higher harmonics necessarily include a wavevector equivalent to (0, 0, 0). This means that some magnetic neutron diffraction peaks can superpose with the nuclear ones if such a harmonic is present in the spin arrangement.

Class 2. Commensurate magnetic structures with two independent primary propagation vectors.

Class 3. Commensurate magnetic structures with three independent primary propagation vectors. Among the structures in classes 2 and 3 with more than one primary propagation vector, those having propagation vectors that are symmetry-related by the MSG operations form an important special set. However, the number of

multi-**k** magnetic structures that are being reported is minimal, and therefore we have not introduced further divisions within classes 2 and 3.

Class 1.1. Incommensurate magnetic structures with a single primary incommensurate propagation wavevector. The symmetry of magnetic structures with incommensurate propagation wavevectors cannot be described using an MSG or Shubnikov group. Their systematic description requires a different methodology. Its symmetry can be described by a magnetic superspace group (MSSG), similar to what happens in the case of incommensurate non-magnetic crystals and quasicrystals (Perez-Mato *et al.*, 2012). The specific form in which incommensurate magnetic structures are stored in *MAGNDATA* using magnetic superspace symmetry is described in detail in a separate publication (Gallego *et al.*, 2016).

3.4. Representation analysis

Commensurate magnetic structures are described in this database under the framework and constraints associated with their MSG, without using the so-called representation method (Bertaut, 1968; Izyumov *et al.*, 1991). However, once a magnetic structure is described under its relevant MSG symmetry and a corresponding magCIF file is prepared, the symmetry mode decomposition of the magnetic structure with respect to the parent structure, in terms of basis spin modes corresponding to the different possible irreducible representations (irreps) of the parent space group, can be done in a straightforward manner with the program *ISODISTORT* (Campbell *et al.*, 2006). Following this procedure, we have obtained for most structures of this collection their irrep mode decomposition, and we have included a brief summary of the magnetic irreps that are active in each phase and their restrictions. Only in the trivial cases for which the assignment of the MSG has a one to one correspondence with the assignment of an irrep has this step often been skipped.

Table 5 lists a set of examples of the information provided on the irrep mode decomposition. The irrep labels are those provided by *ISODISTORT*. This labelling convention is robust and unambiguous, and can be applied through computer-readable irrep listings (Stokes *et al.*, 2013). It has been adopted by the Bilbao Crystallographic Server and by *JANA* (Petříček *et al.*, 2014). This irrep labelling is also consistent with the most extended notation for **k** vectors corresponding to symmetry points, lines and planes of the Brillouin zone (Aroyo *et al.*, 2014). Note that the irreps associated with spin modes, which are odd for time reversal, are distinguished from the analogous non-magnetic ones, which are even for time reversal, by means of the letter `m' as a prefix. For each active irrep, the dimensions of the small and the full representations are given. The factor between these two numbers is the number of **k** vectors in the star of the irrep (Bradley & Cracknell, 1972; Stokes *et al.*, 2013).

If the irrep is multidimensional, the direction of the magnetic order parameter in irrep space is classified as either `general` or `special'. A `general' order parameter direction indicates that the MSG allows any arbitrary combination of the irrep spin basis modes and the MSG is the minimum magnetic symmetry compatible with this irrep distortion, *i.e.* the so-called kernel of the irrep, in contrast with the higher symmetries for some specific irrep subspaces, the so-called irrep epikernels (Ascher, 1977). If the order parameter direction is termed `special', we mean that the symmetry

constraints of the MSG imply the restriction to some specific linear combinations of the irrep spin basis modes, and therefore the spin degrees of freedom of the magnetic phase are fewer than those provided by the full set of irrep spin basis functions.

Table 5
Examples of the available information on the symmetry mode decomposition of the magnetic structures in MAGNDATA.

Compound	Ref.†	Parent SG[a]	k vector(s)	MSG[b]	Irrep(s)	d_s[c]	d_f[d]	O.p.d[e]	Action
$MnTe_2$ (#0.20)	(a)	*Pa-3*	(0,0,0)	*Pa-3* (No. 205.33)	mGM1	1	1	-	Primary
$LiFeGe_2O_6$ (#1.39)	(b)	*$P2_1/c$*	(1/2,0,0)	*P_a2_1/c* (No. 14.80)	mY1+	1	1	-	Primary
ErAuGe (#1.33)	(c)	*$P6_3mc$*	(1/2,0,0)	*P_Cna2_1* (No. 33.154)	mM2	1	3	-	Primary
Mn_3Pt (#0.109)	(d)	*Pm-3m*	(0,0,0)	*R-3m'* (No. 166.101)	mGM4+	3	3	Special	Primary
Na_2MnF_5 (#1.55)	(e)	*$P2_1/c$*	(0,1/2,0)	*P_bc* (No. 7.29)	mZ1	2	2	Special	Primary
$HoMnO_3$ (#1.20)	(f)	*Pnma*	(1/2,0,0)	*P_bmn2_1* (No. 31.129)	mX1	2	2	Special	Primary
$TbMn_2O_5$ (#1.108)	(g)	*Pbam*	(1/2,0,1/4)	*C_am* (No. 8.36)	mG1	2	4	General	Primary
Ca_3LiOsO_6 (#0.3)	(h)	*R-3c*	(0,0,0)	*C2'/c'* (No. 15.89)	mGM3+ mGM2+	2 1	2 1	Special -	Primary Secondary
NiO (#1.6)	(i)	*Fm-3m*	(1/2,1/2,1/2)	*C_c2/c* (No. 15.90)	mL3+ mL2+	2 1	8 4	Special -	Primary Secondary
TmAgGe (#3.1)	(j)	*P-62m*	(1/2,0,0) (1/2,1/2,0) (0,1/2,0)	*P-6'2m'* (No. 189.224)	mM2	1	3	Special-2	Primary
$FePO_4$ (#0.17)	(k)	*Pnma*	(0,0,0)	*$P2_12_12_1$* (No. 19.25)	mGM1+ mGM1-	1 1	1 1	- -	Primary Primary
Bi_2MnRuO_7 (#0.153)	(l)	*Fd-3m*	(0,0,0)	*Fd'd'd* (No. 70.530)	mGM4+ mGM5+	3 3	3 3	Special Special	Primary Primary
$LuFe_4Ge_2$ (#0.140)	(m)	*$P4_2/mnm$*	(0,0,0)	*Pn'n'm* (No. 58.399)	mGM2- GM2+ mGM1-	1 1 1	1 1 1	- - -	Primary Primary Secondary

†References: (*a*) Burlet *et al.* (1997), (*b*) Redhammer *et al.* (2009), (*c*) Baran *et al.* (2001), (*d*) Krén *et al.* (1967), (*e*) Núñez *et al.* (1994), (*f*) Muñoz, Casáis *et al.* (2001), (*g*) Blake *et al.* (2005), (*h*) Calder *et al.* (2012), (*i*) Ressouche *et al.* (2006), (*j*) Baran *et al.* (2009), (*k*) Rousse *et al.* (2003), (*l*) Martínez-Coronado *et al.* (2014), (*m*) Schobinger-Papamantellos *et al.* (2012). [a] Parent space group. [b] Magnetic space group. [c] Dimension of small *irrep.* [d] Dimension of full *irrep.* [e] Order parameter direction.

In the case of irreps with more than one arm in their star of **k** vectors and with **k** equivalent to −**k**, spin arrangements restricted to a single **k** imply a special direction for the order parameter of a rather trivial character. This restriction is introduced automatically in the traditional representation method, when the exploration of spin

arrangements is limited to those coming from the spin basis functions associated with a single **k** of the irrep star. Non-trivial symmetry constraints in 1**k** magnetic structures that are not included in the traditional representation method appear when the star of **k** vectors includes the vector −**k** as non-equivalent and/or when the small irrep is multidimensional. In both cases, the irrep restricted to the symmetry operations that either keep **k** invariant or change it into −**k** (the so-called extended small space group) is multidimensional. The effective order parameter for the single-**k** spin arrangements is therefore multidimensional in these cases and, for special directions within the order parameter space, a higher MSG (irrep epikernel) may be realized. These are the cases that are indicated in the database as having a `special' direction for the irrep, and they are of interest because the correspondence between the MSG and the irrep assignment is not one to one, with different MSGs being possible for the same active irrep.

In the case of multi-**k** structures with several propagation vectors belonging to the same irrep star, even if the small irrep is one dimensional and **k** is equivalent to **−k**, special directions of the order parameter with different MSGs can occur, depending on the way the spin basis functions corresponding to different propagation vectors of the irrep star are combined. These structures are distinguished in the database by denoting them as `special-2' for the direction of the order parameter.

The information on the irrep mode decomposition is completed with the qualification of the active irreps which are listed as `primary' or `secondary'. A symmetry-allowed irrep distortion is identified as primary if the spin modes can be considered as the driving agent for the symmetry break of the magnetic phase, while it is secondary if they are symmetry allowed but their presence in the magnetic ordering can be considered a secondary induced effect, which could be negligible.

In most cases, only one irrep is compatible with the MSG of the structure, and therefore its primary character is obvious. This is the case for the first seven examples in Table 5, where one can see that, when the small irrep is multidimensional, in most cases the magnetic phase corresponds to a special irrep direction, and therefore the description using the MSG implies additional constraints. Other structures have an MSG that is compatible with more than one magnetic irrep [see Ca_3LiOsO_6 (#0.3; Calder *et al.*, 2012) and subsequent entries in Table 5], but one of the possible irreps is the primary one, yielding the symmetry break in the observed MSG. The distinction between primary and secondary irreps has relevance only in this type of structure. Secondary irrep distortions, although symmetry-allowed, are usually absent. They can appear as weak secondary induced effects, and they are often negligible. The absence of these secondary irrep distortions implies that the effective number of spin degrees of freedom of the structure decreases, with respect to those allowed by the MSG, by constraining the model to the spin degrees of freedom of the primary irrep. However, it is important to remark that, in the traditional refinement method, the possible presence of allowed secondary irrep distortions may have been discarded *a priori* without an experimental check. A combined application of magnetic symmetry and representation analysis is especially recommended in these structures. Representation analysis allows the decomposition of the spin degrees of freedom within the relevant MSG into primary and secondary ones, and the performance of a controlled and

systematic check of the significance of possible secondary modes in the spin arrangement. However, the identification of the relevant MSG for the phase is a necessary previous step in order to `symmetry adapt' the spin basis modes of the primary irrep.

The explicit separation of the magnetic degrees of freedom into primary and secondary ones (if these latter exist) within the constraints of an MSG can be done using *ISODISTORT*. In *MAGNDATA*, we have only included some information about the number of degrees of freedom associated with each irrep, and a flag indicating whether the secondary irrep is really present with nonzero amplitude in the distortion. This information does not pretend to be comprehensive. In any case, users can always download the corresponding magCIF and, with the CIF of the appropriate parent phase, obtain in a few minutes with *ISODISTORT* (and previous transformation with *ISOCIF* if the magCIF file is in a non-standard setting) the symmetry mode decomposition of any of the commensurate structures in *MAGNDATA*. A direct link to another program on the Bilbao Crystallographic Server also provides a survey of all compatible irreps (see next section).

Magnetostructural coupling is usually too weak to allow observation of secondary non-magnetic structural displacive distortion modes induced by the magnetic ordering. If they exist in the reported structure, they have generally not been included in the summary of the irrep mode decomposition of the structure, which is limited to the magnetic irreps. Non-magnetic irreps have only exceptionally been included in the irrep summary, as for instance in the case of $LuFe_4Ge_2$ (#0.140; Schobinger-Papamantellos *et al.*, 2012). This compound is reported to exhibit a structural phase transition simultaneously with the magnetic ordering. From its symmetry properties one can deduce that the observed structural distortion is not a magnetic induced effect, as this distortion produces an additional symmetry break that must be taken into account for the MSG of the magnetic phase. Therefore, the non-magnetic irrep associated with this structural distortion should be considered as a primary irrep, and it is listed accordingly in the irrep summary.

3.5. Transition temperature and experiment temperature

If available, the transition temperature below which the reported structure becomes stable is given. This usually coincides with the Néel temperature of a paramagnetic–antiferromagnetic phase transition, but in systems with multiple magnetic phases the temperature given can be the upper temperature bordering a neighbouring magnetic phase. If available, the temperature at which the magnetic diffraction data were measured (experiment temperature) is also listed.

3.6. References

Magnetic structures are often reported without providing a detailed account of the atomic positional structure that has been considered, or if provided, it may correspond to the paramagnetic phase or to a measurement at a different temperature from the one at which the magnetic ordering was measured. In order to have as complete a description of the magnetic structure as possible, we have in most cases used (if available) the atomic positions from the same reference, as retrieved from the

Inorganic Crystal Structure Database (ICSD, 2007), and the ICSD entry number is indicated. If not available, an ICSD entry for the same compound (usually at room temperature) has been employed. In other cases the positional structure has been manually retrieved from the reference. In general, one should be aware that atomic positions are often only approximate, as they may have been determined independently of the magnetic ordering and under different experimental conditions.

3.7. Comments:

The comments that appear for a particular structure are normally reduced to information on the experimental technique used for the data, details of the experimental conditions or the phase diagram of the material, the existence of similar structures *etc*. If the MSG corresponds to a so-called **k**-maximal symmetry (Perez-Mato, 2015) (see next section), this is also stated in the comments. The presence of a magnetic structure in this collection should not be taken as a kind of validation, as we have not performed any cross-check of the proposed structures, and the only requirement was that the model is self-consistent and unambiguous. In fact, the database contains more than one model for some magnetic phases, and they do not necessarily agree. If, according to our analysis, a structure presents some contradictions, compared with either the information given in the same publication or that in other references, these problems are mentioned in the comments. If the way that the structure has been reported strongly indicates that it was fitted without fully exploring all possible spin arrangements, or introducing some strong aprioristic constraints, this may also be mentioned here.

4. Links to other programs

By means of direct links, the relevant data for any entry can be introduced for further analysis into other programs of the Bilbao Crystallographic Server. The most important linked programs are the following:

STRCONVERT. This tool allows automatic online editing, some transformations and different output formats.

MAGNEXT (Gallego *et al.*, 2012). This program provides the systematic absences to be expected on the non-polarized neutron magnetic diffraction diagram due to the MSG of the crystal. The program can also list the symmetry-forced form of the magnetic structure factor for special symmetry directions or planes in reciprocal space. This information can be used to derive additional systematic absences if the orientation of the spins has constraints that are not dictated by the MSG. Possible extra systematic absences due to the restrictions of the magnetic sites to some specific Wyckoff positions are not included. It is important to remark that the systematic absences are expressed in terms of (*h*, *k*, *l*) indices with respect to the reciprocal unit cell of the basis used for the description of the magnetic structure in the present database. This unit cell does not necessarily coincide with that considered in the original publication.

MTENSOR. This program provides the symmetry-adapted form of any crystal tensor property (equilibrium, optical or transport properties). All kinds of crystal tensors (up to eighth rank) can be consulted. The tensor constraints are derived considering the magnetic point group of the structure in the setting (in general non-standard) defined

by the unit cell used in the present database. For example, Fig. 5 reproduces the output of *MTENSOR* for the linear magnetoelectric tensor relating electric polarization and magnetic field for the case of $Ba_2CoGe_2O_7$ (#0.56), the example discussed in §E.2. From the form of the magnetoelectric tensor, one can derive that the application of a magnetic field along **c** is bound to induce some electric polarization along the (1,-1,0) direction, which is the direction of the weak ferromagnetism. Alternatively, the application of the magnetic field along this particular basal direction induces some electric polarization along **c**, which should be added to the ferroelectric spontaneous polarization along this direction. Although in general this magnetoelectric response may be difficult to disentangle from additional magnetoelectric effects due to field-induced reorientation of the spins and domain switching, one must be aware of its existence when interpreting magnetoelectric experiments. Through this link with *MTENSOR*, our database provides the necessary information for any kind of crystal tensor property that may be of interest. This program can also be used to explore tensor switching properties when switching the system to domain-related configurations.

α^T_{ij}		j		
		1	*2*	*3*
i	*1*	0	0	α^T_{13}
	2	0	0	$-\alpha^T_{13}$
	3	α^T_{31}	$-\alpha^T_{31}$	0

Figure 5
The symmetry-adapted form of the magnetoelectric tensor (inverse effect) relating electric polarization and magnetic field, in the form $P_i = \alpha^T_{ij} H_j$, for $Ba_2CoGe_2O_7$ (*MAGNDATA* #0.56) as given by *MTENSOR* through its link with *MAGNDATA*. Note that the setting of the orthorhombic point group symmetry is not standard.

MVISUALIZE. Apart from being a *Jmol*-based visualization tool, with similar features to the online viewer mentioned in §E.2, this separate program, which can work with any magnetic structure introduced with a magCIF file, can be used to produce domain-equivalent structures or to change the description of the structure to any setting/unit-cell basis that may be wished, including the standard setting.

From the knowledge of the parent space group and the MSG of the structure, the program provides a complete set of parent symmetry operations that, applied to the original structure, produce all possible distinct domain-related equivalent structures. These alternative domain-related equivalent descriptions of the magnetic structure can then be visualized and saved as magCIF files.

Let us consider the case of Cs_2CoCl_4 (#1.51; Kenzelmann *et al.*, 2002). The symmetry break of the magnetic ordering in this compound is

$$Pnma1' \longrightarrow P_a 2'_1\left(\mathbf{c}_p, \mathbf{a}_p, \mathbf{b}_p + \mathbf{c}_p; 0, \tfrac{3}{8}, -\tfrac{1}{8}\right) \qquad \text{(E.3)}$$

with the propagation vector **k** = (0,1/2,1/2). The primitive magnetic cell is duplicated with respect to that of the parent lattice, while the point group symmetry reduces from the 16 operations of *mmm*1′ to the four operations in 21′. Hence the index of the magnetic group, as a subgroup of the parent grey group, is 8 and we should expect eight types of domain. The domain-related structures are obtained by transforming the structure stored in the database by the lost symmetry operations of the paramagnetic phase. Only a coset representative for each of the eight cosets of the coset decomposition of the MSG P_a2_1 with respect to the parent group *Pnma*1′ is necessary to obtain the eight distinct domain-related configurations of the magnetic structure with respect to the parent paramagnetic phase. After elimination of the trivial domains obtained by switching all spins to opposite values by the action of the lost time reversal, there are then four non-trivial domains. This means that four distinct but equivalent descriptions of the magnetic structure exist if the parent paramagnetic phase is taken as a common reference. *MVISUALIZE* makes a choice for this set of distinct non-trivial coset representatives (see Fig. 6) and provides, if desired, the magnetic structure models corresponding to each of them (see Fig. 7).

Domain-related equivalent descriptions

MAGNDATA entry: Cs_2CoCl_4 (#1.51)

Magnetic space group P_a2_1 (#4.10) (**c**,**a**,1/2**b**+1/2**c**; 0,3/8,-1/8)
Parent space group *Pnma* (#62) (**a**,**b**,**c**; 0,0,0)
Transformation from parent structure: (**a**,2**b**,2**c**; 0,0,0)

[Magnetic Structure]

Domain-related equivalent structures: coset representatives and conjugated subgroups

The transformation matrices of the table are from the parent space group to the standard setting of the listed magnetic space groups
The coset representatives used to derive the domain-related equivalent structures are expressed in the setting of the parent group

N	Coset representatives		Transformation matrix	Magnetic Structure
	(x,y,z) form	Seitz notation		
1	x,y,z,+1	{ 1 | 0 }	$\begin{pmatrix} 0 & 1 & 0 & 0 \\ 0 & 0 & 1 & 3/4 \\ 2 & 0 & 1 & 7/4 \end{pmatrix}$	Show
2	-x+1/2,-y,z+1/2,+1	{ 2_{001} | 1/2 0 1/2 }		Show
3	-x,-y,-z,+1	{ -1 | 0 }		Show
4	x+1/2,y,-z+1/2,+1	{ m_{001} | 1/2 0 1/2 }		Show

Figure 6
A screenshot of the ouput for Cs_2CoCl_4 (#1.51) listing the chosen set of symmetry operations (coset representatives) in the magnetic phase, whose action on the magnetic structure produces all the distinct non-trivial domain-related spin arrangements, which are physically equivalent.

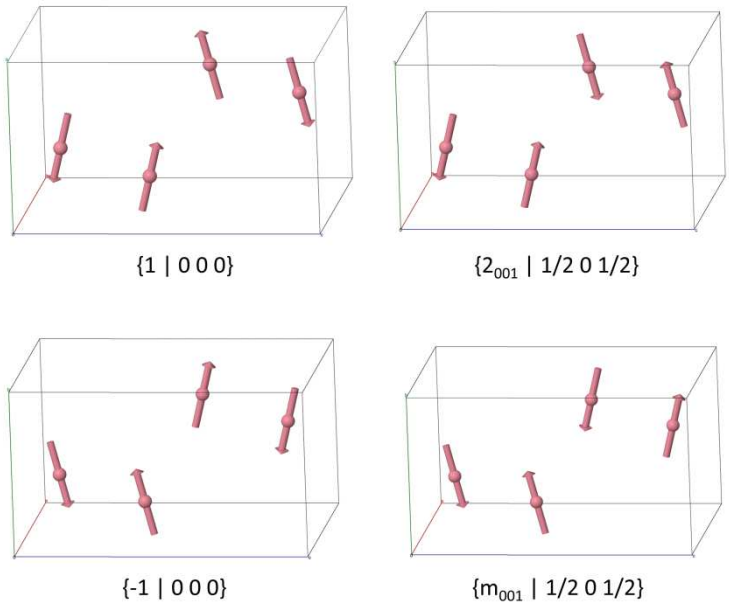

Figure 7
Graphical representation of the four non-trivial domain-related equivalent descriptions of the magnetic structure of Cs_2CoCl_4 (#1.51), as obtained using the corresponding link in *MAGNDATA*. Only the magnetic atoms within a parent unit cell are shown. The spins are repeated in consecutive parent cells with the same or opposite orientation, according to the set of centring translations and anti-translations of the corresponding MSG or, equivalently, according to the phase factor for the propagation vector **k** = (0,1/2,1/2). The lost symmetry operation (coset representative listed in Fig. 6) that has been employed to generate the transformed structure is indicated below each case. Four additional domains, trivially related to those in the figure through the switch of the direction of all spins, complete the set.

Enumeration of the different domain-related descriptions is very important when comparing structures proposed by different studies or when refining the structure. It allows the researcher to enumerate all possible models that are experimentally indistinguishable because of their full equivalence. Particularly in the case of powder diffraction, it is not uncommon to confuse or mix these alternative descriptions of the same model with physically different ones that may fit the experimental data equally well. A systematic determination of all domain-related descriptions not only precludes this confusion, but can also help to detect pseudosymmetry in the model. In Fig. 6 for instance, one can see that the inversion symmetry is only broken by the slight canting of the spins. But the spin *z* component of the Co atoms is 0.4 (2) Bohr magnetons, compared with 1.6 (4) for the *y* component (Kenzelmann *et al.*, 2002). The spin canting that breaks the centrosymmetry of the structure is therefore close to its standard deviation. Cs_2CoCl_4 (#1.51) is one of the few magnetic structures in *MAGNDATA* where the spin arrangement associated with a single multidimensional irrep corresponds to a general direction within the irrep, and the symmetry is reduced to the irrep kernel (see Table 6 in §E.6).

Get_mirreps. This program provides a list of compatible irreps for a given magnetic symmetry break from a parent grey group. It includes all magnetic and non-magnetic irreps of the parent grey group that are allowed to be active in a distorted structure with the symmetry given by the input subgroup. The corresponding wavevectors and

special directions within the irrep spaces are also indicated. Through the direct link to this program, one obtains for each commensurate structure information about all possible primary and secondary irreps that can be relevant. It should be stressed that the program lists *all* compatible irreps from the viewpoint of symmetry, without considering the specificity of the structure. This means that some of these irreps may be irrelevant, because they are not present in the irrep decomposition of the degrees of freedom of the structure.

5. Trend to maximal symmetry: the example of pyrochlore-type structures

A general principle of maximal symmetry is generally at work, and the symmetry of the majority of the structures that are being reported is given by a `maximal subgroup' among the set of possible ones. These most favourable MSGs can be termed `maximal' in the sense that there is no supergroup (subgroup of the parent grey symmetry) that fulfils the same conditions. If only the compatibility condition with the observed propagation vector(s) is taken into account, we denote these most favourable MSGs as `**k**-maximal subgroups', `**k**-maximal MSGs', `**k**-maximal symmetries' *etc.* (Perez-Mato *et al.*, 2015). However, the compatibility condition can be more restrictive if the magnetic atoms occupy special Wyckoff positions, and some of the MSGs compatible with the observed propagation vector(s) can be discarded, either because they force a null magnetic moment at all magnetic sites or because they do not represent any additional degree of freedom with respect to those already allowed by a supergroup.

As an example, Fig. 8 shows the possible MSGs for a magnetic structure with parent space group *Fd*-3*m* (parent MSG *Fd*-3*m*1'), zero propagation vector, and magnetic atoms at the positions 16*c* (0, 0, 0) and/or 16*d* (1/2,1/2,1/2). The figure shows the group–subgroup hierarchy among all the possible symmetries which could be realized. This is the relevant scenario for all magnetic orderings in pyrochlore-type structures that do not break the parent lattice periodicity. In the figure, one can see that there are six possible maximal symmetries in the sense explained above, and three of them are realized in some of the collected structures. Fig. 9 depicts some examples. Although we could not find any experimental structure with any of the other three maximal symmetries, one should be aware that these magnetic structures are often determined with `trial and error' methods, and in some cases it is doubtful that all possible alternative arrangements have been explored and cross-checked. In other cases, powder diffractometry is unable to distinguish between alternative spin modes or their combination, and an arbitrary choice has been made among indistinguishable (but different) configurations (Wills *et al.*, 2006).

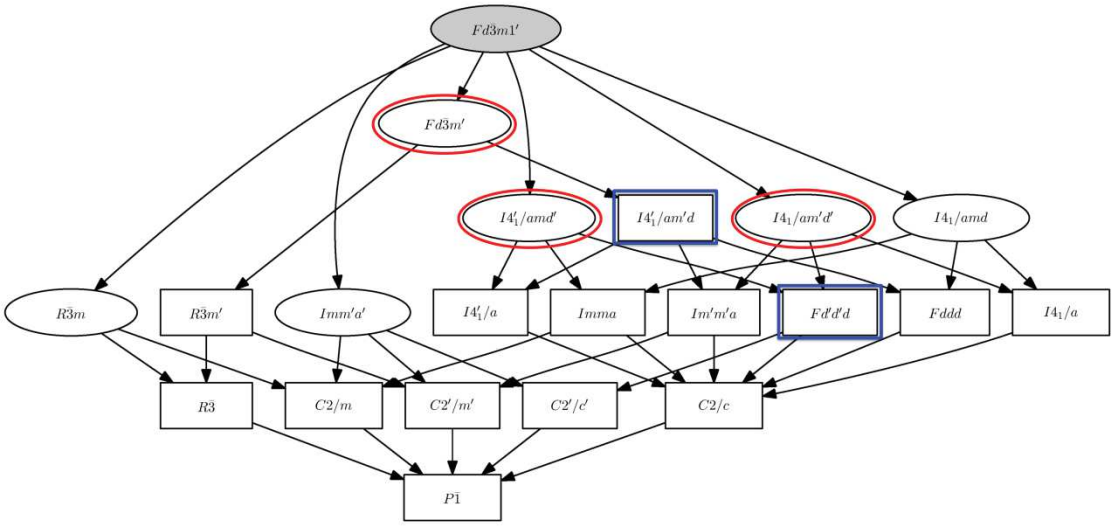

Figure 8

Possible symmetries for a magnetic structure having a parent structure with space group *Fd*-3*m* and a null propagation vector, with the magnetic atoms at sites 16*c* (0, 0, 0) and/or 16*d* (1/2,1/2,1/2). The symmetries are shown as subgroups of the parent grey MSG using standard BNS labels (Stokes & Campbell, 2011), indicating their group–subgroup relationship. Maximal subgroups are surrounded by black ovals. Only one MSG is shown for each conjugacy class of physically equivalent subgroups. The symmetries realized by the experimental pyrochlore structures gathered in *MAGNDATA* are highlighted with red ellipses in the case of maximal symmetries or with blue squares otherwise. (Obtained with *k-SUBGROUPSMAG*; Perez-Mato *et al.*, 2015).

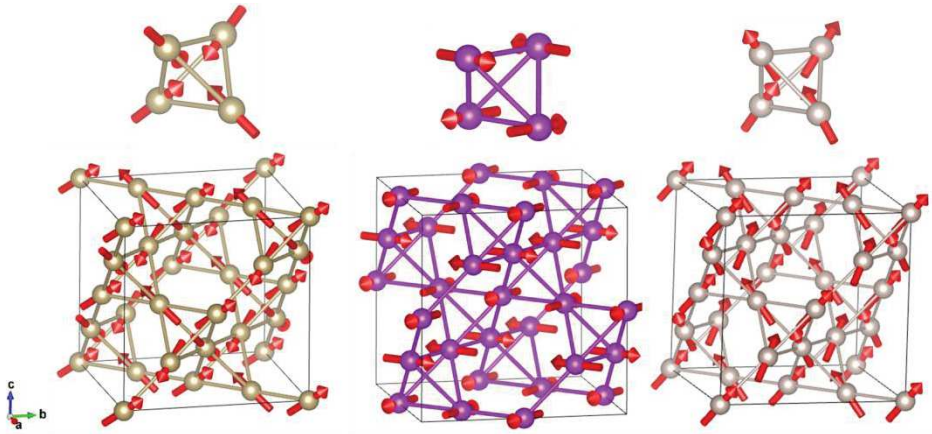

Figure 9

Examples of magnetic structures in *MAGNDATA* having one of the maximal symmetries indicated in Fig. 8, corresponding to $Cd_2Os_2O_7$ (Yamaura *et al.*, 2012), $Gd_2Sn_2O_7$ (Wills *et al.*, 2006) and $Ho_2Ru_2O_7$ (Wiebe *et al.*, 2004).

Only three of the ten pyrochlore-type zero-field magnetic phases with 16*c* or 16*d* as the magnetic site and with **k** = 0, which are present in *MAGNDATA*, do not possess a maximal symmetry in the sense explained above. Two of them have the symmetry $I4_1'/am'd$. As shown in Fig. 8, this group is a subgroup of *Fd*-3*m*' and is therefore not maximal among the possible subgroups. It is, however, maximal among the possible symmetries for magnetic ordering if, according to Landau theory (see §E.3 above), it is

assumed to be triggered by a single irrep. As shown in Fig. 10, this subgroup is indeed one of the two possible maximal symmetries resulting from a spin arrangement according to the two-dimensional irrep GM3+. In general, all maximal MSGs for a given propagation vector and specific magnetic sites are maximal irrep epikernels, but the reverse is not true. Some irrep epikernels of maximal symmetry may be subgroups of one or more MSGs, which are epikernels (or kernels) for another irrep. This is the case in Fig. 10 for the MSG *I*4$_1$'/*am*'*d*, which is a subgroup of *Fd*-3*m*', the kernel of irrep mGM2+ (see Fig. 8). This means that this MSG allows the presence of a secondary mGM2+ spin mode of symmetry *Fd*-3*m*', apart from the primary irrep mode corresponding to mGM3+.

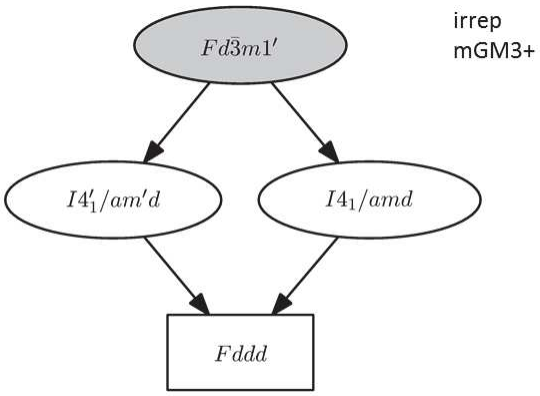

Figure 10
Possible MSGs (epikernels and kernel) for spin arrangements according to the two-dimensional irrep mGM3+ of *Fd*-3*m* (#227), with **k** = 0, showing their group–subgroup relationship. Maximal subgroups are surrounded by black ovals. One single group for each conjugacy class of equivalent subgroups is shown. (Obtained with *k-SUBGROUPSMAG*; Perez-Mato *et al.*, 2015.)

The structure of Bi_2RuMnO_7 (#0.153; Martínez-Coronado *et al.*, 2014) is the only one of the pyrochlore-type structures that could not be classified as having maximal symmetry, in the broad sense summarized in Fig. 8, or in the restrictive sense of a maximal epikernel of a single irrep, as described by Fig. 10. As can be seen in the irrep decomposition summary of this simple collinear structure, this model represents the superposition of spin modes corresponding to two different irreps, namely mGM4+ and mGM5+ (see Table 5), and it is therefore not simple from this viewpoint. It is not clear if the collinearity was an *a priori* assumption or whether more complex models were explored during the refinement. In any case, the authors reporting the structure seem to be unaware of the fact that the proposed collinear model, despite its apparent simplicity, implies the presence of two active primary irreps.

From this example, it becomes clear that an efficient methodology for the structure determination of such a type of complex phase would require the systematic contrast of the experimental data with each of the models corresponding to *all* possible alternative maximal symmetries, monitoring within these symmetries the degrees of freedom corresponding to different irreps if more than one is allowed, and eventually descending to lower MSGs, if necessary.

6. A survey of the collection

MAGNDATA includes a set of sampling and search tools that can be used to explore various properties among the more than 370 collected commensurate structures. Here, we summarize some of the features that can be explored with these tools.

6.1. Experimental technique

While neutron powder diffraction is the main technique for the determination of most of the structures, about one-fifth of them are based on data from neutron single-crystal experiments.

6.2. Structures with a single active primary one-dimensional irrep

About 95% of the structures are single-**k** structures, and 50% of them have a one-dimensional order parameter transforming according to an irrep which is one-dimensional when restricted to the subspace of spin arrangements with the observed propagation vector. In the language of representation analysis, this means that the small irrep is one-dimensional and the propagation vectors **k** and −**k** are equivalent. These are the most simple magnetic structures. The MSG is necessarily **k** maximal in the sense explained in previous sections, and space inversion symmetry is necessarily conserved if existing in the parent phase. Apart from the domains corresponding to possible symmetry-related distinct propagation vectors, only two types of domain exist, which are trivially related by time reversal (switch of all the spins).

6.3. Structures with a single primary multidimensional irrep active

About 100 single-**k** structures have a primary irrep which is multidimensional when restricted to the subspace of spin arrangements for the given propagation vector. The relevant MSG in about 80% of these structures corresponds to an irrep epikernel of maximal symmetry (see §§E.4 and E.5). This means that the spin arrangement includes symmetry-dictated constraints restricting the possible combination of the irrep basis functions. In these structures, the effective point group for the non-magnetic degrees of freedom is lower than the set of parent point group operations keeping the propagation vector invariant, and non-trivial orientational domains with the same propagation vector exist.

6.4. Structures with maximal symmetry

About 76% of the single-**k** commensurate structures have a **k**-maximal symmetry, and if one adds those with their symmetry given by a maximal epikernel of a multidimensional irrep that is not **k** maximal, the number of structures with maximal symmetry within the constraint of a **k** vector or irrep is about 85%. There are therefore about 15% of structures with symmetries that are not maximal in either of these two senses. These cases require either the action of two or more primary irreps or some arbitrariness in the direction taken by the magnetic order parameter, which in these exceptional cases would not be fully dictated by symmetry.

6.5. Structures with exceptional low symmetries

We could only detect eight structures where the direction of the magnetic order parameter within the multidimensional irrep is `general' in the sense explained in §E.4, such that it does not take one of the possible symmetry-dictated directions of higher symmetry. These are listed in Table 6. Most of them are rather complex structures with many spin degrees of freedom, even if they are restricted to a single active irrep [see, for instance, $DyFe_4Ge_2$ (#1.98; Schobinger-Papamantellos *et al.*, 2006) and $Tm_5Ni_2In_4$ (#1.170; Szytuła *et al.*, 2014) in Fig. 11]. Often, the articles accompanying the reports of these structures suggest that the MSG of the model has not been monitored, and models with possible higher symmetries associated with the epikernels of the irrep have not been explored and contrasted with the proposed structure. In some cases, the macroscopic properties of the phases also suggest the possibility of a higher MSG and therefore a special direction for the order parameter. This happens, for instance, with the multiferroics $BiMn_2O_5$ (#1.75; Vecchini *et al.*, 2008), and $TbMn_2O_5$ (#1.108) and $HoMn_2O_5$ (#1.109; Blake *et al.*, 2005), where the direction of the induced electric polarization is along one of the orthorhombic directions, which would be consistent with one of the irrep epikernels. In the case of $BiMn_2O_5$, such an alternative structure of higher symmetry has in fact been reported in another study (#1.74; Muñoz *et al.*, 2002).

Table 6
Single-**k** magnetic structures where the multidimensional order parameter takes a general direction and the symmetry is not maximal for the relevant irrep.

The dimension of the irrep restricted to the subspace of the **k** vector is given in the last column in parentheses, together with the label of the irrep.

Compound	**Ref†**	**k vector**	**Parent SG[a]**	**MSG[b]**	**MPG[c]**	***Irrep* (dim)**
Cs_2CoCl_4 (#1.51)	(a)	(0,1/2,1/2)	*Pnma*	P_a2_1 (4.10)	*21'*	*mT1* (2)
$BiMn_2O_5$ (#1.75)	(b)	(1/2,0,1/2)	*Pbam*	C_am (8.36)	*m1'*	*mU1* (2)
$DyFe_4Ge_2$ (#1.98)	(c)	(1/4,1/4,0)	$P4_2/mnm$	P_ccc2 (27.82)	*mm21'*	*mSM4* (2)
$TbMn_2O_5$ (#1.108)	(d)	(1/2,0,1/4)	*Pbam*	C_am (8.36)	*m1'*	*mG1* (4)
$HoMn_2O_5$ (#1.109)	(d)	(1/2,0,1/4)	*Pbam*	C_am (8.36)	*m1'*	*mG1* (4)
$NiSb_2O_6$ (#1.113)	(e)	(1/2,0,1/2)	$P4_2/mnm$	P_S*-1* (2.7)	*-11'*	*mR1+* (2)
NiS_2 (#1.167)	(f)	(1/2,1/2,1/2)	*Pa-3*	P_S*-1* (2.7)	*-11'*	*mR1+R3+* (4)
$Tm_5Ni_2In_4$ (#1.171)	(g)	(0,1/2,1/2)	*Pbam*	C_am (8.36)	*m1'*	*mT1* (2)

†References: (*a*) Kenzelmann *et al.* (2002), (*b*) Vecchini *et al.* (2008), (*c*) Schobinger-Papamantellos *et al.* (2006), (*d*) Blake *et al.* (2005), (*e*) Ehrenberg *et al.* (1998), (*f*) Yano *et al.* (2016), (*g*) Szytuła *et al.* (2014). [a] Parent space group. [b] Magnetic space group. [c] Magnetic point group.

Among this set of structures of exceptionally low symmetry, there are also quite simple ones such as Cs_2CoCl_4 (#1.51; Kenzelmann *et al.*, 2002), already discussed in §E.4 (see Fig. 7), where the general direction and the deviation from an MSG of higher symmetry are due to a small spin canting, close to its standard deviation. The spin arrangement of $NiSb_2O_6$ (#1.113; Ehrenberg *et al.*, 1998), depicted in Fig. 12(*a*), is also very simple, but its simplicity is deceptive from the point of view of magnetic symmetry. Non-collinear arrangements could conserve higher symmetries, which correspond to the epikernels of the only possible active irrep. Sketches of these alternative models are also shown in Fig. 12. Certainly, the prevalence of the exchange interaction in conjunction with crystal anisotropy may favour the reported collinear

arrangement, despite its larger symmetry reduction. Nevertheless, sometimes it seems that the non-collinear models corresponding to possible higher symmetries have not been fully checked.

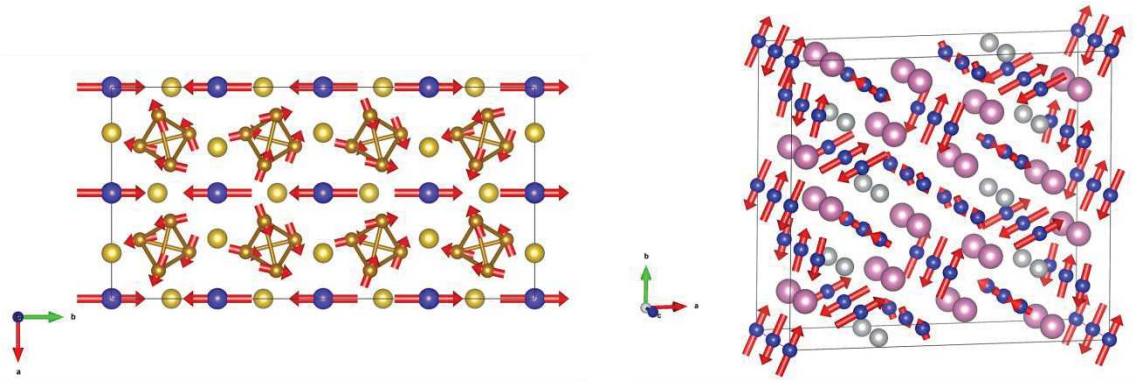

P_ccc2 (-**c**,-**a**,**b**; 3/2,0,0)
$DyFe_4Ge_2$ (#1.98)

C_am (-**b**,-**c**,**a**; 0,0,1/4)
$Tm_5Ni_2In_4$ (#1.170)

Figure 11
The magnetic structures of $DyFe_4Ge_2$ (Schobinger-Papamantellos *et al.*, 2006) and $Tm_5Ni_2In_4$ (Szytuła *et al.*, 2014) as retrieved from *MAGNDATA* (#1.98 and #1.170). These models belong to the few (listed in Table 6) where the magnetic symmetry realized is not maximal for the active irrep.

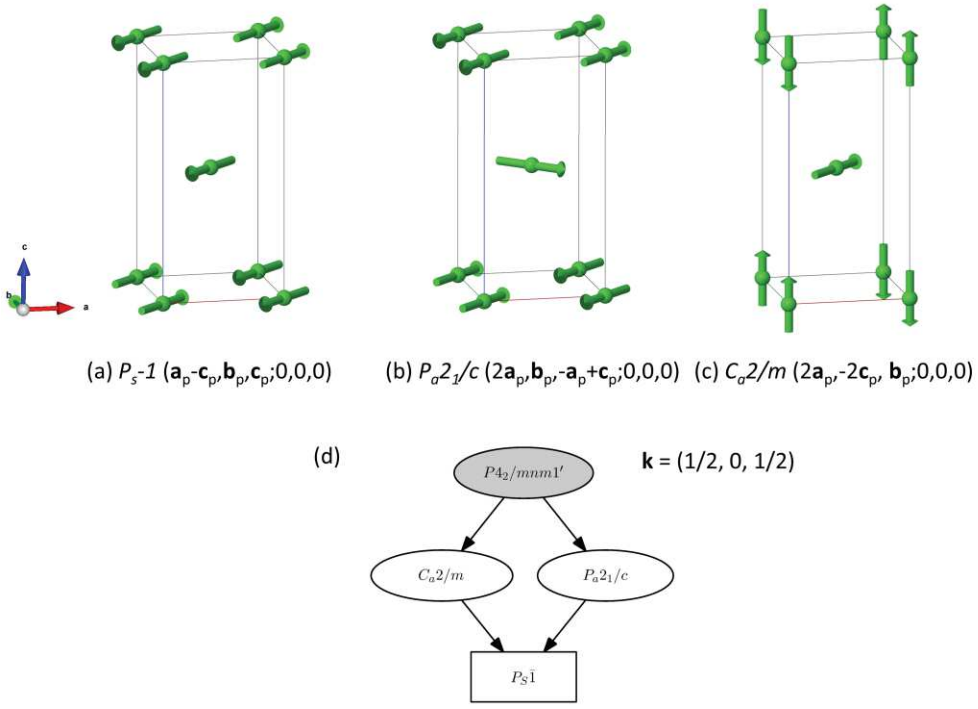

Figure 12
(*a*) A scheme of the collinear magnetic structure reported for $NiSb_2O_6$ (Ehrenberg *et al.*, 1998) (#1.113) with the lowest possible symmetry, despite its collinearity. Only the spins in a parent unit cell are shown; the signs of the spins in consecutive unit cells are determined by the propagation vector (1/2,0,1/2). Its MSG, and a transformation from the parent tetragonal basis to its standard setting, are indicated below the sketch. The magnetic sites at the origin and at the unit-cell centre are symmetry independent and have their three spin components fully free. (*b*) and (*c*) Alternative models with higher symmetry according to the group–subgroup

hierarchy of possible subgroups shown in part (*d*). In the P_a2_1/c symmetry the two Ni sites are symmetry related, only one having its three spin components free, and the arrangement is necessarily non-collinear, except if the easy axis is either along **b** or on the *ac* plane. In the case of the MSG C_a2/m the two sites are independent, with one having the spin restricted along **c** and the other on the *ab* plane, also forcing either a non-collinear arrangement or a null spin in one of the magnetic atoms.

It should be remarked that there are also a few structures where the order parameter direction is termed `general' in the database, but the irrep is a two-dimensional so-called `physically irreducible' representation. Two-dimensional physically irreducible representations do not possess special directions of higher symmetry and have no epikernel, the maximal symmetry being the irrep kernel, realized for any direction of the order parameter. Therefore, in these cases, a general direction for the order parameter is the only one possible, and they have not been included in Table 6.

6.6. Structures with several primary irreps

Most of the structures are the consequence of an order parameter transforming according to a single primary irrep, in agreement with the usual assumption based on the Landau theory of phase transitions. However, about 10% require the action of two or more primary irreps. Table 5 lists the example of $FePO_4$ (#0.17; Rousse *et al.*, 2003), where the spin arrangement includes spin modes corresponding to two one-dimensional irreps, the resulting MSG being the intersection of the kernels of the two irreps, and therefore both irreps being primary. The reason for the presence of two primary irreps is often quite obvious, like the existence of two consecutive phase transitions, or the independent ordering of two different magnetic atoms, but in other cases it is not clear and would require deeper investigation.

The case of $La_2O_2Fe_2OSe_2$ (#1.58; Reehuis *et al.*, 2011) shown in Fig. 13 is especially remarkable. This simple collinear arrangement with propagation vector (1/2,0,1/2) involves two primary irreps and breaks the space inversion of the parent phase with space group $I4/mmm$. The reason is that any of the irreps, if considered alone, would force a null spin in half of the magnetic sites, which are located at Wyckoff position 4*c* of the parent phase. Therefore, the collinear ordering of all atoms is sufficient here to yield a symmetry break into polar symmetry and the system, being a semiconductor, could be expected to exhibit type II multiferroic properties with spin-driven ferroelectricity (Perez-Mato *et al.*, 2016). A similar situation, where the reported collinear arrangement requires two primary irreps, happens in Bi_2RuMnO_7 (#0.153; Martínez-Coronado *et al.*, 2014), already discussed in §E.5.

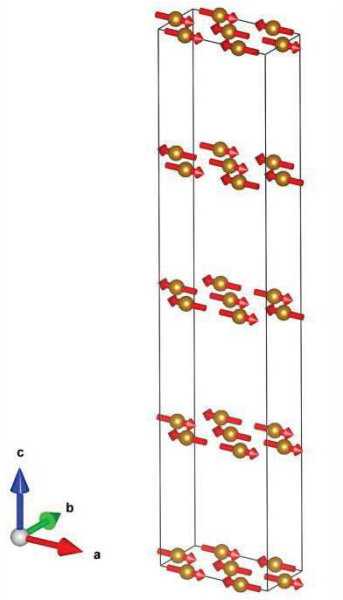

$I4/mmm1' \rightarrow C_cc$ (**a**-**c**,**b**,**c**; 0,0,0)

Figure 13
The collinear magnetic structure of $La_2O_2Fe_2OSe_2$ (Free & Evans, 2010) (#1.58) with an indication of the symmetry break with respect to the paramagnetic phase. Two active primary irreps for the wavevector (1/2,0,1/2) are required in order to have non-null spins at all magnetic sites and the symmetry reduces to a polar monoclinic MSG, with potential multiferroic properties.

6.7. Collinearity and canting

About 50% of the collected structures are collinear, as expected from the usually dominant exchange-type interactions. In contrast with the unusual example of Fig. 13, these collinear arrangements are often compatible with one of the maximal MSGs. Their collinearity can even be part of the constraints of the MSG and in such cases it is symmetry protected [see, for instance, $LiFePO_4$ (#0.95; Rousse *et al.*, 2003) or CrN (#1.28; Corliss *et al.*, 1960)]. In most cases, however, the MSG allows spin components that can break the collinearity. In such cases, assuming collinearity reduces the effective number of spin degrees of freedom with respect to those really allowed by the relevant MSG. The identification of the MSG identifies these possible spin cantings, which are often too weak to be detected, especially in powder experiments. Nevertheless, the collection in *MAGNDATA* includes a good number of structures where they are significant and have been fully characterized (see Fig. 14 for some examples). These structures mostly come from single-crystal studies and it is noticeable that, among the structures that have been determined from single-crystal data, the models with collinearity that is not forced by symmetry amount to only about 10%. This percentage is much larger among the structures determined from powder data.

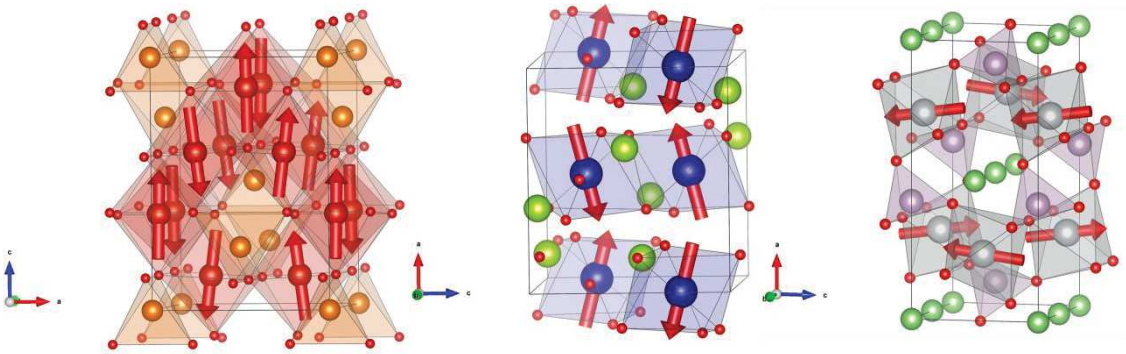

Figure 14
Examples of magnetic structures retrieved from *MAGNDATA* [MgV_2O_4 (#1.138; Wheeler *et al.*, 2010), $CoSe_2O_5$ (#0.119; Melot *et al.*, 2010) and $LiNiPO_4$ (#0.88; Jensen *et al.*, 2009)] with significant spin canting compatible with their MSG. Below each figure, the parent grey group and the MSG of the structure are indicated, including the transformation from the parent basis to the standard setting of the MSG.

An exceptional case is $CoSe_2O_5$, where the results seem to be in contradiction with the general trend: while a powder diffraction study (Melot *et al.*, 2010) reported the structure represented in Fig. 14, with a considerable symmetry-allowed spin canting, a more recent single-crystal study (#0.161; Rodriguez *et al.*, 2016) has refuted the existence of any observable deviation from collinearity.

6.8. Weak ferromagnetics and ferrimagnetics

Any antiferromagnetic phase with a magnetic point group compatible with homogeneous magnetization is susceptible to exhibiting weak ferromagnetism. In other words, weak ferromagnetism can appear in any AFM phase where the cancelling of the global magnetization is not symmetry dictated. In most cases, the symmetry-allowed FM component is too weak to be observed in diffraction experiments, but it is in general detectable in macroscopic measurements. There are about 100 structures with MSGs allowing ferromagnetism, among them the well known systems where weak ferromagnetism was first analysed: α-Fe_2O_3 (#0.66; Hill *et al.*, 2008), $MnCO_3$ (#0.115; Brown & Forsyth, 1967), $CoCO_3$ (#0.114; Brown *et al.*, 1973), $NiCO_3$ (#0.113; Plumier *et al.*, 1983) and $FeBO_3$ (#0.112; Pernet *et al.*, 1970). This large set of structures also includes ferrimagnetic structures, which have more than one symmetry-independent magnetic site, and have their easy axis along an FM direction of the MSG. In principle, weak ferromagnetism can be expected to be especially favourable if the symmetry-allowed FM mode belongs to the same irrep as the primary AFM order parameter, and therefore can be linearly coupled with it, as happens in the classical weak ferromagnets mentioned above. The identification of the primary irrep and its equality or not with that of the FM mode(s) can easily be derived from the information available in *MAGNDATA* on the irrep decomposition of each structure. In any case, the large number of structures fulfilling the necessary symmetry conditions shows that weak ferromagnetism can be a rather common phenomenon, and it can be foreseen if the MSG of the structure is identified.

6.9. Multiferroics

Structures with polar symmetry and with their polarity being induced by the magnetic ordering can easily be retrieved from the collection, by looking for entries with a polar point group and a non-polar one for the parent phase. There are about 40 entries with this property, and those that are insulators fulfil the symmetry condition for being type II multiferroics. They are bound to have some magnetically induced electric polarization (whatever its size) with switching properties coupled with the magnetic order parameter. Many of them are well known multiferroics, but the possible ferroelectric character of a few additional ones has been shown for the first time through the symmetry assignment done in this database. A detailed discussion of these materials is the subject of a separate article (Perez-Mato *et al.*, 2016).

Table 7
Non-polar magnetic phases in MAGNDATA with their transition temperature above 80 K which allow linear magnetoelectric properties if non-metallic. Magnetoelectrics that support non-zero electric polarization at zero field are excluded by the non-polar condition on the MSG. Compounds that to our knowledge are metallic have also been excluded from the list.

Compound	Ref.†	Parent SG[a]	MSG[b]	MPG[c]	T (K)[d]
$FePO_4$ (#0.17)	(a)	*Pnma*	*P2₁2₁2₁* (No. 19.25) ($\mathbf{a}_p$,$\mathbf{b}_p$,$\mathbf{c}_p$; 0,1/2,3/4)	*222*	125
Cr_2O_3 (#0.59)	(b)	*R-3c*	*R-3'c'* (No. 167.106) ($\mathbf{a}_p$,$\mathbf{b}_p$,$\mathbf{c}_p$; 0,0,0)	*-3'm'*	343
Cr_2TeO_6 (#0.76; #0.143)	(c), (d)	*P4₂/mnm*	*Pn'nm* (No. 58.395) ($\mathbf{a}_p$,$\mathbf{b}_p$,$\mathbf{c}_p$; 1/2,1/2,1/2)	*m'mm*	93
$BaMn_2Bi_2$ (#0.89)	(e)	*I4/mmm*	*I4'/m'm'm* (No. 139.536) ($\mathbf{a}_p$,$\mathbf{b}_p$,$\mathbf{c}_p$; 0,0,0)	*4'/m'm'm*	390
$CaMn_2Sb_2$ (#0.92)	(f)	*P-3m1*	*C2'/m* (No. 12.60) ($\mathbf{a}_p$+2$\mathbf{b}_p$,-$\mathbf{a}_p$,$\mathbf{c}_p$; 0,0,0)	*2'/m*	83
Cr_2O_3 (#0.110)	(g)	*R-3c*	*C2'/c* (No. 15.87) (1/3$\mathbf{a}_p$+2/3$\mathbf{b}_p$-4/3$\mathbf{c}_p$,$\mathbf{a}_p$,-1/3$\mathbf{a}_p$-2/3$\mathbf{b}_p$+1/3$\mathbf{c}_p$; 0,1/2,0)	*2'/m*	308
$MnGeO_3$ (#0.125)	(h)	*R-3*	*R-3'* (No. 148.19) ($\mathbf{a}_p$,$\mathbf{b}_p$,$\mathbf{c}_p$; 0,0,0)	*-3'*	120
Fe_2TeO_6 (#0.142)	(i)	*P4₂/mnm*	*P4₂/m'n'm'* (No. 136.503) ($\mathbf{a}_p$,$\mathbf{b}_p$,$\mathbf{c}_p$; 0,0,0)	*4/m'm'm'*	219

†References: (*a*) Rousse *et al.* (2003), (*b*) Brown *et al.* (2002), (*c*) Zhu *et al.* (2014), (*d*) Kunnmann *et al.* (1968), (*e*) Calder *et al.* (2014), (*f*) Ratcliff *et al.* (2009), (*g*) Fiebig *et al.* (1996), (*h*) Tsuzuki *et al.* (1974), (*i*) Kunnmann *et al.* (1968). [a] Parent space group [b] Magnetic space group (transformation to its standard setting from the parent basis indicated) [c] Magnetic point group [d] Transition temperature.

6.10. Magnetoelectrics

There are 56 non-polar structures that have an MSG which forbids zero-field electric polarization but allows linear magnetoelectricity in the case of insulators. Only 14 of them have a transition above 80 K, and this is reduced further to eight if compounds with known metallic properties are excluded. These eight structures are listed in Table 7. The publications where these structures were reported do not mention their

potential magnetoelectricity, with the exception of the well known cases of Cr_2O_3 and Fe_2TeO_6.

6.11. Ferrotoroidics

In recent years, magnetic structures with spin arrangements possessing a nonzero toroidal moment have become the subject of special attention (Schmid, 2001; Spaldin *et al.*, 2008; Ederer & Spaldin, 2007). The development of a spontaneous nonzero toroidal moment, being odd for time reversal and space inversion, is considered a fourth primary ferroic order, the so-called ferrotoroidicity, to be added to the traditional ferromagnetism, ferroelectricity and ferroelasticity. The possible presence of a nonzero toroidal moment in a magnetic structure is restricted by its point group symmetry. The number of magnetic point groups allowing a nonzero macroscopic toroidal moment is quite limited, namely 31 from the 122 possible magnetic point groups. About 60 structures, *i.e.* 15%, have one of these favourable symmetries. If one restricts the sample further to magnetic phases where the symmetry break is such that the primary magnetic order parameter describing the symmetry break has the properties of a toroidal moment, this number is further reduced. Table 8 lists the 29 structures from this set that do not allow electric polarization and/or macroscopic magnetization and can thus be denoted `pure' ferrotoroidic. All possible orientational domains of these structures have a different orientation for the allowed toroidal moment, and the magnetic order parameter is linearly coupled with the so-called toroidal field (**H** × **E**). Domain switching in these systems could in principle be possible with a combined application of magnetic and electric fields.

Table 8
Magnetic structures in *MAGNDATA* that can be classified as `pure' ferrotoroidic phases, with their magnetic order parameter having the transformation properties of a toroidal moment, and the presence of a spontaneous electric polarization and/or macroscopic magnetization being symmetry forbidden.

Compound	Ref.†	Parent SG[a]	MSG[b]	MPG[c]
$U_3Ru_4Al_{12}$ (#0.12)	(a)	*P6$_3$/mmc*	*Cmcm'* (No. 63.461) (**b**$_p$,-2**a**$_p$-**b**$_p$,**c**$_p$; 0,0,0)	*m'mm*
Gd_5Ge_4 (#0.14)	(b)	*Pnma*	*Pnm'a* (No. 62.444) (**a**$_p$,**b**$_p$,**c**$_p$; 0,0,0)	*m'mm*
$EuTiO_3$ (#0.16)	(c)	*I4/mcm*	*Fm'mm* (No. 69.523) (**a**$_p$-**b**$_p$,**a**$_p$+**b**$_p$,**c**$_p$; 0,1/2,1/2)	*m'mm*
$MnTiO_3$ (#0.19)	(d)	*R-3*	*R-3'* (No. 148.19) (**a**$_p$,**b**$_p$,**c**$_p$; 0,0,0)	*-3'*
DyB_4 (#0.22)	(e)	*P4/mbm*	*Pb'am* (No. 55.355) (**b**$_p$,-**a**$_p$,**c**$_p$; 0,0,0)	*m'mm*
$LiFeSi_2O_6$ (#0.28)	(f)	*P2$_1$/c*	*P2$_1$/c'* (No. 14.78) (**a**$_p$,**b**$_p$,**c**$_p$; 0,0,0)	*2/m'*
$Rb_yFe_{2-x}Se_2$ (#0.54)	(g)	*I4/m*	*I4/m'* (No. 87.78) (**a**$_p$,**b**$_p$,**c**$_p$; 0,0,0)	*4/m'*
$K_yFe_{2-x}Se_2$ (#0.55)	(h)	*I4/m*	*I4/m'* (No. 87.78) (**a**$_p$,**b**$_p$,**c**$_p$; 0,0,0)	*4/m'*
Cr_2WO_6 (#0.75)	(i)	*P4$_2$/mnm*	*Pn'nm* (No. 58.395)	*m'mm*

			(**b**$_p$,-**a**$_p$,**c**$_p$; 0,0,0)	
Cr_2TeO_6 (#0.76)	(i)	*P4$_2$/mnm*	*Pn'nm* (No. 58.395) (**a**$_p$,**b**$_p$,**c**$_p$; 1/2,1/2,1/2)	*m'mm*
$KMn_4(PO_4)_3$ (#0.86)	(j)	*Pnam*	*Pnma'* (No. 62.445) (**a**$_p$,**c**$_p$,-**b**$_p$; 0,0,0)	*m'mm*
$NaFePO_4$ (#0.87)	(k)	*Pnma*	*Pnma'* (No. 62.445) (**a**$_p$,**b**$_p$,**c**$_p$; 0,0,0)	*m'mm*
$LiNiPO_4$ (#0.88)	(l)	*Pnma*	*Pnm'a* (No. 62.444) (**a**$_p$,**b**$_p$,**c**$_p$; 0,0,0)	*m'mm*
$CaMn_2Sb_2$ (#0.92)	(m)	*P-3m1*	*C2'/m* (No. 12.60) (**a**$_p$+2**b**$_p$,-**a**$_p$,**c**$_p$; 0,0,0)	*2'/m*
$LiFePO_4$ (#0.95)	(n)	*Pnma*	*Pnma'* (No. 62.445) (**a**$_p$,**b**$_p$,**c**$_p$; 0,0,0)	*m'mm*
Cr_2O_3 (#0.110)	(o)	*R-3c*	*C2'/c* (No. 15.87) (1/3**a**+2/3**b**-4/3**c**,**a**,-1/3**a**-2/3**b**+1/3**c**; 0,1/2,0)	*2'/m*
$CoSe_2O_5$ (#0.119)	(p)	*Pbcn*	*Pb'cn* (No. 60.419) (**a**$_p$,**b**$_p$,**c**$_p$; 0,0,0)	*m'mm*
$MnGeO_3$ (#0.125)	(q)	*R-3*	*R-3'* (No. 148.19) (**a**$_p$,**b**$_p$,**c**$_p$; 0,0,0)	*-3'*
$TbGe_2$ (#0.141)	(r)	*Cmmm*	*Cm'mm* (No. 65.483) (**a**$_p$,**b**$_p$,**c**$_p$; 0,0,0)	*m'mm*
Cr_2TeO_6 (#0.143)	(s)	*P4$_2$/mnm*	*Pn'nm* (No. 58.395) (**b**$_p$,-**a**$_p$,**c**$_p$; 0,0,0)	*m'mm*
Cr_2WO_6 (#0.144)	(s)	*P4$_2$/mnm*	*Pn'nm* (No. 58.395) (**b**$_p$,-**a**$_p$,**c**$_p$; 0,0,0)	*m'mm*
Co_3TeO_6 (#0.145)	(t)	*C2/c*	*C2'/c* (No. 15.87) (**a**$_p$,**b**$_p$,**c**$_p$; 0,0,0)	*2'/m*
$EuZrO_3$ (#0.146)	(u)	*Pnma*	*Pnm'a* (No. 62.444) (**a**$_p$,**b**$_p$,**c**$_p$; 0,0,0)	*m'mm*
$LiFePO_4$ (#0.152)	(v)	*Pnma*	*P2$_1$/c'* (No. 14.78) (-**b**$_p$,-**c**$_p$,**a**$_p$; 0,0,0)	*2/m'*
$CaMnGe_2O_6$ (#0.156)	(w)	*C2/c*	*C2'/c* (No. 15.87) (**a**$_p$,**b**$_p$,**c**$_p$; 0,0,0)	*2'/m*
$TbCoO_3$ (#0.160)	(x)	*Pbnm*	*Pnm'a* (No. 62.444) (-**b**$_p$,**c**$_p$,-**a**$_p$; 0,0,0)	*m'mm*
$CoSe_2O_5$ (#0.161)	(y)	*Pbcn*	*Pb'cn* (No. 60.419) (**a**$_p$,**b**$_p$,**c**$_p$; 0,0,0)	*m'mm*
$NdCrTiO_5$ (#0.162)	(z)	*Pbam*	*Pbam'* (No. 55.356) (**a**$_p$,**b**$_p$,**c**$_p$; 0,0,0)	*m'mm*
$MnPS_3$ (#0.163)	(aa)	*C2/m*	*C2'/m* (No. 12.60) (**a**$_p$,**b**$_p$,**c**$_p$; 0,0,0)	*2'/m*

†References: (*a*) Troć *et al.* (2012), (*b*) Tan *et al.* (2005), (*c*) Scagnoli *et al.* (2012), (*d*) Shirane *et al.* (1959), (*e*) Will & Schafer (1979), (*f*) Redhammer *et al.* (2009), (*g*) Pomjakushin *et al.* (2011), (*h*) Pomjakushin *et al.* (2011), (*i*) Zhu *et al.* (2014), (*j*) López *et al.* (2008), (*k*) Avdeev *et al.* (2013), (*l*) Jensen *et al.* (2009), (*m*) Ratcliff *et al.* (2009), (*n*) Rousse *et al.* (2003), (*o*) Fiebig *et al.* (1996), (*p*) Melot *et al.* (2010), (*q*) Tsuzuki *et al.* (1974), (*r*) Schobinger-Papamantellos *et al.* (1988), (*s*) Kunnmann *et al.* (1968), (*t*) Ivanov *et al.* (2012), (*u*) Avdeev *et al.* (2014), (*v*) Toft-Petersen *et al.* (2015), (*w*) Ding *et al.* (2016), (*x*) Knížek *et al.* (2014), (*y*) Rodriguez *et al.* (2016),

(*z*) Buisson (1970), (*aa*) Ressouche *et al.* (2010). [a] Parent space group [b] Magnetic space group (transformation to its standard setting from the parent basis indicated) [c] Magnetic point group

6.12. Contrast with macroscopic properties

Consistency with observed macroscopic properties can be a stringent test for a magnetic structure, and some of the models collected here are clearly inconsistent from this viewpoint. For instance, this is the case for $LuFe_2O_4$ (#1.0.7; Christianson *et al.*, 2008), which is claimed to be multiferroic, although the symmetry of the reported structure is incompatible with spin-driven or intrinsic ferroelectric properties. Something similar happens with the model of $Cu_3Mo_2O_9$ (#1.129; Vilminot *et al.*, 2009). Its 2'22' point group symmetry would not allow the ferroelectricity and weak ferromagnetism along **a** or **c** that is reported in other work (Hamasaki *et al.*, 2008; Hase *et al.*, 2015). Analogous situations were detected in other structures like $DyVO_3$ (#0.106; Reehuis *et al.*, 2011), Co_3TeO_6 (#0.145 and #1.164; Ivanov *et al.*, 2012) *etc*. In all such cases, the consistency problem is briefly indicated in the comments.

6.13. Secondary modes. Higher harmonics

The MSG of about 10% of the structures allows the presence of secondary irrep spin modes, *i.e.* spin modes transforming according to an irrep which is not that of the order parameter. These spin modes are not necessary for the symmetry break, but they are symmetry allowed and may be present in the structure as a secondary induced effect. These secondary irrep spin distortions, which are expected to be very weak, remain unobserved in most cases, but one must take into account that the traditional representation method used in the refinements, which only considers possible models subject to a single irrep, implies their *a priori* exclusion. In any case, structures with MSGs that allow secondary modes are those where a combined application of the constraints coming from the relevant MSG and from the assumption of a single primary irrep is most convenient, in order to reduce the number of degrees of freedom with respect to the sole application of the MSG symmetry relations.

It is remarkable that secondary modes, generally absent, have large amplitudes in structures where they have been forced *a priori* in the refined model. For instance, this is the case for structures that allow secondary modes corresponding to higher harmonics of the propagation vector, *i.e.* cases where 3**k** is not equivalent to **k**. The 11 structures classified with the labels 1.0.*xxx* in *MAGNDATA* are all of this type. Many of these structures are modelled assuming collinear spin arrangements, where the spin modulus and orientation are maintained at all sites and only its direction can switch sign. These spin arrangements do not fulfil the usual single-irrep assumption and require significant nonzero amplitudes of higher harmonics of the primary spin mode. Magnetic Bragg peaks for odd multiples of the propagation vector should be present in the diffraction diagram, but often these simplified models are assumed without experimental evidence for higher harmonics in the spin wave. The equality of the spin modulus at all sites is generally considered physically more appealing than the single-irrep assumption, which would imply a sinusoidal spin wave. However, one can find both types of approach in the proposed models in the literature. Fig. 15 shows two examples.

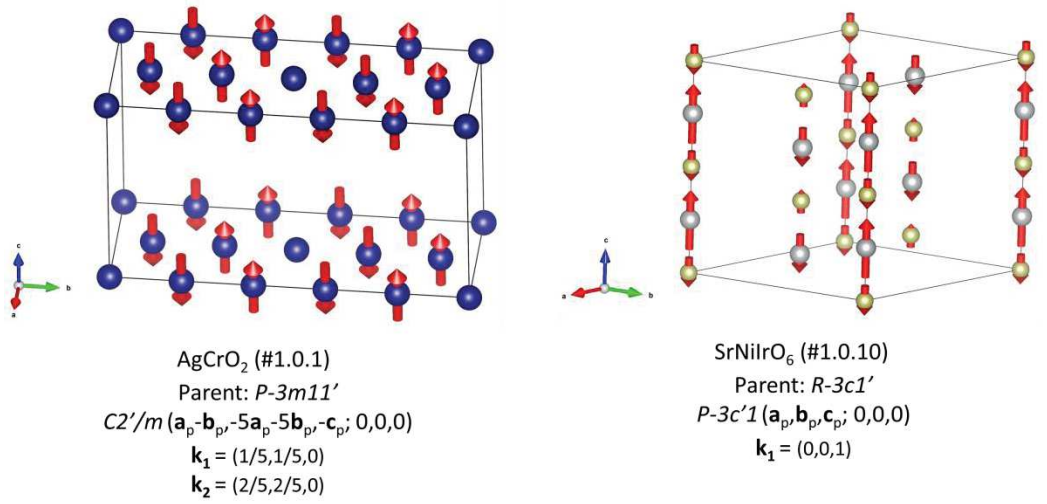

Figure 15
Single-**k** magnetic structures of $AgCrO_2$ (Matsuda *et al.*, 2012) and $SrNiIrO_6$ (Lefrançois *et al.*, 2014) as examples of the two different approaches when dealing with structures with propagation vectors and symmetries that allow the presence of secondary modes in the form of spin wave harmonics. In the first structure, the harmonic with propagation vector 3**k** is necessarily present in the model to produce equality of all spin moduli, while in the second one, a sinusoidal spin wave according to the primary propagation vector is proposed and the symmetry-allowed 3**k** (= 0) component is absent. In both cases, no experimental evidence of a third harmonic seems to exist. Below each structure, the parent grey space group, the MSG and the modulation wavevectors present in the structure are indicated.

6.14. Secondary modes with the primary propagation vector

From the approximately 30 structures with MSGs that allow the presence of secondary modes with the same propagation vector as the primary spin arrangement, there are only six where the amplitude of these secondary degrees of freedom is nonzero. The case of $Er_2Ru_2O_7$ (#0.154; Taira *et al.*, 2003) is an interesting example. Its MSG is $I4_1'/am'd$, *i.e.* it is one of the maximal epikernels of the irrep mGM3+ (see §E.5 and Fig. 10). Fig. 16 shows the reported structure of this compound compared with that of $Er_2Ti_2O_7$ (#0.29; Poole *et al.*, 2007). While the spin arrangement in $Er_2Ti_2O_7$ has been modelled assuming the presence of only the primary irrep mGM3+, and therefore the symmetry-allowed secondary spin mode according to irrep mGM2+ is absent, the spin ordering in $Er_2Ru_2O_7$ has been refined as a collinear arrangement. The simplicity of this second model hides a rather exceptional behaviour when seen in terms of irreps. The collinearity does not imply an MSG different from that of $Er_2Ti_2O_7$, but it requires the presence of a spin mode according to the secondary irrep mGM2+, and with a large specific amplitude correlated with that of the primary active irrep. From the original publication, it is not clear if this rather unusual weight of a secondary irrep mode is the result of an *a priori* collinearity assumption, or whether it was constrasted with a pure mGM3+ model, being then fully supported by the experimental data. The presence of secondary irrep modes of this type in four of the six structures can be traced back to such types of assumption or extrinsic conditions. This is the case for Mn_3GaC (#1.153; Fruchart *et al.*, 1970), where collinearity also forces the presence of a secondary irrep mode, $U_3Ru_4Al_{12}$ (#0.12; Troć *et al.*, 2012), where some specific relative spin orientations not forced by symmetry are included in

the model, and $Tb_2Ti_2O_7$ (#0.77; Sazonov *et al.*, 2013), which is a structure stabilized by an external magnetic field.

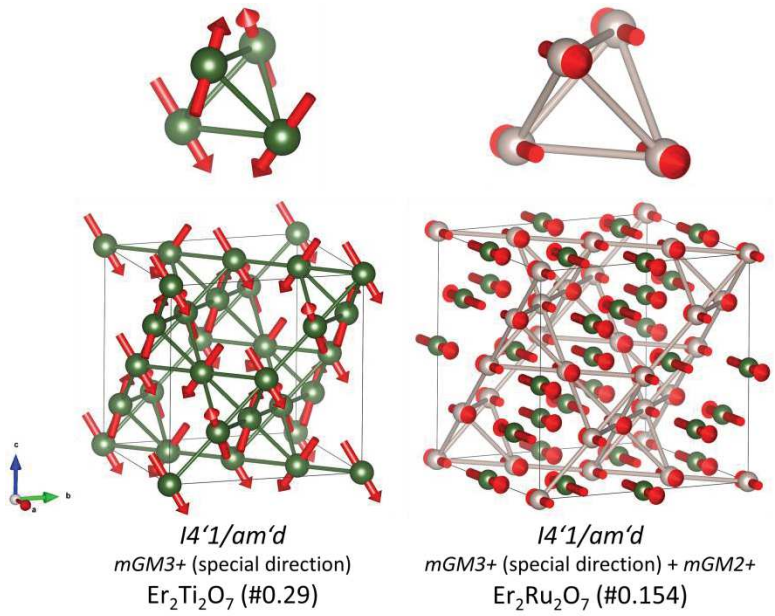

Figure 16
Two magnetic structures complying with the same MSG *I*4'$_1$/*am*'*d*. The structure reported for $Er_2Ti_2O_7$ (Poole *et al.*, 2007) includes a single spin mode with two-dimensional mGM3+ irrep basis functions specialized to this MSG, while the collinear model of $Er_2Ru_2O_7$ (Taira *et al.*, 2003) requires the additional presence of a secondary mGM2+ mode compatible with the same MSG.

Therefore, only two structures in the whole collection include a significant contribution of a secondary irrep mode that was independently monitored and did not originate from some assumption. These are the structures of Cr_2S_3 (#0.5; Bertaut *et al.*, 1968) and $Nd_3Ru_4Al_{12}$ (#0.149; Gorbunov *et al.*, 2016). In both cases, the amplitudes of both primary and secondary modes are comparable, and therefore it does not seem appropriate to consider one of them as an induced secondary effect. Despite the symmetry compatibility of one of the modes with respect to the other, it seems that, in these two cases, one should consider the two spin components as ordering modes associated with two independent primary order parameters.

6.15. Multi-k structures

Reported magnetic structures with more than one propagation vector are scarce. Despite our efforts to find well defined experimental structures in the literature with several independent propagation vectors, the numbers of 2**k** and 3**k** structures that we could collect were only 15 and eight, respectively. These include structures with symmetry-related propagation vectors. Only six 2**k** structures have a parent symmetry relating the two active propagation vectors, while in the case of the 3**k** structures, seven of the eight involve three primary propagation vectors related by the parent symmetry, either cubic or hexagonal. Fig. 17 shows some examples.

It must be stressed that the magnetic symmetry of a commensurate multi-**k** structure is also given by an MSG, having from this viewpoint no essential difference from a

single-**k** structure. The number of independent propagation vectors associated with the spin modulation comes from a comparison with the parent paramagnetic structure, and it is not an intrinsic property of the spin arrangement. The magnetic structure is fully defined by its relevant MSG, its unit cell, and the set of atomic positions and magnetic moments of its asymmetric unit, without any reference to the underlying propagation vectors with respect to the parent structure. For instance, the magnetic structure of NpBi (#3.7; Burlet *et al.*, 1992) represented in Fig. 17 has a parent phase with space group *Fm*-3*m*. The magnetic ordering breaks all the centring translations while keeping the cubic unit cell and results in the MSG *Pn*-3*m'*. This can be described by the condensation of spin waves with the propagation vectors (1, 0, 0), (0, 1, 0) and (0, 0, 1) on the reference paramagnetic face-centred cubic structure. However, the same spin arrangement for the same magnetic sites and with the same MSG can be realized in a magnetic phase having a parent structure with a primitive cubic lattice and space group *Pn*-3*m'*. In such a case, the same spin arrangement would be described as a single-**k** magnetic structure with **k** = 0.

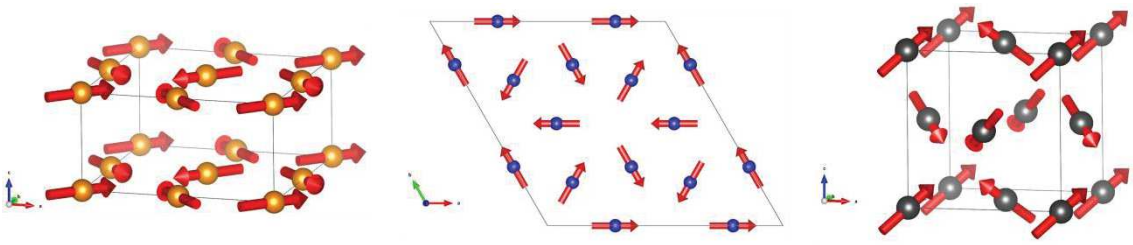

NdMg (#2.14)
Parent: *Pm-3m1'*
P_C4/nbm ($2\mathbf{a}_p$,$2\mathbf{b}_p$,$\mathbf{c}_p$; 0,0,0)
$\mathbf{k}_1$ = (1/2,0,0)
$\mathbf{k}_2$ = (0,1/2,0)

TmAgGe (#3.1)
Parent: *P-62m1'*
P-6'2m' ($2\mathbf{a}_p$,$2\mathbf{b}_p$,$\mathbf{c}_p$; 0,0,0)
$\mathbf{k}_1$ = (1/2,0,0)
$\mathbf{k}_2$ = (1/2,1/2,0)
$\mathbf{k}_3$ = (0,1/2,0)

NpBi (#3.7)
Parent: *Fm-3m1'*
Pn-3m' ($\mathbf{a}_p$,$\mathbf{b}_p$,$\mathbf{c}_p$; 0,0,0)
$\mathbf{k}_1$ = (1,0,0)
$\mathbf{k}_2$ = (0,1,0)
$\mathbf{k}_3$ = (0,0,1)

Figure 17
The magnetic structures of NdMg (Deldem *et al.*, 1998), TmAgGe (Baran *et al.*, 2009) and NpBi (Burlet *et al.*, 1992) as examples of multi-**k** structures with symmetry-related propagation vectors. Below each figure, the parent grey space group, the MSG of the phase and the active independent propagation vectors with respect to the parent structure are indicated.

Multi-**k** structures with symmetry-related **k** vectors are in general indistinguishable from single-**k** structures in powder diffraction experiments. Even in the case of single-crystal studies, the distinction between a multi-**k** and a single-**k** structure with appropriate domain populations can be problematic. Most of the collected multi-**k** structures with symmetry-related **k** vectors correspond to single-crystal studies, but not all [see, for instance, TmAgGe (#3.1; Baran *et al.*, 2009)]. It is generally believed that the diffraction diagrams of single-**k** structures should change considerably under an external magnetic field owing to changes in the domain populations, while those of multi-**k** structures should be rather insensitive. Under this assumption, the study of the variation in a single-crystal diffraction diagram under a magnetic field has become a traditional form of identifying multi-**k** spin arrangements, and was used in the studies of some of the structures collected here.

More than 50 single-**k** structures in this collection have a propagation vector and a parent symmetry such that alternative multi-**k** models would be possible. In most

cases, these multi-**k** models have not been explored as possible alternative models. Usually when confronted with this problem, the single-**k** model is preferred *a priori* and it is the one reported. One should be aware, however, that multi-**k** models could equally well fit the experimental data in most such cases. If an alternative multi-**k** model has also been reported, both have been included in the collection, but this situation rarely happens.

6.16. Multi-axial structures

Sometimes the so-called multi-axial structures, where the spins orientate according to several different fixed directions, are assimilated with the multi-**k** structures. However, multi-axial spin arrangements are not exclusive to multi-**k** structures and they can also be a symmetry-protected feature of single-**k** structures. Fig. 18 shows some examples where multiple axes for the spin orientations are symmetry dictated and a single propagation vector exists with respect to the parent phase.

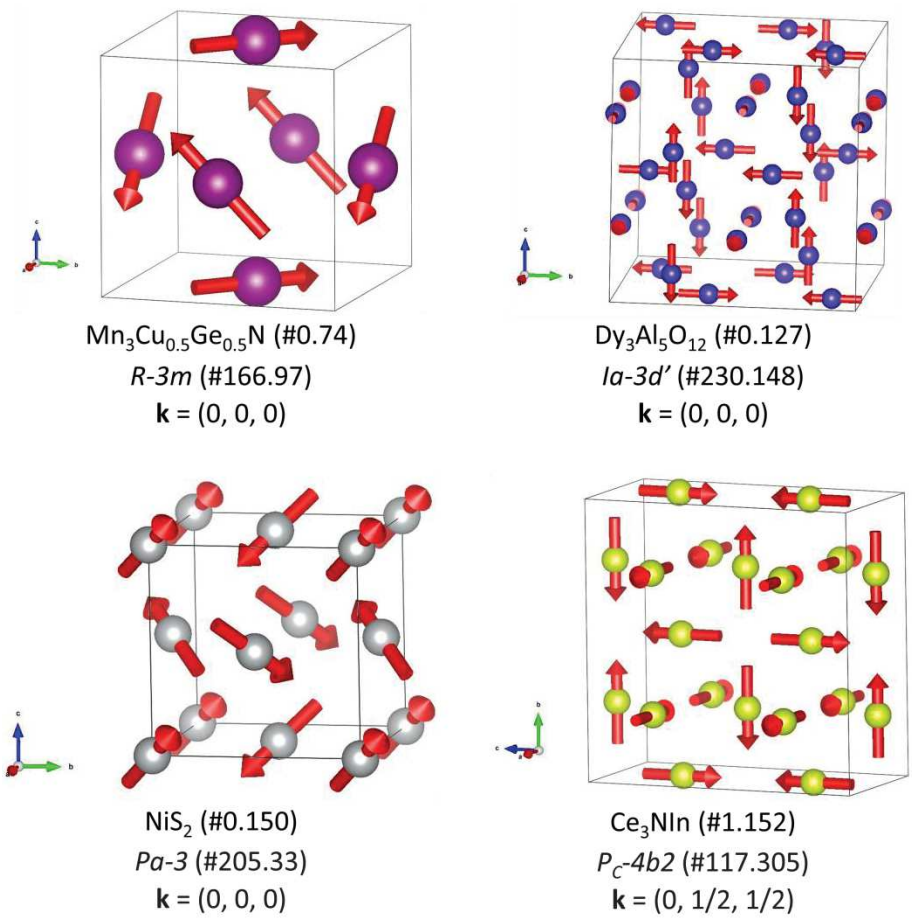

Figure 18
The magnetic structures of $Mn_3Cu_{0.5}Ge_{0.5}N$ (Iikubo *et al.*, 2008), $Dy_3Al_5O_{12}$ (Hastings *et al.*, 1965), NiS_2 (Yano *et al.*, 2016) and Ce_3NIn (Gäbler *et al.*, 2008) as examples of multi-axial structures with a single propagation vector. Below each figure, the label of the corresponding MSG and the propagation vector are indicated.

6.17. Conflicting models

MAGNDATA has more than one magnetic structure for around 50 compounds. In most cases they correspond to different magnetic phases or to the same phase under a different temperature, field *etc*. In other cases they correspond to a different model for the same phase reported by different authors, and the structures are very similar. In a few cases they represent several alternative indistinguishable models that have been reported in the same reference. But in the case of 12 compounds, and for apparently the same phase, this collection has gathered magnetic structures that differ by a significant amount. They are summarized in Table 9.

Table 9
Conflicting structures for the same magnetic phase in MAGNDATA.

In the column headed `Experimental technique', NPD denotes neutron powder diffraction and NSD denotes neutron single-crystal diffraction. In the column headed `SA', a cross (×) indicates that the systematic absences are different for the two proposed models.

Compound	Entries	Ref.†	Parent SG[a]	MSG(s)[b]	Comparison	E.T.[c]	S.a.
$BiMn_2O_5$	1.74 1.75	(a) (b)	*Pbam*	*C$_a$mc2$_1$* *C$_a$m*	Same *irrep* Group-subgroup relation	NPD NSD	-
$CaMnGe_2O_6$	0.156 0.155	(c) (d)	*C2/c*	*C2′/c* *P$_s$-1′*	1 *irrep* and 2 *irreps* models	NPD NPD	-
$CoSe_2O_5$	0.119 0.161	(e) (f)	*Pbcn*	*Pb′cn*	Same *irrep* With and without spin canting	NPD NSD	X
$Cu_3Mo_2O_9$	0.129 0.130	(g) (h)	*Pnma*	*P2$_1$′2$_1$′2$_1$* *Pm′c2$_1$′*	2 *irreps*: one equal, the other different	NPD NPD	X
$EuZrO_3$	0.146 0.147	(i) (j)	*Pnma*	*Pnm′a* *Pn′m′a*	Different easy axis Different single *irrep* ME effect allowed in one of the models	NPD NPD	X
Gd_2CuO_4	0.82 0.104	(k) (l)	*Aeam* *I4/mmm*	*Cm′ca′* *C$_A$ccm*	Different parent symm. Inclusion or not of a structural distortion	NSD NSD	-
$HoMnO_3$	0.33 0.43	(m) (n)	*P6$_3$cm*	*P6$_3$cm* *P6$_3$′cm′*	Different single *irrep*	NPD NSD	-
$LiFePO_4$	0.95 0.152	(o) (p)	*Pnma*	*Pnma′* *P2$_1$/c′*	1-*irrep* and 2-*irreps* models Second *irrep*: small spin canting that breaks the symmetry	NPD NSD	X
$NiTa_2O_6$	1.112 1.172	(q) (r)	*P4$_2$/mnm*	*P$_c$2$_1$/c* *A$_b$ba2*	Group-subgroup relation 2-*irreps*: one equal, the other different	NPD NPD	-
Sr_2IrO_4	1.3 1.77	(s) (t)	*I4$_1$/acd*	*P$_I$cca*	Same *irrep*, same symmetry Without and with canting	NPD NSD	X
$YMnO_3$	0.6 0.44	(u) (n)	*P6$_3$cm*	*P6$_3$cm* *P6$_3$′*	1-*irrep* and 2-*irreps* models. No common *irrep*	NPD NSD	-
$La_{0.333}Ca_{0.667}MnO_3$	1.174 1.175	(v) (w)	*Pnma*	*P$_b$mc2$_1$* *P$_b$mn2$_1$*	Different parent structure, different orientation of the propagation vector	NPD NPD	-

† References: (*a*) Muñoz *et al.* (2002), (*b*) Vecchini *et al.* (2008), (*c*) Ding *et al.* (2016), (*d*) Redhammer *et al.* (2008), (*e*) Melot *et al.* (2010), (*f*) Rodriguez *et al.* (2016), (*g*) Vilminot *et al.* (2009), (*h*) Hase *et al.* (2015), (*i*) Avdeev *et al.* (2014), (*j*) Saha *et al.* (2016), (*k*) Brown & Chatterji (2011), (*l*) Chattopadhyay *et al.* (1992), (*m*) Muñoz, Alonso *et al.* (2001), (*n*) Brown & Chatterji (2006), (*o*) Rousse *et al.* (2003), (*p*) Toft-Petersen *et al.* (2015), (*q*) Law *et al.* (2014), (*r*) Ehrenberg *et al.* (1998), (*s*) Lovesey *et al.* (2012), (*t*) Ye *et al.* (2013), (*u*) Muñoz *et al.* (2000), (*v*) Radaelli *et al.* (1999), (*w*) Fernández-Díaz *et al.* (1999).
[a] Parent space group
[b] Magnetic space group
[c] Experimental technique

In $EuZrO_3$ (Avdeev *et al.*, 2014; Saha *et al.*, 2016), one finds a typical case where the easy axis of a collinear arrangement seems difficult to establish and two different studies report different directions. But, depending on this direction, the relevant MSG changes, and this dictates different magnetostructural properties, like the allowance or not of linear magnetoelectric (ME) effects. Through the direct link to the program *MAGNEXT*, one can also see that the two models imply different systematic absences in the diffraction diagram, which could in principle help to differentiate between the two models. There are also cases where the two models have the same symmetry, and the difference is the presence or not of a significant spin canting fully compatible with the MSG of the structure. We have already mentioned the case of $CoSe_2O_5$ (Melot *et al.*, 2010; Rodriguez *et al.*, 2016), and something similar happens for Sr_2IrO_4 (Lovesey *et al.*, 2012; Ye *et al.*, 2013).

The cases of $BiMn_2O_5$ (Vecchini *et al.*, 2008; Muñoz *et al.*, 2002), already discussed above, and $LiFePO_4$ (Rousse *et al.*, 2003; Toft-Petersen *et al.*, 2015) are representative of situations where the structural models differ only slightly, but this difference breaks the symmetry further, therefore implying an important qualitative difference. In one case it reduces the MSG of the structure to the kernel of the irrep, and in the other it implies the activity of a second primary irrep with a very weak amplitude. A detailed comparison of the two models of the magnetic structure of $BiMn_2O_5$ can be seen in Table 10. One can observe that the deviations of the low-symmetry model from one of higher symmetry are close to their standard deviations, which would imply that the system complies with one of the maximal epikernels of the active irrep. However, apart from the larger magnetic moments of the high-symmetry model, one can see that the spin canting components along **b** for the Mn2 sites have opposite signs in the two structures. It can also be noted that the model of higher symmetry, apart from the moment relations consistent with the indicated irrep epikernel, includes some additional constraints that are not symmetry-forced. Its asymmetric unit has three Mn sites, namely Mn1_1, and two independent sites Mn2_1 and Mn2_2, which are the result of the splitting of the single Mn2 site in the parent *Pbam*1' symmetry. The model reported by Muñoz *et al.* (2002) includes some specific correlation between the components of these two independent sites and has the allowed *z* component of Mn1_1 fixed to zero, but the structure has only a single irrep active and its symmetry is maximal. Therefore, these additional constraints are not justified by either the assumption of a specific irrep spin mode or any other symmetry argument, and they could have been skipped, even if they are fulfilled approximately. This is an example of overconstraints in the structure modelling, an issue discussed below in more detail.

The remaining pairs of structures summarized in Table 9 correspond to models which differ in a higher degree: they have no group–subgroup-related MSGs, different active irreps *etc.* For instance, Fig. 19 shows the two very different magnetic structures proposed for $Cu_3Mo_2O_9$ (Vilminot *et al.*, 2009; Hase *et al.*, 2015). The case of $La_{0.333}Ca_{0.667}MnO_3$ (Radaelli *et al.*, 1999; Fernández-Díaz *et al.*, 1999) is also remarkable. Although the spin arrangements of the two models are very similar, their orientation relative to the parent structure is completely different, both structures having distinct MSGs. A small structural distortion of the parent structure is also oriented differently in the two models. The tetragonal pseudo-symmetry of the parent structure, and especially of the Mn sites, seems to be the cause for these two very

different models being able to fit the diffraction data reasonably well. A model very similar to the one reported by Radaelli *et al.* (1999) has recently been reported for a compound with a similar composition, $La_{0.375}Ca_{0.625}MnO_3$ (#1.173; Martinelli *et al.*, 2016).

Table 10
Comparison of the magnetic structures #1.74 and #1.75, reported for $BiMn_2O_5$ in (Muñoz *et al.*, 2002) and (Vecchini *et al.*, 2008) at 1.5K and 10K, respectively.

The MSG for each structure and the corresponding asymmetric unit for the Mn atoms are listed. The basis ($2\mathbf{a}_p$, $\mathbf{b}_p$, $2\mathbf{c}_p$; 0, 0, 0) with respect to the parent *Pbam* unit cell is used for the description. Only approximate atomic positions are listed. In the case of the model with higher symmetry and smaller asymmetric unit, the spins of symmetry-related atoms are also included for comparison. Structure #1.74 has been transformed to the domain-related equivalent with all spins switched.

Atom				**$BiMn_2O_5$ (#1.75)**					**$BiMn_2O_5$ (#1.74)**				
				***Pbam1'* -> *C$_a$m* ($2a_p$,$-c_p$,$2b_p$;0,0,0)**					***Pbam1'* -> *C$_a$mc2$_1$* ($2c_p$,a_p,$2b_p$;1/8,0,0)**				
Label	***x***	***y***	***z***	**Constr.†**	***M$_x$***	***M$_y$***	***M$_z$***	**|M|**	**Constr.†**	***M$_x$***	***M$_y$***	***M$_z$***	**|M|**
Mn1_1	0.00	0.50	0.37	m_x,m_y,m_z	2.10(3)	-0.33(6)	-0.25(6)	2.14	m_x,m_y,m_z	2.44(10)	-0.6(2)	0.0	2.51
Mn1_2	0.25	0.00	0.13	m_x,m_y,m_z	2.07(3)	0.56(6)	0.08(6)	2.15	$m_x,-m_y,m_z$	2.44	0.6	0.0	2.51
Mn2_1	0.20	0.35	0.25	$m_x,m_y,0$	-2.83(5)	0.33(10)	0.0	2.85	$m_x,m_y,0$	-3.12(9)	-0.8(2)	0.0	3.22
Mn2_3	0.05	0.85	0.25	$m_x,m_y,0$	-2.83(5)	-0.23(10)	0.0	2.84	$m_x,-m_y,0$	-3.12	0.8	0.0	3.22
Mn2_2	0.30	0.65	0.25	$m_x,m_y,0$	2.80(5)	-0.34(9)	0.0	2.82	$-m_x,-m_y,0$	3.12	0.8	0.0	3.22
Mn2_4	0.45	0.15	0.25	$m_x,m_y,0$	-2.74(5)	-0.64(10)	0.0	2.81	$m_x,-m_y,0$	-3.12	0.8	0.0	3.22

† Symmetry constraints on the magnetic moment **M**

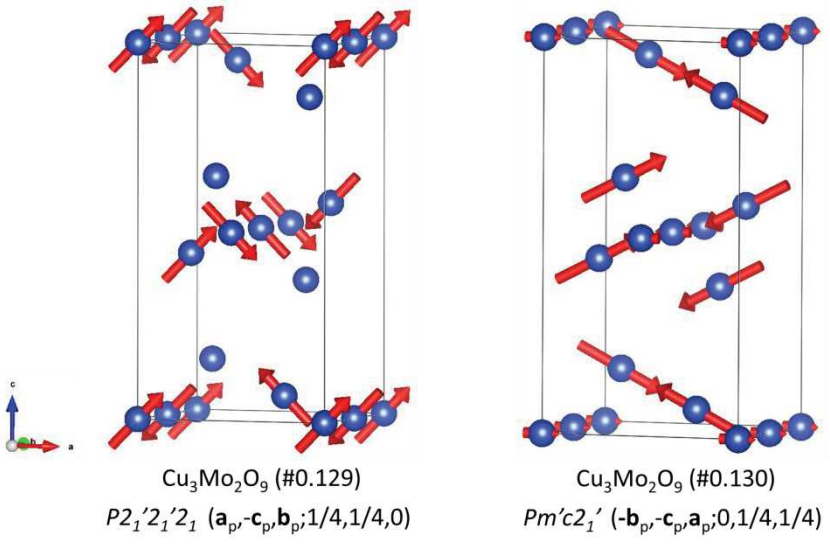

Figure 19
Conflicting magnetic structures for the same phase of $Cu_3Mo_2O_9$ (Vilminot *et al.*, 2009; Hase *et al.*, 2015), with indications of the MSGs and the transformation to the standard setting of each group from the parent *Pnma* basis.

6.18. "Concomitant" structural transitions

About 60% of the collected structures have a magnetic ordering whose symmetry implies some symmetry break for the non-magnetic degrees of freedom. In other words, the MSG of the magnetic structure allows structural distortions forbidden in the parent space group, which can in principle become nonzero through magnetostructural coupling. These include of course the spin-driven multiferroics discussed above. In most cases, the structural distortions that are consistent with the MSG and break the parent space group are too weak to be detected. As they are so rare, if they are detected such distortions are often erroneously considered as a so-called concomitant or simultaneous structural phase transition.

Table 11 summarizes the structures in the collection where such types of concomitant structural distortions have been reported. The effective space group relevant for the non-magnetic degrees of freedom is given by the space group used to label the MSG in the OG setting. Although this collection employs the BNS notation for the MSG labels, a link in the BNS label of the MSG of each entry allows the user to obtain the corresponding OG label and extract from it the effective space group that is relevant for the non-magnetic degrees of freedom. Table 11 indicates this effective space group for the 18 listed structures. The structural distortions of all compounds in Table 11 seem consistent with the corresponding effective space group, except for YFe_4Ge_2 and $LuFe_4Ge_2$ (Schobinger-Papamantellos *et al.*, 2001, 2012). In these two compounds, the reported simultaneous structural symmetry break $P4_2/mnm \rightarrow Pnnm$ cannot be explained as an induced effect of the reported spin arrangement, which without the conjunction of the structural distortion would have a higher MSG. Hence, these two compounds are the only cases in the collection where a genuine simultaneous independent structural phase transition takes place. One must be aware, however, that spin arrangements alternative to those reported could explain the symmetry break observed in these compounds in the non-magnetic structural degrees of freedom as an induced effect, and it seems they were not explored.

Table 11
Structures in *MAGNDATA* where a symmetry-breaking structural distortion is reported to be concomitant with the magnetic transition.

The column headed `Structural distortion' indicates if the structural distortion is fully consistent as an induced effect (`Present'), has been constrained *a priori* by the refined model (`Present partially'), is reported in another reference (`Other reference'), is reported but not characterized (`Reported but not characterized'), or is inconsistent as an induced effect and must be considered an independent structural transition (`Concomitant structural transition?').

Entry	Ref.†	k vector(s)	Parent SG[a]	MSG[b]	ESG[c]	Structural distortion
$BaFe_2As_2$ (#1.16)	(a)	(1/2,1/2,0)	*I4/mmm*	C_Amca (64.480)	*Fmmm*	present
$CaFe_2As_2$ (#1.52)	(b)	(1/2,1/2,0)	*I4/mmm*	C_Amca (64.480)	*Fmmm*	present
CoO (#1.69)	(c)	(1/2,1/2,1/2)	*Fm-3m*	C_c2/c (15.90)	*C2/m*	present
α-Mn	(d)	(1,0,0)	*I-43m*	P_I-42_1c	*I-42m*	present

(#1.85)				(114.282)		
GeV_4S_8 (#1.86)	(e)	(1/2,1/2,0)	*F-43m*	P_ana2_1 (33.149)	$Pmn2_1$	present
$AgCrS_2$ (#1.136)	(f)	(-3/4,3/4,-3/4)	*R3m*	C_cm (8.35)	*Cm*	present
$MnCuO_2$ (#1.57)	(g)	(-1/2,1/2,1/2)	*C2/m*	P_s-1 (2.7)	*P-1*	present
Sr_2CoOsO_6 (#1.72)	(h)	(1/2,1/2,0)	*I4/m*	C_c2/c (15.90)	*C2/c*	present
Ag_2CrO_2 (#1.0.1)	(i)	(1/5,1/5,0) (2/5,2/5,0)	*P-3m1*	*C2'/m* (12.60)	*C2/m*	present - partially
$DyFe_4Ge_2$ (#1.98)	(j)	(1/4,1/4,0)	$P4_2/mnm$	P_ccc2 (27.82)	*Pmm2*	present - partially
NiF_2 (#0.36)	(k)	(0,0,0)	$P4_2/mnm$	*Pnn'm'* (58.398)	*Pnnm*	other reference
$ErVO_3$ (#0.104)	(l)	(0,0,0)	*Pbnm*	$P2_1'/m'$ (11.54)	$P2_1/m$	reported – not characterized
$ErVO_3$ (#0.105)	(m)	(0,0,0)	*Pbnm*	$P2_1/c$ (14.75)	$P2_1/c$	reported - not characterized
$DyVO_3$ (#0.106)	(m)	(0,0,0)	*Pbnm*	$P2_1'/m'$ (11.54)	$P2_1/m$	reported - not characterized
$BaFe_2Se_3$ (#1.120)	(n)	(1/2,1/2,1/2)	*Pnma*	C_ac (9.41)	*Pc*	reported - not characterized
Mn_3CuN (#2.5)	(o)	(1/2,1/2,0) (0,0,0)	*Pm-3m*	*P4/n* (85.59)	*P4/n*	reported - not characterized
YFe_4Ge_2 (#0.27)	(p)	(0,0,0)	$P4_2/mnm$	*Pn'n'm'* (58.399)	*Pnnm*	concomitant structural transition?
$LuFe_4Ge_2$ (#0.140)	(q)	(0,0,0)	$P4_2/mnm$	*Pn'n'm'* (58.399)	*Pnnm*	concomitant structural transition?

†References of the magnetic structures: (*a*) Huang *et al.* (2008), (*b*) Goldman *et al.* (2008), (*c*) Jauch *et al.* (2001), (*d*) Lawson *et al.* (1994), (*e*) Müller *et al.* (2006), (*f*) Damay *et al.* (2011), (*g*) Damay *et al.* (2009), (*h*) Yan *et al.* (2014), (*i*) Matsuda *et al.* (2012), (*j*) Schobinger-Papamantellos *et al.* (2006), (*k*) Brown & Forsyth (1981), (*l*) Chattopadhyay *et al.* (1992), (*m*) Reehuis *et al.* (2011), (*n*) Caron *et al.* (2011), (*o*) Fruchart & Bertaut (1978), (*p*) Schobinger-Papamantellos *et al.* (2001), (*q*) Schobinger-Papamantellos *et al.* (2012).

[b] Parent space group

[c] Magnetic space group

[d] For non-magnetic degrees of freedom

The symmetry-breaking structural distortions of the other 16 structures in Table 11 seem to comply with the expected symmetry constraints resulting from the MSG associated with the spin ordering. Some of them have been refined under the corresponding effective space group and are therefore fully consistent as an induced effect. In a couple of cases, the space group employed in the refinement of the positional structure is a supergroup of the effective space group, and therefore the observed structural distortion is also consistent with the MSG, but it was partially constrained by the assumed model. In some other cases, the structural distortion is

observed and reported, but owing to its weakness it was not characterized and was not included in the magnetic structure.

6.19. Overconstrained structures

The description of magnetic structures in *MAGNDATA* using their MSG allows us to distinguish in the model, in a straightforward form, the constraints that are forced and protected by symmetry from those that are not. Constraints that are not symmetry dictated are very common, and they reduce the number of free parameters with respect to a general model complying with the relevant MSG. There can be good reasons for having a structure with fewer free parameters than those allowed by the associated magnetic symmetry, and some of them have already been discussed above. They can be summarized in the following points:

(i) Collinearity favoured by exchange-type interactions can prevail and strict collinearity can be assumed, despite the MSG allowing non-collinear spin canting. See, for instance, the case of ErAuGe (#1.33; Baran *et al.*, 2001).

(ii) If the magnetic structure has a single active irrep but the resulting MSG allows secondary magnetic irreps, the presence of these additional degrees of freedom is usually negligible and the model can be restricted to the primary irrep (constrained along the direction dictated by the MSG). See, for instance, the case of GdBiPt (#1.111; Müller *et al.*, 2014).

(iii) If several irreps are active, the resulting MSG usually has a very low symmetry. As a consequence, several additional secondary irreps may be symmetry allowed, but they correspond to very weak high-order effects. In such cases, the restriction of the spin arrangement to the primary irreps implies a substantial reduction in the effective number of degrees of freedom. See, for instance, the case of $CsNiCl_3$ (#1.0.4; Yelon & Cox, 1973).

In the traditional representation method, restrictions on the possible combinations of basis spin modes corresponding to the active irrep (or irreps) are usually introduced through a mixture of *ad hoc* simplifications and/or intuitive assumptions combined with trial and error methods. This implies that, in general, the final model may include constraints that cannot be justified on symmetry or physical grounds. Thus, in complex structures the constraints corresponding to a particular irrep epikernel, or the three types of physical restriction mentioned above, are usually mixed up with others that can only be considered convenient simplifications to reduce the number of refinable parameters. An example has already been shown above when discussing the structure of $BiMn_2O_5$ (Muñoz *et al.*, 2002), summarized in Table 10. This kind of simplification is so common that it sometimes seems as if it is introduced automatically without being necessitated by the limitations of the experimental data.

One of the most common contraints not forced by symmetry and present in many structures of this database is the restriction of the modulus of the magnetic moment for the same atomic species to have equal value at sites that are symmetry independent in the paramagnetic phase. This *ad hoc* assumption can often represent a reasonable simplification and can be necessary owing to the lack of sufficient data for a more complex model but, in general, independent sites can have different magnetic

moments and this collection also includes many examples where they have been refined independently.

A more subtle simplifying constraint is the assumption of equal moment modulus at magnetic sites which are symmetry independent in the magnetic phase but come from the splitting of a single orbit in the paramagnetic phase. Traditionally, it has been assumed that, if the propagation vector **k** is not equivalent to −**k**, sites related by operations that transform **k** into −**k** become symmetry split in the magnetic phase. This is not correct in general, as these operations may be maintained within the irrep epikernels. In such cases these sites are kept symmetry related, and therefore the assumption of equal moduli for their magnetic moments is one of the MSG constraints of the phase. In other cases, however, the MSG produces a genuine splitting of the atomic sites, and the assumption of keeping correlated spins is not justified by symmetry arguments. Most of the structures that have genuine split magnetic sites include this simplifying constraint and their spins are assumed to have equal modulus. Table 12 and Fig. 20 summarize the magnetic structure of α-Mn (#1.85; Lawson *et al.*, 1994). This is one of the few examples in the collection where this assumption was not introduced and the refinement was done fully consistent with the active irrep and relevant MSG, with split sites having independent magnetic moment values.

Table 12
The asymmetric unit of the magnetic structure of α-Mn (#1.85; Lawson *et al.*, 1994) as an example of a structure determined including only constraints forced by the MSG with split sites refined independently.

The approximate relations of the magnetic moments at different sites, if fulfilled exactly, cannot be justified by any increase in the symmetry or any additional irrep restriction, as the symmetry is maximal and only one irrep is active.

α-Mn (#1.85), *I-43m1'* -> P_I-42_1c (**b**$_p$,**a**$_p$,-**c**$_p$;0,0,0)

Label	***x***	***y***	***z***	**Constr.**[a]	M_x	M_y	M_z	**|M|**
Mn1	0.00000	0.00000	0.00000	0,0,m_z	0.0	0.0	2.83(13)	2.83
Mn2	0.3192(2)	0.3192	0.3173(3)	m_x,m_x,m_z	0.14(12)	0.14	1.82(6)	1.83
Mn3_1	0.3621(1)	0.3621	0.0408(2)	m_x,m_x,m_z	0.43(8)	0.43	0.43(8)	0.74
Mn3_2	0.3533(2)	0.0333(1)	0.3559(2)	m_x,m_y,m_z	-0.25(10)	-0.25(10)	-0.32(4)	0.48
Mn4_1	0.0921(2)	0.0921	0.2790(3)	m_x,m_x,m_z	0.27(8)	0.27	-0.45(8)	0.59
Mn4_2	0.0895(2)	0.2850(1)	0.0894(2)	m_x,m_y,m_z	-0.08(4)	-0.45(8)	0.48(5)	0.66

[a] Symmetry constraints on **M**

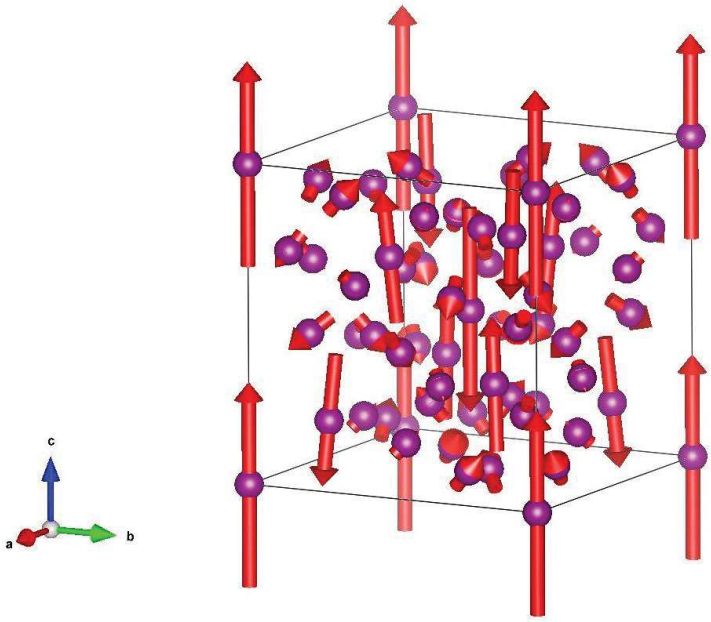

Figure 20
The magnetic structure of α-Mn (#1.85; Lawson *et al.*, 1994), one of the few structures in *MAGNDATA* with a considerable number of independent magnetic sites (some of them symmetry-split by the magnetic order) and which does not include simplifying constraints.

7. Conclusions

We have gathered a digital collection of more than 400 published magnetic structures under the name *MAGNDATA*, where magnetic symmetry is applied as a robust unambiguous common framework for their description, and a preliminary version is used of the so-called magCIF format, which extends the CIF format to magnetic structures. No validation check has been applied to the structures, and inclusion in the collection has only been subject to the requirement that the published model is self-consistent and unambiguous. The collection is freely available at the Bilbao Crystallographic Server (http://www.cryst.ehu.es) and is intended to be a benchmark for a future complete database. This article presents and explains the information that can be retrieved for any of the more than 370 collected commensurate magnetic structures. The various tools that are available for visualization and analysis of each entry have been explained using multiple examples. We have also included a detailed survey of the properties of the collected structures, which shows the power and efficiency of the employed symmetry classification. A subsequent article (Gallego *et al.*, 2016) deals with the more than 40 incommensurate structures that are also included in this collection, using magnetic superspace symmetry as the framework for their description.

We do not have the means to extend *MAGNDATA* to cover all magnetic structures published in the past, or to maintain it and update it regularly for all those published in the future, and therefore this collection does not pretend to become the necessary complete database of all published magnetic structures. However, we hope that this work will stimulate further efforts within the community in the direction of the standardization and unambiguous communication of magnetic structures, with the

aim of making such a database possible in the foreseeable future. Meanwhile, authors who have reported a magnetic structure that is absent from this collection and who are interested in having it included are invited to contact us through the given email address.

Finally, it should be stressed again that the description of many of the structures within a common framework, with full application of their symmetry properties, has in many cases required a complete transformation and reinterpretation of the information provided by the original references. This may have led to errors and misinterpretations. We therefore welcome and will greatly appreciate any report that may point out such problems.

Acknowledgements

The authors thank Branton Campbell and Harold Stokes for very helpful and fruitful interactions. Their programs *ISODISTORT* and *ISOCIF* were some of the basic tools employed during the realization of this work. We are also indebted to V. Petříček for introducing the magCIF format into the communication tools of his program *JANA*. Very helpful comments and suggestions from Juan Rodriguez-Carvajal are also gratefully acknowledged. One of us (JMPM) is especially indebted to J. L. Ribeiro for helpful comments and interchange of information in the early stages of this work, and to W. Sikora for making available the valuable compilation of magnetic structures done in her group in 1976 and 1984. We also acknowledge the work of student Nagore Garcia, and of her supervisor Irene Urcelay-Olabarria, who gathered and reinterpreted some magnetic structures for this collection. The help of D. Khalyavin and V. Pomjakushin for the introduction of some of their published structures into the database is also gratefully appreciated. This work was supported by the Spanish Ministry of Economy and Competitiveness and FEDER funds (project No. MAT2012-34740/MAT2015-66441-P) and by the Government of the Basque Country (project No. IT779-13).

REFERENCES

Aroyo, M. I., Orobengoa, D., de la Flor, G., Tasci, E. S., Perez-Mato J. M. & Wondratschek, H. (2014). *Acta Cryst.* A**70**, 126-137.

Ascher, E. (1977). *J. Phys. C Solid State Phys.* **10**,1365–1377.

Avdeev, M., Kennedy, B. J. & Kolodiazhnyi, T. (2014). *Journal of Physics: Condensed Matter* **26**, 095401.

Avdeev, M., Mohamed, Z., Ling, C. D., Lu, J., Tamaru, M., Yamada, A. & Barpanda, P. (2013). *Inorganic chemistry **52***, 8685-8693.

Baran, S., Hofmann, M., Lampert, G., Stüsser, N., Szytuła, A., Többens, D., Smeibidl, P. & Kausche, S. (2001). *Journal of magnetism and magnetic materials* **236**, 293-301.

Baran, S., Kaczorowski, D., Arulraj, A., Penc, B. & Szytuła, A. (2009). *Journal of Magnetism and Magnetic Materials* **321**, 3256-3261.

Belov, N.V., Neronova, N.N. & Smirnova, T.S. (1957). *Sov. Phys. Crystallogr*. **2**, 311-322.

Bertaut, E.F. (1968). *Acta Crystallogr.* A **24**, 217-231.

Bertaut, E. F., Cohen, J., Lambert-Andron, B. & Mollard, P. (1968). *Journal de Physique* **29**, 813-824.

Bilbao Crystallographic Server. 2013. *MGENPOS: General Positions of Magnetic Space Groups; MWYCKPOS: Wyckoff Positions of Magnetic Space Groups*. http://www.cryst.ehu.es

Blake, G. R., Chapon, L. C., Radaelli, P. G., Park, S., Hur, N., Cheong, S. W. & Rodriguez-Carvajal, J. (2005). *Physical Review B* **71**, 214402.

Bradley, C. J. & Cracknell, A. P. (1972). *The Mathematical Theory of Symmetry in Solids*. Oxford: Clarendon Press.

Brown, I. D. & McMahon, B. (2002). *Acta Cryst. B* **58**, 317-324.

Brown, P. J. & Chatterji, T. (2006). Neutron diffraction and polarimetric study of the magnetic and crystal structures of HoMnO3 and YMnO3. *Journal of Physics: Condensed Matter* **18**, 10085.

Brown, P. J. & Chatterji, T. (2011). *Physical Review B* **84**, 054426.

Brown, P. J. & Forsyth, J. B. (1967). *Proceedings of the Physical Society **92***, 125.

Brown, P. J. & Forsyth, J. B. (1981). *Journal of Physics C: Solid State Physics* **14**, 5171.

Brown, P. J., Forsyth, J. B., Lelievre-Berna, E. & Tasset, F. (2002). *Journal of Physics: Condensed Matter* **14**, 1957

Brown, P. J., Welford, P. J. & Forsyth, J. B. (1973). *Journal of Physics C: Solid State Physics* **6**, 1405.

Buisson, G. (1970). *Journal of Physics and Chemistry of Solids* **31**, 1171-1183.

Burlet, P., Bourdarot, F., Rossat-Mignod, J., Sanchez, J. P., Spirlet, J. C., Rebizant, J. & Vogt, O. (1992). *Physica B: Condensed Matter* **180**, 131-132.

Burlet, P., Ressouche, E., Malaman, B., Welter, R., Sanchez, J. P., & Vulliet, P. (1997). *Physical Review B* **56**, 14013

Calder, S., Lumsden, M. D., Garlea, V. O., Kim, J. W., Shi, Y. G., Feng, H. L., Yamaura, K. & Christianson, A. D. (2012). *Physical Review B* **86**, 054403

Calder, S., Saparov, B., Cao, H. B., Niedziela, J. L., Lumsden, M. D., Sefat, A. S. & Christianson, A. D. (2014). *Physical Review B* **89**, 064417.

Campbell, B.J., Stokes, H.T., Tanner, D.E. & Hatch, D.M. (2006). *J. Appl. Crystallogr*. **39**, 607-614. *ISOTROPY Software Suite.* http://iso.byu.edu

Caron, J. M., Neilson, J. R., Miller, D. C., Llobet, A. & McQueen, T. M. (2011). *Physical Review B* **84**, 180409.

Chattopadhyay, T., Brown, P. J., Roessli, B., Stepanov, A. A., Barilo, S. N. & Zhigunov, D. I. (1992). *Physical Review B* **46**, 5731.

Christianson, A. D., Lumsden, M. D., Angst, M., Yamani, Z., Tian, W., Jin, R., Payzant, E.A., Nagler, S.E. & Mandrus, D. (2008). *Physical Review Letters* **100**, 107601

Corliss, L. M., Elliott, N. & Hastings, J. M. (1960). *Physical Review* **117**, 929.

Damay, F., Martin, C., Hardy, V., André, G., Petit, S. & Maignan, A. (2011). *Physical Review B* **83**, 184413.

Damay, F., Poienar, M., Martin, C., Maignan, A., Rodriguez-Carvajal, J., André, G. & Doumerc, J. P. (2009). *Physical Review B*, **80**, 094410.

Deldem, M., Amara, M., Galéra, R. M., Morin, P., Schmitt, D. & Ouladdiaf, B. (1998). *Journal of Physics: Condensed Matter* **10**, 165.

Ding, L., Colin, C. V., Darie, C., Robert, J., Gay, F. & Bordet, P. (2016). *Physical Review B* **93**, 064423.

Dul, M., Lesniewska, B., Oles, A., Pytlik, L. & Sikora, W. (1997). *Physica B* **234-236**, 790-791.
Ederer, C. & Spaldin, N. A. (2007). *Phys. Rev. B* **76**, 214404
Ehrenberg, H., Witschek, G., Rodriguez-Carvajal, J. & Vogt, T. (1998). *Journal of magnetism and magnetic materials* **184**, 111-115.
Fernandez-Diaz, M. T., Martinez, J. L., Alonso, J. M. & Herrero, E. (1999). *Physical Review B* **59**, 1277.
Fiebig, M., Fröhlich, D. & Thiele, H. J. (1996). *Physical Review B* **54**, R12681.
Free, D. G. & Evans, J. S. (2010). *Physical Review B* **81**, 214433.
Fruchart, D., Bertaut, E. F., Sayetat, F., Eddine, M. N., Fruchart, R. & Senateur, J. P. (1970). *Solid State Communications* **8**, 91-99.
Fruchart, D. & F. Bertaut, E. (1978). *Journal of the Physical Society of Japan* **44**, 781-791.
Gäbler, F., Schnelle, W., Senyshyn, A. & Niewa, R. (2008). *Solid State Sciences*, **10**, 1910-1915.
Gallego, S.V., Tasci, E.S., de la Flor, G., Perez-Mato, J.M. & Aroyo, M.I. (2012). *J. Appl. Crystallogr.* **45**,1236–1247.
Gallego, S.V., Perez-Mato, J.M., Elcoro, L.,Tasci, E.S., Hanson, R.L., Aroyo, M.I. & Madariaga, G. (2016). *J. Appl. Crystallogr.* Submitted.
Glazer, A.M., Aroyo, M.I. & Authier, A. (2014). *Acta Cryst*. A. **70**, 300-302.
Goldman, A. I., Argyriou, D. N., Ouladdiaf, B., Chatterji, T., Kreyssig, A., Nandi, S., Ni, N., Bud'ko, S.L., Canfield, P.C. & McQueeney, R. J. (2008). *Physical Review B* **78**, 100506
Gorbunov, D. I., Henriques, M. S., Andreev, A. V., Eigner, V., Gukasov, A., Fabrèges, X., Skourski, Y., Petříček, V. & Wosnitza, J. (2016). *Physical Review B* **93**, 024407
Hahn, Th. (2002). (Editor). *International Tables for Crystallography Vol. A, Space-Group Symmetry*, 5th ed. Dordrecht: Kluwer Academic Publishers.
Hamasaki, T., Ide, T., Kuroe, H., Sekine, T., Hase, M., Tsukada, I. & Sakakibara, T. (2008). *Phys. Rev. B* **77**, 134419
Hanson, R. (2013). *Jmol: an open-source Java viewer for chemical structures in 3D*. http://www.jmol.org/.
Hase, M., Kuroe, H., Pomjakushin, V. Y., Keller, L., Tamura, R., Terada, N., Matsushita, Y., Dönni, A. & Sekine, T. (2015). *Physical Review B* **92**, 054425
Hastings, J. M., Corliss, L. M. & Windsor, C. G. (1965). *Physical Review* **138**, A176.
Hill, A. H., Jiao, F., Bruce, P. G., Harrison, A., Kockelmann, W. & Ritter, C. (2008). *Chemistry of Materials* **20**, 4891-4899.
Huang, Q., Qiu, Y., Bao, W., Green, M. A., Lynn, J. W., Gasparovic, Y. C., Wu, T. & Chen, X. H. (2008). *Physical Review Letters* **101**, 257003.
Hutanu, V., Sazonov, A., Meven, M., Murakawa, H., Tokura, Y., Bordács, S., Kézsmárki, I. & Náfrádi, B. (2012). *Physical Review B* **86**, 104401
Hwang, J., Choi, E. S., Ye, F., Cruz, C. D., Xin, Y., Zhou, H. D. & Schlottmann, P. (2012). *Physical Review Letters* **109**, 257205.
ICSD (2007). Inorganic Crystal Structure Database. FIZ-Karlsruhe, Germany, and the National Institute of Standards and Technology (NIST), USA. http://www.fiz-karlsruhe.de/icsd.html
Iikubo, S., Kodama, K., Takenaka, K., Takagi, H. & Shamoto, S. (2008). *Physical Review B* **77**, 020409

International Union of Crystallography (2015). *Commission on Magnetic Structures*, http://www.iucr.org/iucr/commissions/magnetic-structures.

Ivanov, S. A., Tellgren, R., Ritter, C., Nordblad, P., Mathieu, R., Andre, G., Golubko, N.V., Politova E.D. & Weil, M. (2012). *Materials Research Bulletin* **47**, 63-72.

Izyumov, Y.A., Naish, V.E. & Ozerov, R.P. (1991). *Neutron Diffraction of Magnetic Materials*. Dordrecht: Kluwer Academic Publishers.

Jauch, W., Reehuis, M., Bleif, H. J., Kubanek, F. & Pattison, P. (2001). *Physical Review B* **64**, 052102

Jensen, T. B. S., Christensen, N. B., Kenzelmann, M., Rønnow, H. M., Niedermayer, C., Andersen, N. H., Lefmann, K., Schefer, J., Zimmermann, M., Li, J., Zarestky, J.L. & Vaknin, D. (2009). *Physical Review B* **79**, 092412

Kenzelmann, M., Coldea, R., Tennant, D. A., Visser, D., Hofmann, M., Smeibidl, P. & Tylczynski, Z. (2002). *Physical Review B* **65**, 144432

Knížek, K., Jirák, Z., Novák, P. & de la Cruz, C. (2014). *Solid State Sciences* **28**, 26-30.

Krén, E., Kádár, G., Pál, L. & Szabó, P. (1967). *Journal of Applied Physics* **38**, 1265-1266.

Kunnmann, W., La Placa, S., Corliss, L. M., Hastings, J. M. & Banks, E. (1968). *Journal of Physics and Chemistry of Solids* **29**, 1359-1364.

Law, J. M., Koo, H. J., Whangbo, M. H., Brücher, E., Pomjakushin, V., & Kremer, R. K. (2014). *Physical Review B* **89**, 014423

Lawson, A. C., Larson, A. C., Aronson, M. C., Johnson, S., Fisk, Z., Canfield, P. C., Thompson, J.D. & Von Dreele, R. B. (1994). *Journal of Applied Physics* **76**, 7049-7051.

Lefrançois, E., Chapon, L. C., Simonet, V., Lejay, P., Khalyavin, D., Rayaprol, S., Sampathkumaran, E.V., Ballou, R. & Adroja, D. T. (2014). *Physical Review B* **90**, 014408

Litvin, D. B. (2013). *Magnetic Group Tables: 1-, 2- and 3-Dimensional Magnetic Subperiodic Groups and Magnetic Space Groups* (Chester: International Union of Crystallography). www.iucr.org/publ/978-0-9553602-2-0

Lopez, M. L., Daidouh, A., Pico, C., Rodríguez-Carvajal, J. & Veiga, M. L. (2008). *Chemistry–A European Journal* **14**, 10829-10838.

Lovesey, S. W., Khalyavin, D. D., Manuel, P., Chapon, L. C., Cao, G. & Qi, T. F. (2012). *Journal of Physics: Condensed Matter* **24**, 496003

Martinelli, A., Ferretti, M. & Ritter, C. (2016). *Journal of Solid State Chemistry* **239**, 99-105.

Martínez-Coronado, R., Alonso, J. A., Cascos, V. & Fernández-Díaz, M. T. (2014). *Journal of Power Sources* **247**, 876-882.

Matsuda, M., de la Cruz, C., Yoshida, H., Isobe, M. & Fishman, R. S. (2012). *Physical Review B* **85**, 144407

Melot, B. C., Paden, B., Seshadri, R., Suard, E., Nénert, G., Dixit, A. & Lawes, G. (2010). *Physical Review* B **82**, 014411

Momma, K. & Izumi, F. (2011). *J. Appl. Crystallogr*. **44**, 1272-1276.

Müller, H., Kockelmann, W. & Johrendt, D. (2006). *Chemistry of materials* **18**, 2174-2180.

Müller, R. A., Lee-Hone, N. R., Lapointe, L., Ryan, D. H., Pereg-Barnea, T., Bianchi, A. D., Mozharivskyj, Y. & Flacau, R. (2014). *Physical Review B*, **90**, 041109

Muñoz, A., Alonso, J. A., Casais, M. T., Martinez-Lope, M. J., Martinez, J. L. & Fernandez-Diaz, M. T. (2002). *Physical Review B* **65**, 144423

Muñoz, A., Alonso, J. A., Martinez-Lope, M. J., Casais, M. T., Martinez, J. L. & Fernandez-Diaz, M. T. (2000). *Physical Review B* **62**, 9498

Muñoz, A., Alonso, J. A., Martínez-Lope, M. J., Casáis, M. T., Martínez, J. L. & Fernandez-Diaz, M. T. (2001). *Chemistry of materials* **13**, 1497-1505.

Muñoz, A., Casáis, M. T., Alonso, J. A., Martínez-Lope, M. J., Martinez, J. L. & Fernandez-Diaz, M. T. (2001). *Inorganic chemistry* **40**, 1020-1028.

Murakawa, H., Onose, Y., Miyahara, S., Furukawa, N. & Tokura, Y. (2010). *Phys. Rev. Lett.* **105**, 137202

Núñez, P., Roisnel, T. & Tressaud, A. (1994). *Solid State Communications* **92**, 601-605.

Oles, A., Kajzar, P., Kucab, M. & Sikora, W. (1976). *Magnetic structures determined by neutron diffaction*. Panstwowe Wydawnictwo Naukowe, Warszawa-Krakow.

Oles, A., Sikora, W., Bombik, A. & Konopka, M. (1984) *Magnetic structure determined by neutron diffraction. Description and Symmetry analysis*. Scientific Bulletins of the Stanislaw Staszic University of Mining and Metallurgy No. 1005, Krakow.

Opechowski, W. & Guccione, R. (1965). *Magnetism*, ed. Rado, GT H Suhl. Vol. II, Part A, pp.105-65. New York: Academic Press

Perez-Mato, J. M., Gallego, S. V., Tasci, E. S., Elcoro, L., de laFlor, G. & Aroyo, M. I. (2015). *Annu. Rev. Mater. Res.* **45,** 13.1-13.32.

Perez-Mato, J. M. & Ribeiro, J. L. (2011). Acta Cryst. A **67**, 264-268.

Perez-Mato, J.M., Ribeiro, J.L., Petricek, V. & Aroyo, M.I.(2012). *Phys. Condens. Matter.* **24**,163201.

Perez-Mato, J. M., Gallego, S. V., Elcoro, L., Tasci, E. S. & Aroyo, M. I. (2016). *J. Phys.: Condens. Matter* **28,** 286001

Pernet, M., Elmale, D. & Joubert, J. C. (1970). *Solid State Communications* **8**, 1583-1587.

Petricek, V., Fuksa, J. & Dusek, M. (2010). *Acta Crystallogr.* A **66**, 649-655.

Petrıcek, V., Dusek, M. & Palatinus, L. (2014). *Z. Krist.* **229**, 345-352.

Plumier, R., Sougi, M. & Saint-James, R. (1983). *Physical Review B* **28**, 4016-4020.

Pomjakushin, V. Y., Pomjakushina, E. V., Krzton-Maziopa, A., Conder, K. & Shermadini, Z. (2011). *Journal of Physics: Condensed Matter* **23**, 156003

Poole, A., Wills, A. S. & Lelievre-Berna, E. (2007). *Journal of Physics: Condensed Matter* **19**, 452201

Radaelli, P. G., Cox, D. E., Capogna, L., Cheong, S. W. & Marezio, M. (1999). *Physical Review B* **59**, 14440

Ratcliff II, W., Sharma, A. L., Gomes, A. M., Gonzalez, J. L., Huang, Q. & Singleton, J. (2009). *Journal of Magnetism and Magnetic Materials* **321**, 2612-2616.

Redhammer, G. J., Roth, G., Treutmann, W., Hoelzel, M., Paulus, W., André, G., Pietzonka, C. & Amthauer, G. (2009). *Journal of Solid State Chemistry* **182**, 2374-2384.

Redhammer, G. J., Roth, G., Treutmann, W., Paulus, W., André, G., Pietzonka, C., & Amthauer, G. (2008).*Journal of Solid State Chemistry* **181**, 3163-3176.

Reehuis, M., Ulrich, C., Prokeš, K., Mat'aš, S., Fujioka, J., Miyasaka, S., Tokura, Y. & Keimer, B. (2011).*Physical Review B* **83**, 064404

Ressouche, E., Kernavanois, N., Regnault, L. P. & Henry, J. Y. (2006). *Physica B: Condensed Matter* **385**, 394-397.

Ressouche, E., Loire, M., Simonet, V., Ballou, R., Stunault, A. & Wildes, A. (2010). *Physical Review B* **82**, 100408

Rodriguez, E.E., Cao, H., Haiges, R. & Melot, B.C. (2016). *Journal of Solid State Chemistry* **236**, 39-44.
Rodriguez-Carvajal, J. (1993). *Physica* B **192**, 55-69.
Rousse, G., Rodriguez-Carvajal, J., Patoux, S. & Masquelier, C. (2003). *Chemistry of materials* **15**, 4082-4090.
Saha, R., Sundaresan, A., Sanyal, M. K., Rao, C. N. R., Orlandi, F., Manuel, P. & Langridge, S. (2016). *Physical Review B* **93**, 014409
Sazonov, A. P., Gukasov, A., Cao, H. B., Bonville, P., Ressouche, E., Decorse, C. & Mirebeau, I. (2013). *Physical Review B* **88**, 184428
Scagnoli, V., Allieta, M., Walker, H., Scavini, M., Katsufuji, T., Sagarna, L., Zaharko, O. & Mazzoli, C. (2012). *Physical Review B*, **86**, 094432
Schmid, H. (2001). *Ferroelectrics* **252**, 41–50.
Schobinger-Papamantellos, P., Buschow, K. H. J. & Rodriguez-Carvajal, J. (2012). *Journal of Magnetism and Magnetic Materials* **324**, 3709-3715.
Schobinger-Papamantellos, P., De Mooij, D. B., & Buschow, K. H. J. (1988). *Journal of the Less Common Metals* **144**, 265-274.
Schobinger-Papamantellos, P., Rodríguez-Carvajal, J., André, G. & Buschow, K. H. J. (2006). *Journal of magnetism and magnetic materials* **300**, 333-350.
Schobinger-Papamantellos, P., Rodríguez-Carvajal, J., André, G., Duong, N. P., Buschow, K. H. J. & Tolédano, P. (2001). *Journal of magnetism and magnetic materials* **236**, 14-27.
Shirane, G., J. Pickart, S. & Ishikawa, Y. (1959). *Journal of the Physical Society of Japan* **14**, 1352-1360.
Shull, C. G. & Smart J. S. (1949). *Phys. Rev.* **76**, 1256-1257.
Spaldin, N. A., Fiebig, M. & Mostovoy, M. (2008). *J. Phys.: Condens. Matter* **20**, 434203
Stokes, H. T. & Campbell, B. J. (2011). *ISO-MAG: Table of magnetic space groups ISOTROPY Software Suite*. http://iso.byu.edu
Stokes, H.T. & Campbell, B.J. (2015) *ISOCIF: Create or modify CIF files, ISOTROPY Software Suite.* http://iso.byu.edu
Stokes, H. T., Campbell, B. J. & Cordes, R. (2013) *Acta Cryst.* A**69**, 388-395
Szytuła, A., Baran, S., Kaczorowski, D., Sikora, W. & Hoser, A. (2014). *Journal of Alloys and Compounds* **617**, 149-153.
Taira, N., Wakeshima, M., Hinatsu, Y., Tobo, A. & Ohoyama, K. (2003). *Journal of Solid State Chemistry* **176**, 165-169.
Tan, L., Kreyssig, A., Kim, J. W., Goldman, A. I., McQueeney, R. J., Wermeille, D., Sieve, B., Lograsso, T.A., Schlagel, D.L., Budko, S.L., Pecharsky, V.K. and Gschneidner, K. A. (2005). *Physical Review B* **71**, 214408
Toft-Petersen, R., Reehuis, M., Jensen, T. B., Andersen, N. H., Li, J., Le, M. D., Laver, M. Niedermayer, C., Klemke, B., Lefmann, K. & Vaknin, D. (2015). *Physical Review B* **92**, 024404
Troć, R., Pasturel, M., Tougait, O., Sazonov, A. P., Gukasov, A., Sułkowski, C. & Noël, H. (2012). *Physical Review B* **85**, 064412
Tsuzuki, K., Ishikawa, Y., Watanabe, N. & Akimoto, S. (1974). *Journal of the Physical Society of Japan* **37**, 1242-1247.
Vecchini, C., Chapon, L. C., Brown, P. J., Chatterji, T., Park, S., Cheong, S. W. & Radaelli, P. G. (2008). *Physical Review B* **77**, 134434
Vilminot, S., André, G. & Kurmoo, M. (2009). *Inorganic chemistry* **48**, 2687-2692.

Wheeler, E. M., Lake, B., Islam, A. N., Reehuis, M., Steffens, P., Guidi, T. & Hill, A. H. (2010). *Physical Review B* **82**, 140406

Wiebe, C. R., Gardner, J. S., Kim, S. J., Luke, G. M., Wills, A. S., Gaulin, B. D., Greedan, J.E., Swainson, I., Qiu, Y. & Jones, C. Y. (2004). *Physical Review Letters*, *93*(7), 076403

Will, G. & Schafer, W. (1979). *Journal of the Less Common Metals* **67**, 31-39.

Wills, A. S., Zhitomirsky, M. E., Canals, B., Sanchez, J. P., Bonville, P., de Réotier, P. D. & Yaouanc, A. (2006). *Journal of Physics: Condensed Matter 18*, L37-L42.

Yamaura, J., Ohgushi, K., Ohsumi, H., Hasegawa, T., Yamauchi, I., Sugimoto, K., Takeshita, S., Tokuda, A., Takata, M., Udagawa, M., Takigawa, M., Harima, H., Arima, T. & Hiroi, Z. (2012). *Physical Review Letters* **108**, 247205

Yan, B., Kumar Paul, A., Kanungo, S., Reehuis, M., Hoser, A., Többens, D.M., Schnelle, W., Williams, R.C., Lancaster, T., Xiao, F., Möller, J.S., Blundell, S.J., Hayes, W., Felser, C. & Jansen, M. (2014). *Phys. Rev. Lett.* **112**, 147202

Yano, S., Louca, D., Yang, J., Chatterjee, U., Bugaris, D.E., Chung, D.Y., Peng, L., Grayson, M. & Kanatzidis, M.G. (2016). *Physical Review B* **93**, 024409

Ye, F., Chi, S., Chakoumakos, B. C., Fernandez-Baca, J. A., Qi, T. & Cao G. (2013). *Physical Review B* **87**, 140406

Yelon, W. B. & Cox, D. E. (1973). *Physical Review B* **7**, 2024-2027.

Zhu, M., Do, D., Cruz, C. D., Dun, Z., Zhou, H. D., Mahanti, S. D. & Ke, X. (2014). *Physical review letters* **113**, 076406

ANEXO F

Gallego S. V., Perez-Mato J. M., Elcoro L., Tasci E. S., Hanson R. M., Aroyo M. I., Madariaga G. *J. Appl. Cryst*. **49**, 1941-56 (2016) DOI: 10.1107/S1600576716015491

MAGNDATA: towards a database of magnetic structures. II. The incommensurate case

Samuel V. Gallego[a], J. Manuel Perez-Mato[a]*, Luis Elcoro[a], Emre S. Tasci[b], Robert M. Hanson[c], Mois I. Aroyo[a] and Gotzon Madariaga[a]

[a]Departamento de Fisica de la Materia Condensada, Facultad de Ciencia y Tecnología, Universidad del País Vasco (UPV/EHU), Apartado 644, 48080 Bilbao, Spain, [b]Department of Physics Engineering, Hacettepe University, 06800 Ankara, Turkey, and [c]Department of Chemistry, St Olaf College, Northfield, MN 55057. *Correspondence e-mail: jm.perez-mato@ehu.es

Edited by G. Kostorz, ETH Zurich, Switzerland (Received 1 July 2016; accepted 3 October 2016; online 21 October 2016)

Keywords: magnetic structures database; *MAGNDATA*; incommensurate magnetic structures; magnetic superspace groups; Bilbao Crystallographic Server; superspace symmetry; irreducible representations.

Abstract:

A free web page under the name *MAGNDATA*, which provides detailed quantitative information on more than 400 published magnetic structures, has been made available at the Bilbao Crystallographic Server (http://www.cryst.ehu.es). It includes both commensurate and incommensurate structures. In the first article in this series, the information available on commensurate magnetic structures was presented [Gallego, Perez-Mato, Elcoro, Tasci, Hanson, Momma, Aroyo & Madariaga (2016). *J. Appl. Cryst.* **49**, 1750–1776]. In this second article, the subset of the database devoted to incommensurate magnetic structures is discussed. These structures are described using magnetic superspace groups, *i.e.* a direct extension of the non-magnetic superspace groups, which is the standard approach in the description of aperiodic crystals. The use of magnetic superspace symmetry ensures a robust and unambiguous description of both atomic positions and magnetic moments within a common unique formalism. The point-group symmetry of each structure is derived from its magnetic superspace group, and any macroscopic tensor property of interest governed by this point-group symmetry can be retrieved through direct links to other programs of the Bilbao Crystallographic Server. The fact that incommensurate magnetic structures are often reported with ambiguous or incomplete information has made it impossible to include in this collection a good number of the published structures which were initially considered. However, as a proof of concept, the published data of about 30 structures have been re-interpreted and transformed, and together with ten structures

where the superspace formalism was directly employed, they form this section of *MAGNDATA*. The relevant symmetry of most of the structures could be identified with an epikernel or isotropy subgroup of one irreducible representation of the space group of the parent phase, but in some cases several irreducible representations are active. Any entry of the collection can be visualized using the online tools available on the Bilbao server or can be retrieved as a magCIF file, a file format under development by the International Union of Crystallography. These CIF-like files are supported by visualization programs like *Jmol* and by analysis programs like *JANA* and *ISODISTORT*.

1. Introduction

Under the name *MAGNDATA* we have collected on the Bilbao Crystallographic Server (http://www.cryst.ehu.es) comprehensive information on more than 400 magnetic structures, both commensurate and incommensurate. *MAGNDATA* has been developed as a proof of concept for the development of a database of magnetic structures based on the systematic application of magnetic symmetry. This task has been done within the framework of the efforts of the Commission on Magnetic Structures of the IUCr (International Union of Crystallography, 2015) for achieving a standard in the communication of magnetic structures and an extension of the CIF format (Brown & McMahon, 2002) to magnetic structures. For a detailed description of the context under which this small database has been developed, we refer to our previous article (Gallego *et al.*, 2016), where we presented and discussed the section of *MAGNDATA* devoted to commensurate structures. This has more than 360 entries, and the structures are described within the framework of the symmetry relations described by the magnetic space groups (MSGs), also called Shubnikov groups (Litvin, 2013; Stokes & Campbell, 2011). *MAGNDATA* also includes about 40 incommensurate structures (see Fig. 1) which require a different methodology, with their symmetry being given by magnetic superspace groups (MSSGs). Here, we present and discuss the main features of this second part of the collection. We concentrate on the explanation of the information available for each structure, and the way this information can be retrieved and analysed.

The symmetry of magnetic structures with incommensurate propagation vector(s) cannot be described by an MSG (Litvin, 2013; Stokes & Campbell, 2011). Its symmetry is given instead by a superspace group (Petříček *et al.*, 2010; Perez-Mato *et al.*, 2012). The superspace formalism was developed decades ago to describe the symmetry properties of aperiodic crystals, *i.e.* incommensurate crystals and quasicrystals, and it has become the standard approach for any quantitative analysis of these systems (Janssen *et al.*, 2006, 2007; Van Smaalen, 2007; Stokes *et al.*, 2011; Janssen & Janner, 2014). Although it was clear from the beginning (Janner & Janssen, 1980) that the new concept was also extensible and applicable to incommensurate magnetic structures, superspace symmetry has been underutilized in the characterization of magnetic order until very recently, when computer programs which make use of the so-called magnetic superspace groups were developed (Petříček *et al.*, 2014; Campbell *et al.*, 2006; Perez-Mato *et al.*, 2015). Using these symmetry groups defined in a $(3 + d)$-dimensional superspace (d is the number of rationally independent propagation vectors in the modulation), incommensurately magnetic structures can be described

following a crystallographic methodology, similar to the case of non-magnetic incommensurately modulated crystals and quasicrystals. For a review of the properties and application of MSSGs, see Perez-Mato *et al.* (2012). The use of magnetic superspace symmetry ensures a robust and unambiguous description of both atomic positions and magnetic moments within a common unique formalism, and this is the approach followed in *MAGNDATA*.

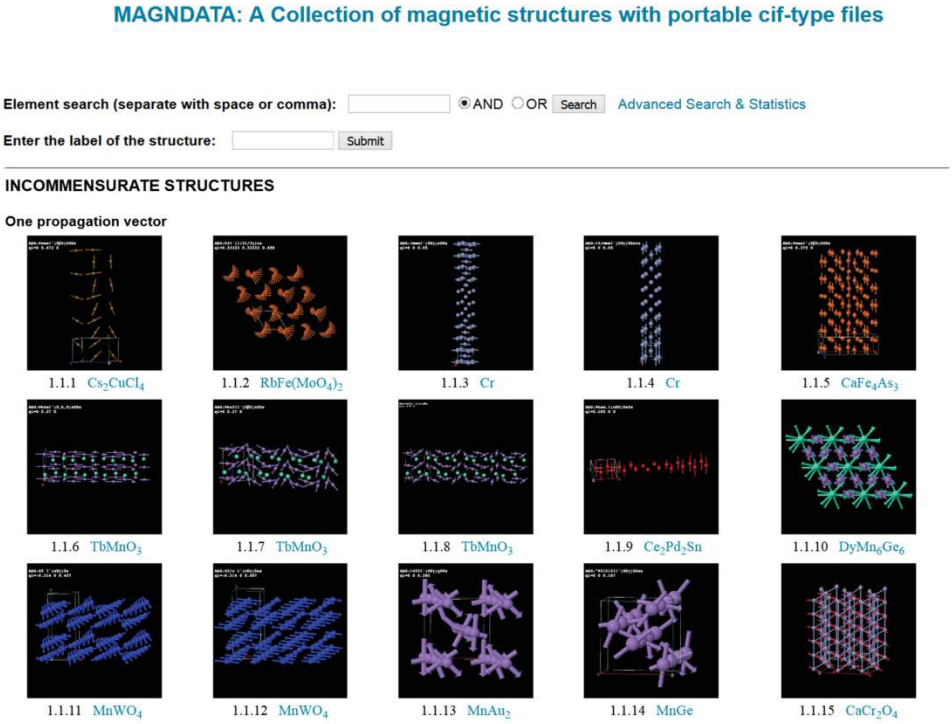

Figure 1
A screenshot, with a partial view of the online icon list of the incommensurate magnetic structures that can be retrieved from *MAGNDATA*.

The CIF format was extended years ago for the case of non-magnetic incommensurate crystals and their superspace symmetry (Brown & McMahon, 2002; Madariaga, 2005). The magCIF file format that is being developed by the Commision on Magnetic Structures of the IUCr has also extended the CIF format to incommensurate magnetic structures with the inclusion of the features associated with the MSSGs (International Union of Crystallography, 2015). We could therefore employ a preliminary version of the magCIF file format not only for commensurate magnetic structures but also for incommensurate structures. For the moment, only structures with a single rational independent incommensurate propagation vector have been included, which means that their superspace symmetry is described by a (3 + 1)-dimensional superspace group. Extension to structures with (3 + d)-dimensional superspace symmetry with d > 1 is, however, straightforward.

2. Description of incommensurate magnetic structures

Under the superspace formalism, the data items defining an incommensurate magnetic structure with a single rationally independent incommensurate propagation vector are the following:

(i) A unit cell that defines the average lattice periodicity of the magnetic ordering if the incommensurate modulation is taken out. This lattice acts as a reference, and its unit cell is called the basic unit cell.

(ii) A primary incommensurate propagation vector (also termed modulation wavevector in the usual superspace formalism).

(iii) The magnetic (3 + 1)-dimensional superspace group (MSSG), which defines the symmetry of the phase. The symmetry operations of this group define both the symmetry relations between the average positions of the atoms within the average lattice, and those between their spin, displacive and occupational modulations. These symmetry relations are expected to be satisfied within the whole thermodynamic stabilitity range of the incommensurate phase. The fourth dimension included in these groups represents the argument of the modulation functions, and a translation along this internal coordinate corresponds to a global shift of the phase of all modulation functions.

(iv) The average atomic positions (in relative units with respect to the basic unit cell) and average magnetic moments (if the atom is magnetic) of a set of atoms in the basic unit cell that are not symmetry related and form an asymmetric unit. The average position and average magnetic moments of any other atom in the unit cell can be derived from those of the asymmetric unit through the application of the symmetry operations of the MSSG defined in (iii). The term `average' is used here to denote the periodic magnetic structure that would be obtained if the reported incommensurate modulated distortions present in the structure were cancelled. This average periodic structure, also called the basic structure in the traditional language of superspace formalism, acts as a reference for both the magnetic and structural modulations, where by construction $k = 0$ terms are not included. This average structure, usually obtained from a refinement considering all diffraction peaks, is to be distinguished from the structure that could be obtained in a refinement in which only the main reflections are used.

(v) Atomic modulation functions for the atoms in the asymmetric unit in (iv), from which the atomic modulation functions of any other atom in the basic unit cell can be derived through the application of the symmetry operations of the MSSG defined in (iii).

These five items constitute the basic information that is stored for any of the incommensurate magnetic structures gathered in *MAGNDATA* and this is the essential part of the corresponding magCIF file that can be downloaded. It should be remarked that some of the programs supporting commensurate magCIF files that were mentioned by Gallego *et al.* (2016) do not yet support magCIF files of incommensurate structures. Among those that are fully compatible, the most important ones are *Jmol* (Hanson, 2013), *ISOCIF* (Stokes & Campbell, 2014), *ISODISTORT* (Campbell *et al.*, 2006) and *JANA* (Petříček *et al.*, 2014).

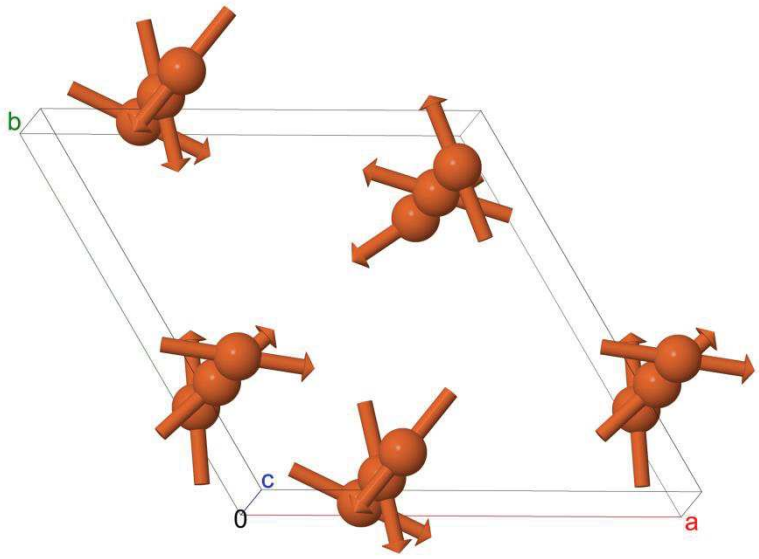

Figure 2
A schematic diagram of the incommensurate magnetic structure of $Ba_3NbFe_3Si_2O_{14}$ (Marty *et al.*, 2008), showing only the Fe atoms in three consecutive basic unit cells along **c**, as retrieved from *MAGNDATA* (#1.1.17) using its *Jmol* visualization tool.

Table 1
Symmetry operations of the MSSG *P*3211′(00γ)000*s* describing the superspace symmetry of the magnetic structure of $Ba_3NbFe_3Si_2O_{14}$ (#1.1.17; Marty *et al.*, 2008)

The MSSG label is obtained from a direct extension of the notation convention used for non-magnetic superpace groups (Janssen *et al.*, 2006), which essentially agrees with that employed by *ISODISTORT* (Campbell *et al.*, 2006) and *JANA* (Petříček *et al.*, 2014). The MSSG label included in *MAGNDATA* is only illustrative, as there are no standard labels and the group is fully defined by the provided list of symmetry operations.

N	(*x1,x2,x3,x4*,±1)	Seitz notation
1	*x1,x2,x3,x4*,+1	{1 | 0}
2	*-x2,x1-x2,x3,x4*,+1	$\{3^{+}_{001} \mid 0\}$
3	*-x1+x2,-x1,x3,x4*,+1	$\{3^{-}_{001} \mid 0\}$
4	*x2,x1,-x3,-x4*,+1	$\{2_{110} \mid 0\}$
5	*x1-x2,-x2,-x3,-x4*,+1	$\{2_{100} \mid 0\}$
6	*-x1,-x1+x2,-x3,-x4*,+1	$\{2_{010} \mid 0\}$
7	*x1,x2,x3,x4*+1/2,-1	{1' | 0, 0, 0, 1/2}
8	*-x2,x1-x2,x3,x4*+1/2,-1	$\{3'^{+}_{001} \mid 0, 0, 0, 1/2\}$
9	*-x1+x2,-x1,x3,x4*+1/2,-1	$\{3'^{-}_{001} \mid 0, 0, 0, 1/2\}$
10	*x2,x1,-x3,-x4*+1/2,-1	$\{2'_{110} \mid 0, 0, 0, 1/2\}$
11	*x1-x2,-x2,-x3,-x4*+1/2,-1	$\{2'_{100} \mid 0, 0, 0, 1/2\}$
12	*-x1,-x1+x2,-x3,-x4*+1/2,-1	$\{2'_{010} \mid 0, 0, 0, 1/2\}$

As an example, Tables 1, 2 and 3 present the data available in *MAGNDATA* for the incommensurate magnetic structure of $Ba_3NbFe_3Si_2O_{14}$ reported by Marty *et al.* (2008)

and depicted in Fig. 2. These data are sufficient for a full definition of this structure. The following remarks are important with respect to these data.

2.1 Symmetry operations

The list of symmetry operations (see Table 1) is the only obligatory information in a magCIF file with respect to symmetry, and it fully defines the MSSG of the structure. Operations are described with respect to the basic unit cell that defines the average lattice. They are given in a form similar to the symmetry operations of the magnetic space groups, which was explained in the previous article on the commensurate section of *MAGNDATA* (Gallego *et al.*, 2016). A direct extension of the standard notation for non-magnetic superspace groups (Janssen *et al.*, 2006) is used. Each symmetry operation is described by the transformation of a general four-dimensional position (x_1, x_2, x_3, x_4) plus the `−1/+1' symbol to indicate the inclusion or not of time reversal (second column of Table 1); this is also the format used in the magCIF files. For a better direct visualization of the operations, *MAGNDATA* also includes an alternative generalized Seitz notation (last column in Table 1), where the point-group operations are indicated with labels that can be easily interpreted (Glazer *et al.*, 2014).

The linear transformation of the components (x_1, x_2, x_3, x_4) associated with any symmetry operation of an MSSG can be expressed in the matrix form

$$\left(\begin{array}{ccc|c} & \mathbf{R} & & \begin{matrix}0\\0\\0\end{matrix} \\ \hline h_1 & h_2 & h_3 & R_I \end{array}\right)\begin{pmatrix} x_1 \\ x_2 \\ x_3 \\ x_4 \end{pmatrix} + \begin{pmatrix} t_1 \\ t_2 \\ t_3 \\ t_4 \end{pmatrix}, \qquad \text{(F.1)}$$

where **R** is a 3×3 matrix corresponding to a crystallographic three-dimensional point-group operation expressed in the basic unit-cell basis. The value of R_I (either +1 or −1) and the integers (h_1, h_2, h_3) are fully determined by **R** and the value of the incommensurate propagation vector **k** according to the relation

$$\mathbf{k}\cdot\mathbf{R} = R_I\mathbf{k} + \mathbf{H}_\mathrm{R} \qquad \text{(F.2)}$$

where $\mathbf{H}_\mathrm{R}$ is a reciprocal lattice vector of the average structure, given by the integer components (h_1, h_2, h_3) in the reciprocal basis of the basic unit cell. In the example of Table 1, $\mathbf{H}_\mathrm{R}$ = (0, 0, 0) for any operation. The vector $\mathbf{H}_\mathrm{R}$ can have nonzero components (h_1, h_2, h_3) if the propagation vector lies on the Brillouin zone surface, with some commensurate fractional components. The Seitz notation for the generic operation in equation (F.1) is {**R**′ | t_1, t_2, t_3, t_4} or {**R** | t_1, t_2, t_3, t_4}, depending on the additional action of time reversal or not, where **R** now stands for the corresponding three-dimensional point-group operation. As shown in equation (F.2), the point-group operations present in the MSSG either keep the propagation vector invariant (R_I = +1) or change it to its opposite value (R_I = −1), in both cases modulo the basic reciprocal lattice.

2.2. Average structure

The set of operations {**R** | t_1, t_2, t_3} and {**R**′ | t_1, t_2, t_3}, which can be derived from the set of operations of the MSSG, define a three-dimensional MSG in the basis given by the chosen basic unit cell, which describes the symmetry of the average structure. This average structure, as an ordinary commensurate magnetic structure, is defined by the values of the atomic positions and magnetic moments of a chosen asymmetric unit (see Table 2). The three-dimensional MSG resulting from the operations in Table 1 is *P*3211′, and this is the label used as the first part of the MSSG label. It is a grey space group, as all operations are present in the group both with and without time reversal. This is the symmetry of the average structure, and therefore all average magnetic moments are necessarily zero. The list of average atomic positions for the asymmetric unit in our example is given in Table 2. As in most incommensurate structures, the average magnetic moments are forced by symmetry to be zero and are not explicitly listed. In general, if not appearing in the table they should be taken as zero. The average commensurate structure can be reconstructed from Table 2 and the given unit cell by making use of the superspace group operations listed in Table 1. The effective space group to be used can be extracted from this table.

Table 2
Average atomic positions (average magnetic moments are all zero) of symmetry-independent atoms in the incommensurate magnetic structure of $Ba_3NbFe_3Si_2O_{14}$ (#1.1.17; Marty *et al.*, 2008).

Unit cell *a* = 8.539 (1), *b* = 8.539 (1), *c* = 5.2414 (1) Å, α = 90, β = 90, γ = 120°, MSSG *P*3211′(00γ)000*s* (see Table 1).

Label	Atom type	*x*	*y*	*z*	Multiplicity
Fe1	Fe	0.24964(4)	0	0.5	3
Ba1	Ba	0.56598(2)	0	0	3
Nb1	Nb	0	0	0	1
Si1	Si	0.666667	0.333333	0.5220(1)	2
O1	O	0.666667	0.333333	0.2162(4)	2
O2	O	0.5259(2)	0.7024(2)	0.3536(3)	6
O3	O	0.7840(2)	0.9002(2)	0.7760(3)	6

2.3. Modulation functions

The modulation of any atomic quantity **A** for any atom with respect to its average value is in general given by a periodic modulation function (of period 1) $\mathbf{A}_\mu(x_4)$ along a single variable x_4, such that the value of the quantity **A** of atom μ in the primitive unit cell **L** is given by the value of the modulation function $\mathbf{A}_\mu(x_4)$ for $x_4 = \mathbf{k}\cdot(\mathbf{L} + \mathbf{r}_\mu)$, where $\mathbf{r}_\mu$ is the position of atom μ within the primitive unit cell. The modulation functions may be anharmonic, and they are parameterized as Fourier series in terms of cosine and sine functions. Thus, for any component *i* of **A**, the modulation function is defined by the real amplitudes $A_{\mu i\cos n}$ and $A_{\mu i\sin n}$ describing the modulation function in the form

$$A_{\mu i}\left(x_4\right) = \sum_n A_{\mu i\cos n}\cos\left(2\pi n x_4\right) + A_{\mu i\sin n}\sin\left(2\pi n x_4\right) \qquad \text{(F.3)}$$

In the case of structural modulations, a Fourier series may be ill-suited to describing the complex anharmonic modulations that are often present in aperiodic crystals, and quite a number of alternative basis functions are used for the parameterization of the modulation functions (Petříček *et al.*, 2014, 2016). In the case of magnetic modulations, however, the Fourier decomposition of equation (F.3) reduces in most cases to a first harmonic, or is limited to a few terms. In our example, a single harmonic is present in the spin modulation, and its Fourier cosine and sine amplitudes for the single symmetry-independent Fe atom are reproduced in Table 3.

Table 3
Amplitudes of the cosine and sine functions describing the spin modulation function of the only symmetry-independent magnetic atom in the incommensurate magnetic structure of $Ba_3NbFe_3Si_2O_{14}$ (#1.1.17; Marty *et al.*, 2008).

MSSG *P*3211′(00γ)000*s* (see Table 1). **k** = (0, 0, 0.143). Magnetic moment components along the crystallographic axes are given in Bohr magnetons.

	Magnetic moment Fourier Cos coeffs						**Magnetic moment Fourier Sin coeffs**					
Atom	**Symmetry constraints**			**Numerical values**			**Symmetry constraints**			**Numerical values**		
	x	***y***	***z***	***x***	***y***	***z***	***x***	***y***	***z***	***x***	***y***	***z***
Fe1	M_{xcos1}	0	0	4	0.0	0.0	M_{xsin1}	$2M_{xsin1}$	M_{zsin1}	-2.31	-4.62	0.0

For instance, one can see in Table 3 for our example that the cosine amplitudes of the Fe1 spin modulation are forced to be zero except for the *x* component, while the sine amplitudes for the *x* and *y* components are forced to have a 1:2 ratio and a *z* component is also allowed. This means that the amplitude of the sine modulation of the spin of the Fe atom at the position (*x*, 0, 1/2) is on a plane perpendicular to the **a** direction, while the spin cosine modulation is along **a**. In other words, the spin modulation is forced by symmetry to follow a mixed screw/cycloid modulation, the plane of the elliptical spin rotation being in general oblique to the propagation vector along **c**, with its plane director of type (*u*, 2*u*, *v*). One can then see in Table 3 that the model reported by Marty *et al.* (2008) has additional restrictions not forced by symmetry: it is a circular screw modulation, with the plane of the spin rotation perpendicular to the **c** direction and a spin modulus of approximately 4 μ_B. This means that the amplitude of $M_{z\sin1}$ is zero, and the nonzero values of $M_{x\sin1}$ and $M_{y\sin1}$ are correlated with the value of $M_{x\cos1}$ to produce a sine component along (1, 2, 0) with the same amplitude of 4 μ_B. (Note that our parameterization has forced the inclusion of non-significant digits for these amplitudes $M_{x\sin1}$ and $M_{y\sin1}$). The symmetry constraints reproduced in Table 3 show that the value of $M_{x\sin1}$ is, however, independent of $M_{x\cos1}$, and a nonzero value of $M_{z\sin1}$ for Fe1 is also allowed, as these additional variables do not break the superspace symmetry. Thus, the number of free parameters in the most general model of the spin modulation under this symmetry is three instead of one. Not only can the plane of rotation of the spins be oblique with respect to the propagation direction, but the rotation can also be elliptical, instead of circular. To our knowledge this more general model has never been tested, but an alternative model for the same phase has been proposed by Scagnoli *et al.* (2013). This second model indeed includes a nonzero M_z modulation. Unfortunately, some quantitative details in the description of the spin modulations seem to be missing and we have been unable to interpret the model fully and transform it to an unambiguous

description within the superspace formalism. It seems, however, that the modulated spin structure proposed by Scagnoli *et al.* (2013) is not a mere improvement of the one reported by Marty *et al.* (2008), corresponding to nonzero values for the additional free variables mentioned above. The spin modulations of the structure reported by Scagnoli *et al.* (2013) do not seem to keep a constant rotation plane. Hence, its superspace symmetry must be different from that of the model proposed by Marty *et al.* (2008), and the two models are therefore in contradiction. This is a clear example where the systematic use of magnetic superspace symmetry becomes a fundamental tool in *MAGNDATA* to classify and compare different models for incommensurate magnetic structures.

2.4. Symmetry relations between modulation functions

The Fe1 site in the average structure has a multiplicity of 3, *i.e.* there are two other Fe sites within the unit cell with spin modulations that are symmetry related to that of Fe1 defined in Table 3. Optionally, *MAGNDATA* can explicitly show these symmetry-related modulations in the same format. The general equation relating the spin modulation functions of two atoms ν and μ, through an MSSG operation {**R** | **t**, t_4}, such that {**R** | **t**}$\mathbf{r}_\nu = \mathbf{r}_\mu$ (modulo an average lattice translation), is (see Perez-Mato *et al.*, 2012)

$$\mathbf{M}_\mu\left(R_I x_4 + t_4 + \mathbf{H}_{\boldsymbol{R}}\cdot\mathbf{r}_\nu\right) = \pm\det\left(\boldsymbol{R}\right)\boldsymbol{R}\mathbf{M}_\nu\left(x_4\right) \qquad \text{(F.4)}$$

where the parameters in equation (F.4) have been defined above in the context of equations (F.1) and (F.2). The ± sign depends on the operation being either {**R** | **t**, t_4} or {**R**′ | **t**, t_4}. It is important to remark that the parameterization chosen in the superspace formalism, with the correspondence between the continuous coordinate x_4 and the factor $\mathbf{k}\cdot(\mathbf{L} + \mathbf{r}_\mu)$ when particularized for a specific atom, makes the symmetry relation defined by equation (F.4) independent of the choice made for atoms μ and ν among those equivalent by lattice translations of the average structure. This avoids a frequent source of confusion and ambiguity in the traditional description using the factor **k**·**L**. Table 4 shows the three average sites forming the orbit derived from the Fe1 site in the asymmetric unit and their corresponding modulation functions, as given in *MAGNDATA*. The table explicitly shows the relation of the modulation parameters of the two additional atoms with those of Fe1, as derived from the general equation (F.4). This relation forces a 120° pattern of their spins on each plane along **c**. It is important to remark that the so-called triangular chirality (Marty *et al.*, 2008) of the spin helical modulations is dictated by the MSSG, with the relation of the spin helicities of the three modulations being unique. The MSSG is chiral (as it is the space group of the paramagnetic phase) and the enantiomeric form, which is described under the same MSSG, will have opposite chirality for both the atomic positions and the spin modulations. The helicities of all spin modulations in the enantiomeric form will be opposite but maintain their relative signs, as dictated by the MSSG. The triangular chirality defined by Marty *et al.* (2008) is therefore the same for both enantiomeric forms.

The symmetry constraints of the Fe1 spin modulation discussed in §F.2.3 also come from the general condition expressed by equation (F.4) for the operations that keep the Fe1 site invariant. The average position of this site is invariant for the operation

$\{2_{100} \mid 0, 0, 0, 0\}$ (see Table 1), and equation (F.4) particularized for this symmetry operation yields the constraints of the Fe1 moment modulation that reduce the possible free parameters of the spin modulation from six to three.

Table 4
The set of atoms in the unit cell related by symmetry to the chosen independent magnetic atom Fe1 of $Ba_3NbFe_3Si_2O_{14}$, listed in Table 2 (#1.1.17), and the symmetry-related amplitudes of the cosine and sine functions describing their spin modulation functions, according to the MSSG *P*3211'(00γ)000*s*, defined in Table 1.

Magnetic moments are given in Bohr magnetons.

Atom	***x***	***y***	***z***
1	0.24964	0.00000	0.50000
2	0.00000	0.24964	0.50000
3	0.75036	0.75036	0.50000

	Magnetic moment Fourier Cos coeffs						**Magnetic moment Fourier Sin coeffs**					
Atom	**Symmetry constraints**			**Numerical values**			**Symmetry constraints**			**Numerical values**		
	x	***y***	***z***	***x***	***y***	***z***	***x***	***y***	***z***	***x***	***y***	***z***
1	M_{xcos1}	0	0	4.0	0.0	0.0	M_{xsin1}	$2M_{xsin1}$	M_{zsin1}	-2.31	-4.62	0.0
2	0	M_{xcos1}	0	0.0	4.0	0.0	$-2M_{xsin1}$	$-M_{xsin1}$	M_{zsin1}	4.62	2.31	0.0
3	$-M_{xcos1}$	$-M_{xcos1}$	0	-4.0	-4.0	0.0	M_{xsin1}	$-M_{xsin1}$	M_{zsin1}	-2.31	2.31	0.0

The parameterization within the superspace formalism expressed by equation (F.3) essentially coincides with the traditional so-called **k**-vector description, employed for instance in the *FullProf* suite (Rodríguez-Carvajal, 1993) for incommensurate magnetic structures. The differences can be considered minor, namely the use of $\mathbf{k}\cdot(\mathbf{L} + \mathbf{r}_\mu)$ instead of $\mathbf{k}\cdot\mathbf{L}$ as the variable of the Fourier wavefunction, and the use of cosine and sine functions instead of expressing the Fourier series as complex exponentials. It is, however, the introduction of symmetry relations between the modulation functions, as given by equation (F.4) for each symmetry operation of the MSSG, and the resulting constraints for the modulations of atoms at special positions that make the major difference from traditional parameterization. For the sake of future reference, as the parameterization employed in *FullProf* is one of the most commonly used, we include in Appendix F.A a transcription of the symmetry relations resulting from an MSSG operation and described by equation (F.4) into the parameterization employed by Basireps in *FullProf*.

2.5. Assignment of the MSSG

Computer tools for the efficient application of magnetic superspace symmetry have only been made available very recently (Petříček *et al.*, 2010, 2014). Hence, the use of magnetic superspace symmetry is still rare and incommensurate magnetic structures are usually reported without controlling the possible symmetry of the model, or exploring the constraints consistent with different possible alternative MSSGs. Following the traditional representation method (Bertaut, 1968; Izyumov *et al.*, 1991), the structures are often described using basis spin functions associated with a single irreducible representation (irrep) of the parent space group, but in many cases several

MSSGs are possible for a single active irrep (Perez-Mato *et al.*, 2012, 2015), and therefore the symmetry assignment becomes ambiguous if the proposed model for the spin modulations is not reported in full detail. In principle, any reported incommensurate structure can be transformed into a symmetry-based description under an MSSG, if the average structure and atomic modulations are given without ambiguity. In the worst situation, it may happen that all modulation functions are symmetry independent, and the resulting MSSG is then limited to the minimum possible superspace symmetry with its point group reduced to 1 or 11′. However, in many cases it is very difficult to extract a detailed account of all spin atomic modulations. In particular, the relative phase shifts between the spin modulations of different atoms are often absent or ambiguous in the published reports, making strenuous or even impossible the transformation of the published models into the symmetry-based unified description of this database. This has made it particularly difficult to include incommensurate structures in this collection compared with commensurate ones.

As in the commensurate case, instead of identifying the relevant MSSG with a bottom-up process, we have in most cases followed a reverse methodology, exploring the possible MSSGs for the known propagation vector and identifying the one relevant for the reported structure. For this purpose, we have used either the representation analysis tool available in *JANA* (Petříček *et al.*, 2014), which determines the possible MSSGs that can result from the action of a single irrep, or *ISODISTORT* (Campbell *et al.*, 2006), which can also determine the possible MSSGs for the cases where several irreps are active. Both programs can provide a magCIF file for each of the models corresponding to these possible alternative symmetries, and they can then be compared with the published structure. Similarly to the commensurate case (Gallego *et al.*, 2016), the relevant MSSG could be easily identified in this way in most cases, except for the above-mentioned structures where the information provided in the publication is insufficient or ambiguous. Once the MSSG was identified, the process was completed by transforming the structure and modulation parameters of the original publication to the parameterization employed in the description under this MSSG. The final model, with these transformed parameters and any convenient complementary information, was then added to a magCIF file and introduced into the database.

In most cases, a label for the MSSG is included. This is given by extending the labelling rules used for non-magnetic superspace groups, and in general it does not uniquely determine the operations of the group. An MSSG label in general has the form [SG](k_1, k_2, k_3)*ab*…, where [SG] is the standard label of the MSG of the average structure, (k_1, k_2, k_3) is a generic expression of the most general form allowed by the MSSG for the incommensurate propagation vector, and *a*, *b*,… are an ordered set of zeros and/or letters that define the value of t_4 that the MSSG associates with each symmetry operation represented in the label [SG], following the same order. The zeros in this set of symbols are assigned not only to the operations with $t_4 = 0$, but also to those for which $R_I = -1$, as for them the value of t_4 is not intrinsic and depends on the origin chosen along x_4. Thus, the MSSG of our example in Table 1 is *P*3211′(00γ)000*s*, indicating that the average structure has the grey MSG *P*3211′, *i.e.* it is non-magnetic, the average magnetic moments being zero. The `000*s*' at the end shows that the

threefold rotation 3^+ has $t_4 = 0$, while the symbol *s* associated with 1′ indicates that time reversal is maintained combined with a 1/2 translation along x_4, *i.e.* the operation {1′ | 0, 0, 0, 1/2} belongs to the MSSG. For other fractional values of t_4, different letters are used following the same convention as in non-magnetic superspace groups (Janssen *et al.*, 2006).

The presence in the incommensurate propagation vector of some commensurate simple components like 1/2 can introduce into the symmetry relations described by equation (F.4) nonzero values for the vectors $\mathbf{H}_R$. This makes the symmetry relations rather complex, with the phase shifts between modulations depending explicitly on the specific value of the atomic positions. This complication can be avoided by using a supercell for the basic structure, where the commensurate part of the propagation vector becomes a reciprocal lattice vector, and the effect of this part of the propagation vector is instead introduced by a centring of the supercell in the (3 + 1) superspace. Thus, for instance, an incommensurate propagation vector (1/2, 0, γ) on a structure with a basic primitive unit cell (*a*, *b*, *c*) can be replaced by (0, 0, γ), if the basic unit cell is chosen to be 2*a*, *b*, *c* and a centring {1 | 1/2, 0, 0, 1/2} is included instead in the MSSG, which equally ensures that the modulations in two consecutive original basic unit cells along **a** have their phases shifted by π (or 1/2 for x_4). If the MSSG includes this kind of centring involving internal space, the [SG] label of the basic space group has an initial letter *X*, instead of the usual letters employed in ordinary space groups for indicating the centring type (Janssen *et al.*, 2006).

It is important to stress that, in contrast with the non-magnetic superspace groups, there is no listing of all possible MSSGs. Therefore, there is no setting of the MSSGs that can be taken as standard. The list of the symmetry operations of the MSSG compulsorily included in a magCIF file is therefore more fundamental than in the commensurate case, in order to define the magnetic symmetry of the structure unambiguously.

In most cases, we keep as the average unit cell that of the original publication, except for cases where we have avoided the presence of commensurate components in the propagation vector through a multiplication of the reference average unit cell accompanied by appropriate centring operations, as explained above.

2.6. Ubiquity of the symmetry operation {1′ | 0, 0, 0, 1/2}

All single-*k* incommensurate structures necessarily have the symmetry operation {1′ | 0, 0, 0, 1/2} within their MSSG (Perez-Mato *et al.*, 2012). This is reflected in the MSSG label by the presence of a grey magnetic space group label in the first part and an *s* at the end of the label. This superspace symmetry operation is due to the fact that any single harmonic modulation in any system remains invariant if the action of time reversal is followed by a global phase shift π (or 1/2 in x_4 units) of the modulation. The presence of this invariance as a symmetry property of the whole phase implies the well known restriction of single-*k* anharmonic incommensurate magnetic structures, such that any anharmonicity of the magnetic modulation within the same thermodynamic phase can only be developed through odd harmonics. See, for instance, the case of HoMgPb (*MAGNDATA* reference #1.1.32; Lemoine *et al.*, 2012), where the third and fifth harmonics have been refined. The additional presence of a **k** = 0 component or

even harmonics in the magnetic modulation breaks the symmetry operation {1′ | 0, 0, 0, 1/2}, and this can only be explained by the independent action of two propagation vectors, with the magnetic phase thus being a 2*k* phase, although its symmetry is still described by a (3 + 1)-dimensional MSSG. This is, for instance, the case of the modulated structure reported for $DyMn_6Ge_6$ (#1.1.10; Rodriguez-Carvajal & Bouree, 2012) where, apart from the incommensurate propagation vector, a **k** = 0 magnetic component has been observed and the MSSG of the structure can be labelled as *P*62′2′(00γ)*h*00 (the letter *h* means that t_4 = 1/6 for the sixfold rotation). This is the only entry where the MSSG does not include the operation {1′ | 0, 0, 0, 1/2}.

2.7. Structural modulations

As in the commensurate case, the non-magnetic degrees of freedom are also subject to the magnetic symmetry group of the phase. The use of the MSSG in the parameterization of the structure makes explicit all non-magnetic degrees of freedom released by the magnetic ordering, which may be significant if the magnetoelastic coupling is strong enough. Thus, if the MSG of the average structure is lower than the parent grey group, new free parameters are present in the listing of its asymmetric unit. The MSSG in general will also allow structural modulations, which are subject to symmetry correlations analogous to those of equation (F.4), except for the fact that the inclusion of time reversal in the operation is irrelevant. Thus, the atomic displacive modulations (if present) of two symmetry-related atoms ν and μ must be related according to the equation

$$\mathbf{u}_\mu\left(R_I x_4 + t_4 + \mathbf{H}_{\boldsymbol{R}}\cdot\mathbf{r}_\nu\right) = \boldsymbol{R}\mathbf{u}_\nu\left(x_4\right) \tag{F.5}$$

while for the modulation of a scalar quantity, such as the occupancy probability or the atomic charge of the sites, the following relation is required:

$$\rho_\mu\left(R_I x_4 + t_4 + \mathbf{H}_{\boldsymbol{R}}\cdot\mathbf{r}_\nu\right) = \rho_\nu\left(x_4\right) \tag{F.6}$$

These equations, particularized for the operation {1′ | 0, 0, 0, 1/2}, imply the restriction of the structural modulations to even harmonics (Perez-Mato *et al.*, 2012). This constraint of magnetoelastic effects is often observed in single-*k* incommensurate magnetic structures, and its universal validity for this kind of structure becomes apparent if superspace symmetry is considered.

Even-order diffraction satellites showing the presence of magnetically induced structural modulations are often observed, but their weakness has hampered any quantitative analysis. Equations (F.5) and (F.6), however, imply that strong specific correlations between magnetic modulation and induced structural modulations should be expected, and this can help to approach the problem of its characterization.

The symmetry-dictated division between odd magnetic and even structural Fourier terms in the modulations can also happen in incommensurate magnetic structures where the paramagnetic phase is an incommensurate structure with an intrinsic structural modulation. This is the case for CeRuSn (#1.1.35; Prokes *et al.*, 2014), where the paramagnetic phase is a monoclinic incommensurate structure with propagation vector **k** = (0, 0, 0.35) and the magnetic propagation vector is **k**/2. The resulting

magnetic phase has structural and magnetic modulations complying with an MSSG for the propagation vector **k**/2, which also describes the constraints of the intrinsic structural modulation that has only even Fourier terms.

2.8. Visualization and analysis

The output page for each structure includes an image obtained using *Jmol* (Hanson, 2013) with only the magnetic atoms. A link to an online three-dimensional viewer (Perez-Mato *et al.*, 2015) that uses *JSmol*, the JavaScript version of *Jmol*, is also available (see Fig. 3). This online tool makes directly accessible the simplest and most important commands of *Jmol* through specific buttons, while the innumerable commands available to manipulate and analyse the graphical representation can be applied through a command window or a pop-up console. The visualization options include the possibility of shifting the global modulation phase both statically or dynamically (*phase shift* and *phase sliding* buttons) in order to have access to all the configurations realized along the modulation. The latest version of *Jmol* fully supports MSSGs and accepts magCIF files as input files. Therefore, the database entries can also be visualized and analysed locally using *Jmol*, provided that the user has previously downloaded this free open-source Java program.

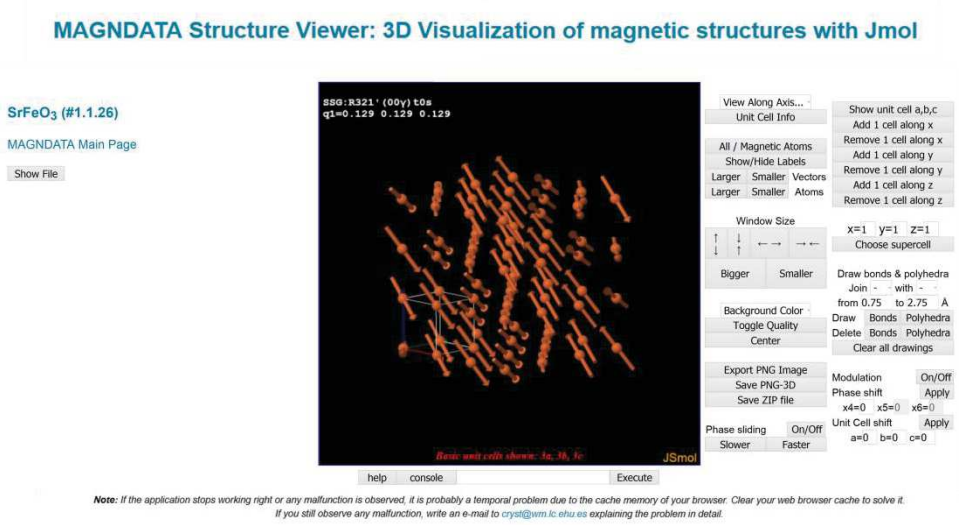

Figure 3
A screenshot of the online visualization of the incommensurate magnetic structure $SrFeO_3$ (#1.1.26; Reehuis *et al.*, 2012).

3. Additional information

Apart from the minimal information necessary to build up the magnetic structure in three-dimensional space, *MAGNDATA* provides additional important data for each entry. This information is also included in the corresponding magCIF file that can be downloaded (local tags beyond the official magCIF dictionary are used for some of the items). We list and discuss here the most important items.

3.1. Magnetic point group

The magnetic point group associated with an incommensurate magnetic structure can be derived in a straightforward manner from the knowledge of its MSSG, simply by taking the rotation or roto-inversion operations, combined (or not) with time reversal, which are present in the group. This information is very important, as the magnetic point group governs the macroscopic crystal tensor properties. As in the commensurate case, a direct link to *MTENSOR*, another program on the Bilbao Crystallographic Server, then allows the user to explore, for this specific point group and the setting used for the structure, the symmetry constraints that should be present in the macroscopic tensorial magnetic, structural or magneto-structural properties.

3.2. Parent space group, and the relationship between the basic unit cell and the unit cell of the parent phase

Although a magnetic structure is in principle fully defined by the data discussed in the previous section, as in the commensurate case (Gallego *et al.*, 2016), the knowledge of the symmetry of its parent paramagnetic structure is fundamental to characterize the possible domains and the switching properties of the material. Therefore, this parent space group is given as additional information. Information about the relationship between the basis used for this reference parent phase and the basic unit cell employed is also included. This is given under the heading `Transformation from parent structure'.

If the point group of the MSSG is a strict subgroup of the point group of the parent phase, structural ferroic properties are to be expected in the incommensurate magnetic phase. Thus, for instance, in the example of $Ba_3NbFe_3Si_2O_{14}$ (#1.1.17; Marty *et al.*, 2008) the parent space group is *P*321, *i.e.* its magnetic point group is 321', which is also the point group of the MSSG. Therefore, there is no point-group symmetry break and no distinct domains are expected, except those produced by the loss of coherence in the modulation (in 1*k* incommensurate structures, the usual trivial domains related by time reversal with opposite spins are just the same structure with its free global modulation phase shifted by π, or by 1/2 in x_4 units).

On the other hand, if we take the case of $MnSb_2O_6$ (#1.1.38; Johnson *et al.*, 2013), the point-group symmetry break with respect to the parent phase is 321' → 21', and domains related by the lost threefold rotation are to be expected. Note that in *MAGNDATA* we use in general for the average structure a unit-cell basis as close as possible to that of the parent space group. Thus, in this example the parent cell is maintained, and the `Transformation from parent structure' is the identity transformation, although the monoclinic axis of the MSSG is along (1, 0, 0) of the parent trigonal lattice. In this example, knowledge of the symmetry break from a non-polar to a polar point-group symmetry is sufficient to expect this material to behave as a type II multiferroic, with a magnetically induced electric polarization along the monoclinic axis of the MSSG.

The spins in $MnSb_2O_6$ follow cycloids along the **c** direction (see Fig. 4), which is a typical geometry that introduces polarity at a local level (Perez-Mato *et al.*, 2015) and which has been identified in quite a number of incommensurate multiferroics (Tokura *et al.*, 2014). However, it is important to stress that the presence of spin cycloids is not

sufficient for a polar symmetry. The symmetry of magnetic structures is a global property and there are other structures with spin cycloids, such as Cs_2CuCl_4 (#1.1.1; Coldea *et al.*, 1996), which are centrosymmetric and therefore non-polar. In this second case, the spin cycloids are related through the MSSG symmetry operations, such that the space inversion is maintained with symmetry-related cycloids of opposite chirality. In fact, in this second example, compared with the parent symmetry, one can see that the magnetic ordering does not break at all the point-group symmetry of the system (see Fig. 4).

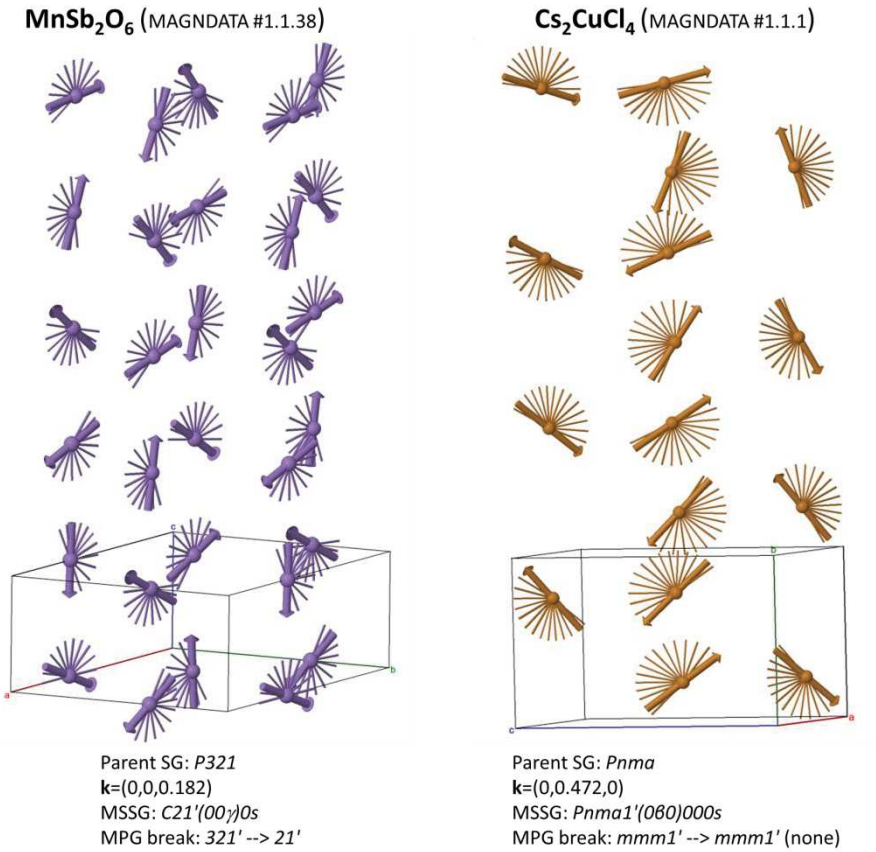

Figure 4
The spin arrangements in the magnetic structures of $MnSb_2O_6$ (#1.1.38; Johnson *et al.*, 2013) and Cs_2CuCl_4 (#1.1.1; Coldea *et al.*, 1996), as given by the online *Jmol* visualization tool of *MAGNDATA*, with an indication of their symmetry properties. Both structures exhibit spin cycloids. In the first case these produce a symmetry break into a polar symmetry, while in the second case the centrosymmetric parent point-group symmetry is maintained, through the MSSG symmetry relations between cycloids of opposite chirality. A partial trail of the spin value for a shift in the free global phase of the modulation is depicted, to show the rotation plane and chirality of each cycloid.

3.3. Representation analysis

In accordance with the Landau theory of phase transitions, the magnetic ordering in most of the magnetic phases of this collection has an order parameter transforming according to a single irrep of the parent symmetry group (odd for time reversal, when considered as a representation of the magnetic parent grey group). In fact, as mentioned above, in most cases the original structure determination was done

following the traditional representation method, where the possible spin waves are restricted to a single irrep and, if necessary, the process is extended to include additional ones.

The information on the activity of one or more irreps in the spin ordering and its relation to the MSSG of the structure that is being used in the database can be found in the comments included for each entry and/or in a table with the heading `Active irreps'. The irrep labels are those employed in *ISODISTORT*, which have also been adopted by *JANA* and by other programs on the Bilbao Crystallographic Server.

Finally, similar to the commensurate structures, each entry also includes information (if available) on the transition and experimental temperatures, references for the positional structure, and some complementary comments; see Gallego *et al.* (2016) for more details. In particular, it should also be stressed here that many incommensurate magnetic structures have been reported without providing a detailed account of the average structure that has been assumed as the reference for the modulation. In such cases, an average structure has been taken from other sources, and the corresponding reference has been included.

4. Magnetic superspace symmetry *versus* irrep descriptions

As mentioned above, in order to transform each structure to the symmetry-based unified description of this collection, its MSSG has been identified, if not given in the original reference, by exploring the possible MSSGs that can be realized if the magnetic arrangement complies with one or more irreps of the parent grey group. The MSSG that corresponds to the correlations between the spin modulations introduced in the model has then been detected.

The relation of the MSSG description to that using irreps has been discussed in detail by Perez-Mato *et al.* (2012, 2015). The database includes examples of the two different situations that can happen if a single irrep is active, given below.

(i) *A one-to-one correspondence exists between the irrep and the MSSG.* In this case, adapting the spin wave to fulfil the transformation conditions of a single irrep spin mode for the active irrep is in principle fully equivalent to the introduction of the symmetry constraints of the corresponding MSSG. However, this does *not* mean in general that the traditional form in which the representation method is being used introduces into the reported model equivalent restrictions to those of the corresponding MSSG. The reason for the difference between the two approaches in these simple cases is that the irrep-dictated transformation properties of the spin waves with respect to the operations that transform **k** into −**k** are usually disregarded. The irrep decomposition of the magnetic configuration space is usually done considering the so-called small irreps associated with the small space group $G_{\mathbf{k}}$, formed by the operations of the parent group that keep the propagation vector **k** invariant. However, the operations of the parent group that invert **k** imply in general additional restrictions on the possible form of a spin wave transforming according to a specific irrep. For instance, atomic sites related by these operations do not necessarily split [see equations (F.18*a*) and (F.18*b*) in Appendix F.A]. This problem was already pointed

out within the framework of the Landau theory of some incommensurate magnetic phases (Harris *et al.*, 2008; Harris, 2007), and its relevance for a proper comparison of the superspace symmetry formalism with the representation method was discussed by Perez-Mato *et al.* (2012, 2015). In general, the MSSG symmetry properties of a single-*k* spin modulation transforming according to a single irrep are defined for all operations of what we call the extended small group $G_{\mathbf{k},-\mathbf{k}}$, which includes both the operations that maintain or invert the propagation vector.

As an example, let us consider the case of $NaFeSi_2O_6$ (#1.1.36; Baum *et al.*, 2015), which has parent space group *C*2/*c* and propagation vector (0, 0.78, 0). This propagation vector is along the Brillouin zone (BZ) line LD, with its small space group reduced to *C*2, and two possible irreps depending on the one-dimensional small irrep being even or odd for the binary rotation. The inversion and the mirror plane transform **k** into −**k**, and therefore the two possible magnetic (full) irreps are two-dimensional, namely mLD1 and mLD2 in the notation of *ISODISTORT* (Campbell *et al.*, 2006). It is a general property that incommensurate spin modulations with the transformation properties of an irrep that is two-dimensional when restricted to the (**k**, −**k**) subspace have superspace symmetry properties described by a single MSSG. In these cases there is a one-to-one correspondence between the irrep and this MSSG (Perez-Mato *et al.*, 2012). This is illustrated graphically in Fig. 5 for our example. Each possible irrep results in one single MSSG, and the corresponding symmetry relations and constraints on the spin waves can be derived from the general relation of equation (F.4).

The only symmetry-independent magnetic atom, Fe1(1), in the parent phase of $NaFeSi_2O_6$ is at Wyckoff position 4*e* (0, *y*, 1/4). It is therefore invariant for the symmetry operation $\{2_{010} \mid 0, 0, 1/2\}$. This symmetry operation is conserved either as $\{2_{010} \mid 0, 0, 1/2, 0\}$ in the MSSG corresponding to mLD1 or as $\{2_{010} \mid 0, 0, 1/2, 1/2\}$ in the MSSG of mLD2. In the first case, equation (F.4) forces the modulation to be longitudinal with the spin constrained along the **b** direction, the first harmonic amplitudes being reduced to the two parameters $M_{y\cos 1}$ and $M_{y\sin 1}$. In the second case, *i.e.* the irrep mLD2, the operation $\{2_{010} \mid 0, 0, 1/2, 1/2\}$ forces a transverse modulation, with four free parameters ($M_{x\cos 1}$, 0, $M_{z\cos 1}$) and ($M_{x\sin 1}$, 0, $M_{z\sin 1}$). Both MSSGs include the inversion operation which, for a convenient choice of origin along the internal space x_4, can be expressed without any shift along x_4 as $\{-1 \mid 0, 0, 0, 0\}$. Equation (F.4) particularized for the inversion implies that the modulation amplitudes of Fe1(2) (see Fig. 5) are related to those of Fe1(1), in the form $M_{\alpha\cos 1}$[Fe1(2)] = $M_{\alpha\cos 1}$[Fe1(1)] and $M_{\alpha\sin 1}$[Fe1(2)] = −$M_{\alpha\sin 1}$[Fe1(1)] for α = *x*, *y*, *z*, for any of the two irreps/MSSGs. Therefore, the magnetic modulation does not split the Fe sites, and both MSSGs keep a single symmetry-independent site, with two and four free parameters for mLD1 and mLD2, respectively, to describe the Fe spin modulations. For comparison, the traditional representation approach yields four and eight parameters for the spin basis functions, respectively, which by fixing the global arbitrary phase of the incomensurate modulation reduce to three and seven.

It should be remarked that, in the MSSG description, the arbitrary global phase of the modulation is fixed by the setting used for the MSSG, if it contains operations transforming **k** into −**k**. The origin along x_4 is fixed by the choice of the t_4 values of

these operations. The structure of $NaFeSi_2O_6$ reported by Baum *et al.* (2015) corresponds to the MSSG *C*2/*c*1′(0β0)*s*0*s* (irrep mLD2), but the model reported by Baum *et al.* (2015) includes additional constraints, as the spin arrangement is collinear and the number of refined parameters has been limited to three. Note however that the irrep, or equivalently the MSSG, allows more complex arrangements, including transverse helical ellipsoidal modulations.

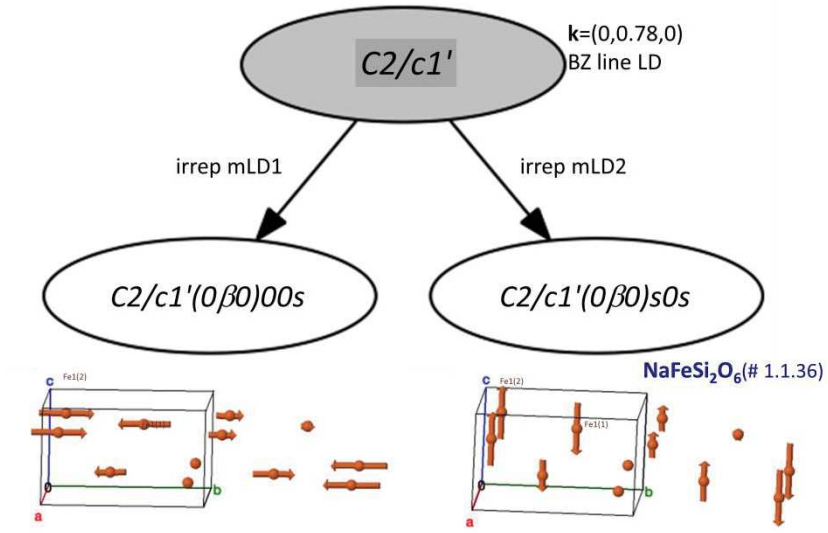

Figure 5
Possible MSSGs for an incommensurate magnetic structure with parent space group *C*2/*c* and propagation vector (0, 0.78, 0) (line LD of the BZ), resulting from the condensation of a spin wave transforming according to one of the two possible irreps. The two possible groups, one for each irrep, are depicted as maximal subgroups of the parent grey group. A partial view of the Fe spin modulation reported for $NaFeSi_2O_6$ (#1.1.36; Baum *et al.*, 2015) is represented below its MSSG, compared with the alternative model corresponding to the other irrep or MSSG. In both cases, the spin modulations of the atoms Fe1(1) and Fe1(2), which are symmetry related by the space inversion in the parent phase, keep a symmetry relation through the MSSG. While the mLD1 longitudinal wave has two free parameters to fit, the transverse mLD2 wave has four free parameters, and its collinearity is not symmetry protected. Transverse helical modulations or more complex phase relations are possible within the same irrep/MSSG.

In contrast with the commensurate case, an incommensurate spin arrangement transforming according to a single irrep, and having the MSSG symmetry associated with this irrep, can imply phase relations between the modulations of atoms that are symmetry independent in the parent space group (Perez-Mato *et al.*, 2012). This may sound paradoxical, but it is a special property of incommensurate structures and the symmetry associated with the phase shift of their modulation. In order that two incommensurate basis functions associated with symmetry-independent atoms correspond to a single spin mode transforming according to a single irrep, their relative phases should be correlated. Unfortunately, this single irrep condition, which is part of the constraints of the associated MSSG, is often not considered. This is a recurrent problem encountered when translating reported incommensurate structures into the superspace formalism. For example, the compound $CaFe_4As_3$ (#1.1.5; Manuel *et al.*, 2010) has four independent Fe sites of type 4*c* (*x*, 1/4, *z*) in the parent space group *Pnma* and was reported to have centrosymmetric properties in the incommensurate

phase. The irrep mY1 with **k** = (0, 0.375, 0) associated with its spin arrangement constrains the spin modulations to be longitudinal, but the transformation properties of this irrep by the inversion operation also force the modulations for the four independent Fe atoms to be in phase (Perez-Mato *et al.*, 2012). The modulation phases of the different sites were refined, however (Manuel *et al.*, 2010), and reached relative values close to zero or π, as expected from the centrosymmetric MSSG associated with a single irrep mode. Accordingly, to keep a centrosymmetric symmetry we had to ignore the small deviations from these values when introducing the structure into the database.

(ii) *Several alternative MSSGs are possible, depending on how the spin basis functions of the irrep are combined*. If the active irrep restricted to the extended small group $G_{\mathbf{k},-\mathbf{k}}$ has a dimension larger than two, more than one MSSG is in general possible, depending on the direction taken by the order parameter within the irrep space. This implies that specific linear combinations of the irrep spin basis modes can yield different MSSGs (so-called irrep epikernels), while an arbitrary combination of the whole set of basis modes reduces the symmetry to the minimum possible MSSG for the irrep (the so-called irrep kernel) (Perez-Mato *et al.*, 2012, 2015). The refined models are usually obtained by introducing *ad hoc* restrictions on the combination of irrep spin basis modes or without using irreps, simply assuming simple models following a trial-and-error approach. In many cases these restrictions make the model comply with one of the several possible MSSGs.

An example is the magnetic structure reported for $SrFeO_3$ (#1.1.26; Reehuis *et al.*, 2012), shown in Fig. 3. Having a paramagnetic cubic phase with space group *Pm*-3*m*, the reported magnetic structure has a propagation vector of type (*u*, *u*, *u*), *i.e.* it lies along the line LD of the Brillouin zone, and the active irrep is mLD3. Fig. 6 shows the group–subgroup hierarchy of all possible MSSGs which can result from the action of a magnetic order parameter transforming according to mLD3. Six different superspace symmetries are in principle possible for the magnetic phase. The magnetic atom sits at the origin, and the irrep decomposition of its magnetic representation for this propagation vector is mLD3(4) + mLD2(2), where the dimensions of the irreps restricted to the extended small group $G_{\mathbf{k},-\mathbf{k}}$ are indicated in parentheses. The subspace of mLD3-type spin configurations is therefore spanned by four independent basis modes. As shown in Fig. 6, if these modes are combined arbitrarily the superspace symmetry is reduced to a minimum triclinic group, while very specific combinations can maintain either the trigonal symmetry or centrosymmetric monoclinic symmetries with the monoclinic axis perpendicular to the propagation vector. The model reported for $SrFeO_3$ corresponds to one of these three maximum symmetries, and a single free parameter is to be refined. The magnetic modulation breaks space inversion and maintains the trigonal symmetry compatible with the propagation vector, but keeps the system non-polar owing to the binary rotations perpendicular to the propagation vector that are also preserved.

As shown in Fig. 6, some of the possible MSSGs resulting from a single active irrep may have degrees of freedom associated with secondary irreps having compatible epi-kernels, which are supergroups of this particular MSSG. For instance, this is the case for the MSSG *C*2/*m*1′(α,0,γ)0*ss*, which implies two free parameters in the spin

modulation, but if restricted to the mLD3 irrep only one parameter is necessary, the second one corresponding to a secondary symmetry-compatible longitudinal spin component transforming according to mLD2.

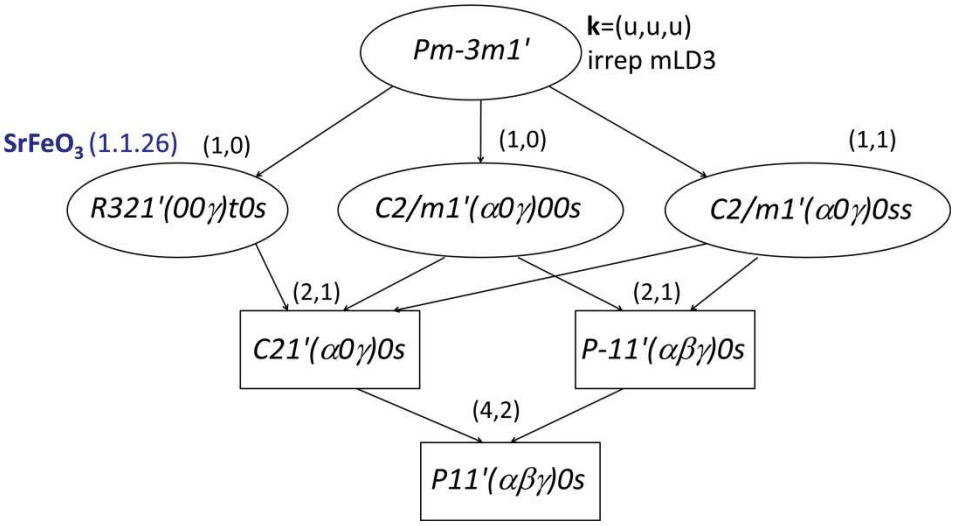

Figure 6
Possible MSSGs for an incommensurate magnetic structure with parent space group *Pm*-3*m* and active irrep mLD3, with its propagation vector on the symmetry line LD (*u*, *u*, *u*) of the BZ. The groups are depicted showing their group–subgroup hierarchy and only one subgroup per conjugacy class is shown. The set of integers (*n*, *m*) above each group indicates the degrees of freedom of the spin wave for a magnetic atom at the origin under each symmetry, separating those associated with the irrep mLD3(*n*) from those with mLD2(*m*), these latter corresponding to possible secondary spin modes if $m \neq 0$. The MSSG of the magnetic phase of $SrFeO_3$ (#1.1.26; Reehuis *et al.*, 2012) is indicated.

The database also contains structures whose spin modulation corresponds to the superposition of two primary irreps, the resulting MSSG being the intersection of the irrep epikernels associated with each irrep. This intersection depends in general on the relative phase shift between the two irrep spin modulations (Perez-Mato *et al.*, 2012), and again various MSSGs are possible even if the two primary irreps separately result in a single possible MSSG. Among these cases, one has to include those with spin modulations corresponding to a single irrep but with arbitrary relative phase shifts between the basis functions, which decrease the resulting MSSG, breaking all operations that transform **k** into −**k**. These structures must be considered the result of the action of two distinct order parameters transforming according to the same irrep. The possibility of reducing the symmetry through the superposition of irrep modes of the same irrep is a peculiarity of incommensurate structures, not present in the commensurate case.

5. Summary of the structures in the collection

Table 5 summarizes the symmetry properties of the incommensurate structures gathered in this collection. The first 13 cases in the list are structures where the magnetic point group does not vary with respect to the paramagnetic phase. No ferroic properties are therefore to be expected. No twinning can exist, not even the

simple case of spin switching. In all these cases a single primary irrep is active and its small irrep is one dimensional, such that there is a one-to-one correspondence between the MSSG and the irrep; once the active irrep has been identified, the identification of the corresponding MSSG is rather straightforward. These structures have usually been refined assuming some simple form for the modulation as helical, cycloidal, sinusoidal *etc*. This kind of modulation usually complies with the MSSG associated with the active irrep, except in cases like that of $CaFe_4As_3$, discussed in the previous section, but they often include additional restrictions that are not forced by the MSSG or by the reduction to a single irrep. For instance, this is the case for $CaCr_2O_4$ (#1.1.15; Damay *et al.*, 2010), where the most general spin modulation under its MSSG is a set of elliptical cycloidal modulations with opposite chiralities by pairs and with the normal to its rotation plane being allowed to be oblique on the plane perpendicular to the propagation vector. However, the cycloids of the reported model lie on the *ac* plane, and it is not mentioned if a more general orientation was explored and checked. A similar situation occurs in the case of $Ba_3NbFe_3Si_2O_{14}$ (Marty *et al.*, 2008), discussed in §F.2.

Table 5
A list of the incommensurate magnetic structures included in *MAGNDATA*, with a summary of their symmetry properties

Compounds having no point-group symmetry break are listed first. The dimension of the small irrep is given with an asterisk in those cases where the refined model includes restrictions that are not symmetry forced and apparently have not been fully assessed. Type II multiferroics are indicated with the suffix (MFII).

Material	Ref†	Parent[a]	prop. vector	MSSG[b]	MPG[c]	Pr.[d]	Sm.[e]
Cs_2CuCl_4 (#1.1.1)	(*a*)	*Pnma* (#62)	(0,0.472,0)	*Pnma1'(0□0)000s*	*mmm1'*	1	1
$CaFe_4As_3$ (#1.1.5)	(*b*)	*Pnma* (#62)	(0,0.475,0)	*Pnma1'(0□0)000s*	*mmm1'*	1	1
$TbMnO_3$ (#1.1.6)	(*c*)	*Pbnm* (#62)	(0,0.27,0)	*Pbnm1'(0,β,0)s00s*	*mmm1'*	1	1*
$MnWO_4$ (#1.1.12)	(*d*)	*P2/c* (#13)	(-0.214,0,0.457)	*X2/c1'(α0γ)0ss*	*2/m1'*	1	1
$CaCr_2O_4$ (#1.1.15)	(*e*)	*Pbnm* (#62)	(0,0,0.477)	*Pbnm1'(00γ)s00s*	*mmm1'*	1	1*
$Ba_3NbFe_3Si_2O_{14}$ (#1.1.17)	(*f*)	*P321* (#150)	(0,0,0.143)	*P3211'(00γ)000s*	*321'*	1	1*
$NdFe_3B_4O_{12}$ (#1.1.18)	(*g*)	*R32* (#155)	(0,0,1.502)	*R321'(00γ)t0s*	*321'*	1	1
UPtGe (#1.1.19)	(*h*)	*Imm2* (#44)	(0.554(1),0,0)	*Imm21'(α00)0s0s*	*mm21'*	1	1
Li_2IrO_3 (#1.1.20)	(*i*)	*Fddd* (#70)	(0.5768(3),0,0)	*Fddd1'(α00)0s0s*	*mmm1'*	1	1
$PrNi_2Si_2$ (#1.1.34)	(*j*)	*I4/mmm* (#139)	(0,0,0.87)	*I4/mmm1'(00γ)00sss*	*I4/mmm1'*	1	1
CeRuSn (#1.1.35)	(*k*)	*C2/m* (#12)	(0,0,0.175)	*C2/m1'(α0γ)0ss*	*2/m1'*	1	1
$NaFeSi_2O_6$ (#1.1.36)	(*l*)	*C2/c* (#15)	(0,0.78,0)	*C2/c1'(0θ0)s0s*	*2/m1'*	1	1*

$Ca_3Co_2O_6$ (#1.1.39)	(*m*)	*R-3c* (#167)	(0,0,1.02)	*R-3c1'(00γ)00s*	*-3m1'*	1	1
Cr (#1.1.4)	(*n*)	*Im-3m* (#229)	(0,0,0.95)	*I4/mmm1'(00γ)00sss*	*I4/mmm1'*	1	1
Ce_2Pd_2Sn (#1.1.9)	(*o*)	*P4/mbm* (#127)	(0.105,0,0)	*Pbam1'(α00)0s0s*	*mmm1'*	1	1
MnGe (#1.1.14)	(*p*)	*$P2_13$* (#198)	(0,0,0.167(4))	*P2121211'(00γ)00ss*	*2221'*	1	1*
$TmCu_2Ge_2$ (#1.1.23)	(*q*)	*I4/mmm* (#139)	(0.117,0.117,0)	*Fmmm1'(α00)0s0s*	*mmm1'*	1	1
CeMgPb (#1.1.27)	(*r*)	*I4/mmm* (#139)	(0.448,1/2,0)	*I112/m1'(αβ0)00s*	*2/m1'*	1	1*
TmMgPb (#1.1.28)	(*r*)	*I4/mmm* (#139)	(0.412,0,0)	*Immm1'(α00)0s0s*	*mmm1'*	1	1
ErMgPb (#1.1.29)	(*r*)	*I4/mmm* (#139)	(0.816,0,0)	*Immm1'(α00)0sss*	*mmm1'*	1	1
$RbFe(MoO_4)_2$ (#1.1.2) (MFII)	(*s*)	*P-3* (#147)	(1/3,1/3,0.458)	*P31'(1/31/3γ)ts*	*31'*	1	2
$MnAu_2$ (#1.1.13)	(*t*)	*I4/mmm* (#139)	(0,0,0.283)	*I4221'(00γ)q00s*	*4221'*	1	2
$CeRhIn_5$ (#1.1.16)	(*u*)	*I4/mmm* (#139)	(1/2,1/2,0.297)	*P4221'(1/2,1/2,γ)q00s*	*4221'*	1	2
$CeAuAl_3$ (#1.1.33)	(*v*)	*I4mm* (#107)	(0,0,0.52)	*I41'(00γ)qs*	*41'*	1	2
FeOCl (#1.1.40)	(*w*)	*Pmmn* (#59)	(0.286,1/2,0)	*X2/n1'(αβ0)00s*	*2/m1'*	1*	2
Cr (#1.1.3)	(*n*)	*Im-3m* (#229)	(0,0,0.95)	*Immm1'(00γ)s00s*	*mmm1'*	1	2
$SrFeO_3$ (#1.1.26)	(*x*)	*Pm-3m* (#221)	(0.129,0.129 ,0.129)	*R321'(00γ)t0s*	*321'*	1	2
$TbMnO_3$ (#1.1.7) (MFII)	(*c*)	*Pbnm* (#62)	(0,0.27,0)	*Pbn211'(0β0)s00s*	*mm21'*	2	1,1
$TbMnO_3$ (#1.1.8) (MFII)	(*c*)	*Pbnm* (#62)	(0,0.27,0)	*Pbn211'(0b0)s00s*	*mm21'*	2	1,1
$MnWO_4$ (#1.1.11) (MFII)	(*d*)	*P2/c* (#13)	(-0.214,0,0.457)	*X21'(α0γ)0s*	*21'*	2	1,1
Li_2IrO_3 (#1.1.21)	(*y*)	*Cccm* (#66)	(0.57(1),0,0)	*C2221'(α00)s00s*	*2221'*	2*	1,1
$Sr_3Fe_2O_7$ (#1.1.22)	(*z*)	*Im-3m* (#229)	(0.1416,0.1416,0)	*X2221'(α,α,0)s00s*	*2221'*	2*	1,1
CrAs (#1.1.24)	(*aa*)	*Pnma* (#62)	(0,0,3562)	*P2121211'(00γ)00ss*	*2221'*	2*	1,1
TbMgPb (#1.1.30)	(*r*)	*I4/mmm* (#139)	(0.843(1),0,0)	*I2/m1'(αβ0)00s*	*2/m1'*	2	1,1
DyMgPb (#1.1.31)	(*r*)	*I4/mmm* (#139)	(0.841(1),0.016(1) ,0)	*I2/m1'(αβ0)00s*	*2/m1'*	2	1,1
HoMgPb (#1.1.32)	(*r*)	*I4/mmm* (#139)	(0.835,0,0)	*I2/m1'(αβ0)00s*	*2/m1'*	2	1,1
$MnSb_2O_6$ (#1.1.38) (MFII)	(*bb*)	*P321* (#150)	(0,0,0.182)	*C21'(00γ)0s*	*21'*	2	1,1
$LiFeAs_2O_7$ (#1.1.25)	(*cc*)	*C2* (#5)	(0.709,0,0.155)	*C11'(αβγ)0s*	*11'*	2(2x1)	1,1

$NaFeSi_2O_6$ (#1.1.37) (MFII)	(*l*)	*C2/c* (#15)	(0,0.78,0)	*C21'(0θ0)ss*	*21'*	2(2x1)	1,1
$DyMn_6Ge_6$ (#1.1.10)	(*o*)	*P6/mmm* (#191)	(0,0,0.1651)	*P62'2'(00γ)h00*	*62'2'*	2	2,1

† References for the magnetic structures: (*a*) Coldea *et al.* (1996), (*b*) Manuel *et al.* (2010), (*c*) Kenzelmann *et al.* (2005), (*d*) Urcelay-Olabarria *et al.* (2013), (*e*) Damay *et al.* (2010), (*f*) Marty *et al.* (2008), (*g*) Janoschek *et al.* (2010), (*h*) Mannix *et al.* (2000), (*i*) Biffin, Johnson, Choi *et al.* (2014), (*j*) Blanco *et al.* (2010), (*k*) Prokes *et al.* (2014), (*l*) Baum *et al.* (2015), (*m*) Agrestini *et al.* (2008), (*n*) Perez-Mato *et al.* (2012), (*o*) Rodriguez-Carvajal & Bouree (2012), (*p*) Makarova *et al.* (2012), (*q*) Penc *et al.* (2012), (*r*) Lemoine *et al.* (2012), (*s*) Kenzelmann *et al.* (2007), (*t*) Herpin & Meriel (1961), (*u*) Bao *et al.* (2000), (*v*) Adroja *et al.* (2015), (*w*) Hwang *et al.* (2000), (*x*) Reehuis *et al.* (2012), (*y*) Biffin, Johnson, Kimchi *et al.* (2014), (*z*) Kim *et al.* (2014), (*aa*) Keller *et al.* (2015), (*bb*) Johnson *et al.* (2013), (*cc*) Rousse *et al.* (2013).

[a] Parent space group

[b] Magnetic superspace group

[c] Magnetic point group

[d] Number of primary irreps

[e] Dimension of small irrep

The remaining structures with a single active primary irrep break the parent point-group symmetry and can be classified into three sets:

(i) Structures where the direction of the propagation vector is the only agent of this symmetry reduction, with the extended small space group $G_{\mathbf{k},-\mathbf{k}}$ being a strict subgoup of the parent space group, while the active small irrep is one dimensional. Also in these cases, there is a one-to-one correspondence between the small irrep and the MSSG, but this latter only keeps the point-group symmetry corresponding to $G_{\mathbf{k},-\mathbf{k}}$, which is lower than that of the parent phase. There are seven cases of this type.

(ii) Structures where the propagation vector does not break the parent symmetry, $G_{\mathbf{k},-\mathbf{k}}$ coinciding with the full parent space group, and the reduction of the point-group symmetry being due to the fact that the active irrep is multidimensional. This is the case for the magnetic structures of $RbFe(MoO_4)_2$ (#1.1.2), $MnAu_2$ (#1.1.13), $CeRhIn_5$ (#1.1.16), $CeAuAl_3$ (#1.1.33) and FeOCl (#1.1.40). Their MSSG is one of the epikernels of maximum symmetry of the active irrep. It is remarkable that the spin modulations in these structures are circular helical modulations and they are symmetry protected (see Fig. 7). This contrasts with other entries in the collection, where the regular spin helical or cycloidal spin arrangement which has been reported is not symmetry dictated and other more complex arrangements are possible for the same irrep and the same MSSG. For instance, this is the case for MnGe (#1.1.14; Makarova *et al.*, 2012), where the Mn atom occupies a general position and therefore its spin modulation has no symmetry restriction, while the refinement was done assuming pure helical modulations.

The case of FeOCl (#1.1.40) within this set is also representative of the problems that have arisen when transforming the published structures into an unambiguous symmetry-based description. According to our interpretation, the figures in the publication show spin cycloids with chiralities that are inconsistent with the corresponding equations in the text. We therefore had to decide which of the two

representations was the correct one, and finally considered the equations to be more reliable.

(iii) Structures where the propagation vector and a multidimensional irrep are both agents of the point-group symmetry break. This is the case for $SrFeO_3$ (#1.1.26), discussed in the previous section, and also for Cr (#1.1.3).

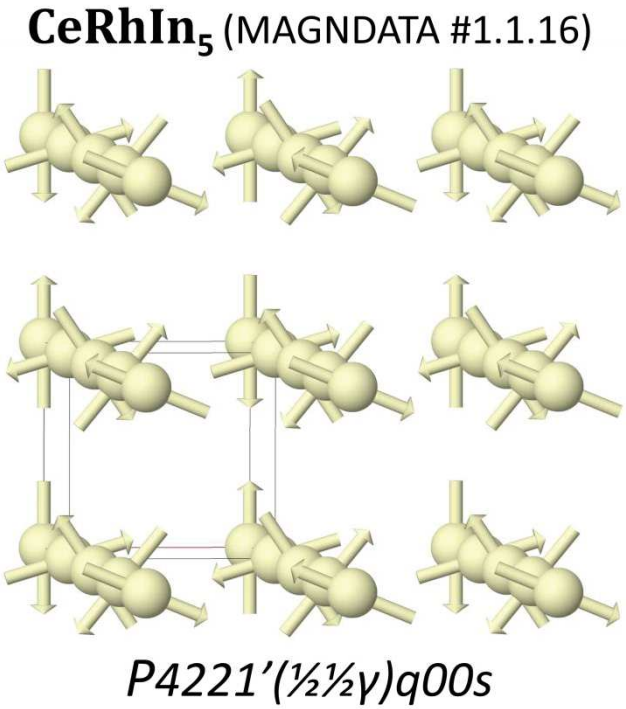

Figure 7
The incommensurate magnetic structure of $CeRhIn_5$ (#1.1.16; Bao *et al.*, 2000), with helical spin modulations that are symmetry dictated by the superspace symmetry of the phase. Only Ce atoms are shown. The label of its MSSG is indicated. The space group of the paramagnetic phase is *P*4/*mmm* and the incommensurate propagation vector is of type (1/2, 1/2, γ). The spin modulation breaks space inversion but maintains a non-polar point-group symmetry. This MSSG is one of seven possible for the magnetic order parameter active in this phase, corresponding to a four-dimensional irrep.

The remaining 13 structures involve the presence of spin modulations according to two irreps. In all cases except one, the two irreps refer to the same propagation vector. The superposition of two irreps implies in general a drastic symmetry reduction. This set includes those structures where the symmetry reduction takes place through the superposition of two spin modes transforming according to the same irrep, mentioned in the previous section. Two cases of this type have been collected, namely $LiFeAs_2O_7$ (# 1.1.25) and $NaFeSi_2O_6$ (#1.1.37). In the case of $NaFeSi_2O_6$ (Baum *et al.*, 2015), the condensation of two independent order parameters transforming according to the same irrep seems well established, as this phase is preceded by another one with a single order parameter belonging to this irrep (see #1.1.36). In contrast, the model of $NaFeSi_2O_6$ (#1.1.37) was derived following the traditional representation method, where irrep restrictions coming from the operations transforming **k** into −**k** are not

considered, and a more symmetrical model with a single irrep order parameter was not tested.

The last structure in the list, $DyMn_6Ge_6$ (#1.1.10), is the only case where the incommensurate irrep superposes with a **k** = 0 spin modulation. As mentioned above, this implies that the operation {1′ | 0, 0, 0, 1/2}, present in all other structures, is absent, and the MSG of the average structure does not include the time-reversal operation. In contrast with all the other cases, the atomic magnetic moments therefore have nonzero average values. Typical incommensurate systems belonging to this class, with an additional **k** = 0 spin mode and a non-grey point-group symmetry, are all structures with conical spin modulations.

The magnetic point-group symmetry change between the paramagnetic and magnetic structures listed in Table 5 for each structure governs its possible ferroic properties. In particular, a symmetry break from a non-polar to a polar point-group symmetry is sufficient to have the symmetry conditions for a type II multiferroic, if it is an insulator. In general, a necessary (but not sufficient) condition for a non-polar/polar symmetry break is either a multidimensional small irrep for the magnetic order parameter, or the presence of two or more primary irreps, if their small irrep is one dimensional. As shown in Table 5, this collection includes five type II multiferroics. In four of them the symmetry break involves the superposition of two primary irreps ($TbMnO_3$, $MnWO_4$, $MnSb_2O_6$ and $NaFeSi_2O_6$), and only in the case of $RbFe(MO_4)_2$ is a single multidimensional primary irrep active (actually, it is a physically irreducible representation). It is important to stress that the multiferroic character of these phases can be derived directly from knowledge of the magnetic point group of the magnetic structure compared with that of the paramagnetic phase, without appealing to any particular mechanism. An additional important fact to note is that the presence of the symmetry operation {1′ | 0, 0, 0, 1/2} in all single-*k* incommensurate structures precludes the existence in these phases of any linear magnetoelectric or magnetoelastic effect within a single domain, the magnetic point-group of these phases being grey.

6. Conclusions

As a final word of caution, we should stress that the transformation to the unambiguous quantitative description used in this database has in many cases required an exercise in the interpretation of the tables, equations and/or figures in the original publications, and this may have been incorrect. Often, some clear ambiguities or inconsistencies were detected in the data, and the transformation of the proposed structure to a fully unambiguous description under a certain MSSG required some additional assumptions on our part. In such cases, comments describing the problem are included both on the entry web page and in the magCIF file. Our interpretation of some of the publications may therefore be defective and we would greatly appreciate any report of such types of problem.

Finally, we stress, as we did in our previous paper (Gallego *et al.*, 2016), that this collection does not pretend to become a complete and updated database of all published incommensurate magnetic structures. We lack the means for such an

endeavour. However, we hope that this work will stimulate further efforts within the community in the direction of the standardization and unambiguous communication of incommensurate magnetic structures through files in magCIF format, with the aim of making such a database possible in the not-too-distant future. Meanwhile, authors having published any incommensurate magnetic structure that is absent from this collection, and who are interested in having it included, are invited to contact us through the given email address.

APPENDIX F.A

Superspace symmetry relations using the parameterization of FullProf

In the superspace description, for single-*k* modulations, the spin modulation of a representative atom ν in the unit cell of the basic structure is expressed as

$$\mathbf{M}^{\nu}\left(x_4\right)=\mathbf{M}_0^{\nu}+\sum_{n=1,\ldots}\left[\mathbf{M}_{\sin n}^{\nu}\sin\left(2\pi n x_4\right)+\mathbf{M}_{\cos n}^{\nu}\cos\left(2\pi n x_4\right)\right], \tag{F.7}$$

with the value of the magnetic moment $\mathbf{M}^{\nu}_{\mathbf{L}}$ of atom ν in unit cell **L** being given by

$$\mathbf{M}_{\mathbf{L}}^{\nu}=\mathbf{M}^{\nu}\left[x_4=\mathbf{q}\cdot\left(\mathbf{L}+\mathbf{r}_{\mu}\right)\right], \tag{F.8}$$

Here **k** is the propagation vector and $\mathbf{r}_{\nu}$ is the position of atom ν within the unit cell. All quantities are real, and they are decomposed into three components along the crystallographic directions:

$$\begin{aligned}\mathbf{M}_{\sin n}^{\nu}&=\left(M_{x\sin n}^{\nu},M_{y\sin n}^{\nu},M_{z\sin n}^{\nu}\right),\\ \mathbf{M}_{\cos n}^{\nu}&=\left(M_{x\cos n}^{\nu},M_{y\cos n}^{\nu},M_{z\cos n}^{\nu}\right),\end{aligned} \tag{F.9}$$

In *FullProf* (Basireps), this spin modulation is expressed instead as

$$\mathbf{M}_{\mathbf{L}}^{\nu}=\mathbf{M}_0^{\nu}+\sum_{n}\left[\mathbf{S}_{n\mathbf{k}}^{\nu}\exp\left(-i2\pi n\mathbf{k}\cdot\mathbf{L}\right)+\mathbf{S}_{n\mathbf{k}}^{\nu *}\exp\left(i2\pi n\mathbf{k}\cdot\mathbf{L}\right)\right], \tag{F.10}$$

Note the explicit minus sign for the Fourier amplitude $\mathbf{S}^{\nu}_{\mathbf{k}}$ associated with **k**. Comparing the two expressions, the following relation exists between the two types of parameter:

$$2\mathbf{S}_{n\mathbf{k}}^{\nu}\exp\left(i2\pi n\mathbf{k}\cdot\mathbf{r}_{\nu}\right)=\mathbf{M}_{\cos n}^{\nu}+i\mathbf{M}_{\sin n}^{\nu}, \tag{F.11}$$

and for a single harmonic

$$2\mathbf{S}_{\mathbf{k}}^{\nu}\exp\left(i2\pi\mathbf{k}\cdot\mathbf{r}_{\nu}\right)=\mathbf{M}_{\cos 1}^{\nu}+i\mathbf{M}_{\sin 1}^{\nu}, \tag{F.12}$$

If we call:

$$\mathbf{S}_{\mathbf{k}}^{\nu}=\left[S\left(\mathbf{k}\right)_x^{\nu},S\left(\mathbf{k}\right)_y^{\nu},S\left(\mathbf{k}\right)_z^{\nu}\right], \tag{F.13}$$

then

$$\mathbf{M}^{\nu}_{\cos 1} = 2\,\mathrm{Re}\left\{\left[S(\mathbf{k})^{\nu}_{x}, S(\mathbf{k})^{\nu}_{y}, S(\mathbf{k})^{\nu}_{z}\right]\exp\left(i2\pi\mathbf{k}\cdot\mathbf{r}_{\nu}\right)\right\},$$
$$\mathbf{M}^{\nu}_{\sin 1} = 2\,\mathrm{Im}\left\{\left[S(\mathbf{k})^{\nu}_{x}, S(\mathbf{k})^{\nu}_{y}, S(\mathbf{k})^{\nu}_{z}\right]\exp\left(i2\pi\mathbf{k}\cdot\mathbf{r}_{\nu}\right)\right\}, \quad \text{(F.14)}$$

If {**R**, θ | **t**, t_4} is a symmetry operation, where θ is −1 or +1 depending on whether the operation includes time reversal or not, and a second atom μ is related to atom ν such that {**R** | **t**} $\mathbf{r}_{\nu} = \mathbf{r}_{\mu} + \mathbf{L}$ (with **L** some particular lattice translation), then the Fourier amplitudes of atom μ are related to those of atom ν by

$$\mathbf{M}^{\mu}\left(R_I x_4 + t_4 + \mathbf{H}_{\mathrm{R}}\cdot\mathbf{r}_{\nu}\right) = \theta\det(\mathbf{R})\,\mathbf{R}\cdot\mathbf{M}^{\mu}\left(x_4\right), \quad \text{(F.15)}$$

where R_I (+1 or −1) and the reciprocal lattice vector $\mathbf{H}_R$ are defined by the relation

$$\mathbf{k}\cdot\mathbf{R} = R_I\mathbf{k} + \mathbf{H}_{\mathrm{R}}, \quad \text{(F.16)}$$

Equation (F.15) implies that

$$\mathbf{M}^{\nu}_{\cos 1} + i\mathbf{M}^{\nu}_{\sin 1} = \exp\left[i2\pi\left(t_4 + \mathbf{H}_{\mathrm{R}}\cdot\mathbf{r}_{\nu}\right)\right]\times\theta\det(\mathbf{R})\,\mathbf{R}\cdot\left(\mathbf{M}^{\nu}_{\cos 1} + R_I i\mathbf{M}^{\nu}_{\sin 1}\right), \quad \text{(F.17)}$$

or, in terms of the *FullProf* (Basireps) parameters,

$$\mathbf{S}^{\mu}_{\mathbf{k}} = \theta\det(\mathbf{R})\,\mathbf{R}\mathbf{S}^{\nu}_{\mathbf{k}}\exp\left[-i2\pi\mathbf{k}\cdot\left(\mathbf{r}_{\mu} - \mathbf{r}_{\nu}\right)\right]\times\exp\left[i2\pi\left(t_4 + \mathbf{H}_{\mathrm{R}}\cdot\mathbf{r}_{\nu}\right)\right], \quad \text{(F.18a)}$$

if R_I = +1, and

$$\mathbf{S}^{\mu}_{\mathbf{k}} = \theta\det(\mathbf{R})\,\mathbf{R}\mathbf{S}^{\nu *}_{\mathbf{k}}\exp\left[-i2\pi\mathbf{k}\cdot\left(\mathbf{r}_{\mu} + \mathbf{r}_{\nu}\right)\right]\times\exp\left[i2\pi\left(t_4 + \mathbf{H}_{\mathrm{R}}\cdot\mathbf{r}_{\nu}\right)\right], \quad \text{(F.18b)}$$

if R_I = −1.

However, the two atomic positions are related in the form

$$\mathbf{k}\cdot\mathbf{r}_{\mu} - R_I\mathbf{k}\cdot\mathbf{r}_{\nu} = \mathbf{k}\cdot\mathbf{t} + \mathbf{H}_{\mathrm{R}}\cdot\mathbf{r}_{\nu}, \quad \text{(F.19)}$$

Equations (F.18*a*) and (F.18*b*) can then be put as

$$\mathbf{S}^{\mu}_{\mathbf{k}} = \theta\det(\mathbf{R})\,\mathbf{R}\mathbf{S}^{\nu}_{\mathbf{k}}\exp\left(-i2\pi\mathbf{k}\cdot\mathbf{t}\right)\exp\left(i2\pi t_4\right), \quad \text{(F.20a)}$$

if R_I = +1, and

$$\mathbf{S}^{\mu}_{\mathbf{k}} = \theta\det(\mathbf{R})\,\mathbf{R}\mathbf{S}^{\nu *}_{\mathbf{k}}\exp\left(-i2\pi\mathbf{k}\cdot\mathbf{t}\right)\exp\left(i2\pi t_4\right), \quad \text{(F.20b)}$$

if R_I = −1.

Note that these equations depend on the value of **t** in {**R** | **t**}, which implies a dependence on the choice made for atom μ among the set of atoms equivalent by lattice translations of the basic structure. Equations (F.20*a*) and (F.20*b*) can be used to introduce a certain superspace symmetry operation when using *FullProf* (Basireps), but

it has to be applied systematically, including all atoms in an orbit and all the operations of the superspace group.

F.A1. Example: inversion operation

If the system has an inversion centre {−1 | 0, 0, 0, 0} and two atoms are related by this inversion operation, so that $\mathbf{r}_\mu = -\mathbf{r}_\nu$, then their Fourier amplitudes according to equations (F.20*a*) and (F.20*b*) must be related in the form

$$\mathbf{S}_{\mathbf{k}}^{\mu} = \mathbf{S}_{\mathbf{k}}^{\nu *}. \tag{F.21}$$

However, if by convenience one is using as a representative for atoms μ the atom fulfilling $\mathbf{r}_\mu = -\mathbf{r}_\nu + (1, 0, 0)$, then {**R** | **t**} in equations (F.20*a*) and (F.20*b*) becomes {−1 | 1, 0, 0} and the relation of equation (F.21) must be changed to

$$\mathbf{S}_{\mathbf{k}}^{\mu} = \mathbf{S}_{\mathbf{k}}^{\nu *} \exp\left[-i2\pi\mathbf{k}\cdot(1,0,0)\right]. \tag{F.22}$$

This dependence on the atom representative is not present in the superspace parameterization, where for any **k** which does not include commensurate components making $\mathbf{H}_R \neq 0$ the relation is

$$\begin{aligned} \mathbf{M}_{\cos 1}^{\mu} &= \mathbf{M}_{\cos 1}^{\nu}, \\ \mathbf{M}_{\sin 1}^{\mu} &= -\mathbf{M}_{\sin 1}^{\nu}. \end{aligned} \tag{F.23}$$

If the inversion centre and atom ν lie at the origin, such that μ = ν for {−1 | 0, 0, 0, 0}, then its spin Fourier amplitude should be real:

$$\mathbf{S}_{\mathbf{k}}^{\mu} = \mathbf{S}_{\mathbf{k}}^{\mu *}. \tag{F.24}$$

However, if atom ν lies at (1/2, 0, 0), then the relevant MSSG operation is {−1 | 1, 0, 0, 0} and the same phase factor as in equation (22) appears. This phase shift only implies that, in fact, all modulations for atoms lying on inversion centres are in phase, considering their relative positions. Indeed, in the superspace parameterization, the invariance of atom μ for an MSSG operation {−1 | **t**, 0}, whatever the value of **t**, implies that $M^{\mu}_{\sin 1} = 0$ (if $\mathbf{H}_R = 0$). The application of the MSSG operations transforming **k** into −**k** with a given value of t_4 implies a specific choice of the global phase of the modulation. As this phase is arbitrary, the important result is that all atoms lying on inversion centres should be in phase.

Acknowledgements

The authors thank Branton Campbell and Harold Stokes for very helpful and fruitful interactions. The use of their program *ISODISTORT* and its constant improvements and extensions have been fundamental for the realization of this work. We are also indebted to V. Petříček for introducing the magCIF format into the communication tools of his program *JANA* which, as explained above, was used extensively to produce preliminary magCIF files of the structures. Very helpful comments and suggestions from Juan Rodriguez-Carvajal are also gratefully acknowledged. One of us (JMPM) is

also especially indebted to J. L. Ribeiro for helpful comments and interchange of information in the early stages of this work. This work was supported by the Spanish Ministry of Economy and Competitiveness and FEDER funds (project Nos. MAT2012-34740 and MAT2015-66441-P) and the Government of the Basque Country (project IT779-13).

References

Adroja, D. T., de la Fuente, C., Fraile, A., Hillier, A. D., Daoud-Aladine, A., Kockelmann, W., Taylor, J. W., Koza, M. M., Burzuri, E., Luis, F., Arnaudas, J. I. & del Moral, A. (2015). *Phys. Rev B* **91**, 134425.

Agrestini, S., Chapon, L. C., Daoud-Aladine, A., Schefer, J., Gukasov, A., Mazzoli, C., Lees, M. R. & Petrenko, O. A. (2008). *Phys. Rev. Lett*. **101**, 097207.

Bao, W., Pagliuso, P. G., Sarrao, J. L., Thompson, J. D., Fisk, Z., Lynn, J. W. & Erwin, R. W. (2000). *Phys. Rev. B* **62**, R14621.

Baum, M., Komarek, A. C., Holbein, S., Fernandez-Diaz, M. T., Andre, G., Hiess, A., Sidis, Y., Steffens, P., Becker, P., Bohaty, L. & Braden, M. (2015). *Phys. Rev. B* **91**, 214415.

Bertaut, E. F. (1968). *Acta Crystallogr. Sect. A* **24**, 217-231.

Biffin, A., Johnson, R. D., Choi, S., Freund, F., Manni, S., Bombardi, A., Manuel, P., Gegenwart, P. & Coldea, R. (2014a). *Phys. Rev B* **90**, 205116.

Biffin, A., Johnson, R. D., Kimchi, I., Morris, R., Bombardi, A., Analytis, J. G., Vishwanath, A. & Coldea, R. (2014b). *Phys. Rev. Lett*. **113**, 197201.

Blanco, J. A., Fak, B., Ressouche, E., Grenier, B., Rotter, M., Schmitt, D., Rodriguez-Velamazan, J. A., Campo, J. & Lejay, P. (2010). *Phys. Rev B* **82**, 054414.

Brown, I. D. & McMahon, B. (2002). *Acta Cryst. B* **58**, 317-324.

Campbell, B. J., Stokes, H. T., Tanner, D. E. & Hatch, D. M. (2006). *J. Appl. Crystallogr.* **39**, 607-614. http://stokes.byu.edu/isodistort.html.

Coldea, R., Tennant, D. A., Cowley, R. A., McMorrow, D. F., Dorner, B. & Tylczynski, Z. (1996). *J. Phys.: Condens. Matter* **8**, 7473-7491.

Damay, F., Martin, C., Hardy, V., Maignan, A., Gilles, A., Knight, K., Giblin, S. R. & Chapon, L. C. (2010). *Phys. Rev. B* **81**, 214405

Gallego, S. V., Perez-Mato, J. M., Elcoro, L., Tasci, E. S., Hanson, R. M., Momma, K., Aroyo, M. I. & Madariaga G. (2016). *J. Appl. Cryst.* (to be published).

Glazer, A. M., Aroyo, M. I. & Authier, A. (2014). *Acta Crystallogr. Sect. A* **70**, 300-302.

Hanson, R. (2013). *Jmol: an open-source Java viewer for chemical structures in 3D*. http://www.jmol.org/.

Harris, A. B. (2007). *Phys. Rev. B* **76**, 054447.

Harris, A. B., Kenzelmann, M., Aharony, A. & Entin-Wohlman, O. (2008). *Phys. Rev. B* **78**, 014407.

Herpin, A. & Meriel, P. (1961). *J. Phys. Radium* **22**, 337-348

Hwang, S. R., Li, W.-H., Lee, K. C., Lynn, J. W. & Wu, C.-G. (2000). *Phys. Rev. B* **62**, 14157.

IUCr (2015). *Commission on Magnetic Structures*, International Union of Crystallography, http://www.iucr.org/iucr/commissions/magnetic-structures.

Izyumov, Y. A., Naish, V. E. & Ozerov, R. P. (1991). *Neutron Diffraction of Magnetic Materials*. Dordrecht, Netherlands: Kluwer Acad.

Janner, A. & Janssen, T. (1980). *Acta Crystallogr. Sect. A* **36**, 408-415.
Janoschek, M., Fischer, P., Schefer, J., Roessli, B., Pomjakushin, V., Meven, M., Petricek, V., Petrakovskii, G. & Bezmaternikh, L. (2010). *Phys. Rev B* **81**, 094429.
Janssen, T., Janner, A., Looijenga-Vos, A. & de Wolff, P. M. (2006). *International Tables for Crystallography*, Vol. C: *Mathematical, Physical and Chemical Tables*. ed. E. Prince, p. 907-955. Dordrecht, Netherlands: Kluwer Acad.
Janssen, T., Chapuis, G. & de Boissieu, M. (2007). *Aperiodic Crystals: From Modulated Phases to Quasicrystals*. IUCr Monogr. Crystallogr. No. 20. Oxford, UK: Oxford Univ. Press.
Janssen, T. & Janner, A. (2014). *Acta Crystallogr. Sect. B* **70**, 617-651.
Johnson, R. D., Cao, K., Chapon, L. C., Fabrizi, F., Perks, N., Manuel, P., Yang, J. J., Oh, Y. S., Cheong, S. W. & Radaelli, P. G. (2013). *Phys. Rev. Lett*. **111**, 017202.
Keller, L., White, J. S., Frontzek, M., Babkevich, P., Susner, M. A., Sims, Z. C., Sefat, A. S., Ronnow, H. M. & Rüegg, Ch. (2015). *Phys. Rev B* **91**, 020409(R).
Kenzelmann, M., Harris, A. B., Jonas, S., Broholm, C., Schefer, J., Kim, S. B., Zhang, C. L., Cheong, S.-W., Vajk, O. P. & Lynn, J. W. (2005). *Phys. Rev. Lett*. **95**, 087206.
Kenzelmann, M., Lawes, G., Harris, A. B., Gasparovic, G., Broholm, A., Ramirez, P., Jorge, G. A., Jaime, M., Park, S., Huang, Q., Shapiro A. Y. & Demianets, L. A. (2007). *Phys. Rev. Lett*. **98**, 267205.
Kim, J.-H., Jain, A., Reehuis, M., Khaliullin, G., Peets, D. C., Ulrich, C., Park, J. T., Faulhaber, E., Hoser, A., Walker, H. C., Adroja, D. T., Walters, A. C., Inosov, D. S., Maljuk, A. & Keimer, B. (2014). *Phys. Rev. Lett*. **113**, 147206.
Lemoine, P., Verniere, A., Venturini, G., Mareche, J. F., Capelli, S. & Malaman, B. (2012). *J. Magn. Magn. Mater.* **324**, 2937-2952.
Litvin, D. B. (2013). *Magnetic Group Tables: 1-, 2- and 3-Dimensional Magnetic Subperiodic Groups and Magnetic Space Groups*. Chester, UK: International Union of Crystallography. http://www.iucr.org/publ/978-0-9553602-2-0.
Madariaga, G. (2005). *International Tables for Crystallography Volume G: Definition and exchange of crystallographic data*, First edition, Chapter 4.3, p. 270. Dordrecht, Netherlands: Kluwer Acad.
Makarova, O. L., Tsvyashchenko, A. V., Andre, G., Porcher, F., Fomicheva, L. N., Rey, N. & Mirebeau, I. (2012). *Phys. Rev. B* **85**, 205205.
Mannix, D., Coad, S., Lander, G. H., Rebizant, J., Brown, P. J., Paixao, J. A., Langridge, S., Kawamata, S. & Yamaguchi, Y. (2000). *Phys. Rev. B* **62**, 3801.
Manuel, P., Chapon, L. C., Todorov, I. S., Chung, D. Y., Castellan, J.-P., Rosenkranz, S., Osborn, R., Toledano, P. & Kanatzidis, M. G. (2010). *Phys. Rev. B* **81**, 184402.
Marty, K., Simonet, V., Ressouche, E., Ballou, R., Lejay, P. & Bordet, P. (2008). *Phys. Rev. Lett*. **101**, 247201.
Penc, B., Gerischer, S., Hoser, A. & Szytula, A. (2012). *J. Magn. Magn. Mater.* **324**, 657-659.
Perez-Mato, J. M., Ribeiro, J. L., Petricek, V. & Aroyo, M. I. (2012). *J. Phys. Condens. Matter.* **24**, 163201.
Perez-Mato, J. M., Gallego, S. V., Tasci, E. S., Elcoro, L., de la Flor, G. & Aroyo, M. I. (2015). *Annu. Rev. Mater. Res*. **45**, 13.1-13.32.
Petricek., V., Fuksa, J. & Dusek, M. (2010). *Acta Crystallogr. Sect. A* **66**, 649-655.
Petrıcek, V., Dusek, M. & Palatinus, L. (2014). *Z. Krist.* **229**(5), 345-352.

Petricek, V., Eigner, V., Dusek, M. & Cejchan, A. (2016). *Zeitschrift für Kristallogr. - Crystalline Materials* **231**, 301-312

Prokes, K., Petricek, V., Ressouche, E., Hartwig, S., Ouladdiaf, B., Mydosh, J. A., Hoffman, R.-D., Huang, Y.-K. & Pöttgen, R. (2014). *J. Phys.: Condens. Matter* **26**, 122201.

Reehuis, M., Ulrich, C., Maljuk, A., Niedermayer, Ch., Ouladdiaf, B., Hoser, A., Hofmann, T. & Keimer, B. (2012). *Phys. Rev. B* **85**, 184109.

Rodríguez-Carvajal, J. (1993). *Phys. B Condens. Matter*, **192**, 55–69.

Rodriguez-Carvajal, J. & Bouree F. (2012). *EPJ Web of Conferences* **22**, 00010.

Rousse, G., Rodriguez-Carvajal, J., Wurm, C. & Masquelier, C. (2013). *Phys. Rev B* **88**, 214433.

Scagnoli, V., Huang S. W., Garganourakis, R. A., de Souza, R. A., Staub, U., Simonet, V., Lejay, P. & Ballou, R. (2013). *Phys. Rev*. *B* **88**, 104417.

Stokes, H. T. & Campbell, B. J. (2011a). *ISO-MAG: table of magnetic space groups*. *ISOTROPY Software Suite.* http://iso.byu.edu.

Stokes, H. T., Campbell, B. J. & van Smaalen, S. (2011b). *Acta Cryst. A* **67**, 45-55

Stokes, H. T. & Campbell, B. J. (2014). *ISOCIF: create or modify CIF files*. *ISOTROPY Software Suite*. http://iso.byu.edu.

Tokura, Y., Seki, S. & Nagaosa, N. (2014). *Rep. Prog. Phys.* **77,** 076501.

Urcelay-Olabarria, I., Perez-Mato, J. M., Ribeiro, J. L., Garcia-Munoz, J. L., Ressouche, E., Skumryev, V. & Mukhin, A. A. (2013). *Phys. Rev. B* **87**, 014419.

Van Smaalen, S. (2007). *Incommensurate Crystallography.* IUCr Monogr. Crystallogr. No. 21. Oxford, UK: Oxford Univ. Press.